

Design and Synthesis of Purine Isosteres as Inhibitors of Nek2 and CDK2

This thesis is submitted to Newcastle University
for the degree of doctor of philosophy

David Michael Turner

April 2013

Declaration

The research described within this document was performed between October 2009 and October 2012 in the Medicinal Chemistry Laboratories, Bedson Building, Northern Institute for Cancer Research, Newcastle University, Newcastle-upon-Tyne, UK, NE1 7RU. This research was conducted in collaboration with scientists at the University of Leicester, Henry Welcome Building, Lancaster Rd, Leicester, LE1 9HN and the CR UK Centre for Cancer Therapeutics, The Institute of Cancer Research, 15 Cotswold Rd, Sutton, Surrey, UK, SM2 5NG and 237 Fulham Road, London, SW3 6JB.

All research described within this thesis is original in content, and does not incorporate any material or ideas previously published or presented by other authors except where due reference is given.

No part of this thesis has been previously submitted for a degree, diploma or any other qualification at any other university.

Acknowledgements

Firstly, I would like to thank my supervisors Dr Céline Cano, Professor Roger Griffin, Professor Bernard Golding and Dr Ian Hardcastle for their continued support and guidance throughout my PhD and during the construction of my thesis. I am very grateful for all the opportunities that I have had whilst studying at the NICR, and feel that my experience has helped to shape my future career path.

Additionally, I am very grateful to Dr Karen Haggerty and Carlo Bawn for their technical expertise and assistance during my PhD. I would also like to say thank you to all the members of the group and particularly the Nek2 team, who have made my time here at Newcastle University an unforgettable experience; Santosh Adhikari, Lauren Barrett, Dr Ruth Bawn, Annalisa Bertoli, Dr Tim Blackburn, Dr Benoit Carbain, Sarah Cully, Honorine Lebraud, Nicholas Martin, Dr Chris Matheson, Dr Elisa Meschini, Duncan Miller, Dr Stephanie Myers, Dr Sara Payne, James Pickles, Dr Tommy Rennison, Dr Charlotte Revill, Dr Jen Ricci, Andrew Shouksmith, Dr Kate Smith, Judith Unterlass, Dr Chris Wong, Bian Zhang and Dr Andrey Zaytsev.

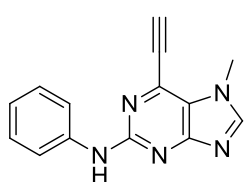
I would like to acknowledge all of the collaborators on the Nek2 and CDK2 projects including Professor Herbie Newell and Lan-Zhen Wang at the NICR and Dr Swen Holder and Katherine Boxall at the Institute of Cancer Research (ICR). I would also like to thank Dr Richard Bayliss and Dr Sharon Yeoh for their supervision and patience during my structural biology placement at the University of Leicester.

I want to express my gratitude to the Engineering and Physical Sciences Research Council (EPSRC) and Cancer Research UK for their generous funding of my PhD, and on-going research at the NICR.

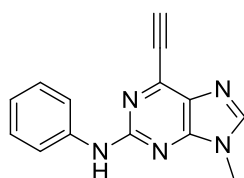
Finally, I would like to thank my parents Bob and Christine Turner and my girlfriend Kirsty Jackson for their continued support and encouragement throughout my studies.

Abstract

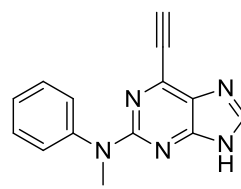
Nek2 and CDK2 are serine/threonine protein kinases that are implicated in cell cycle control and cancer. The Nek family of enzymes contains 11 known serine/threonine protein kinases (Nek1-11) and are involved in mitotic cell cycle control. There is evidence that of these 11 kinases, Nek2, Nek6, Nek7 and Nek9 play an important role in the regulation of mitotic events through microtubule control. Particular interest has been placed upon Nek2, which has been shown to have a critical role in mitosis, assisting centrosome disjunction. 6-Ethynyl purine **39**, was identified as a sub-micromolar irreversible inhibitor of Nek2 ($IC_{50} = 150$ nM), exhibiting good selectivity over other members of the Nek family. It was believed that this compound formed a triplet of H-bonds with the amino acids of the Nek2 ATP-binding site hinge region *via* the 2-amino N-H, the purine N^3 and the imidazole N^9H , allowing an initial non-covalent binding interaction, which facilitates subsequent covalent modification. To validate this binding motif and to act as control compounds, *N*-methylated purines **52-54** were synthesised, along with the 2-phenoxy purine **55** and the 2-benzylpurine **56**. These compounds were all essentially inactive in the Nek2 inhibition assay, which demonstrated that the purine 2-amino N-H group and imidazole N^9H were essential for non-covalent binding interactions.



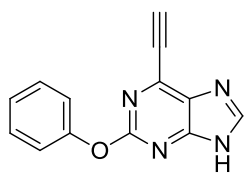
52
Nek2; $IC_{50} > 50$ μ M
CDK2; $IC_{50} > 100$ μ M



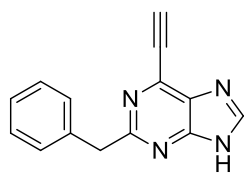
53
Nek2; $IC_{50} = 28.3$ μ M
CDK2; $IC_{50} > 100$ μ M



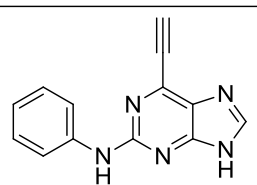
54
Nek2; $IC_{50} > 10$ μ M
CDK2; $IC_{50} > 100$ μ M



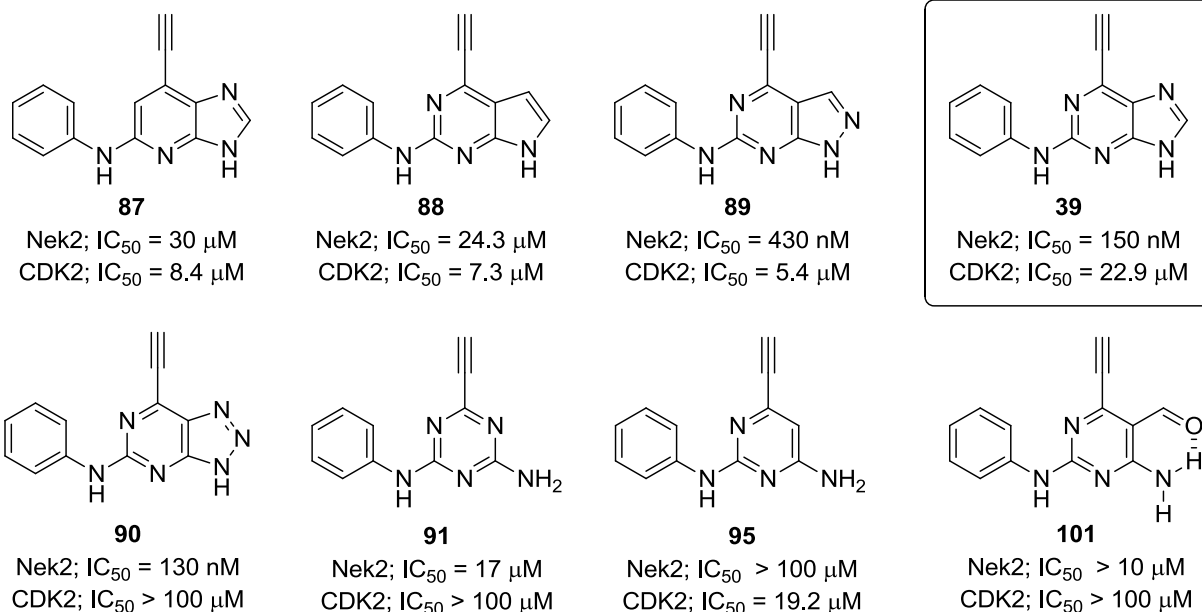
55
Nek2; $IC_{50} > 10$ μ M
CDK2; $IC_{50} > 100$ μ M



56
Nek2; $IC_{50} > 10$ μ M
CDK2; $IC_{50} > 100$ μ M



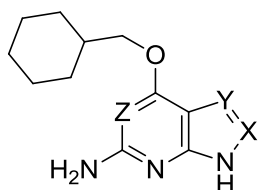
39
Nek2; $IC_{50} = 150$ nM
CDK2; $IC_{50} = 22.9$ μ M



To investigate the influence of the purine heterocycle upon Nek2 inhibitory activity and ethynyl group reactivity, heterocyclic derivatives of **39** were synthesised. Deazapurines **87** and **88** were weakly active in the Nek2 inhibition assay (IC₅₀ = 30 μM and 24 μM, respectively), whilst pyrazolopyrimidine **89** and triazolopyrimidine **90** had sub-micromolar activity comparable with the parent purine **39**. The 5-formylpyrimidine **101** and triazine **91** were modest inhibitors of Nek2 (IC₅₀ = > 10 μM and 17 μM, respectively). By contrast, pyrimidine **95** (10% inhibition at 100 μM) demonstrated weak Nek2 inhibitory activity.

Quantitative ¹H NMR (q¹H-NMR) kinetic studies were performed to model the reaction of ethynyl-functionalised heterocycles with Cys-22 at the Nek2 ATP-binding site. Compounds **54**, **56**, and **88-89** were reacted with *N*-acetylcysteine methyl ester in DMSO-*d*₆ at 24 °C under *pseudo* first order reaction conditions. The most reactive compounds were triazolopyrimidine **90** and pyrazolopyrimidine **89**. The 2-benzylpurine **56** and *N*-methylanilinopurine **54** had moderate reactivity, comparable with the parent purine **39**. The least reactive compound was pyrrolopyrimidine **88**, which was approximately 150-fold less reactive than purine **39**.

CDK2 is a member of the cyclin-dependent kinase (CDK) family of enzymes and a mediator of cell cycle progression. Of the 11 known human CDKs, four (CDK1, CDK2, CDK4 and CDK6) have been directly implicated in cell cycle regulation. Mutation of genes coding for CDKs are common in a variety of cancers, making CDKs attractive chemotherapeutic targets. Purines **249** and **37** were identified as moderate ($IC_{50} = 17 \mu M$) and potent ($IC_{50} = 5 nM$) ATP-competitive inhibitors of CDK2, respectively. The focus of this research was to determine whether subtle changes to the core heterocycle would allow retention of CDK-inhibitory activity.



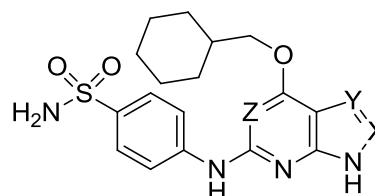
249, Purine; CDK2; $IC_{50} = 17 \mu M$
(X = CH, Y = N, Z = N)

254, Imidazopyridine; CDK2; $IC_{50} = 18 \mu M$
(X = CH, Y = N, Z = CH)

255, Pyrrolopyrimidine; CDK2; $> 100 \mu M$
(X = CH, Y = CH, Z = N)

256, Pyrazolopyrimidine; CDK2; $IC_{50} = 13 \mu M$
(X = N, Y = CH, Z = N)

257, Triazolopyrimidine; CDK2; $IC_{50} = 18 \mu M$
(X = N, Y = N, Z = N)



37, Purine; CDK2; $IC_{50} = 5 nM$
(X = CH, Y = N, Z = N)

250, Imidazopyridine; CDK2; $IC_{50} = 140 nM$
(X = CH, Y = N, Z = CH)

251, Pyrrolopyrimidine; CDK2; $IC_{50} = 26 nM$
(X = CH, Y = CH, Z = N)

252, Pyrazolopyrimidine; CDK2; $IC_{50} = 18 nM$
(X = N, Y = CH, Z = N)

253, Triazolopyrimidine; CDK2; $IC_{50} = 3 nM$
(X = N, Y = N, Z = N)

CDK2 inhibitors based on the pyrazolopyrimidine and triazolopyrimidine heterocycles (**256**, **252**, **257** and **253**) were of comparable potency with the corresponding purines (**249** and **37**). The most potent compound was triazolopyrimidine **253** with an IC_{50} value of 3 nM against CDK2. Interestingly, the pyrrolopyrimidine **255** proved only weakly active ($IC_{50} > 100 \mu M$), whereas the functionalised pyrrolopyrimidine **251** had potent CDK2 inhibitory activity ($IC_{50} = 26 nM$). Finally, imidazopyridine **254** exhibited activity comparable with purine **249**; however, imidazopyridine **250** was found to be approximately 30-fold less potent ($IC_{50} = 140 nM$) than the parent **37**, for reasons that remain unclear.

Abbreviations

A	AChE	Acetylcholinesterase
	ADP	Adenosine diphosphate
	AK-A	Aurora kinase-A
	AK-B	Aurora kinase-B
	Akt	See PKBb
	APC/C	Anaphase-promoting complex
	Asp	Aspartic acid
B	ATP	Adenosine triphosphate
	Bcl-2	B-cell lymphoma 2
	Bicd2	Protein bicaudal D homolog 2
	BRCA1	Breast cancer 1, early onset
	BRCA2	Breast cancer 2, early onset
	BTEA.NO2	Benzyltriethylammonium nitrate
	BTK	Bruton's tyrosine kinase
C	BUB1	Budding uninhibited by benzimidazoles 1
	CC	Coiled-coiled
	CDK	Cyclin-dependent kinase
	Chk1	Checkpoint kinase 1
	Chk2	Checkpoint kinase 2
	cLog <i>P</i>	Calculated partition coefficient
	CML	Chronic myelogenous leukemia
	C-Nap1	Centrosomal Nek2 associated protein
	COSY	Correlation spectroscopy
	Cys	Cysteine
D	DABCO	1,4-Diazabicyclo[2.2.2]octane
	dec.	Decomposed
	DIPEA	Diisopropylethylamine (Hünig's base)
	DISC	Death-inducing signalling complex
	DMP	Dess–Martin periodinane
	DNA	Deoxyribonucleic acid
E	ECM	Extracellular matrix
	EDC.HCl	<i>N</i> -(3-Dimethylaminopropyl)- <i>N'</i> -ethylcarbodiimide hydrochloride
	EGFR	Epidermal growth factor receptor
	ELSD	Evaporative light scattering detection
	EPSRC	Engineering and physical sciences research council
	ERK	Extracellular signal-regulated kinase
	Esp1	Separin
	EWG	Electron withdrawing group
F	FDA	Food and Drug Administration
	Flk-1	Foetal liver kinase-1
	FTIR	Fourier transform infra-red spectroscopy
G	GC	Gas chromatography

	GF	Growth factor
	GI ₅₀	Concentration required to inhibit cell growth by 50%
	Gln	Glutamine
	GIST	Gastrointestinal stromal tumour
	GSH	Glutathione
	GSK-3 β	Glycogen synthase kinase-3 β
H	Hec1	Highly expressed in cancer protein-1
	HEK293	Human embryonic kidney 293 cells
	HER2	Human epidermal growth factor receptor 2
	HFF	Human foreskin fibroblast cell line
	HMGA2	High mobility group AT-hook 2
	HPLC	High performance liquid chromatography
	HPV	Human papilloma virus
	HRMS	High resolution mass spectrometry
	HTT	Thyroid hyalinising trabecular tumour
	HuCCT1	Human cholangiocellular carcinoma cell line
I	IBX	2-Iodobenzoic acid
	IC ₅₀	The half maximal inhibitory concentration
	Ile	Isoleucine
	Inh-2	Inhibitor protein-2
	IPA	Isopropanol
	IR	Infrared
K	kDa	Kilodalton
L	LC-MS	Liquid chromatography mass spectrometry
	Leu	Leucine
	LRMS	Low resolution mass spectrometry
	Lys	Lysine
	LZ	Leucine zipper
M	MAD1	Mitotic spindle assembly checkpoint protein 1
	MAD2	Mitotic spindle assembly checkpoint protein 2
	MAPK	Mitogen-activated protein kinase
	MAPKK	Mitogen-activated protein kinase kinase
	<i>m</i> CPBA	Meta-chloroperoxybenzoic acid
	MDM2	Mouse double minute 2 homolog
	Met	Methionine
	MHz	Megahertz
	MAO	Monoamine oxidase
	MP	Melting point
	MPLC	Medium pressure liquid chromatography
	mRNA	Messenger ribonucleic acid
	MTOC	Microtubule organisation centre
	MW	Microwave
N	NBS	<i>N</i> -Bromosuccinimide
	NCS	<i>N</i> -Chlorosuccinimide

	Nek	NIMA related kinase gene-2
	NIMA	Never in mitosis gene-A
	Nlp	Ninelin-like protein
	NMR	Nuclear magnetic resonance
	NOE	Nuclear Overhauser effect
O	OBD	Optimal biologically effective dose
P	PARP-1	Poly (ADP-ribose) polymerase-1
	PCC	Pyridinium chlorochromate
	pc-Nap1	Phospho-C-Nap1
	PKBb	Protein kinase B beta
	PI-3K	Phosphoinositide 3-kinase
	Plk	Polo-like kinase
	PP1	Protein phosphatase 1
	ppm	Parts per million
	PPI	Protein-protein interaction
	pRb	Retinoblastoma protein
Q	qNMR	Quantitative NMR
R	RNA	Ribonucleic acid
	RaNi	Raney nickel
	RP	Reverse phase
	RSK2	Ribosomal s6 kinase
	RT	Room temperature
	RTK	Receptor tyrosine kinase
S	SAC	Spindle assembly checkpoint
	SAR	Structure-activity relationship
	SD	Standard deviation
	Ser	Serine
	siNEK2	Nek2 silencing RNA
	S _N Ar	Nucleophilic aromatic substitution
T	TBAN	Tetrabutylammonium nitrate
	TBDMS	<i>tert</i> -Butyldimethylsilyl
	TFAA	Trifluoroacetic anhydride
	THP	Tetrahydropyran
	TIPS	Triisopropylsilyl
	TLC	Thin layer chromatography
	tPSA	Topological polar surface area
	TSP-1	Thrombospondin-1
	Tyr	Tyrosine
U	U2OS	Human osteosarcoma cell line
	UPLC	Ultra performance liquid chromatography
	UV	Ultraviolet
V	VEGF-A	Vascular endothelial growth factor A

Table of Contents

Chapter One: Cancer in Human Health and Disease.....	16
1.1 Cancer Epidemiology.....	16
1.2 Pathophysiology of Cancer	16
1.2.1 Sustained Proliferative Signalling	18
1.2.2 Evading Growth Suppressors.....	19
1.2.3 Activating Invasion and Metastasis	19
1.2.4 Enabling Replicative Immortality	20
1.2.5 Inducing Angiogenesis	21
1.2.6 Resisting Cell Death.....	23
1.3 Small-Molecule Chemotherapeutic Agents in the Treatment of Cancer	24
1.3.1 Cytotoxic Cancer Chemotherapy	24
1.4 Targeted Cancer Chemotherapy	27
Chapter Two: Targeting Protein Kinases with Small-molecule Inhibitors	29
2.1 The Role of Protein Kinases in Cell Signalling.....	29
2.2 ATP-Competitive Inhibition of Protein Kinases	30
2.3 Irreversible Enzyme Inhibition.....	32
2.3.1 Safety of Irreversible inhibitors	33
2.3.2 Mechanisms of Covalent Enzyme Inhibition.....	33
2.3.3 Affinity Label Enzyme Inactivators	34
2.3.4 Mechanism-Based Inhibitors	35
2.3.5 Differences in the Therapeutic Window of Reversible and Irreversible Enzyme Inhibitors.....	36
2.3.6 Targeting Cysteine Thiols with Electrophilic Drugs	38
2.4 Kinase Inhibition – beyond the ATP-binding pocket.....	38
2.4.1 Allosteric Enzyme Inhibitors	38
2.4.2 Targeting Protein-Protein Interactions.....	39

2.5 Resistance to Small-molecule Kinase Inhibitors	40
2.6 Functionalised Purines as Kinase Inhibitors	42
Chapter Three: Mitotic Kinases and Cell Cycle Control	44
3.1 The Eukaryotic Cell Cycle.....	44
3.2 Molecular Mechanisms of Mitosis	45
3.3 The Centrosome Cycle	48
3.4 Centrosome Instability and Cancer.....	50
3.5 Targeting Mitosis in Cancer Chemotherapy.....	51
3.6 Protein Kinases and Cell Cycle Progression	51
3.7 Cyclin-Dependent Kinases (CDKs).....	51
3.7.1 CDKs in Cell Cycle Control	52
3.8 Aurora Kinases	53
3.9 Polo-like kinases (Plks).....	53
3.10 Never in Mitosis Gene-A Related Kinases (Neks)	54
Chapter Four: Targeting Nek2 with Small-Molecule Chemotherapeutic Agents	57
4.1 Nek2 is Implicated in Chromosomal Instability and Cancer	57
4.2 Nek2 Induces Centrosome Splitting at the G ₂ /M Transition.....	57
4.3 Nek2 in the Regulation of the Centrosome Associated Protein Nlp.....	59
4.4 Structural Features of Nek2 Kinase	59
4.5 Nek2 Regulation of the Spindle Assembly Checkpoint (SAC)	60
4.6 Nek2 is Implicated in Chromatin Condensation	62
4.7 Inhibition of Nek2 Results in Decreased Tumour Cell Growth	62
4.8 ATP-Competitive Reversible Inhibitors of Nek2	64
4.9 Oxindole Based Irreversible Inactivators of Nek2 Kinase	64
4.10 Purines as Irreversible Inhibitors of Nek2	67
Chapter Five: Synthesis of Purine Isosteres as Inhibitors of Nek2	69
5.1 Development of Purine-Based Irreversible Inhibitors of Nek2	69

5.2 Nek2 Putative Binding Mechanism	70
5.3 Reversibility of the Nek2-Cys-22 Covalent Complex	71
5.4 Structure-Activity Relationship Studies with 6-Ethynyl-2-Phenylaminopurine (39)	73
5.4.1 Synthesis of N^7 - and N^9 -Methyl-2-Phenylaminopurines (52) and (53).....	73
5.4.2 Synthesis of <i>N</i> -Methylanilinopurine (54).....	77
5.4.3 Synthesis of 2-Phenoxypurine (55)	78
5.4.4 Synthesis of 2-Benzylpurine (56)	81
5.5 Synthesis of Purine Isosteres	83
5.5.1 Synthesis of Imidazo[4,5- <i>b</i>]pyridine (87)	84
5.5.2 Synthesis of 7 <i>H</i> -Pyrrolo[2,3- <i>d</i>]pyrimidines (88) and (231).....	92
5.5.3 Synthesis of 1 <i>H</i> -Pyrazolo[3,4- <i>d</i>]pyrimidines (89) and (154)	98
5.5.4 Synthesis of 3-Methyl-1 <i>H</i> -pyrazolo[3,4- <i>d</i>]pyrimidine (165).....	103
5.5.5 3 <i>H</i> -[1,2,3]Triazolo[4,5- <i>d</i>]pyrimidines (90) and (232).....	106
5.5.6 Synthesis of 1,3,5-Triazine-based Nek2 inhibitors (91-94).....	112
5.5.7 Synthesis of Pyrimidine-Based Nek2 Inhibitors.....	114
5.5.8 Synthesis of 5-Halopyrimidines	119
5.5.9 Synthesis of 5-Formylpyrimidine (101).....	121
Chapter Six: Biological Evaluation of Nek2 Inhibitors	126
6.1 Structure-Activity Relationship Studies for 6-Ethynyl-2-Phenylaminopurine (39)	126
6.1.1 N^7 - and N^9 -Methylpurines (52) and (53)	126
6.1.2 Investigating the Requirement of the 2-Amino H-Bond of Purine (39) for Nek2 Inhibitory Activity.....	131
6.2 Ethynyl-Substituted Heterocyclic Derivatives of Purine (39) as Irreversible Nek2 Inhibitors.....	132
6.2.1 Imidazo[4,5- <i>b</i>]pyridine (87).....	132
6.2.2 7 <i>H</i> -Pyrrolo[2,3- <i>d</i>]pyrimidines (88) and (231)	132

6.2.3 1 <i>H</i> -Pyrazolo[3,4- <i>d</i>]pyrimidines (89) and (154).....	134
6.2.4 3-Methyl-1 <i>H</i> -Pyrazolo[3,4- <i>d</i>]pyrimidine (165).....	137
6.2.5 3 <i>H</i> -[1,2,3]Triazolo[4,5- <i>d</i>]pyrimidines (90) and (232).....	138
6.2.6 1,3,5-Triazine Based Nek2 Inhibitors	141
6.2.7 Pyrimidine Based Nek2 Inhibitors	142
6.2.8 5-Formylpyrimidine (101)	143
Chapter Seven: ¹ H-qNMR Kinetic Experiments of Irreversible Nek2 Inhibitors.....	145
7.1 Introduction to Quantitative ¹ H NMR (qNMR) Spectroscopy.....	145
7.2 Prerequisites for Successful qNMR Analysis.....	145
7.3 Optimisation of Relaxation Time - Inversion Recovery Experiment	147
7.4 qNMR Kinetic Analysis of Irreversible Nek2 Inhibitors	150
7.5 qNMR Kinetic Analysis – Results.....	152
7.5.1 Reaction of 2-Benzylpurine (56) with <i>N</i> -Acetylcysteine Methyl Ester (239)	152
7.5.2 Reaction of 2-Methylanilinopurine (54) with Thiol (239)	154
7.5.3 Reaction of Pyrrolopyrimidine (88) with Thiol (239).....	156
7.5.4 Reaction of Pyrazolopyrimidine (89) with Thiol (239)	158
7.5.5 Reaction of Triazolopyrimidine (90) with Thiol (239)	160
7.6 Discussion	162
7.7 Future qNMR Studies to Investigate the Reaction of Ethynyl-Functionalised Heterocycles with <i>N</i> -Acetylcysteine Methyl Ester (239).....	163
Chapter Eight: Synthesis of Purine Isosteres as Inhibitors of CDK2.....	164
8.1 The Role of CDK2 in Cell Cycle Regulation.....	164
8.2 Cell Cycle-Independent Functions of CDK2	165
8.3 CDK2 as a Target for Cancer Chemotherapy	165
8.4 SAR Studies with ATP-Competitive Heterocyclic CDK2 Inhibitors.....	166
8.5 Synthesis of Heterocyclic Derivatives of (249) and (37)	168
8.5.1 Synthesis of Imidazo[4,5- <i>b</i>]pyridines (254) and (250)	169

8.5.2 Synthesis of 7 <i>H</i> -Pyrrolo[2,3- <i>d</i>]pyrimidines (251) and (255).....	173
8.5.3 Synthesis of 1 <i>H</i> -Pyrazolo[3,4- <i>d</i>]pyrimidines (252) and (256)	179
8.5.4 Synthesis of 3 <i>H</i> -[1,2,3]Triazolo[4,5- <i>d</i>]pyrimidines (253) and (257)	180
8.6 CDK2-Inhibitory Activity for Isosteres of 2-Amino-6-Cyclohexylmethoxypurine	181
8.7 CDK2 IC ₅₀ Determination of Alternative Heterocycles Based on Purine (37)	182
8.8 Potentiation of Cisplatin Cytotoxicity by NU2058 (249) and Analogues.....	183
Chapter Nine: Conclusions and Future Work	187
9.1 Design and Synthesis of Irreversible Inactivators of Nek2	187
9.2 qNMR Kinetic Analysis of Irreversible Nek2 Inhibitors	189
9.3 Design and Synthesis of ATP-Competitive CDK2 Inhibitors	190
Chapter Ten: Experimental Section	192
10.1 Solvents and Reagents.....	192
10.2 Equipment and Analysis	192
10.2.1 Analytical Techniques	192
10.2.2 Microwave Reactions	193
10.2.3 Chromatography	193
10.2.4 Analytical High Performance Liquid Chromatography	193
10.2.5 Small-Molecule <i>X-ray</i> Crystallography	194
10.3 Biological Evaluation of Nek2 and CDK2 inhibitors.....	194
10.3.1 Nek2 Biochemical Assay	194
10.3.2 CellTiter-Blue Assay for Cell Growth Inhibition.....	196
10.3.3 CDK2/Cyclin A3 Biochemical Assay	197
10.3.4 Nek2 Protein Crystallography.....	198
10.4 Index of Synthesised Compounds	198
10.5 General Procedures.....	203
Appendix	318

i - Small-Molecule <i>X-ray</i> Crystallography Data	318
ii - ¹ H-qNMR Experimental Data.....	340
Bibliography	347

Chapter One: Cancer in Human Health and Disease

1.1 Cancer Epidemiology

Cancer is a disease characterised by loss of normal cell function resulting in rapid uncontrolled cell proliferation and growth.¹ Cancer has become the major cause of death globally with an estimated 7.6 million fatalities attributed to cancer in 2008 alone.² It is predicted that this figure will continue to rise to over 13.1 million by the year 2030, making new cancer drug development an area of crucial interest.² There are over two hundred forms of cancer, and it is known that cancer can develop in almost every tissue type, with the most common forms being breast, lung, colorectal and prostate cancer.^{1,3}

A normal healthy cell may become cancerous through the accumulation of genetic mutations resulting in loss of cell differentiation and uncontrolled proliferation. These mutations may be present at birth, or more commonly are the result of chronic exposure to genotoxic stimuli such as chemical carcinogens (e.g. asbestos and tobacco smoke), viruses (e.g. human papilloma virus (HPV)) or physical carcinogens (e.g. UV light and ionising radiation).² The human body has evolved mechanisms to protect against genetic damage, and most often cells bearing these abnormalities are quickly destroyed or repaired. It is rare that a single mutation will result in malignancy, as this is usually a multistep process requiring the accumulation of many mutations of different genes over time. It is for this reason that 75% of all new cases of cancer in the UK are diagnosed in patients aged 60 and over.⁴

1.2 Pathophysiology of Cancer

For a cell to become malignant it must develop errors in the regulation of homeostasis through mutations that favour enhanced growth and proliferation.⁵ These mutations may be viewed as minor changes to the DNA sequence through point mutations (single base substitution), or larger scale changes such as translocations, deletions, and amplifications which alter chromatin structure.⁴

Mutations become problematic when they accumulate, causing disruption of the cell cycle through oncogene activation or removal of vital tumour suppressor gene

function.⁴ Oncogenes (e.g. RAS and ERK) are genes that are highly and/or abnormally expressed in tumour tissue and are known to induce cancer in cells. These genes derive from proto-oncogenes through a function-altering mutation.⁶ Tumour suppressor genes (e.g. p53 and BRCA1) are key regulatory genes that function to prevent carcinogenesis. As with all genes, there are two copies of each individual proto-oncogene or tumour suppressor gene present in every cell. Mutation of both alleles of these genes is required to alter function, which is why mutations that give rise to cancer are usually somatic and occur over long periods of time. Inherited mutations may occur when a defective gene is passed down from a parent to their offspring. The remaining dominant allele maintains function; however, individuals are at increased risk of developing cancer.^{1,6}

The transition of normal healthy cells to a neoplastic state is a complex process requiring the acquisition of a number of traits. In 2000, Hanahan and Weinberg proposed six acquired capabilities of cells that induce oncogenesis.⁷ This was updated in 2011 to include the traits shown in Figure 1.⁵ In the following section, each trait will be discussed to provide an overview of the events preceding malignancy.

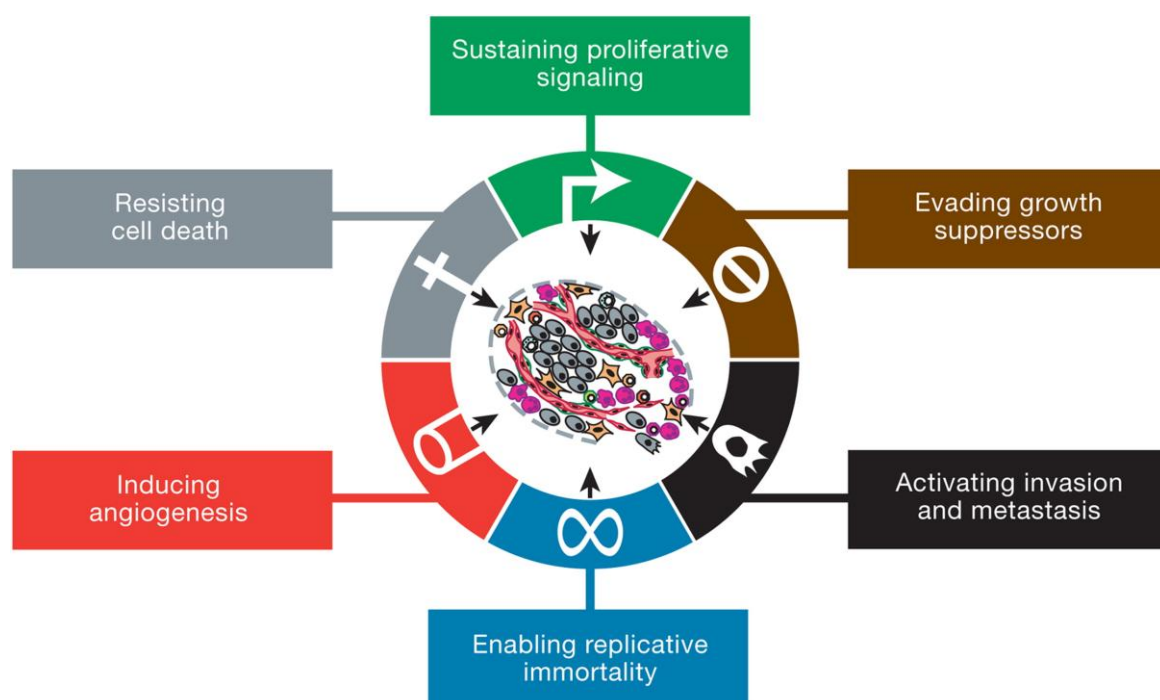


Figure 1 - Hallmarks of cancer as described by Hanahan and Weinberg 2011.⁵

1.2.1 Sustained Proliferative Signalling

Cells in a dormant non-proliferative state may become active through mitogenic signalling. This signalling occurs *via* transmembrane receptors that detect growth factors, extracellular matrix components and cell-cell adhesion molecules. External signals are then transmitted across the cell membrane to promote growth and proliferation.^{5,7} In healthy cells these processes are tightly regulated and essential for maintaining homeostasis. In cancerous cells this control system is compromised, resulting in aberrant signalling to favour sustained proliferation.⁵

Premalignant epithelial cells must acquire multiple mutations before malignancy develops. The process of tumour progression occurs over several stages and requires multiple growth factors. These are small polypeptide molecules that bind to transmembrane receptors causing activation of proliferative signalling cascades (e.g. mitogen-activated protein kinase (MAPK) and phosphoinositide 3-kinase (PI-3K)) to favour transcription and ultimately clonal expansion.⁸ The expression of growth factors (GFs) in normal healthy cells is a highly regulated process and functions through a paracrine mode of action. In cancer cells this regulation is lost, allowing cells to evade proliferative control and develop self-sufficiency in growth signals, leading to sustained proliferative signalling.⁷

A method of achieving self-sufficiency is through mutations that induce GF secretion in neoplastic cells. By generating their own GFs, cancer cells may be stimulated to continually replicate through autocrine signalling.⁹ Alternatively, tumour cells can exploit the presence of ambient GFs and become hypersensitised through the increased expression of receptor tyrosine kinases (RTKs) (e.g. epidermal growth factor receptor (EGFR)) at the cell surface. This allows cancerous cells to proliferate in the presence of low levels of GFs that would not normally permit replication.^{7,10,11} Overexpression of these receptors, or the expression of mutated receptors, has been implicated in ligand-independent proliferative signalling.^{12,13} GF-independent induction of cell proliferation may also occur through downstream activation of intrinsic signalling cascades. An example of this is the activation of B-Raf protein, which when mutated stimulates the Raf-mitogen-activated protein (MAP)-kinase pathway resulting in cell proliferation.^{5,14}

1.2.2 Evading Growth Suppressors

Negative regulation of growth and proliferation is an essential component of normal cell homeostasis, designed to prevent malignant transformation. It has been demonstrated experimentally in mice that signalling cascades that orchestrate growth suppression often contain established tumour suppressor genes.⁵ These suppressor genes are frequently mutated in cancers, resulting in inactivation, and permitting unregulated growth. Two key tumour suppressor genes that regulate cell proliferation and are commonly mutated in cancers are the genes coding for retinoblastoma-associated protein (pRb) and p53. The gene coding for pRb receives primarily extracellular signals, which are interpreted and combined to make the decision whether a cell should be allowed to grow and proliferate, or enter a state of senescence. pRb is an important checkpoint protein, restricting progression beyond the G₁ stage of the cell cycle.^{15,16} Cancer cells with mutated pRb lack this vital gatekeeper, allowing cells to enter a persistent proliferative state.⁵ By contrast, the gene coding for p53 (TP53) responds to intracellular stress and damage signalling pathways by monitoring the level of free nucleotide bases, glucose and oxygen, as well as the intensity of growth-promoting signals. If conditions are deemed sub-optimal, TP53 forces the cell into a state of senescence until conditions are returned to normal. Additionally, If significant cellular damage is detected, TP53 can activate apoptotic signalling pathways resulting in programmed cell death.¹⁷ Somatic mutations of TP53 are very common in human cancer.¹⁸

1.2.3 Activating Invasion and Metastasis

Metastasis involves a series of events that allow transport of cancerous cells from a primary tumour to distant parts of the body, resulting in the formation of secondary tumours. Tumour metastasis is associated with poor prognosis and is the primary cause of cancer-related deaths.¹⁹⁻²¹ Surgical treatment of metastatic tumours is rarely attempted due to the systemic distribution of the disease. Treatment usually involves a combination of chemotherapy, hormone therapy and radiation; however, success is limited, and this treatment functions primarily as a palliative solution.²²

The first stage in the process of metastasis is the invasion of surrounding tissue by neoplastic cells. To facilitate this, a change in the tumour phenotype must occur that causes a loss of cell adhesion through disruption of cell-cell interactions and cell-extracellular matrix (ECM) binding (Figure 2).^{23,24} Proteases are recruited that cause degradation of the ECM, which liberates growth factors and chemokines favouring cell motility.²² Liberated cells are then able to enter the blood stream or lymphatic system *via* the tumour blood vessels.²¹ Cells are transported systemically until reaching the site of dissemination where they arrest through the use of specific adhesion factors or, more commonly, owing to size restriction in the capillaries.²² At this point malignant cells may extrude from the vessel (extravasation) and enter surrounding tissue. If these cells survive the microenvironment of the tissues in which they reside, secondary tumour formation may occur through cell growth and proliferation.¹⁹⁻²²

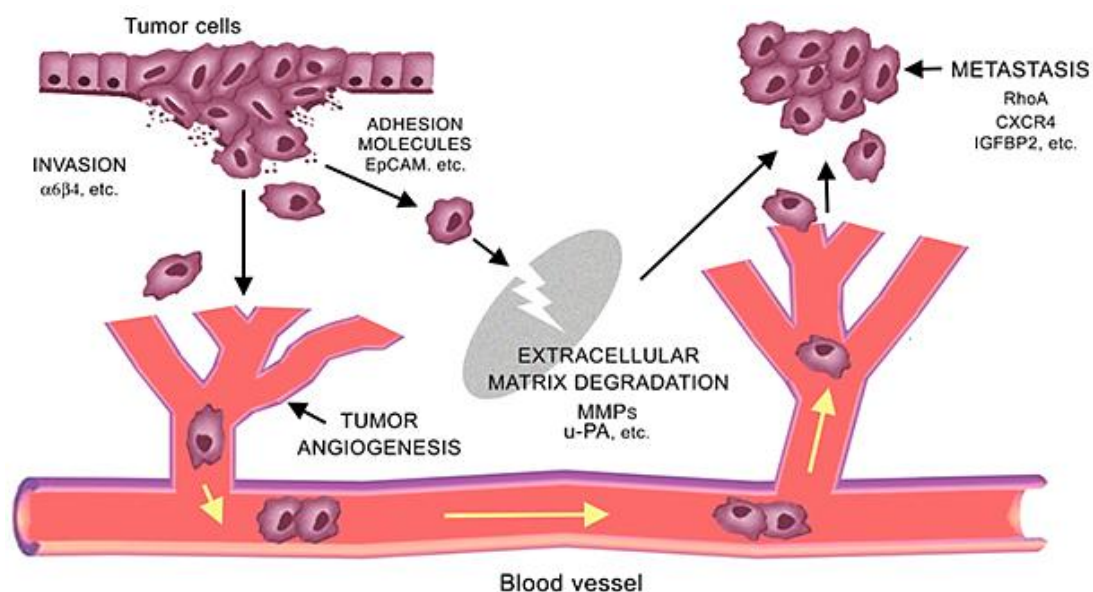


Figure 2 – Schematic representation of tumour metastasis (adapted from Pai *et al.*).²⁵

1.2.4 Enabling Replicative Immortality

The chromosomes of normal cells contain repetitive nucleotide sequences (TTAGGG) known as telomers that protect against genomic instability, and hence malignancy, through the prevention of chromosomal degradation.²⁶ With each subsequent round of the cell cycle, telomer length decreases until eventually the protective telomer cap is removed.²⁷ This may cause cells to enter a non-replicative

state (senescence) or to proceed to a crisis phase due to end-on chromosome ligation, arrest of the cell cycle and activation of apoptotic signalling cascades.⁵ Telomerase is a DNA polymerase that functions to increase telomere length, thus enhancing the replicative potential of cells. Expression of telomerase is generally low in somatic cells; however, telomerase is expressed at significant levels in approximately 90% of immortalised cells including T-lymphocytes and tumour cells.⁵ Overexpression of telomerase allows tumour cells to subvert senescence and apoptosis through the prevention of telomere shortening, enabling replicative immortality. Interestingly, recent findings have suggested that delayed telomerase upregulation in preneoplastic cells that allows telomere shortening, may induce mutations leading to malignancy. It is suggested that subsequent activation of telomerase stabilised these cells allowing immortality and tumour progression.^{5,28}

1.2.5 Inducing Angiogenesis

As tumour volume expands beyond a small population of cells, there is an elevated demand for nutrients and oxygen as well as increased waste production.²⁹ Up until this point, metabolic needs are met by passive diffusion at a rate proportional to tumour surface area (Figure 3, **A**). The level of diffusion becomes insufficient for further growth at a tumour size of 1-2 mm, and, as such, many tumours remain dormant and do not develop further.^{30,31} To expand beyond these biophysical constraints a tumour must establish its own blood supply through a process known as angiogenesis.^{5,7,31}

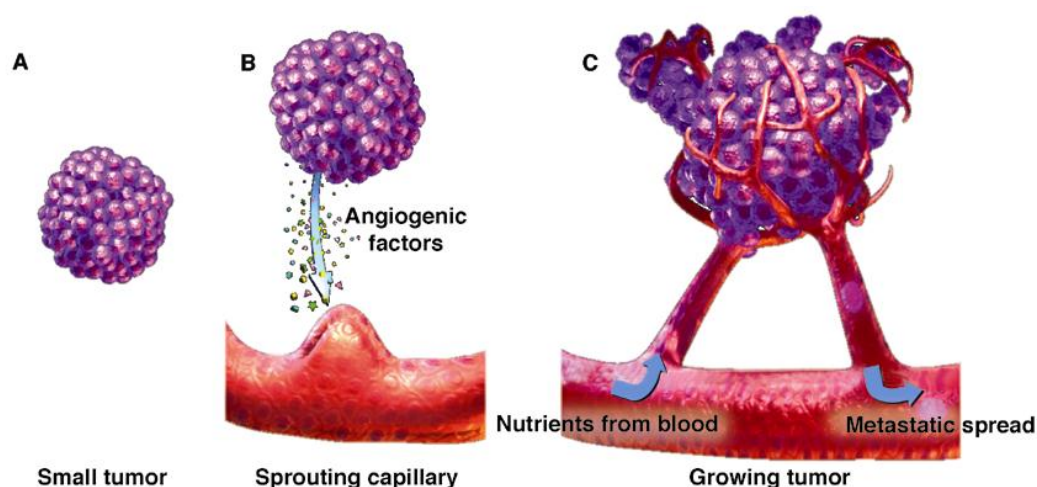


Figure 3 – Schematic representation of tumour angiogenesis (adapted from Siemann).³²

At gestation, normal healthy cells undergo embryonic vasculogenesis allowing formation of the vascular tree. This primary network of blood vessels is adapted and modified to ensure suitable delivery of nutrients throughout the body.^{29,33} Subsequent changes to the vascular structure are required for growth and repair and occur through angiogenesis. In normal tissue this process is highly regulated and controlled by a number of pro- and anti-angiogenic signalling cascades.³⁴ By contrast, the balance of angiogenic signals in vascular tumours is disrupted to favour angiogenesis in a process known as an 'angiogenic switch'.^{5,34} As an avascular tumour grows in size, angiogenesis may be activated through the release of angiogenic factors that bind to surrounding host blood vessels to induce capillary formation (Figure 3, **B**). These capillaries infiltrate the tumour body providing nutrients and oxygen to satisfy metabolic demands (Figure 3, **C**).^{29,31} Unlike normal angiogenesis, which is transient, tumour angiogenesis remains constantly active favouring rapid vascularisation and growth. Tumour vasculature appears irregular, convoluted and poorly formed as growth is unregulated.³⁴ These vessels are also highly permeable with little basal membrane or cellular junctions when compared to normal blood vessels. Tumour vessels are therefore an ideal conduit for carcinoma cells to enter the circulatory system, possibly allowing the development of metastatic tumours.³⁵

A major inducer of tumour angiogenesis is vascular endothelial growth-factor-A (VEGF-A),³¹ and mRNA coding for VEGF-A is greatly up-regulated in the majority of human cancers. Similarly, elevated levels of VEGF and its partner receptor Flk-1 have been reported in metastatic colon cancer at levels proportional to tumour vascularisation.³⁶ VEGF-A is a well characterised 34-42 kDa glycoprotein that functions as a cytokine, binding to and activating three structurally related type III receptor tyrosine kinases (VEGFRs 1-3 also known as FLT1, KDR and FLT4, respectively).^{37,38} In doing so, a number of downstream effects occur *via* signalling cascades. VEGF-A can induce angiogenesis through a number of mechanisms including elevated endothelial cell proliferation, increased vascular permeability, lattice formation, promotion of endothelial cell migration, and chemotaxis of vascular precursor cells.³⁸ Elevated VEGF-A gene expression in tumours may occur as a consequence of oncogenic signalling and/or hypoxia-induced cellular stress.⁵

A number of factors exist to control angiogenesis by inhibiting proangiogenic signalling cascades. One such molecule is thrombospondin-1 (TSP-1), a matricellular glycoprotein known to regulate cell proliferation, migration and apoptosis.^{5,39} These processes require the formation of cell surface multi-protein complexes to enable signal transduction. It is the role of TSP-1 to enable correct orientation and composition of these complexes by specific interaction with growth factors and cytokines, as well as components of the extracellular matrix and cell membrane. In doing so, TSP-1 can neutralise proangiogenic signals, thereby suppressing tumour growth.³⁵

A second protein critical for inhibition of tumour angiogenesis is p53, a protein expressed by the gene TP53. p53 is a well-established tumour suppressor gene essential for maintaining genomic stability.⁴⁰ Among numerous additional tumour suppressive functions, p53 may limit angiogenesis through induction of cell-cycle arrest and initiation of apoptosis. Additionally, p53 is able to inhibit hypoxia-induced angiogenesis by preventing activation of proangiogenic growth factors such as VEGF.⁴¹ Mutation of genes coding for antiangiogenic ligands are a leading cause of the angiogenic switch, resulting in increased tumour vasculisation and growth.

1.2.6 Resisting Cell Death

Apoptosis is a method of programmed cell death employed to remove redundant, damaged or infected cells. This process is essential for foetal development as well as in homeostasis, and as a form of defence against DNA damage and pathogens in adult tissue.^{42,43} Apoptosis involves a series of interconnected biochemical events that enable selective caspase activation in cells labelled for destruction.⁴⁴ Caspases are proteolytic enzymes that induce apoptosis, causing cells to shrink, undergo chromatin degradation, and eventually break apart into small fragments known as vesicles which are later phagocytosed and destroyed.⁴³ There are two major pathways involved in apoptosis, the extrinsic receptor-mediated pathway and the intrinsic mitochondrial pathway. The extrinsic pathway is activated by extracellular ligands that induce assembly of the death-inducing signalling complex (DISC) and stimulate receptor oligomerization. The intrinsic mitochondrial pathway induces apoptosis through modification of pro- and anti-apoptotic signalling *via* the regulatory

B-cell lymphoma 2 (Bcl-2) family of proteins.⁵ This allows apoptosome formation due to mitochondrial release of cytochrome c, which triggers a signalling cascade resulting in caspase activation and ultimately apoptosis.⁴⁴ The evasion of apoptosis in tumour cells may occur through activation of specific oncogenes with antiapoptotic functions (e.g. c-Myc) or disablement of pro-apoptotic tumour suppressor genes (e.g. Chk1/Chk2 and p53) allowing rapid expansion of the cell population.⁴⁴⁻⁴⁶ Modulation of apoptosis through targeting of the underlying cell death signalling pathways or removal of endogenous apoptotic inhibitors in tumour cells may have a therapeutic benefit for the treatment of cancers.¹⁷ Most therapeutic agents of this type are in the early stages of clinical development; however, there is substantial interest in the development of these compounds for use in combination with established cancer chemotherapeutic agents.⁴⁷

1.3 Small-Molecule Chemotherapeutic Agents in the Treatment of Cancer

The treatment of cancer may consist of localised treatments such as surgery and radiotherapy, or systemic treatment through the use of chemotherapeutic drugs. It is the goal of the majority of anticancer drugs currently in development, to prevent tumour progression by inhibiting cell growth and division (cytostatic drugs) or killing tumour cells (cytotoxic drugs).⁴ There are two broad classes of cancer chemotherapeutic agents, traditional cytotoxic drugs, and targeted therapies.

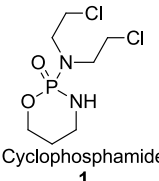
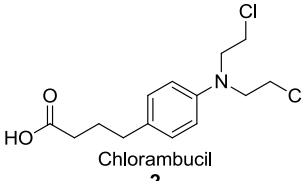
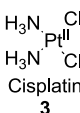
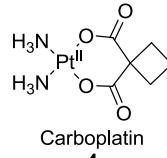
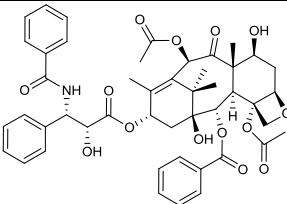
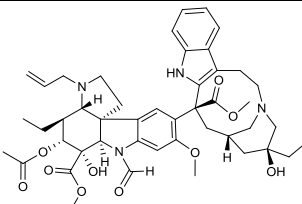
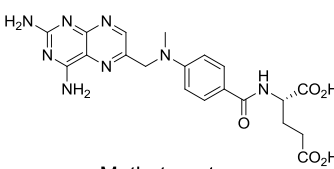
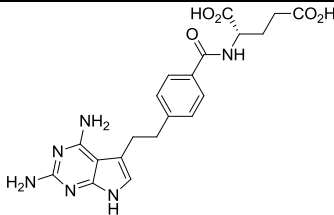
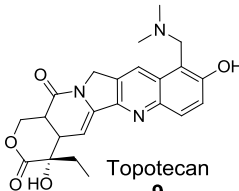
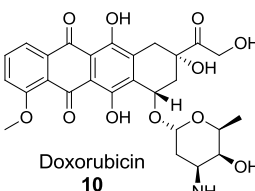
1.3.1 Cytotoxic Cancer Chemotherapy

Conventional cytotoxic anticancer drugs non-specifically target enzymes and macromolecules (e.g. DNA) causing toxicity and ultimately cell death. Once administered, these compounds are distributed systemically and accumulate in cells with high proliferative activity. This causes greater susceptibility to drug induced toxicity in cancer cells as they are rapidly dividing and, as such, have high metabolic demands.⁴⁸ However, a disadvantage of cytotoxic cancer chemotherapy is that compounds are indiscriminately cytotoxic, and therefore induce toxicity in all rapidly dividing cells including those found in the gut epithelium, bone-marrow and hair-follicles. This gives rise to the classical toxicities associated with cancer chemotherapy, such as gastrointestinal disturbance, myelosuppression and

alopecia.⁴⁸⁻⁵⁰ These side-effects can result in substantial patient discomfort and may in some cases be dose-limiting.

Table 1. shows a selection of traditional cytotoxic drugs used in the treatment of cancer. The choice of the correct chemotherapeutic regime is greatly dependent upon the type of cancer, drug resistance and side-effects of treatment. Traditional cytotoxic cancer chemotherapeutics remain an important part of the arsenal of anticancer drugs.

Table 1. Examples of common cytotoxic agents used in the treatment of cancer

Class	Structure/Name	
DNA-alkylating agent (Nitrogen mustards)	 Cyclophosphamide 1	 Chlorambucil 2
	 Cisplatin 3	 Carboplatin 4
Mitotic inhibitor (taxanes and vinca alkaloids)	 Paclitaxel 5	 Vincristine 6
	 Methotrexate 7	 Pemetrexed 8
Topoisomerase inhibitor	 Topotecan 9	 Doxorubicin 10

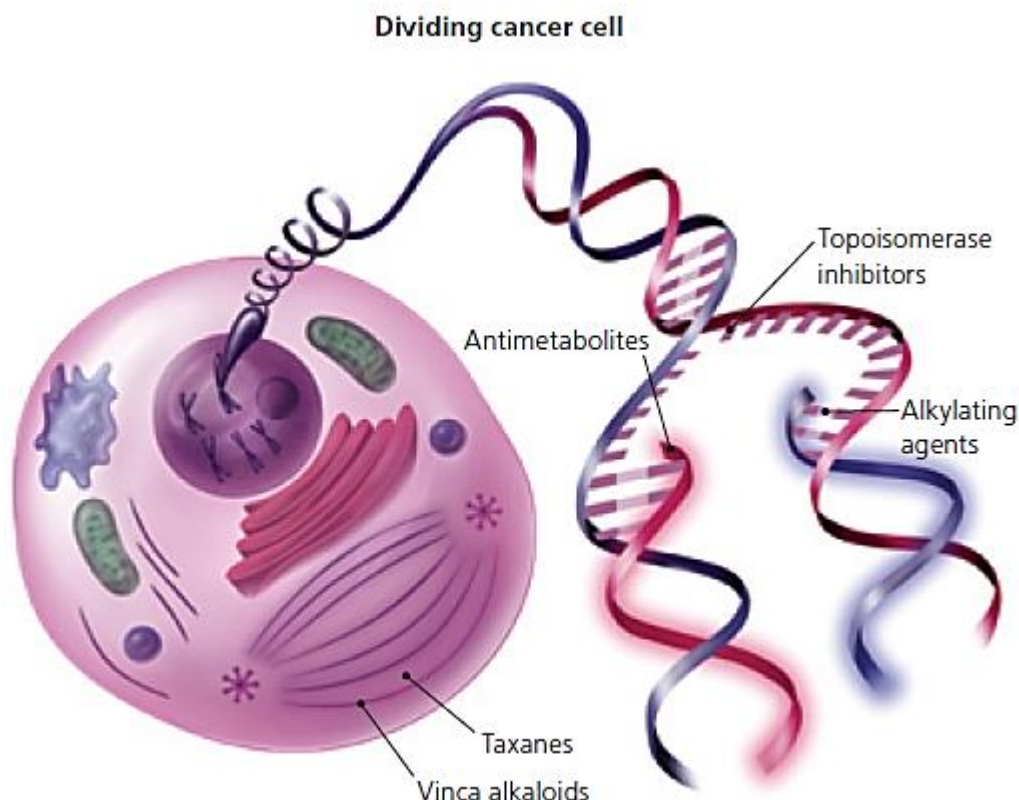


Figure 4 – Cytotoxic cancer chemotherapy.⁴⁹

Traditional cytotoxic agents work by inhibiting cell division. Figure 4 shows the various classes of cytotoxics. Antimetabolites (e.g. methotrexate **7** and pemetrexed **8**) prevent DNA replication by inhibiting nucleic acid formation. Topoisomerase inhibitors (e.g. topotecan **9** and doxorubicin **10**) prevent relaxation of DNA supercoiling. Alkylating agents including nitrogen mustards (e.g. cyclophosphamide **1** and chlorambucil **2**) and platinum based compounds (e.g. cisplatin **3** and carboplatin **4**) form single and double strand breaks in DNA through alkylation of purine bases. Finally, taxanes (e.g. paclitaxel **5**) and vinca alkaloids (e.g. vincristine **6**) inhibit mitosis by disrupting microtubule function.⁴⁹

As mentioned previously, it is difficult to avoid nonspecific-cytotoxicity with traditional cytotoxic drugs. Also, due to systemic distribution and indiscriminate drug binding, a large dose of compound is often required to achieve a therapeutic concentration at the tumour site. To combat this and improve selectivity, several mechanistically new cytotoxic drug targeting approaches have been adopted to elevate drug accumulation in cancerous cells.⁵¹ One such approach is to target subtle differences

in tumour physiology such as enzyme expression, hypoxia and pH, by designing compounds that exploit these differences.

1.4 Targeted Cancer Chemotherapy

Over the past 20 years cancer research has advanced dramatically. A detailed understanding of the molecular and genetic processes responsible for oncogenesis has allowed the discovery of new targeted anticancer therapies. Unlike traditional cytotoxics, targeted chemotherapy is directed towards specific enzymes/pathways critical for tumour progression.⁵² These pathways include targets such as growth factors, signalling molecules, cell-cycle proteins and processes involved in apoptosis and angiogenesis.^{5,7,48} An attractive feature of targeted chemotherapy is the potential for low cytotoxicity in normal healthy tissue, whilst maintaining good efficacy against neoplastic cells leading to a broader therapeutic window.^{50,53} Unlike cytotoxic therapy, which is administered at the maximum tolerated dose, targeted therapy is given at the optimal biologically effective dose (OBD). This is the dose level designed to 'saturate' the target causing inactivation. In many cases this will be substantially lower than the maximum tolerated dose. It is unnecessary to further increase the dose as this may result in needless toxicity.⁵⁴ Targeted therapy is often cytostatic as cell proliferation and/or metastasis is prevented without significant tumour regression.⁵⁵ Long dosing regimens are often required, and, as such, orally active drugs with minimal chronic side-effects are most desirable.⁵⁴

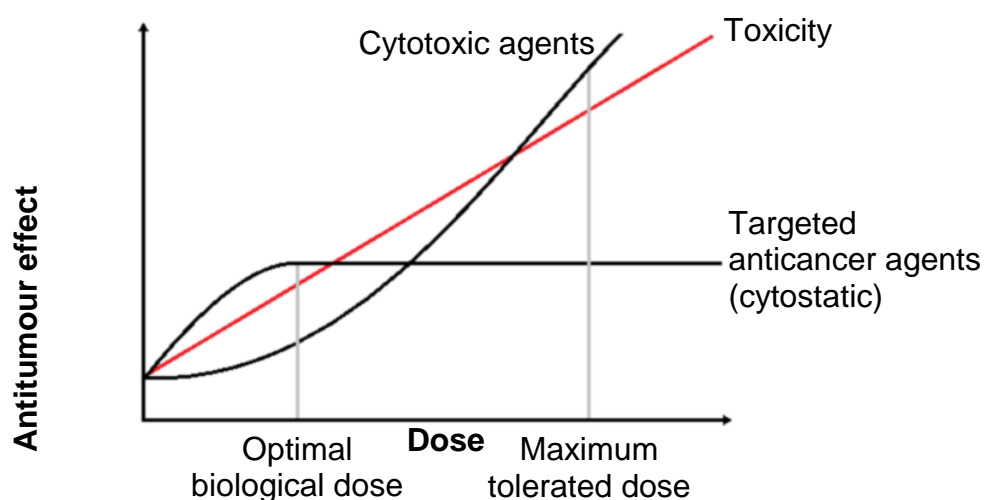
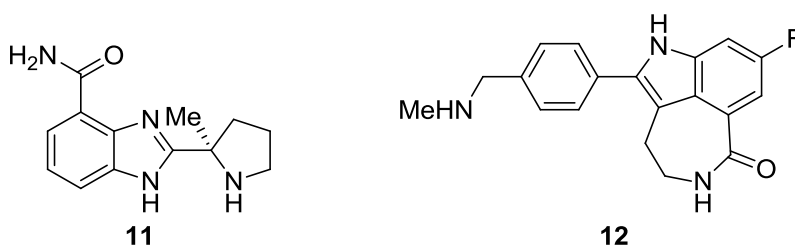


Figure 5 – Comparing the dose response of cytotoxic and targeted cancer chemotherapeutic agents.⁵⁴

Figure 5 shows a typical dose-response for targeted anticancer agents and conventional cytotoxic therapy. As described previously, a disadvantage of cytotoxics is dose limiting toxicity. The graph shows that the antitumour effect of cytotoxic drugs increases with elevated dose alongside toxicity (shown in red) until the maximum tolerated dose is reached. By contrast, when the dose of a targeted anticancer agent is increased the optimal biological dose is obtained at target saturation. After this point no improvement in antitumour activity is observed and toxicity rapidly rises.⁵⁴



It is possible to combine the benefits of both traditional cytotoxic therapy and molecular targeted therapies through a multi-agent approach. The aim of multi-agent cancer therapy is to resensitise drug resistant cancerous cells or enhance the activity of conventional drug and radiation therapies.⁵⁶ A good example of this is the use of the poly(ADP-ribose) polymerase-1 (PARP)-1 inhibitors veliparib (ABT-888) **11** and rucaparib (AG-014699) **12**, which have been shown to potentiate DNA damage *in-vivo* when co-administered with the topoisomerase-I poison topotecan **9**.^{57,58} Unfortunately, the effectiveness of current PARP-1 inhibitors when used in combination therapy, is often limited due to high toxicity, which illustrates the difficulties in the design and instigation of a successful multi-agent chemotherapeutic regime.⁵⁹

Chapter Two: Targeting Protein Kinases with Small-molecule Inhibitors

2.1 The Role of Protein Kinases in Cell Signalling

The sequencing of the human genome was completed in 2003, allowing identification of the 20-25,000 genes that make up human DNA.⁶⁰ From this, a group of 518 genes, collectively known as the kinome, was identified that coded for human protein kinases.⁶¹ The kinome can be broadly divided into the protein kinase and lipid kinase families of enzymes based upon their catalytic specificity.^{20, 21} Additionally, protein kinases may be further subdivided into serine/threonine protein kinases and tyrosine kinases due to their substrate activity. However, there are instances where a protein kinase does not fit into a single class, an example of which are the mitogen activated protein kinase kinases (MAPKKs), which are dual-specificity kinases and interact with both threonine and tyrosine residues of their substrate proteins.⁶² Kinases are located on cell membranes, within the cytoplasm and inside the nucleus of all cells.

Protein kinases are essential enzymes that maintain homeostasis, allowing cells and tissues to respond to changes in their environment through a complex series of interlinked phosphorylation events. This is possible because kinases have a pivotal role in the control of cell physiology through many processes, including cell cycle regulation, cell differentiation and programmed cell death.⁶³ These processes are controlled by kinase-mediated signal transduction through the transfer of γ -phosphate from ATP to the hydroxyl groups of a serine, threonine or tyrosine residues of substrate proteins (Figure 6).^{61,62,64} Substrate specificity is maintained because phosphate transfer requires the correct orientation of both ATP and the substrate protein.⁶⁵

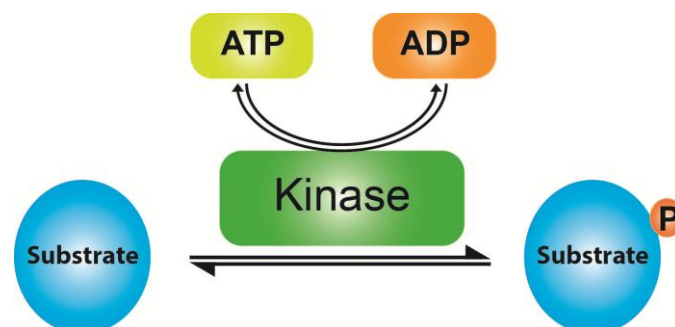


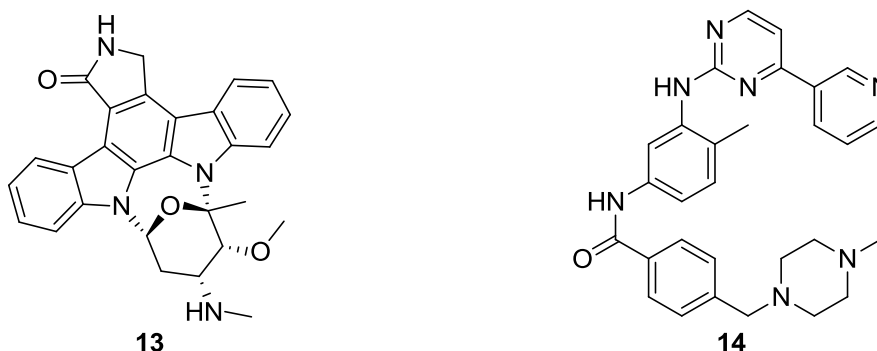
Figure 6 – Schematic representation of protein phosphorylation by a kinase

Mammalian protein kinases are highly conserved families of enzymes containing 250-300 amino acid residues within the kinase domain. Recent advances in biophysical analysis techniques such as NMR spectroscopy and X-ray protein crystallography have allowed the structural elucidation of many kinases, thereby revealing significant structural similarities. Kinases consist of two globular polypeptide lobes connected by the enzyme active-site. The N-terminal lobe consists of a β -sheet and an α -helix, whereas the larger C-terminal lobe is composed primarily of α -helices and an additional activation loop of 25-35 amino acid residues between the conserved residues Asp-Phe-Gly (DFG) and the less conserved Ala-Pro-Glu (APE) motif.⁶⁵ The orientation of the DFG motif is important for enzyme activation, and it has been suggested that the DFG aspartate residue is used to chelate Mg^{2+} , which assists in ATP-binding and γ -phosphate transfer.⁶⁵ At the core of the kinase molecule is the catalytic domain and the conserved ATP-binding pocket. Within this site lies the 'hinge' region, a peptidic backbone that forms H-bonding interactions with the purine N¹ and C⁶-NH₂ group of ATP. Additional hydrophobic interactions are formed through nonpolar aliphatic groups, which further improve binding of ATP.⁶⁵

Kinase-mediated protein phosphorylation is essential for cell signalling. Expression of mutated or dysfunctional kinases as a result of genetic damage may elicit abnormal cell signalling leading to disease. In the last 20 years there has been much interest in the role of kinases in human disease. It has been estimated that more than 400 human diseases are linked to modified kinase activity.⁶⁶ Aberrant kinase activity can result in the development of poorly differentiated cells with a survival advantage, leading to rapid cell proliferation and eventually malignancy.^{63,67} Selectively targeting kinases to modulate activity is an appealing cancer chemotherapeutic strategy, and has been used successfully for the inhibition of both tyrosine kinases and serine/threonine kinases.⁶²

2.2 ATP-Competitive Inhibition of Protein Kinases

The design of targeted and selective inhibitors of human protein kinases is a major goal of chemotherapeutic research.⁶⁵ As described previously, the ATP-binding domain is relatively highly conserved between kinase family members, and this is reflected in the difficulty of designing selective ATP-competitive kinase inhibitors.⁶⁸



One of first ATP-competitive kinase inhibitors to be discovered was the natural product staurosporine **13**. This compound was found to bind within the ATP pocket of kinases and demonstrated potent inhibitory activity. An important consequence of this was the observation that ATP-competitive ligands such as **13**, could compete with the high cellular concentration of endogenous ATP due to increased binding affinity, causing enzyme inhibition.⁶⁸ This was later discovered to be due to additional binding interactions between **13** and unoccupied sub-pockets within the kinase ATP-binding domain. Interestingly, regardless of its bulky size, **13** was found to be a pan-kinase inhibitor that inhibits >90% of all known kinases.⁶⁹ This lack of selectivity made **13** a poor drug candidate due to unwanted toxicity.⁶⁸ The first potent and selective ATP-competitive inhibitor that received clinical approval was imatinib **14** in 2001. This drug selectively targets the BCR-Abl tyrosine kinase associated with the Philadelphia chromosome, and has been approved for the treatment of chronic myelogenous leukemia (CML) and gastrointestinal stromal tumours (GIST).^{70,71}

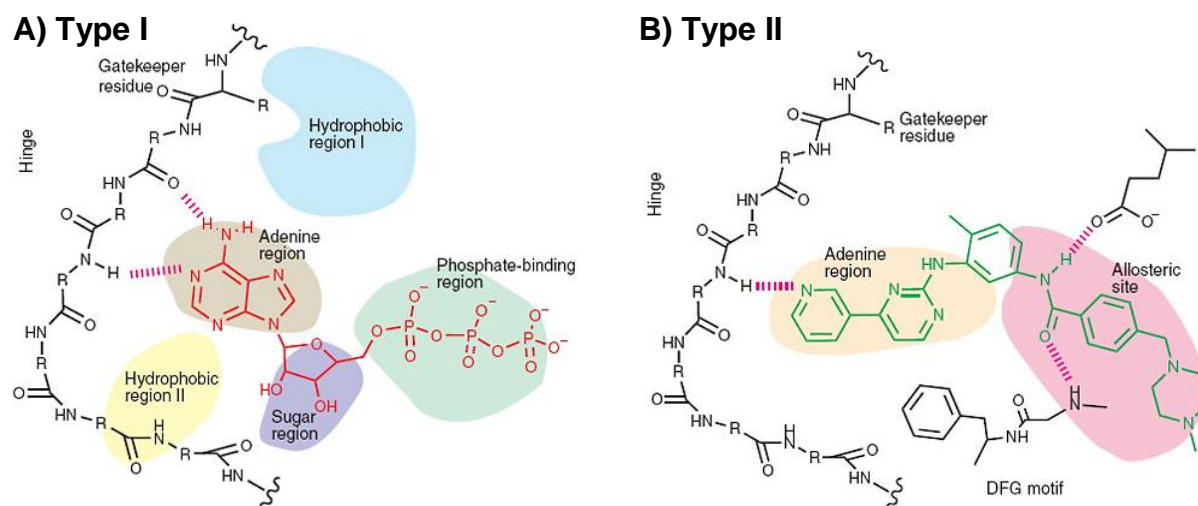


Figure 7 - Comparison of type I (A) and II (B) binding modes of ATP-competitive kinase inhibitors.⁷²

There are several classes of ATP-competitive kinase inhibitors, the most common of which are the type I and type II inhibitors, based upon their binding mode (Figure 7).⁷² Type I inhibitors make up the majority of established ATP-competitive inhibitors and target kinases in their active conformation. Type I ligands mimic the binding of ATP and contain a heterocyclic scaffold that binds to the kinase hinge region through H-bond interactions. This binding is assisted by additional hydrophobic interactions between the heterocyclic moiety and the surrounding hydrophobic regions, and does not require direct interactions with the DFG motif (Figure 7, **A**).^{72,73} Type II kinase inhibitors also occupy the ATP-binding site; however, these compounds bind to the inactive kinase conformation *via* alternative H-bonding and hydrophobic interactions. This is possible due to a change in the orientation of the kinase activation loop, resulting in a 'DFG-out' conformation that facilitates binding *via* additional interactions with the DFG motif. An example of this binding mode is shown for the binding of imatinib **14** to the tyrosine kinase BCR-Abl (Figure 7, **B**). Compounds that inhibit kinases in their inactive form are often highly potent as they prevent kinase activation and subsequent ATP-binding.^{72,73}

2.3 Irreversible Enzyme Inhibition

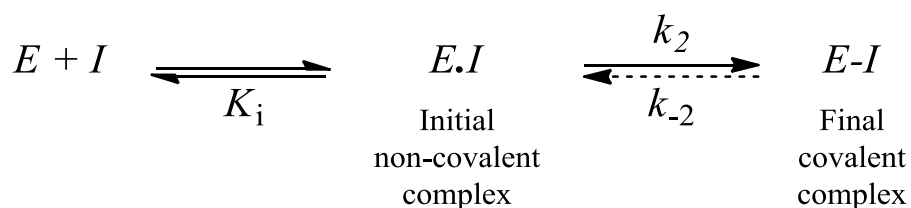
Compounds that cause irreversible inhibition of the activity of a biological target through covalent modification have, until recently, been unpopular as drug candidates through fears of off-target toxicity.⁷⁴ Early approaches to the design of covalent enzyme inhibitors targeted catalytic nucleophiles within the active-site. This can lead to selectivity problems between different enzyme classes, making this approach unattractive.⁷⁴ A resurgence of interest in covalent irreversible inhibitors has occurred recently, owing to the human genome project, advances in structure based-design, and structural bioinformatics.⁷⁴ Modern irreversible enzyme inhibitors (inactivators) are designed to selectively target non-catalytic residues that are poorly conserved between families of enzymes.⁷⁵ Rational design of the ligand using techniques such as *X-ray* protein crystallography allows optimisation of the initial non-covalent binding interaction. The choice of electrophilic 'warhead' is also essential and reactivity must be tuned to prevent reactions with endogenous nucleophiles (e.g. GSH) while maintaining good target specificity.^{76,77}

2.3.1 Safety of Irreversible inhibitors

There are inevitably reservations over the safety of inherently electrophilic drugs and therapeutic agents that are metabolically activated to electrophilic species. Many pharmaceutical companies avoid this class of compound entirely, designating electrophilic groups as known toxicophores.⁷⁸ A major concern regarding the safety of these compounds is as a consequence of the potential for random or prolonged covalent binding of the reactive species. Whilst this may result in acute toxicity, an additional problem is that such compounds may bring about an immune response through haptenization of proteins, and a possible result of this is autoimmune toxicity.^{76,78,79} These safety concerns can be minimised through the design of weakly electrophilic targeted covalent inhibitors. In contrast to highly reactive electrophilic compounds, which are likely to target a broad spectrum of proteins, weakly electrophilic compounds often need to adopt an initial non-covalent binding interaction with the target protein prior to activation, which reduces off-target binding.⁷⁶

2.3.2 Mechanisms of Covalent Enzyme Inhibition

Equation 1 shows a general mechanism of covalent enzyme inhibition. An initial reversible non-covalent interaction must first occur between the ligand (*I*) and enzyme (*E*). This positions the electrophilic group of the ligand in close proximity to a nucleophilic site within the target enzyme to give a complex (*E.I*). A bond forming reaction (k_2) then occurs resulting in covalent modification to give the final covalent complex (*E-I*). For truly irreversible inhibitors, the rate of breakdown of the final covalent complex (k_{-2}) will equal zero, resulting in permanent enzyme inhibition. In contrast, reversible or slowly reversible covalent inhibitors have a k_{-2} value that governs the off-rate of the ligand, and therefore the persistence of the enzyme inhibitor complex (*E - I*).⁷⁶



Equation 1 – Schematic of irreversible enzyme inhibition (adapted from Singh *et al.*).⁷⁶

This type of initial non-covalent enzyme-ligand interaction is referred to as approximation because the nucleophilic group of the enzyme and the electrophilic group of the ligand are placed in close proximity to one another. This lowers the activation energy of the reaction due to decreased enthalpy (ΔH^0), which is caused by a reduction in rotational energy of the bound ligand.⁷⁵

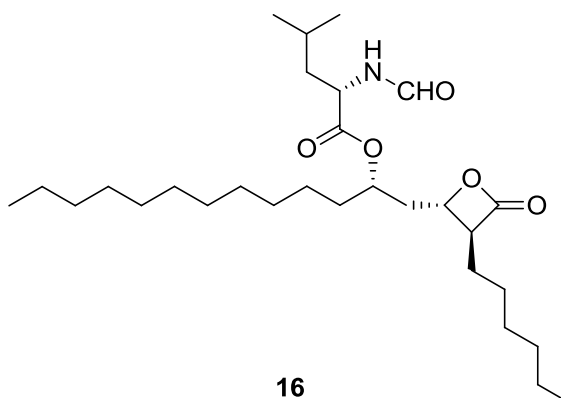
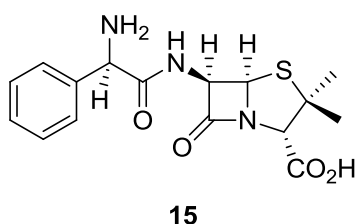
Irreversible binding of drugs is particularly advantageous for the circumvention of drug-induced resistance arising by mutation of the ligand-binding site following treatment with a reversible inhibitor.^{76,80} Although mutations may affect the rate of formation of the initial non-covalent complex, with sufficient time and exposure to the irreversible inhibitor the target protein can be effectively inhibited.⁷⁶

2.3.3 Affinity Label Enzyme Inactivators

Affinity label enzyme inactivators are time-dependent irreversible inhibitors that are often structurally similar to the enzyme's natural substrate.⁷⁵ These compounds bind to the enzyme active-site and form covalent bonds with amino acid side chains often by acylation or alkylation reactions, thus occupying the substrate-binding domain causing irreversible inactivation. As with all electrophilic compounds, affinity labels have the disadvantage of potential toxicity through reaction of the functional group with endogenous nucleophiles. However, although these compounds may form an initial non-covalent complex (*E.I*) with off-target enzymes and other ligands (e.g. GSH), covalent modification is often not possible unless a nucleophilic group is present and correctly orientated within the enzyme active-site. Additionally, the reaction of this nucleophile will occur at a far greater rate than with off-target proteins (typically 10^8 times faster) due to substrate activation, which may improve selectivity.⁷⁵ An advantage of this is the possibility of achieving selectivity between families of enzymes with poorly conserved nucleophilic amino acids within the substrate-binding domain.

There are three important features of compounds designed as affinity label enzyme inhibitors. Firstly, it is essential that the ligand forms an initial reversible binding interaction with the enzyme (or cofactor) binding-site. This non-covalent binding should be rate-limiting up until enzyme saturation, at which point increasing inhibitor

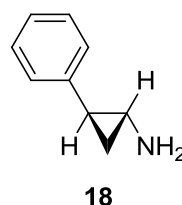
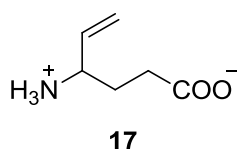
concentration should not increase the rate of reaction.^{75,81} A second important feature is that increasing the concentration of a reversible ligand for the target enzyme, such as the natural substrate or cofactor, should reduce the rate at which enzyme inactivation occurs. This is due to competition between inhibitor and substrate for access to the enzyme active-site prior to forming the final covalent complex. Finally, it is desirable to screen structurally unrelated compounds that contain an identical electrophilic functional group to the affinity label, but that do not form the enzyme inhibitor complex. This helps to confirm selectivity and establish that inhibition is a two-stage process assisted by initial non-covalent interactions, and not arising as a result of non-specific binding of the reactive electrophile.⁸¹ Selected examples of affinity labeling agents include the beta-lactam antibiotic, ampicillin (**15**), and the anti-obesity drug, orlistat (**16**).



2.3.4 Mechanism-Based Inhibitors

An alternative strategy for the design of irreversible enzyme inhibitors is to use a mechanism-based approach, also known as ‘suicide’ inhibition. In this situation, an unreactive drug serves as a substrate for the target enzyme, which causes activation *via* the normal catalytic process, for example phosphorylation. This results in the formation of a reactive species that behaves as an affinity label, leading to irreversible inactivation of the target enzyme.⁷⁵ Alternatively, the reactive species formed may not be a covalent modifier, but instead a compound that binds much more strongly than the parent molecule through enhanced non-covalent interactions with the target enzyme, causing slowly reversible inhibition.

Mechanism-based inactivators have an advantage over affinity labels as there is a reduced risk of non-specific covalent modification and hence toxicity. This is because such agents remain inert until they are activated through enzyme-mediated activation. It is desirable that the enzyme that activates a mechanism-based inhibitor is also the target of inhibition as this provides high enzyme specificity and low toxicity. However, this is not always possible and the activated species may be released from the enzyme active-site allowing reaction with alternative proteins, which may cause toxicity.⁷⁵ Examples of mechanism-based enzyme inactivators include the anticonvulsant drug, vigabatrin (**17**), and the antidepressant drug tranylcypromine (**18**).



2.3.5 Differences in the Therapeutic Window of Reversible and Irreversible

Enzyme Inhibitors

An ATP-competitive kinase inhibitor is only able to modify the action of its target enzyme when it is bound in the ATP-binding pocket. As such, the biological efficacy of reversible ATP-competitive kinase inhibitors is largely dependent upon the lifetime of the enzyme-ligand-complex (residence time) rather than ligand affinity.⁸² In addition to ADME properties, the residence time has a profound influence upon the half-life ($t_{1/2}$) and frequency of dose required to maintain a therapeutic concentration of drug at the enzyme active-site. The pharmacodynamic effect of reversible therapeutic agents is therefore greatly influenced by pharmacokinetic factors. This is demonstrated in the dose-response curve shown in Figure 8, where multiple doses of an inhibitor may be required to achieve an effective dose. A disadvantage of this approach is that a high systemic level of inhibitor may be required to maintain a therapeutic dose, which can result in toxicity.⁷⁷

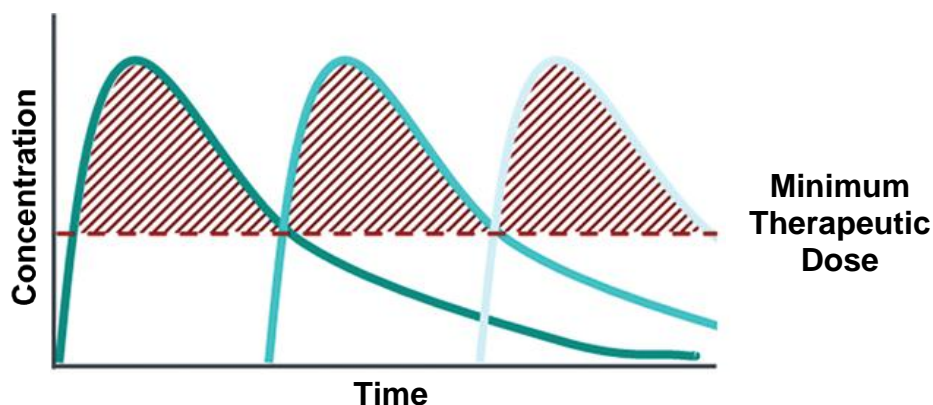


Figure 8 – Pharmacodynamics of reversible enzyme inhibitors (adapted from Barf and Kaptein).⁷⁷

Irreversibly targeting enzymes through the use of agents that covalently modify the active-site can have a dramatic effect upon the pharmacodynamic effect of enzyme inhibition. For this class of inhibitor, it is the enzyme turnover (*de novo* synthesis) rather than the pharmacokinetics that drives pharmacodynamics, because the ligand often remains permanently bound to the enzyme active-site. As such, irreversible inhibitors invariably have a longer duration of action than reversible inhibitors and require less frequent dosing as shown (Figure 9), which may reduce systemic toxicity.⁷⁷ A further advantage of irreversible inhibitors is that pharmacokinetic issues, such as rapid clearance and plasma protein binding, may be reduced because the pharmacodynamic action of these compounds is often retained after systemic removal of the drug. However, this can also be a disadvantage if transient inhibition or short residence times are required.⁷⁴

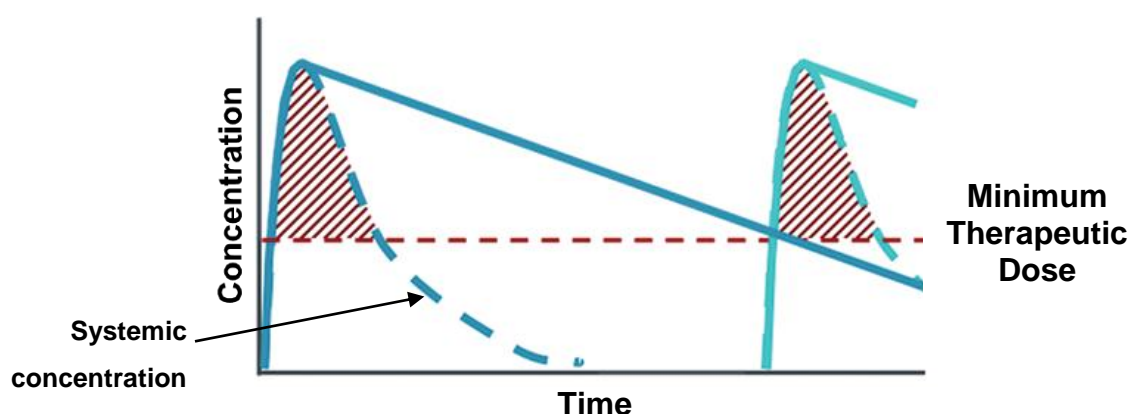


Figure 9 – Pharmacodynamics of irreversible enzyme inhibition (adapted from Barf and Kaptein).⁷⁷

2.3.6 Targeting Cysteine Thiols with Electrophilic Drugs

Cysteine (Cys) is one of the least abundant amino acid residues but also one of the most important. Cys residues are often found at functionally critical locations within proteins and, as such, mutation can often have catastrophic results that can lead to genetic diseases such as cancer. The roles of Cys are diverse and include structure-stabilisation, binding of cofactors, catalytic activity and regulatory activity.⁸³ Cys is distinct from other amino acids in that the thiol is able to form covalent disulfide bonds that are essential for protein stability and folding.⁸⁴ In addition, thiol-dependent regulation of cellular processes is possible due to redox control. The Cys thiol, when subjected to oxidative stress, may be readily oxidised to a number of products including disulfides, sulfenic acids, sulfinic acids and sulfonic acids.⁸⁵ This can result in upregulation of cytoprotective cellular responses such as increased cell proliferation or signal transduction, as well as negative responses, e.g. growth inhibition and cell death.⁸⁶

2.4 Kinase Inhibition – beyond the ATP-binding pocket

2.4.1 Allosteric Enzyme Inhibitors

An alternative strategy for the design of kinase inhibitors is to target sites other than the ATP-binding pocket with non-competitive inhibitors.⁸⁷ Many enzymes contain additional binding domains distinct from the active-site, known as allosteric sites. Interaction of endogenous ligands, known as effectors, with allosteric domains induces conformational changes at the active-site which alters substrate affinity. Binding of negative effector ligands reduces substrate binding whilst binding of positive effector ligands enhances enzyme activity. These effectors form part of signalling cascades and allow the modulation of enzyme activity. Targeting allosteric binding sites with small-molecule inhibitors is challenging as these sites are difficult to characterise, and unlike active-site inhibitors there are usually no small-molecule natural ligands (e.g. ATP) upon which to base inhibitor design. It is for these reasons that the majority of known allosteric inhibitors were discovered serendipitously.⁸⁸ Despite these challenges, allosteric modulators offer the potential of compounds with

high selectivity and fewer side effects than active-site directed inhibitors due to reduced binding site similarities between kinases.⁸⁹

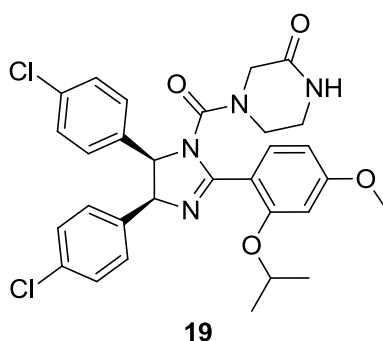
2.4.2 Targeting Protein-Protein Interactions

An emerging area of chemotherapeutic research is the design of ligands that modulate protein-protein interactions (PPIs). These interactions are essential for almost all biological processes; however, the formation of abnormal protein complexes is strongly associated with cancer and other diseases. As such, there is much interest in the design of small-molecule inhibitors that selectively disrupt protein complex formation in an attempt to restore normal cellular function.⁹⁰

Until recently, protein-protein targets have been viewed as high risk owing to the difficulties in designing ligands that bind to this primary interaction site.⁹¹ A major challenge of designing small-molecule inhibitors that target PPIs is that the binding site is often large and featureless. Mimicking this type of interaction is therefore problematic as protein binding is often facilitated by a multitude of weak interactions over a large surface area (600-1300 Å²).⁹² A strategy to overcome this hurdle is to design inhibitors that target critical points of interaction upon the binding surface rather than deep pockets, of which there are few. Additionally, it has been reported that some PPIs are made through smaller regions of high binding energy ('hot-spots'), which may be targeted by small-molecule inhibitors.⁹² Selectivity of these compounds is of particular concern, as if the same interaction points appear upon the surface of other proteins, off-target effects and toxicity may occur.⁹¹

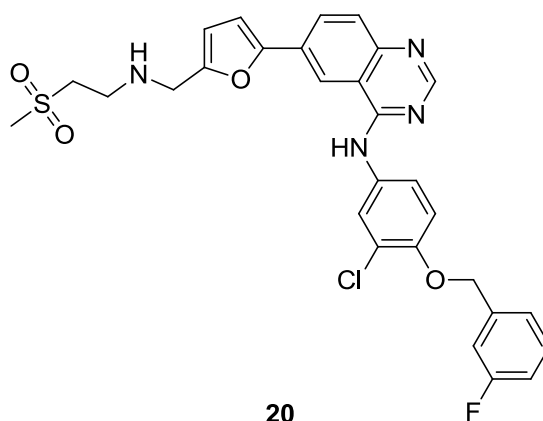
The MDM2-p53 complex is an example of a PPI that is implicated in cancer and currently under investigation as a potential cancer therapeutic target. As described previously, p53 is an essential tumour suppressor protein, which is activated in response to cellular stress (e.g. DNA damage) and functions to prevent replication of cells with aberrant gene expression.⁹³ MDM2 is a key modulator of p53 activity and an established oncoprotein. Binding of MDM2 to p53 causes deactivation and proteasomal degradation of p53, preventing p53 induced cell cycle arrest *etc.*⁹³⁻⁹⁵ It is possible to restore the function of p53 by disrupting the MDM2-p53 interaction with

small-molecule inhibitors. An example of a compound that can achieve this is nutlin-3 **19**, which is currently in preclinical development as an inhibitor of MDM2-p53.⁹⁶



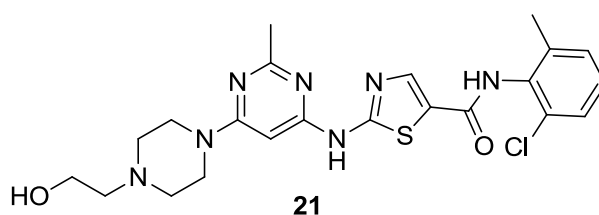
2.5 Resistance to Small-molecule Kinase Inhibitors

Due to the rapid proliferation and genetic instability of cancer cells, it is common that mutations occur in response to anticancer therapy that can lead to drug resistance.⁹⁷ The speed at which these changes in drug susceptibility occur greatly influences the clinical efficacy of treatment. Additionally, the types of mutations that confer resistance are usually limited to those that conserve enzyme function.⁹⁸ One method of acquired drug resistance is through enhanced gene expression of a target protein in response to cellular stress associated with treatment. This causes elevated expression of the target kinase, which compensates for the intracellular concentration of inhibitor. Alternatively, redundant pathways may be activated due to increased expression of downstream signalling proteins that assume the role of the targeted kinase.⁹⁹ An example of this can be observed in the treatment of breast cancer with lapatinib **20**, a small-molecule inhibitor of the tyrosine kinase HER2 (ErbB2), where drug resistance typically occurs after approximately 12 months.¹⁰⁰



A mutation in the amino acid sequence of the kinase ATP-binding site may result from selective pressure caused by drug treatment, favouring a resistant phenotype. One common mutation is a change in the gate-keeper residue to prevent drug molecules entering the ATP-binding pocket. The gate-keeper residue is an amino acid that controls access to a hydrophobic domain within the ATP-binding pocket through size exclusion.⁷³ This hydrophobic region is often the target of small-molecule inhibitors, which form lipophilic interactions that enhance binding affinity. For example, a mutation that confers resistance to imatinib **14** in CML occurs through substitution of Thr-315 in BCR-Abl tyrosine kinase by larger amino acid residues such as Ile, Asp or Asn. This causes steric clashes and loss of a vital H-bond preventing binding of imatinib.¹⁰¹ Another example of a mutation in response to molecular targeted cancer therapy occurs following treatment with compounds that bind to kinases in their inactive conformation. Mutations of the amino acid sequence of these kinases can destabilise the DFG loop causing persistent kinase activation, and preventing binding of inhibitors.¹⁰¹

The selective pressure of molecular targeted therapy can facilitate drug resistance.⁹⁷ A strategy to combat this is to design second generation inhibitors that target the mutated enzyme form or, alternatively, inhibitors with such high binding affinity for the wild-type target that mutation has a minimal impact upon binding. An example of this is dasatinib **21**, a potent tyrosine kinase BCR-Abl inhibitor with 325-fold greater activity than imatinib **14**, and used in the treatment of imatinib-resistant CML.¹⁰²



An alternative strategy is to target multiple kinases either through combination therapy or a single agent approach. This treatment strategy has the potential for increased potency and reduced drug resistance. However, it is often difficult to balance potency with off-target activity and toxicity.⁹⁷

2.6 Functionalised Purines as Kinase Inhibitors

The naturally occurring purines adenine and guanine have important roles in numerous life processes. There has been a large degree of interest in the modification of the purine scaffold to create chemical probes and pharmaceutical agents to understand and treat a multitude of conditions several of which are shown below (Figure 10).¹⁰³ The substituents on the purine ring structure (Figure 10, R₁-R₇) can easily be modified and large libraries of modified purines have been prepared for high-throughput screening, allowing the discovery of potent and selective inhibitors of a variety of targets. As a result of these screens, a number of purine based drug candidates have progressed to clinical trials for the treatment of cancer and other diseases.

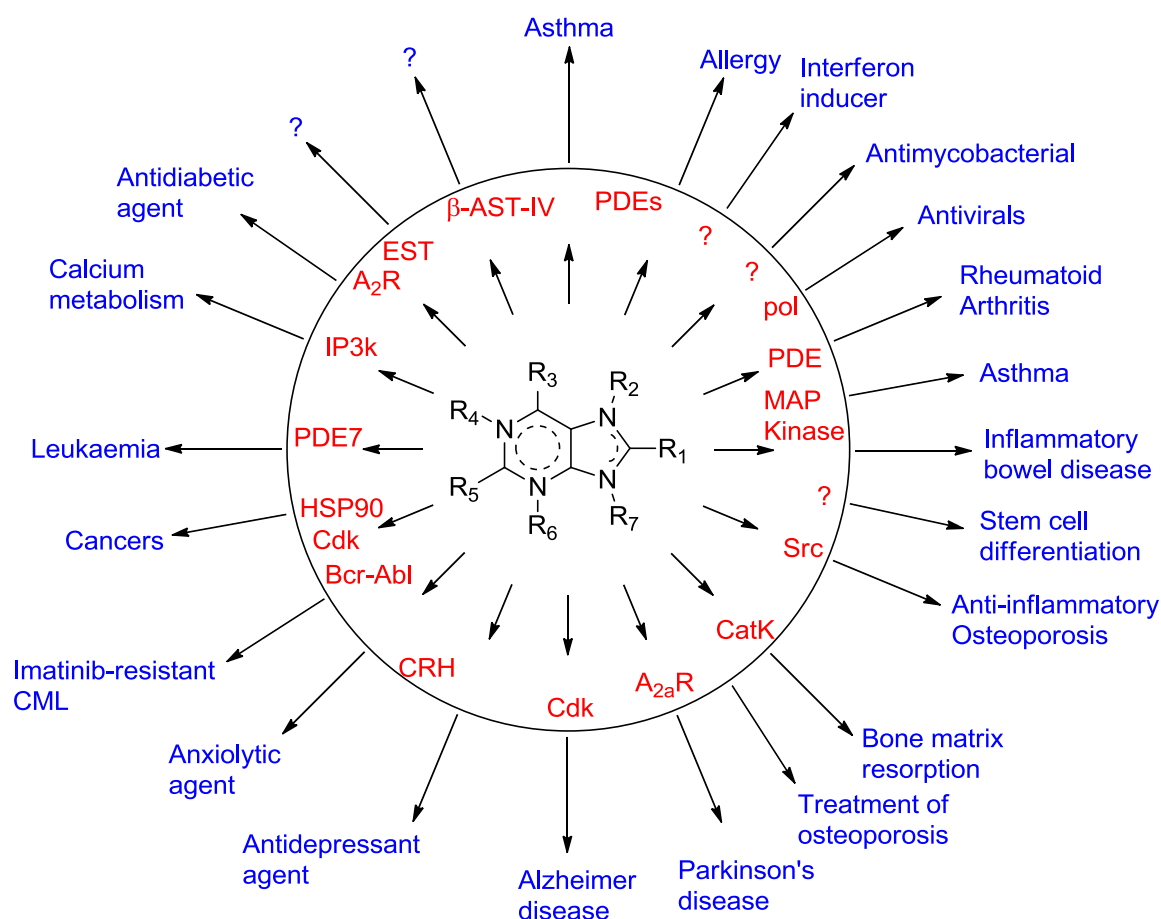


Figure 10 – Purines in the treatment of disease (adapted from Legraverend and Grierson).¹⁰³

As purine compounds have high natural abundance throughout the body, it is challenging to gain selectivity in related families of enzymes. This is emphasised by

the fact that an estimated 7% of all proteins expressed by genes, rely upon naturally occurring purines as co-factors or substrates.¹⁰³

Purine analogues are an important class of kinase inhibitors, of use for the treatment of diseases including cancer (Figure 10). By competing with the natural substrate (ATP) for the ATP-binding domain, these compounds are able to cause kinase inhibition, which prevents downstream phosphorylation events, thus allowing modulation of specific metabolic pathways.¹⁰⁴ However, as the ATP-binding domain is often conserved amongst kinase family members, it may be difficult to gain good selectivity using inhibitors that mimic the binding of ATP. Compounds that lack selectivity may elicit off-target effects which could lead to toxicity. As such, it is important to screen kinase inhibitors against a comprehensive panel of additional kinases.¹⁰³ Nevertheless, by modifying substituents on the purine ring to exploit non-conserved features of the target kinase, it is possible to develop highly potent compounds with minimal off-target activity. This is greatly assisted by recent advances in *X-ray* crystallography, which have allowed the development of inhibitors using a structure based design approach.¹⁰⁵

Chapter Three: Mitotic Kinases and Cell Cycle Control

3.1 The Eukaryotic Cell Cycle

Mitotic cell division has evolved as a series of interconnected biological events known collectively as the cell cycle, which facilitates DNA replication and the even distribution of chromosomes.^{106,107} Control of this cycle is achieved through phosphorylation-mediated signalling cascades and restriction check-points, and cancer may arise due to mutation of signalling genes resulting in hyperactivation. Similarly, mutation of genes coding for checkpoint-control proteins may prevent cell cycle regulation, causing genomic instability.¹⁰⁸ As such, proteins of the cell cycle are attractive cancer therapeutic targets.

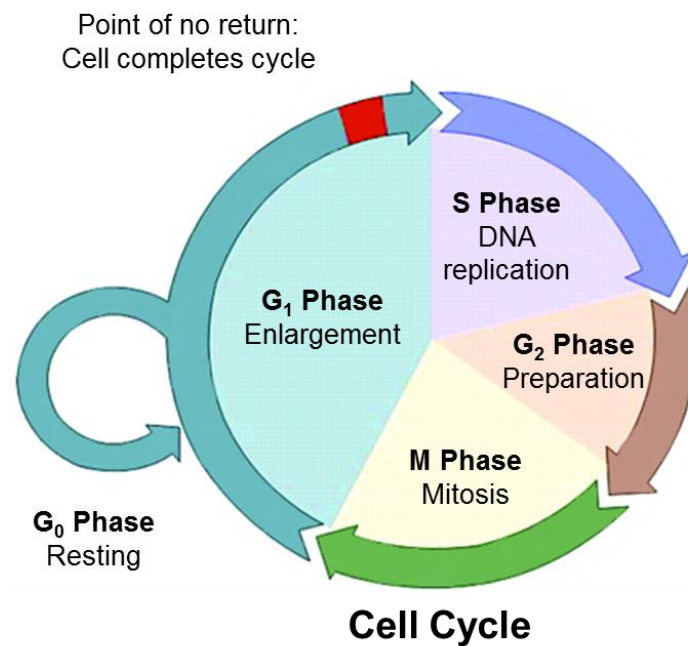


Figure 11 - Schematic representation of the mitotic cell cycle.

The mitotic cell cycle is divided into an ordered sequence of events known as G₀, G₁, S, G₂ and M (Figure 11). In the first stage of the cell cycle (G₁), cells experience a period of growth during which essential proteins and enzymes (e.g. DNA polymerases) are synthesised for use in subsequent phases.¹⁰⁹ G₁ serves as the first of two restriction checkpoints that control cell cycle progression. At this point, cells may either progress to S-phase or enter a phase of quiescence (G₀) if required. Cells in G₀ may survive in this state for extended periods of time maintaining function

but remaining dormant and non-proliferative. These cells can be stimulated to re-enter the cell cycle when required, returning to G_1 through activation/silencing of key regulatory genes.¹¹⁰ After G_1 , the cell enters the S-phase of the cell cycle, during which the synthesis of DNA, centrosomes, histones and key enzymes required for chromosome replication takes place. The role of the S-phase is to produce two identical sets of chromosomes and centrosome pairs for use in mitosis. It is essential that both DNA replication and centrosome duplication occur only once with each subsequent cycle to prevent aneuploidy, the abnormal distribution of chromosomes.¹¹¹ Following S-phase, there is a second gap phase known as G_2 . This is the final stage of the interphase component of the cell cycle, and is characterised by rapid growth resulting in elevated expression of the numerous cellular components required for mitosis. Prior to the G_2/M transition, there is a second restriction checkpoint. At this point DNA is assessed for errors by a number of proteins including p53 and CDKs. If errors are found, they are either repaired or the cell is destroyed by apoptosis.¹¹² The final stage of the cell cycle is the mitotic (M) phase, which allows chromosome segregation and cell division, resulting in the production of two identical daughter cells.

3.2 Molecular Mechanisms of Mitosis

Mitosis is a highly-ordered sequence of biophysical processes that facilitate separation and distribution of chromosome pairs in somatic cells prior to division (cytokinesis). Errors in mitosis are a leading cause of aneuploidy and genetic instability. A number of regulatory processes protect against these errors and more often than not abnormal cells are swiftly removed through apoptosis. Failure to correct these errors or eliminate affected cells can have disastrous consequences, leading to cancer and other diseases.¹¹¹

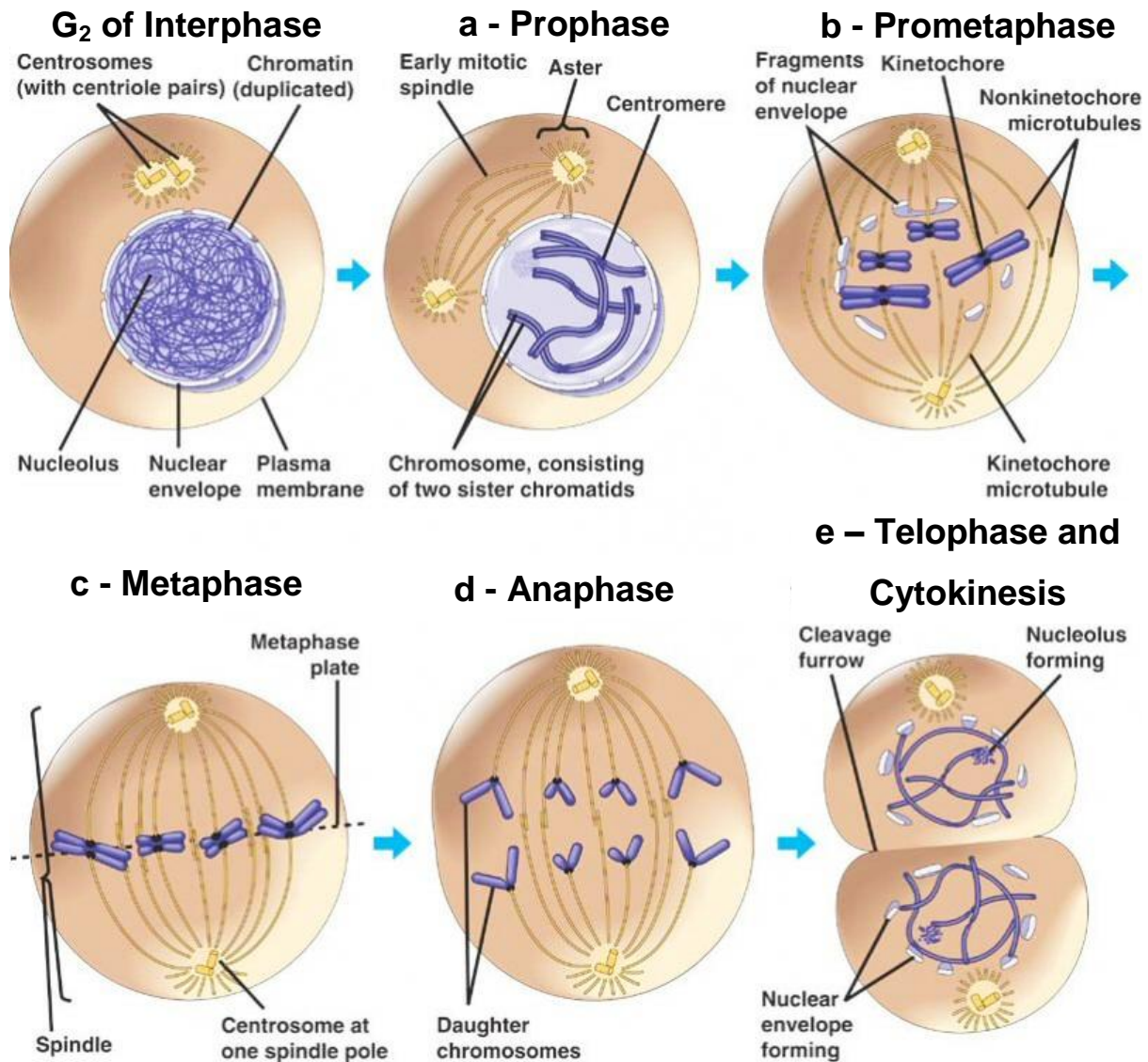


Figure 12 – Stages of mitotic cell division.¹¹³

Following completion of both the S- and G₂-phases of the cell cycle, cells proceed into the mitotic phase (M-phase) allowing cell replication and division. The first stage of mitosis is prophase, during which chromosome condensation occurs (Figure 12a). Simultaneously, cytoplasmic organelles known as centrosomes separate and migrate to opposite poles of the cell, where they recruit γ -tubulin and form the microtubule organising centres (MTOCs) in preparation for mitotic spindle formation. Finally, fully condensed chromosomes begin to interact with mitotic spindle fibres through tubulin polymerisation, signifying the end of the prophase and the onset of prometaphase.¹¹⁴ It is essential that correct chromosome condensation occurs to prevent truncation and allow accurate separation of sister chromatids.¹¹⁵

During prometaphase, the nuclear membrane becomes hyperphosphorylated causing it to fragment and release the chromatid pairs from the nucleus. Three distinct sets of microtubule spindle fibres protrude from the MTOCs towards the cell cortex through microtubule polymerisation (Figure 12b). These microtubules form the mitotic machinery required for chromosome segregation.¹¹⁶ One set of microtubules, the kinetochore microtubules, attach to the chromatids forming protein structures (kinetochores), which are essential for chromosome segregation. Each individual chromatid is attached to a single centrosome *via* these kinetochore microtubules ensuring correct segregation at later stages of mitosis. A second set of microtubules, the astral microtubules, do not connect to a kinetochore but are instead used to position mitotic machinery with the aid of motor proteins (dyneins). The third set of microtubules, known as polar microtubules, form interdigitate links with microtubules at the opposite pole of the cell. These microtubules are assisted by motor proteins and help facilitate cell division.

The cell progresses from prometaphase to metaphase when all chromosomes are attached to kinetochore microtubules (Figure 12c). At this point, chromosome pairs begin the process of chromosome 'congression' during which chromosomes translocate to the 'equator' of the cell and align along the metaphase plate.^{1,114} To ensure all kinetochore microtubules are correctly attached prior to mitotic progression, chromosomes are checked by the spindle assembly checkpoint (SAC) which consists of a number of cell cycle kinases including: CDK1, Aurora-B, MPS1, BUB1 and BUB1B.^{111,117}

Once the requirements of the SAC are met, the cell enters anaphase (Figure 12d) during which the centromere connecting sister chromatids is cleaved by the enzyme separin (also known as Esp1).^{118,119} Up until this point of the cell cycle separin is inhibited by the chaperone protein securin. Upon entry into anaphase, securin is labelled for destruction through ubiquitination by the anaphase promoting complex (APC/C) allowing separin activation.^{118,119} After cleavage of the centromere, chromosome segregation occurs through the actions of microtubules and motor proteins.¹¹⁴ There are two major processes that facilitate this separation, termed anaphase A and anaphase B. During anaphase A, kinetochore microtubules shorten, drawing the attached chromosomes towards opposite centrosomes. By contrast,

during anaphase B, centrosomes are driven apart through spindle elongation.^{120,121} Finally, the kinetochore is broken down, freeing the daughter chromosomes.¹¹⁶

At this point the cell enters telophase (Figure 12e). The nuclear envelope reforms around the condensed chromosomes from residual vesicles of the parent nuclear envelope, to produce two independent nuclei at opposite ends of the cell. The cell then initiates cytokinesis beginning with formation of the cleavage furrow. Simultaneously, chromosomes de-condense, and finally the cytoplasm divides resulting in two genetically identical daughter cells.¹¹⁴ The cell cycle is now complete and the newly produced daughter cells proceed to enter interphase in a new cell cycle.¹¹⁶

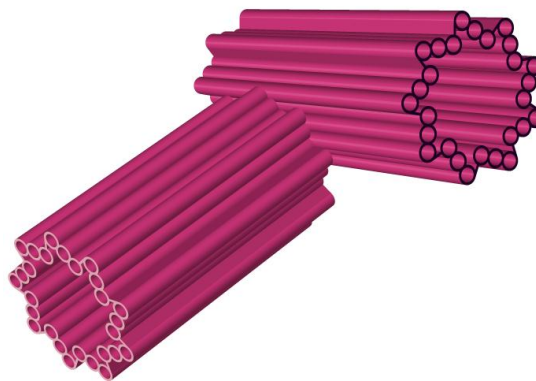


Figure 13 - Schematic representation of a centrosome.¹²²

3.3 The Centrosome Cycle

The centrosome cycle is a key component of cell physiology that functions in concert with the cell cycle. The role of the centrosome cycle is to facilitate the semi-conservative replication of a cytoplasmic organelle known as the centrosome. The centrosome has a vital role as the major microtubule-organising centre (MTOC) of cells in higher-organisms.^{123,124} Centrosomes control microtubule dynamics allowing precise control of organelle transport, cell shape, polarity and motility. Centrosomes are particularly important for cell replication and assist mitosis through their role in spindle pole assembly and cytokinesis.¹²⁵

The centrosome is an organelle located within the cytoplasm near the nucleus of cells, which consists of two orthogonal barrel-shaped centrioles each containing nine microtubule triplets (Figure 13) in a 9-fold axis of symmetry.¹²⁵⁻¹²⁷ These

microtubules reside within the pericentriolar material – a highly organised matrix of proteins required for microtubule nucleation through the recruitment of γ -tubulin.¹²⁶

During the cell cycle the structure of the centrosome is precisely altered to facilitate centrosome duplication. These structural alterations correspond to specific events of the cell cycle and are collectively termed the centrosome cycle (Figure 14). Each centrosome cycle takes one complete cell cycle, resulting in a single replication of the centrosome in a semi-conserved process.^{127,128}

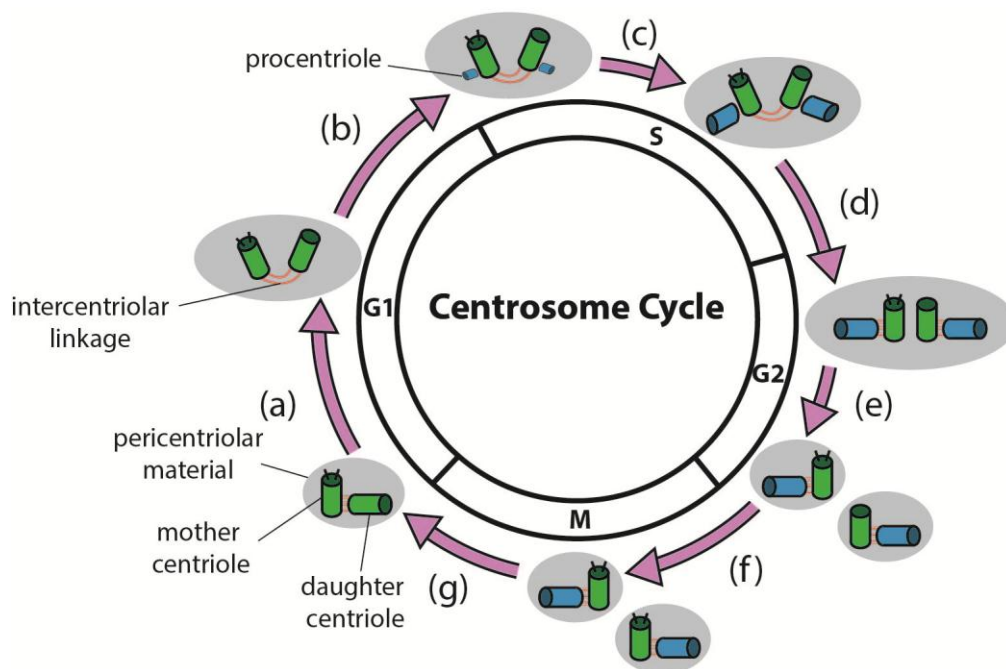


Figure 14 – The centrosome cycle (adapted from Crasta and Surana).¹²⁷

Figure 14 shows a schematic representation of the centrosome cycle. This commences at G_1 with the centrosome pair consisting of a mother and daughter centriole. The mother centriole contains additional distil and sub-distil appendages, and was formed a minimum of two cycles ago. The daughter centriole was formed in the previous cycle and is deemed immature, as it does not yet possess these appendages.^{124,127} (a) To begin replication, the centrioles lose their orthogonal orientation, remaining interconnected *via* a flexible connector known as the intercentriolar linkage.¹²⁷ (b) As the cell enters the S-phase of the cell cycle the centrioles nucleate secondary immature centrioles (procentrioles) (shown in blue) orthogonal to the parent centrioles. (c) The procentrioles elongate forming daughter centrioles (shown in blue). (d) The cell then enters G_2 and the intercentriolar linkage

is cleaved. (e) At the G₂/M transition the centrioles split and the pericentriolar material divides allowing the newly formed centrosome pairs to separate. (f) The daughter centriole from the start of the cycle then matures gaining distal and sub-distal appendages consisting of a range of proteins including: cenexin, ninein, CEP110 and ϵ -tubulin.¹²⁷ (g) At this point the cycle is complete and centrosomes migrate to opposite poles of the cell to form the mitotic spindle, prior to entry into mitosis.

3.4 Centrosome Instability and Cancer

Progress through the centrosome cycle is highly regulated by p53 and a number of cell cycle protein kinases including CDKs and aurora kinases.¹²⁹ Centrosome stability is critical for the even distribution of chromosomes during mitosis, and it is essential that at the point of entry into mitosis there are exactly two centrosome pairs present within the cell.¹²⁸

In human cells the required number of chromosome pairs is 23. Aberrant distribution of these chromosomes between parent and daughter cells is a common result of mitotic errors, brought about through dysfunctional centrosome replication. Failures in centrosome replication prior to the onset of mitosis can be catastrophic. In most instances, cells will not divide but instead return to interphase resulting in polyploidy – the presence of extra chromosome pairs.¹³⁰ By contrast, the presence of additional centrosome pairs can induce the production of a multipolar spindle, resulting in a myriad of daughter cells each with a randomly distributed aberrant mixture of chromosomes.¹³⁰ In either case, genetic imbalances occur, which under normal circumstances prove fatal to cell survival due to intervention by apoptosis-inducing defence mechanisms. Cells that evade these defence mechanisms and survive may exhibit an altered phenotype, giving rise to aggressive growth and the invasive properties most often associated with cancerous cells.¹²⁸ Interestingly, cells that lack centrosomes entirely may still engage in bipolar spindle assembly, although there is an increased risk of cleavage failure during mitosis.^{130,131}

3.5 Targeting Mitosis in Cancer Chemotherapy

Preventing cell cycle progression by targeting mitotic events is an effective cancer therapeutic strategy. Conventional cytotoxic drug classes such as taxanes and *vinca* alkaloids (see p25) target microtubules and prevent accurate spindle formation and chromosome alignment through stabilisation or destabilisation of tubulin, respectively. This causes targeted cells to remain at the spindle assembly checkpoint phase of mitosis, and they cannot progress into anaphase resulting in mitotic arrest and apoptosis.¹³² These therapies, although effective, are known to produce many side effects and toxicity due to binding of microtubules involved in processes required to maintain cell physiology and function.¹³³ It is therefore desirable to develop modulators of mitosis that have good selectivity and do not interfere with tubulin function. One possible approach is to target mitotic protein kinases involved in tumour progression using molecular targeted therapy.

3.6 Protein Kinases and Cell Cycle Progression

Errors in cell cycle modulation can induce rapid proliferation and is often associated with malignant transformation. A major function of protein kinases is to monitor and regulate cell cycle progression, preventing errors in DNA duplication and chromosome segregation that would otherwise cause abnormal cell division and the development of cancer.¹¹⁷ In the following section four families of important cell cycle kinases will be discussed, namely CDKs, aurora kinases, Plks and the Nek family.

3.7 Cyclin-Dependent Kinases (CDKs)

The CDK family of enzymes consists of 13 serine/threonine protein kinases, many of which have important roles in cell cycle progression and checkpoint control.¹³⁴ The level of CDK expression generally remains constant throughout the cell cycle; however, CDK activation is precisely regulated by a number of processes (Figure 15), including binding of partner cyclins, phosphorylation, proteinogenic inhibition by CDKIs and ubiquitin-mediated proteolytic degradation.¹³⁵⁻¹³⁷ Monomeric CDKs are essentially inactive but become activated upon binding of a partner cyclin to form a heterodimeric protein complex. CDK activity is vastly increased due the formation of

targeting domains, which allow additional binding interactions and control substrate specificity.^{138,139} Mutation of genes coding for CDKs and their binding partners are known to cause unscheduled cell proliferation, genomic instability and aneuploidy, and is associated with tumour progression.¹³⁷ Additionally, elevated CDK expression has been shown to be common in cancer.

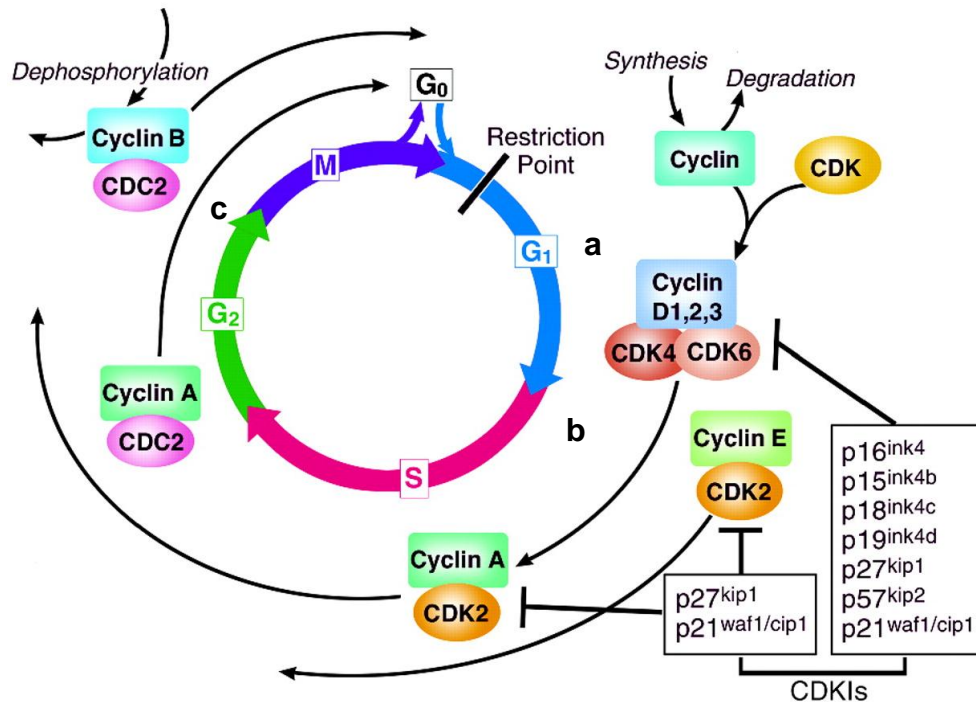


Figure 15 – Cell cycle dependent regulation of CDK activity.¹³⁶

3.7.1 CDKs in Cell Cycle Control

At the G₁ phase of the cell cycle, CDK4 or CDK6, forms a complex with D-type cyclins, which facilitates centrosome replication. Progression from G₁ to the S phase is then catalysed by the CDK2/cyclin-E complex allowing chromosome replication. At the G₂/S checkpoint, CDK2 complexes with cyclin-A, which changes its substrate specificity ensuring that all cellular components are correct prior to entry into mitosis (M). CDK1/cyclin-B then functions to facilitate the transition from G₂ to M. Not all members of the CDK family are thought to be necessary for cell cycle progression; indeed the three interphase CDKs (CDK2, CDK4 and CDK6) are only required for proliferation of certain cell types (e.g. CDK2 for germ cells,¹⁴⁰ CDK4 for pancreatic β -cells¹⁴¹ and CDK6 for haematopoietic cells).¹⁴² Contrary to this, CDK1 has been shown to be essential for cell division. Defects that induce aberrant CDK activity

may give cells a proliferative advantage, and are closely linked to cancer. By targeting CDKs with small-molecule inhibitors it is hoped that such activity may be prevented through the restoration of checkpoint control, causing cell cycle arrest and possibly apoptosis.¹⁴³ As such, CDKs have received considerable interest in the field of cancer therapeutics.¹⁴⁴

3.8 Aurora Kinases

The aurora kinases are a highly conserved class of three kinases (aurora A,B and C) that assist mitotic spindle formation through regulation of centrosome replication, microtubule-kinetochore attachment, spindle checkpoint and cytokinesis.¹⁴⁵ The most comprehensively studied member of this family of kinases is aurora A, which is located at the centrosomes, and assists mitotic spindle pole assembly and centrosome maturation to facilitate cell cycle progression.^{146,147} Aurora B is localised at the chromosomes and forms part of the spindle assembly checkpoint and chromosome passenger complex.¹¹⁷ The major roles of aurora B are to ensure correct kinetochore-microtubule attachment as well as facilitating chromosome segregation and cytokinesis.^{117,148} Inhibition of aurora B has been shown to cause polyploidy by removal of a critical spindle checkpoint, causing an early exit from mitosis without cytokinesis.¹⁴⁹ Aurora C is not well studied but is suspected to be important for mitosis as it is found to accumulate at the centrosome. It has been suggested that the role of aurora C is highly analogous to aurora B and may in-fact be a redundant pathway.¹⁴⁵ Drugs that target these kinases are thought to cause deregulation of microtubule dynamics, and may offer a therapeutic alternative to patients who do not respond to antimitotic agents.¹⁵⁰

3.9 Polo-like kinases (Plks)

The Plk family of enzymes are serine/threonine protein kinases that have a role in the cell cycle and are known to be associated with cancer.¹⁵¹ The four members of the mammalian Plk family include Plk1 (*Xenopus* Plx1), Plk2 (serum-inducible kinase (Snk)), Plk3 (fibroblast growth factor inducible kinase (Fnk)/ proliferation related kinase (Prk)) and Plk4/Sak. Biochemical and genetic *in-vivo* experiments have

indicated the role of Plks in a number of events that occur during the cell cycle including: mitotic spindle formation, chromosome segregation, cytokinesis and numerous activation and regulatory roles. There is evidence that Plk1 is associated with cell proliferation linked to cancer formation. Studies with the mouse NIH3T3 cell line, which overexpresses murine Plk1, demonstrated a transformed phenotype with the presence of multinucleated cells resulting in tumour formation in nude mice. Plk1 overexpression in human cancer has also been linked to aggressive growth and poor clinical outcome.¹⁵¹ Plk1 has therefore become a target of considerable interest and its inhibition may prove useful in cancer chemotherapy. The exact function of Plk2 is less well known, although studies in mice indicate a role in centriole duplication. Plk3 is thought to assist G₁/S progression through enhancement of cyclin E expression. Finally, Plk4 is known to be an essential regulator of centriole duplication.¹⁵²

3.10 Never in Mitosis Gene-A Related Kinases (Neks)

Never in mitosis gene-A (NIMA), was first identified in the filamentous fungus *Aspergillus nidulans*. In this fungus the function of NIMA is to facilitate the G₂/M transition and entry into mitosis. In humans, the closest relatives of NIMA are the NIMA related kinase (Nek) family of serine/threonine protein kinases, of which there are 11 known members (Nek1-11). Each member of the Nek family exhibits a broad similarity to NIMA due to possession of a highly conserved N-terminal catalytic domain. Contrary to this, amino acid residues found at the carboxyl terminus are quite different, suggesting that during the evolution of NIMA, its function has diversified away from G₂/M progression into a more complex process.¹⁵³ This is further exemplified by the existence of multiple Nek kinases, many with alternative functions to NIMA.¹⁵⁴ The most closely related Nek kinase member to NIMA is the NIMA related kinase gene 2 (Nek2), which shares a 44% amino acid homology with the NIMA catalytic domain. To date, none of the Nek family of enzymes have demonstrated a functional homologue of NIMA; however, initial characterisation studies have implicated Nek2 in cell cycle control and microtubule organisation.¹⁵⁴ Nek2 function will be reviewed in greater detail in chapter four.

In addition to Nek2, other members of the Nek family of enzymes may also prove to be viable therapeutic targets. Nek8 and Nek9 form a subfamily, as they are suspected to both possess the regulator of chromosome condensation domain 1 (RCC1) and a close structural homologue at the kinase domain (Figure 16). A structural difference observed between Nek8 and Nek9 is that Nek9 exhibits a coiled-coiled domain, which is believed to allow additional protein-protein interactions. Additionally, Nek8/9 are structurally similar to Nek2, which suggests that they have a related function. Contrary to this, the Nek1/3 subfamilies appear the most distinct and are likely to have the greatest difference in function.¹⁵³

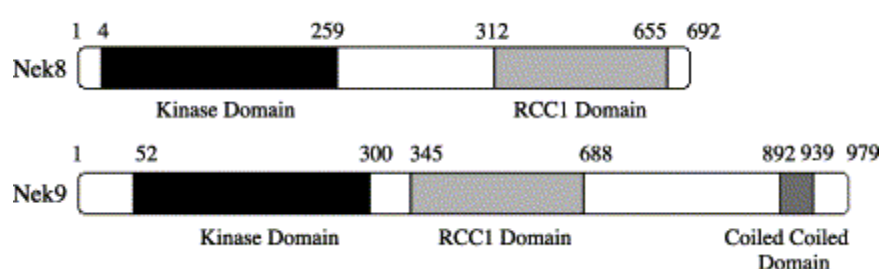


Figure 16 – Structural similarities between Nek8 and Nek9 coding domains.¹⁵³

Nek8 is thought to be associated with human cancer. The exact function of Nek8 in humans remains unknown, although predictions have been made using murine Nek8.¹⁵³ In mice, mutation of the Nek8 coding gene resulted in the production of oversized cells with multiple nuclei. In an additional study, the expression of Nek8 was down regulated in zebrafish embryos using anti-sense DNA, resulting in the formation of pronephric cysts. This suggests that Nek8 is involved in the cell cycle and that its disruption leads to further downstream cellular complications.¹⁵⁵ It has been demonstrated that the expression of Nek8 in normal human tissue is limited, whereas in human breast carcinoma cells Nek8 is over-expressed.¹⁵³ The result of this over-expression is a reduction in the concentration of endogenous actin and elevated CDK1/CyclinB1 levels further suggesting Nek8's involvement at the G₂/M transition of the cell cycle.

As described previously, Nek9 contains a coiled-coiled domain. It has been demonstrated that this difference in structure to Nek8 facilitates interactions between Nek9 and additional binding partners, including the GTPase Ran, Nek6, Nek7 and

Bicd2. This suggests Nek9 may have additional roles in the regulation of chromosomal microtubule organisation and alignment.¹⁵³

Other members of the Nek kinases include Nek1, which has been shown to interact with polycystic kidney disease proteins, and may have a role in the DNA damage response pathway. Nek3 is believed to associate with Vav2 and modulate prolactin receptor signalling but is not involved in the cell cycle. Neks 4, 5 and 10 currently have no known function.¹⁵⁶ Nek6 and Nek7 are closely related to each other and form a subfamily within the Nek kinases. It is thought that these kinases are activated by the C-terminal tail of Nek9, which causes phosphorylation and allosteric binding.^{157,158} Inhibition of Nek6 causes apoptosis by inducing arrest at the metaphase stage of mitosis.^{156,158} Nek11 is the most recently discovered member of the Nek family, and is known to be activated in response to DNA damage / stress. Inhibition of Nek11 by caffeine in HeLaS3 cells has been shown to minimise cell lethality at the S-phase, suggesting that Nek11 may help regulate the G₁/S phase checkpoint.^{156,159} Aside from Nek2, Neks 6, 7 and 9 appear to have the greatest potential as targets for therapeutic agents.¹¹⁷ Each of these kinases is implicated in cell cycle control and has shown elevated expression in various tumour types.

Chapter Four: Targeting Nek2 with Small-Molecule Chemotherapeutic Agents

4.1 Nek2 is Implicated in Chromosomal Instability and Cancer

Genetic instability is a common characteristic of cancerous cells. It is brought about due to defects in DNA repair and/or changes in DNA content, through errors that occur during the chromosome segregation phase of mitosis.¹ A common feature of cancer cells is missing or extra chromosomes (aneuploidy). Cells exhibiting aneuploid defects are at increased risk of developing chromosome instability, which can result in unregulated cell growth and division, causing malignant transformation.^{154,160} Cells with aberrant regulation of Nek2 activity are more likely to develop aneuploidy, and as such have an increased likelihood of malignant transformation.¹⁶¹ This has been reflected in studies that demonstrated a 2-5 fold increase in Nek2 coding gene expression in breast and cervical carcinomas as well as lymphomas, when compared with healthy cells.¹⁵⁴

4.2 Nek2 Induces Centrosome Splitting at the G₂/M Transition

Nek2 is a serine/threonine protein kinase that is implicated in centrosome disjunction and mitotic spindle formation. Nek2 is localised at the centrosomes and is expressed in a cell cycle-dependent manner. At G₁, the level of cellular Nek2 is low; however, upon transition into the S-phase of the cell cycle a marked increase in Nek2 expression is observed. The level of cellular Nek2 peaks at the G₂/M transition and then rapidly declines upon entry into mitosis due to proteolysis.¹⁶² It is believed that Nek2 plays an important catalytic role in the phosphorylation of proteins involved in centriolar cohesion. Upon phosphorylation, centrosome segregation occurs by breakage of the intercentriolar linkage allowing mitotic entry (Figure 17).

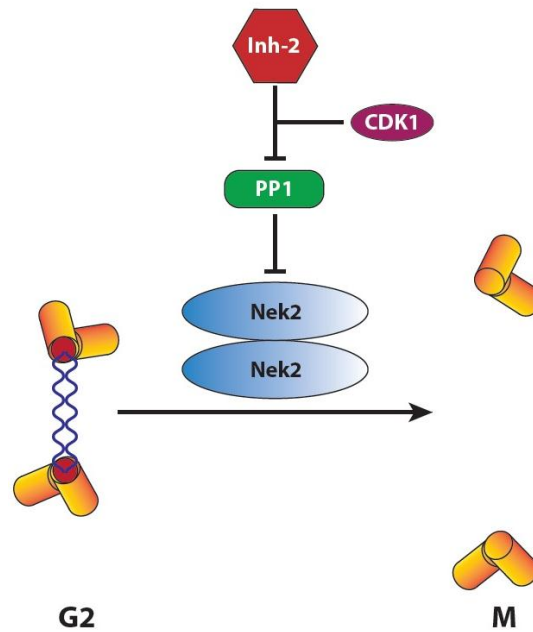


Figure 17 - Schematic representation of Nek2 mediated centriole disjunction (adapted from O'Regan *et al.*).¹⁶³

The intercentriolar linker is a bridged structure that connects the two centrosome pairs (Figure 17). This structure consists of at least two proteins, including rootletin (shown in blue) and centrosomal Nek2 associated protein 1 (C-Nap1) (shown in red). C-Nap1 has been shown to locate at the end of the centriole during interphase and behaves as an attachment site for rootletin, which links the centrosome pairs.¹⁶⁴ During entry into mitosis (G_2/M) Nek2 is activated following inhibition of protein phosphatase 1 (PP1) by inhibitor-2 protein (Inh-2), which may be assisted by CDK1 (Figure 17). It is thought that PP1 functions to remove phosphate groups from Nek2 and its substrate proteins which modulates Nek2 activity.^{123,165} Once active, Nek2 phosphorylates C-Nap1 and rootletin causing conformational changes that favour centrosome splitting. After separation, the centriole pairs are transported to opposite poles of the mitotic cell by microtubule-based motor proteins in preparation for mitotic spindle formation.¹⁶³ Upon entry into mitosis, Nek2 is ubiquitinated and rapidly undergoes proteasomal degradation by anaphase promoting complex (APC/C).¹²³

4.3 Nek2 in the Regulation of the Centrosome Associated Protein Nlp

In addition to the Nek2 substrates rootletin and C-Nap1 described previously, ninein-like-protein (Nlp) has recently been identified as a substrate of Nek2. Nlp is located at the centrosome and functions to induce microtubule nucleation through the recruitment of γ -tubulin and gamma-tubulin complex component 4 (hGCP4).¹⁶⁶ Correct nucleation of the microtubules is essential for centrosome maturation, as well as accurate spindle assembly and mitotic progression.¹⁶⁷ Overexpression of Nlp is known to cause the formation of aggregates around the centrosomes leading to mitotic defects, which has been associated with chromosome instability and malignant transformation.^{168,169} It is the role of regulatory enzymes such as Plk-1 to prevent aberrant Nlp activity, which is achieved by phosphorylation of Nlp causing its removal from the centrosome.¹⁷⁰ *In vitro* and *in vivo* studies have demonstrated that Nek2 phosphorylation of Nlp occurs in a similar way to Plk1 phosphorylation, albeit at an alternative phosphorylation site. Interestingly, inhibition of Nek2 has been shown to disrupt Plk1 mediated phosphorylation of Nlp, which suggests that Nek2 may activate Nlp allowing Plk1 binding.¹⁷⁰ Additionally, Nlp is known to have an important role in cell division, as phosphorylation of Nlp by aurora-B is thought to be vital for cytokinesis.¹⁶⁷

4.4 Structural Features of Nek2 Kinase

It has been established that cellular Nek2 exists as a homodimeric pair of enzymes. This dimerisation enables *trans*-autophosphorylation of serine residues at the C-terminal region *via* a dimerization domain known as the leucine zipper (LZ), which facilitates Nek2 activation.¹⁷¹ Interestingly, it has been shown that this leucine zipper is essential for Nek2 substrate activity, and removal through deletion or mutation causes a reduction in centrosome splitting in U2OS cells.¹⁷¹

There are two splice variants of Nek2 (Nek2A and Nek2B), the structures of which are shown in Figure 18. A major component of each isoform is a conserved N-terminal kinase domain (shown in green), which is required for catalytic activity. Additionally both isoforms contain a leucine zipper (LZ), which allows dimerisation. Nek2A differs from Nek2B in that it is longer and contains a C-terminal regulatory

domain consisting of a protein phosphatase binding site (PP1c) alongside a coiled-coiled domain (CC), and destruction domains (KEN-box and D-box).¹²³ The function of the CC domain in Nek2A is currently unknown; however, it has been suggested that this site has a role in centrosome disjunction.¹⁶⁵

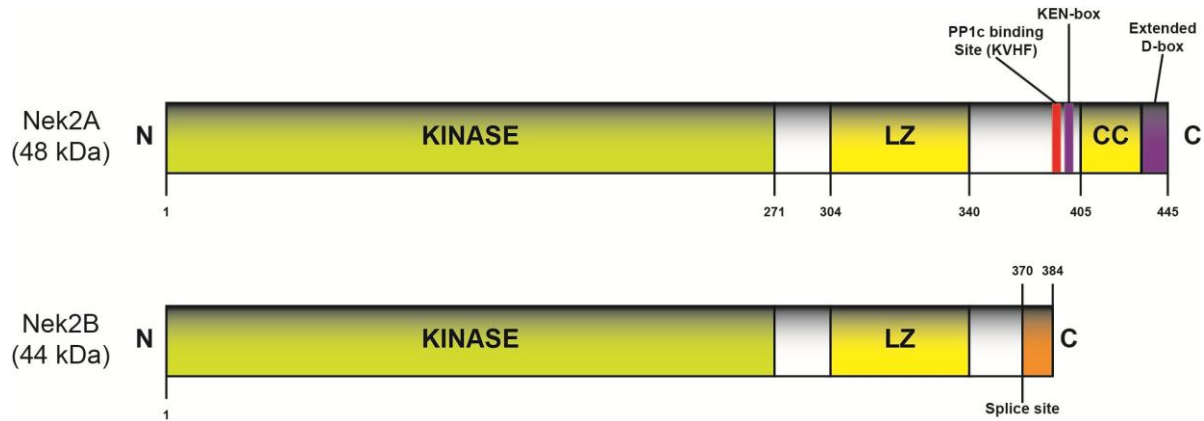


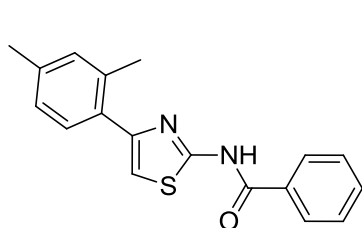
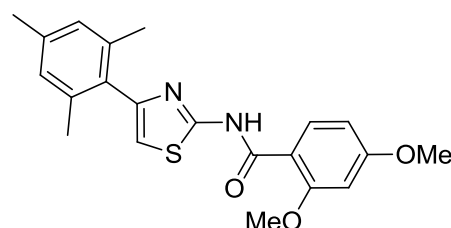
Figure 18 - Schematic representation of Nek2A and Nek2B (adapted from Fry).¹²³

Expression of Nek2A and Nek2B is cell cycle dependent but also distinct for each isoform. Upon entry into mitosis, Nek2A is quickly removed by APC/C following ubiquitination of the C-terminal domain. As this site is not present in the shorter Nek2B isoform, Nek2B levels remain elevated during mitosis suggesting functional differences.^{123,165}

4.5 Nek2 Regulation of the Spindle Assembly Checkpoint (SAC)

The spindle assembly checkpoint (SAC) is an essential regulator of mitosis that ensures correct attachment of microtubules to the kinetochore of chromosomes prior to progression from metaphase to anaphase. Mutations that cause incorrect SAC regulation can induce errors in chromosome segregation, and is strongly associated with the development of aneuploidy and chromosome instability.¹⁷² Nek2 has been implicated in spindle checkpoint control through phosphorylation of the proteins 'highly expressed in cancer 1' (Hec1), 'mitotic arrest deficient 1' (MAD1) and 'mitotic arrest deficient 2' (MAD2).¹⁷³

Hec1 is an established oncogene and is over-expressed by a number of human cancers. Overexpression of Hec1 in human carcinoma has been associated with a poor clinical outcome, and therefore inhibition of Hec1 poses an attractive target for therapeutic agents. Hec1 functions to regulate mitotic spindle formation between kinetochores and centrosomes.¹⁷⁴ To function correctly, Hec1 must first be activated through phosphorylation of Ser-165 in a cell cycle-dependent manner at the G₂/M transition. It has been demonstrated in yeast cells using scNek2/Kin3, a Nek2 functional homologue, that Hec1 is a substrate of Nek2 and phosphorylation at Ser-165 is essential for Hec1 function. However, it has also been shown that this phosphorylation occurs in the absence of scNEk2/Kin3, suggesting a redundant compensatory pathway.¹⁷³ Loss of Hec1 phosphorylation is known to cause errors in chromosome segregation ultimately resulting in reduced cell proliferation and increased cell death, which was demonstrated through the use of Hec1 silencing siRNA studies.¹⁷⁵ A screen of approximately 24,000 compounds led to the discovery of the aryl thiazolylbenzamide compounds INH1 **22** and INH2 **23**, which demonstrated Hec1 inhibitory activity but had low potency and aqueous solubility. SAR studies revealed that a central thiazolyl ring, coupled to a hydrophobic aryl ring and a polar arylamide were critical for activity and analogues of the two lead compounds focused on modification of this scaffold to improve pharmacokinetic properties. Although these compounds were not inhibitors of Nek2, they demonstrated that disruption of the downstream effects of Nek2 inhibition can induce chromosome misalignment leading to cell death.¹⁷⁴

**22****23**

Like Hec1, MAD1 and MAD2 are also mitotic checkpoint proteins that are localised at the kinetochore. It has been demonstrated that MAD2 is a substrate for Nek2 phosphorylation, which is thought to allow regulation of the SAC, thus preventing premature entry into anaphase.¹⁷⁶ Additional studies are required to further elucidate the role of Nek2 in SAC regulation.

4.6 Nek2 is Implicated in Chromatin Condensation

Aside from an established role in mitosis, Nek2 has also been implicated in chromatin condensation during meiosis.^{177,178} Di Agostino observed that activation of the mitogen-activated protein kinase (MAPK) pathway in mouse spermatocytes, caused subsequent activation of p90Rsk2 and Nek2 through a kinase signalling cascade.¹⁷⁷ Additional studies by Sette showed that the MAPK pathway is essential for efficient chromatin condensation.¹⁷⁹ A key enzyme in this pathway is high mobility group AT-hook 2 (HMGA2), which has been shown to be a substrate for Nek2 by *in vitro* studies.¹⁷⁹ HMGA2 binds to DNA at areas rich in adenine-thymine (AT) base pairs. The function of HMGA2 is to regulate transcription, which is achieved by causing conformational changes in chromatin facilitating further protein binding.¹⁸⁰ Upon phosphorylation, HMGA2 has a decreased affinity for DNA which may cause its release from chromatin allowing further condensation.¹⁷⁷

4.7 Inhibition of Nek2 Results in Decreased Tumour Cell Growth

In vivo studies in mice have shown that Nek2 inhibition may induce a reduction in tumour growth. In these experiments, nude mice were inoculated with human cholangiocellular carcinoma cells (HuCCT1).¹⁸¹ Cholangiocarcinoma is a form of liver cancer that is rare in the western world, but is becoming increasingly common in southeast Asia. Four weeks after inoculation, mice bearing tumours were selected and treated (20 µmol/L) with either Nek2 silencing siRNA in cell matrix, a non-silencing siRNA in cell matrix or cell matrix alone, once a week for 3 weeks (Figure 19, **a**). Upon completion of treatment, tumour volumes were determined periodically, for 12-weeks following inoculation. Mice treated with Nek2 silencing siRNA experienced an approximate 50% reduction in tumour cell growth when compared with control mice.¹⁸¹ Additionally, it was shown that Nek2 inhibition in these tumours led to a reduction of cell division and increased cell death. To confirm that these results were a result of Nek2 inhibition, an immunoblot analysis was performed, which showed that Nek2 was effectively inhibited in treated mice by siNek2 27 (a Nek2 silencing siRNA) but was still active in the tumours from control mice (Figure 19, **b**).

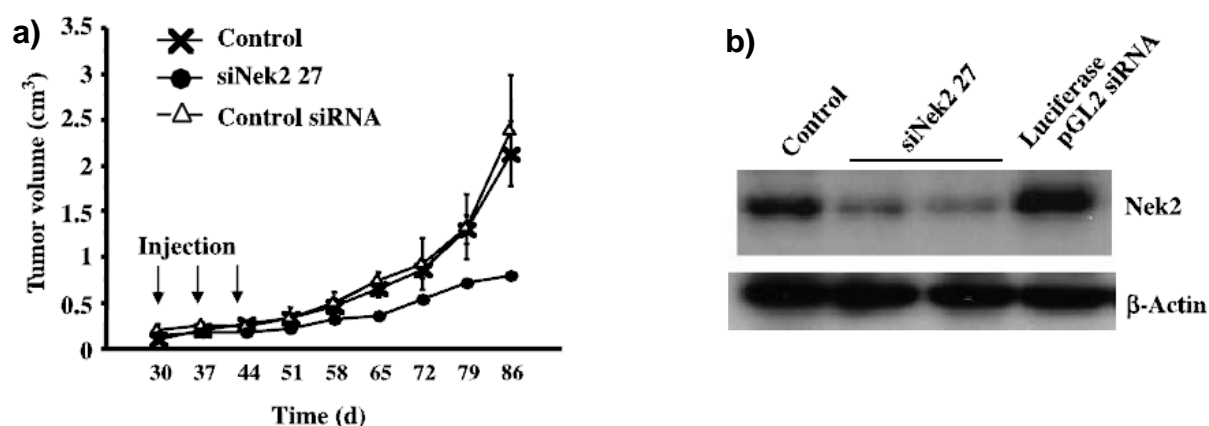


Figure 19 - Inhibition of Nek2 by Nek2 silencing siRNA.¹⁸¹

In vitro studies were conducted using alternative tumour cell lines including, thyroid hyalinising trabecular tumour (HTT) cells and the bile duct carcinoma cell line (TFK1). Whilst Nek2 siRNA induced cell death in TFK1 cells analogous to the HuCCT cell line, there was limited evidence that Nek2 inhibition reduced the viability of HTT cells (Figure 20). These results suggest that the therapeutic potential of Nek2 may be limited to responsive cell lines.¹⁸¹

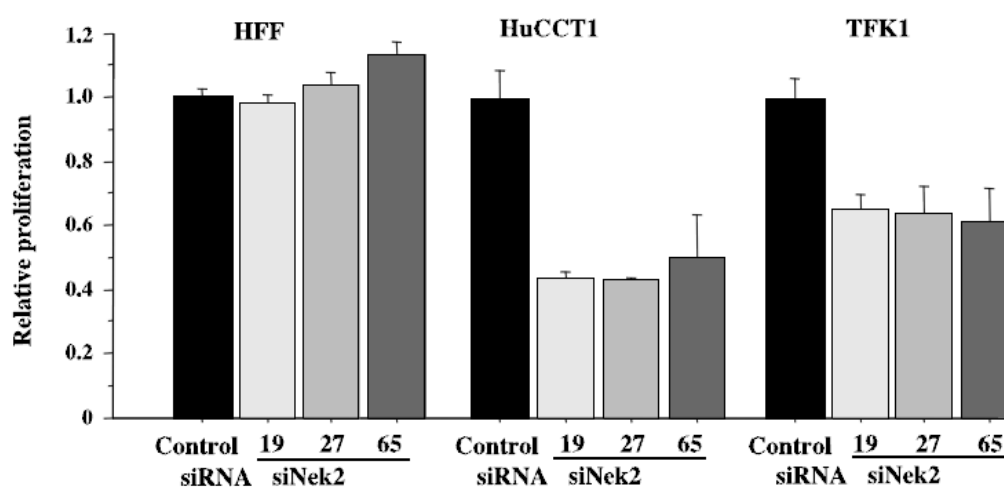
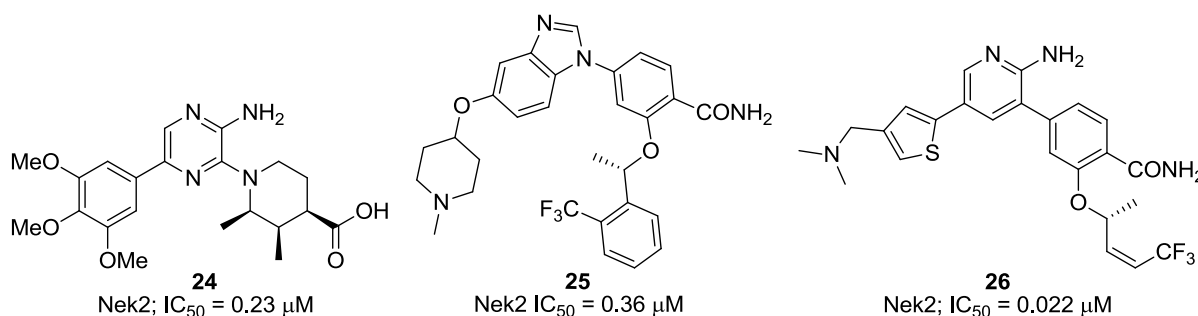


Figure 20 - Effect of Nek2 inhibition on HFF, HuCCT1 and TFK1 cell lines.¹⁸¹

4.8 ATP-Competitive Reversible Inhibitors of Nek2



Pyrazine **24** is a member of an aminopyrazine series of ATP-competitive reversible inhibitors that binds to an inactive form of Nek2.¹⁸² Nek2 phosphorylation, and hence activation, is prevented causing the enzyme to remain in an inactive state. An advantage of binding in this way, is that an increased window of opportunity exists for successful drug-target interactions, which may improve efficacy. Whilst this compound was shown to have sub-micromolar Nek2 inhibitory activity ($IC_{50} = 230$ nM) and good selectivity for Nek2 over other kinases, the pyrazine series was essentially inactive in cells due to poor membrane permeability.¹⁸²

Compound **25** represents a series of Nek2 inhibitors based upon the benzimidazole heterocycle. This compound was found to have sub-micromolar Nek2 inhibitory activity ($IC_{50} = 360$ nM) and good cell permeability. Unfortunately, this compound series was highly lipophilic and lacked good structure-activity relationships (SARs), preventing further advances of Nek2 inhibition.¹⁸³ Additionally, this series was found to lack cellular activity, which was attributed to inadequate Nek2 inhibitory activity.¹⁸⁴

Recently, a potent selective series of Nek2 inhibitors with improved lipophilicity was discovered based upon a hybrid of pyrazine **24** and benzimidazole **25**.¹⁸⁴ Of this series, aminopyridine **26** had the highest Nek2 inhibitory activity ($IC_{50} = 22$ nM), and showed promising cellular activity. It is hoped that this compound will help further elucidate the function of Nek2 and its involvement in the cell cycle.¹⁸⁴

4.9 Oxindole Based Irreversible Inactivators of Nek2 Kinase

The first reported irreversible inhibitor of Nek2 with cellular activity was described by Henise and Taunton in 2011.¹⁸⁵ This compound was based upon the oxindole

inhibitor SU11652 **27**, which is an ATP-competitive Nek2 inhibitor with poor kinase selectivity.¹⁸⁵ The oxindole heterocycle and the pyrrole ring of **27** form a triplet of hydrogen bonds with the Nek2 hinge region, which is vital for potent Nek2 inhibition. It was determined that modifications of the 3', 4' and 5' positions of the pyrrole ring were tolerated, and it was hoped that functionalisation of these positions would allow increased Nek2 selectivity due to the presence of a non-conserved cleft within the Nek2 ATP-binding domain, which could be occupied by small alkyl substituents. The 6- and 7-positions of the oxindole ring form close contacts with the Nek2 methionine gatekeeper residue (Met-86), and therefore were unsuitable for functionalisation. Interestingly, the 5-chloro group of **27** was estimated to be approximately 6 Å from Cys-22. The close proximity of the reactive Cys residue suggested that covalent modification and hence irreversible Nek2 inhibition might be achievable through the inclusion of electrophilic groups at this position (Figure 21).

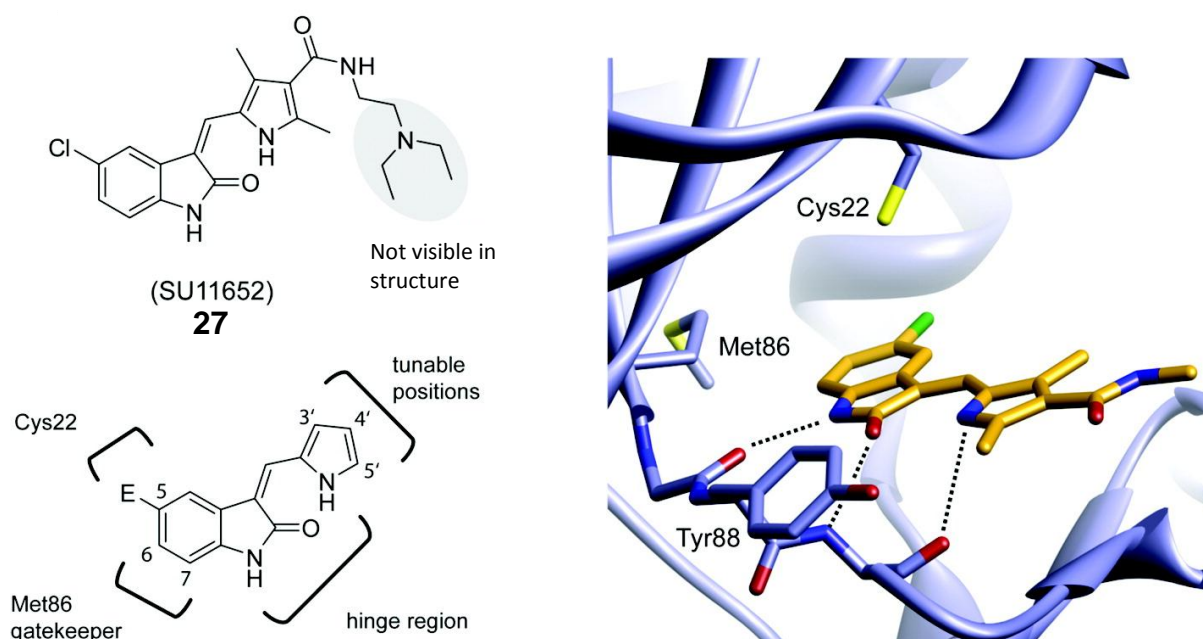


Figure 21 - Design of oxindole based irreversible inhibitors of Nek2.¹⁸⁵

A structure-based design approach led to the synthesis of a small library of compounds based upon **27**, with a range of electrophilic groups at the oxindole 6-position. These included chloromethylketone **28**, chloroacetamide **29**, and a range of compounds containing Michael acceptor groups **30-34** (Figure 22). Of these, propyneamide **34** and chloromethylketone **28** were found to be the most potent, with IC₅₀ values of 920 nM and less than 6 nM, respectively.¹⁸⁵

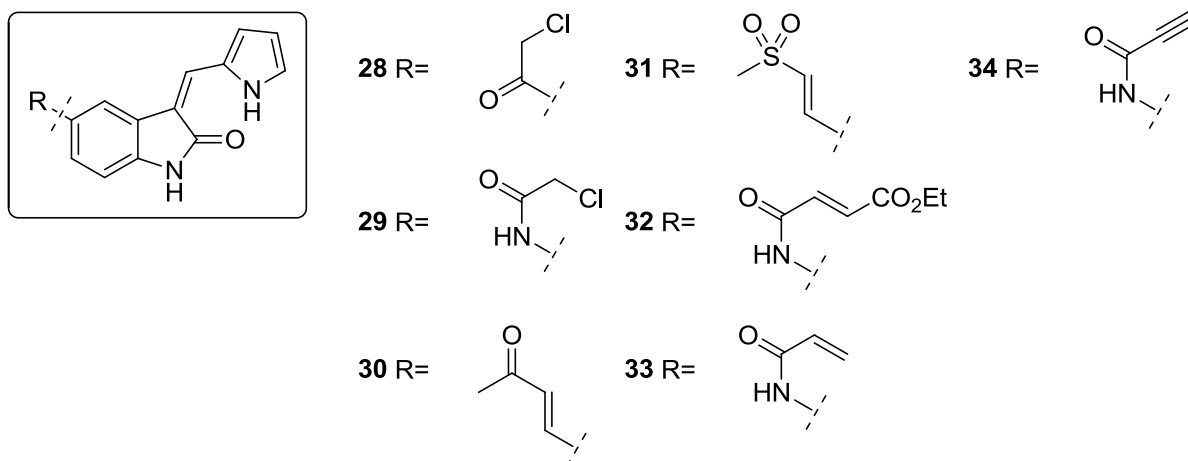
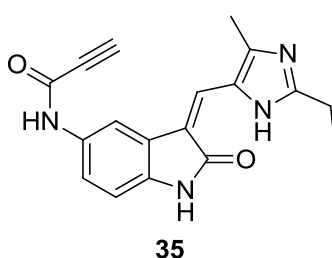


Figure 22 - First generation irreversible Nek2 inhibitors.¹⁸⁵

Unfortunately, these compounds were found to be non-selective and were also low-nanomolar inhibitors of CDK1. To attempt to improve selectivity, further modifications were investigated leading to the discovery of alkylimidazole **35**. This compound was found to retain Nek2 inhibitory activity ($\text{IC}_{50} = 700 \text{ nM}$) and demonstrated excellent selectivity over CDK1 ($\text{IC}_{50} = >20 \text{ }\mu\text{M}$), which was found to be due to the presence of the ethyl substituent on the imidazole ring. Covalent modification of Cys-22 within the Nek2 ATP-binding domain was confirmed by time-dependent inhibition studies and mass-spectrometry analysis of **35** bound to Nek2. Additionally, site-directed mutagenesis studies with the Nek2 C22V mutant (Cys-22 \rightarrow Val-22), demonstrated a substantial reduction of Nek2 inhibitory activity of **35** compared with wild-type Nek2.¹⁸⁵



Finally, *in vitro* immunoprecipitation kinase assays in A549 lung cancer cells, showed that **35** inhibited cellular Nek2 (92% at $5 \text{ }\mu\text{M}$). Interestingly, it was observed that despite inhibition of Nek2, these cells were able to enter mitosis and form intact bipolar spindles. These results suggest that Nek2 is either not essential for entry into mitosis, or that only low levels of Nek2 are required for mitotic progression.¹⁸⁵

4.10 Purines as Irreversible Inhibitors of Nek2

The use of the purine heterocycle as a basis for Nek2 inhibitors arose from *X-ray* crystal structural analysis of the interaction between the pyrrole-indolinone compound SU11652 **27** with the Nek2 ATP-binding site (Figure 23). SU11652 was designed as an ATP-competitive tyrosine kinase inhibitor; however, activity had also been observed for a variety of serine/threonine kinases including Nek2.¹⁸⁶ The crystal structure of **27** bound to Nek2 three key H-bond interactions with the Nek2 Hinge region (Figure 24).¹⁵² In addition to this, hydrophobic interactions are observed with the Met-86 gatekeeper residue. Both **27** and its fluorine derivative SU11248 **36**, demonstrated activity against Nek2 but poor kinase selectivity.¹⁵²

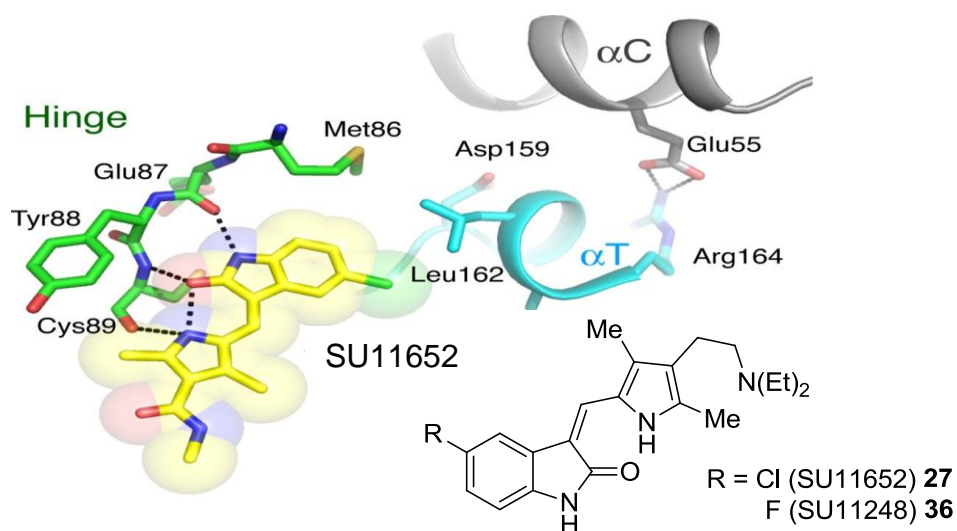


Figure 23 - H-bond interactions of **23** and **32** with Nek2 ATP-binding domain.¹⁵²

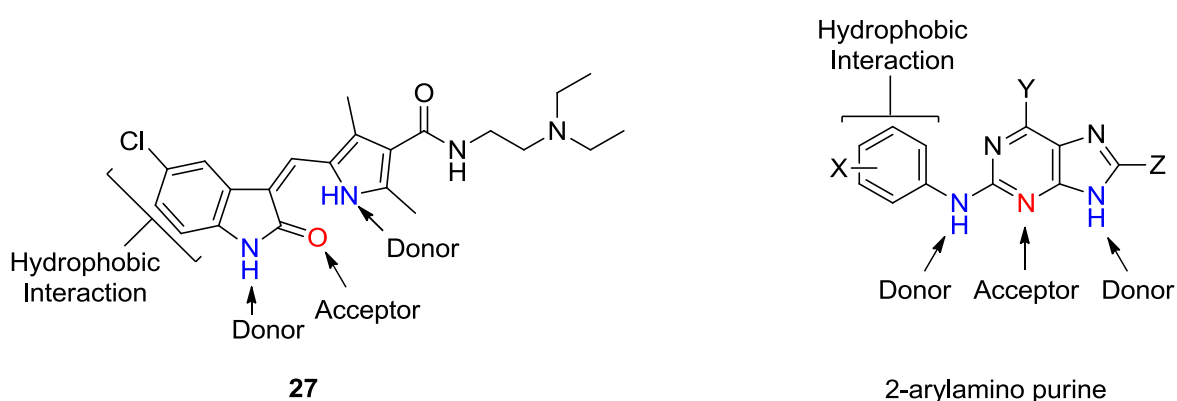


Figure 24 - Comparison of **27** with a purine template.

As CDK2 and Nek2 are both members of the serine/threonine family of protein kinases, their ATP-binding domains have a degree of structural homology. It was established that that CDK2 could be inhibited by functionalised purines, which form a

H-bond triplet with amino acids of the hinge region of the ATP-binding domain, and it was thought that these compounds may also have Nek2-inhibitory activity.¹⁸⁷ A screen of purine-based CDK2 inhibitors against Nek2, revealed NU6102 **37** (see chapter five) as a modest inhibitor of Nek2 ($IC_{50} = 20.9 \mu M$) with potent CDK2 inhibitory activity ($IC_{50} = 5 nM$). As such, **37** was selected as a hit compound with the aim of designing out CDK2 activity to give a potent and selective inhibitor of Nek2. **37** was thought to act as a reversible inhibitor of Nek2 by competing for the ATP-binding domain. In this instance, it was known that the Nek2 ATP-binding domain contained a cysteine residue (Cys-22) that was not present in CDK2. It was hypothesised that the thiol group of Cys-22 may be correctly orientated to allow covalent reaction with a bound purine that contained an electrophilic ethynyl group at the 6-position. The conjugate addition of sulfur containing nucleophiles to 6-ethynyl purines had been demonstrated previously by Hocke.¹⁸⁸ However, to our knowledge this approach to irreversible enzyme inhibition had not been reported previously. To synthesise an irreversible inhibitor of Nek2 it was necessary to design a compound that could covalently modify the Nek2 ATP-binding domain, thus permanently preventing binding of the natural substrate. As the crystal structures of both CDK2 and Nek2 had already been determined it was possible to utilise a structure-based approach for the design of an irreversible inhibitor of Nek2 with selectivity over CDK2. Traditional drug design has often adopted a random approach involving the screening of numerous compounds. By contrast, an intelligent design approach uses structural biology to identify key structural features within the binding site of the target enzyme or receptor. Ligands can then be designed with the assistance of bioinformatics and molecular modelling to contain functional groups correctly positioned to interact with these motifs with the aim of producing a potent selective inhibitor.¹⁸⁹ This approach led to the discovery of the 6-ethynylpurine **40** (see chapter five), which is a potent Nek2 inhibitor ($IC_{50} = 56 nM$) with excellent selectivity over CDK2 ($IC_{50} = 11.8 \mu M$).

Chapter Five: Synthesis of Purine Isosteres as Inhibitors of Nek2

5.1 Development of Purine-Based Irreversible Inhibitors of Nek2

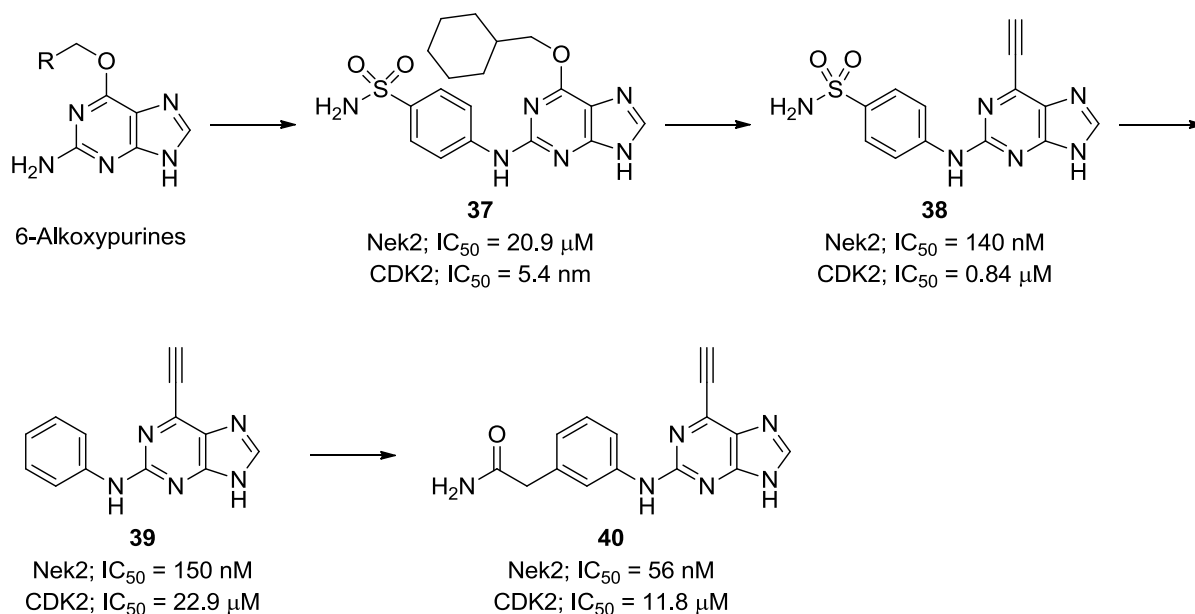


Figure 25 - Development of purine based Nek2 inhibitors at the NICR.

A medium-throughput screen of approximately 250 compounds identified 6-alkoxypurines as modest inhibitors of Nek2. Purine **37**, a potent CDK2 inhibitor (IC_{50} = 5.0 nM), demonstrated Nek2 inhibitory activity in the micromolar range (IC_{50} = 20.9 μ M). Investigations into modification of the 2-aryl amino and 6-alkoxy groups led to the identification of **38**. This compound was a potent inhibitor of Nek2 (IC_{50} = 140 nM) with 6-fold selectivity over CDK2. Interestingly, **38** exhibited a time-dependent Nek2 inhibition profile characteristic of irreversible enzyme inhibition. However, **38** was essentially inactive in cells due to poor physicochemical properties. Removal of the sulfonamide functionality gave **39**, which was a potent Nek2 inhibitor (IC_{50} = 150 nM) with selectivity over CDK2 and displayed growth inhibitory activity *in vitro* (GI_{50} ; SKBR3 cells = 0.33 μ M). This compound was taken forward as an early hit, assayed in the 'Dundee Kinase Screen' against a panel of 121 kinases, and found to be remarkably selective for Nek2. Unfortunately, **39** had sub-optimal cellular properties including high lipophilicity ($cLogP$ = 2.93) and poor aqueous solubility. A structure-based design approach led to the discovery of **40** a potent and selective irreversible Nek2 inhibitor with good cellular growth-inhibitory activity (GI_{50} ; SKBR3 cells = 2.2 μ M) and acceptable drug-like properties. The additional acetamide functional group

possibly serves to make H-bond interactions with Ser-96 and Asp-93 within the Nek2 ATP-binding domain (Figure 26).

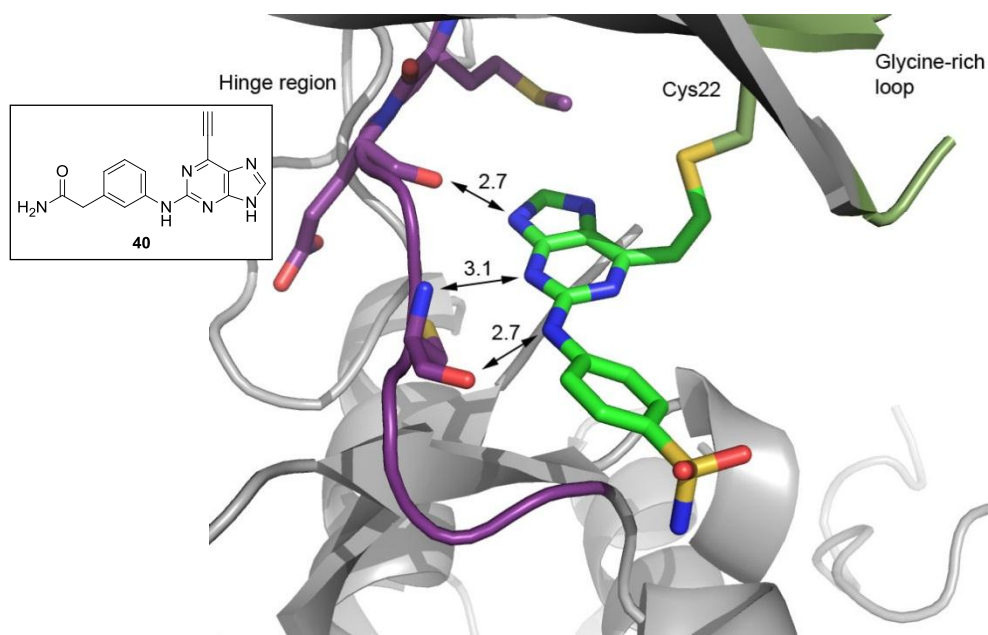


Figure 26 X-ray crystal structure showing irreversible covalent modification of Cys-22 within the Nek2 ATP-binding domain by **40**.

5.2 Nek2 Putative Binding Mechanism

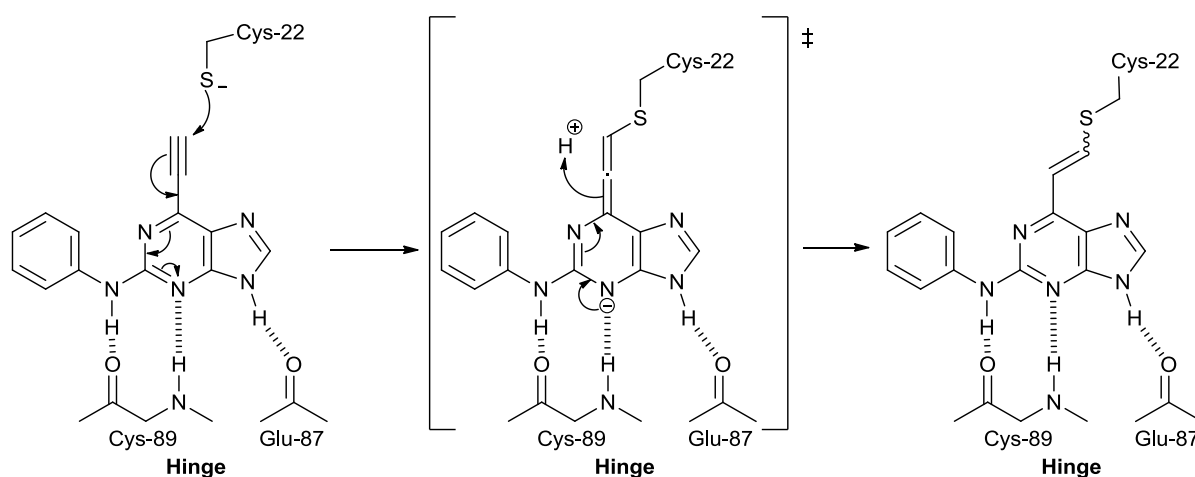


Figure 27 – Mechanism of Nek2 inactivation by 6-ethynylpurines.

The 6-ethynylpurine series has been shown to irreversibly inhibit Nek2 through covalent modification of Cys-22 within the Nek2 ATP-binding domain. An initial reversible ATP-competitive binding interaction between the ligand and the Nek2 hinge region occurs *via* a triplet of H-bonds (Figure 27). The resulting enzyme-

inhibitor complex is believed to position the electrophilic 6-ethynyl group at *ca.* 120° relative to Cys-22, which is the optimum angle of nucleophilic attack.¹⁹⁰ 'Partial protonation' of the purine *N*³ *via* a H-bond may also facilitate covalent modification.¹⁹¹ The covalently bound ligand occupies the Nek2 ATP-binding domain causing irreversible inactivation of Nek2.

5.3 Reversibility of the Nek2-Cys-22 Covalent Complex

Rather than being true irreversible inhibitors of Nek2 it has been suggested that 6-ethynylpurines such as **39** may form an initial covalent complex that is slowly hydrolysed to give the aldehyde **46** (Figure 28). Indeed, preliminary studies have identified a compound with a mass suggesting the presence of **46**; however, further work is required to confirm this.

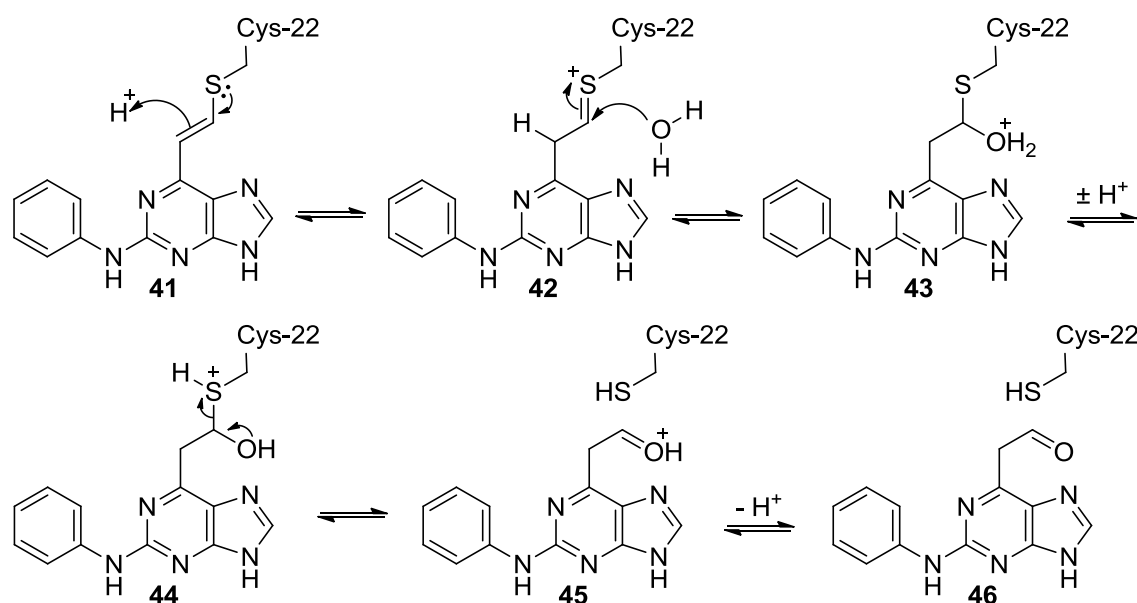


Figure 28 - Putative mechanism for the hydrolysis of the Nek2-inhibitor complex.

An example of this type of enzyme inhibition occurs with physostigmine **47**, a carbamate-based reversible acetylcholinesterase (AChE) inhibitor.¹⁹² The mechanism of action of this drug is shown in Figure 29. A reversible enzyme-inhibitor complex forms, which is followed by carbamylation of the serine hydroxyl group of AChE causing irreversible enzyme inhibition. The covalently bond between the enzyme and the inhibitor is then hydrolysed to give the active enzyme, methylamine and CO₂.¹⁹³

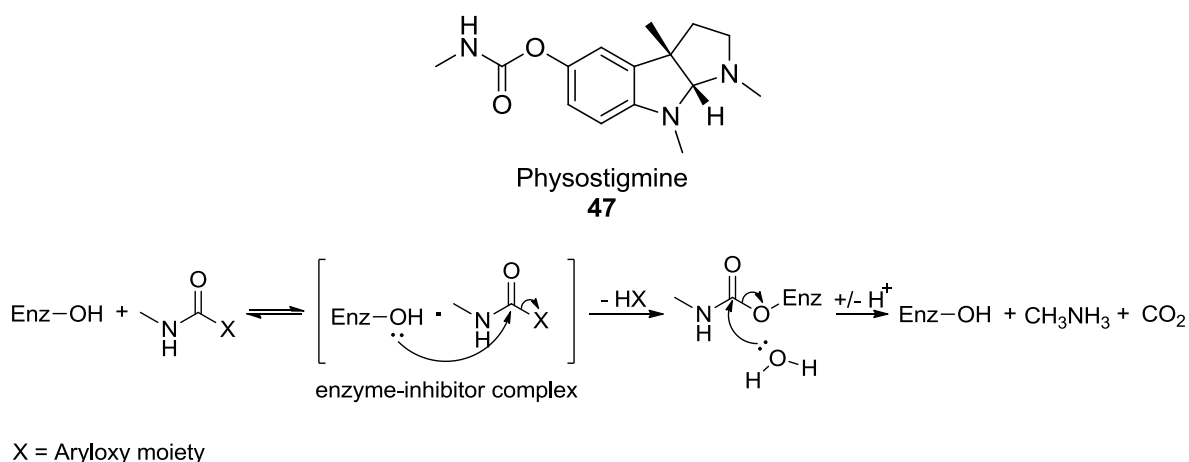
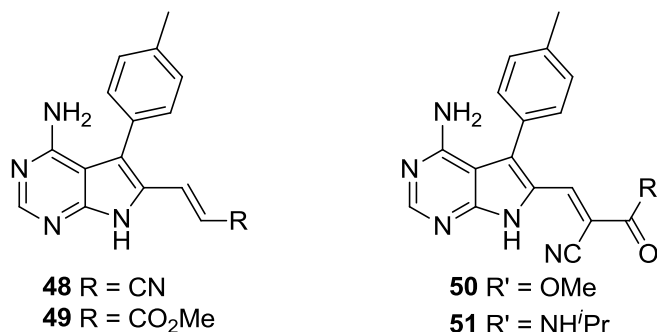


Figure 29 - Inhibition of AChE by physostigmine.

Additionally, early work by Pritchard *et al.* showed that it was possible to react *N*-butanethiol with 2-cyanoacrylates at physiological pH via an addition-elimination reaction.¹⁹⁴ However, attempts to isolate or characterise products proved unsuccessful, possibly due to the reaction being rapidly reversible.^{194,195} Recently, this has been further investigated through the design of reversible covalent inhibitors of p90 ribosomal protein S6 kinase (RSK2) using acrylamide-based pyrrolopyrimidines (**48-51**).¹⁹⁵



A benefit of 'reversibly' targeting enzymes with electrophiles is that the advantages of irreversible inhibitors are often retained, e.g. high selectivity and long residence times, whilst disadvantages such as toxicity associated with covalent modification may be reduced.^{77,195}

5.4 Structure-Activity Relationship Studies with 6-Ethynyl-2-Phenylaminopurine (39)

Phenylaminopurine (39)

A series of 2-arylamino-purine derivatives was synthesised to further evaluate the importance of H-bond interactions in the initial non-covalent binding interaction with Nek2. The first compounds to be synthesised were the N^7 - and N^9 -methylpurines **52** and **53**, which allowed investigations into the $N^9\text{H} \cdots \text{O}=\text{C}$ (Glu-87) H-bond. The role of the $2\text{-NH} \cdots \text{O}=\text{C}$ (Cys-89) H-bond was evaluated through the synthesis of the 2-*N*-methyl- (**54**), 2-phenoxy- (**55**) and 2-benzyl- (**56**) purine derivatives respectively (Figure 30).

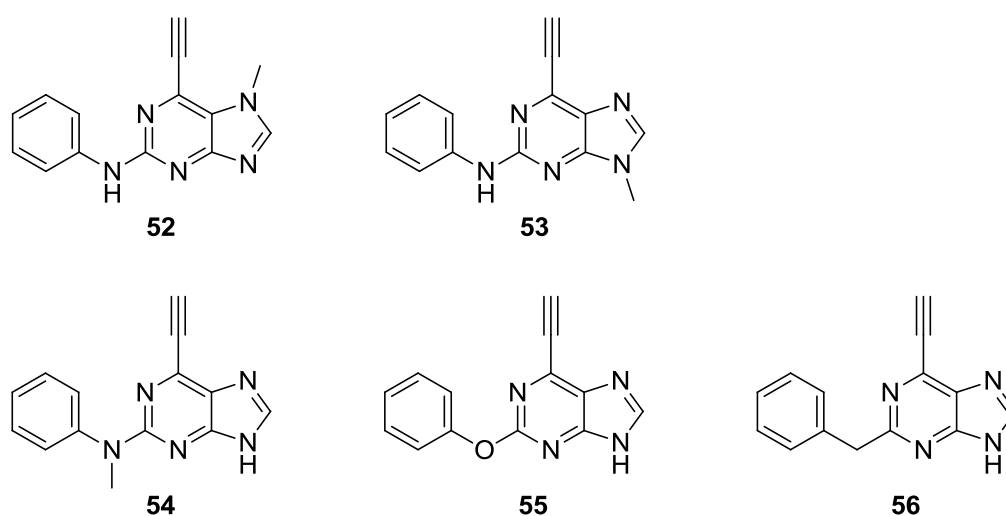


Figure 30 – SAR studies of purine **39**.

5.4.1 Synthesis of N^7 - and N^9 -Methyl-2-Phenylaminopurines (**52**) and (**53**)

The N^7 - and N^9 -methyl derivatives of **39** were synthesised to further investigate the binding mode of this series of compounds, and provided inactive control compounds for further biological evaluation. Methylation at the N^7 - or N^9 -position removes a crucial H-bond between the purine and the hinge region of the Nek2 ATP-binding domain (Figure 31). This bond is likely critical for Nek2 inhibition as it positions the substrate in an orientation that facilitates attack of Cys-22 on the 6-ethynyl group. This approach was used previously within the group during the design of CDK2 inhibitors.¹⁹⁶

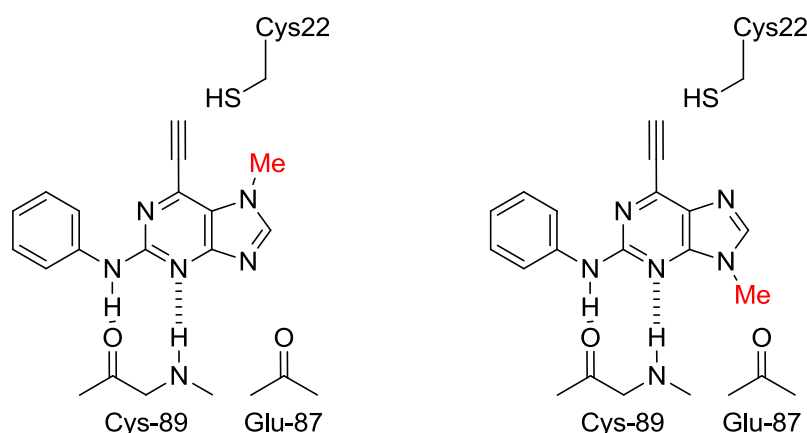
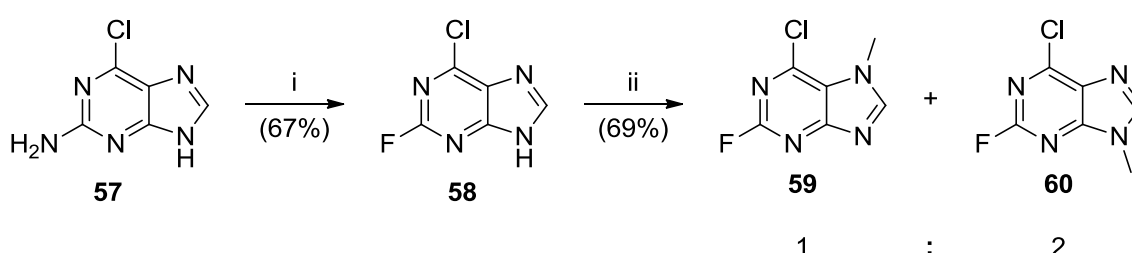


Figure 31 - Methylation of **39** a removes crucial hydrogen bond.

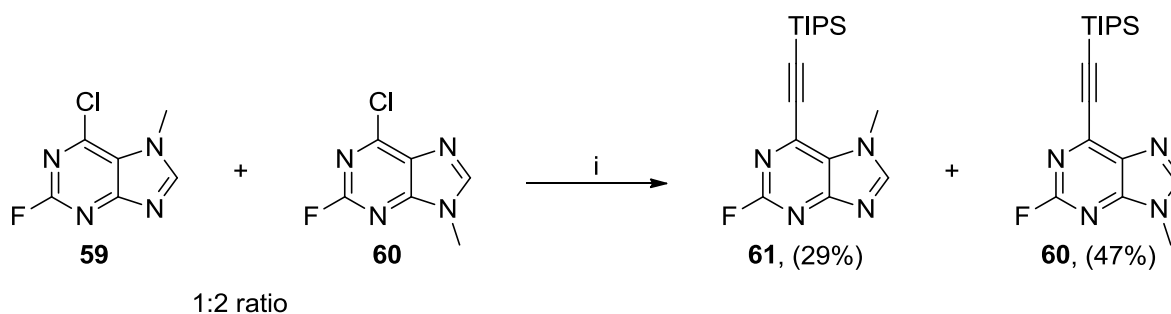


Reagents and conditions: i) NaNO_2 , HBF_4 , $0^\circ\text{C} - \text{RT}$, 18 h; ii) MeI , K_2CO_3 , DMF , RT , 18 h.

Scheme 1.

The Balz-Schiemann reaction allows the conversion of aromatic amines into the respective fluoro derivative *via* a diazonium intermediate.¹⁹⁷ Traditionally this reaction is performed in a two-step procedure, with isolation of the diazonium intermediate as the tetrafluoroborate salt, followed by heating to induce fluorodediazotization.¹⁹⁸ Whilst this method can facilitate the preparation of aryl fluorides in good yield, the hazards associated with heating large quantities of a diazonium salt and the poor yields obtained with thermally sensitive substrates made this method unsuitable for the conversion of **57** to **58**. Instead, a one-pot approach using NaNO_2 in $\text{HBF}_4(\text{aq})$ was used, allowing the preparation of **58** in 67% yield.¹⁹⁸

Direct *N*-methylation of fluorochloropurine **58** using methyl iodide in basic conditions, gave an inseparable mixture of the *N*⁷- and *N*⁹-methylpurines **59** and **60** in a ratio of 1:2, respectively (observed by ^1H -NMR spectroscopy). The mixture of **59** and **60** was used in the Sonogashira cross coupling of TIPS-acetylene, which allowed separation of regioisomers **61** and **62** with an overall yield of 76%.

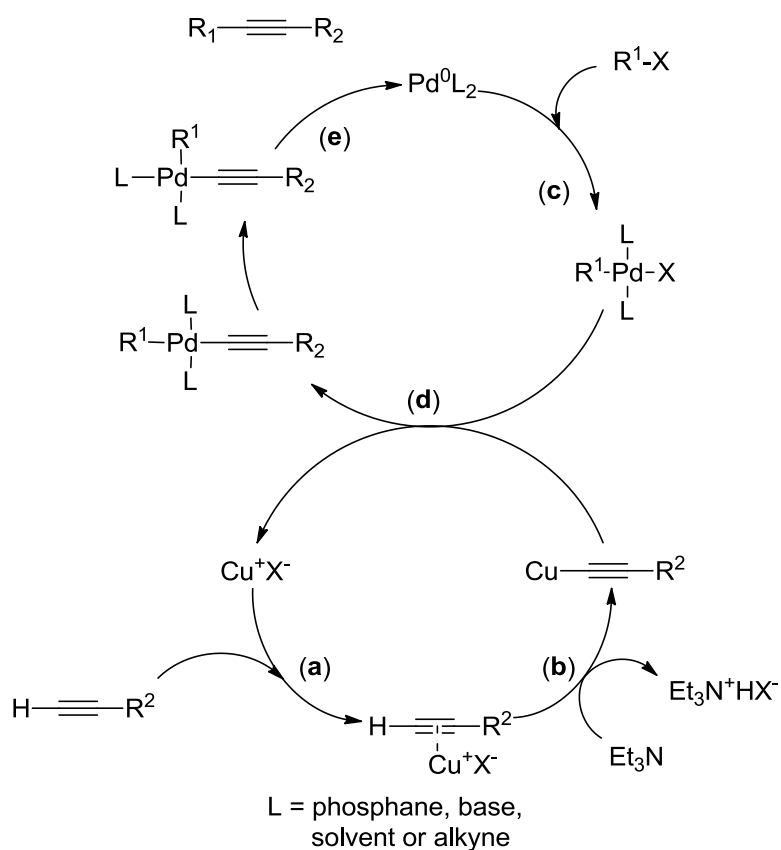


Reagents and conditions: i) TIPS-acetylene, Pd(PPh₃)Cl₂ (5 mol%), CuI (5 mol%), Et₃N, THF, RT, 18 h.

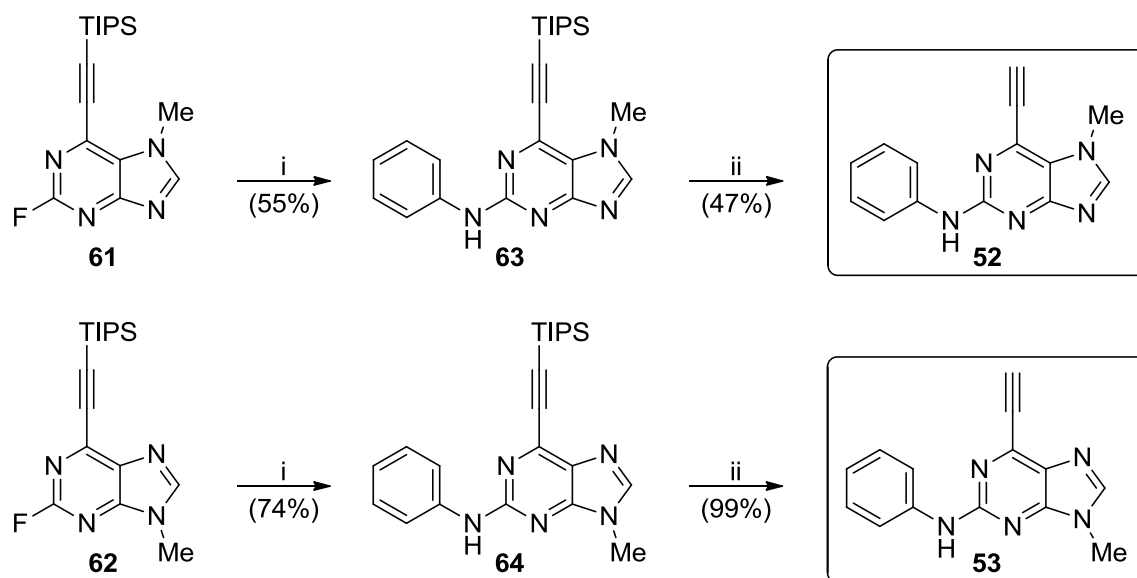
Scheme 2.

The Sonogashira reaction allows the coupling of terminal acetylenes with aryl halides. The reaction involves the application of a palladium (0) (Pd⁰) complex which can be used directly or generated *in situ* through oxidation of palladium (II) (Pd^{II}). Copper (I) iodide (CuI) is added as a co-catalyst, together with an organic base such as Et₃N to quench acidic side-products and generate the active palladium species (Pd⁰).¹⁹⁹ An inert N₂ atmosphere is maintained throughout to stabilise the intermediate metal complex and prevent oxidation.

The Sonogashira reaction proceeds through two separate catalytic cycles (Scheme 3). Copper iodide coordinates to the acetylene (**a**) which is then deprotonated by Et₃N allowing generation of the alkynyl copper species and removal of the hydrogen halide side-product (**b**). Simultaneously, Pd⁰ oxidatively inserts into the aryl-halide species forming the Pd^(II) intermediate (**c**). A transmetalation reaction occurs between alkynyl-copper and the newly formed Pd^(II) complex resulting in transmetalation and regeneration of copper (I) iodide (**d**). Finally, reductive elimination results in product formation and regeneration of the palladium catalyst (**e**).¹⁹⁹



Scheme 3 - Sonogashira cross-coupling mechanism.



Reagents and conditions: i) PhNH_2 , TFA, TFE, 75°C , 18 h; ii) TBAF, THF, RT, 30 min.

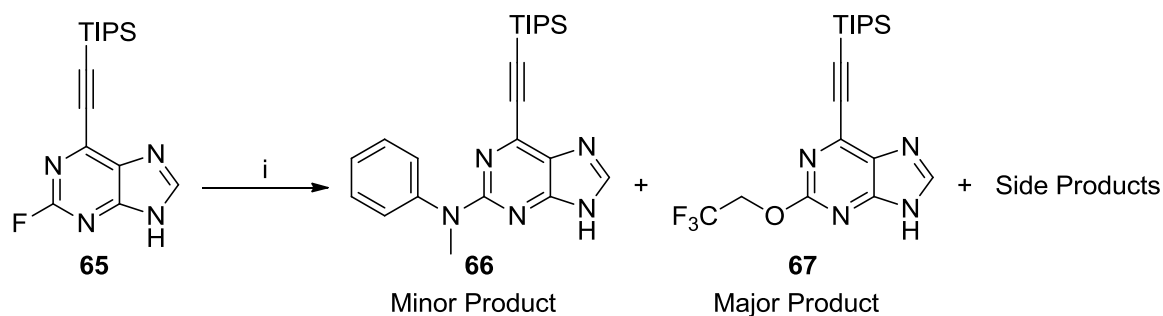
Scheme 4.

An acid-catalysed $\text{S}_{\text{N}}\text{Ar}$ reaction allowed coupling of aniline to **61** and **62**, giving 2-arylamino-4-alkynylpurines **63** and **64** in moderate (55%) to excellent (74%) yield, respectively. The use of TFE as a solvent in this reaction is advantageous as it is thought to allow

solvation of fluoride, resulting in increased reactivity.^{200,201} It was determined that 2.5 equivalents of TFA was optimum to catalyse the reaction, and this quantity of TFA allows protonation of purine N^1 or N^3 ($pK_a = 2.5$) with minimal protonation of the less basic aniline NH_2 ($pK_a = 4.6$). The final stage of this synthesis was deprotection of the terminal acetylene from **63** and **64**. The TIPS protecting group can be readily removed with fluoride and a convenient source of fluoride is TBAF, which has advantages over other sources of fluoride such as HF and KF in terms of safety and solubility. An interesting finding was that yields for reactions of N^7 -methylpurines **61** and **63** were lower than those observed in the synthesis of the N^9 -methylpurine **53**, which is likely due to reduced stability for reasons that remain unclear.

5.4.2 Synthesis of *N*-Methylanilinopurine (**54**)

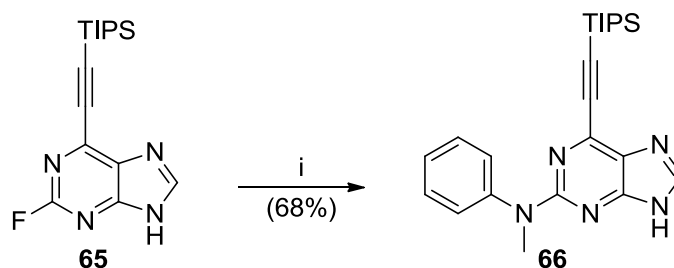
The *N*-methylanilinopurine derivative **54** was synthesised to address the role of the 2-arylamino NH of parent purine **39**, which forms a H-bond interaction with Cys-89 of the Nek2 ATP-binding domain. If this H-bond was found to be unnecessary for inhibitor binding, the possibility of further modification at this position was to be investigated.



Reagents and conditions: i) *N*-Methylaniline, TFA, TFE, 75 °C, 18 h.

Scheme 5.

Coupling of *N*-methylaniline with purine **65** under standard conditions (Scheme 5) proved unsuccessful owing to multiple side-products, the most prominent of which was the TFE ether **67**.



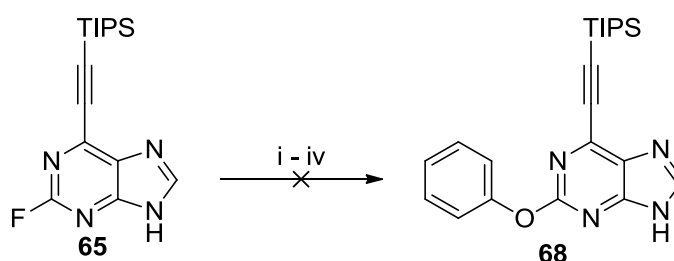
Reagents and conditions: i) *N*-Methylaniline, TFA, Toluene, MW 160 °C, 4 h.

Scheme 6.

Replacement of TFE by toluene proved an effective solution to this problem as it is non-nucleophilic and has a comparable boiling point (111 °C). It was also found that this reaction benefitted from microwave heating, allowing formation of **64** in a yield of 68% (Scheme 6).

5.4.3 Synthesis of 2-Phenoxypurine (**55**)

To further investigate the role of the purine C²-NH in the binding interaction, the 2-phenoxypurine derivative **55** was synthesised. In this compound, the donor aniline NH is replaced by an acceptor oxygen. The phenoxy moiety was also predicted to attenuate reactivity of the ethynyl group *via* electron donation to the purine. By making the ethynyl group less reactive it was hoped that selectivity for Nek2 would be improved.



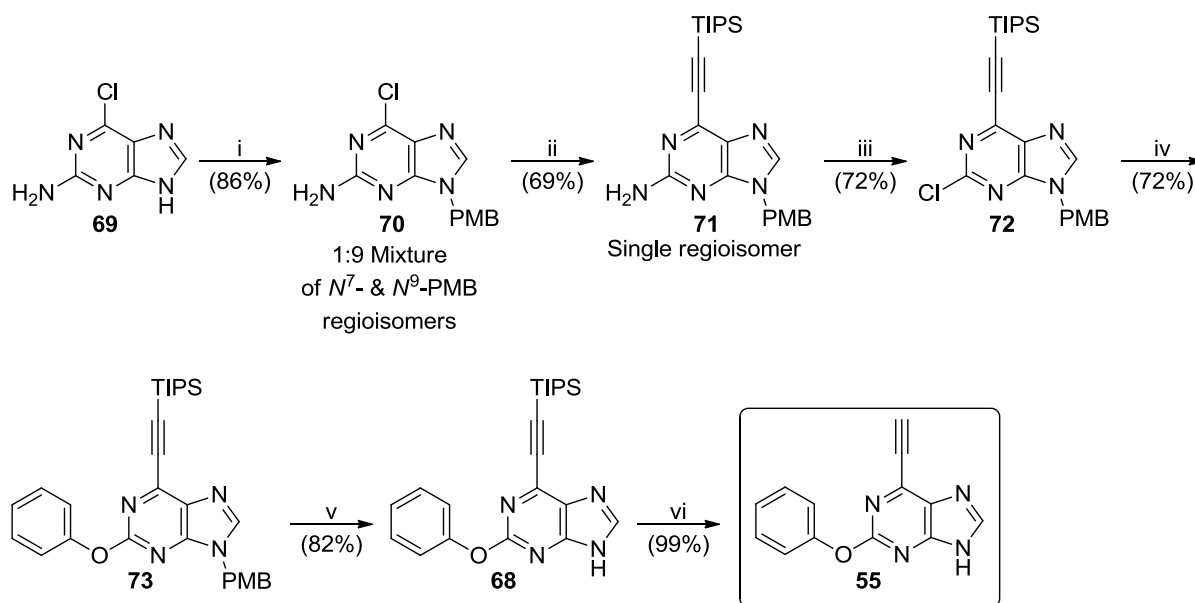
Reagents and conditions: i) Phenol, TFA, TFE, 85 °C, 18 h; ii) Phenol, TFA, Toluene MW 160 °C, 4 h; iii) Phenol, MW 180 °C, 1 h; iv) Phenol, NaH, THF, 80 °C, 30 min.

Scheme 7.

Initial attempts to couple phenol directly with purine **65** were unsuccessful, resulting in little if any product formation alongside a multitude of side-products. The standard TFA/TFE coupling conditions that worked well for reactions with anilines, failed when

phenol was the substrate, owing to displacement of fluoride by trifluoroethanol to give **67**. Using toluene in place of TFE resulted in no observed reaction, even with prolonged heating at high temperatures (160 °C, 8 h). In addition, modifying the number of equivalents of TFA used to catalyse the reaction was investigated. However, even with 20-equivalents of TFA no product formation (**68**) was observed. An alternate approach was to generate phenoxide using a base, thus enhancing nucleophilicity. Literature examples using this method are reportedly high yielding and rapid, but in this case only degradation was observed, possibly due to instability of the TIPS protecting group of **65**.

As phenol was too unreactive for an acid-mediated coupling reaction and base catalysed reactions led to degradation, a mild Pd catalysed approach was investigated.

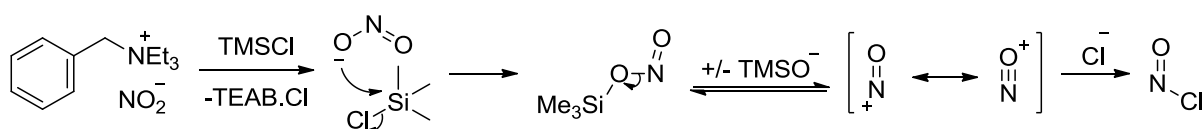


Reagents and Conditions: i) PMBCl, K₂CO₃, DMF, 65 °C, 18 h; ii) TIPS-acetylene, Pd(PPh₃)Cl₂ (5 mol%), CuI (5 mol%), Et₃N, THF, RT, 18 h; iii) Benzyltriethylammonium nitrite, TMSCl, DCM; iv) Phenol, K₃PO₄, Pd(OAc)₂ (2 mol%), XPhos (3 mol%), Toluene, 100 °C, 1 h; v) TFA, 75 °C, 3 h; vi) TBAF, THF, RT, 2 h.

Scheme 8.

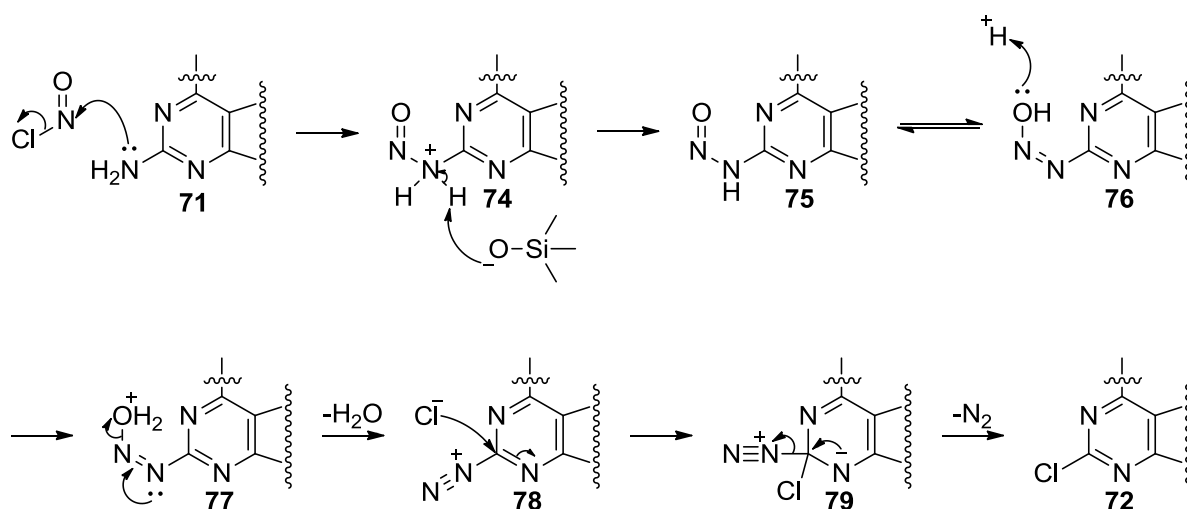
The 9-position of 2-amino-6-chloropurine **69** was protected as the PMB derivative **70** using standard conditions.²⁰² This resulted in an inseparable mixture of PMB-regioisomers of the *N*⁷- and *N*⁹-products in a 1:9 ratio, respectively, (observed by ¹H-NMR spectroscopy). This mixture was taken forward into the Sonogashira reaction,

which did not reach completion even after additional catalyst and further equivalents of TIPS-acetylene were added. It was interesting to note that only a single product **71** was isolated, suggesting that the *N*⁷-PMB regioisomer was unreactive owing to the proximity of the bulky protecting group to the 6-chloro substituent of **67**. A modified Sandmeyer reaction was then performed using benzyltriethylammonium nitrite (BTEA.NO₂), which gave 2-chloropurine **72**.²⁰³



Scheme 9 - Generation of nitrosyl chloride from benzyltriethylammonium nitrite

There is much debate over the mechanism of the copper-free Sandmeyer reaction, although the reaction is thought to be initiated through the generation of nitrosyl chloride, which in this case may be formed from the reaction of benzyltriethylammonium nitrite with TMSCl (Scheme 9).²⁰⁴



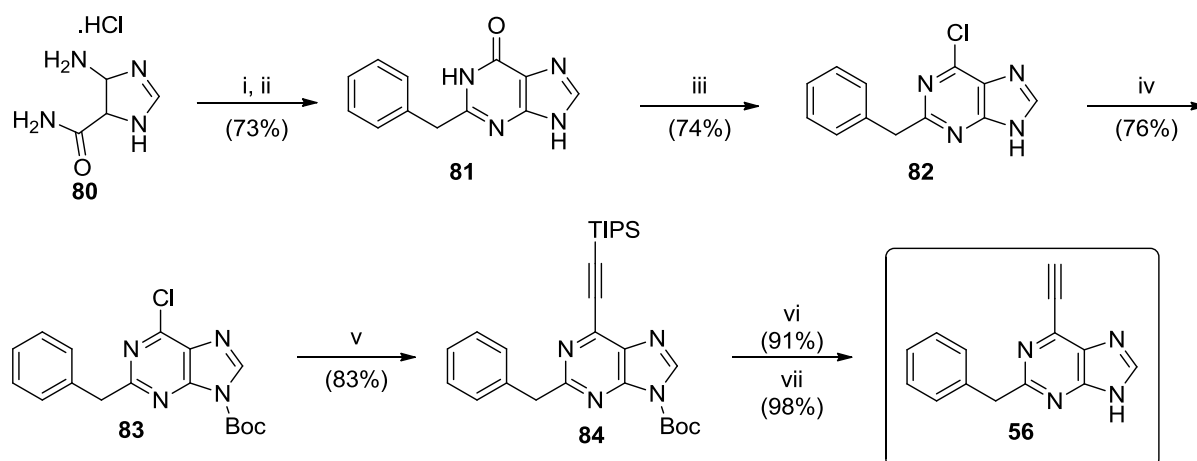
Scheme 10 - Chlorodediazotisation reaction mechanism

A diazotisation reaction occurs by reaction of 2-aminopurine **71** with nitrosyl chloride. This results in the charged species **74**, which is deprotonated by TMSO⁻ to form nitrosamine **75**, and tautomerizes to give **76**. A protonation occurs followed by loss of water to form diazonium **78**. Finally an S_NAr reaction with endogenous chloride causes loss of dinitrogen and formation of 2-chloropurine **72**.²⁰⁴ This method of chlorodediazotisation is particularly suited to substrates such as **71**, due to the mild reaction conditions, which allowed preparation of **72** in 72% yield.

A Buchwald-Hartwig etherification²⁰⁵ of **72** allowed rapid coupling of phenol in a yield of 72%, and the PMB protecting group of **73** was then removed with TFA. Finally, the TIPS protecting group of **68** was removed with TBAF to give 6-ethynylpurine **55** in near quantitative yield (99%).

5.4.4 Synthesis of 2-Benzylpurine (56)

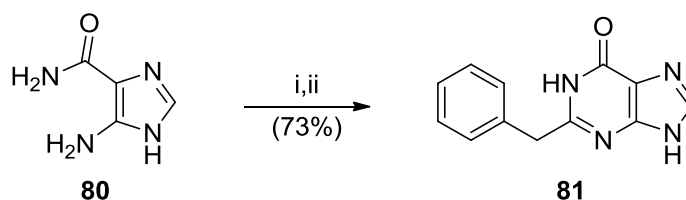
The final modification at the C² position to be investigated was the replacement of the aniline NH of **39** with a methylene group to give 2-benzylpurine **56**. It was hoped that the non-conjugated benzyl group would potentiate the reactivity of the 6-ethynyl group towards electrophiles. Additionally, removal of the aniline NH renders this compound an excellent probe molecule to further investigate the importance of the aniline H-bond interaction.



Reagents and Conditions: i) Phenylacetic acid, EDC.HCl, DMAP, Pyridine/DMF, 70 °C, 18 h; ii) NaOH (2 M), 100 °C, 1 h; iii) SOCl₂, DMF, CHCl₃, 65 °C, 2 h; iv) Boc₂O, DMAP, DCM, RT, 1 h; v) TIPS-acetylene, Pd(PPh₃)Cl₂ (5 mol%), Cul (5 mol%), Et₃N, THF, RT, 4 h; vi) TFE, 85 °C, 3 h; vii) TBAF, THF, RT, 15 min.

Scheme 11.

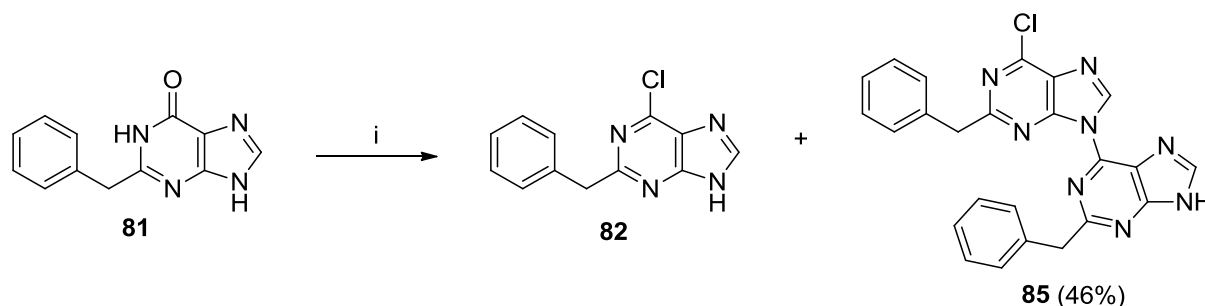
The reaction scheme was designed to allow rapid synthesis of **56** in high yield using a modification of an established synthetic route.^{196,206}



Reagents and conditions: i) Phenylacetic acid, EDC.HCl, DMAP, DMF, Pyridine, 70 °C, 18 h; ii) 2 M NaOH, 100 °C, 30 min.

Scheme 12.

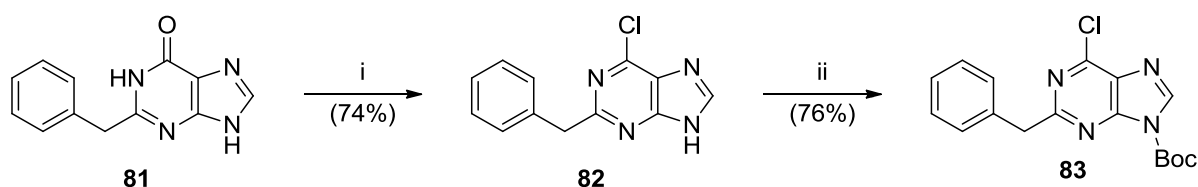
The first stage of the reaction scheme was the formation of the purine heterocycle using a modified literature procedure.²⁰⁶ EDC was chosen as the coupling agent due to the aqueous solubility of the starting material and by-product, which simplified purification.



Reagents and conditions: i) POCl₃, 110 °C, 3h.

Scheme 13.

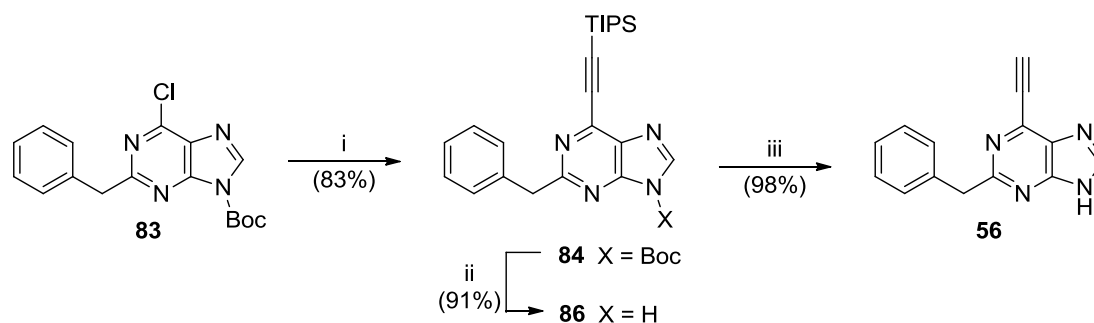
An initial attempt to chlorinate the purine 6-position of **81** was made using standard conditions employing POCl₃. A small amount of 2-benzylpurine **82** was observed by LC-MS and TLC; however, the major reaction product was the homodimeric compound **85**. After aqueous workup, none of the desired product **82** remained in the reaction mixture and the homodimeric product **85** was isolated in 46% yield. It is likely that the acidic conditions of the reaction, and subsequent aqueous work-up, catalyse formation of **85** via protonation of the purine *N*¹- or *N*³-positions.



Reagents and conditions: i) SOCl₂, DMF, CHCl₃, 65 °C, 90 min; ii) Boc₂O, DMAP, DCM, RT, 18 h.

Scheme 14.

Milder reaction conditions were achieved using SOCl₂ and DMF in chloroform.²⁰⁶ The reaction proceeds through the *in situ* generation of the Vilsmeier reagent and resulted in 80% of **82** with no observable formation of the undesired homodimeric product **85**. However, a disadvantage of using DMF in a chlorination reaction such as this is that dimethylcarbamoyl chloride (DMCC) is formed, which is a potential human carcinogen.²⁰⁷



Reagents and conditions: i) TIPS-acetylene, Pd(PPh₃)Cl₂ (5 mol%), Cul (5 mol%), Et₃N, THF, RT, 4 h; ii) TFE, 85 °C, 3 h; iii) TBAF, THF, RT, 15 min.

Scheme 15.

The purine *N*⁹-position of **83** was then protected as the Boc carbamate in 76% yield. A Sonogashira reaction using standard conditions coupled the TIPS-ethynyl group to give **84**. The Boc protecting group was removed through thermolytic cleavage using TFE as a solvent. An advantage of this deprotection method was that all unwanted by-products are volatile and were thus removed by evaporation to give 2-benzylpurine **86** in 91% yield.²⁰⁸ The final stage of this reaction scheme was removal of the TIPS protecting group using TBAF in THF to furnish **56** in almost quantitative yield.

5.5 Synthesis of Purine Isosteres

A major aim of this project was to investigate alternative heterocycles to the purine as irreversible inhibitors of Nek2. These compounds allow entry into novel patent space, and in many cases provide new vectors which can be further functionalised. These include the C⁶-position of imidazopyridine **87**, the C⁵- and C⁶-positions of pyrrolopyrimidine **88**, and C³-position of pyrazolopyrimidine **89** (indicated in red), which may lead to more potent inhibitors. It was hoped that by altering the number of nitrogen atoms in the heterocycle it would also be possible to modulate the reactivity of the electrophilic ethynyl group, to balance Nek2 reactivity with selectivity over endogenous thiol containing proteins. A further consequence of changing the heterocycle was that physicochemical properties such as Log*P* and topological polar surface area (tPSA) could be modified without significantly altering the overall shape of the ligand. This may allow discovery of a potent Nek2 inhibitor with improved

pharmacokinetics, and hence more favourable drug-like properties than the parent purine **39**.

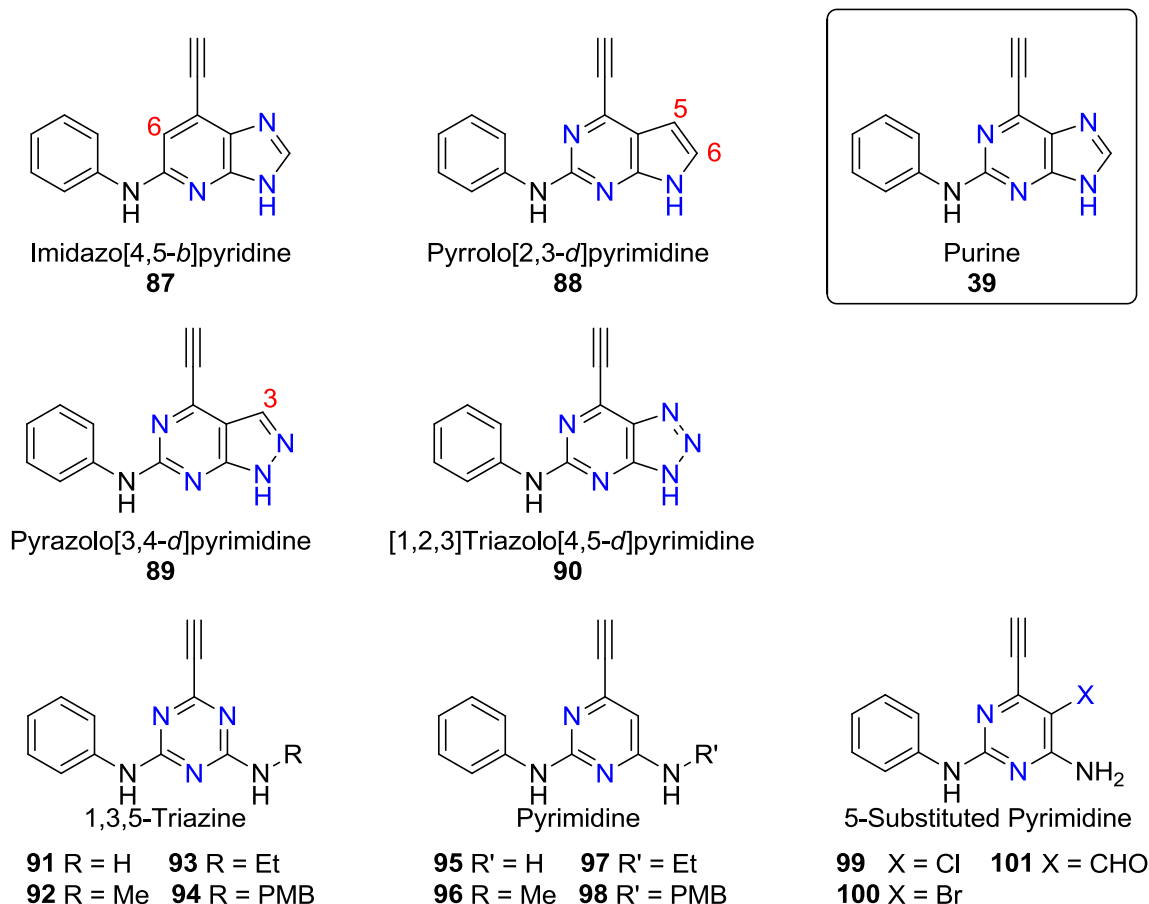
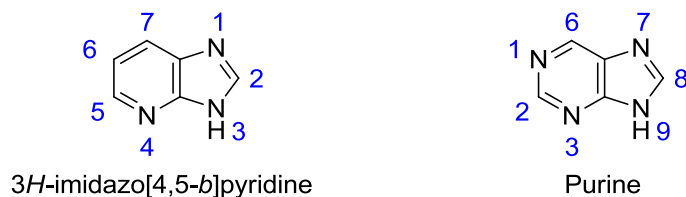


Figure 32 – Alternative heterocycles as inhibitors of Nek2.

5.5.1 Synthesis of Imidazo[4,5-*b*]pyridine (**87**)



Removal of the purine N^1 nitrogen to give the imidazopyridine core heterocycle alters the electronic character of the ring system by increasing electron density. A direct consequence of this should be attenuation in reactivity of the conjugated electrophilic ethynyl group towards nucleophiles. This can be useful in the design of electrophilic irreversible inhibitors, and allows the potential to fine-tune reactivity away from endogenous nucleophiles such as GSH whilst maintaining target activity. Additionally, by exchanging the pyrimidine ring for a pyridine the C^6 position is

available for further functionalisation. It is interesting to note the difference in calculated tPSA and cLogP between the more lipophilic imidazopyridine **87** and the parent purine **39** (Figure 33).

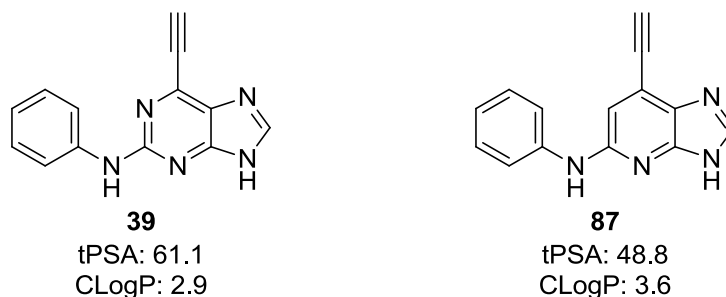
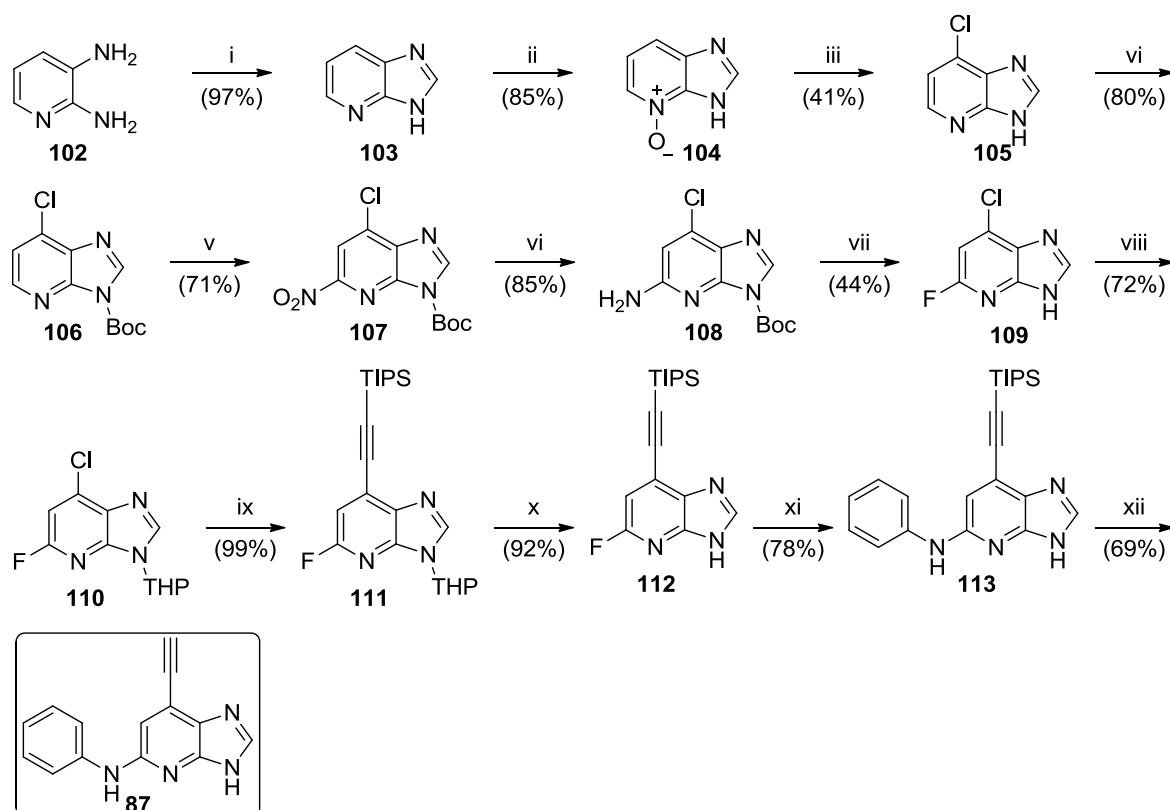


Figure 33 - Comparison of the calculated physicochemical properties of purine **39** and imidazopyridine **87**.

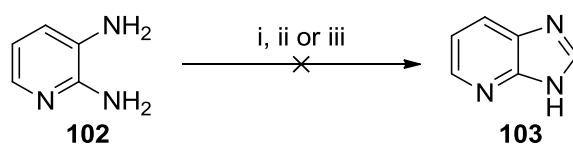
Little literature precedent exists for the synthesis of 5,7-bifunctionalised imidazopyridines, and a literature search revealed no compounds that contain an ethynyl functionality at the 7-position. The difficulties encountered during the synthesis of compound **87** perhaps help to explain why this heterocycle is less studied than the corresponding purine.



Reagents and Conditions: i) $(\text{EtO})_3\text{CH}$, TFA, TFE, MW 140 °C, 15 min; ii) *m*CPBA, CHCl_3 , RT, 18 h; iii) POCl_3 , MW 140 °C, 15 min; iv) Boc_2O , DMAP, THF, RT, 3 h; v) TBAN, TFAA, DCM, 0 °C, 1 h; vi) RaNi , H-cube (40 °C, 1 mL/min), 0.05 M solution in DCM; vii) NaNO_2 , HBF_4 , 0 °C-RT, 1 h; viii) DHP, CSA, EtOAc , 60 °C, 18 h; ix) TIPS-acetylene, Cs_2CO_3 , $\text{PdCl}_2(\text{MeCN})_2$ (10 mol%), XPhos (30 mol%), MeCN, 80 °C, 2 h; x) TFA, IPA, H_2O , 100 °C, 18 h; xi) $\text{PhNH}_2\cdot\text{HCl}$, TFE, 100 °C, 7 days; xii) TBAF, THF, RT, 5 min.

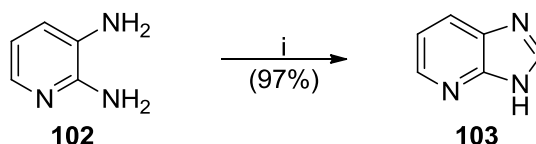
Scheme 16.

A synthetic strategy was developed for the preparation of imidazopyridine **87** based upon syntheses developed by Schelling *et al.* and Deghati *et al.*^{209,210} The first stage of this reaction scheme entails formation of the imidazo[4,5-*b*]pyridine core heterocycle. Several attempts were made using literature procedures (Scheme 17), none of which produced satisfactory results and often lead to multiple side-products and difficult isolation.²¹¹



Reagents and conditions: i) $(\text{EtO})_3\text{CH}$, 150 °C, 3 h; ii) $(\text{EtO})_3\text{CH}$, 3 Å molecular sieves, DMF, 220 °C, 1 h; iii) 2-(ethoxymethylene)malononitrile, AcOH, 120 °C, 1 h.

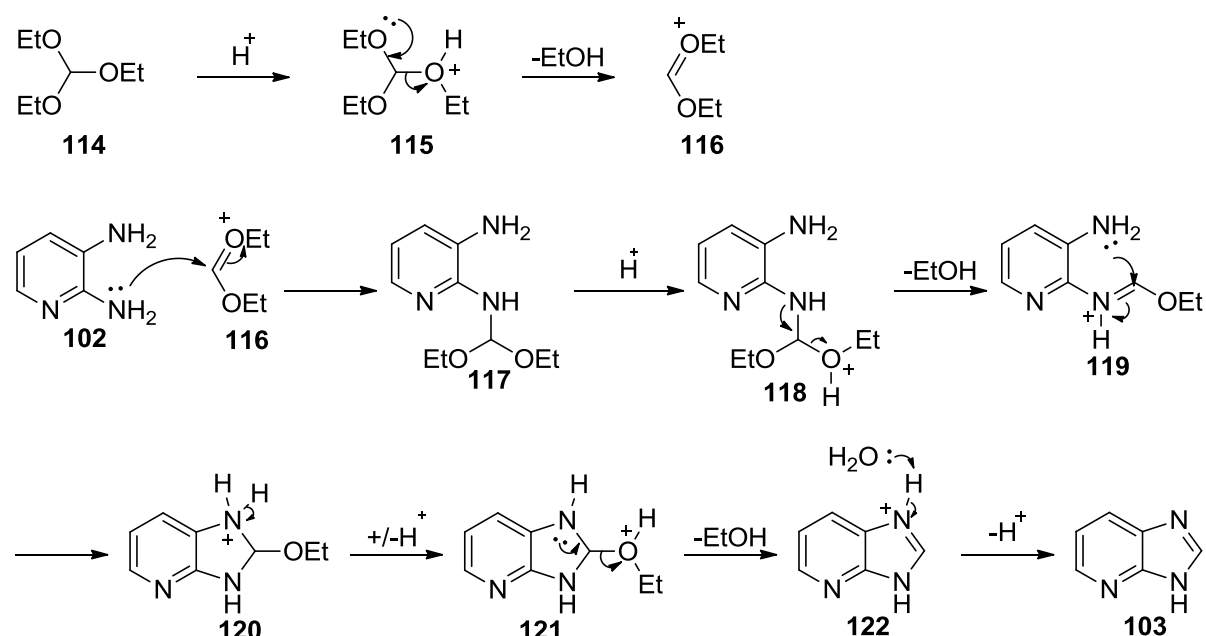
Scheme 17.



Reagents and conditions: i) $(\text{EtO})_3\text{CH}$, TFA, TFE, MW 140 °C, 15 min.

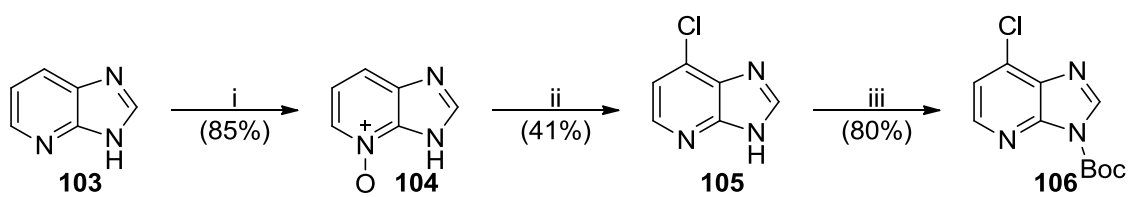
Scheme 18.

By using triethyl orthoformate **114** in TFE with a catalytic amount of TFA (5 mol%) it was possible to prepare imidazopyridine **103** in almost quantitative yield. Although this reaction proceeds well using conventional heating, it was found that with microwave assisted heating the reaction was accelerated and produced less of the imine intermediate **119** observed as a side-product (Scheme 19).



Scheme 19 – Formation of imidazo[4,5-*b*]pyridine heterocycle.

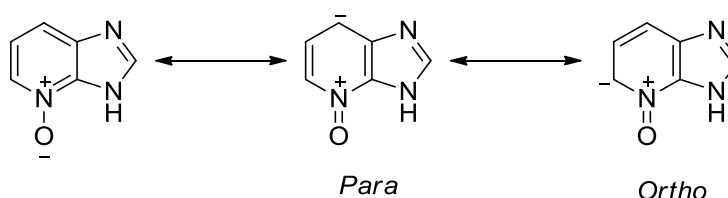
The reaction is initiated by loss of EtOH from **114** to give the reactive oxonium species **115**. One of the exocyclic amine groups from pyridine **102** then attacks *via* a nucleophilic addition to form hemiacetal **117**. The hemiacetal is protonated by TFA followed by E_2 elimination of EtOH to form iminium **119**. An intramolecular cyclisation occurs, followed by proton transfer to furnish tetrahedral intermediate **121**. Finally, an elimination of ethanol gives imidazopyridine **103**.



Reagents and conditions: i) *m*CPBA, CHCl₃, RT, 18 h; ii) POCl₃, MW 140 °C, 15 min; iii) Boc₂O, DMAP, THF, RT, 3 h.

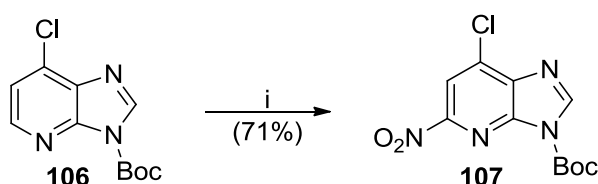
Scheme 20.

To allow functionalisation, the imidazopyridine *N*-oxide **104** was prepared by reaction of imidazopyridine **103** with *m*CPBA.²¹² The *N*-oxide **104** is a dipolar species and the electrons of the oxygen atom are delocalised into the pyridine ring system (Scheme 21). The overall result of this is activation of the *ortho*- and *para*-positions of the pyridine ring to electrophilic attack.



Scheme 21 - Imidazopyridine *N*-oxide resonance structures (adapted from Ochi).²¹³

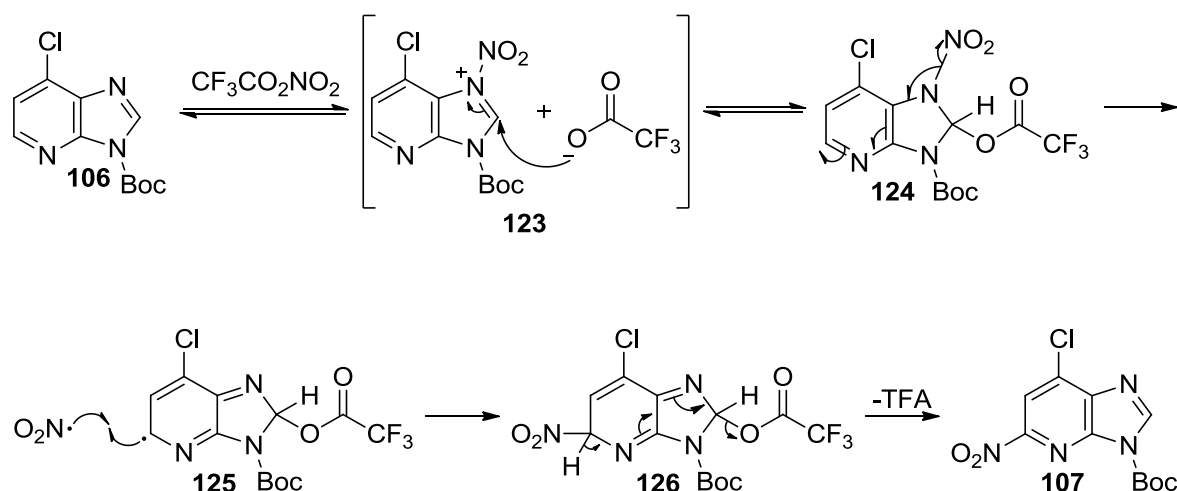
Treatment of imidazopyridine *N*-oxide **104** with POCl₃ gave a 2:1 mixture of the *para*- and *ortho*-chloroimidazopyridines, respectively, which were separated by selective precipitation resulting in imidazopyridine **105** in 41% yield.²¹¹ The imidazole nitrogen was then protected as the carbamate to furnish **106** in good yield (80%).



Reagents and conditions: i) TBAN, TFAA, DCM, 0 °C, 1 h.

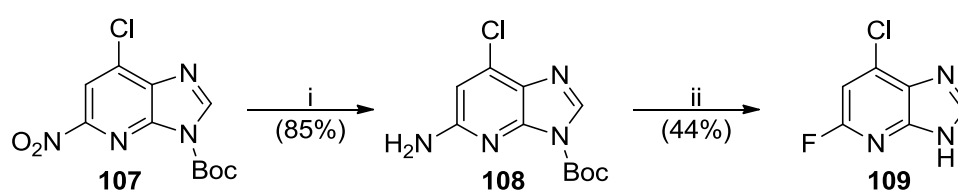
Scheme 22.

Mild regioselective nitration of **106** with tetra-*N*-butylammonium nitrate (TBAN) and trifluoroacetic anhydride (TFAA) gave nitro compound **107**.²¹⁰ Interestingly, when the *N*³ position was protected with THP rather than Boc no reaction was observed, suggesting the electron-withdrawing carbamate group may facilitate nitration.



Scheme 23 – Radical mediated nitration of imidazopyridine **106**.²¹⁴

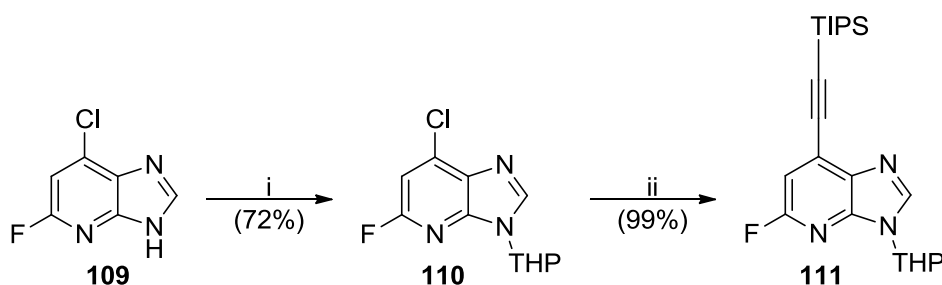
It was originally speculated that the reaction was initiated by the homolytic cleavage of trifluoroacetyl nitrate formed during the TBAN/TFAA reaction, resulting in the generation of nitro and a trifluoroacetyl radicals.²¹⁰ However, more recent studies revealed that trifluoroacetyl nitrate reacts directly with **106** forming the 7-nitramine intermediate **124** (Scheme 23).²¹⁴ **124** undergoes homolytic cleavage, resulting in formation of $\cdot\text{NO}_2$ and the aryl radical **125**, which react through a radical termination to form tetrahedral intermediate **126**. Interestingly, the nitration of **106** is selective for the 2-position due to stabilisation of the aryl radical by the *para*-chloro substituent.^{210,214} The final step of this reaction mechanism is liberation of TFA from the unstable intermediate **126** to give the desired product **107**.



Reagents and conditions: i) RaNi , H-cube (40 °C, 1 mL/min), 0.05 M solution in DCM; ii) NaNO_2 , $\text{HBF}_4(\text{aq})$, 0 °C – RT, 1 h.

Scheme 24.

The nitro group of **107** was reduced to the respective amine using an H-cube[®] continuous flow hydrogenation unit. 7-Chloro-5-fluoroimidazopyridine **108** was prepared in a reasonable overall yield of 44% through a one-pot tandem carbamate deprotection and fluorodediazotisation sequence using Balz-Schiemann conditions.

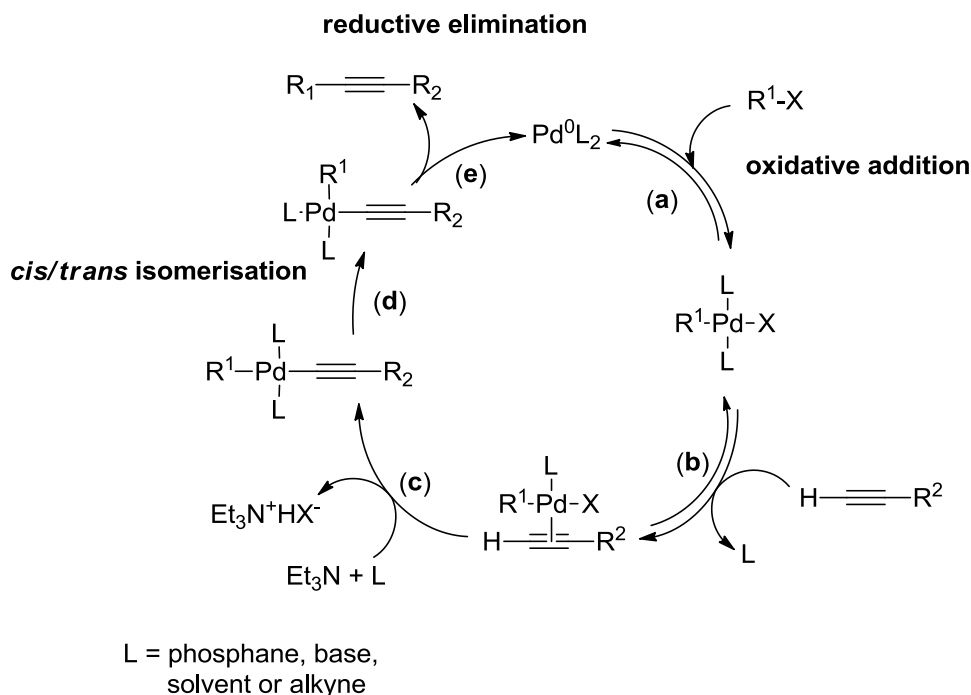


Reagents and conditions: i) DHP, CSA, EtOAc, 60 °C, 18 h; ii) TIPS-acetylene, Cs₂CO₃, PdCl₂(MeCN)₂ (10 mol%), XPhos (30 mol%), MeCN, 80 °C, 2 h.

Scheme 25.

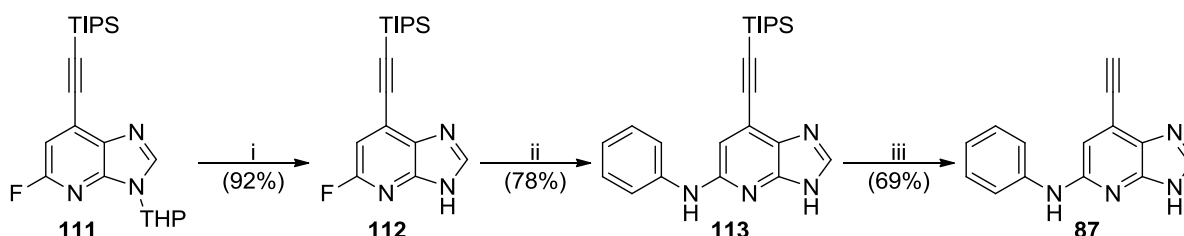
The imidazopyridine NH of **109** was protected as the THP-derivative **110**. A Sonogashira reaction of **110** was attempted unsuccessfully using standard Pd(PPh₃)Cl₂ / CuI conditions. It is possible that failure of this reaction was due to the electron rich nature of the imidazopyridine ring system of **110**, which prevents palladium insertion. It has been suggested that the rate determining step of the Sonogashira reaction is initial oxidative addition of the Pd⁰ into the Ar-halogen bond.²¹⁵ An end-on ligation of the halogen to the palladium is believed to precede this and could be viewed as electron donation. Therefore electron-rich substrates are likely to form a more stable Pd complex, requiring greater activation energy to proceed to the subsequent oxidative addition stage of the cycle. The reaction was heated, but this led to decomposition of the starting material (**110**).

Alternative conditions were sought, and a copper-free method developed by Buchwald *et al.* for coupling terminal acetylenes and electron rich heteroarenes proved a suitable alternative, allowing the synthesis of **111** in near quantitative yield.²¹⁵ A disadvantage of the copper based Sonogashira reaction is the potential for Glaser oxidative dimerization of terminal acetylenes.²¹⁶ Replacement of CuI with a suitable ligand eliminates this side reaction.



Scheme 26 - Copper free Sonogashira coupling of terminal acetylenes with aryl halides.²¹⁷

The mechanism for the copper-free Sonogashira reaction of terminal acetylenes compounds with aryl halides (Scheme 26) is likely to proceed *via* a mechanism similar to the traditional Sonogashira reaction. The reaction is initiated by oxidative addition of Pd^0 into the aryl halide (a) followed by a reversible coordination of the alkyne π -system to the palladium complex (b) resulting in an alkyne- Pd^{II} complex. The now acidic, acetylene proton is removed by a base, for example Et_3N , allowing ligand coordination (c). A *cis/trans* isomerisation occurs (d) followed by reductive elimination (e), which reforms the active Pd^0 species and releases the newly formed arylethynyl product.

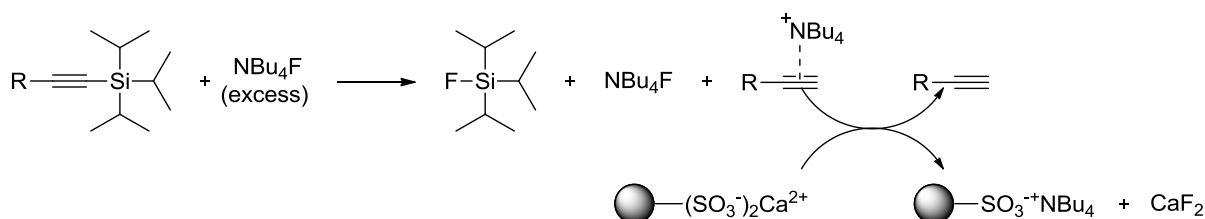


Reagents and conditions: i) TFA, IPA, H_2O , 100 °C, 18 h; ii) $\text{PhNH}_2\cdot\text{HCl}$, TFE, 100 °C, 7 days; iii) TBAF, THF, RT, 5 min.

Scheme 27.

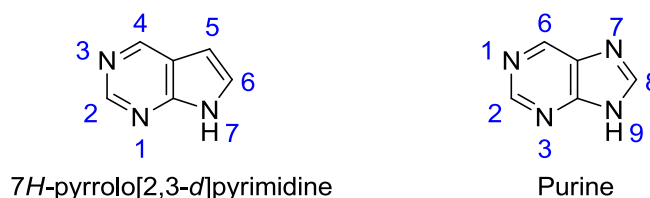
Removal of the THP protecting group from **111** was achieved in 92% yield.²¹⁸ Displacement of the 5-fluoro group of **112** with aniline using standard TFA/TFE conditions was unsuccessful, and gave no observable product formation. However, reaction of **112** with aniline hydrochloride in TFE was successful, albeit slow, resulting in **113** in 78% yield.

The final stage of this reaction scheme was the TBAF-mediated deprotection of **113** to give imidazopyridine **87**. The reaction was successful; however, after purification ¹H-NMR spectroscopy confirmed TBAF contamination of the product. Residual TBAF was removed using a calcium sulfonate scavenger resin, which had been developed previously to address this problem.²¹⁹ It is likely that residual TBAF from the reaction mixture coordinates to either the ethynyl group or a heterocyclic nitrogen atom of **87**. Addition of the scavenger resin removes TBAF from the reaction mixture by forming calcium fluoride and polymeric tetrabutylammonium sulfonate (Scheme 28), which are removed by filtration.^{219,220}



Scheme 28 - Removal of TBAF contamination with calcium sulfonate resin.²²⁰

5.5.2 Synthesis of 7H-Pyrrolo[2,3-d]pyrimidines (**88**) and (**231**)



The second deazapurine compound to be investigated was the pyrrolopyrimidine **88**. In this compound, the role of the purine *N*⁷ was investigated. Compared with the imidazopyridine **87**, removal of this nitrogen should lead to attenuation of ethynyl reactivity due to increased electron density. However, it was unclear if this nitrogen was essential for Nek2-inhibitory activity. Calculated tPSA and cLog*P* values (Figure

34) are almost identical to those obtained for imidazopyridine **87**, showing the increased lipophilicity of pyrrolopyrimidine **88** compared with the parent purine **39**.

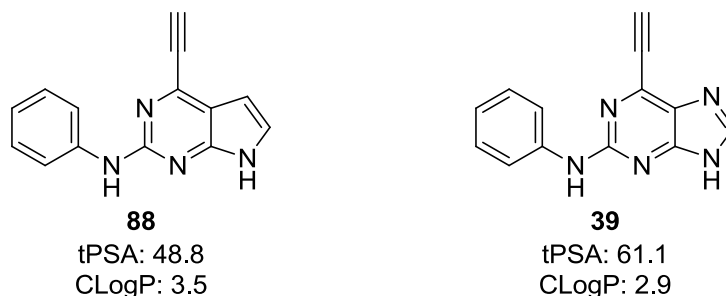
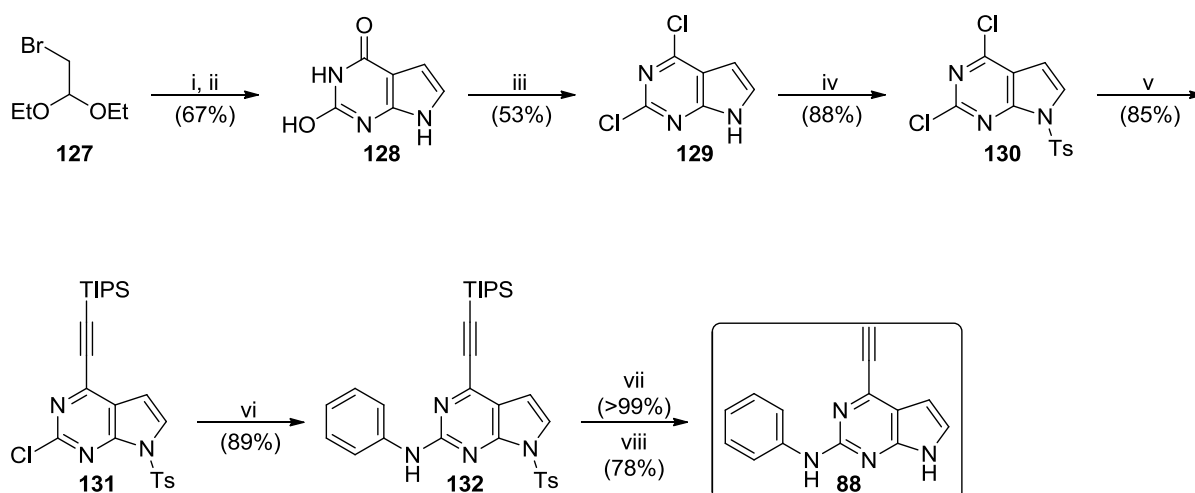


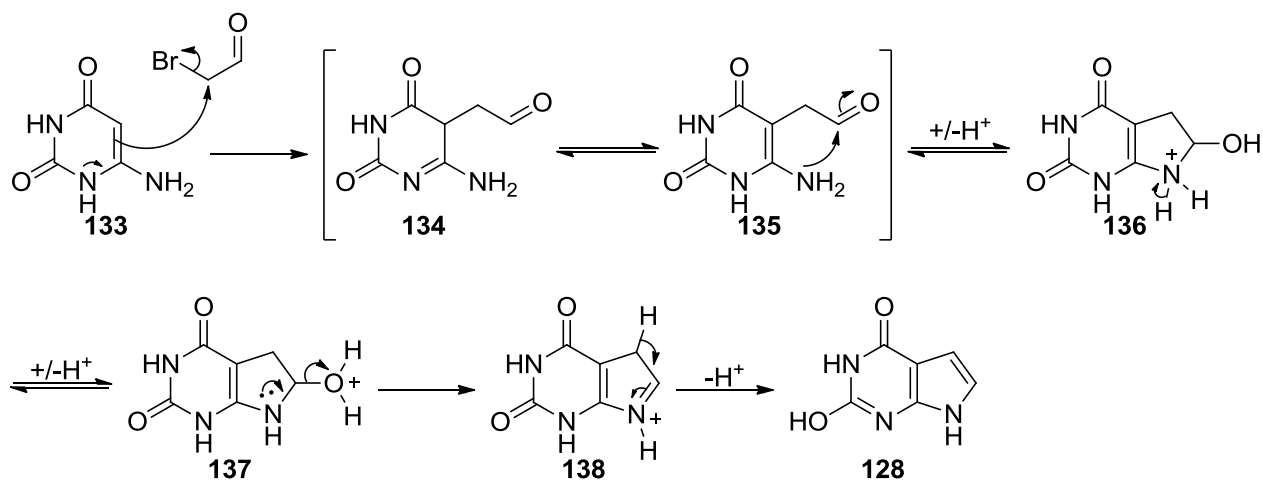
Figure 34 - Comparison of the calculated physicochemical properties of purine **39** and pyrrolopyrimidine **88**.



Reagents and Conditions: i) $\text{HCl}_{(\text{aq})}$, 90 °C, 30 min; ii) **133**, NaOAc, 100 °C, 5 h; iii) PhPOCl_2 , 220 °C, 5 h; iv) TsCl, DMAP, Et_3N , DCM, RT, 1 h; v) TIPS-acetylene, $\text{Pd}(\text{PPh}_3)_2\text{Cl}_2$ (5 mol%), CuI (5 mol%), Et_3N , THF, RT, 48 h; vi) PhNH_2 , TMSCl, *n*-BuOH, 116 °C, 72 h; vii) Cs_2CO_3 , MeOH, THF, 0 °C, 18 h; viii) TBAF, THF, RT, 15 min.

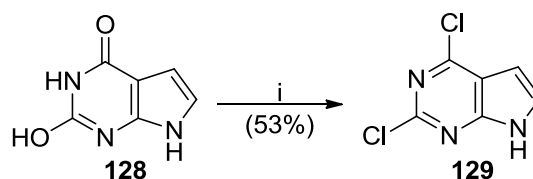
Scheme 29.

Bromoacetaldehyde was prepared *in situ* through hydrolysis of bromoacetaldehyde diethylacetal **127** using aqueous HCl. 2-Aminouracil **133** was then added to give pyrrolopyrimidine **128** in 67% yield. A proposed reaction mechanism is shown in Scheme 30. In the first stage of this reaction an electrophilic aromatic substitution of **133** with bromoacetaldehyde occurs, followed by intramolecular cyclisation and loss of water gave imine **139**, which tautomerizes to the more stable 2-hydroxypyrrolopyrimidine **128**.²²¹



Scheme 30 – Formation of 7H-pyrrolo[2,3-d]pyrimidine (**128**)

An alternative mechanism for this reaction could be for the exocyclic NH_2 of **133** to attack the CHO of bromoacetaldehyde first, followed by an intramolecular $\text{S}_{\text{N}}2$ reaction. It would be interesting to monitor this reaction *in situ* using ^1H -NMR spectroscopy, to gain a detailed understanding of the reaction mechanism through the identification of key intermediates.

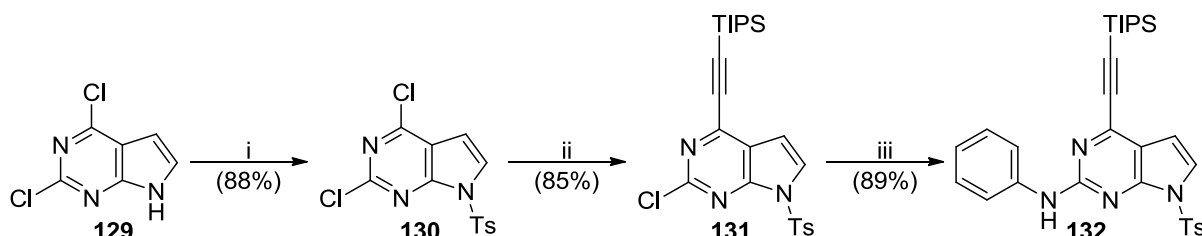


Reagents and Conditions: i) PhPOCl_2 , $220\text{ }^\circ\text{C}$, 5 h.

Scheme 31.

The next stage of the reaction scheme involved chlorination of pyrrolopyrimidine **128**. This reaction was attempted using phosphorus oxychloride (POCl_3) as a chlorinating agent, but there were multiple side-products and low product formation was observed. Refluxing in POCl_3 is one of the most common methods for performing chlorodehydroxylation reactions. This method is useful but limited by the somewhat low boiling point of POCl_3 ($107\text{ }^\circ\text{C}$) which can be insufficient for some reactions. A solution to this problem is to heat the reaction mixture in a sealed vessel, or more recently through microwave irradiation. Both methods allow higher temperatures, but the hazards and impracticalities involved in the scale-up of such techniques limited their usefulness for this particular reaction. An alternative to POCl_3 is phosphorus pentachloride (PCl_5), which has a much higher boiling point ($180\text{ }^\circ\text{C}$) but this reagent

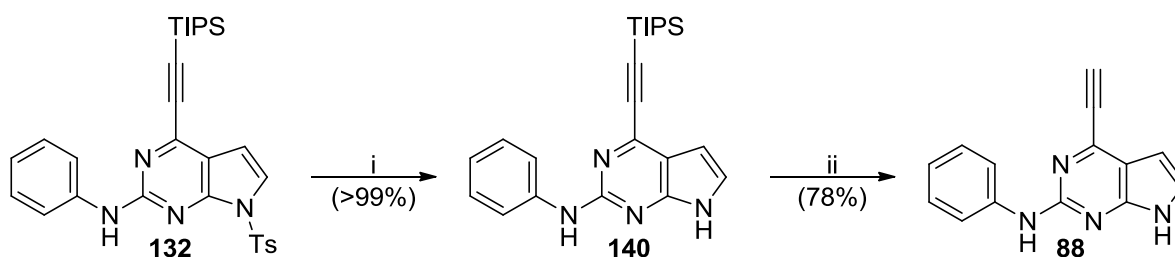
can also act as an oxidative chlorinating agent through displacement of aromatic protons. Using phenylphosphonic dichloride (PhPOCl_2) solves both problems as it is a non-oxidative chlorinating agent that boils at $258\text{ }^\circ\text{C}$.²²² In this reaction PhPOCl_2 was used successfully to synthesise the dichloropyrrolopyrimidine **129** from **128** in 53% yield.



Reagents and conditions: i) TsCl , DMAP, Et_3N , DCM, RT, 1 h; ii) TIPS-acetylene, $\text{Pd}(\text{PPh}_3)_2\text{Cl}_2$ (5 mol%), CuI (5 mol%), Et_3N , THF, RT, 48 h; iii) PhNH_2 , TMSCl , $n\text{-BuOH}$, $116\text{ }^\circ\text{C}$, 72 h.

Scheme 32.

THP protection of the pyrrolopyrimidine 7-NH was unsuccessful; however, tosyl protection proved a suitable alternative to give **130** in 88% yield. The next stage of the reaction scheme was the regioselective Sonogashira coupling of TIPS acetylene to **130**. Initial concerns over selectivity between coupling at the desired 4-position and undesired 2-position of **130** were unfounded. It is likely that this selectivity is due to increased electrophilicity of the 4-position making palladium insertion more energetically favourable.²²³ Using standard Sonogashira cross-coupling conditions, **131** was formed in 85% yield with no observable side-products. Aniline was coupled to **131** through an acid catalysed $\text{S}_{\text{N}}\text{Ar}$ reaction. A literature procedure using trimethylsilyl chloride (TMSCl) in butanol, to generate anhydrous HCl , worked well, resulting in **132** in 89% yield, with no observable cleavage of the tosyl or TIPS protecting groups.



Reagents and conditions: i) Cs_2CO_3 , MeOH, THF, $0\text{ }^\circ\text{C}$, 18 h; ii) TBAF, THF, RT, 15 min.

Scheme 33.

The final stages of the reaction scheme entailed removal of the tosyl and TIPS protecting groups from **132** and **140**, respectively. It was important to remove the

tosyl protecting group first to prevent side reactions with the ethynyl group. Standard tosyl deprotection methods require harsh conditions, e.g. NaOH in alcohol-based solvents at high temperatures, nucleophiles such as Gilman's reagent (PhMe_2SiLi), reducing agents including Red-Al or dissolving metal reductions with lithium or sodium in ammonia or methanol.²²⁴ The presence of the TIPS ethynyl moiety of **132** makes these methods unsuitable in this case. A mild selective deprotection method was achieved using Cs_2CO_3 in a mixture of MeOH and THF. Methoxide generated *in situ* attacks the sulfonyl group resulting in cleavage of the tosyl protecting group. The by-product of this reaction methyl *p*-toluenesulfonate (MeOTs), reacts further to form tosic acid and dimethyl ether.²²⁴ Using literature conditions (RT, 15 min) the reaction proceeded rapidly, but in modest yield (39%), due to multiple side-products owing to TIPS deprotection. By cooling the mixture to 0 °C the reaction progressed more slowly (18 h vs. 15 min) but no side-products were observed, and an almost quantitative yield of **140** was achieved. Finally the TIPS protecting group was removed with TBAF to give **88** in 78% yield. There was concern that the TIPS-ethynyl group of **88** may have been introduced at the 2-position during the Sonogashira reaction (Scheme 32) rather than at the required 4-position. However, the X-ray crystal structure of **88** (Figure 35) confirmed that the proposed structure of **88** was correct. It is interesting to note the H-bond interactions between molecules of **88** via the pyrrolopyrimidine N¹ and N⁷ positions.

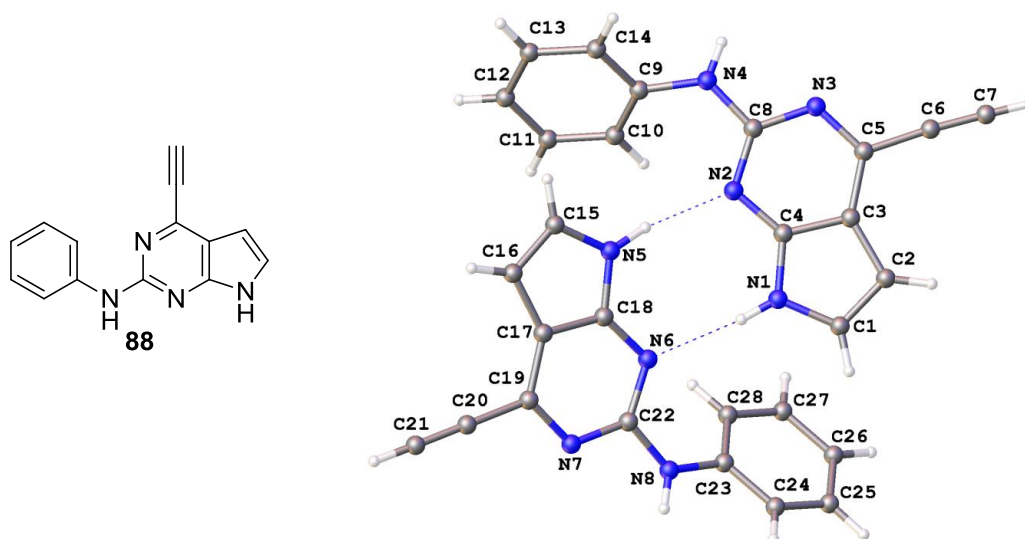
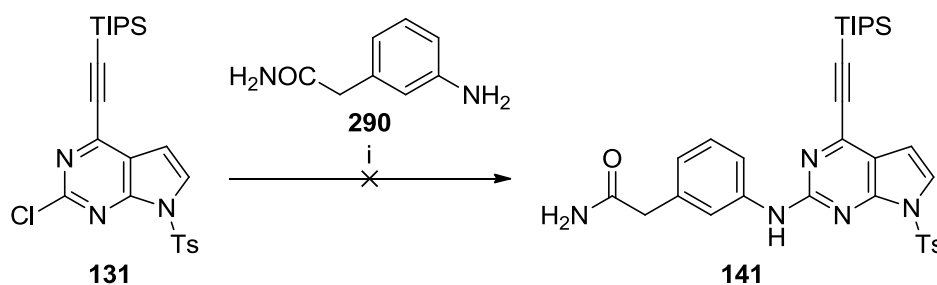


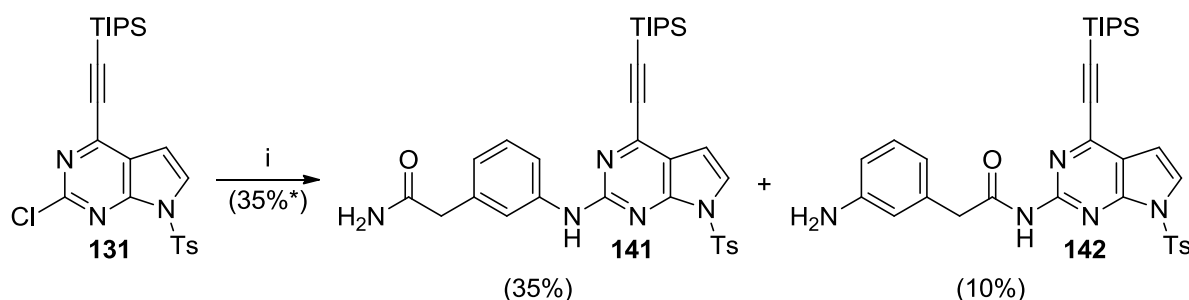
Figure 35 - X-ray crystal structure of pyrrolopyrimidine **88**.



Reagents and conditions: i) **290**, TMSCl, *n*-BuOH, 116 °C, 72 h.

Scheme 34.

Synthesis of the functionalised derivative **141** proved problematic. It was found that the S_NAr coupling conditions that worked well in the synthesis of **132**, resulted in no observable product formation even with prolonged reaction times and microwave assisted heating (140 °C, 6 h). TFA/TFE coupling conditions were attempted but also failed.

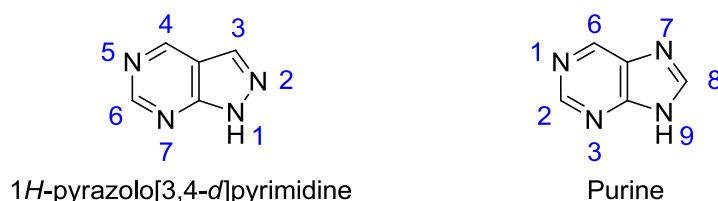


* = Isolated yield of **141**

Reagents and conditions: i) **290**, Pd₂(dba)₃ (4 mol%), XPhos (4 mol%), K₂CO₃, MeCN, 80 °C, 2 h.

Scheme 35.

Buchwald-Hartwig coupling was employed successfully to give a separable mixture of the desired product **141** (35%) and the undesired acetamide coupled product **142** (10%). A literature review of coupling conditions revealed that the choice of ligand and Pd source are critical in selectivity during Buchwald-Hartwig type aminations.²²⁵ With further optimisation and careful choice of ligand/catalyst, it is likely that selectivity and yield could have been improved substantially. However, as there was sufficient material to complete the reaction scheme, this was not investigated further.

5.5.3 Synthesis of 1*H*-Pyrazolo[3,4-*d*]pyrimidines (**89**) and (**154**)

The 1*H*-pyrazolo[3,4-*d*]pyrimidine heterocycle has found application as an important scaffold in many fields of drug discovery, including oncology, antibacterial research and in compounds used to promote histamine release.²²⁶ Pyrazolo[3,4-*d*]pyrimidines can in many cases mimic the purine scaffold whilst subtly changing the overall electronic character of the heterocycle.²²⁷ The C³-position of the pyrazolopyrimidine also offers a synthetic 'handle' which may be functionalised providing access to areas of chemical space previously unavailable. In addition, replacement of the imidazole of the purine by a pyrazole may facilitate alternative H-bond interactions. Interestingly, calculated tPSA and cLog*P* values (Figure 36) are very similar to those obtained for the parent purine **39** suggesting similar physicochemical properties. It was unclear if any difference in reactivity would be observed between the pyrazolopyrimidine and purine ethynyl groups, and whether this would impact upon Nek2-inhibitory activity.

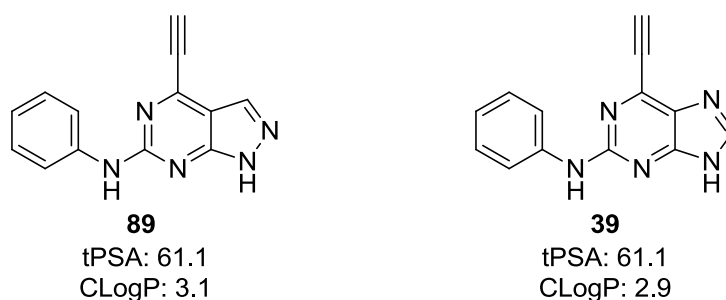
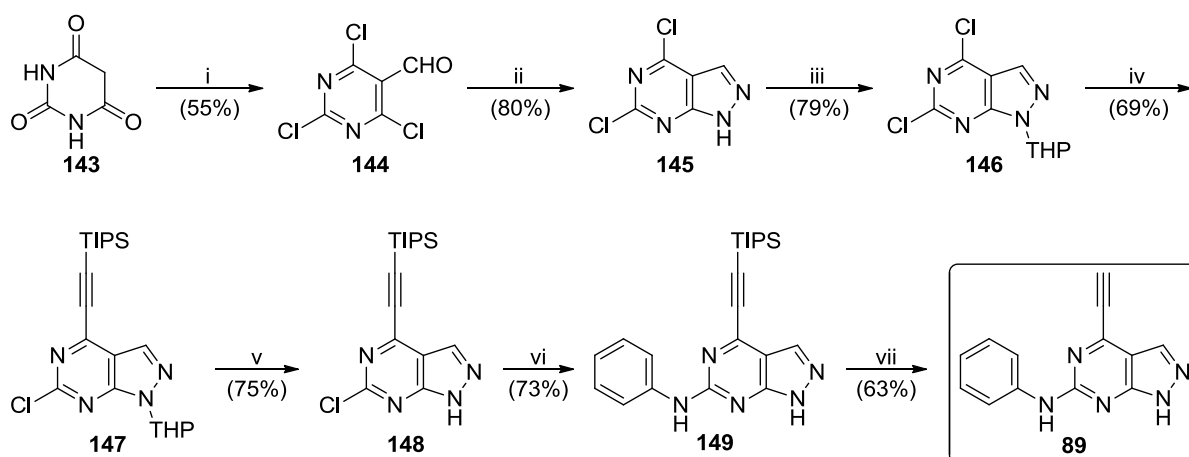


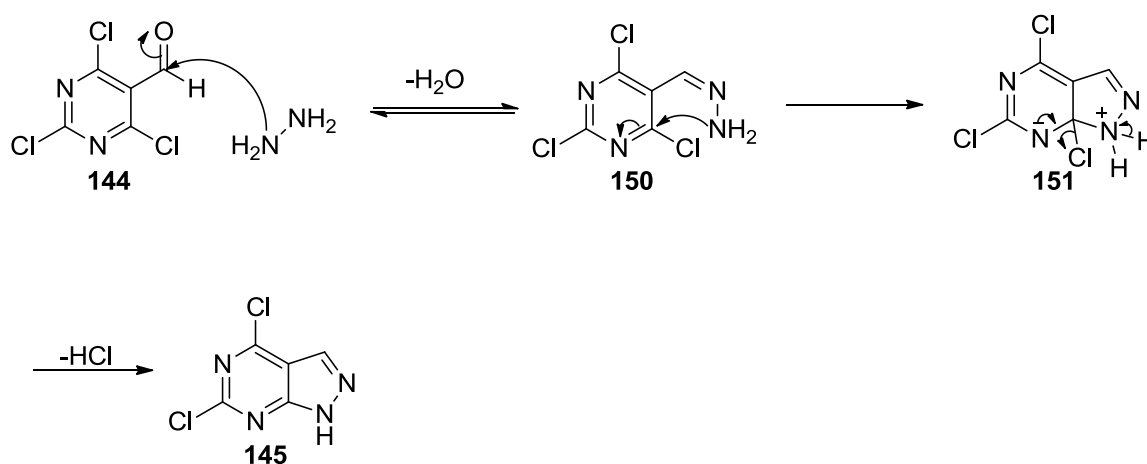
Figure 36 - Comparison of the calculated physicochemical properties of purine **39** and pyrazolopyrimidine **89**.



Reagents and Conditions: i) POCl_3 , DMF, 110°C , 4 h; ii) $\text{N}_2\text{H}_4\cdot\text{H}_2\text{O}$, MeOH, -30°C , 6 h; iii) DHP, CSA, EtOAc, 55°C , 16 h; iv) TIPS-acetylene, $\text{Pd}(\text{PPh}_3)_2\text{Cl}_2$ (5 mol%), CuI (5 mol%), Et_3N , THF, RT, 18 h; v) TFA, TFE, H_2O , 100°C , 6 h; vi) PhNH_2 , TFA, TFE, 100°C , 18 h; vii) TBAF, THF, RT, 15 min.

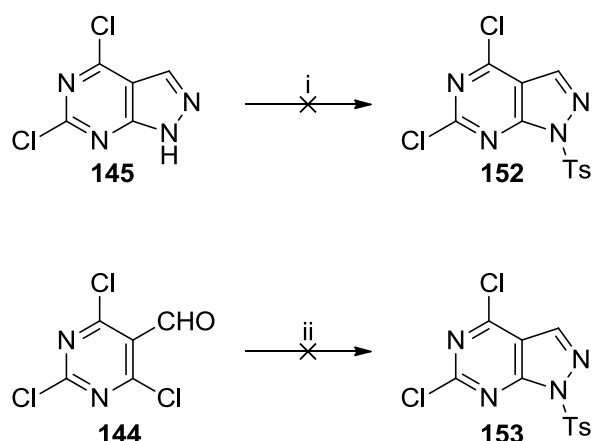
Scheme 36.

Barbituric acid **143** was reacted with freshly prepared Vilsmeier reagent, generated *in situ* reaction of POCl_3 and DMF, resulting in formylation of the C^5 position. Further heating gave the desired 2,4,6-trichloropyrimidine-5-carbaldehyde **144** (55%).²²⁸



Scheme 37 – Formation of the pyrazolopyrimidine heterocycle.

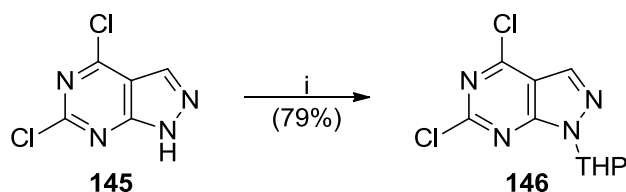
Cyclisation of **144** with hydrazine hydrate in MeOH was used to generate pyrazolopyrimidine **145**.²²⁸ It is unclear whether the hydrazine first attacks the C^5 -formyl group to form the hydrazone intermediate **150** (as shown in Scheme 37), or if an $\text{S}_{\text{N}}\text{Ar}$ reaction precedes this due to the reactive 4/6 chlorine atoms of the pyrimidine ring system. However, as both synthetic routes inevitably lead to pyrazolopyrimidin **145**, this was not further investigated.



Reagents and conditions: i) TsCl, Et_3N , DMAP, DCM; ii) TsNHNH₂, MeOH, -30 °C, 6 h.

Scheme 38.

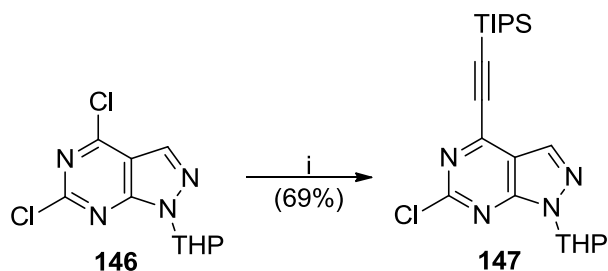
Initial attempts to protect the pyrazole ring NH of **145** as the tosyl derivative **152** were unsuccessful due to decomposition of both starting materials and product. An alternative approach using tosylhydrazide (TsNHNH₂) in place of hydrazine hydrate at the cyclisation step was also attempted with pyrimidine **144**, in an effort to introduce the tosyl protecting group. However, this reaction also proved unsuccessful.



Reagents and conditions: i) DHP, CSA, EtOAc, 55 °C, 16 h.

Scheme 39.

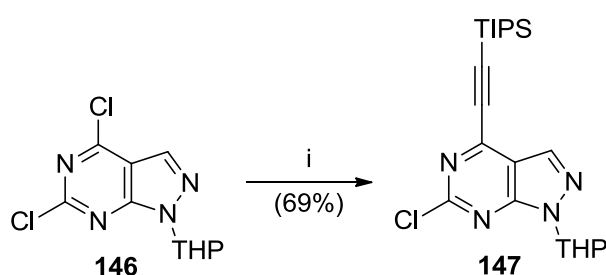
THP protection of pyrazolopyrimidine **145** using standard conditions proved a suitable alternative to tosyl protection, allowing the preparation of **146** in 79% yield.



Reagents and conditions: i) TIPS-acetylene, Pd(PPh₃)₂Cl₂ (5 mol%), CuI (5 mol%), Cs₂CO₃, DMF, MW 45 °C, 10 min.

Scheme 40.

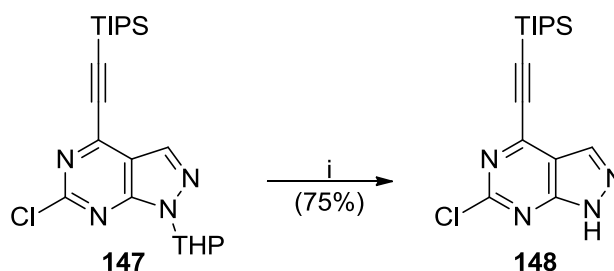
A literature review for Sonogashira cross-coupling conditions of pyrazolopyrimidines with terminal acetylenes, identified a mild and selective microwave-assisted method to couple the TIPS ethynyl group at the desired C⁴-position of **146**. The reaction was performed in DMF, which efficiently absorbs microwave radiation, and Cs₂CO₃ was used as base. An advantage of microwave over conventional heating is that localised superheating of the catalyst can occur, often leading to increased reaction rates and catalytic turnover. These conditions worked well for small scale reactions (ca. 50 mg) resulting in a 69% yield of pyrazolopyrimidine **147**. However, larger scale reactions (>100 mg) were found to be capricious and low yielding (<30%).



Reagents and conditions: i) TIPS-acetylene, Pd(PPh₃)₂Cl₂ (5 mol%), CuI (5 mol%), Et₃N, THF, RT, 18 h.

Scheme 41.

Fortunately, the Sonogashira conditions previously developed for the purine system were a suitable alternative, allowing the synthesis of **147** in 69% yield. 1D NOE ¹H-NMR spectroscopic analysis of **147** was attempted to determine whether the correct regioisomer had been obtained, as it was hoped that an interaction between the C³-pyrazole proton and a methyl proton of the TIPS group of **147** would be detectable. A very faint signal was observed, but it was unclear whether this was significant. Attempts were made to grow crystals of **147** for X-ray crystallography using a variety of conditions, none of which were successful. It was decided to persevere with the synthesis of pyrazolopyrimidine **89** in the hope that it would be possible to grow crystals of a subsequent synthetic product.



Reagents and conditions: i) TFA, TFE, H₂O, 100 °C, 6 h.

Scheme 42.

Removal of the THP protecting group from **133** was unsuccessful when 2-propanol (IPA) was used as a solvent, as the reaction would only proceed to ca. 50% completion (observed by LC-MS analysis). When IPA was replaced by TFE, the reaction proceeded to completion due possibly to the higher acidity of TFE. In the remaining steps the aniline side chain was coupled using standard TFA/TFE conditions, followed by removal of the TIPS group. In each case yields and reaction times were comparable with the parent purine.

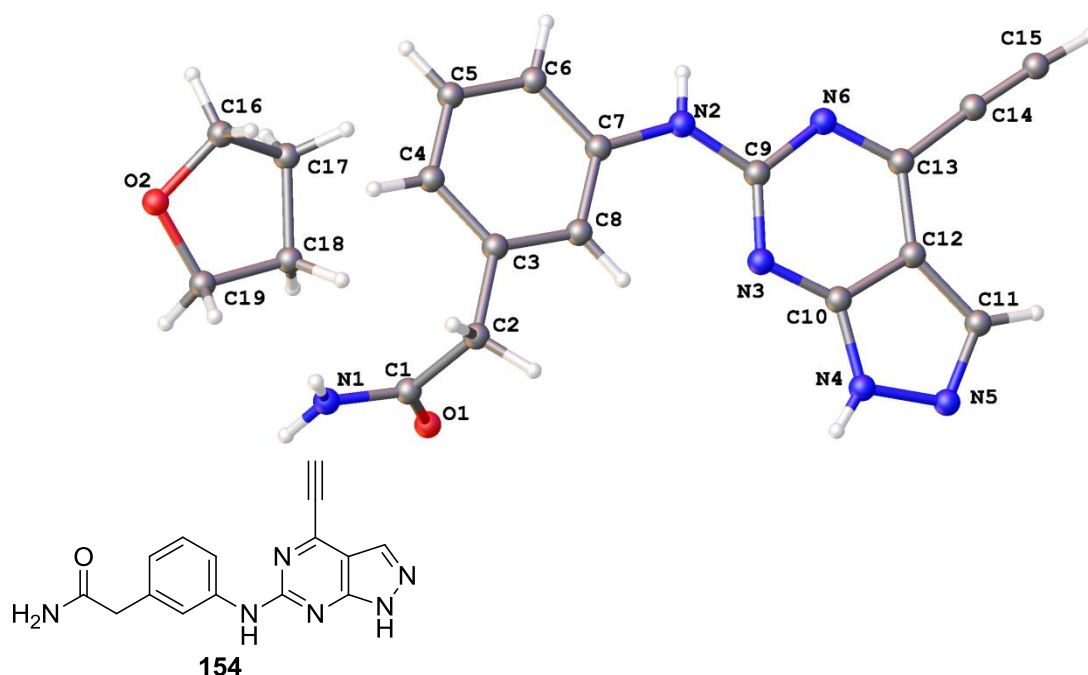
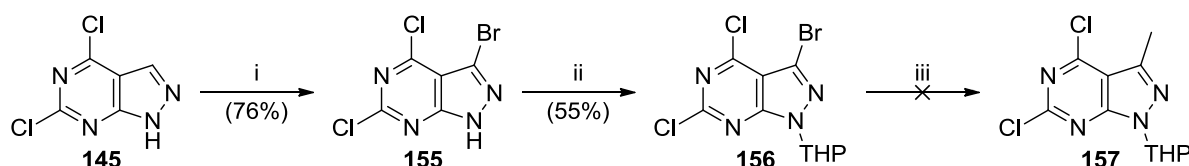


Figure 37 - X-ray crystal structure of pyrazolopyrimidine 154.

A small-molecule *X-ray* crystal structure was successfully solved for pyrazolopyrimidine **154** following crystallisation from THF (Figure 37). This confirmed that the product was the correct regioisomer.

5.5.4 Synthesis of 3-Methyl-1*H*-pyrazolo[3,4-*d*]pyrimidine (**165**)

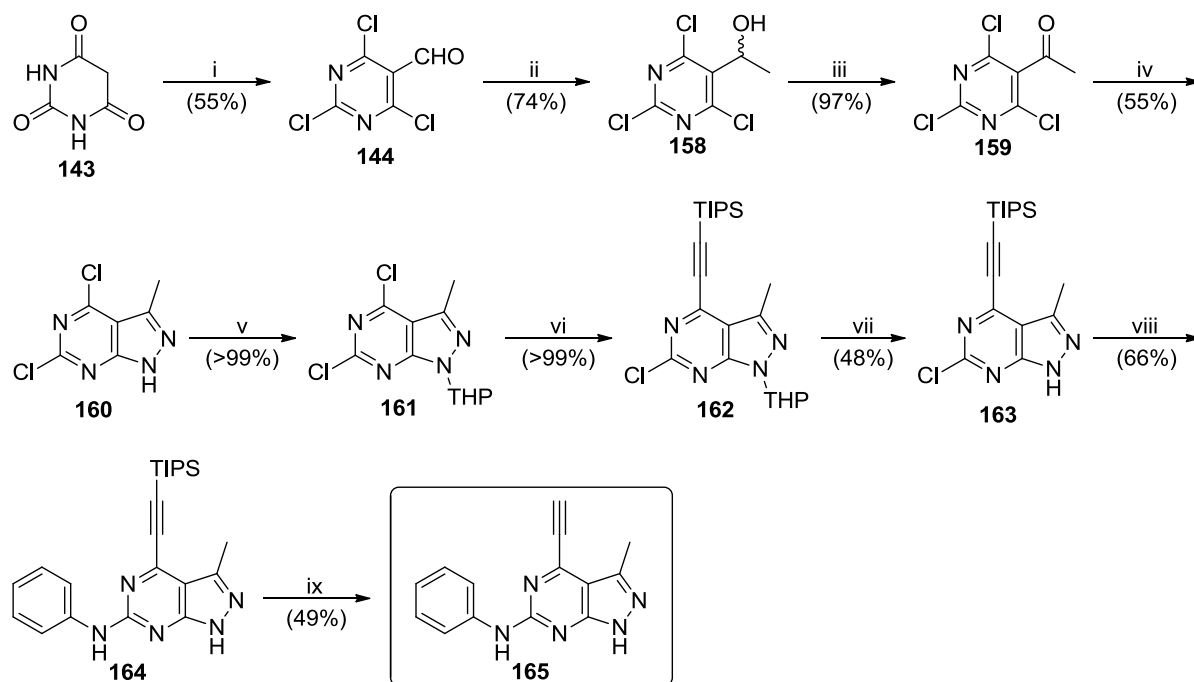
As the pyrazolopyrimidine derivative **89** was found to have Nek2 inhibitory activity comparable with the purine **39** (IC₅₀ values of 430 nM vs. 150 nM respectively), it was decided to investigate modification of the C³ position of **89**. The initial objective was to synthesize the C³ methyl derivative **165** as the simplest modification, to determine whether further elaboration at this position would be tolerated.



Reagents and conditions: i) NBS, MeCN, 100 °C, 15 min; ii) DHP, CSA, EtOAc, 65 °C, 18 h; iii) Trimethylboroxine, Pd(PPh₃)₃ (10 mol%), Cs₂CO₃, Toluene, MW 140 °C, 1 h.

Scheme 43.

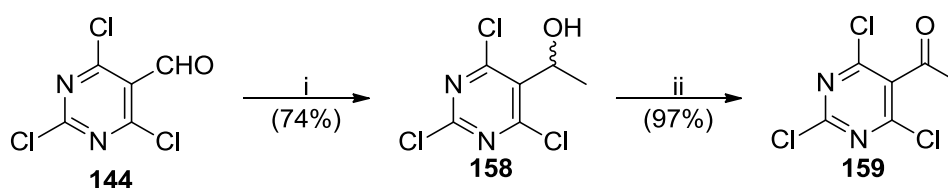
The 3-bromo derivative **155** was prepared by electrophilic aromatic substitution of **145** with NBS. This compound **155** was unstable, and was used directly in the THP protection step to give the stable THP-amine **156** (55%). It was hoped that palladium insertion would favour the 3-bromo position of **156** over the chloro substituents, thus allowing selective alkylation. However, attempts at Suzuki couplings using trimethylboroxine and a variety of bases and palladium catalysts were unsuccessful, leading to no observable product (**157**) formation.



Reagents and Conditions: i) POCl_3 , DMF, $110\text{ }^\circ\text{C}$, 4 h; ii) MeMgBr , THF, $0\text{ }^\circ\text{C}$ – RT, 1 h; iii) DMP, DCM, RT, 2 h; iv) $\text{N}_2\text{H}_4\cdot\text{H}_2\text{O}$, MeOH, $-15\text{ }^\circ\text{C}$, 6 h; v) DHP, CSA, EtOAc; vi) TIPS-acetylene, $\text{Pd}(\text{PPh}_3)_2\text{Cl}_2$ (5 mol%), CuI (5 mol%), Et_3N , THF, RT, 18 h; vii) TFA, TFE, H_2O , $100\text{ }^\circ\text{C}$, 18 h; viii) PhNH_2 , TFA, TFE, $85\text{ }^\circ\text{C}$, 18 h; ix) TBAF, THF, RT, 15 min.

Scheme 44.

As such, an alternative synthetic route to **165** was devised by incorporating the methyl group into the pyrazolopyrimidine scaffold early in the synthesis using Grignard chemistry (Scheme 44). An advantage of this approach was that all of the subsequent chemistry had been previously optimised during the synthesis of pyrazolopyrimidine **89**.

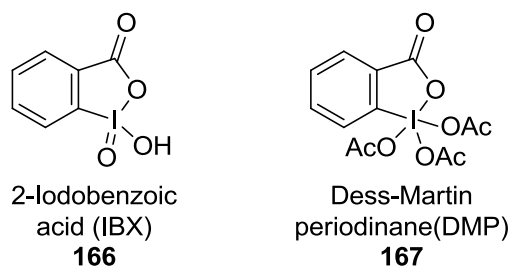


Reagents and conditions: i) MeMgBr , THF, $0\text{ }^\circ\text{C}$ – RT, 1 h; ii) DMP, DCM, RT, 2 h.

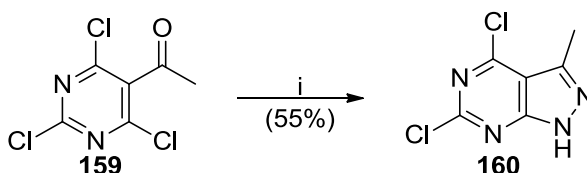
Scheme 45.

Reaction of 2,4,6-trichloropyrimidine-5-carbaldehyde **144** with methyllmagnesium bromide (MeMgBr) resulted in a rapid and clean conversion into the respective alcohol **158** in 74% yield. The wide range of commercially available Grignard reagents renders this method an attractive approach to introduce a variety of alkyl

groups at the 3-position. The newly formed alcohol **158** required oxidation to the ketone **159** prior to cyclisation with hydrazine. Many methods are available to perform this reaction, including Swern oxidation or the use of chromium based oxidising agents, but due to concerns as to the stability of **158**, a much milder approach was needed. To date, hypervalent iodine reagents have proven useful for the oxidation of primary and secondary alcohols to their respective aldehydes and ketones. These reagents facilitate mild chemoselective oxidation, without the need for highly toxic heavy metal oxidising agents such as the chromium (VI) based oxidising agents (e.g. pyridinium chlorochromate (PCC)).²²⁹ The most commonly used hypervalent iodine reagents are 2-iodoxybenzoic acid (IBX, **166**) and Dess-Martin periodinane (DMP, **167**). IBX has been reported as explosive which may limit its use for large scale reactions.^{229,230} However, Dess and Martin have suggested that residual potassium bromate (KBrO₃), or another impurity from the synthesis of this compound, may be responsible for its potentially explosive nature and that pure IBX should be relatively stable.^{229,230}



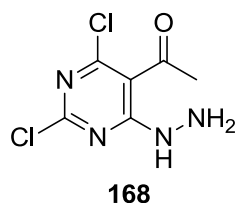
A major disadvantage of **166** is that it has very poor solubility in most common organic solvents, which can reduce rates of reactions.²³⁰ By contrast **167**, the triacetoxo derivative of **166**, has far greater solubility increasing its usefulness as an oxidising agent. In this reaction, **167** was used successfully to convert alcohol **158** into ketone **159** in excellent yield (97%).



Reagents and conditions: i) N₂H₄·H₂O, MeOH, -15 °C, 6 h

Scheme 46.

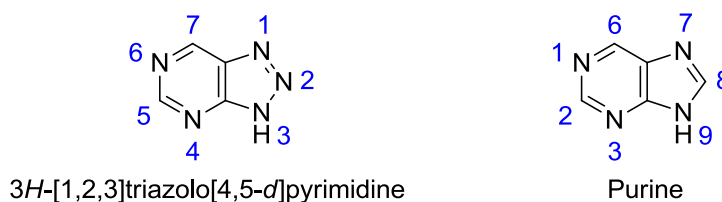
Cyclisation of **159** with hydrazine to form pyrazolopyrimidine **160** was initially attempted using the conditions established previously ($-30\text{ }^{\circ}\text{C}$, 18 h); however, it was found that the reaction could not be driven to completion. It was interesting to note that the arylhydrazine intermediate **168** was observed (by LC-MS), suggesting that the 4-chloro position is more reactive than the 5-acetyl moiety of **159**.



The reaction mixture was warmed to $-15\text{ }^{\circ}\text{C}$ resulting in consumption of the starting material **159** and intermediate **168**. The yield was lower than for the reaction of the formyl derivative **144** with hydrazine (55% vs. 80%), which was attributed to formation of a number of uncharacterised side-products arising as a result of the increased temperature and decreased reactivity of the carbonyl group of **168**.

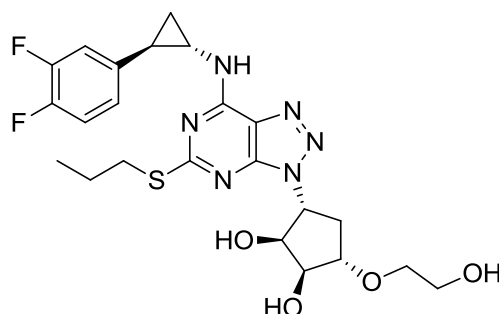
The subsequent reaction steps proceeded in yields similar to those for the synthesis of pyrazolopyrimidine **89**, to give the target compound **165**.

5.5.5 3*H*-[1,2,3]Triazolo[4,5-*d*]pyrimidines (**90**) and (**232**)



In the 3*H*-[1,2,3]triazolo[4,5-*d*]pyrimidine scaffold, C⁸ of the purine imidazole has been replaced by nitrogen to form an azapurine. It was thought that this would elicit a significant electron-withdrawing effect, thus potentiating the reactivity of the 7-ethynyl group. Whilst this could lead to enhancement of Nek2-inhibitory activity, there was also a possibility that this might lead to significant off-target activity. Additionally, there were concerns as to the stability of this heterocycle, although examples of clinical candidates based upon this heterocycle are reported, e.g. **169** (Ticagrelor), a triazolopyrimidine-based inhibitor of ADP-induced platelet aggregation developed by

AstraZeneca. This compound was recently approved for the treatment of acute coronary syndromes.²³¹



Ticagrelor (*Brilinta*)
169

A comparison of the tPSA and cLogP values of **90** with **39** (Figure 38) suggested a reduction in lipophilicity and an increase in polar surface area compared with the parent purine.

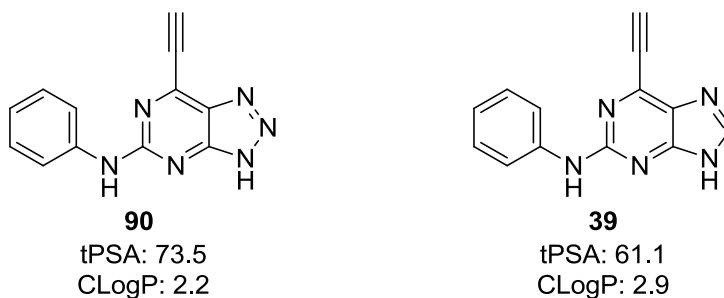
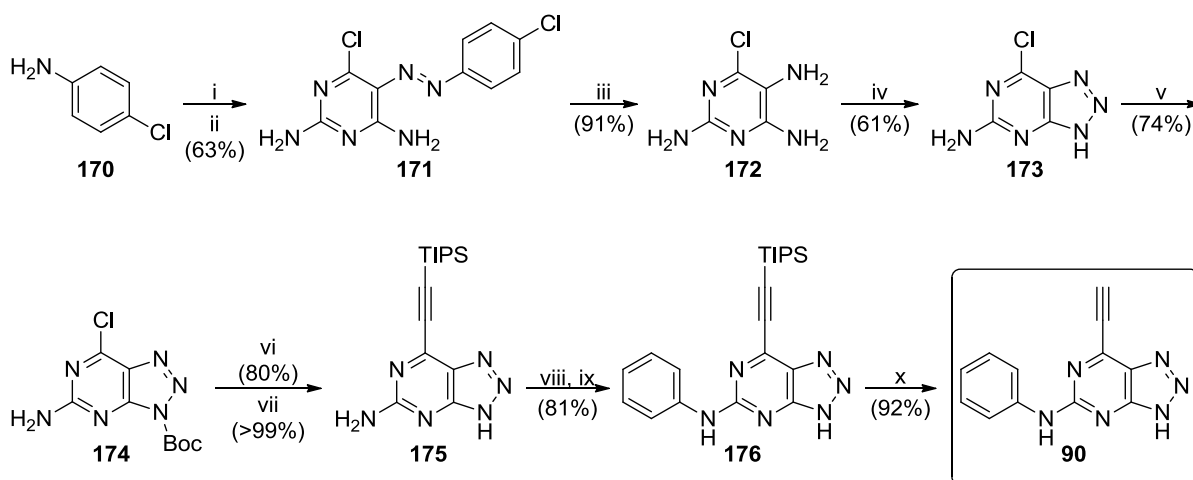


Figure 38 - Comparison of the calculated physicochemical properties of parent purine **39** and triazolopyrimidine **90**.

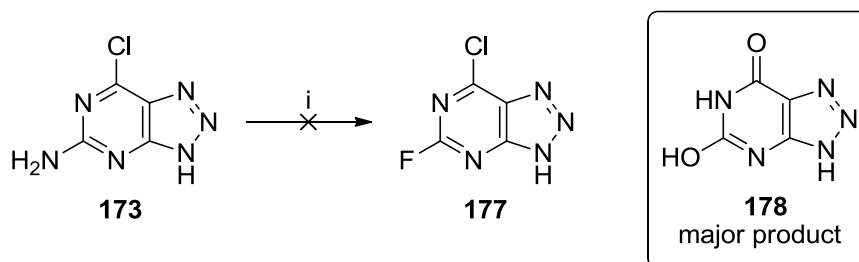
The synthesis of triazolopyrimidine **90** was particularly challenging owing to the inherent instability of this heterocycle. This required the development of mild conditions for each step of the reaction sequence.



Reagents and Conditions: i) NaNO_2 , HCl(aq) , H_2O , $0\text{ }^\circ\text{C}$, 30 min; ii) **177**, AcOH , NaOAc , H_2O , $0\text{ }^\circ\text{C}$ – RT, 18 h; iii) Zn , AcOH , THF , RT, 15 min; iv) NaNO_2 , AcOH , H_2O , $0\text{ }^\circ\text{C}$ – RT, 1 h; v) Boc_2O , DMAP , THF ; vi) TIPS-acetylene , $\text{Pd(PPh}_3)_2\text{Cl}_2$ (5 mol%), CuI (5 mol%), DIPEA , THF , RT, 18 h; vii) TFE , $75\text{ }^\circ\text{C}$, 1 h; viii) $\text{Benzyltriethylammonium nitrite}$, TMSCl , DCM , $0\text{ }^\circ\text{C}$ – RT, 1 h; ix) PhNH_2 , DMSO , $70\text{ }^\circ\text{C}$, 96 h; x) TBAF , THF , $0\text{ }^\circ\text{C}$, 1 h.

Scheme 47.

A solution of the diazonium salt of *p*-chloroaniline was prepared by reaction of **170** with NaNO_2 in aqueous HCl at $0\text{ }^\circ\text{C}$, and added to 4-chloro-2,6-diaminopyrimidine (**177**) to give the azo compound **171**, which was isolated and reduced to triaminopyrimidine **172**.^{232,233} Pyrimidine **172** was found to be unstable and prolonged storage resulted in formation of a dark purple side-product, possibly through *N*-oxidation. This derivative was therefore stored at reduced temperature under nitrogen or used immediately in the reaction with NaNO_2 to form triazolopyrimidine **173**.

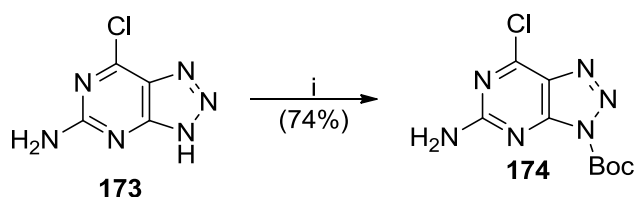


Reagents and conditions: i) NaNO_2 , $\text{HBF}_4(\text{aq})$, $0\text{ }^\circ\text{C}$ – RT.

Scheme 48.

Introduction of the 2-fluoro group in **173** using Balz-Schiemann conditions (Scheme 48) proved unsuccessful, resulting in very little formation of **177**, and the production of numerous side-products of which the major product was

dihydroxytriazolopyrimidine **178**. It is likely that fluoro compound **177** was unstable to the harsh reaction conditions and so an alternative synthetic route was developed.



Reagents and conditions: i) Boc_2O , DMAP, THF, RT, 18 h.

Scheme 49.

The TIPS-ethynyl group was introduced to **174** prior to addition of the aniline to reduce stability issues. THP protection of the triazole ring of **173** was attempted, but led to a mixture of triazole regioisomers making purification difficult. Regioselective Boc protection of **173** gave **174** in 74% yield. The X-ray crystal structure of **174** confirmed the Boc group was added regioselectively to **173** at the 3-position (Figure 39). Triazolopyrimidine **174** was unstable in the presence of solvents such as MeOH, and decomposition was found to occur when stored in air at RT. It was therefore important that **174** was stored under nitrogen at reduced temperature prior to use.

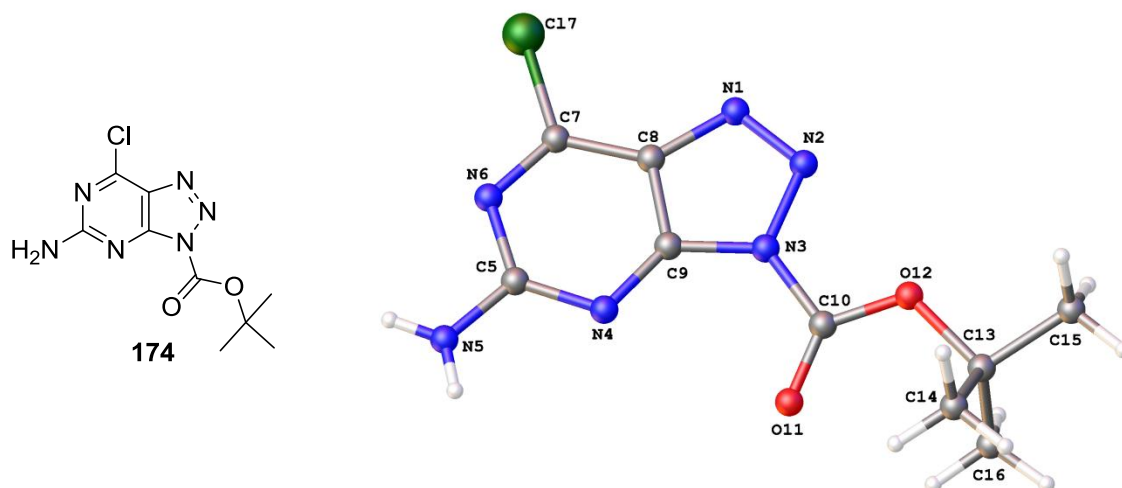
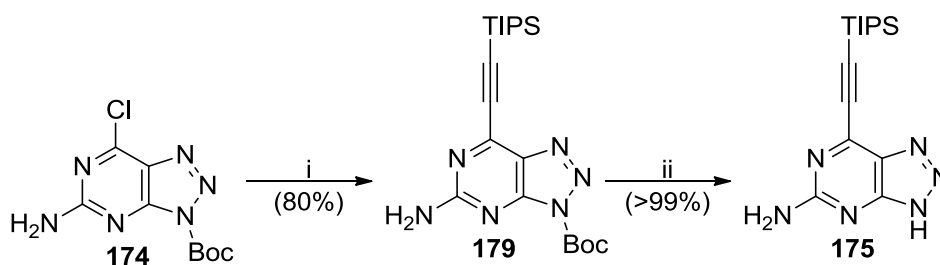


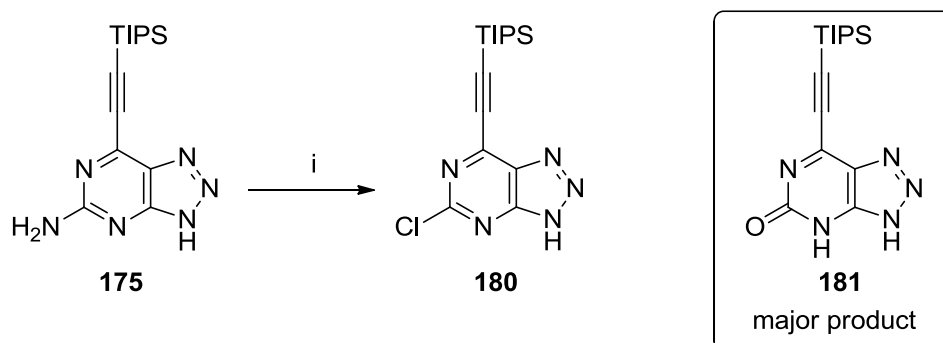
Figure 39 - X-ray crystal structure of **174** confirms regioselective protection of the triazolopyrimidine N^3 as the Boc carbamate.



Reagents and conditions: i) TIPS-acetylene, $\text{Pd}(\text{PPh}_3)_2\text{Cl}_2$ (5 mol%), CuI (5 mol%), DIPEA , THF , RT , 18 h; ii) TFE , 75°C , 1 h

Scheme 50.

The TIPS-ethynyl group was introduced at the 7-position of **174** under Sonogashira conditions. The reaction proceeded optimally when DIPEA was used as a base, as this minimised side-product formation, and the Boc protecting group was removed quantitatively from **179** by refluxing in TFE . A variety of copper-mediated Sandmeyer type reaction conditions were attempted to replace the amino group of **175** by chloro-, bromo- or iodo-substituents, but all were unsuccessful owing to decomposition of **175**.

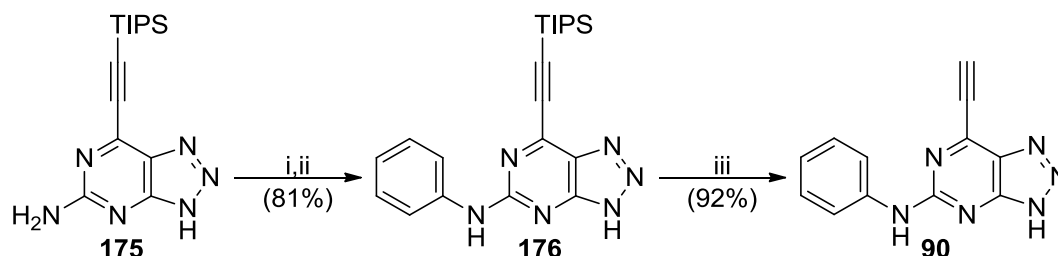


Reagents and conditions: i) SOCl_2 , LiCl , isoamyl nitrite, DMA , 0°C – RT , 1 h.

Scheme 51.

A copper-free modified Sandmeyer chlorination reaction was attempted on amine **175** using SOCl_2 , LiCl and isoamyl nitrite in DMA to form the 5-chloro compound **180** (Scheme 51).²³⁴ It is believed that this reaction is initiated through *in situ* formation of nitrosyl chloride followed by chlorodediazotisation analogous to the benzyltriethylammonium nitrite-mediated chlorodediazotisation strategy described previously (Scheme 9). Although this reaction was successful, it was found to be unreliable and low yielding (16%). Hydroxy derivative **181** was also observed as a major side-product due to adventitious water. Purification of **180** was difficult as the

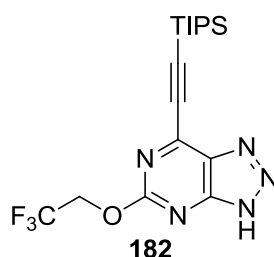
compound was found to be unstable to liquid chromatography conditions. The multitude of side-products made it impractical to use the crude product **180** directly for the next reaction step.



Reagents and conditions: i) Benzyltriethylammonium nitrite, TMSCl, DCM, 0 °C – RT, 1 h; ii) PhNH₂, DMSO, 70 °C, 96 h; iii) TBAF, THF, 0 °C, 1 h.

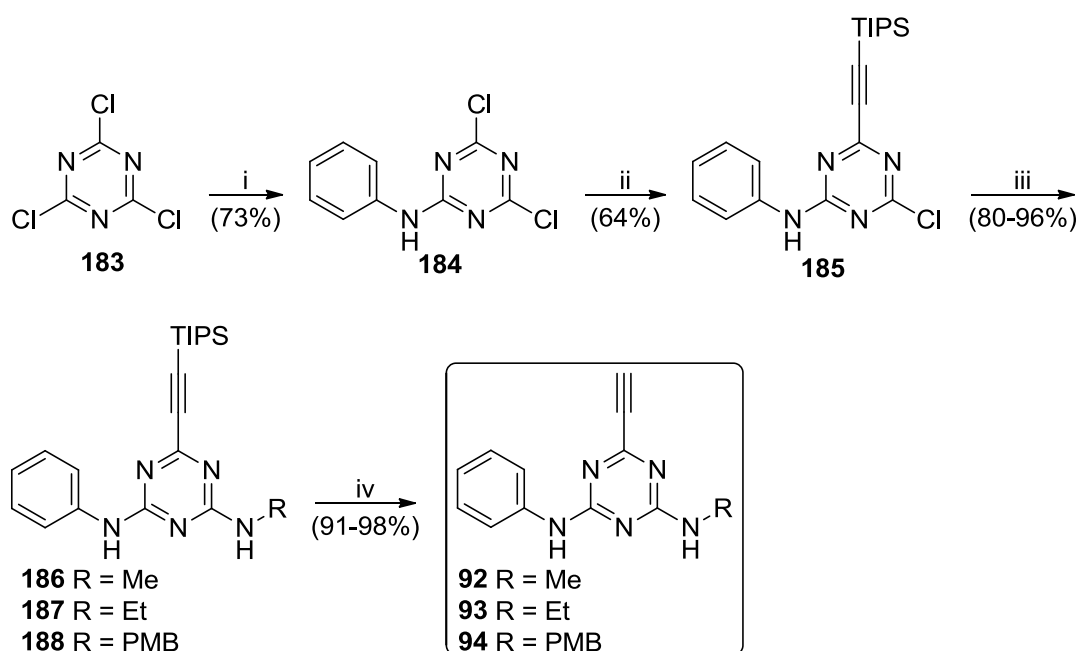
Scheme 52.

The benzyltriethylammonium nitrite-mediated method (Scheme 10) of chlorination was found to be a suitable alternative for the preparation of **180**, proceeding smoothly and with no observable side-products.²⁰⁰ An aqueous work up removed residual benzyltriethylammonium nitrite and hydrolysed TMSCl to TMSOH, which was removed by evaporation. Silica based MPLC was attempted, but again it was found that compound **180** was unstable, and so the crude product **180** was used directly for the reaction with aniline without further purification. Initial attempts at this reaction using TFE as a solvent, with the addition of TFA, resulted in rapid formation of **176** (30 min), together with several by-products including the TFE ether derivative **182**. Reaction at lower temperature and in the absence of TFA was investigated, but no improvements were observed. This problem was resolved by performing the reaction in a 1 M solution of aniline in DMSO. Finally, the TIPS protecting group was removed from **176** using TBAF in THF. The reaction was performed at reduced temperature (0 °C) due to concerns over the stability of **90**.



5.5.6 Synthesis of 1,3,5-Triazine-based Nek2 inhibitors (**91-94**)

A rapid, concise and high yielding synthesis of trifunctionalised 1,3,5-triazines was developed. The rationale for synthesising this heterocycle was to investigate the importance of the imidazole ring for potency. It was hoped that the electron-deficient triazine heterocycle would increase the reactivity of the conjugated acetylene towards Cys-22 within the Nek2-ATP-binding domain leading to increased Nek2 inhibitory activity. A small library of alkylamines (**91-94**) was synthesised to investigate structure-activity relationships.

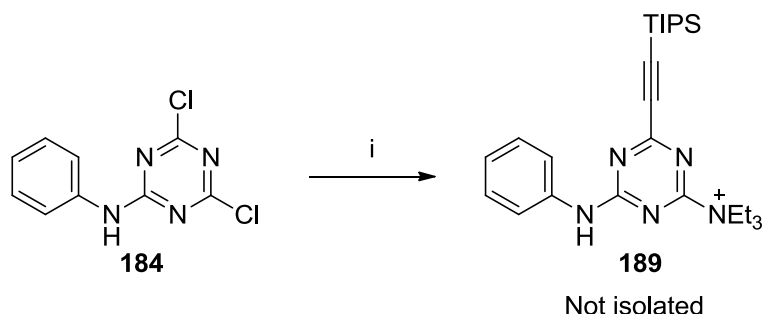


Reagents and Conditions: i) PhNH_2 , K_2CO_3 , THF, 0°C – RT, 1 h; ii) TIPS-acetylene, $\text{Pd}(\text{PPh}_3)_2\text{Cl}_2$ (5 mol%), CuI (5 mol%), DIPEA, THF, RT, 18 h; iii) RNH_2 , THF, RT, 3 h; iv) TBAF, THF.

Scheme 53.

A thermally controlled $\text{S}_{\text{N}}\text{Ar}$ reaction of cyanuric chloride **183** with aniline gave dichlorotriazine **184** exclusively in 73% yield.²³⁵ Standard Sonogashira conditions were attempted to couple TIPS-acetylene with triazine **184** (Scheme 54); however, in addition to coupling of the TIPS ethynyl group to furnish **185**, a side reaction with

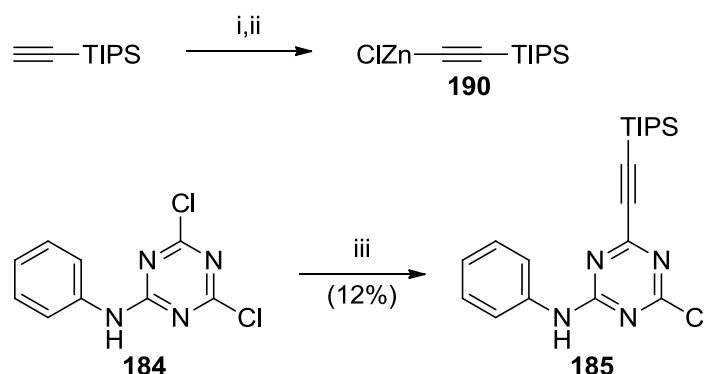
triethylamine led to the quaternary ammonium species **189** as the major product (observed by LC-MS analysis).



Reagents and conditions: i) TIPS-acetylene, Pd(PPh₃)₂Cl₂ (5 mol%), CuI (5 mol%), Et₃N, THF, RT, 18 h.

Scheme 54.

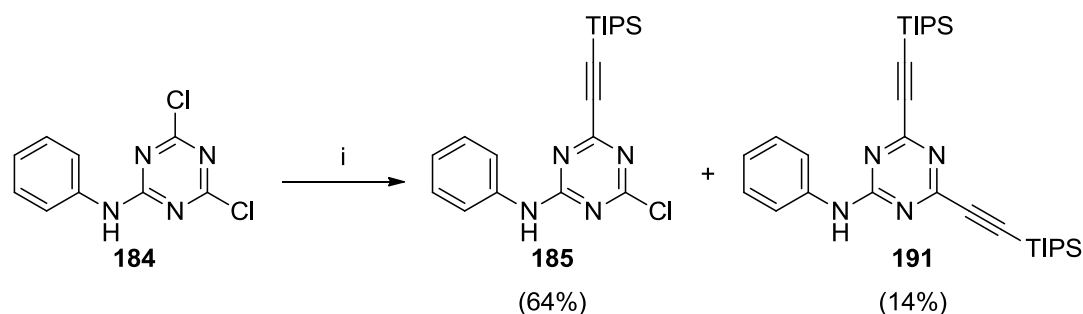
Zinc acetylide **190** was prepared from TIPS-acetylene and used in a Negishi coupling reaction with triazine **184** (Scheme 55). Anilinothiazine **185** was obtained in low yield (12%) together with multiple side-products, as such, an alternative route was developed.²³⁶



Reagents and conditions: i) TIPS-acetylene, *n*-BuLi, THF, -78 °C, 30 min.; ii) ZnCl₂; iii) **190**, Pd(PPh₃)₄ (30 mol%), THF, -78 °C – RT, 1 h.

Scheme 55.

Sonogashira coupling of triazine **184** with TIPS-acetylene in the presence of DIPEA gave triazine **185** in 64% yield, with a 14% yield of the undesired disubstituted compound **191** (Scheme 56), which was separable from **185** by RP-MPLC.



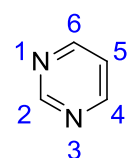
Reagents and conditions: i) TIPS-acetylene, Pd(PPh₃)₂Cl₂ (5 mol%), Cul (5 mol%), DIPEA, THF, RT, 18 h.

Scheme 56.

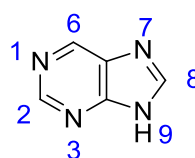
A range of alkylamines were then coupled to **184** including MeNH₂, EtNH₂ and PMBNH₂ in high yield (80-96%). Synthesis of the parent amine derivative **91** was achieved by TFA-mediated PMB deprotection of **188**. Finally, the TIPS protecting group was removed with TBAF to give the target triazines **91-94** in 91-98% yield.

5.5.7 Synthesis of Pyrimidine-Based Nek2 Inhibitors

Pyrimidines are able to participate in a number of unique reactions due to their electronic structure. For example, the carbon atoms at the 2-,4- and 6-positions are activated to S_NAr type reactions due to electron deficiencies in the π -system caused by localisation of electrons at N^{1/3}. This is further enhanced as the ring nitrogens are positioned *meta* with respect to one another, resulting in a cumulative effect. Additionally, the electron rich ‘semi-aromatic’ 5-position may participate in electrophilic aromatic substitution reactions with suitable electrophiles (e.g. *N*-bromosuccinimide).²³⁷



Pyrimidine



Purine

To further investigate the potential application of 6-membered ring heterocycles as inhibitors of Nek2, a small library of pyrimidine derivatives was synthesised. As for the triazine series, it was essential to maintain the triplet of H-bonds with the Nek2 hinge region. It was also important that the 6-ethynyl and 2-anilino groups were

present in target molecules analogous to purine **39**. A range of amines was investigated at the pyrimidine 4-position as well as several 5-halogenated derivatives (Figure 40). It was unclear how Nek2 inhibitory activity would compare to the parent purine **39** or triazines **91-94**. However, due to the increased electron density of the pyrimidine series it was suspected that an attenuation of ethynyl group reactivity would be observed.

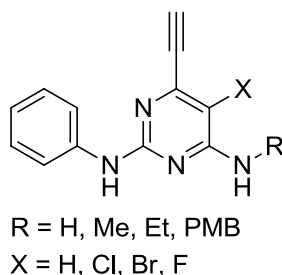
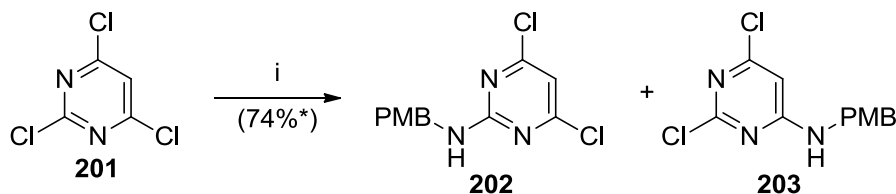


Figure 40 – Pyrimidine-based Nek2 inhibitors.

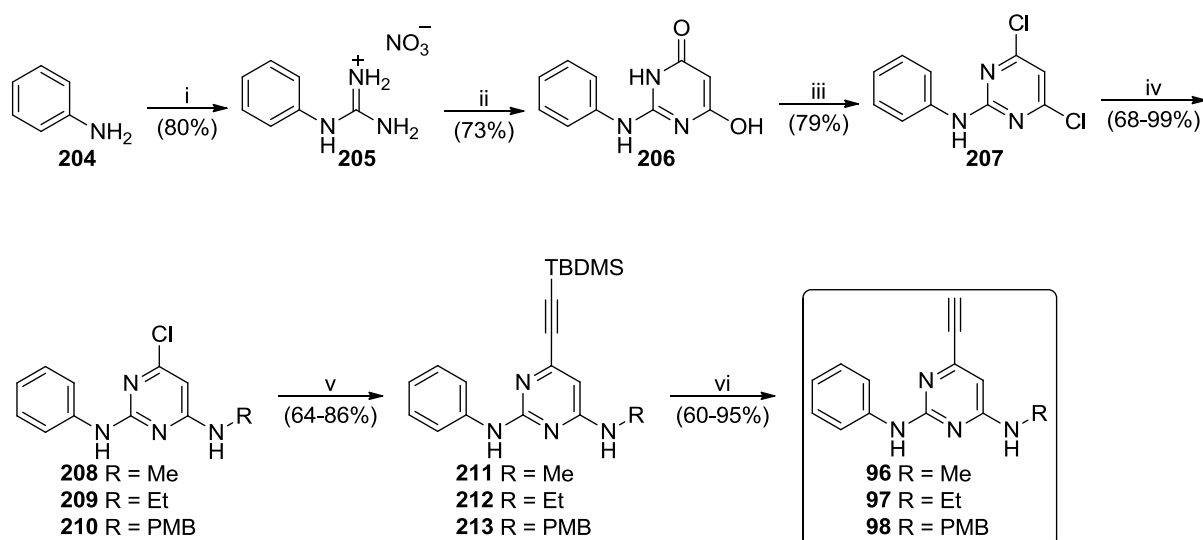
An initial synthetic route based upon that of the 1,3,5-triazines was attempted starting from 2,4,6-trichloropyrimidine **201**. However, this strategy was found to be unsuitable due to poor regioselectivity (Scheme 57)



Reagents and conditions: i) PMBNH₂, K₂CO₃, THF, 0 °C – RT, 15 min.

Scheme 57.

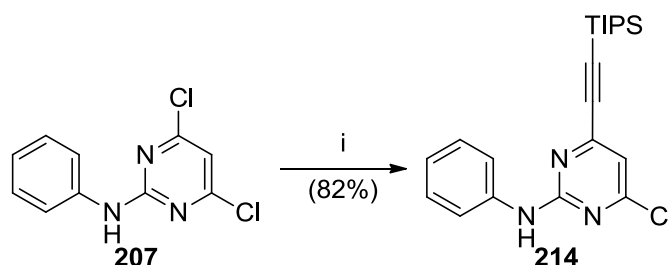
A synthetic route was devised that incorporated the aniline side chain at the start of the synthesis (Scheme 58), thus preventing regioselectivity issues. A further advantage of this approach was that final derivatization occurs towards the end of the scheme, aiding library synthesis.



Reagents and Conditions: i) Cyanamide, HNO_3 , EtOH, 100 °C, 16 h; ii) Diethyl malonate, NaOMe, MeOH, RT, 18 h; iii) POCl_3 , MW 140 °C, 20 min; iv) RNH_2 , THF, RT, 18 h; v) **216**, $\text{Pd}(\text{PPh}_3)_4$ (10 mol%), Cs_2CO_3 , Dioxane, MW 140 °C, 2 h; vi) TBAF, THF, RT, 15 min.

Scheme 58.

Aniline was reacted with cyanamide in the presence of nitric acid to form phenylguanidine nitrate **205**.²³⁸ A Pinner pyrimidine synthesis gave the pyrimidine **206** which was treated with POCl_3 to give dichloropyrimidine **207**.²³⁹

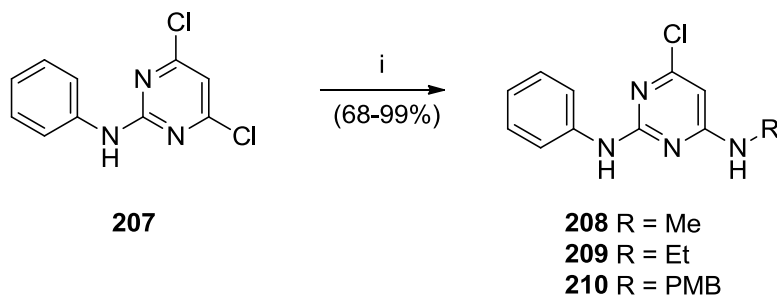


Reagents and conditions: i) TIPS-acetylene, $\text{Pd}(\text{PPh}_3)_2\text{Cl}_2$ (10 mol%), Et_3N , CuI, THF, RT, 18 h.

Scheme 59.

Sonogashira coupling of the TIPS ethynyl group with **207** was successful; however, upon coupling of the ethynyl group, all attempted amine additions failed. It is likely that the exchange of the electron-withdrawing chloro group of **207** for an electron-donating acetylene reduced the reactivity of pyrimidine **214**. A variety of conditions were attempted to facilitate this reaction, including microwave irradiation of a solution of **214** in neat PMBNH_2 and deprotonation of the amine with NaH to increase nucleophilicity. Unfortunately, in each case no reaction was observed. A copper-

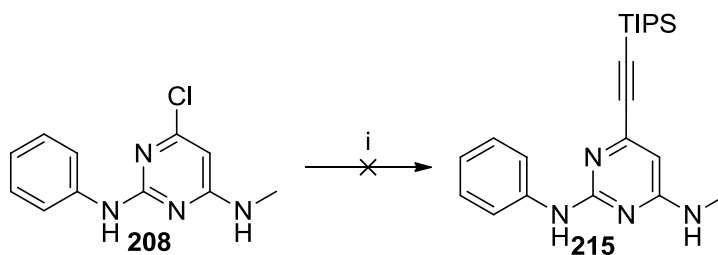
based Ullmann coupling reaction of **214** with MeNH_2 was also attempted but led to decomposition. A number of palladium-mediated Buchwald amination conditions were attempted, but again decomposition of **214** was observed.



Reagents and conditions: i) RNH_2 , THF, RT, 18 h

Scheme 60.

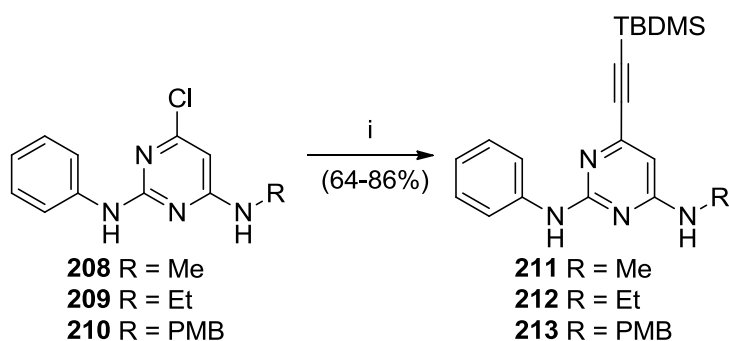
It was decided to attempt to couple the amine functional group to pyrimidine **207** prior to the Sonogashira reaction, in the hope that the increased electron deficiency, due to the presence of two chloro substituents in pyrimidine **207**, would facilitate the reaction (Scheme 60). Interestingly, after a single addition of amine no further reaction took place. It was therefore possible to use multiple equivalents of amine, which reduced the reaction time and negated the need for an additional base.



Reagents and conditions: i) TIPS-acetylene, $\text{Pd}(\text{PPh}_3)_2\text{Cl}_2$ (5 mol%), Et_3N , CuI (5 mol%), THF, RT, 18 h.

Scheme 61.

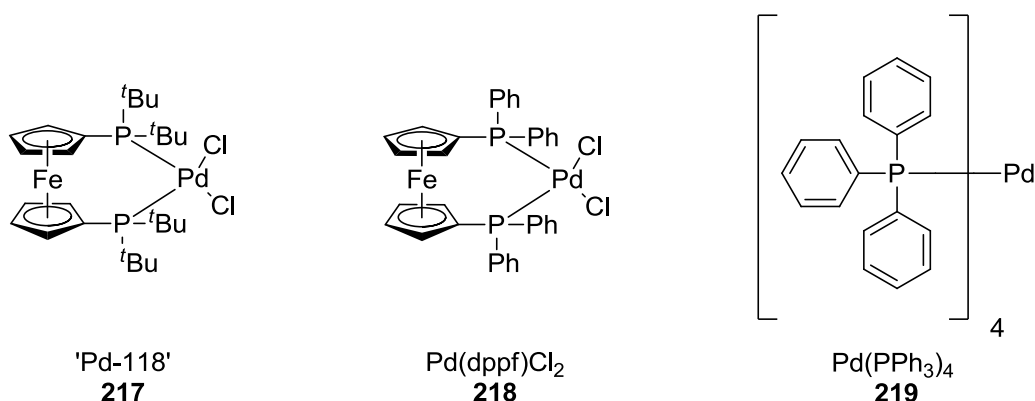
Unfortunately, after introduction of the amino group the subsequent Sonogashira reaction became disfavoured (Scheme 61). It is possible that the increased electron density of pyrimidine **208** stabilises the intermediate Pd complex preventing oxidative addition.²¹⁵ Attempts at heating the reaction resulted in decomposition, as did the reaction using Buchwald's copper free Sonogashira method.²²⁵



Reagents and conditions: **i** **216**, Pd(PPh₃)₄ (10 mol%), Cs₂CO₃, dioxane, MW 140 °C, 2 h.

Scheme 62.

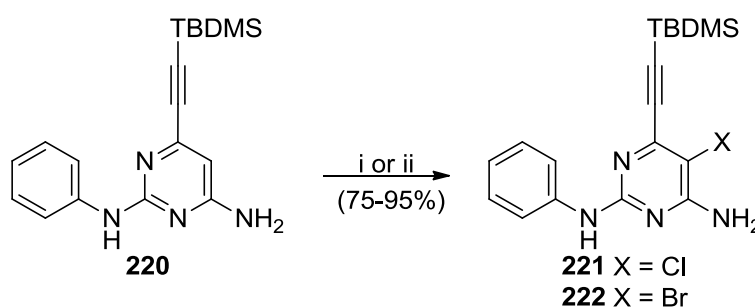
A key step in this reaction scheme was the Suzuki coupling of the TBDMS acetylene pinacolborane **216** to 6-chloropyrimidines **208–210** (Scheme 62). Early experiments using the highly active ‘Pd-118’ **217** and moderately active Pd(dppf)Cl₂ **218** catalysts resulted in modest product formation, and a number of side-products including dehalogenated pyrimidines. Pd(PPh₃)₄ **219** was found to be better suited for this reaction and resulted in clean conversion to the pyrimidine **213**. Unfortunately, the reaction could not be driven to completion even with prolonged heating, stoichiometric amounts of catalyst and 3 equivalents of **216**. This problem was resolved through the use of microwave-assisted heating. Reactions were conducted at 140 °C for 2 h, and optimised to require 0.1 equivalent of Pd(PPh₃)₄ and 1.5 equivalents of **216**. Yields of **211–213** were variable, ranging from 64–88%, albeit with minimal side-product formation.



To obtain the aminopyrimidine **95**, the PMB protected derivative **213** was refluxed in TFA, resulting in clean deprotection to afford pyrimidine **220**. In the final stage, the TBDMS group was removed from pyrimidines **211–213** and **220** with TBAF in THF in a method analogous to that employed for TIPS group deprotection.

5.5.8 Synthesis of 5-Halopyrimidines

A series of 5-halopyrimidines was investigated based upon aminopyrimidine **95**. It was hoped that inclusion of electron-withdrawing halogen groups such as fluoro, chloro and bromo would enhance the reactivity of the ethynyl group and increase Nek2 inhibitory activity. In addition, these halogen groups could be used in future chemistry to further investigate the effect of modifications at the pyrimidine 5-position on Nek2 inhibition.

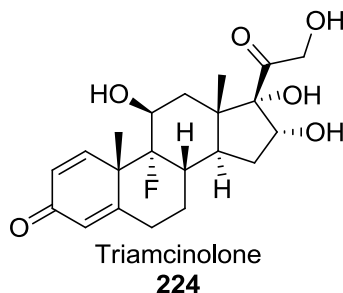
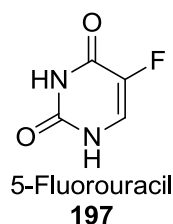


Reagents and conditions: i) NCS, MeCN, MW 100 °C, 30 min; ii) NBS, MeCN, MW 100 °C, 30 min.

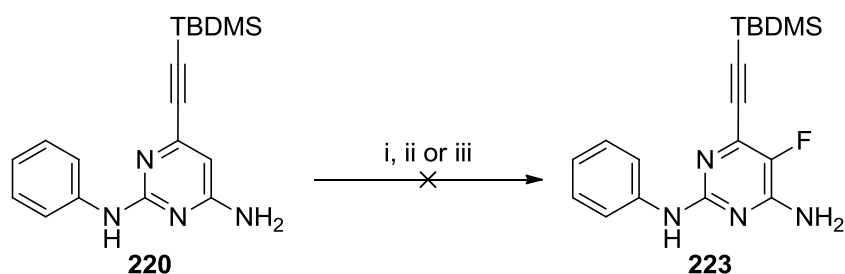
Scheme 63.

Electrophilic aromatic substitution of the pyrimidine 5-position of **220** was achieved using *N*-chlorosuccinimide (NCS) or *N*-bromosuccinimide (NBS) to afford the 2-chloro- and 2-bromopyrimidine derivatives **221** and **222**, respectively. Electrophilic halogenating agents such as NCS and NBS are convenient, easy to handle, and allow selective halogenation of the pyrimidine ring in good yield.

The final 5-halopyrimidine derivative to be synthesised was the 5-fluoro pyrimidine. The inclusion of fluorine in chemotherapeutic compounds is increasingly common, and can have a profound effect upon toxicity and potency.²⁴⁰ Compounds containing a fluoride atom may behave as antimetabolites as the C-F bond can mimic C-H, whilst preventing metabolism. An example is 5-fluorouracil **197**, which is a mechanism-based irreversible inhibitor of thymidylate synthase used in cancer chemotherapy. Additionally, inclusion of fluoride into the structure of corticosteroids can greatly increase the half-life by enhancing the lipid-water solubility ratio. An example of this is the corticosteroid triamcinolone **224**, which is known for its long duration of action.²⁴¹



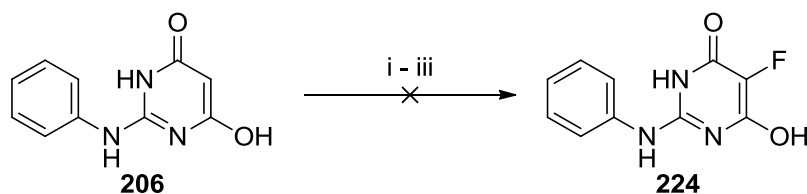
Several attempts were made to synthesise the 5-fluoropyrimidine **223** using N-F based electrophilic fluorinating agents (Scheme 64).²⁴⁰ Regrettably, none of the attempted fluorinations were successful due to decomposition of pyrimidine **220**, and it was decided to attempt to introduce the fluorine atom at an earlier stage in the synthetic scheme.



Reagents and conditions: i) Selectfluor™, MeCN, MW 100 °C, 4 h; ii) 1-Fluoropyridinium tetrafluoroborate, MeCN, MW 100 °C, 4 h; iii) 1-Fluoro-2,4,6-trimethylpyridinium tetrafluoroborate MeCN, MW 100 °C, 4 h.

Scheme 64.

Dihydroxypyrimidine **206** was chosen as the starting material, as this compound should have has increased reactivity towards electrophiles due to higher electron density. However, this compound failed to react with any of the fluorinating agents even with prolonged heating at elevated temperatures (140 °C, 6 h) (Scheme 64). The decision was therefore made to abandon the synthesis of 5-fluoropyrimidine **224** in favour of more synthetically accessible targets.



Reagents and conditions: i) Selectfluor™, MeCN, MW 100 °C, 4 h; ii) 1-Fluoropyridinium tetrafluoroborate, MeCN, MW 100 °C, 4 h; iii) 1-Fluoro-2,4,6-trimethylpyridinium tetrafluoroborate MeCN, MW 100 °C, 4 h.

Scheme 65.

5.5.9 Synthesis of 5-Formylpyrimidine (101)

The final pyrimidine compound synthesised was the 5-formylpyrimidine **101**. Previous work by Marchetti *et al* demonstrated that **225** is a potent inhibitor of CDK2. An intramolecular H-bond between the amino N-H and formyl oxygen forms a pseudocycle. The remaining N-H, is thereby orientated towards the hinge region resulting in a 'purine-mimetic' structure with enhanced competitive binding at the CDK2 ATP-binding domain.²⁴² It was hoped that the pseudocyclic conformation of **225** would be retained in the 6-ethynyl compound **101**, resulting in an increase in potency (Figure 41). It is likely that the electron-withdrawing effect of the formyl group would also enhance reactivity of the terminal 6-ethynyl group of **101**, assisting attack of Cys-22 within the Nek2 ATP-binding domain.

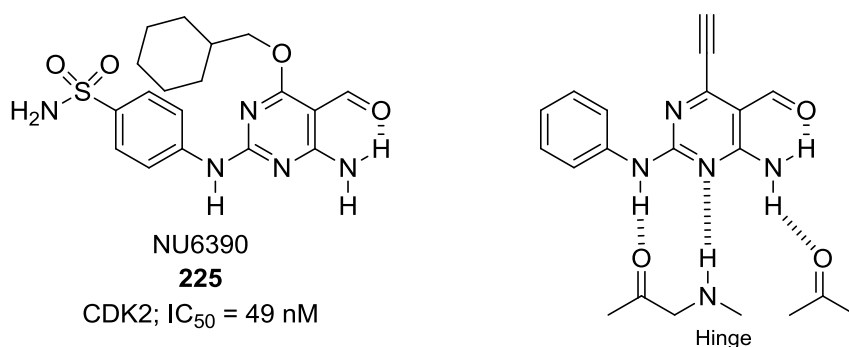
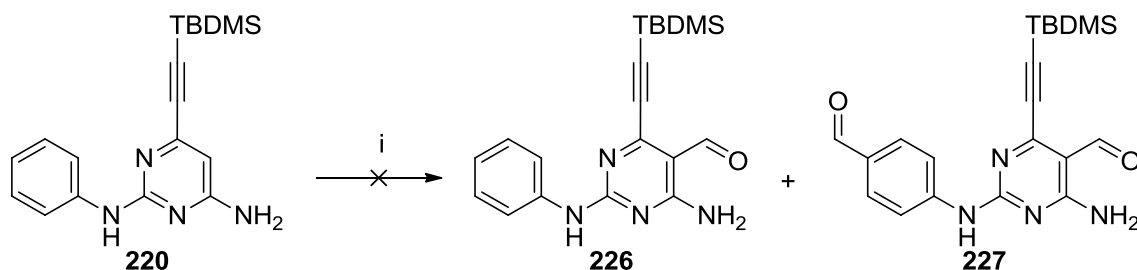


Figure 41 - 5-Formylpyrimidines as purine mimetics.

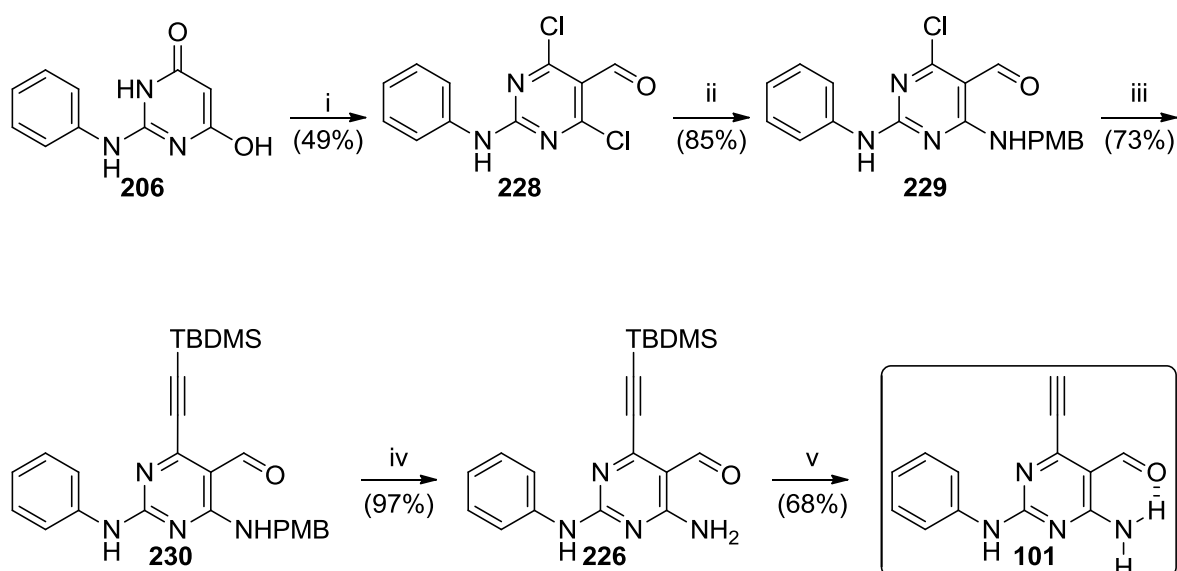
An initial strategy for introduction of the 5-formyl group was to conduct a Vilsmeier-Haack reaction on compound **220**. Standard conditions with DMF in POCl₃ led to decomposition of pyrimidine **220**, and a milder method was attempted using the

isolated (chloromethylene)dimethyliminium chloride (Vilsmeier salt) in MeCN. At room temperature no reaction occurred so the reaction mixture was heated (100 °C, 30 min), which resulted in a small amount of the desired formyl product **226** together with di-aldehyde side-product **227** (Scheme 66).



Reagents and conditions i) Vilsmeier salt, MeCN, RT - 100 °C, 4 h.

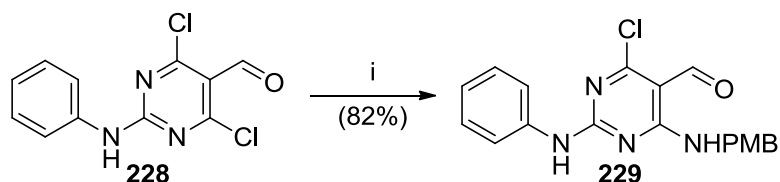
Scheme 66.



Reagents and Conditions: i) POCl₃, DMF, 0 °C – 110 °C, 3 h; ii) PMBNH₂, DIPEA, THF, RT, 1 h; iii) **216**, Pd(PPh₃)₄ (10 mol%), Cs₂CO₃, dioxane, MW 140 °C, 2 h; iv) TFA, 80 °C, 18 h; v) TBAF, THF, RT, 15 min.

Scheme 67.

To improve selectivity, the formyl group was introduced at an earlier stage of the synthesis (Scheme 67), which allowed selective 5-formylation of pyrimidine **228**. It was important to maintain the temperature at 0 °C and to use a single equivalent of DMF in the reaction to ensure regioselectivity and monoformylation of **206**.



Reagents and conditions: i) PMBNH₂, DIPEA, THF, RT, 1 h.

Scheme 68.

The next stage in the reaction was the coupling of PMBNH₂ to pyrimidine **228** (Scheme 68), which adds the 4-amino group. It was interesting to note the increased reactivity of the formyl compound (**288**) when compared to the unsubstituted pyrimidine **207**. Using multiple equivalents of PMBNH₂ led to displacement of both chloro groups from pyrimidine **228**. By contrast, using a single equivalent of PMBNH₂ resulted in a slow reaction, which did not reach completion presumably due to HCl liberated during the reaction. By adding 1 equivalent of DIPEA, this problem was resolved, allowing rapid preparation of pyrimidine **229** in 85% yield. The remaining steps including the Suzuki reaction, PMB deprotection and TBDMS deprotection, proceeded in similar yields to those for the non-formylated series.

2D-COSY ¹H-NMR spectroscopic analysis was performed on 5-formylpyrimidine **101** to confirm the presence of the desired intramolecular H-bond between the 5-formyl oxygen and the 4-amino NH (Figure 42). The data clearly showed that the two amino protons (a) and (b) had distinct chemical environments and coupled with one another, strongly suggesting that an intramolecular H-bond was present in the molecule.

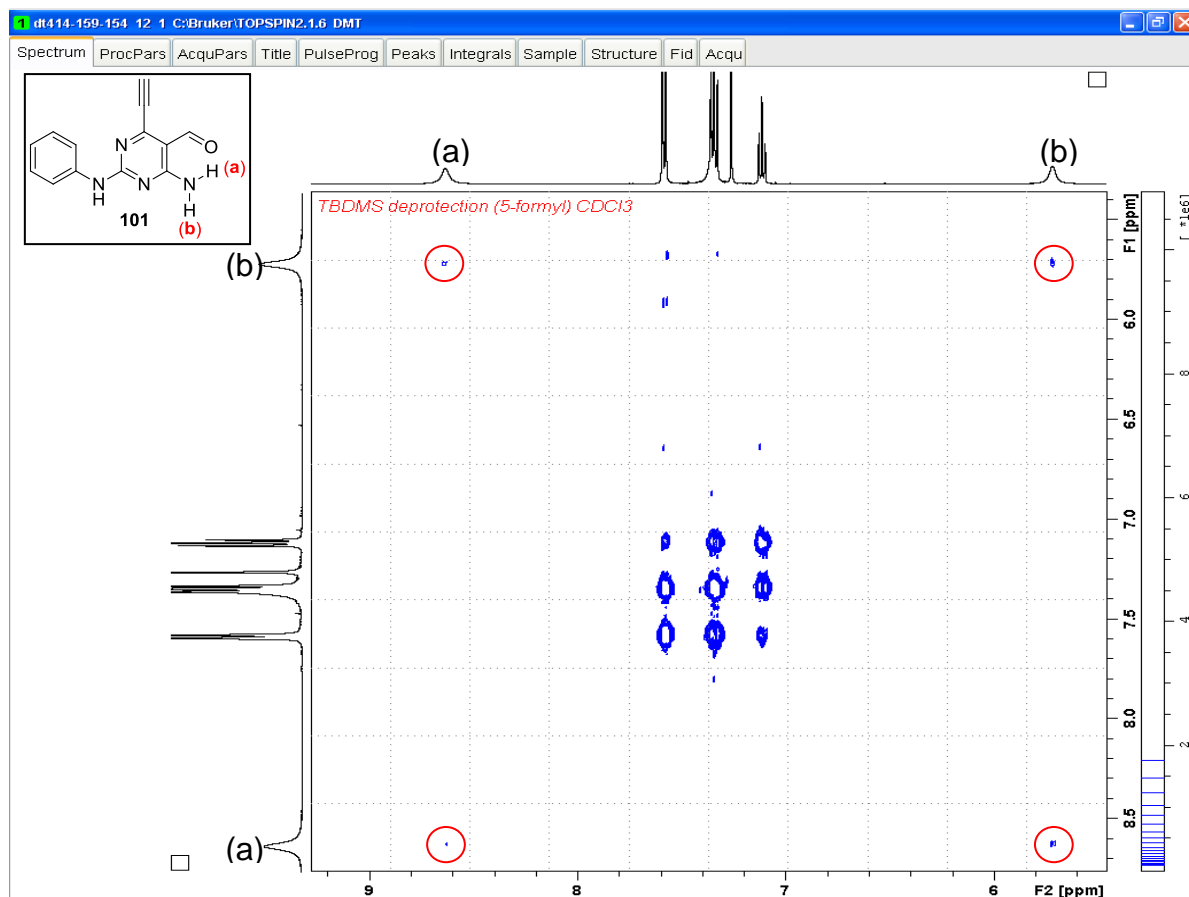


Figure 42 – 2D-COSY ^1H -NMR analysis of **101**.

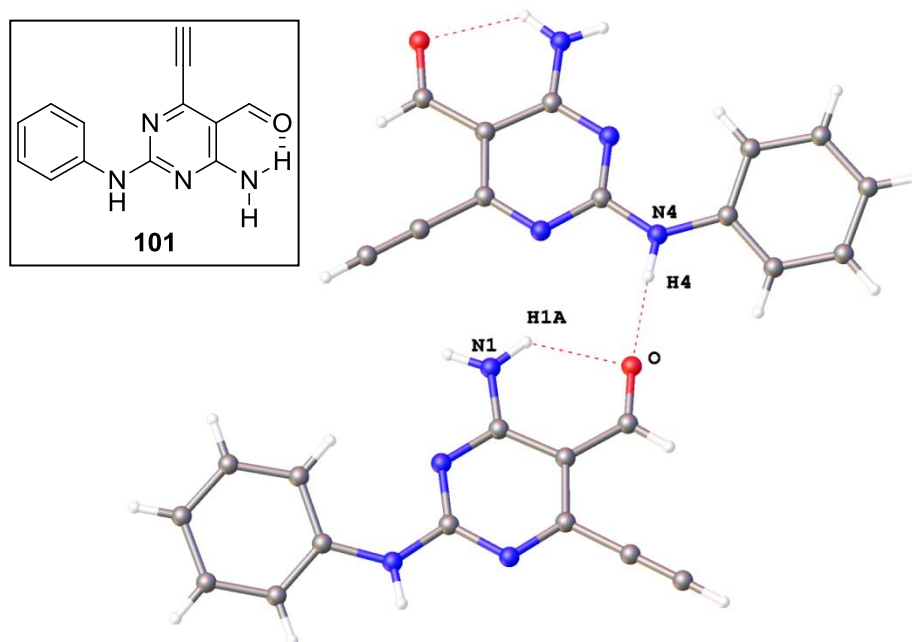


Figure 43 - The X-ray crystal structure of **101** confirmed the presence of an intramolecular H-bond between the carbonyl oxygen and the 4-amino NH.

Crystals of **101** were prepared by dissolution in EtOAc followed by gradual solvent evaporation. The small-molecule *X-ray* crystal structure of **101** was solved (Figure 43), which confirmed the presence of the expected intramolecular hydrogen bond between the 5-formyl oxygen and the 4-amino NH.

Chapter Six: Biological Evaluation of Nek2 Inhibitors

6.1 Structure-Activity Relationship Studies for 6-Ethynyl-2-Phenylaminopurine

(39)

6.1.1 *N*⁷- and *N*⁹-Methylpurines (**52**) and (**53**)

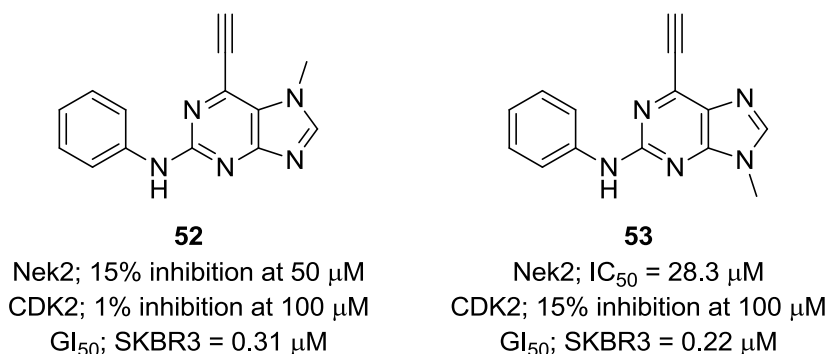


Figure 44.

Compounds **52** and **53** were evaluated for Nek2 inhibitory activity. Methylation of either imidazole nitrogen greatly reduced potency due to loss of a critical H-bond. Interestingly, the *N*⁹-methyl compound **53** was found to retain some activity (Nek2; IC₅₀ = 28.3 μ M). This suggests that the *N*⁹H H-bond interaction with the hinge is not essential for Nek2 inhibitory activity, although it is important for an initial non-covalent binding interaction. By contrast, compound **52** was essentially inactive (Nek2; 15% inhibition at 50 μ M). A consequence of methylation of the *N*⁷-position is that the *N*⁹-nitrogen becomes an H-bond acceptor rather than a donor. This could potentially produce a repulsive effect with the amino acids of the Nek2 hinge region within the ATP-binding domain. Compounds **52** and **53** were also found to be essentially inactive in the CDK2 counter-screen.

In vitro time dependent-inhibition studies of Nek2 were performed using compounds **52** and **53**. Figure 45 shows the percentage of Nek2 inhibition over a range of concentrations and times. Compound **53** was an irreversible inhibitor of Nek2 as demonstrated by the increase in potency relative to incubation time (Figure 45, **a**). By contrast, the level of Nek2 inhibition by compound **52** was not time dependent

Figure 45, **b**), suggesting that this compound has little/no irreversible inhibitory activity at the observed pre-incubation times and concentrations.

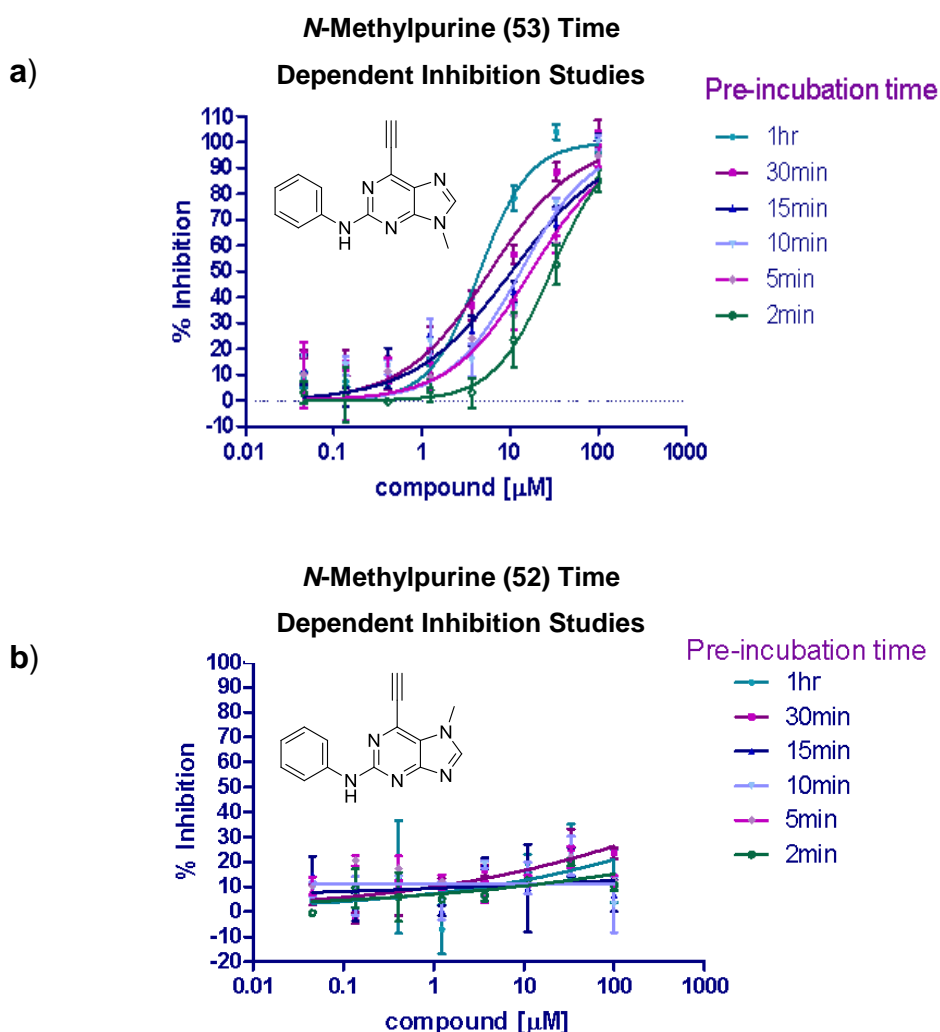
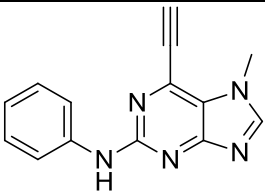
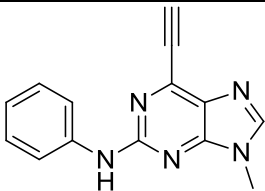
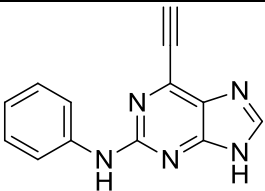


Figure 45 - *in vitro* Nek2 inhibition studies with *N*-methylpurines **53** and **52**, performed at the NICR.

To ascertain whether compounds **52** and **53** were control compounds for the parent purine **39** they were screened in a number of cancer cell lines known to have elevated Nek2 expression (Table 2). These cell lines included: human breast cancer cell lines MDAMB231 and SKBR3, human osteosarcoma cell line (U2OS) and the transformed cell line human embryonic kidney 293 (HEK293). If growth inhibition was due to inhibition of Nek2 these compounds would be expected to have poor cellular potency and hence a high GI_{50} value. Compounds **52** and **53** possessed cellular activity comparable with the parent purine **39** in all cell lines assayed, with the exception of HEK293. In this cell line the *N*⁷-methypurine **52** was found to be 12-

fold less active than the parent **39**. Interestingly, the *N*⁹-methypurine **53** was found to have growth-inhibitory activity comparable with the parent purine **39**. Cellular activity in the absence of Nek2 inhibitory activity suggests that growth inhibition may be due to an off-target effect rather than as a result of Nek2 inhibition.

Table 2 – Growth inhibition studies with *N*-Methylpurines **52** and **53**, performed at the NICR.^a

Assay/Cell Line GI ₅₀ or IC ₅₀ (μM)	 52	 53	 39
Nek2	15% inhibition at 50 μM	28.3	0.15
MDAMB231	1.7	0.9	1.1
U2OS	1.4	1.4	1.8
HEK293	1.2	>0.05	0.1
SKBR3	0.31	0.22	0.33

^a Compounds **52** and **53** are weak inhibitors of Nek2 but demonstrated cellular growth inhibitory activity comparable to the parent purine **39**.

C-Nap1 is a substrate for Nek2 phosphorylation and a component of the intercentriolar linkage. Depletion of cellular Nek2 through irreversible inhibition causes a reduction in phospho-C-Nap1 (pC-Nap1) concentration.^{123,163} *In vitro* phospho-C-Nap-1 (pC-Nap1) assays with *N*-methylpurines **52** and **53** were performed in U2OS cells, allowing a comparison of cellular Nek2 inhibitory activity and growth inhibition with the parent purine **39** (Figure 46).

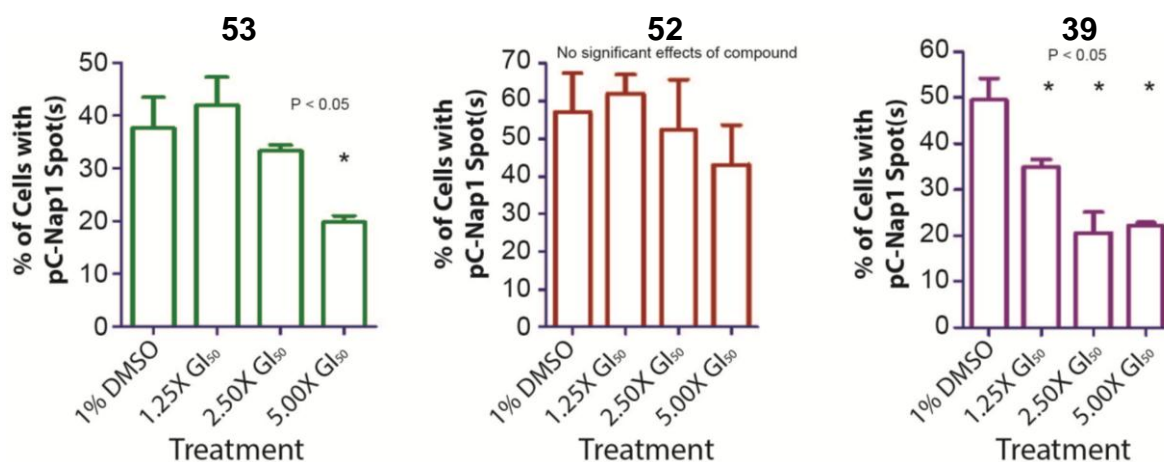


Figure 46 – *In vitro* pC-Nap1 assay with *N*-methylpurines (**53**, **52**, **39**), performed at the NICR.

In the pC-Nap1 assay, U2OS cells were synchronized for 16 h, washed, and incubated in the presence of the desired compound for 4 h. The cells were then stained to visualize γ -tubulin and pC-Nap1, which allows pC-Nap1 co-localised with the centrosomes to be counted. Each compound was titrated at varying multiples of the GI_{50} until no change of pC-Nap1 was observed. The results from the pC-Nap1 assays (Figure 46) demonstrate that the *N*⁹-methylpurine **53** showed dose-dependent inhibition when titrated at greater than 1.25x its GI_{50} . By contrast, the *N*⁷-methylpurine **52** did not inhibit Nek2 even at 5x the GI_{50} . The parent purine **39** also produced a dose response but at lower concentrations than compound **53**. Studies at 5x the GI_{50} of **39** failed to cause further reduction in pC-Nap1 levels, suggesting that a compensatory pathway may be in place permitting C-Nap1 phosphorylation in the absence of Nek2.

Figure 47 shows a direct comparison of growth-inhibitory activity between parent purine **39** and *N*-methylpurines **52** and **53** in SKBR3 cells over a range of concentrations. The cellular potency of all three compounds follows a very similar trend independent of Nek2 inhibitory activity. These findings increase the likelihood that growth inhibition is due to off-target activity, rather than as a result of Nek2-inhibitory activity.

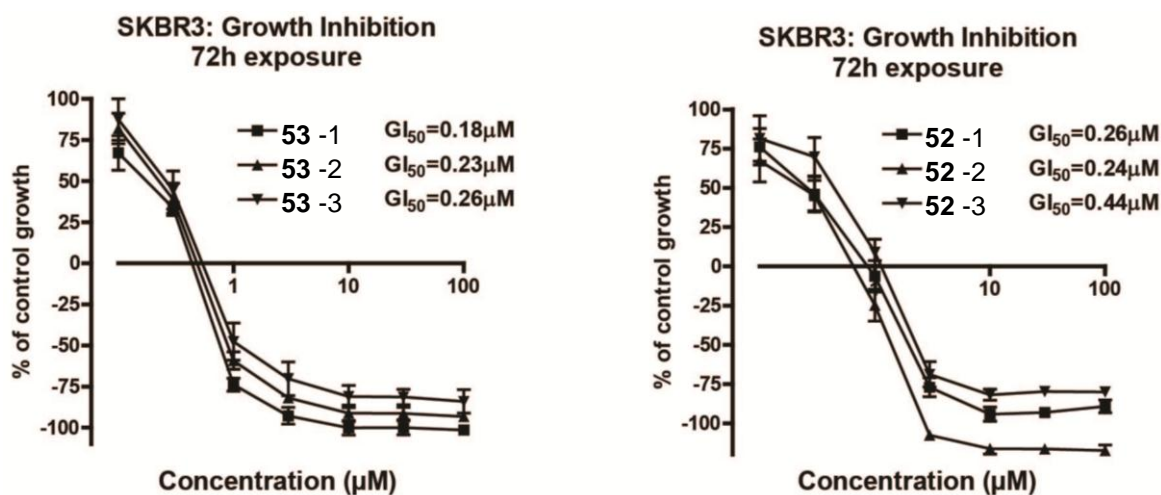
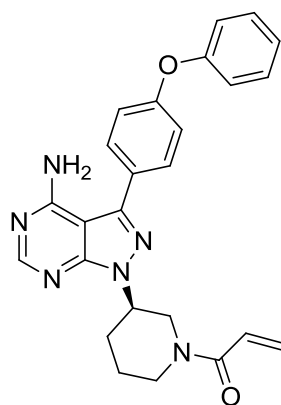


Figure 47 - SKBR3 Growth Inhibition Assays of *N*-Methylpurines **52** and **53**, performed at the NICR.

N-Methylpurines **52** and **53** were screened against a panel of 121 kinases (single point determination at 1 μM) to assess kinase selectivity. Nek2-inhibitory activity was

observed to be higher for both compounds **52** and **53** (29% and 64% inhibition at 1 μ M respectively) than for the Caliper assay (15% inhibition at 50 μ M and 28 μ M, respectively). This is likely because these compounds exhibit time-dependent inhibition kinetics and, as such, the incubation time of the assay affects the observed potency. In addition to Nek2 inhibition, compounds **52** and **53** showed inhibitory activity of greater than 30% at 1 μ M in Bruton's tyrosine kinase (BTK) and aurora kinase A (AK-A).

BTK is a Tec family kinase involved in B-lymphocyte development, differentiation and cell signalling. There is evidence to suggest that BTK is a mediator of proinflammatory signals which has led to interest in the development of selective BTK inhibitors for the treatment of autoimmune diseases (e.g. rheumatoid arthritis) and B-cell malignancies.²⁴³⁻²⁴⁶ BTK contains a non-conserved Cys residue (Cys-481) within the ATP-binding domain which may be targeted by electrophiles. Ibrutinib (PCI-32765) **230** is an example of an orally active irreversible BTK inhibitor that is currently in phase II clinical trials for the treatment of B-cell non-Hodgkin lymphoma.²⁴³⁻²⁴⁶



Ibrutinib (PCI-32765)
230

In addition to BTK inhibitory activity, *N*⁷-methylpurine **52** was found to have moderate aurora kinase A (AK-A) (34% at 1 μ M) activity. As mentioned previously (chapter 3), AK-A is a cell cycle kinase that facilitates mitotic spindle assembly. It is possible that inhibition of AK-A could cause cell cycle arrest and growth inhibition.

6.1.2 Investigating the Requirement of the 2-Amino H-Bond of Purine (**39**) for Nek2 Inhibitory Activity

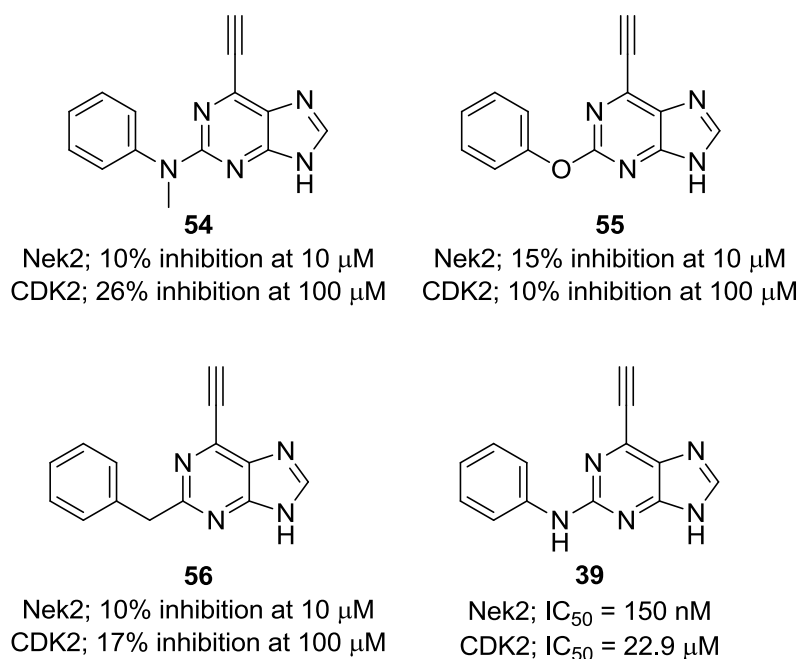


Figure 48.

Evaluation of **54** in Nek2 and CDK2 inhibition assays revealed that methylation of the 2-arylamino group was not tolerated resulting in a large reduction in both Nek2 and CDK2 activity compared with the parent purine **39**. However, it was unclear if this loss of potency was due to a reduction in binding affinity as a result of removal of a critical H-bond interaction, or simply a steric clash arising from the methyl group. To address this, additional modifications of the purine 2-position were investigated. Replacement of the aniline NH in **39** by oxygen in **55** caused a substantial reduction of potency in both the Nek2 and CDK2 assays. This suggests that H-bond acceptor groups at the C²-position are not tolerated and, as such, this series was abandoned. 2-Benzylpurine **56** showed reduced inhibitory activity against both Nek2 and CDK2 compared with the parent purine **39**, which is likely due to loss of the 2-NH hydrogen bond interaction with Cys-89 of the Nek2-ATP-binding domain. In combination with the results from the 2-methylanilino-6-ethynylpurine **54** and the 2-phenoxy-6-ethynylpurine **55** this indicates that the aniline NH of the parent purine **39** is required for potent Nek2 inhibitory activity and likely enhances the initial non-covalent ATP-competitive binding interaction.

6.2 Ethynyl-Substituted Heterocyclic Derivatives of Purine (**39**) as Irreversible Nek2 Inhibitors

6.2.1 Imidazo[4,5-*b*]pyridine (**87**)

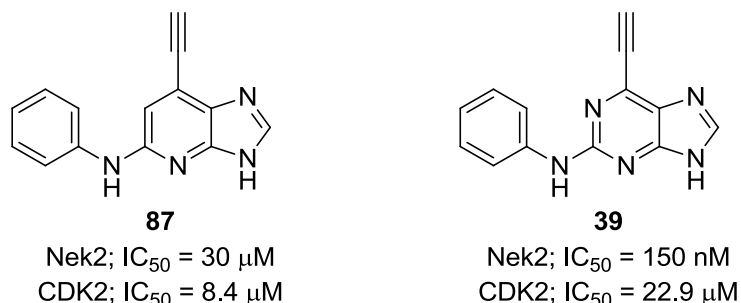


Figure 49.

A 200-fold reduction in Nek2 activity was observed for **87** compared with **39** alongside a slight gain in CDK2 inhibitory activity. It is possible that the increased electron density of the imidazopyridine heterocycle may attenuate ethynyl reactivity preventing covalent modification by Cys-22 at the Nek2 ATP-binding domain. Additionally, the increased electron density relative to purine **39** may also raise the pKa of the aniline side chain NH causing it to become less acidic. This could reduce the H-bond interactions between the ligand and the Nek2 hinge region. These results suggest that the purine *N*¹ nitrogen is important for Nek2 inhibitory activity.

6.2.2 7*H*-Pyrrolo[2,3-*d*]pyrimidines (**88**) and (**231**)

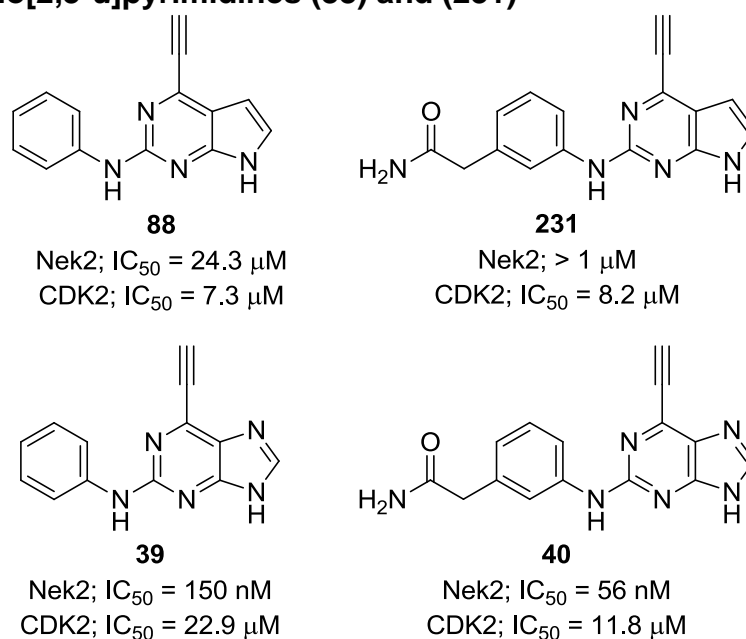


Figure 50 – Comparison of potency between pyrrolopyrimidine and purine heterocycles.

Pyrrolopyrimidines **88** and **231** had substantially lower Nek2 inhibitory activity than the parent purines **39** and **40**. Similar to imidazopyridine **87**, it was likely that the increased electron density due to loss of a nitrogen atom from the heterocycle compared with the purine reduces the reactivity of the ethynyl group towards nucleophilic attack. A slight increase in CDK2 inhibitory activity was observed for both compounds, although this increase was highest in pyrrolopyrimidine **88**.

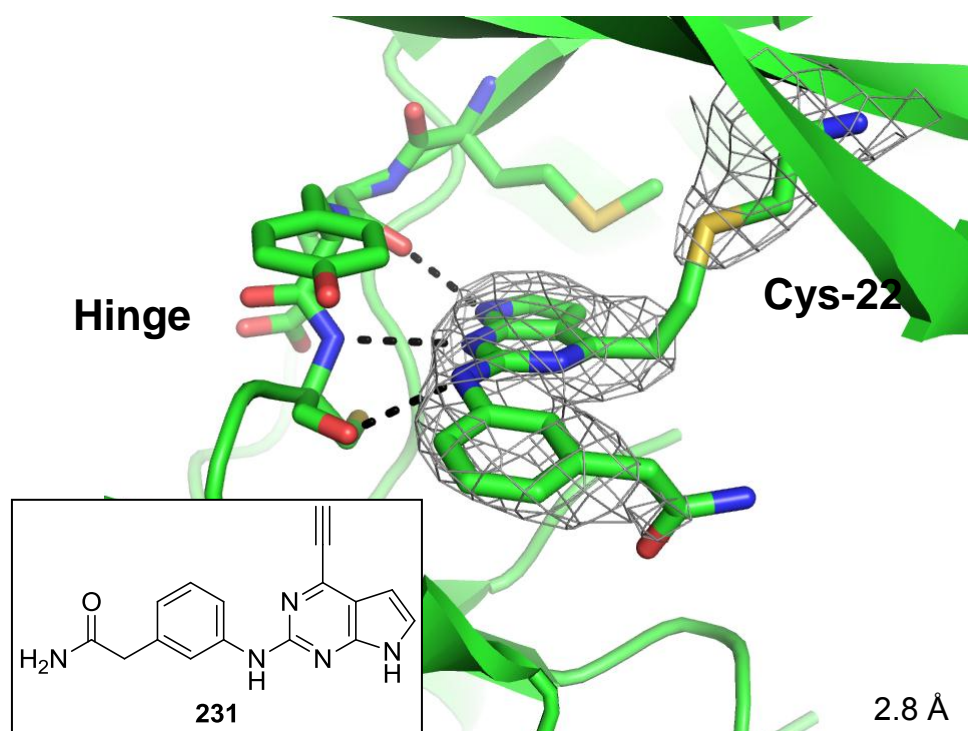


Figure 51 – X-ray crystal structure of **231** in complex with Nek2. Electron density (grey wire mesh) was observed suggesting **231** bound within the Nek2 ATP-binding domain; however, there was insufficient electron density to confirm covalent modification of Cys-22. Note: ene-sulfide bond was modelled to show its predicted position, but was not observed.

The Nek2 X-ray co-crystal structure (Figure 51) showed compound **231** bound within the Nek2 ATP-binding domain. The triplet of hydrogen bonds between the ligand and the Nek2 hinge region was maintained through the pyrrolopyrimidine N^1 and N^7 as well as the aniline amino NH group. However, this compound did not appear to be covalently bound to Cys-22, since electron density between the ligand and Cys-22 was not visible (Figure 51). It is likely that **231** is therefore a reversible inhibitor of Nek2 and did not covalently modify Nek2 during the crystal soak. To further

investigate this possibility, *in-vitro* Nek2 time-dependent inhibition studies should be performed using compound **231**.

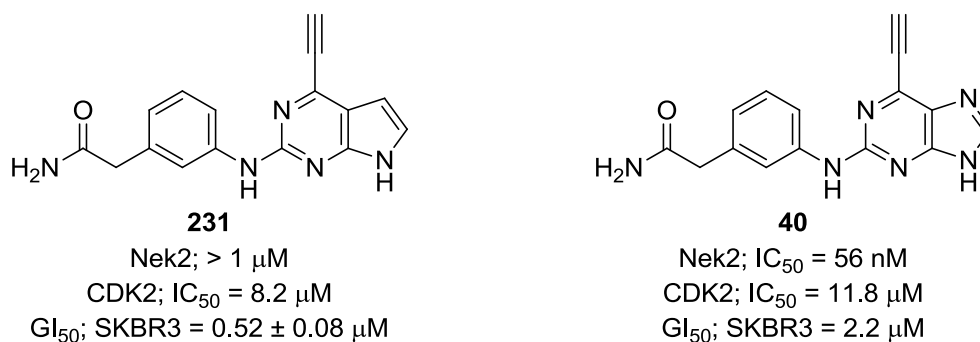


Figure 52.

Pyrrolopyrimidine **231** was evaluated for growth inhibitory activity in SKBR3 cells, and although essentially inactive in the Nek2 assay, **231** had sub-micromolar growth inhibitory activity. This supports the suggestion that growth inhibitory activity may be independent of Nek2 activity and due to off-target effects.

6.2.3 1*H*-Pyrazolo[3,4-*d*]pyrimidines (**89**) and (**154**)

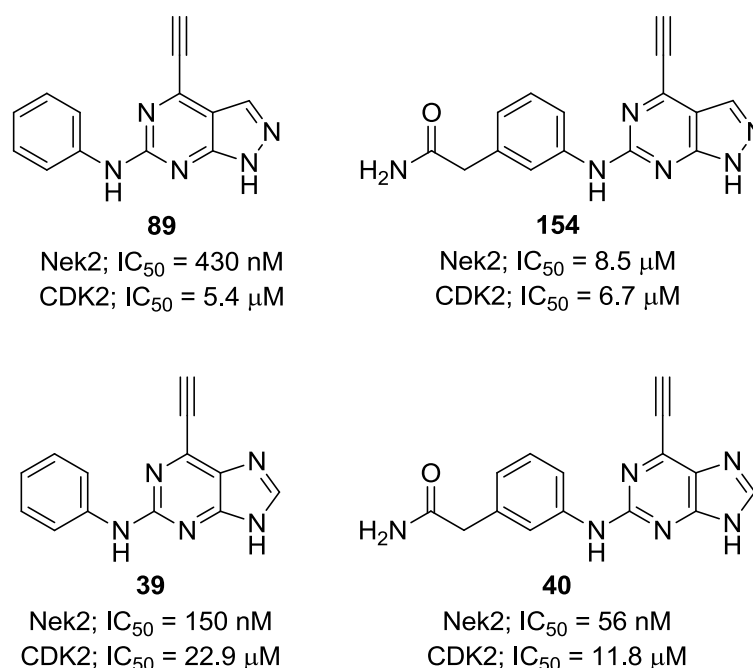


Figure 53 – Comparison of potency between pyrazolopyrimidine and purine heterocycles.

Biological evaluation revealed that the unsubstituted aniline derivative **89** was a sub-micromolar Nek2 inhibitor (430 nM) with good selectivity over CDK2. A 3-fold loss in

Nek2 inhibitory activity was observed when compared with the parent purine **39** (IC_{50} = 150 nM) but this was deemed negligible. Interestingly, the acetamide derivative **154** was found to have modest Nek2 inhibitory activity (8.5 μ M) and CDK2 activity (6.7 μ M) compared with the parent purine **40**, and a 150-fold loss in activity was observed. It was unclear why the unsubstituted pyrazolopyrimidine **89** retained activity when the functionalise pyrazolopyrimidine **154** did not. Both compounds **89** and **154** were analysed in Nek2 co-crystallisation studies to determine whether an alternative binding mode was possible in either case.

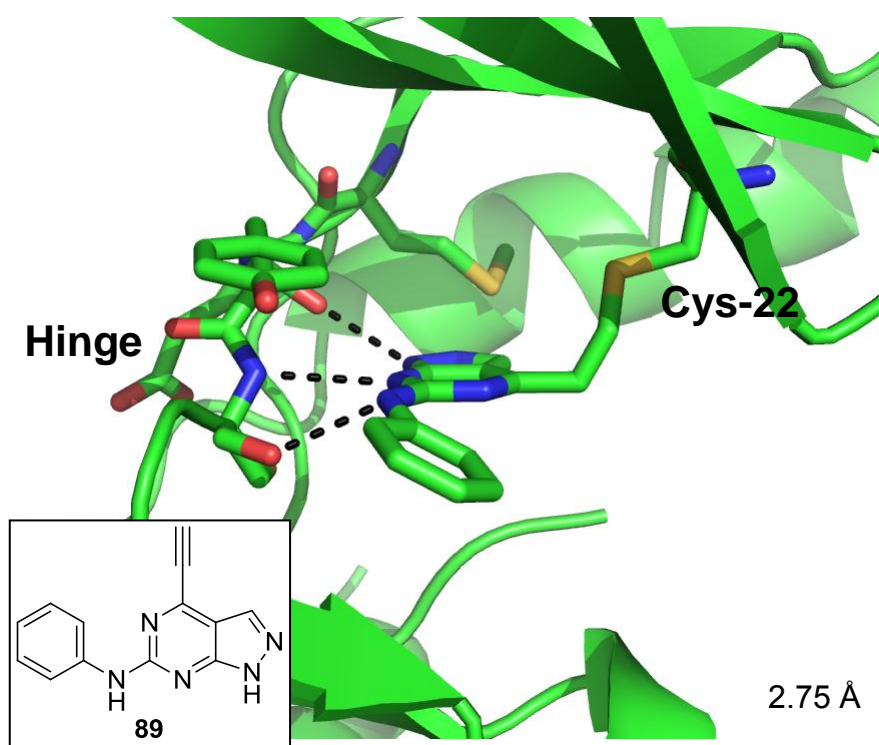


Figure 54 - X-ray crystal structure of **89** in complex with Nek2 suggested covalent modification of Cys-22. Note: further refinement is required to confirm ene-sulfide bond geometry.

The Nek2 X-ray co-crystal structure (Figure 54) showed that pyrazolopyrimidine **89** clearly covalently bound to Cys-22, with a triplet of H-bonds arising with the hinge region of the ATP-binding domain. This is the expected binding motif that is shared with the parent purine **39**.

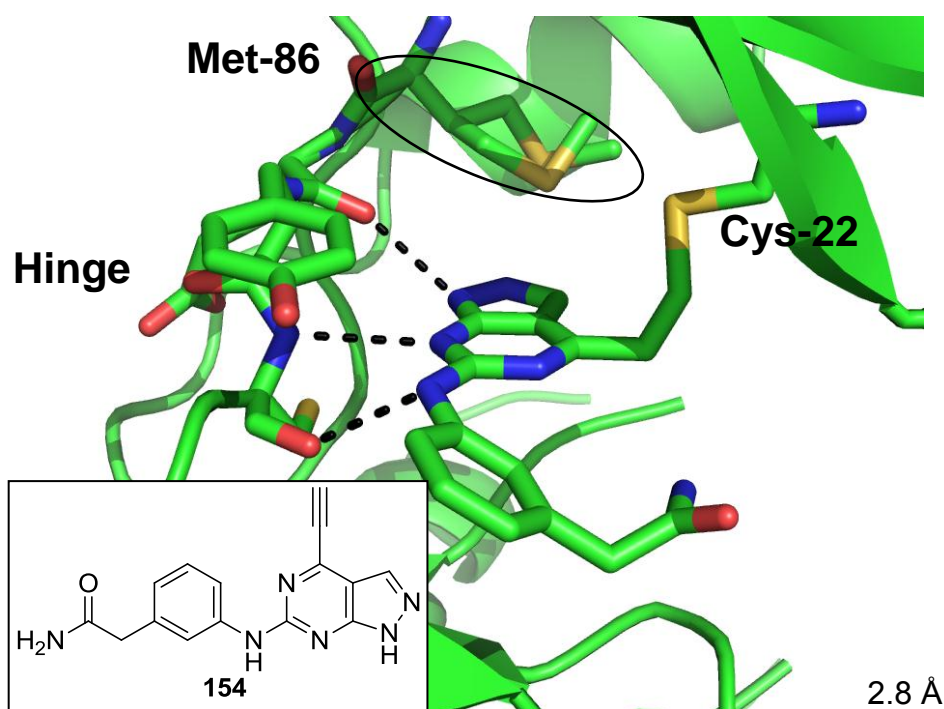


Figure 55 - X-ray crystal structure of **154** in complex with Nek2 suggested covalent modification of Cys-22. Note: further refinement is required to confirm ene-sulfide bond geometry.

Pyrazolopyrimidine **154** was seen to bind to Nek2 in a very similar way to the unsubstituted pyrazolopyrimidine **89** (Figure 55), and it is unclear why there is a difference in potency between the two compounds **89** and **154**. One possibility is that a slight steric clash is observed between the pyrazole nitrogen of the functionalised pyrazolopyrimidine **154** and Met-86 gatekeeper residue, reducing non-covalent binding. Indeed, a small degree of unusual electron density was observed around Met-86 and the model was adjusted to accommodate both conformations of Met-86; however, it remains unclear if a steric clash is responsible for the reduction in potency.

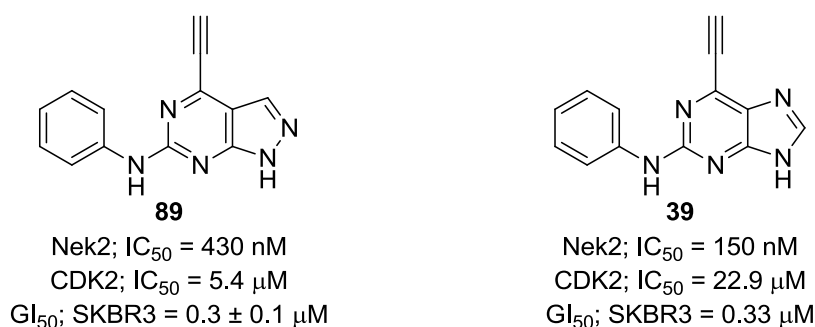


Figure 56.

Pyrazolopyrimidine **89** demonstrated growth inhibitory activity comparable with the parent purine **39**; however, it is uncertain whether if this activity was due to Nek2

inhibition or an off-target effect. Further biological screening of **89** is therefore required to address this.

6.2.4 3-Methyl-1*H*-Pyrazolo[3,4-*d*]pyrimidine (**165**)

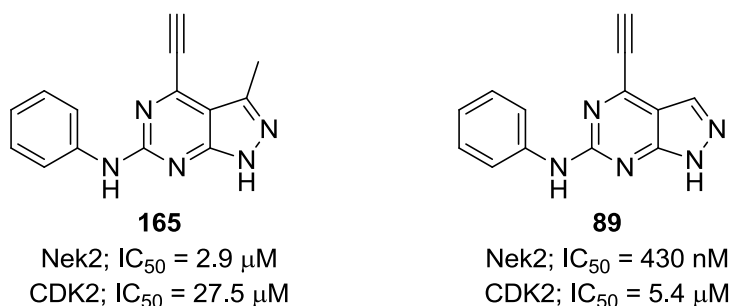


Figure 57.

It was determined that the methyl group at the 3-position of **165** was not tolerated and resulted in a 7-fold reduction in Nek2 inhibitory activity when compared with the parent pyrazolopyrimidine **89**. To identify why this simple modification resulted in such a loss in potency this compound was analysed in Nek2 *X-ray* co-crystal studies. Additionally, CDK2 inhibitory activity was also reduced from 5.4 μM to 27.5 μM.

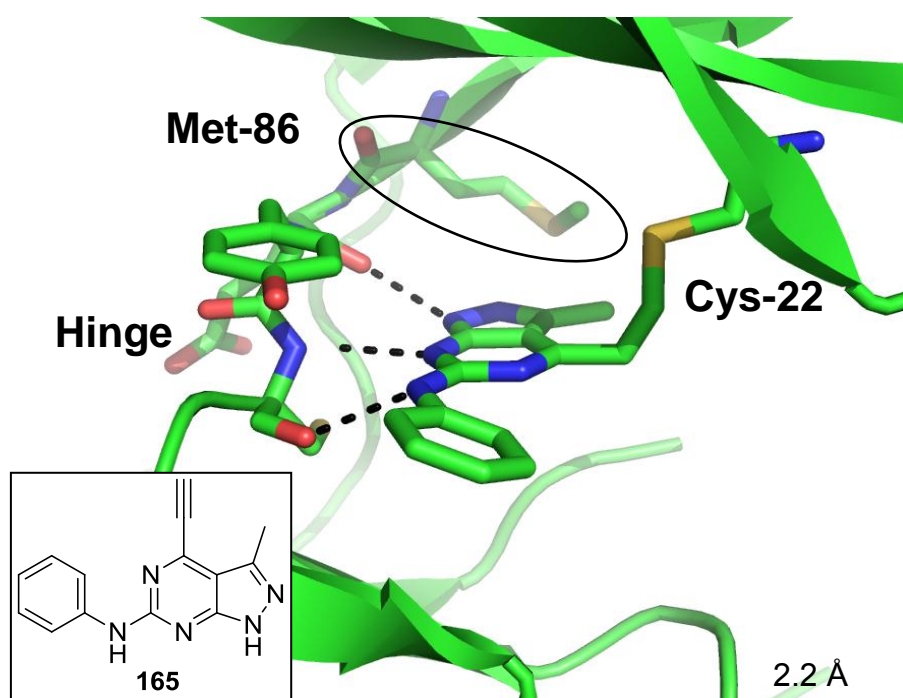


Figure 58 - The *X-ray* crystal structure of **165** in complex with Nek2 suggested covalent modification. A steric clash with the C³-methyl group of **165** causes the side chain of the Met-86 gatekeeper residue to flip, resulting in reduced binding efficiency. Note: further refinement is required to confirm ene-sulfide bond geometry.

The Nek2 crystal structure (Figure 58) showed that compound **165** covalently modified Cys-22 of Nek2 and bound in a similar orientation to the parent pyrazolopyrimidine **89**. However, one clear observed difference was the orientation of the Nek2 gatekeeper residue Met-86, which was flipped when compared with the conventional binding motif. It is likely that a steric clash with the 3-methyl group of **165** forces the methionine side-chain to realign in order to accommodate the ligand. This causes an energetic penalty, and is likely responsible for the reduction in activity when compared with the unsubstituted compound **89**. In light of this observation, it was decided that there would be no benefit in investigating further substituents at the 3-position (e.g. Et, *i*-Pr, halogens *etc.*).

6.2.5 3*H*-[1,2,3]Triazolo[4,5-*d*]pyrimidines (**90**) and (**232**)

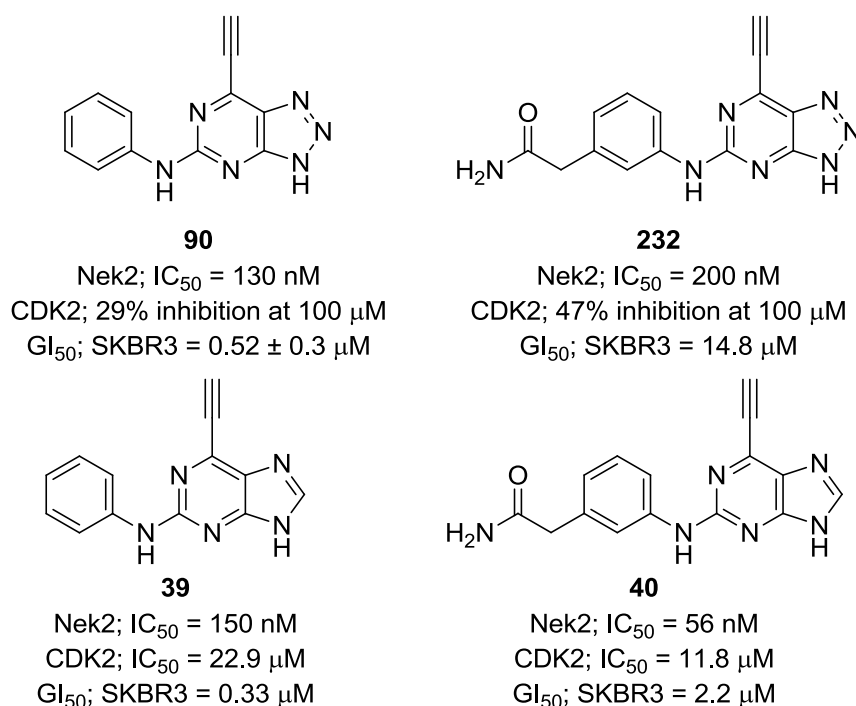


Figure 59 – Comparison of potency between triazolopyrimidine and purine heterocycles.

Triazolopyrimidine **90** possessed similar Nek2 inhibitory activity to the parent purine **39** and was weakly active against CDK2. The functionalised aniline derivative **232** showed a 4-fold reduction in Nek2 inhibitory activity when compared to purine **40**, and was also poorly active in the CDK2 assay. Cell based assays in the SKBR3 cell line showed that **90** had similar cellular potency to the parent purine **39**. By contrast,

the cellular activity of triazolopyrimidine **232** was found to be considerably higher than the parent purine **39** (14.8 μM vs. 2.2 μM , respectively). It is possible that triazolopyrimidine **232** had weak growth inhibitory activity due to its high calculated polar surface area of 116.6 (tPSA purine = 104.2) and low cLogP value of 0.54 (cLogP purine = 1.24) (Figure 60), which may prevent **232** from crossing cell membranes.

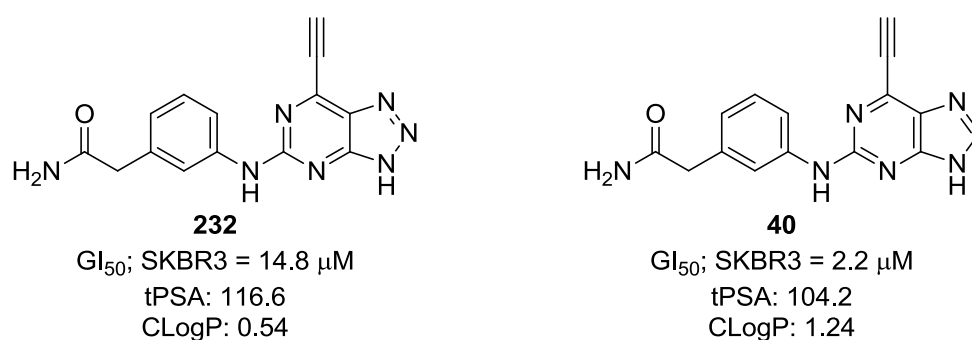


Figure 60.

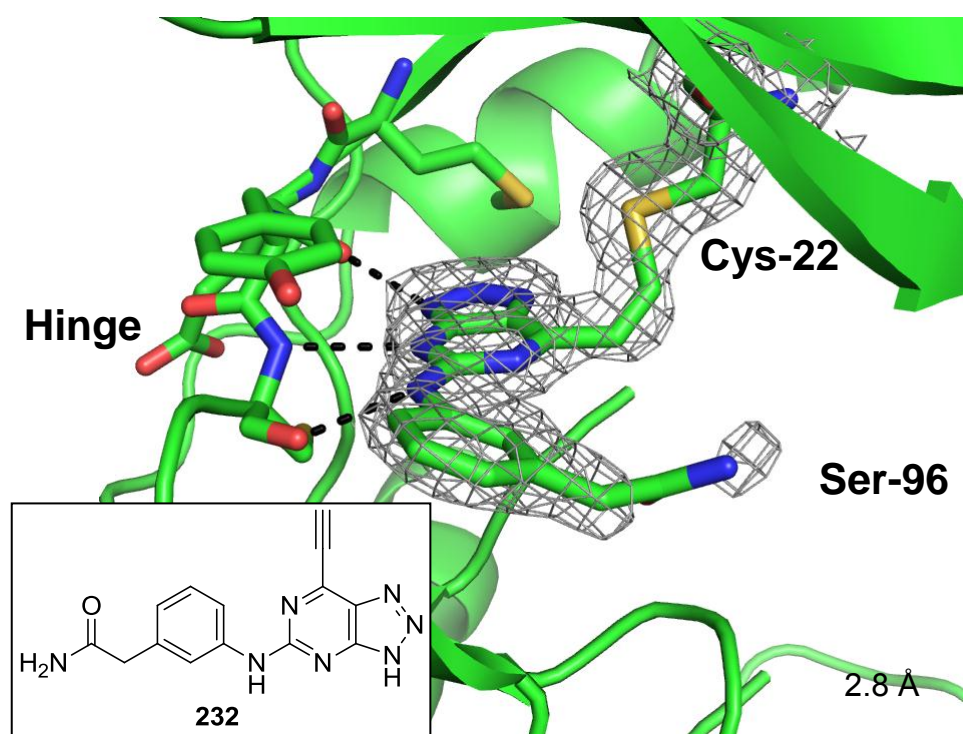


Figure 61 - X-ray crystal structure of **232** in complex with Nek2. Covalent modification of Cys-22 was clearly visible; however, further refinement is required to confirm presence of the ene-sulfide bond.

Triazolopyrimidine **232** covalently modified Cys-22 of the Nek2 ATP-binding domain, which provides evidence that **232** is an irreversible Nek2 inhibitor (Figure 61). The binding orientation of **232** was very similar to the parent purine **40**, as

triazolopyrimidine **232** made H-bond interactions with Cys-89 and Glu-87 of the Nek2 hinge region *via* the triazolopyrimidine heterocycle and the 5-amino NH group. The acetamide side chain was poorly resolved due to flexibility and rotation of this group. However, there was a small degree of electron density in the vicinity of the triazolopyrimidine side chain, which suggested that the acetamide functional group was orientated towards the hydroxyl group of Ser-96, indicating the presence of a possible H-bond interaction.

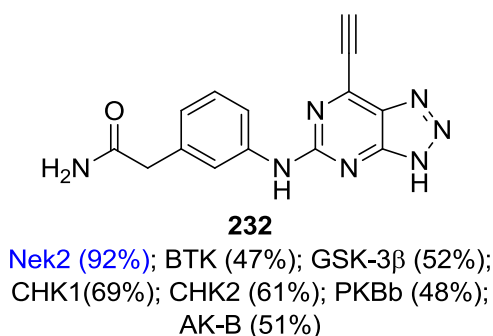


Figure 62 – Kinase selectivity screen of triazolopyrimidine **232** showing percentage inhibition (single point determination 1 μ M).

Triazolopyrimidine **232** was screened against a panel of 121 kinases to assess kinase selectivity (Figure 62). Nek2 inhibition of 92% was observed, alongside significant inhibition of only 6 other kinases indicating good selectivity. As for the *N*-methylpurines **48** and **49**, triazolopyrimidine **232** was an inhibitor of BTK (47% inhibition at 1 μ M), which was possibly due to covalent modification of Cys-481 within the BTK ATP-binding domain. A second Cys containing kinase that was inhibited by **232** was glycogen synthase kinase 3 β (GSK-3 β) (52% inhibition at 1 μ M). GSK-3 β is a Ser/Thr protein kinase involved in numerous physiological processes including glycogen metabolism and gene transcription.²⁴⁷ There has been much interest in the development of small-molecule inhibitors of GSK-3 β for the treatment of diabetes mellitus, due to its role in glycogen metabolism.²⁴⁸ Additionally, GSK-3 β contains a non-conserved Cys residue (Cys-199) located within the ATP-binding domain that is susceptible to covalent modification by electrophiles. Recently, halomethylketones (Figure 63) have been identified as irreversible inactivators of GSK-3 β that function through alkylation of Cys-199.^{249,250} It is not unreasonable to suggest that triazolopyrimidine **232** binds in a similar orientation to these ligands and covalently modifies Cys-199 within the GSK-3 β ATP-binding domain.

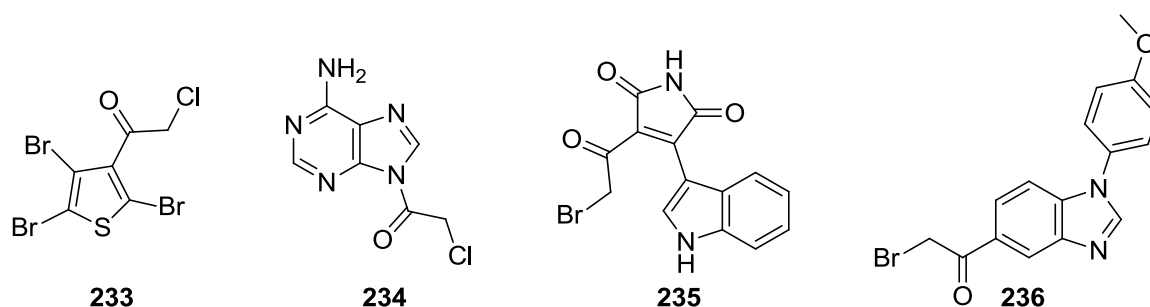


Figure 63 – Halomethylketones that covalently modify Cys-199 of GSK-3 β .

Additionally, the serine/threonine protein kinases Chk1 and Chk2 were inhibited by 69% and 61%, respectively. The function of Chk1/2 is to regulate checkpoint signalling during the cell cycle, particularly in response to DNA damage. Interestingly, both Chk1 and Chk2 have been implicated in cancer and there is currently growing interest in the development of small-molecule inhibitors that target these kinases.⁴⁶ Triazolopyrimidine **232** was also found to be a low-micromolar inhibitor of protein kinase B (PKB β) (48% inhibition at 1 μ M). PKB β (also known as Akt) is a signalling protein that has a role in metabolism, cell cycle control and apoptosis.²⁵¹ PKB β has been described as an attractive cancer chemotherapeutic target due to its influence on the proliferation and survival of tumour cells.^{252,253} Finally, aurora kinase B (AK-B) inhibitory activity of 51% was observed, which is similar to the value obtained for *N*-methylpurine **48** (30% inhibition at 1 μ M).

6.2.6 1,3,5-Triazine Based Nek2 Inhibitors

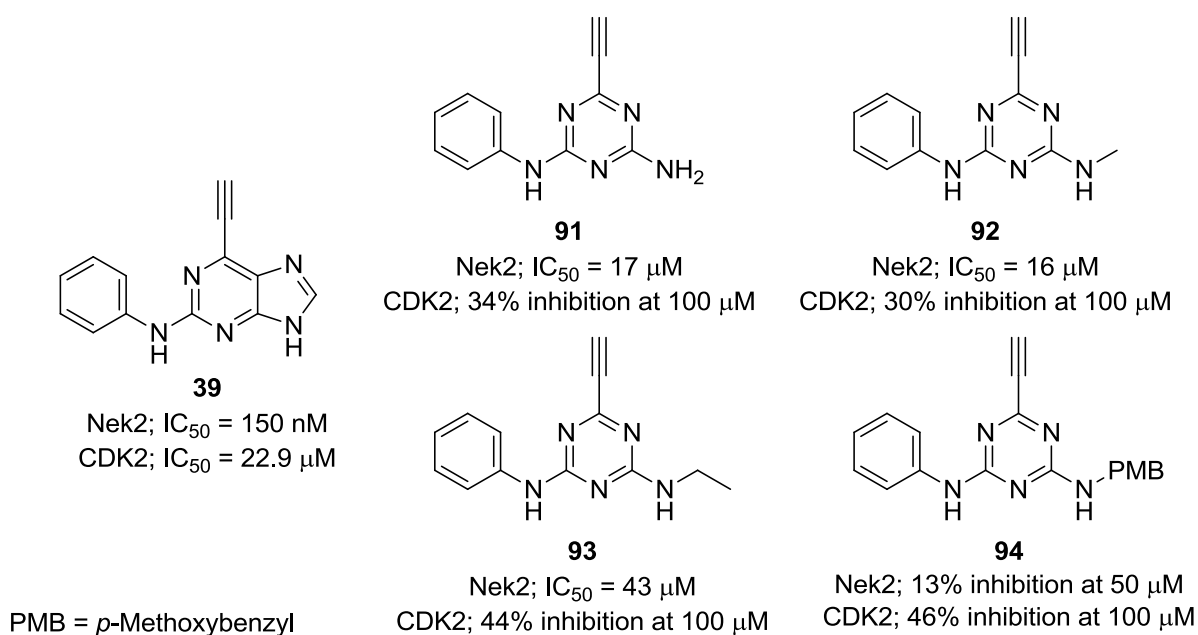


Figure 64 – Comparison of potency between triazines **91-94** and parent purine **39**.

Biological evaluation of the triazine series revealed that the unsubstituted amine derivative **91** and *N*-methylamine **93** were modest inhibitors of Nek2 with 17 μM and 16 μM Nek2 inhibitory activity, respectively. Extension of the *N*-alkyl chain was not tolerated as demonstrated by the reduction in potency of the *N*-ethylamine derivative **93** (Nek2; IC_{50} = 43 μM) and *N*-PMB-amine **94** (Nek2; 13% inhibition at 50 μM). This is likely due to a steric clash with the Met-86 gatekeeper residue of the Nek2 ATP-binding domain. All compounds were found to be essentially inactive in the CDK2 inhibition assay.

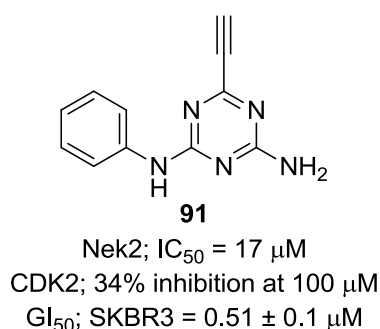


Figure 65.

Growth inhibition studies of compound **91** in SKBR3 cells gave a GI_{50} value of 0.51 ± 0.1 μM . Due to the poor Nek2 inhibitory activity (Nek2; IC_{50} = 17 μM) it is unlikely that growth inhibition is due to Nek2 inhibition, but rather, as a result of off-target activity. Further screening of this compound would be required to confirm this.

6.2.7 Pyrimidine Based Nek2 Inhibitors

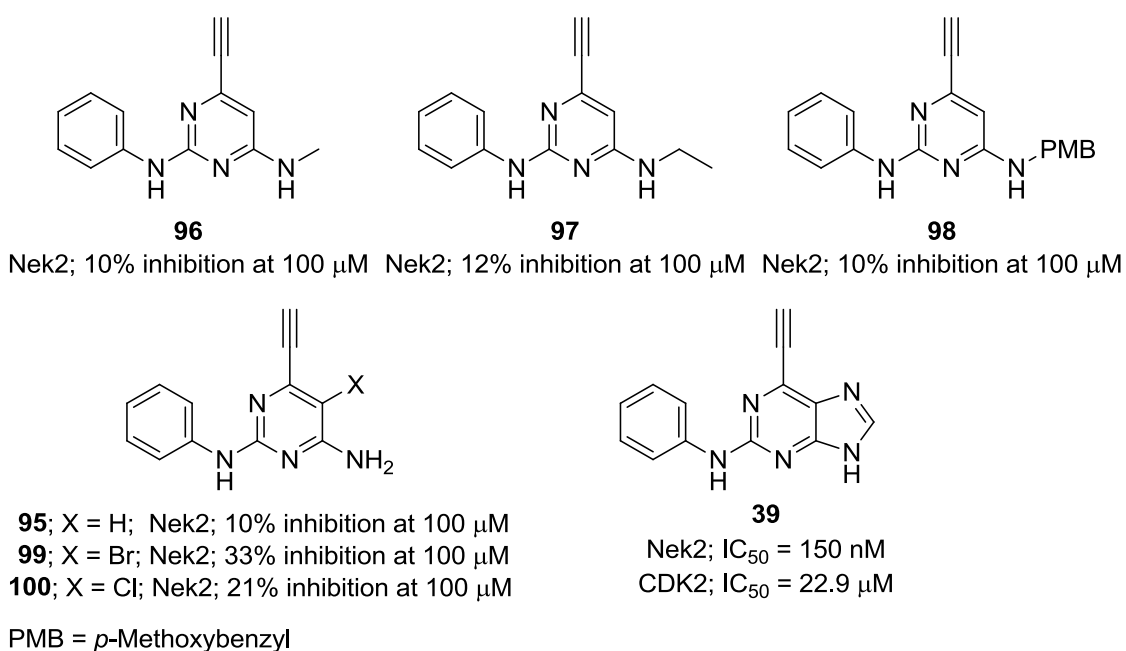
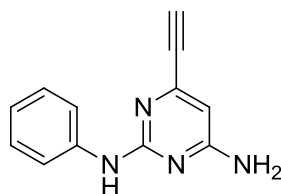


Figure 66 – Comparison of potency between pyrimidine series and parent purine **39**.

The pyrimidine series were found to be very weak inhibitors of Nek2, with IC_{50} values in excess of 100 μM observed for all compounds. It was suspected that the pyrimidine 4-amino group of this series cannot effectively mimic the purine N^9 H-bond interaction between **39** and the Nek2 hinge region, which reduces the initial ATP-competitive binding.

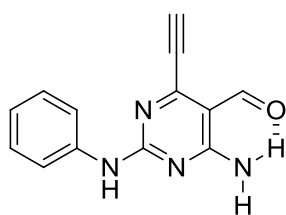
**95**

Nek2; 10% inhibition at 100 μM
 CDK2; IC_{50} = 19.2 μM
 GI_{50} ; SKBR3 = 4.9 ± 0.6 μM

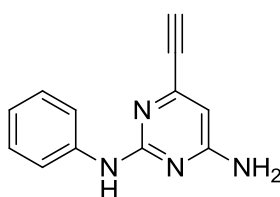
Figure 67.

Interestingly, pyrimidine **95** demonstrated moderate growth inhibitory activity in SKBR3 cells (GI_{50} = 4.9 ± 0.6 μM) despite exhibiting poor Nek2 inhibitory activity. To determine if off-target binding of pyrimidine **95** is responsible for this growth inhibition it would be useful to perform a selectivity screen against a broad panel of kinases.

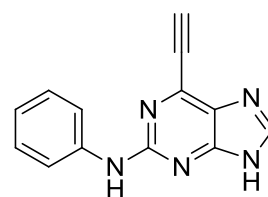
6.2.8 5-Formylpyrimidine (**101**)

**101**

Nek2; 40% inhibition at 10 μM
 CDK2; 43% inhibition at 100 μM
 GI_{50} ; SKBR3 = 0.47 ± 0.15 μM

**95**

Nek2; 10% inhibition at 100 μM
 CDK2; IC_{50} = 19.2 μM
 GI_{50} ; SKBR3 = 4.9 ± 0.6 μM

**39**

Nek2; IC_{50} = 150 nM
 CDK2; IC_{50} = 22.9 μM
 GI_{50} ; SKBR3 = 0.33 μM

Figure 68 – 5-Formylpyrimidine **101** has increased potency compared with pyrimidine **95** but lower Nek2 inhibitory activity than the parent purine **39**.

The formylpyrimidine compound **101** was assayed for Nek2- and CDK2-inhibitory activity. A 70-fold reduction in Nek2 inhibitory activity of **101** was observed when compared with the parent purine **39**. However, compound **101** was 40-fold more potent than pyrimidine **95**. A reduction in CDK2 inhibitory activity was also observed.

It is interesting to note that the 5-formylpyrimidine **101** was found to be 10-fold more potent in cells (GI_{50} ; SKBR3 = $0.47 \pm 0.15 \mu\text{M}$) than the non-formylated pyrimidine **95** (GI_{50} ; SKBR3 = $4.9 \pm 0.6 \mu\text{M}$) although it is unclear if this is due to Nek2 inhibition or an off-target effect.

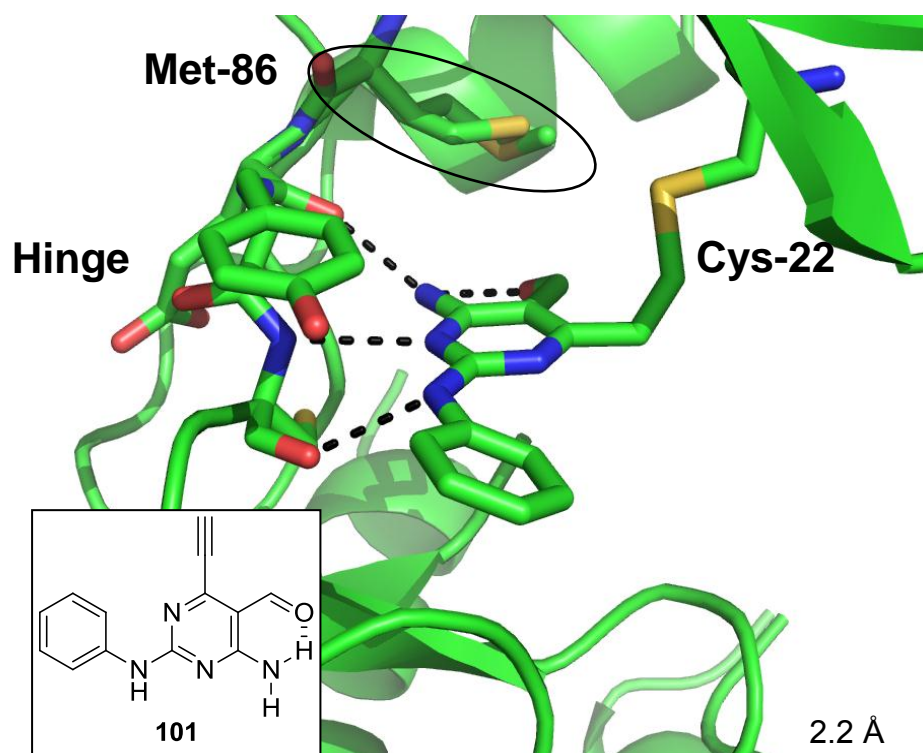


Figure 69 - X-ray crystal structure of **101** in complex with Nek2 suggested covalent modification of Cys-22. The side chain of the Met-86 gatekeeper residue was found to be present in both the conventional and flipped orientations. Note: further refinement is required to confirm ene-sulfide bond geometry.

Figure 69 showed covalent modification of Cys-22 by the pyrimidine 6-ethynyl group of **101**. The ligand binding was similar to that of the parent purine and the hinge H-bond interaction was clearly visible. The Met-86 gatekeeper residue was modelled in both the conventional and flipped orientation as the electron density suggested both conformers were present. A steric clash with Met-86 could therefore possibly explain the reduction in potency versus the parent purine **39**.

Chapter Seven: ^1H -qNMR Kinetic Experiments of Irreversible Nek2 Inhibitors

7.1 Introduction to Quantitative ^1H NMR (qNMR) Spectroscopy

NMR spectroscopy is commonly used as a primary method of measurement to allow structural elucidation of molecules.²⁵⁴ The first reported use of qNMR was by Hollis in 1963 for pharmaceutical analysis of commercial analgesics consisting of aspirin, phenacetin and caffeine.²⁵⁵ qNMR is now established as a vitally important technique in a range of fields, and is routinely used to characterise the composition of a variety of analytes including pharmaceutical preparations, natural products, peptides, agrochemicals, food products and biofluids (metabolomics).²⁵⁴ qNMR is a non-destructive method of analysis which has low uncertainty in quantification.²⁵⁶ Alternative approaches to quantification include high performance liquid chromatography (HPLC) and gas chromatography (GC). These analytical methods are commonly used for quantitative sample analysis, particularly within the pharmaceutical industry. However, as these techniques rely upon the physicochemical differences of analytes rather than structural complexity, good chromatographic properties are required for accurate analysis. Additionally, mixtures of polar compounds with low molecular weights and poor chromophores can be particularly problematic, and often require high levels of optimisation to obtain good chromatographic separation and accurate quantification. By comparison, qNMR analysis of these types of compounds is often relatively straightforward.²⁵⁷ A further advantage of qNMR over chromatographic analysis techniques is the ease of sample preparation. qNMR can be used to rapidly analyse complex mixtures such as urine or plasma, often with minimal sample preparation.²⁵⁶

7.2 Prerequisites for Successful qNMR Analysis

There are a number of prerequisites for accurate quantitative NMR analysis. The first of these is the choice of analysis peak. The signal intensity (I) observed after an NMR experiment directly relates to the number of nuclei (N) responsible for said signal multiplied by the spectrometer constant (K_s), as shown in the equation

($I = K_s \cdot N$). To allow accurate qNMR measurement of peak intensity, it is essential that this peak be distinct from others around it in order to prevent overlap. This is known as “purity of the NMR signal”.²⁵⁴

Early NMR instruments suffered from low sensitivity and precision of quantification, which made qNMR experiments disfavoured. This is not an issue for modern instruments as there are a number of methods for maximising sensitivity, including high-field strength (>400 MHz instrument), gradient shimming techniques for improved spectra quality, and specialised probes. To optimise the accuracy of integration it is essential that the baseline noise is minimal to allow the maximum signal-to-noise ratio. A way of doing this is by using inverse- or cryo-probes which can increase the signal-to-noise by more than ten-fold. However, these probes are expensive and can make this approach cost-prohibitive. A simpler and more economical solution to improve the signal-to-noise ratio is to increase the concentration of analyte by reducing the volume of solvent, although this is limited by the solubility of the analyte in the chosen solvent. Finally, increasing the number of scans can be used to enhance the signal-to-noise ratio.²⁵⁴ This may not be appropriate for kinetic experiments as the ratio of reactants and products is dynamic, which may result in inaccurate data collection.

A problem often encountered during qNMR experiments is the presence of spinning side bands caused by variations in the magnetic field. These peaks appear either side of a genuine signal at a distance directly proportional to the frequency of rotation. In standard qNMR experiments these are avoided by simply preventing sample rotation.²⁵⁴ This is not possible in the case of a kinetic experiment where sample homogenisation is important. In our experiments spinning side bands were not a problem owing to the high field strength (500 MHz) of the instrument used, and the nature of the peak being investigated (ethynyl C-H).²⁵⁸

A further consideration is the presence of ^{13}C satellite peaks. These interfering peaks appear at the sides of a genuine peak and arise from $^1\text{H}/^{13}\text{C}$ coupling between adjacent nuclei. ^{13}C satellites can be avoided through heteronuclear decoupled experiments or, as our experiments, by using an instrument of high field strength (>400 MHz).^{254,258}

7.3 Optimisation of Relaxation Time - Inversion Recovery Experiment

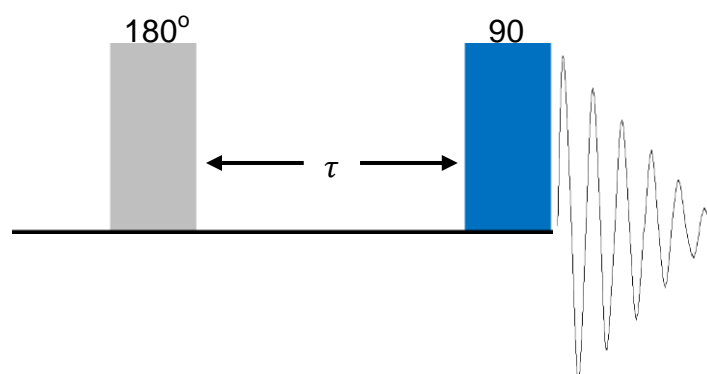


Figure 70 - NMR inversion recovery pulse sequence (adapted from Claridge).²⁵⁹

It is important to calculate the longitudinal relaxation time (T_1) of nuclear spin in-order to guarantee the best possible signal. The maximal theoretical recovery of magnetisation (99.33%) after a 90° rf pulse is obtained after a period of at least $5T_1$. One may determine the value of T_1 in seconds (T_1 s) through inversion recovery sequence experiments (Figure 70). A 180° rf pulse is used to disrupt the nuclear spin from its thermal equilibrium causing inversion of the spin population from $z+$ to $z-$, which results in a negative signal (Figure 71, **A – B**). The system responds to offset this change and re-establish equilibrium, through the loss of energy in the form of heat. As the spin populations precess from $-z$ towards the x - y intercept the signal is reduced to zero and then recovers to $+z$ (Figure 71, **B – C**). Magnetisation along the z plane is unobservable, so after a period of time (τ) a second pulse of 90° is used to return the vector to the x - y plane (Figure 71, **C – D**).²⁵⁹

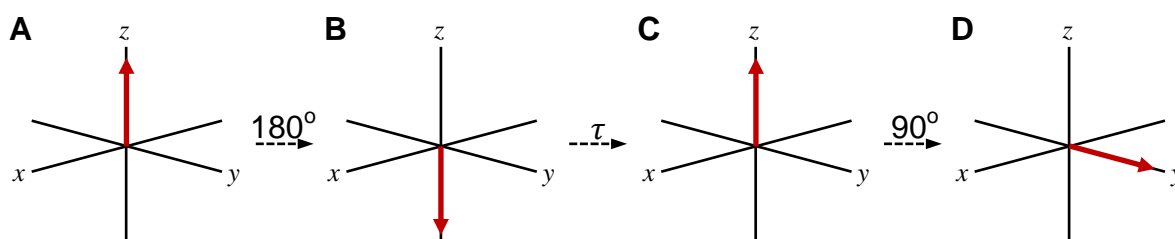


Figure 71 - Inversion recovery sequence (adapted from Claridge).²⁵⁹

If $\tau = 0$, there is no recovery of spin population, and thus the magnetisation vector remains at $-z$ (Figure 72, **A – B**). A 90° pulse is then used causing the spin

population to precess from $-z$ to $-y$ with the maximum possible signal intensity (Figure 72, **B – C**). This results in a negative or ‘inverted’ spectrum.

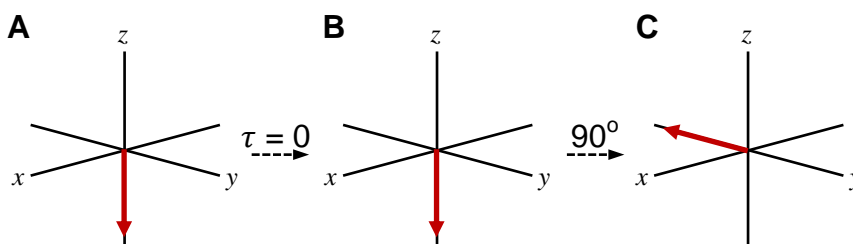


Figure 72.

By contrast, gradually increasing the value of τ to the point where $\tau_\infty > 5T_1$ allows complete relaxation to occur, resulting in the maximum positive signal at $+y$ (Figure 73, **A – C**).²⁵⁹

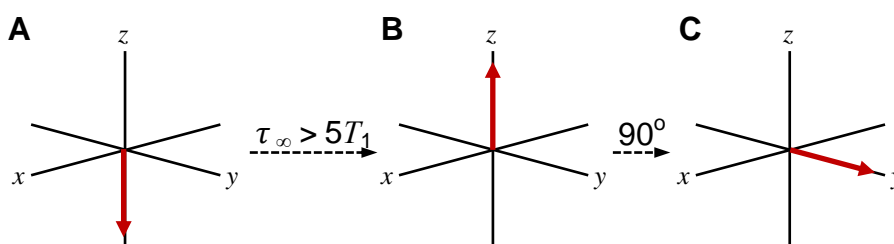


Figure 73.

Accurate calculation of T_1 in most cases is both time consuming and unnecessary due to the variety of nuclei and T_1 s values observable within the analyte. It is possible to quickly estimate T_1 by monitoring the disappearance of signals during the recovery of spin population.

The Bloch theory of NMR (Equation 2) states that recovery of $+z$ magnetisation (M_z) is exponential and can be described using Equation 2.

$$\frac{dM_z}{dt} = \frac{(M_0 - M_z)}{T_1}$$

Therefore:

$$M_z = M_0(1 - e^{-t/T_1})$$

Equation 2 - Bloch Equation (adapted from Claridge).²⁵⁹

M_0 represents the magnetisation at thermal equilibrium. The time taken for this process to occur is represented by the constant T_1 . This equation can be modified to calculate the intensity of magnetisation (M_t) as shown in Equation 3.

$$M_t = M_0(1 - 2e^{-\tau/T_1})$$

Equation 3.

When the longitudinal magnetisation reaches the x - y intercept (at time τ_{null}) the population difference equals zero, resulting in an M_t value also of zero. The above equation can therefore be rearranged to give:

$$\tau_{null} = T_1 \ln 2$$

Therefore:

$$T_1 = \frac{\tau_{null}}{\ln 2} = 1.443 \tau_{null}$$

Equation 4.

An inversion recovery experiment was used to determine the optimum relaxation time for the ethynyl C-H of purine **56** (Figure 74). The experiment was run using the pulse program shown in Figure 70, whilst incrementally increasing the recovery time (τ) between pulses until a positive signal for the ethynyl C-H was observed. An initial recovery time of zero ($\tau = 0$) (shown in black) was used to obtain the maximum negative signal. The recovery time (τ) was gradually increased until the signal for the ethynyl C-H proton was no longer visible (τ_{null}), which occurred at a time of 4 s (shown in orange). For this compound a relaxation time (T_1) of 5.8 s was obtained using Equation 4. To obtain the maximum theoretical recovery of magnetisation, and obtain the strongest possible signal, this value was multiplied by 5 to give an optimum relaxation time of 28.9 s.

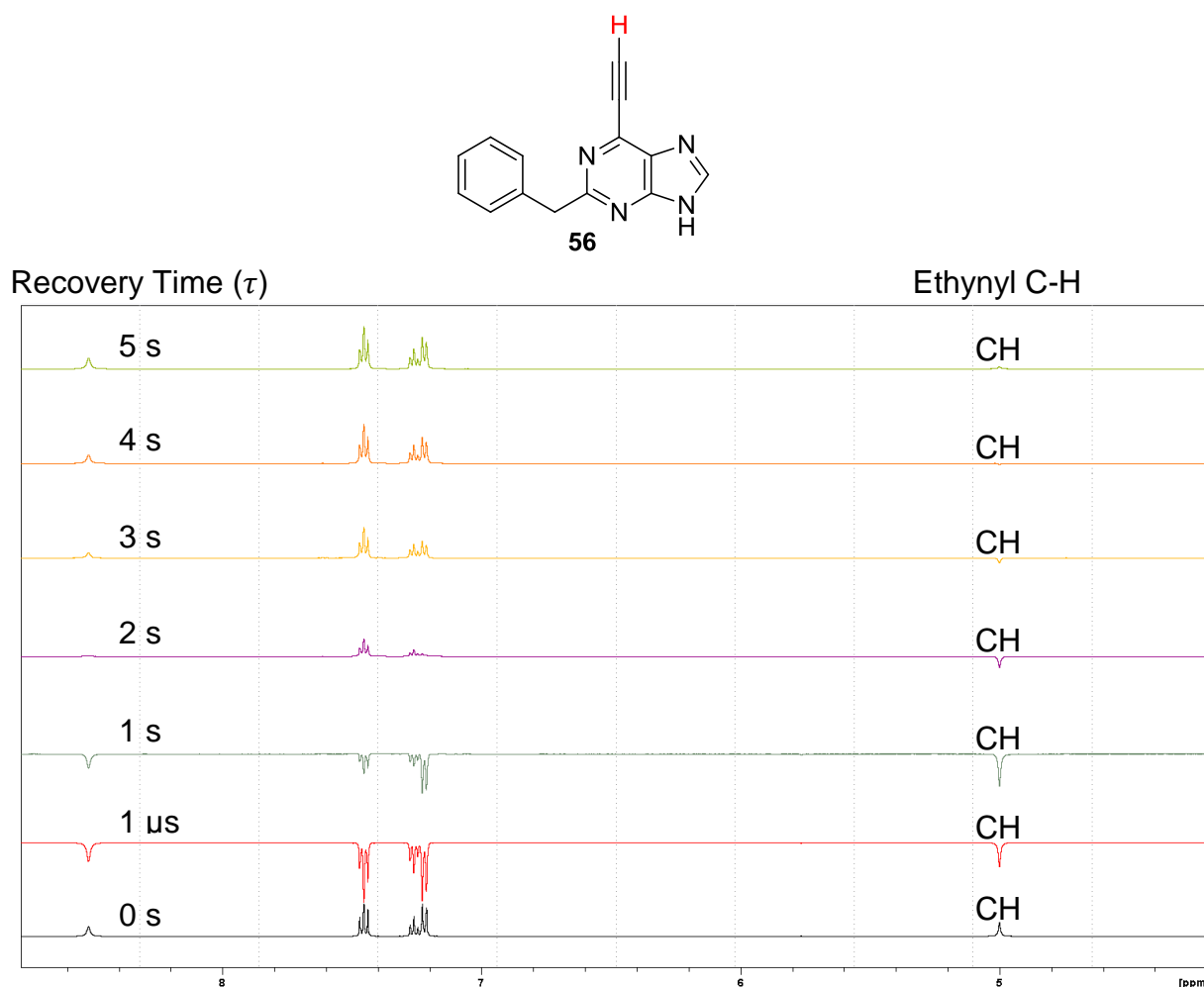


Figure 74 - ^1H -NMR inversion recovery experiment for purine **56**.

7.4 qNMR Kinetic Analysis of Irreversible Nek2 Inhibitors

Before commencing the qNMR experiment, there were a number of considerations necessary for the design of the reaction. Firstly, the choice of deuterated solvent is of importance. Initial attempts were made using D_2O as the reaction solvent to mimic physiological conditions. Unfortunately, D_2O was found to be unsuitable for use in this reaction due to the poor solubility of reagents.²⁶⁰ $\text{DMSO-}d_6$ proved a suitable alternative as it provided excellent solubility, and the residual solvent peak is at 2.50 ppm (^1H NMR) which does not interfere with analysis. Sample concentration was another important factor that needed to be addressed. As stated previously, to improve the signal-to-noise ratio, sample concentration may be increased, but factors such as solubility and availability of starting materials limit the achievable concentration.²⁵⁴ A concentration of 6 mmol/L was found to provide a good balance between these two factors, and so this concentration was chosen for all experiments.

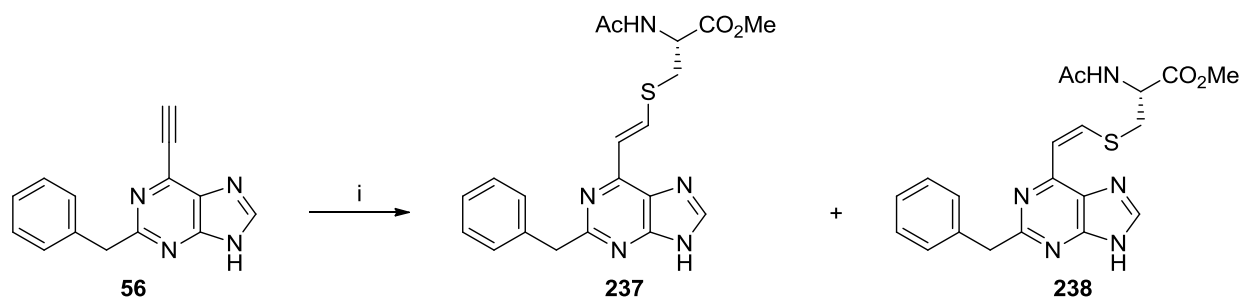
Finally, the temperature at which the reaction is performed is closely related to the overall rate of reaction. It was determined that a temperature of 24 °C allowed analysis of 6-ethynylpurine **39** over a period of 4-5 h, providing multiple analysis points that were ideal for accurate rate measurement.²⁶⁰

N-Acetylcysteine methyl ester **239** was chosen as a suitable nucleophile for this reaction due to the similar reactivity of its thiol group to that of Cys-22 within the Nek2 ATP-binding domain. A 10-fold excess of **239** relative to the ethynyl compound was used to ensure that *pseudo*-first-order kinetics were maintained. A *pseudo*-first-order reaction is a second-order reaction that utilises a large excess of one reagent (>10-fold). In doing so, no appreciable change in the concentration of this reagent is observed, which greatly simplifies calculation of the apparent rate constant k' from the equation: $\text{rate} = k' \cdot [A]$.²⁶¹

1,4-Diazabicyclo[2.2.2]octane (DABCO) was chosen as a base owing to its simple NMR profile and good solubility in DMSO- d_6 . 0.30 mole equivalents of DABCO were sufficient to catalyse the reaction of 6-ethynylpurine **56** and thiol **239** at an observable rate.²⁶⁰ It is thought that DABCO deprotonates **239** to form the thiolate, which is approximately 100-fold more reactive than the parent thiol.²⁶⁰ Although the uncatalysed reaction still proceeds, the DABCO-catalysed reaction is more kinetically favoured, resulting in rate enhancement without alteration of reaction order.²⁶²

An appropriate internal standard is vital for successful qNMR analysis. The NMR signal from the internal standard must appear in a distinct region of the NMR spectra for accurate quantification. The standard should also have good solubility in the chosen solvent, be chemically inert, and have low volatility so that the concentration remains constant throughout the experiment.²⁵⁶ DMF fulfilled all of these criteria and was chosen as the internal standard. One mole equivalent of DMF was used, which allowed baseline-correction based upon the formyl proton at 7.95 ppm (^1H NMR, DMSO- d_6). Reaction progress was observed by monitoring the change in intensity over time of the terminal ethynyl C-H of the electrophiles **54**, **56**, **88**, **89**, and **90** relative to the DMF internal standard.

7.5 qNMR Kinetic Analysis – Results

7.5.1 Reaction of 2-Benzylpurine (56) with *N*-Acetylcysteine Methyl Ester (239)

Reagents and Conditions: i) **239**, DABCO, DMF, DMSO- d_6 , 24 °C, analysed every 10 min.

Scheme 69.

The first compound to be investigated was the 2-benzylpurine derivative **56**. It was predicted that replacement of the electron-donating aniline conjugated to the purine for **39**, by the non-conjugated benzyl group **56** might increase reactivity of the 6-ethynyl group to nucleophilic attack. Using the conditions previously established for 6-ethynypurine **39**, **56** was successfully reacted with **239**. The reaction reached completion after approximately 2 h and obeyed *pseudo*-first-order kinetics as shown by the linear relationship observed between $\ln[\mathbf{56}]$ and time (Figure 75).

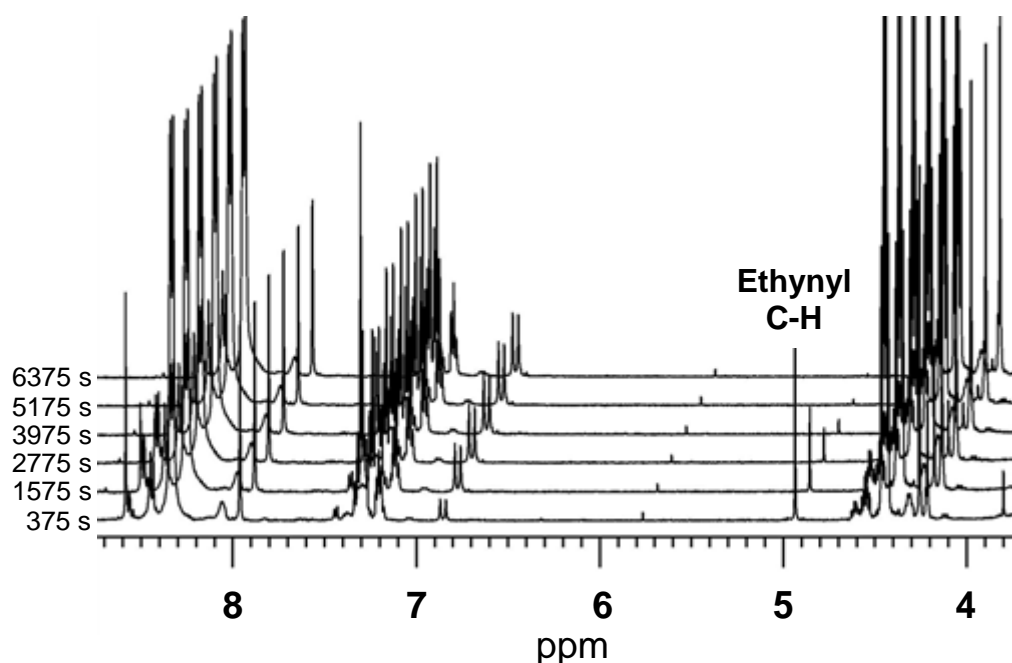


Figure 75 - ^1H -NMR spectrum (500 MHz) stacked plot showing consumption of **56**.

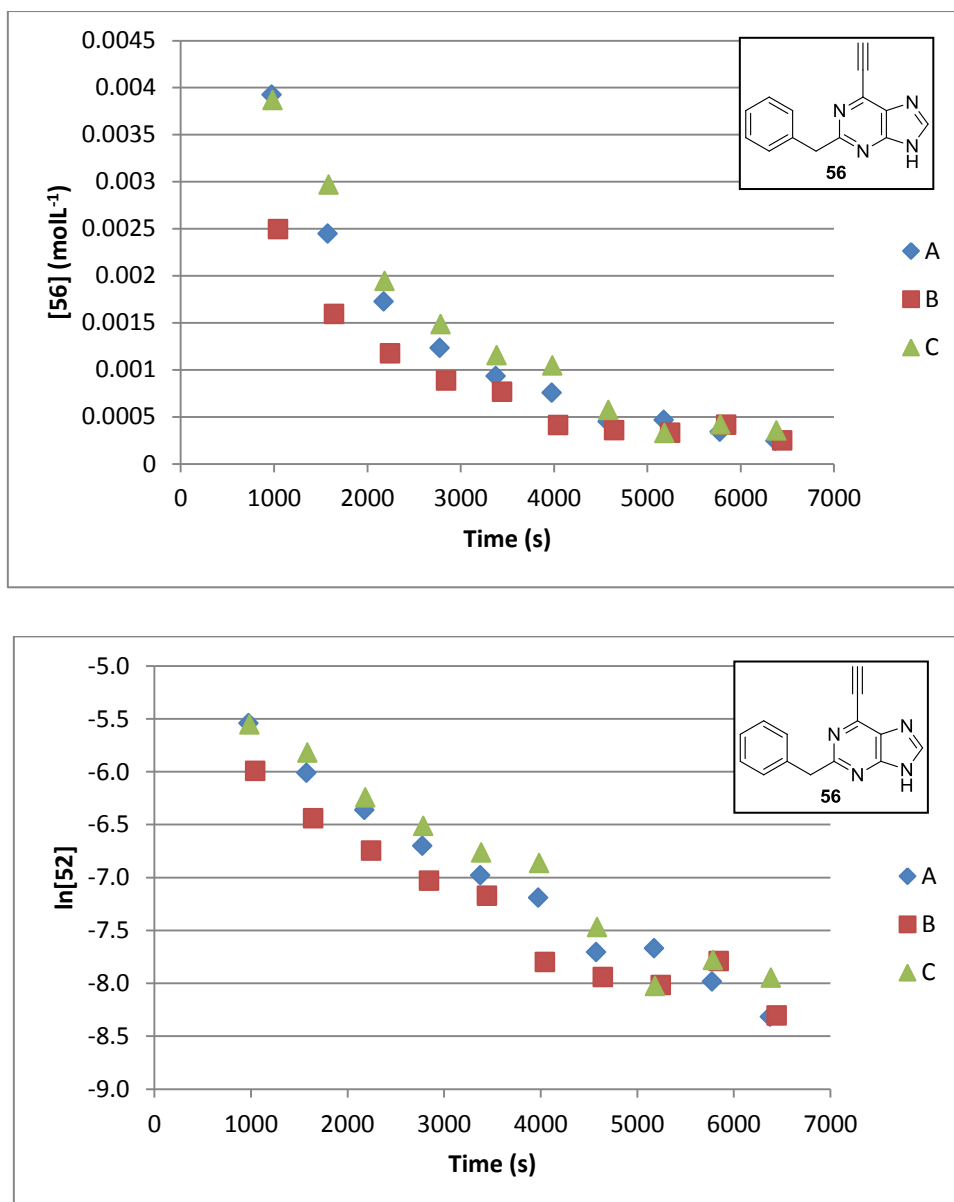


Figure 76 – Consumption of benzylpurine **56** following reaction with *N*-acetylcysteine methyl ester (**239**). The reaction was performed in triplicate (A-C) and was monitored through the disappearance of the ethynyl proton at δ 4.94 using ¹H-NMR (500 MHz, DMSO).

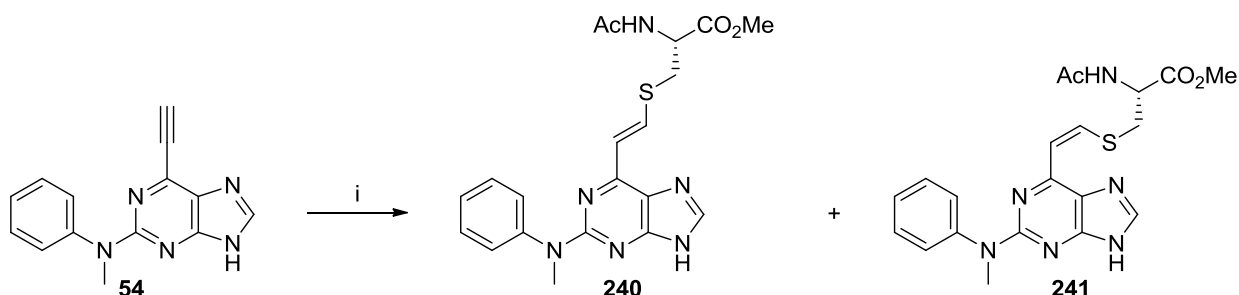
Table 3 - Apparent rate constants (k') and half-life (s) for the reaction of **56** with **239**.

ID	k' ($\times 10^{-4} \text{ s}^{-1}$)	R^2	$t_{1/2}$ (s)
a	5.00	0.9832	1386
b	4.90	0.9203	1415
c	4.80	0.9564	1444

Using these data the average value of k' was determined as $4.90 \times 10^{-4} \text{ s}^{-1}$ with a standard deviation (SD) of $1.0 \times 10^{-5} \text{ s}^{-1}$. Interestingly, despite predictions of a

marked increase in the rate of reaction when compared to parent purine **39** ($k' = 4.6 \times 10^{-4} \text{ s}^{-1}$), no significant gain in reactivity was observed with **56**. The average half-life ($t_{1/2}$) was determined as $1415 \pm 29 \text{ s}$. The coefficient of determination (R^2) ranged from 0.9203-0.9832, indicating a good fit for the data.

7.5.2 Reaction of 2-Methylanilinopurine (**54**) with Thiol (**239**)



Reagents and Conditions: i) **239**, DABCO, DMF, $\text{DMSO-}d_6$, 24°C , analysed every 10 min.

Scheme 70.

The conditions used previously (0.30 mole equivalents DABCO) were employed for the reaction of the 2-methylanilino-6-ethynylpurine **54** with thiol **239**. The reaction proceeded more slowly than for the parent purine **39** and did not reach completion after 5 h. Data analysis was thus limited to the first 160 minutes of the reaction as no useful information was obtained after this time-point. This compound obeyed *pseudo*-first-order kinetics as shown through the linear relationship between $\ln[(\mathbf{54})]$ and time (Figure 78).

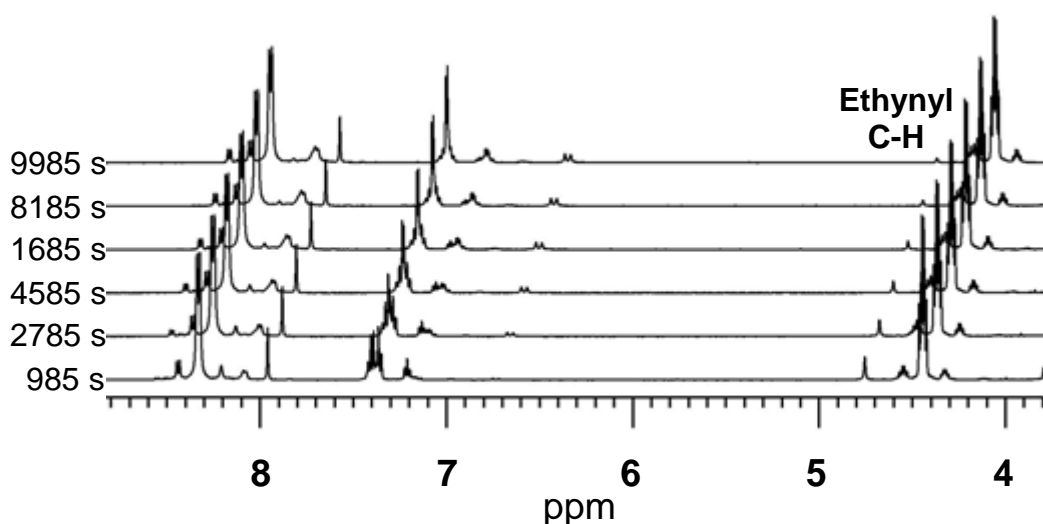


Figure 77 - ^1H -NMR spectrum (500 MHz) stacked plot showing consumption of **54**.

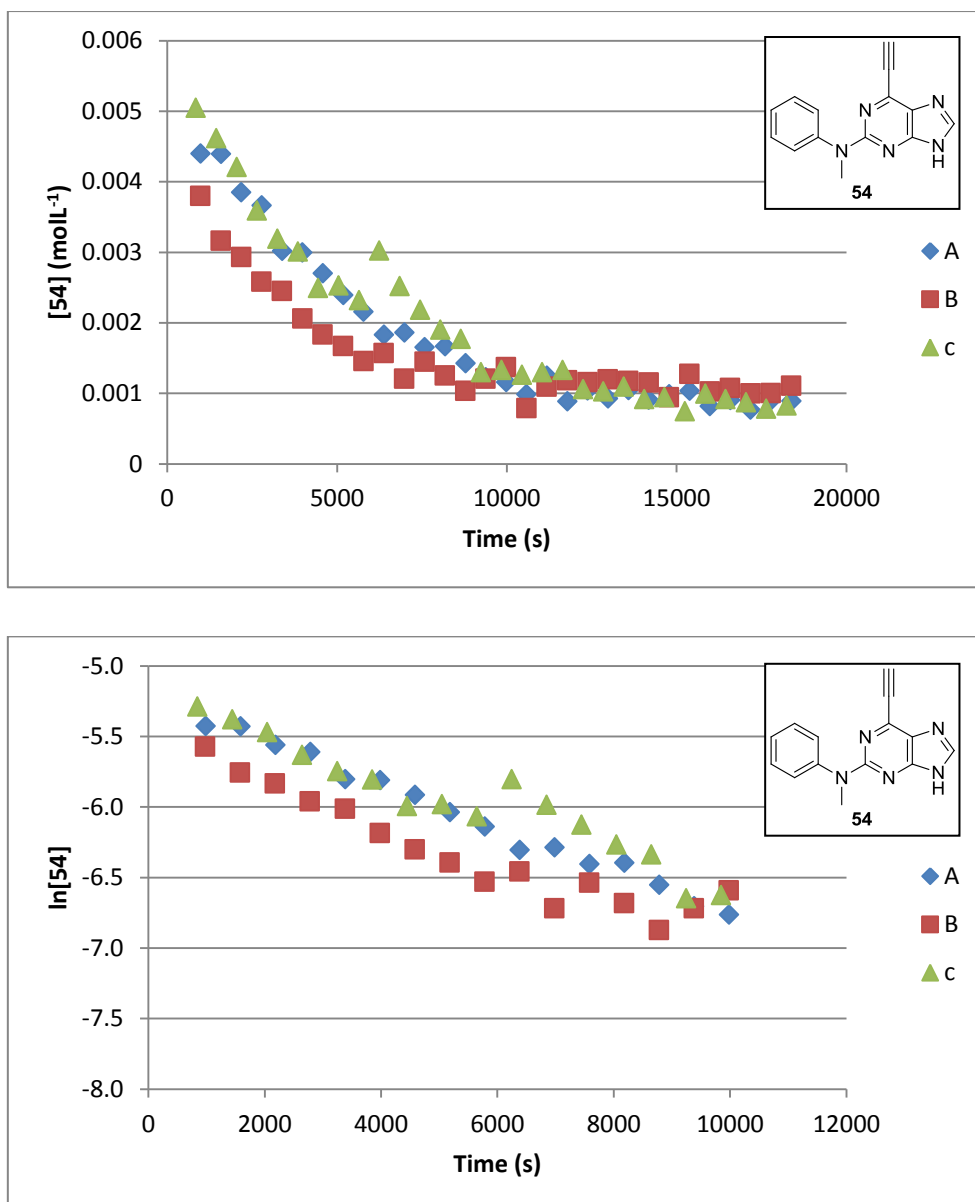


Figure 78 – Consumption of *N*-methylanilino-purine **54** following reaction with *N*-acetylcysteine methyl ester (**239**). The reaction was performed in triplicate (A-C) and was monitored through the disappearance of the ethynyl proton at δ 4.75 using ¹H-NMR (500 MHz, DMSO).

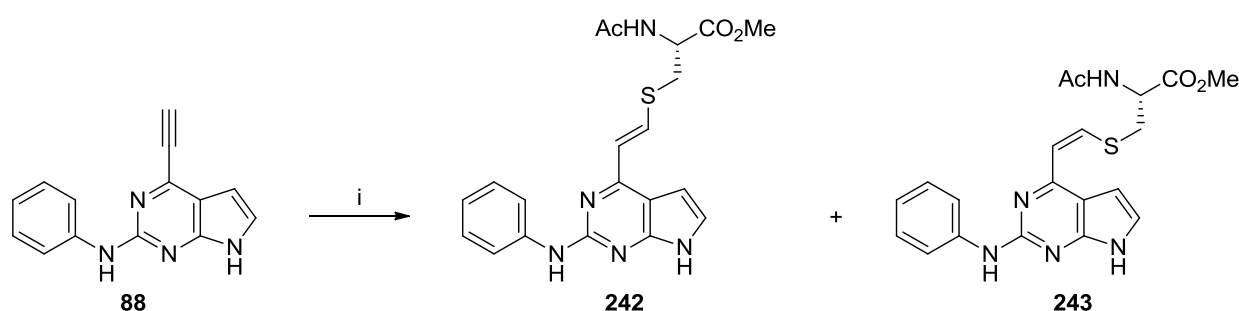
Table 4 - Apparent rate constants (k') and half-life for the reaction of **54** with **239**.

ID	$k'(\times 10^{-4} \text{ s}^{-1})$	R^2	$t_{1/2} \text{ (-s)}$
a	1.50	0.9895	4621
b	1.30	0.8869	5332
c	1.30	0.9141	5332

The average k' value was $1.40 \times 10^{-4} \text{ s}^{-1}$ with an SD of $1.2 \times 10^{-5} \text{ s}^{-1}$. This value is 4-fold lower than the k' value obtained for **56**. It is possible that the electron-donating

character of the conjugated side chain of **54** increases the overall electron density of the purine core, reducing the electrophilicity of the 6-ethynyl group and hence reactivity towards thiol **239**. The average $t_{1/2}$ was determined as 5072 ± 410 s. The relatively high SD value indicates a lack of consistency between datasets, and additional repeat reactions would likely lower this value leading to a more accurate dataset. The R^2 values range from 0.8869 – 0.9895 indicating a good data fit.

7.5.3 Reaction of Pyrrolopyrimidine (**88**) with Thiol (**239**)



Reagents and Conditions: i) **239**, DABCO, DMF, DMSO- d_6 , 24 °C, analysed every 10 min.

Scheme 71.

The first of the alternative heterocycles to be investigated was pyrrolopyrimidine **88**. This compound had shown modest Nek2-inhibitory activity ($IC_{50} = 24 \mu M$) which was attributed to the low electrophilicity of the ethynyl group due to increased electron density relative to the parent purine **39**. This compound proved particularly unreactive, and after 5 h the reaction had reached approximately 50% conversion of pyrrolopyrimidine **88** to the *E* and *Z* alkenes **242** and **243**. *Pseudo*-first-order kinetics was observed as indicated by the linear relationship between $\ln[88]$ and time (Figure 80).

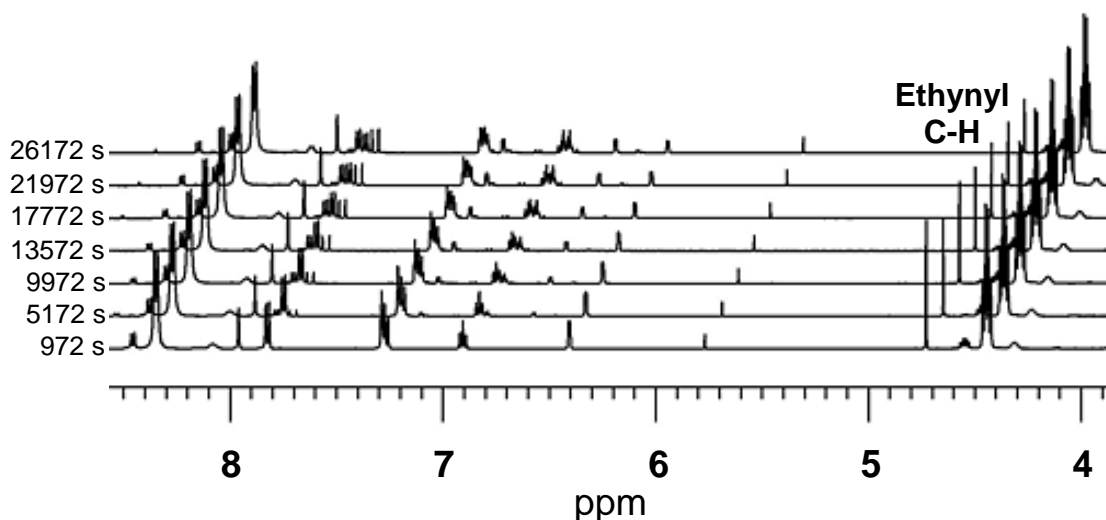


Figure 79 - 1H -NMR spectrum (500 MHz) stacked plot showing consumption of **88**.

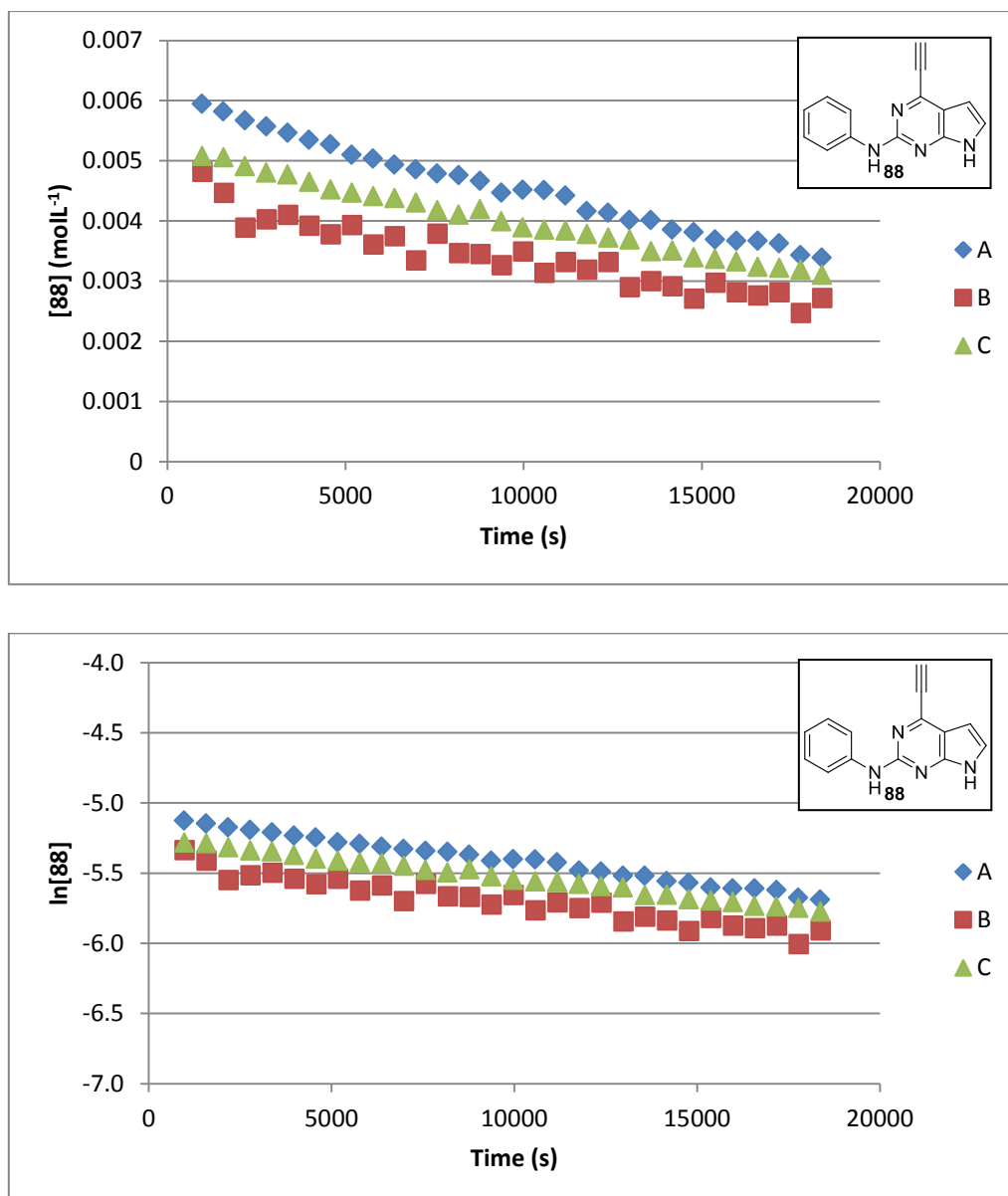


Figure 80 – Consumption of pyrrolopyrimidine **88** following reaction with *N*-acetylcysteine methyl ester (**239**). The reaction was performed in triplicate (A-C) and was monitored through the disappearance of the ethynyl proton at δ 4.71 using ¹H-NMR (500 MHz, DMSO).

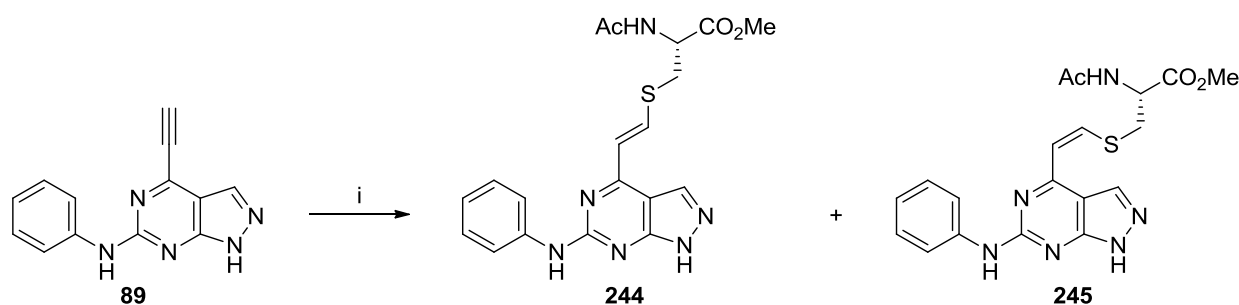
Table 5 - Apparent rate constants (k') and half-life for the reaction of **88** with **239**.

ID	$k'(\times 10^{-4} \text{ s}^{-1})$	R^2	$t_{1/2} \text{ (-s)}$
a	0.031	0.9939	22360
b	0.030	0.9187	23105
c	0.028	0.9951	24755

Pyrrolopyrimidine **88** was the least reactive compound investigated. An average k' value of $3.0 \times 10^{-6} \text{ s}^{-1}$ was obtained with an SD of $1.5 \times 10^{-6} \text{ s}^{-1}$. This compound was

150-fold less reactive than the parent purine **39** ($k' = 4.46 \times 10^{-4} \text{ s}^{-1}$) and had a $t_{1/2}$ of $6.5 \pm 0.34 \text{ h}$.²⁶⁰ The R^2 values range from 0.9187 – 0.9951 indicating a good data fit. These results demonstrate the need for an electron deficient heterocycle to maintain ethynyl reactivity towards electrophilic thiols.

7.5.4 Reaction of Pyrazolopyrimidine (**89**) with Thiol (**239**)



Reagents and Conditions: i) **239**, DABCO, DMF, DMSO- d_6 , 24 °C, analysed every 10 min.

Scheme 72.

The second alternative heterocycle to be investigated was pyrazolopyrimidine **89**. This compound had potent irreversible Nek2-inhibitory activity ($\text{IC}_{50} = 430 \text{ nM}$) comparable with the parent purine **39** ($\text{IC}_{50} = 150 \text{ nM}$). Initial reaction attempts using 0.30 mole equivalents of DABCO resulted in consumption of pyrazolopyrimidine **89** at a rate too fast for accurate observation. By reducing the concentration of DABCO to 0.03 mole equivalents the reaction proceeded at a slower rate, allowing monitoring over a period of 2 h. Due to insufficient availability of **89** it was only possible to perform a single repeat reaction rather than two repeats, as is convention.

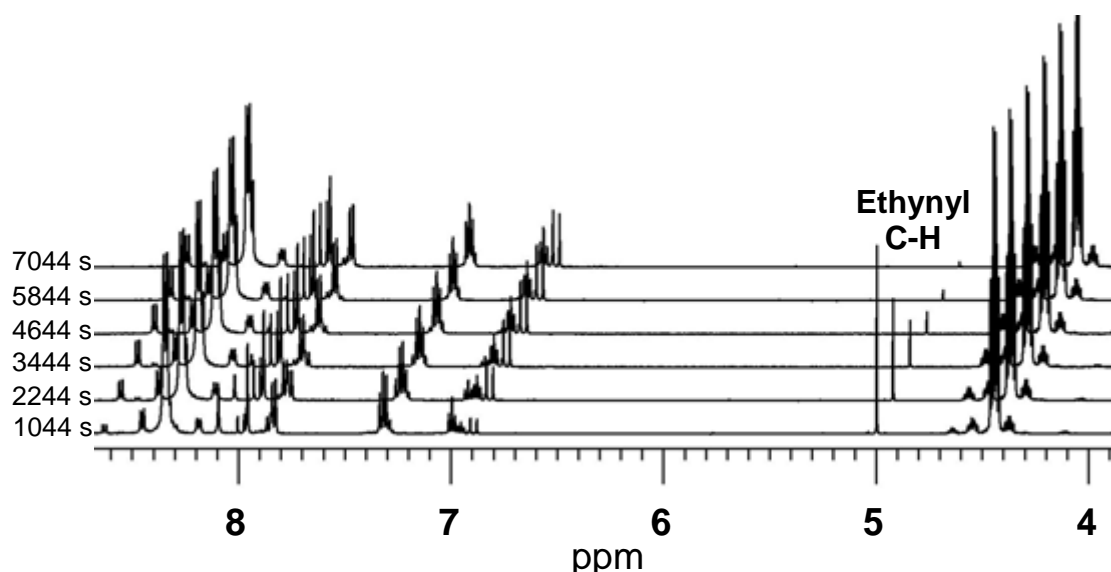


Figure 81 - ^1H -NMR spectrum (500 MHz) stacked plot showing consumption of **89**.

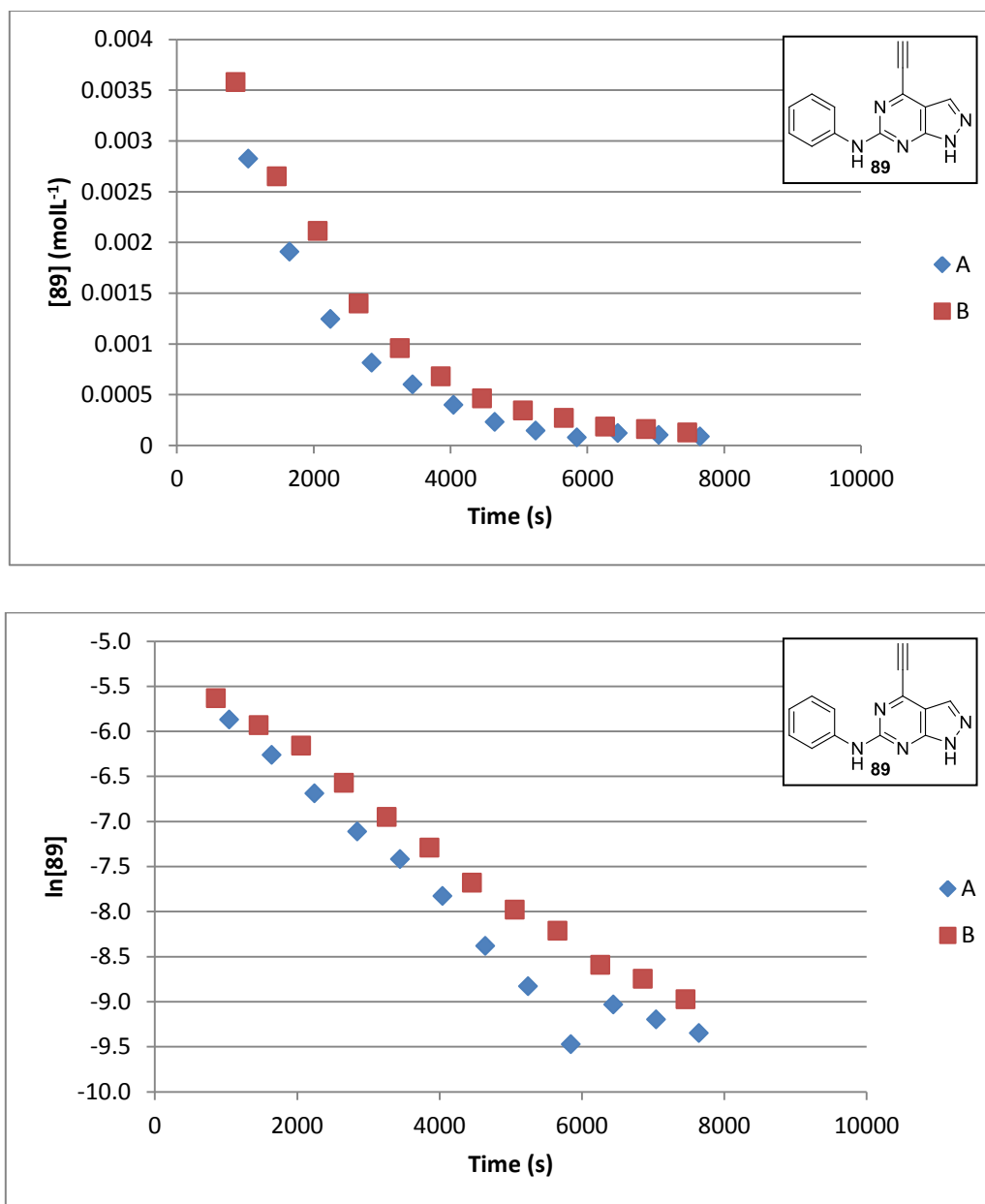


Figure 82 – Consumption of pyrazolopyrimidine **89** following reaction with *N*-acetylcysteine methyl ester (**239**). The reaction was performed in duplicate (A and B) and was monitored through the disappearance of the ethynyl proton at δ 4.98 using ¹H-NMR (500 MHz, DMSO).

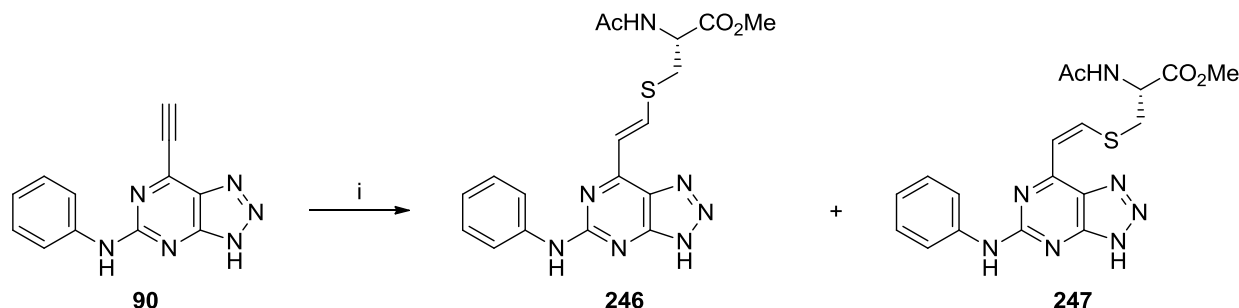
Table 6 - Apparent rate constants (k') and half-life for the reaction of **89** with **239**.

ID	$k'(\times 10^{-4} \text{ s}^{-1})$	R^2	$t_{1/2} \text{ (-s)}$
a	5.29	0.9408	1218
b	5.69	0.9937	1310

The average k' value of **89** was determined as $5.49 \times 10^{-4} \text{ s}^{-1}$ (SD of $2.82 \times 10^{-5} \text{ s}^{-1}$) demonstrating a high rate of reaction with thiol **239**. Compound **89** obeyed *pseudo*-

first order kinetics and had an average $t_{1/2}$ of 1263 ± 65 s. The R^2 values of the dataset ranged from 0.9408-0.9937 indicating a good data fit.

7.5.5 Reaction of Triazolopyrimidine (90) with Thiol (239)



Reagents and Conditions: i) **239**, DABCO, DMF, DMSO-*d*₆, 24 °C, analysed every 10 min.

Scheme 73.

The final heterocycle to be investigated was the triazolopyrimidine derivative **90**. This compound was found to be a potent irreversible inhibitor of Nek2 ($IC_{50} = 130$ nM), and this was attributed to the electron-deficient heterocycle enhancing ethynyl reactivity towards thiol nucleophiles. Early reactions using 0.03 mole equivalents of DABCO proceeded very rapidly, and the reaction was complete within 30 minutes. Standard qNMR methodology was inadequate as only 3 data points were collected per experiment which was insufficient for accurate analysis. The solution to this problem was to reduce the number of scans from 8 to 4, which shortened the overall experiment time and increased the number of data points collected.

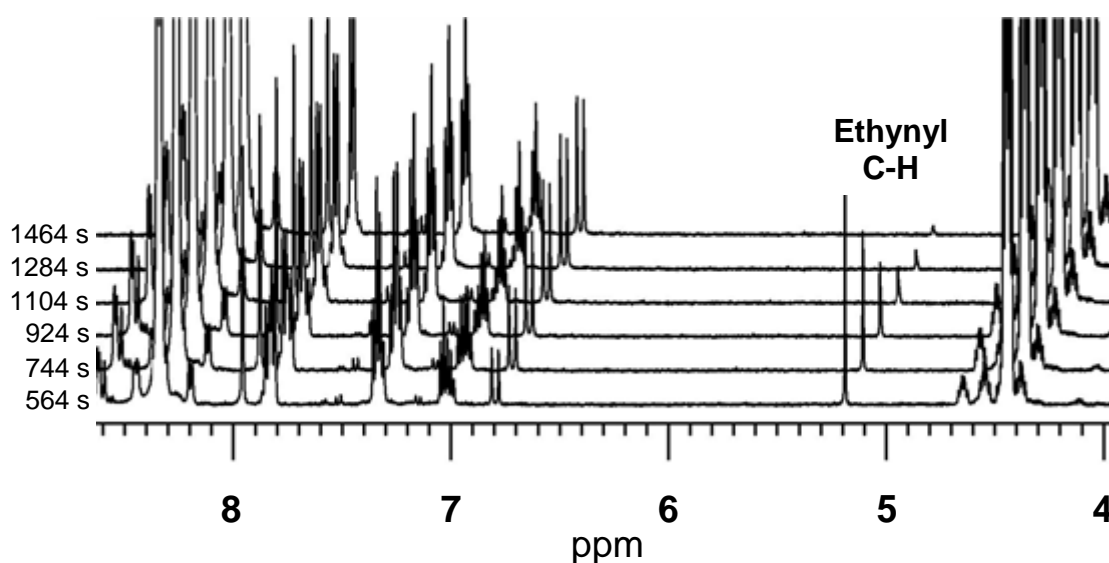


Figure 83 - ¹H-NMR spectrum (500 MHz) stacked plot showing consumption of **90**.

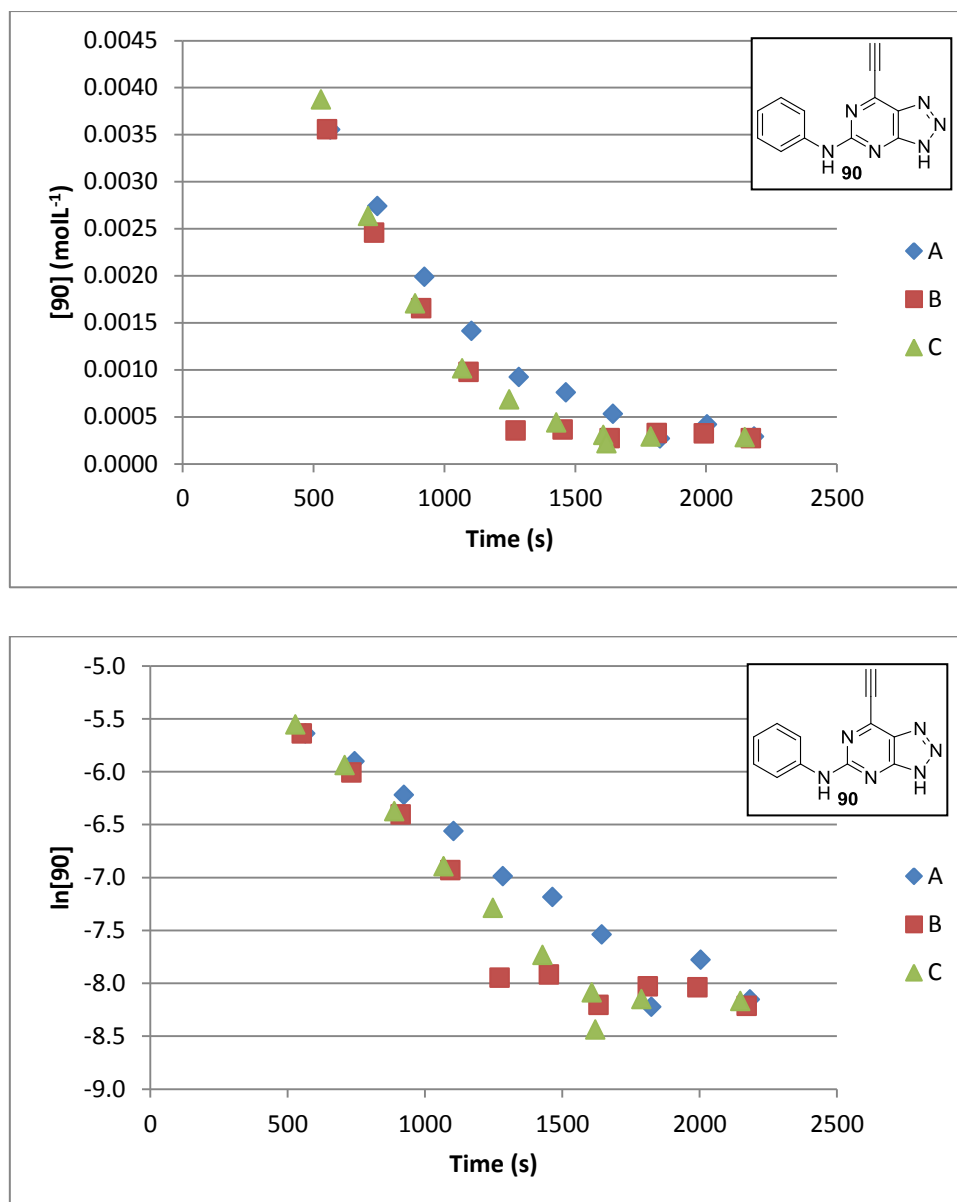


Figure 84 – Consumption of triazolopyrimidine **90** following reaction with *N*-acetylcysteine methyl ester (**239**). The reaction was performed in triplicate (A-C) and was monitored through the disappearance of the ethynyl proton at δ 5.19 using ¹H-NMR (500 MHz, DMSO).

Table 7 - Apparent rate constants (k') and half-life for the reaction of **90** with **239**.

Triazolopyrimidine **90** was more than 3-fold more reactive than pyrazolopyrimidine

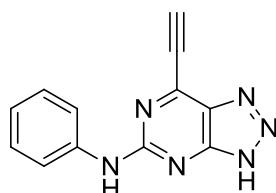
ID	$k'(\times 10^{-4} \text{ s}^{-1})$	R^2	$t_{1/2}$ (-s)
A	16.5	0.9524	420
B	16.6	0.8291	419
C	19.0	0.8882	365

89 and had an average k' value of $17.4 \times 10^{-4} \text{ s}^{-1}$ (SD = $1.42 \times 10^{-4} \text{ s}^{-1}$). The average $t_{1/2}$ was only $401 \pm 31 \text{ s}$ and the R^2 value ranged from 0.8291 - 0.8882 indicating

acceptable fit. Quality of data could possibly be improved by further increasing the number of data points and discounting data after 1600 s. However, this was not possible with the instrumentation available.

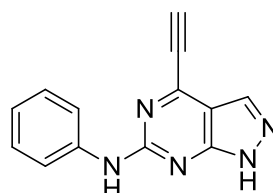
7.6 Discussion

High Reactivity



90

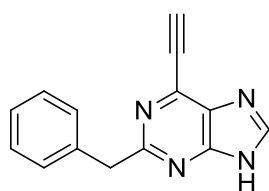
Nek2; IC_{50} = 130 nM
 $k' = 1.7 \times 10^{-3} \text{ s}^{-1}$



89

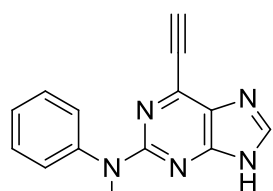
Nek2; IC_{50} = 430 nM
 $k' = 5.5 \times 10^{-4} \text{ s}^{-1}$

Moderate Reactivity



56

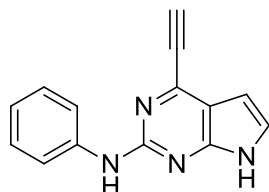
Nek2; 10% inhibition at 10 μM
 $k' = 4.6 \times 10^{-4} \text{ s}^{-1}$



54

Nek2; 10% inhibition at 10 μM
 $k' = 1.4 \times 10^{-4} \text{ s}^{-1}$

Low Reactivity



88

Nek2; IC_{50} = 24.3 μM
 $k' = 3.0 \times 10^{-6} \text{ s}^{-1}$

Note: Reaction of compounds **90** and **89** with *N*-acetylcysteine methyl ester required 0.03 equivalents of DABCO, whereas compounds **56**, **54** and **88** used 0.30 equivalents of DABCO

^1H -qNMR spectroscopy was successfully used to investigate the influence of modifications at the purine 2-position upon conjugate addition of thiol **239** to 6-ethynyl purines **54** and **56**. It was discovered that methylation of the 2-amino group resulted in a 4-fold reduction in the rate of the Michael addition of thiol **239** when compared with the parent purine **39**. By contrast, replacement of the 2-anilino group of **39** by a benzyl group **56** resulted in no significant change in reactivity. These results suggest that the reduction in Nek2 inhibitory activity observed for **54** and **56** ($IC_{50} > 10 \mu\text{M}$) when compared with parent purine **39** ($IC_{50} = 150 \text{ nM}$) is not due to attenuation of ethynyl reactivity.

A number of heterocyclic derivatives of 6-ethynyl purine **39** were also investigated. Pyrrolopyrimidine **88** was the least reactive compound examined and was approximately 150-fold less reactive than the parent purine **39**. The low reactivity of the ethynyl group of **88** may explain why this compound was such a poor inhibitor of Nek2 ($IC_{50} = 24.3 \mu M$). The pyrazolopyrimidine and triazolopyrimidine compounds **89** and **90**, respectively, had the highest rates of reactivity with thiol **239** and required only 0.03 equivalents of the DABCO catalyst. The most reactive compound was the triazolopyrimidine **90**, which is likely due to the high electron deficiency of this heterocycle. Interestingly, **90** had similar Nek2 inhibitory activity to the parent purine **39** ($IC_{50} = 130 \text{ nM}$ and 150 nM , respectively) despite a large increase in the reactivity of the ethynyl group of **90**.

7.7 Future qNMR Studies to Investigate the Reaction of Ethynyl-Functionalised Heterocycles with *N*-Acetylcysteine Methyl Ester (**239**)

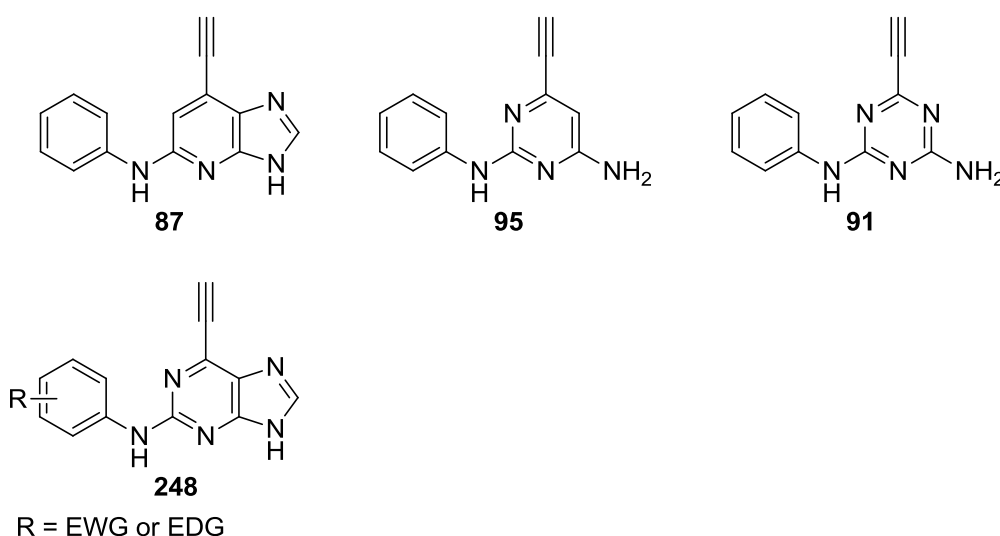


Figure 85.

To further investigate the influence of the conjugated heterocycle upon ethynyl reactivity it would be interesting to perform qNMR experiments using imidazopyrimidine **87**, pyrimidine **95**, and triazine **91** as substrates for reaction with thiol **239**. Additionally, studies of functionalised purine derivatives with electron withdrawing/donating groups positioned around the aniline ring (**248**) should be attempted to help understand the importance of the aniline side chain for good ethynyl reactivity. In combination with Nek2 IC_{50} values, qNMR could prove a valuable tool in the screening of future electrophilic Nek2 inhibitors.

Chapter Eight: Synthesis of Purine Isosteres as Inhibitors of CDK2

8.1 The Role of CDK2 in Cell Cycle Regulation

CDK2 is a serine/threonine protein kinase that functions principally at the G₁/S phase of the cell cycle.²⁶³ CDK2 has two partner cyclins – cyclin E and cyclin A, which regulate CDK2 function. The CDK2/cyclin-E complex is at its highest level during the G₁/S transitions and it was initially thought that CDK2 and cyclin-E were essential for cell cycle progression through inhibition of the retinoblastoma protein (pRb).¹⁴⁰ pRb is a tumour suppressor protein that arrests cells at G₁/S preventing cell cycle progression. This is achieved as pRb causes inactivation of E₂F family members, which in-turn prevents DNA transcription. Inactivation of pRb by hyperphosphorylation causes the release of transcription factors, which favour cell cycle progression.²⁶⁴

Upon progression into the S-phase of the cell cycle, CDK2/cyclin-E induces cyclin-E autophosphorylation. The newly formed phosphorylated cyclin-E is ubiquitinated, which enables proteasomal degradation by F-box protein FBW7.^{140,265} CDK2 then binds cyclin-A, which changes its substrate specificity. The resulting CDK2/cyclin-A complex phosphorylates the protein cell division cycle 6 (Cdc6), causing Cdc6 to translocate to the cytoplasm of the cell, which may prevent further DNA replication.²⁶⁶ Additionally, CDK2/cyclin-A has been implicated in mitotic progression due to its ability to phosphorylate endogenous Cdh1, which allows the accumulation of cyclin-B in preparation for the G₂/M transition.²⁶⁷

A further cell cycle dependent role of CDK2 is in the control of centrosome duplication. As described previously (Chapter 3), the duplication of centrosomes for mitosis is a highly ordered process and is achieved *via* the centrosome cycle.¹²⁵ Studies show that CDK2, together with partner cyclins E and A, may facilitate centrosome replication through the phosphorylation of proteins involved in the centrosome cycle.^{128,268,269}

8.2 Cell Cycle-Independent Functions of CDK2

In addition to facilitating cell cycle progression, it has been established that CDK2 has a number of secondary roles that are independent of the cell cycle. One such role is in the DNA damage response pathway, which enables DNA repair. In response to DNA damage, cell cycle progression is prevented due to cells not meeting the criteria of checkpoint controls at G₁, S, or G₂/M. This allows time to repair DNA damage or activate apoptosis in-order to prevent errors in mitosis.²⁷⁰ In response to DNA damage, p21^{Cip1/Waf1} is activated by the tumour suppressor p53.²⁷¹ Binding of p21 to CDK2/cyclin-E causes CDK2 inhibition and induces cell cycle arrest at the G₁/S checkpoint, which prevents replication of damaged DNA.²⁷⁰ Interestingly, it has been demonstrated in CDK2 depleted cells that CDK1/cyclin-B was also a substrate for p21 and compensates for CDK2 inactivation at the G₁/S transition.²⁷² However, CDK1 was not able to faithfully repair DNA to the extent that CDK2 can resulting in delayed DNA replication.²⁷⁰ These findings suggest CDK2 may have an important role in the DNA repair pathway through the binding of additional substrates.

8.3 CDK2 as a Target for Cancer Chemotherapy

Early *in vitro* cellular studies using a dominant negative (DN) CDK2 construct, demonstrated that in the absence of CDK2, cell cycle progression was halted at the G₁/S transition.²⁷³ This observation suggested CDK2 is essential for the initiation of DNA synthesis in higher eukaryotes, which made CDK2 a priority target. However, later research cast doubt upon the viability of CDK2 as a cancer chemotherapeutic target due to its non-essential role in cell proliferation.^{140,274,275} CDK2 inhibitory studies using antisense oligonucleotides or CDK2 siRNA showed sustained cell proliferation in the absence of CDK2.²⁷⁴ Additionally, CDK2 knockout mice were found to be viable, indicating that CDK2 is not essential. However, it was found that these mice were sterile indicating the importance of CDK2 in mouse germ cell maturation and meiosis.^{140,275} A possible explanation for the apparent viability of cells in the absence of CDK2, was that a redundant pathway was in place, which compensates for CDK2 inactivation. This was later confirmed in studies that demonstrated that in the absence of CDK2, CDK1 is able to compensate and

maintain cell cycle progression through the binding of cyclin-A.²⁷⁶ Interestingly, inhibition of both CDK1 and CDK2 caused cells to arrest in G₂. Despite the apparent non-essential role of CDK2 in cell proliferation, inhibitors of CDK2 may still be of use as targeted anticancer agents particularly in patients with specific tumour genotypes that give rise to predisposed drug sensitivity.¹³⁴ Additionally, due to the secondary functions of CDK2 in the control of DNA damage repair pathways and centrosome duplication CDK2 remains an interesting target for the treatment of cancer.²⁷⁰

8.4 SAR Studies with ATP-Competitive Heterocyclic CDK2 Inhibitors

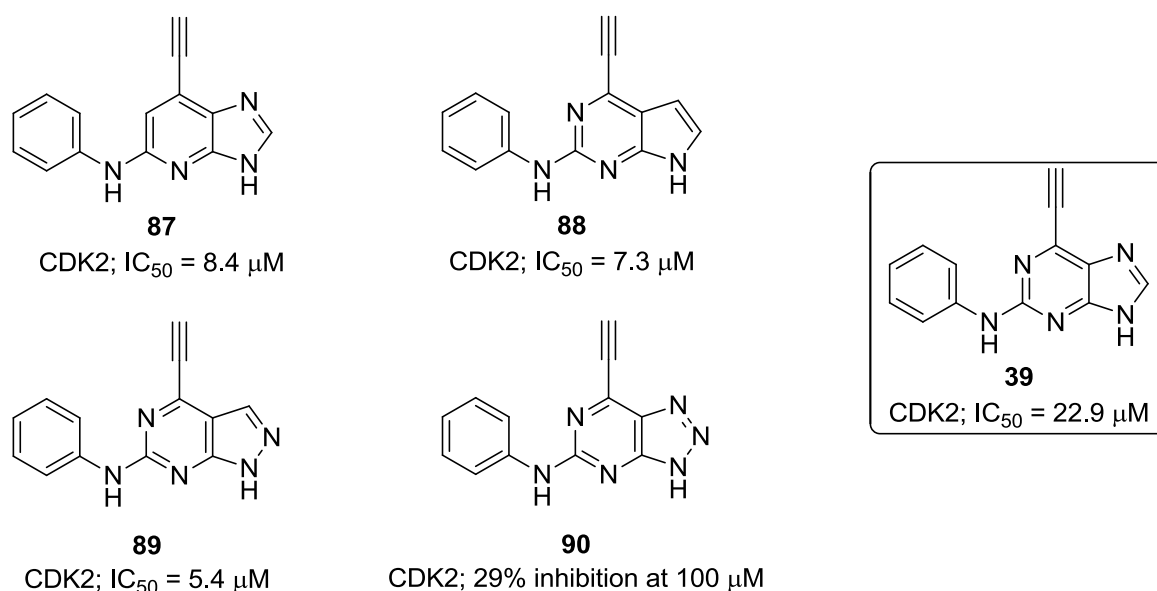
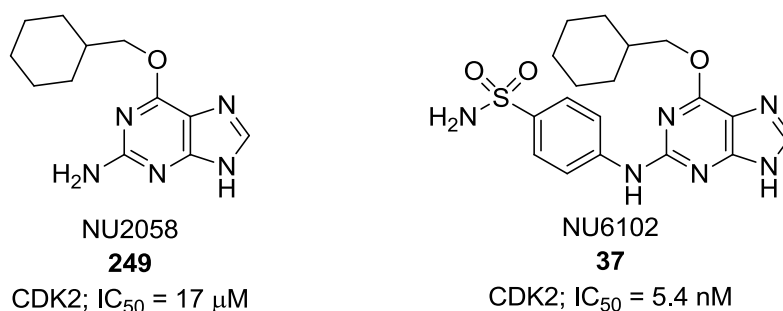
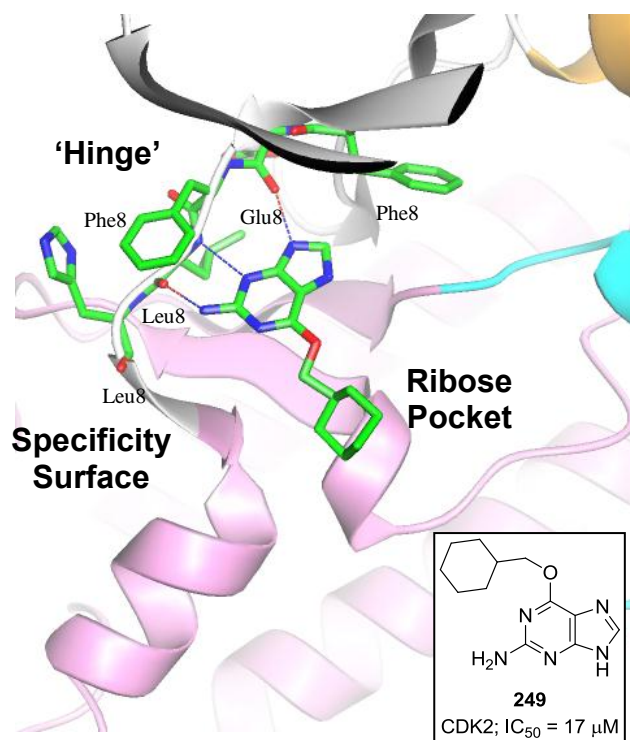


Figure 86.

It was of interest to note the differences in CDK2-inhibitory activity observed between the parent purine **39** and the heterocycle derivatives **87-90**. The imidazopyridine **87**, pyrrolopyrimidine **88** and pyrazolopyrimidine **89** derivatives were found to have increased potency compared with the parent 6-ethynylpurine **39** whereas triazolopyrimidine **90** was essentially inactive as a CDK2 inhibitor. To investigate this further the corresponding heterocyclic derivatives of NU6102 **37**, a potent CDK2 inhibitor (IC₅₀ = 5.4 nM), were synthesised. Derivatives of NU2058 **249**, a modest CDK2 inhibitor (IC₅₀ = 17 μM) known to potentiate cisplatin cytotoxicity, were also synthesised and evaluated for both CDK2 inhibitory activity and their ability to enhance cisplatin cytotoxicity.

**Figure 87.**

The optimum substituent at the purine 6-position was previously identified as cyclohexylmethoxy, which makes hydrophobic interactions within the ribose pocket of the CDK2 ATP-binding domain (Figure 88).²⁷⁷ Non-covalent binding to the backbone of Glu-81 and Leu-83 within the CDK2 hinge region is facilitated by a triplet of H-bonds with the 2-amino group and *N*³- and *N*⁹-positions of purine **249**. This hydrogen bonding motif has been shown previously to be essential for CDK2-inhibitory activity.²⁷⁷

**Figure 88** - Binding interactions of **249** within the CDK2 ATP-binding domain.²⁷⁷

A structure based design approach based upon **249**, led to the discovery of **37** (IC₅₀ = 5 nM), a potent and selective CDK2 inhibitor. The 2-arylamino group of **37** occupies a hydrophobic region and forms π -stacking interactions with the kinase

surface.²⁷⁷ The *para*-sulfonamide substituent further improves binding by making additional H-bond interactions with the side chain oxygen and backbone nitrogen of Asp-86 at the specificity surface (Figure 89).²⁷⁷

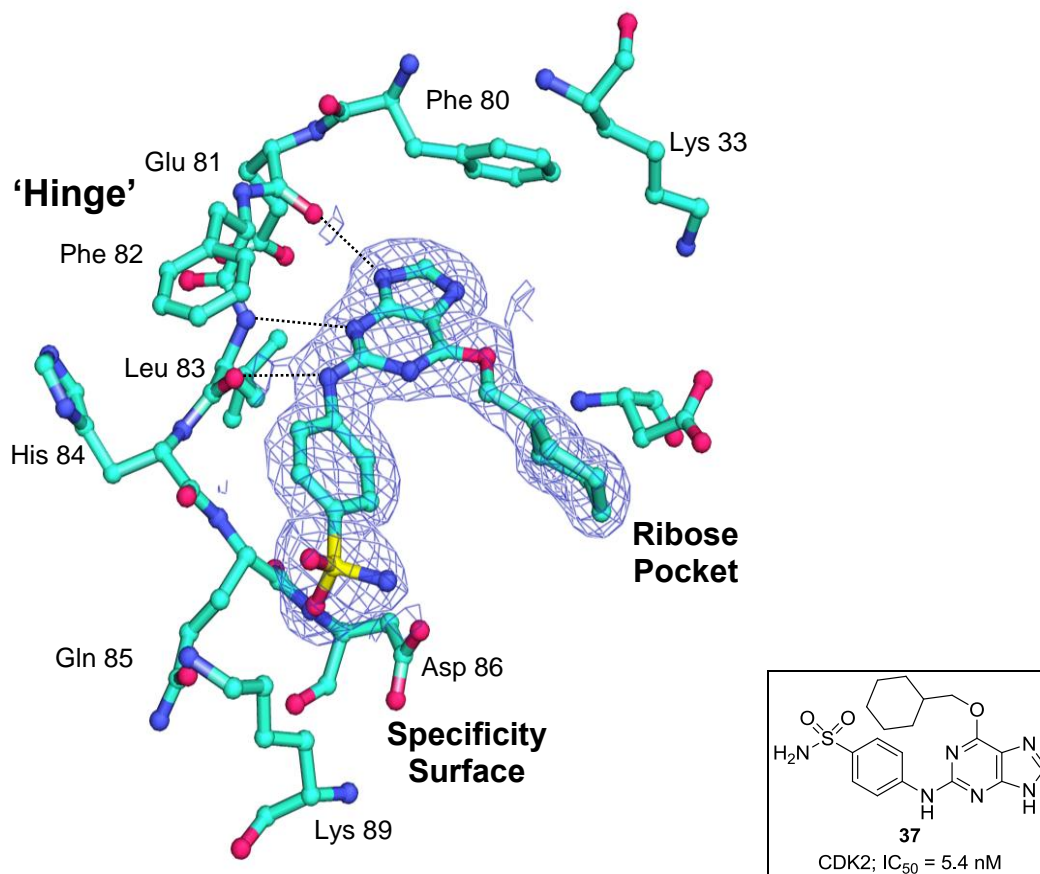


Figure 89 – X-ray crystal structure of purine **37** in complex with CDK2.²⁷⁷

8.5 Synthesis of Heterocyclic Derivatives of (**249**) and (**37**)

Synthetic strategies were developed for the preparation of imidazo[4,5-*b*]pyridine, 7*H*-pyrrolo[2,3-*d*]pyrimidine, 1*H*-Pyrazolo[3,4-*d*]pyrimidine and 3*H*-[1,2,3]Triazolo[4,5-*d*]pyrimidine derivatives of **249** and **37** (Figure 90). Unlike the Nek2 inhibitors which contained an electrophilic ethynyl group at the purine 6-position, these compounds were designed to be ATP-competitive CDK2 inhibitors. Variations in the potency of these compounds may therefore reflect changes in H-bond interactions at the CDK2 ATP-binding domain leading to subtle differences in the binding mode, which would help to further establish SAR and may allow the discovery of a new potent and selective series of CDK2 inhibitors.

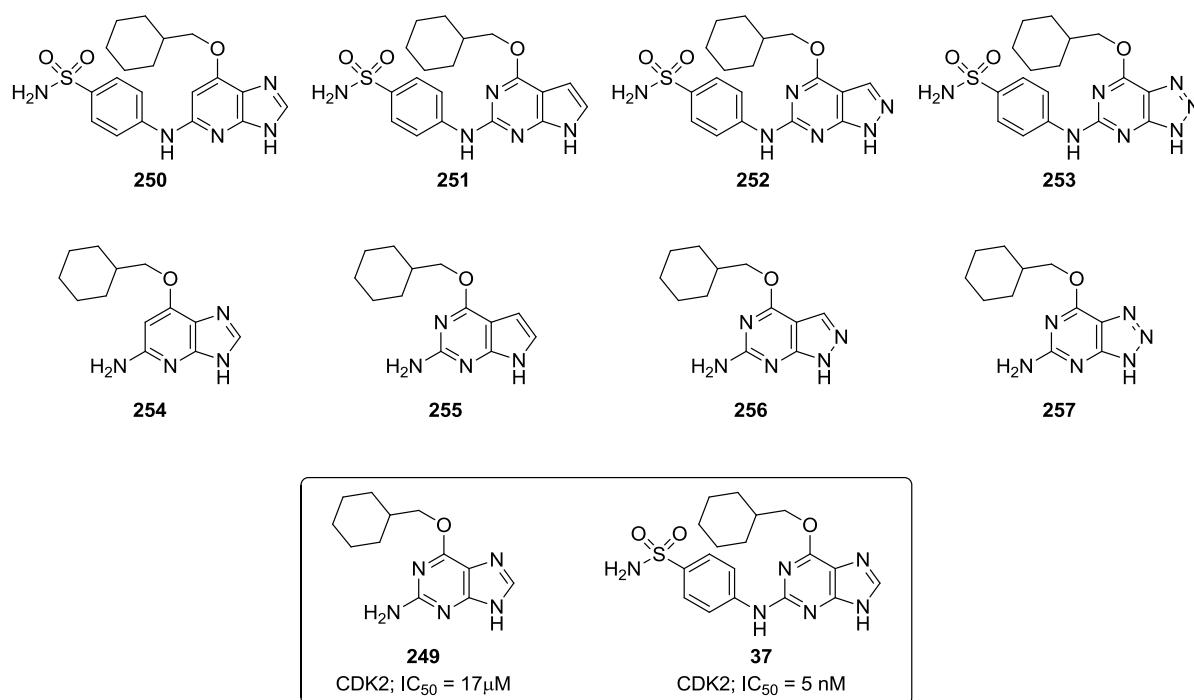
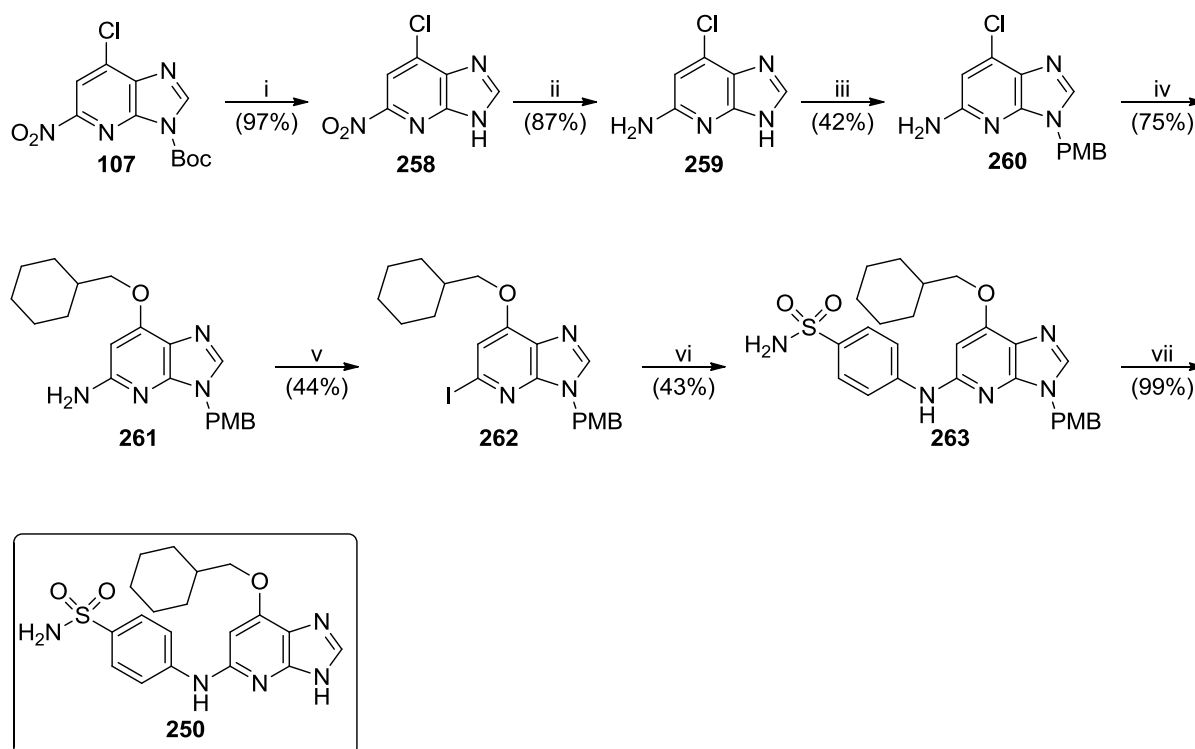


Figure 90 - Heterocyclic derivatives of purines **249** and **37**.

8.5.1 Synthesis of Imidazo[4,5-*b*]pyridines (**254**) and (**250**)

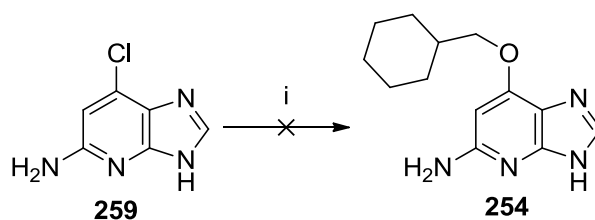
A synthetic strategy was developed for the preparation of imidazopyridines **249** and **37** based upon the synthesis of ethynylimidazopyridine **87** (Scheme 16). Unlike the ethynyl series, which used an S_NAr reaction to couple the aniline side chain, this synthesis was designed to include a Buchwald amination step, which was hoped to improve the yield and shorten reaction times.



Reagents and Conditions: i) TFE, 85 °C, 1 h; ii) Fe, AcOH:H₂O:EtOH (1:5:15) 90 °C, 1 h; iii) PMBCl, K₂CO₃, DMF, 60 °C, 18 h; iv) Sodium cyclohexylmethoxide, DMSO, MW 100 °C, 2 h; v) Diiodomethane, isoamyl nitrite, CuI, THF, 80 °C, 4 h; vi) Sulfanilamide **264**, Pd₂(dba)₃ (4 mol%), XPhos (4 mol%), K₂CO₃, MeCN, 85 °C, 6 h; vii) TFA, 85 °C, 4 h.

Scheme 74.

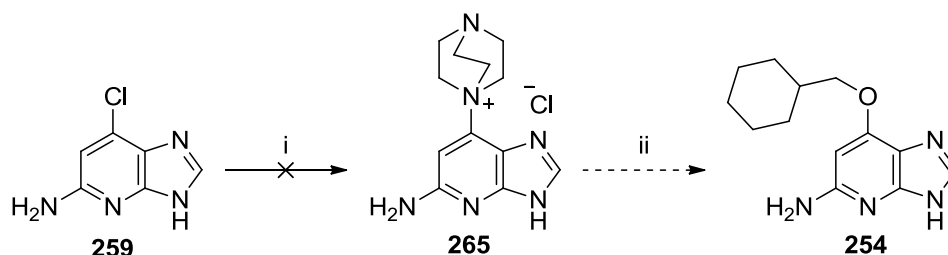
Imidazopyridine **107** was prepared as described previously (Scheme 16). The Boc protecting group was removed by heating to reflux in TFE, which gave **258** in near quantitative yield.²⁰⁸ It was not possible to reduce the nitro group of **258** using the conditions previously employed due to low solubility of both starting material and product. However, an alternative approach using 2.2 equivalents of iron powder in a mixture of EtOH, water and AcOH (15:5:1) selectively reduced of the nitro group to furnish **259** in 87% yield.



Reagents and conditions: i) Sodium cyclohexylmethoxide, DMSO, 0 °C - 100 °C, 1 h.

Scheme 75.

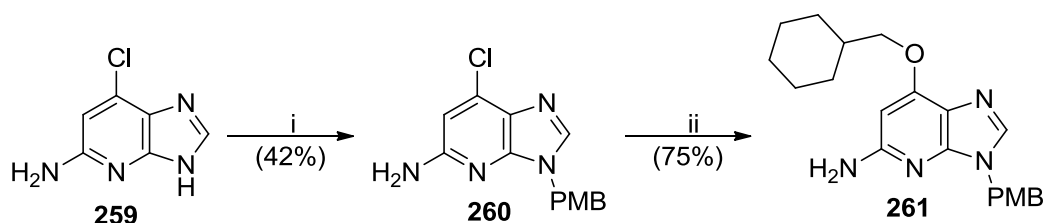
An initial attempt to couple cyclohexylmethoxide (prepared by treatment of cyclohexylmethanol with NaH) with imidazopyridine **259** was made using a literature procedure that was utilised for the synthesis of the purine **249** (Scheme 77).²⁷⁸ No reaction was observed at room temperature (48 h) and so the temperature was gradually increased (0 °C – 100 °C) resulting in decomposition of **259** and the formation of multiple side-products.



Reagents and conditions: i) DABCO, DMSO, RT – 60 °C, 48 h; ii) sodium cyclohexylmethoxide, DMSO, RT - 100 °C, 48 h.

Scheme 76.

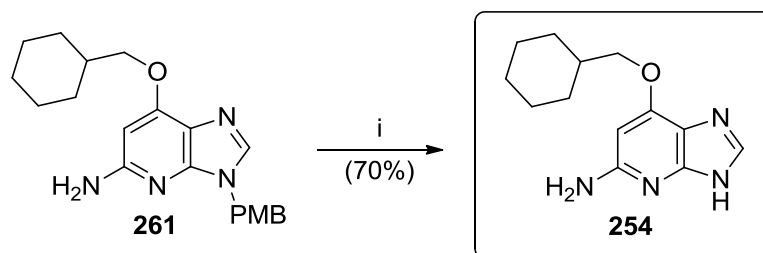
An alternative approach was to form the ‘DABCO-imidazopyridine’ salt **265**, which could be used in the reaction with cyclohexylmethoxide to form imidazopyridine **254**. It was reported that the relative rate of reaction for purines was increased *ca.* 10-fold for the displacement of the DABCO salt, when compared with the purine derivative **259**.²⁷⁹ The reaction of DABCO with imidazopyridine **259** resulted in no reaction so heating was attempted but this led to degradation of **259** and the formation of a multitude of side-products. It is likely that the electron-rich π -system of imidazopyridine **259** makes S_NAr reactions difficult. However, there are literature examples of successful S_NAr reactions between **259** and primary amines.²⁰⁹ In an attempt to prevent side-product formation it was decided to protect the N^3 position of **259** as the PMB derivative **260** (Scheme 77).



Reagents and conditions: i) PMBCl, K_2CO_3 , DMF, 60 °C, 18 h; ii) sodium cyclohexylmethoxide, DMSO, MW 100 °C, 2 h.

Scheme 77.

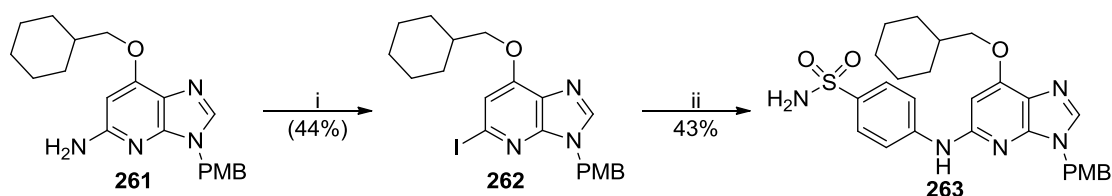
Imidazopyridine **259** was successfully protected as the PMB amine **260** in moderate yield (42%). The PMB derivative **260** was then treated with cyclohexylmethoxide in DMSO. After stirring overnight at RT a small amount of product **261** was observed by LC-MS analysis. Microwave irradiation of the reaction mixture (100 °C, 2 h) resulted in consumption of the starting material with minimal side-product formation, to give **261** in 75% yield. The PMB group of **261** was readily removed with TFA to provide **254** in 70% yield (Scheme 78).



Reagents and conditions: i) TFA, 75 °C, 2 h.

Scheme 78.

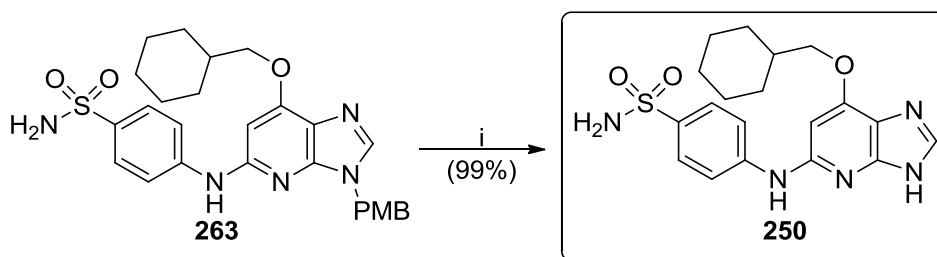
To allow further functionalisation at the 5-position, the iodo-species **262** was formed from imidazopyridine **261** through a Sandmeyer type reaction with diiodomethane, isoamyl nitrite and CuI in THF.²⁸⁰ This was followed by a Buchwald-Hartwig amination of **262** to couple the sulfanilyl side chain, furnishing **263** in 43% yield.



Reagents and conditions: i) Diiodomethane, isoamyl nitrite, CuI, THF, 80 °C, 4 h; ii) Sulfanilamide **264**, Pd₂(dba)₃ (4 mol%), XPhos (4 mol%), K₂CO₃, MeCN, 85 °C, 6 h.

Scheme 79.

Final PMB deprotection was achieved by treatment of **263** with TFA to give **250** in excellent yield (99%) (scheme 80).

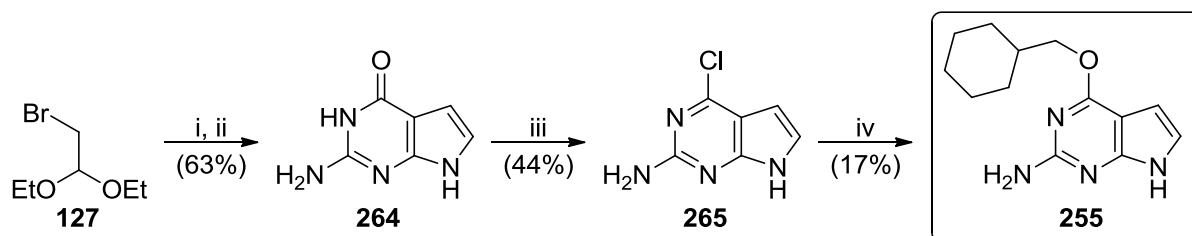


Reagents and conditions: i) TFA, 85 °C, 4 h.

Scheme 80.

8.5.2 Synthesis of 7H-Pyrrolo[2,3-d]pyrimidines (251) and (255)

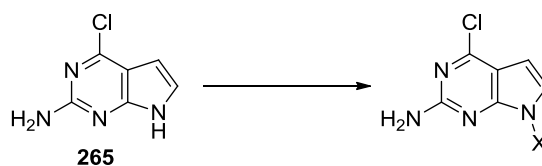
The synthesis of pyrrolopyrimidine derivatives **251** and **255** was developed starting from 2,6-diaminopyrimidin-4(3*H*)-one (**266**). Cyclisation of **266** with bromoacetaldehyde formed pyrrolopyrimidinone **264** in 63% yield. Chlorination was achieved by heating **264** in POCl₃, which gave 4-chloro derivative **265** (44% yield). The coupling of cyclohexylmethoxide with **265** proved particularly problematic and no observable reaction occurred at room temperature. However, using microwave assisted heating (170 °C, 5 h) it was possible to synthesise **255** in a 17% isolated yield together with a number of uncharacterised side-products.



Reagents and Conditions: i) HCl_(aq), 90 °C, 30 min; ii) **266**, NaOAc, H₂O, 80 °C, 3 h; iii) POCl₃, 110 °C, 5 h; iv) Sodium cyclohexylmethoxide, DMSO, MW 170 °C, 5 h.

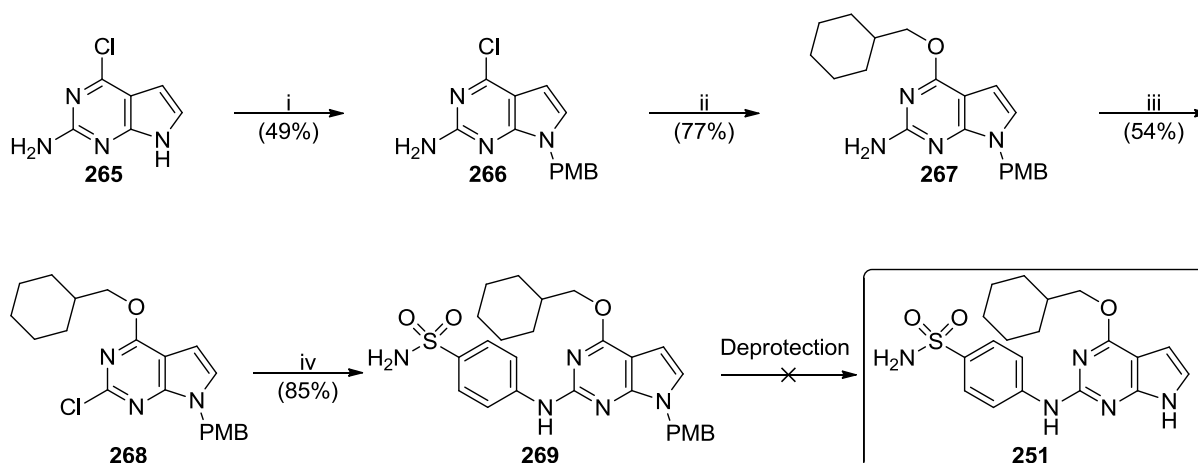
Scheme 81.

Purification of **255** was difficult and scale-up to more than 100 mg was equally problematic. It was hoped that protection of the pyrrolopyrimidine *N*⁷-position of **265** would improve the yield by preventing side reactions.

Table 8 - Protection of the pyrrolopyrimidine *N*⁷-position of **265**

Protecting Group (X)	Protection Conditions	Yield	Deprotection Conditions	Stable During Coupling of Cyclohexylmethoxide
Ts	TsCl, Et ₃ N, THF RT, 18 h	85%	NaOH/MeOH Gilman Reagent Na/NH ₃	No
TIPS	TIPSCl, NaH, THF -78 °C – RT, 18 h	71%	TFA TBAF	No
<i>t</i> -Boc	Boc ₂ O, DMAP, THF 0 °C – RT, 2 h	80%	TFA	No
PMB	PMBCl, NaH, DMF -78 °C – RT, 18 h	49%	TFA	Yes
<i>o</i> -NB	<i>o</i> -NBBBr, NaH, DMF -78 °C – RT, 18 h	63%	UV irradiation	No
SEM	SEMCl, NaH, MeCN -30 °C – RT, 18 h	74%	TFA TBAF	Yes

The tosyl-, trimethylsilyl- and *t*-Boc-protected derivatives of **265** were synthesised, and in each case protection of the pyrrolopyrimidine 7-position was selective and high yielding (71-85%). Unfortunately, none of these protecting groups withstood the conditions used during subsequent coupling of the cyclohexylmethoxide at the 4-position.



Reagents and conditions: i) PMBCl, NaH, DMF, 0 °C - RT, 18 h; ii) sodium cyclohexylmethoxide, THF, 0 °C - RT, 18 h; iii) isoamyl nitrite, SOCl₂, LiCl, THF, RT, 3 h; iv) sulfanilamide **264**, Pd₂(dba)₃ (4 mol%), XPhos (4 mol%), K₂CO₃, MeCN, 80 °C, 4 h.

Scheme 82.

The next protecting group investigated for the protection of **265** was PMB. This group was coupled in a reasonable yield of 49% (Scheme 82), which enabled attachment of the cyclohexylmethoxy group to **266** using standard conditions, furnishing **267** in 77% yield. A modified Sandmeyer chlorodediazotisation type reaction gave the chloro compound **268**, which was used in the Buchwald-Hartwig coupling of sulfanilamide **264** to give **269** in excellent yield (85%). The final reaction step entailed removal of the PMB protecting group from **269**. Regrettably, after several failed attempts using a range of conditions (Figure 91) this group could not be removed and this approach was abandoned.

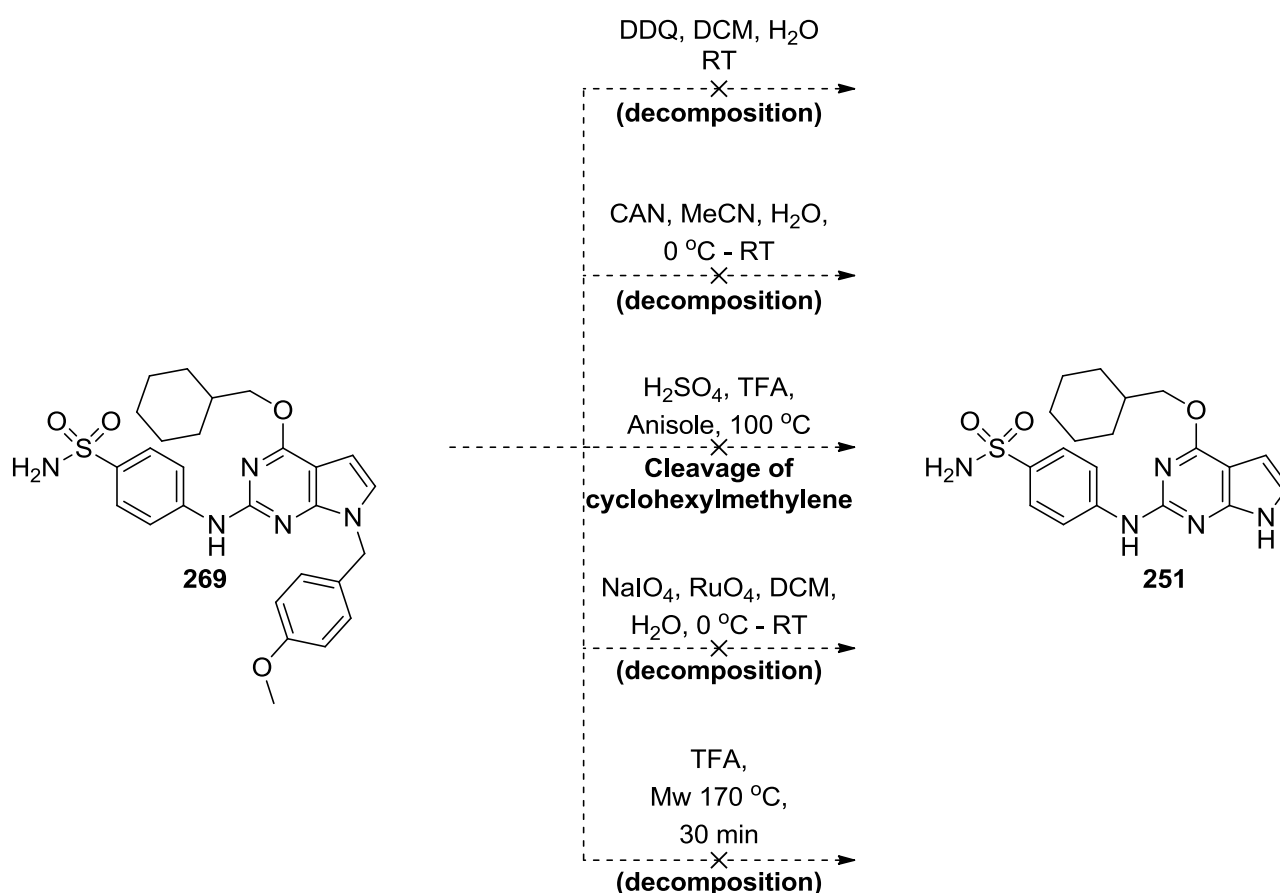
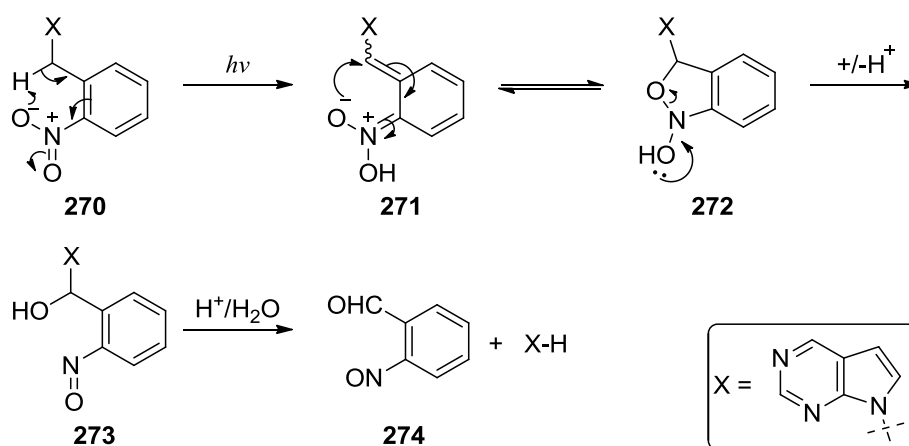


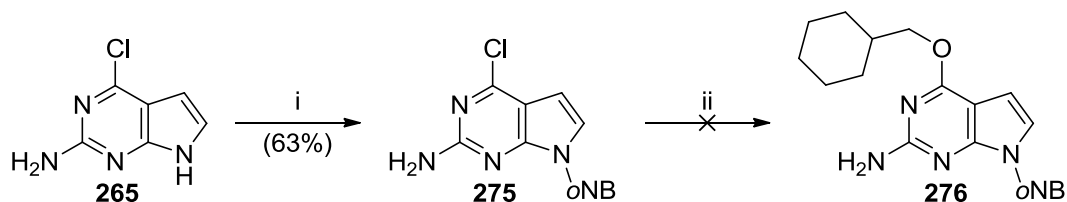
Figure 91 – Attempted removal of the PMB protecting group from **269**.

An alternative protecting group investigated for the protection of **265** was *ortho*-nitrobenzyl (*o*-NB), a photolabile protecting group which can be removed easily using UV radiation. The likely mechanism of this deprotection has been extensively studied, both experimentally and theoretically, and is shown in Scheme 83.^{281,282}



Scheme 83 - Photolytic cleavage of the *o*-NB protecting group from pyrrolopyrimidines (Adapted from Il'ichev *et al.*).²⁸²

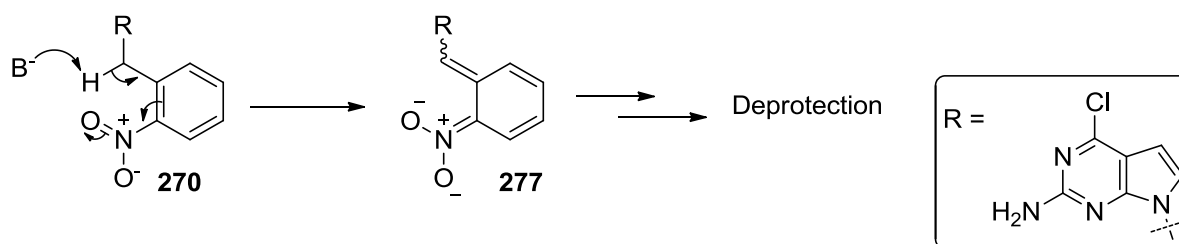
A photoreaction induces a proton transfer and tautomerization of the 2-nitrobenzyl group of **270** resulting in nitro tautomer **271**. A cyclisation then forms the acetal intermediate **272**, which ring opens to give the hemiacetal **273**. The hemiacetal **273** is then hydrolysed resulting in removal of the protecting group to give the unprotected pyrrolopyrimidine and 2-nitrosobenzaldehyde **274**.



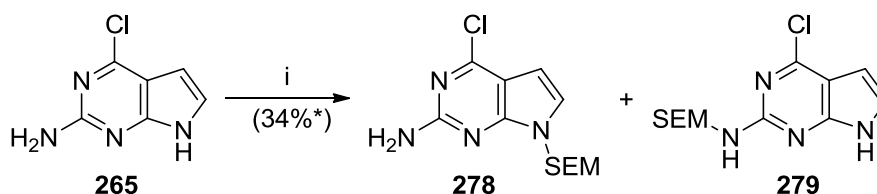
Reagents and conditions: i) *o*-NBBBr, NaH, DMF, 0 °C - RT, 18 h; ii) sodium cyclohexylmethoxide, THF, 0 °C - RT, 18 h.

Scheme 84.

Protection of pyrrolopyrimidine **265** at the *N*⁷-position with *o*-NB proceeded in 63% yield. However, when the coupling of the cyclohexylmethoxide group was attempted the *o*-NB group was removed with no observable product (**276**) formation. A possible explanation for this finding is that the benzylic proton of **270** is sufficiently acidic to be removed by the strongly basic sodium cyclohexylmethoxide (Scheme 84). The resulting carbanion may then tautomerise to the intermediate **277** resulting in removal of the *o*-NB group analogous to the photodeprotection mechanism (Scheme 85).

**Scheme 85.**

The final protecting group to be investigated was 2-(trimethylsilyl)ethoxymethyl (SEM). Previous work within the research group demonstrated that SEM could be successfully used for the protection of *N*-pyrrole groups.²⁸³ There was also limited literature precedent for the use of SEM as a protecting group for pyrrolopyrimidines.²⁸⁴

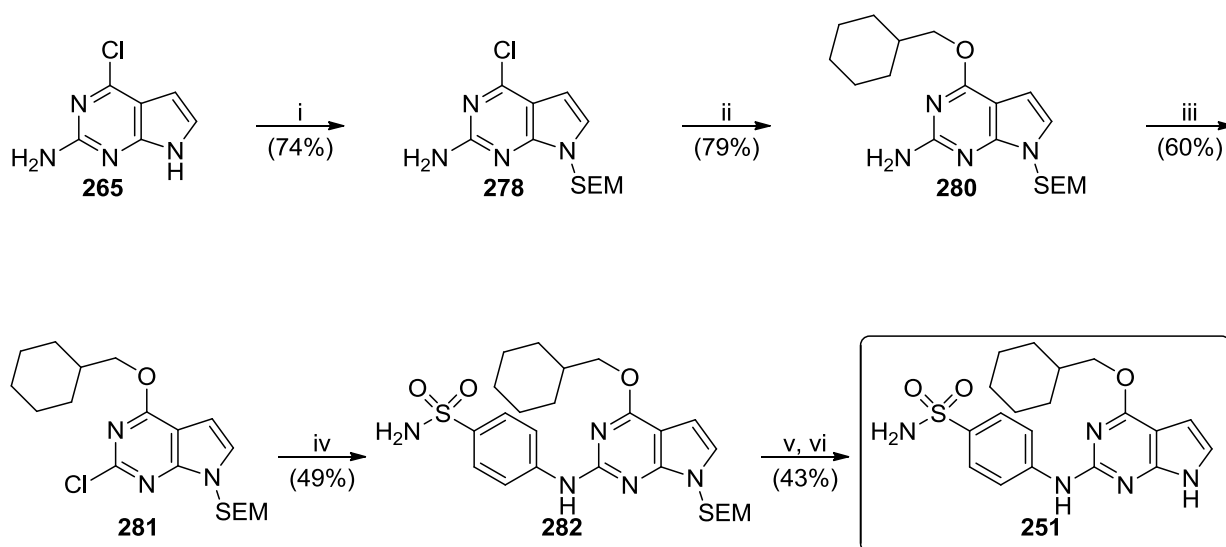


* = isolated yield of **279**

Reagents and conditions: i) SEMCl, NaH, MeCN, RT, 18 h.

Scheme 86.

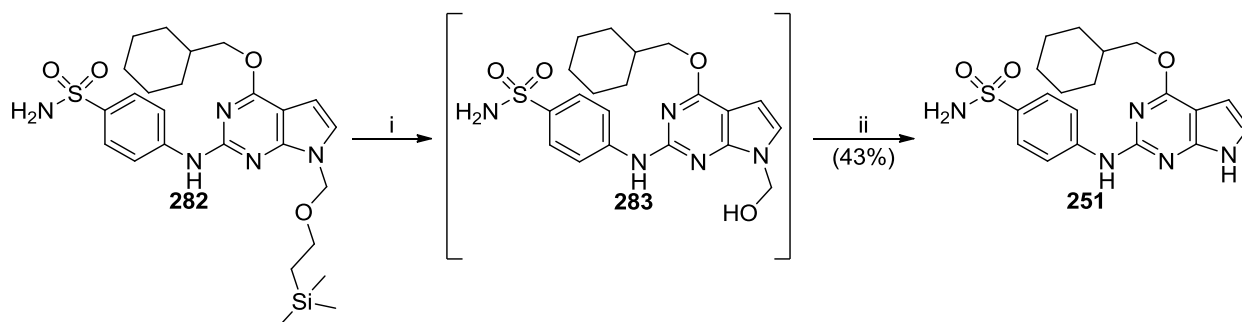
SEM protection of pyrrolopyrimidine **265** was attempted. Initially this reaction was performed at RT resulting in a mixture of regioisomers **278** and **279** in a 1:1 ratio (Scheme 86). By cooling the reaction mixture to 0 °C formation of the unwanted regioisomer **279** was avoided, allowing the isolation of **278** in 74% yield (Scheme 87).



Reagents and Conditions: i) SEMCl, NaH, MeCN, 0 °C – RT, 18 h; ii) Sodium cyclohexylmethoxide, THF, 0 °C – RT, 18 h; iii) Isoamyl nitrite, SOCl₂, LiCl, THF, RT, 3 h; iv) Sulfanilamide **264**, Pd₂(dba)₃ (4 mol%), XPhos (4 mol%), K₂CO₃, MeCN, 80 °C, 4 h; v) TFA, RT, 18 h; vi) NH₄OH, MeCN, H₂O, RT, 1 h.

Scheme 87.

Following SEM protection of **265**, the cyclohexylmethoxy group was introduced to give **278** in 79% yield. This was followed by a modified Sandmeyer chlorodediazotization and finally a Buchwald-Hartwig amination with sulfanilamide **264** to give pyrrolopyrimidine **282**.



Reagents and conditions: i) TFA, RT, 18 h; ii) NH₄OH, MeCN, H₂O, RT, 1 h.

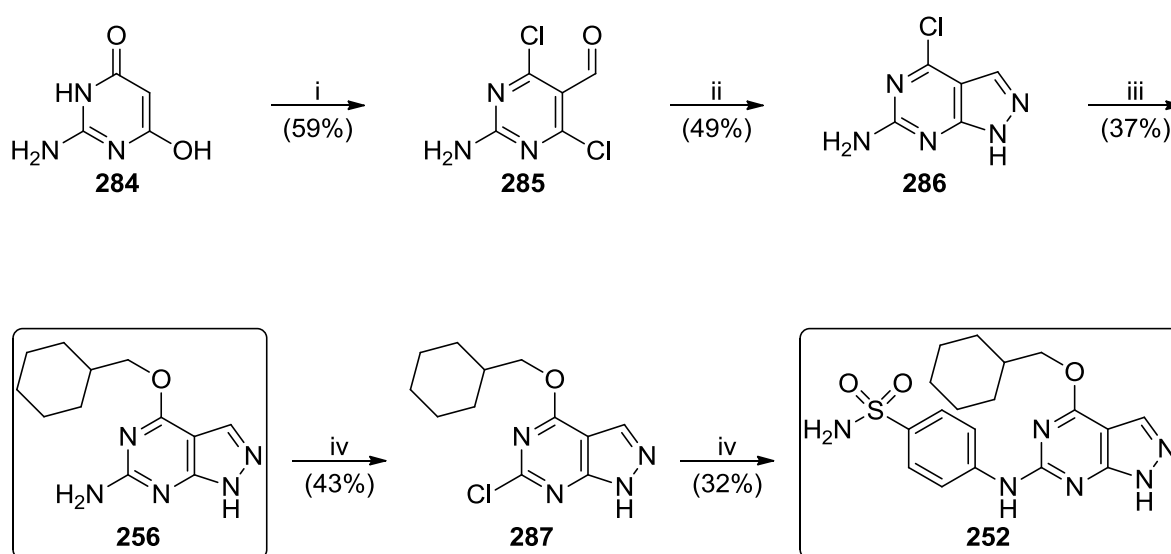
Scheme 88.

Attempted final removal of the SEM protecting group from **282** by stirring with TBAF in THF at room temperature resulted in no reaction. The reaction mixture was gradually heated to reflux (70 °C, 24 h) but without success. A literature example of pyrrolopyrimidine SEM deprotection using this method has been reported, and it was unclear why the reaction was unsuccessful with **282**.²⁸⁴ However, treatment of **282**

with TFA resulted in the formation of hemiacetal **283** which was fully deprotected with aqueous ammonia in MeCN, to give the target pyrrolopyrimidine derivative **251**.

8.5.3 Synthesis of 1*H*-Pyrazolo[3,4-*d*]pyrimidines (**252**) and (**256**)

A concise synthesis of pyrazolopyrimidines **252** and **256** was developed based upon a literature procedure (Scheme 89).²²⁸



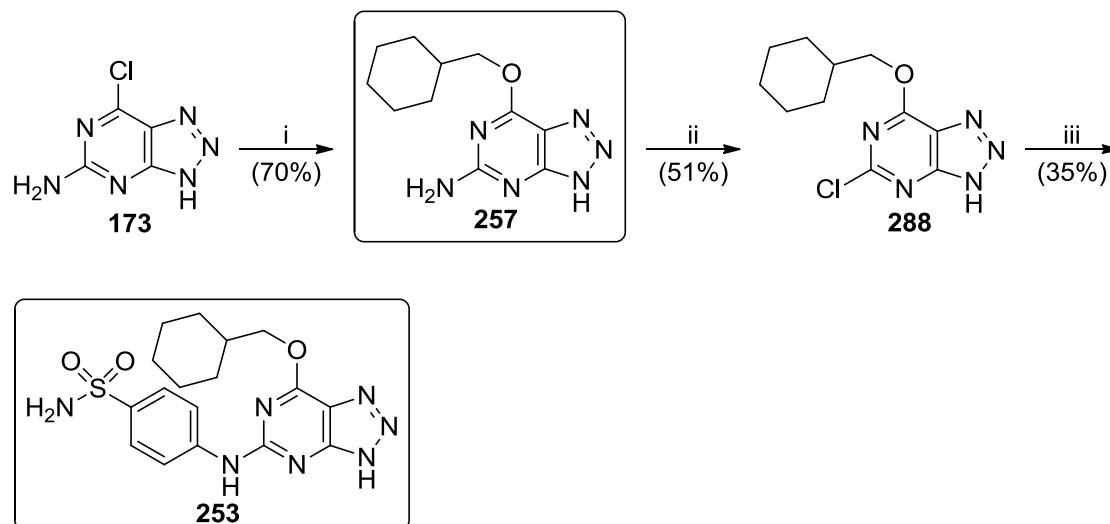
Reagents and Conditions: i) POCl₃, DMF, 110 °C, 3 h; ii) N₂H₄·H₂O, Et₃N, THF, H₂O, 50 °C, 1 h; iii) Sodium cyclohexylmethoxide, DMSO, 100 °C, 30 min; iv) Isoamyl nitrite, LiCl, SOCl₂, DMA, 0 °C – RT, 6 h; v) Sulfanilamide **264**, TFA, TFE, 80 °C, 48 h.

Scheme 89.

A tandem Vilsmeier-Haack/chlorodehydroxylation reaction of **284** gave dichloropyrimidine **285** in moderate yield (59%). Cyclisation with hydrazine hydrate gave pyrazolopyrimidine **286**, which was reacted with cyclohexylmethoxide to give derivative **256** in 37% yield. A modified Sandmeyer chlorodediazotization reaction was then used which furnished 6-chloro derivative **287** in 43% yield. Finally, an acid catalysed S_NAr reaction with sulfanilamide **264** was used to give the target pyrazolopyrimidine **252** in 32% yield.

8.5.4 Synthesis of 3*H*-[1,2,3]Triazolo[4,5-*d*]pyrimidines (**253**) and (**257**)

A synthetic route to triazolopyrimidines **253** and **257** was developed starting from **173**, which was prepared as summarised in Scheme 90.



Reagents and Conditions: i) Sodium cyclohexylmethoxide, DMSO, RT, 18 h; ii) Isoamyl nitrite, LiCl, SOCl₂, DMA, 0 °C – RT, 6 h; iii) Sulfanilamide **264**, TFA, TFE, 80 °C, 2h.

Scheme 90.

Triazolopyrimidine **173** was reacted with cyclohexylmethoxide in DMSO to give derivative **257** in 70% yield. Sandmeyer chlorodehydroxylation gave **288**, which was unstable to chromatography and used directly in the next reaction without further purification. The final step was an acid-catalysed S_NAr reaction of **288** with sulfanilamide **264** to give derivative **253** in 35% yield. It is likely that had the starting material been pure, this reaction would have been much higher yielding as no significant side-products were observed.

8.6 CDK2-Inhibitory Activity for Isosteres of 2-Amino-6-Cyclohexylmethoxypurine

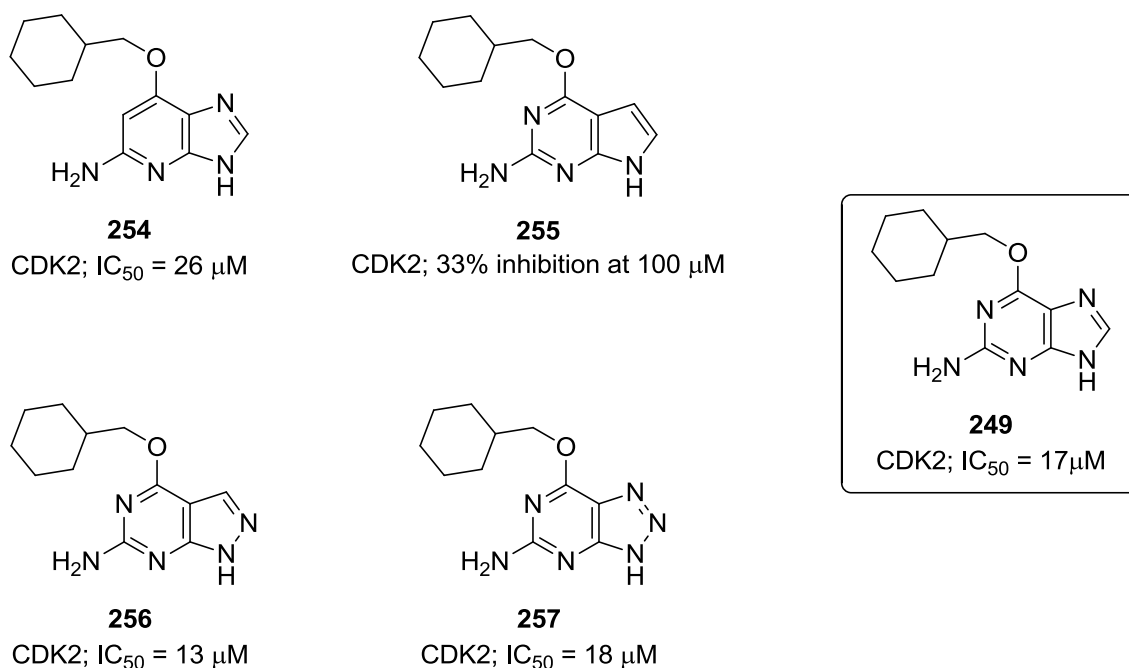


Figure 92.

Biological evaluation of the heterocyclic derivatives of purine **249** revealed compounds **254**, **256** and **257** demonstrated CDK2-inhibitory activity comparable with the parent purine **249**, whereas pyrrolopyrimidine **255** was essentially inactive for reasons that remain elusive. One possible explanation is that the purine **249** makes an interaction within the CDK2 active-site by virtue of the N^7 , which is lost in the pyrrolopyrimidine derivative **255**. Another possibility is that the H-bond made by the pyrrolopyrimidine NH may be weaker than that of the corresponding nitrogen of the other heterocyclic derivatives, which could lead to an alternative binding orientation. To further elucidate this, it would be interesting to compare the co-crystal structures of these compounds in complex with CDK2. Additionally, it would be interesting to investigate modifications of the alkoxy-group for each heterocyclic series to determine if trends in CDK2 inhibitory activity were heterocycle dependent.

8.7 CDK2 IC₅₀ Determination of Alternative Heterocycles Based on Purine (**37**)

A range of heterocyclic derivatives of the potent CDK2 inhibitor NU6102 (**37**) (IC₅₀ = 5 nM) were synthesised and evaluated for CDK2-inhibitory activity (Figure 93). These compounds were designed to serve as pharmacological probes to further evaluate CDK2 as a prospective cancer chemotherapeutic target.

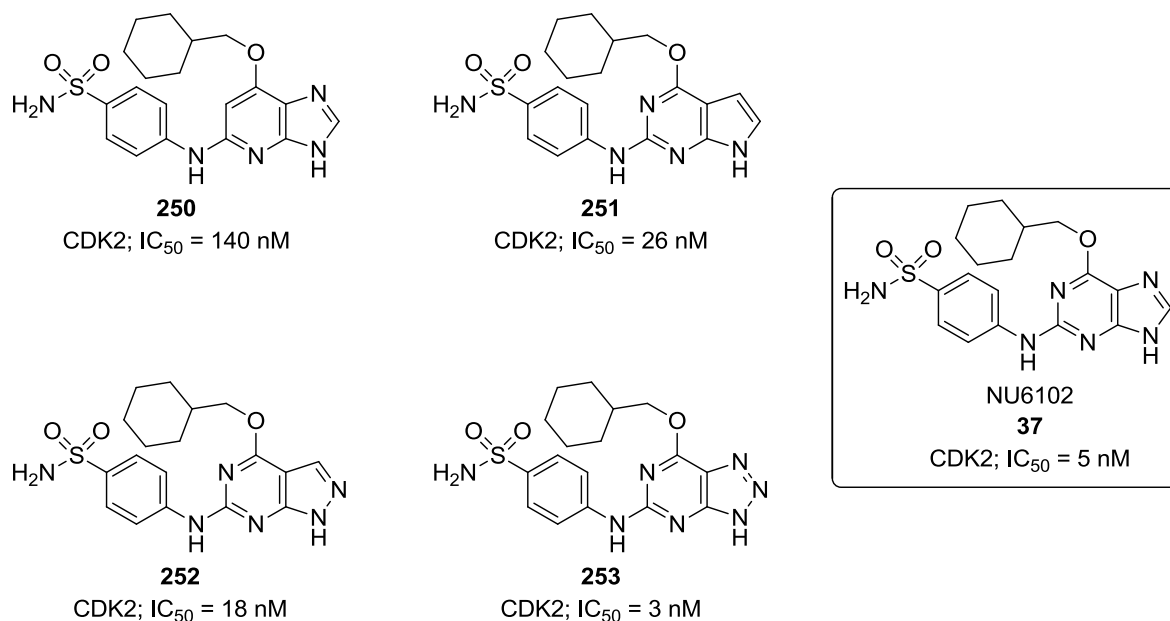


Figure 93.

Imidazopyridine **250** was found to be 28-fold less active than the parent purine **37**, whereas pyrrolopyrimidine **251** was 5-fold less active. This result was surprising considering that the NU2058 (**249**) derivative **255** was essentially inactive, which demonstrates the importance of the additional sulfanilamide H-bond interactions of these compounds. A possible explanation for the reduction in potency of **250** and **251** when compared with purine **37** could be reduced H-bonding between the heterocycle and amino acids or water molecules present at the CDK2 ATP-binding domain caused by removal of the purine *N*¹ or *N*⁷ nitrogen from these heterocycles. As such, it would be interesting to compare the *X-ray* co-crystal structures of these compounds bound to CDK2 with that of purine **37**. Pyrazolopyrimidine **252** had similar CDK2 inhibitory activity (IC₅₀ = 18 nM) to the purine **37**. The most potent compound was triazolopyrimidine **253** (IC₅₀ = 3 nM) which was equipotent with the parent purine **37**.

Future work would include growth inhibition assays to determine if potency towards CDK2 translates into cellular activity. Screening of these compounds against a panel of kinases would allow observation of differences in the kinase selectivity profile for each compound.

8.8 Potentiation of Cisplatin Cytotoxicity by NU2058 (249) and Analogues

Cisplatin (**3**) is a member of a family of platinum containing drugs that have found widespread use in the treatment of cancer.²⁸⁵ Although cisplatin is effective in many tumour types, it is particularly effective for the treatment of testicular cancer with curative rates in excess of 90%.²⁸⁶ The mechanism of cisplatin uptake into cells is not fully understood, although it is believed that the drug can cross cell membranes through a combination of active transport and passive diffusion.²⁸⁶ Once inside the nucleus of the cell, cisplatin forms DNA adducts by covalent modification of purine bases predominantly at the *N*⁷-position. A second covalent modification results in a 1,2- or 1,3-intrastrand crosslink, or in some instances interstrand crosslinks (Figure 94).²⁸⁶ A consequence of this may be DNA damage due to impaired cell replication, inhibition of transcription, cell-cycle arrest, activation of DNA repair pathways and apoptosis.²⁸⁶

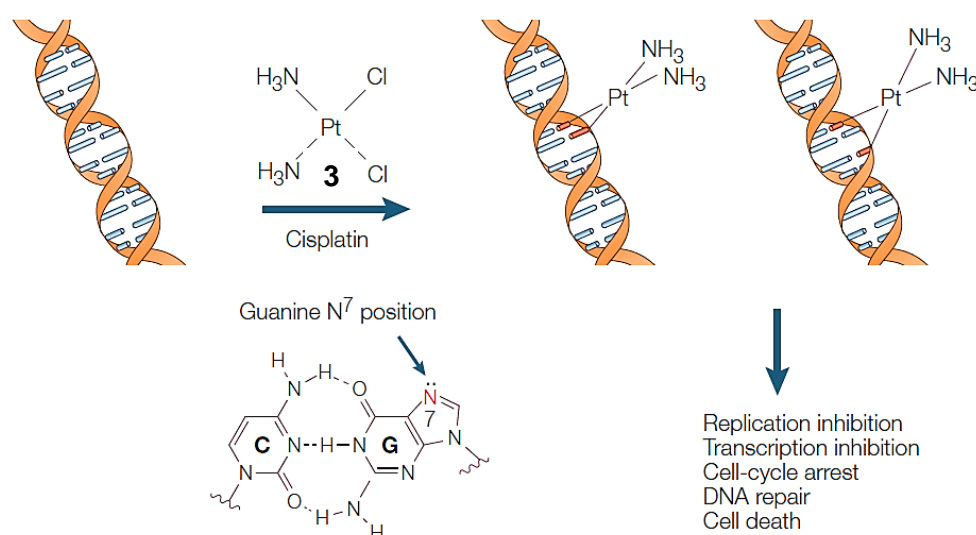


Figure 94 - Cisplatin causes cell death through the formation of DNA adducts (adapted from Wang).²⁸⁶

Cisplatin has been shown to be an effective treatment for some tumour types but has limited clinical use in others. In addition, previously responsive cancers may develop resistance due to changes in cell signalling causing increased DNA repair, altered cellular transport and enhanced drug efflux.²⁸⁵ Another limiting factor in the treatment of cancers with platinum containing compounds is the propensity for toxicity. Cisplatin and derivatives are known to have numerous side-effects including nephrotoxicity, emetogenesis and neurotoxicity.^{286,287} An effective strategy to combat both drug resistance and toxicity is to target the pathways involved in these processes. By doing so it may be possible to increase drug potency whilst minimising toxicity. Similarly, by targeting pathways involved in cisplatin induced resistance it may be possible to render an otherwise ineffective drug active.²⁸⁵

Previous studies have demonstrated that NU2058 (**249**), a modest CDK2 inhibitor ($IC_{50} = 17 \mu M$) can potentiate cisplatin-induced cytotoxicity *in vitro*.²⁸⁸ It was initially hypothesised that increased cytotoxicity was as a result of CDK2 inhibition, but this was later disproved by comparative studies with NU6230 (**289**), a structurally related CDK2 inhibitor with similar potency ($IC_{50} = 18 \mu M$), and NU6102 (**37**), a potent and selective CDK2 inhibitor ($IC_{50} = 5 \text{ nM}$) (Figure 95).²⁸⁵

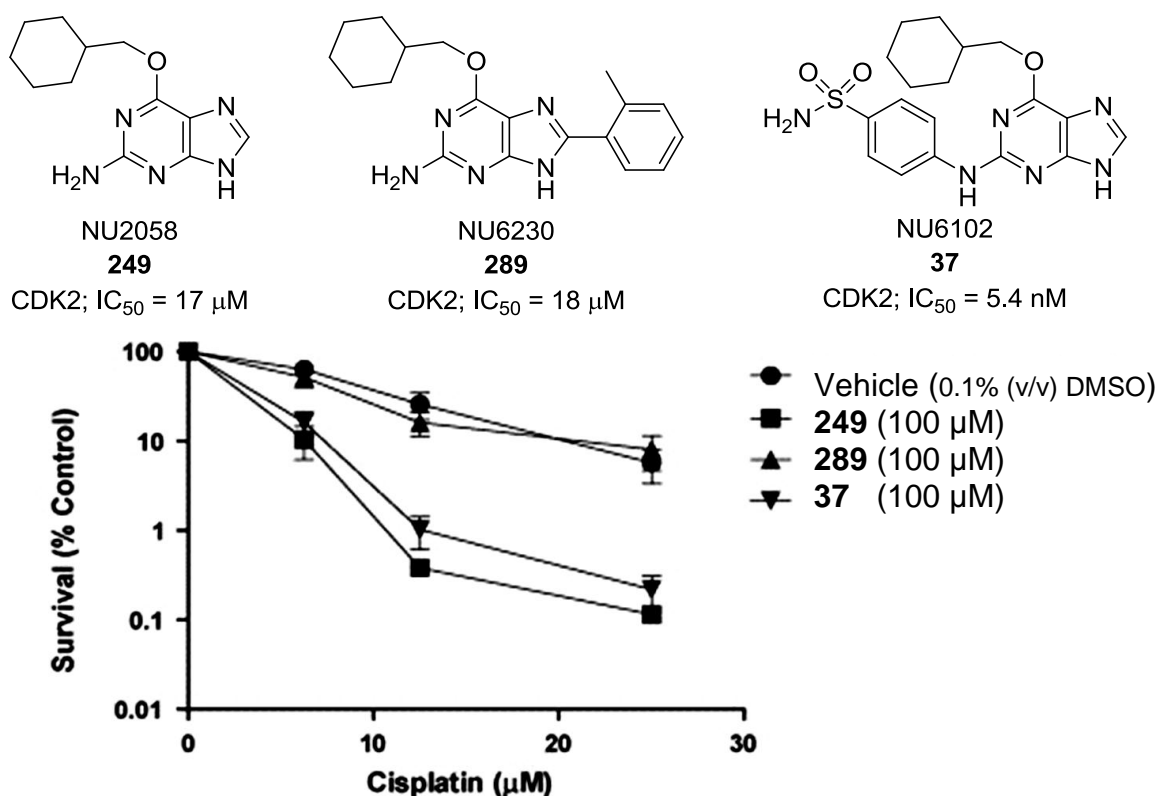


Figure 95 - **249** and **37** potentiate cisplatin cytotoxicity *in vitro* (adapted from Harrison).²⁸⁵

Head and neck squamous carcinoma cells (SQ20b) were treated with the appropriate purines for 2 h at 100 μ M, followed by exposure to cisplatin for an additional 2 h. All compounds were found to be non-toxic when administered in the absence of cisplatin. LC_{50} values (the concentration of drug required to reduce plating efficiency by 50%) were determined and compared with a vehicle control of cisplatin alone.²⁸⁵ The dose modification factor (DMF) (ratio of vehicle control and combined treated LC_{50} value) was determined for each compound. It was revealed that **249** potentiated cisplatin cytotoxicity with a DMF value of 3.1. Similarly, NU6102 **37** enhanced cisplatin cytotoxicity with a DMF value of 2.3. Interestingly, this compound was substantially more potent than **249** as a CDK2 inhibitor but had similar activity in the cisplatin combination cytotoxicity assay. Cells treated with **289** and cisplatin showed no significant increase in cytotoxicity. Cellular assays confirmed that **289** had similar cellular CDK2 inhibitory activity to **249**, suggesting that cisplatin potentiation is independent of CDK2 inhibition.²⁸⁵

The mechanism for the potentiation of cisplatin cytotoxicity by **249** remains unknown. It has been suggested that **249** may attenuate cellular transport of cisplatin, causing accumulation and thus resulting in an increase in the number of DNA adducts. A second possibility is that **249** modulates DNA repair pathways through interactions with an as of yet unidentified target resulting in enhanced cytotoxicity.²⁸⁵ A similar assay was used to evaluate the ability of derivatives **255**, **256** and **257** to potentiate cisplatin cytotoxicity (Figure 96).

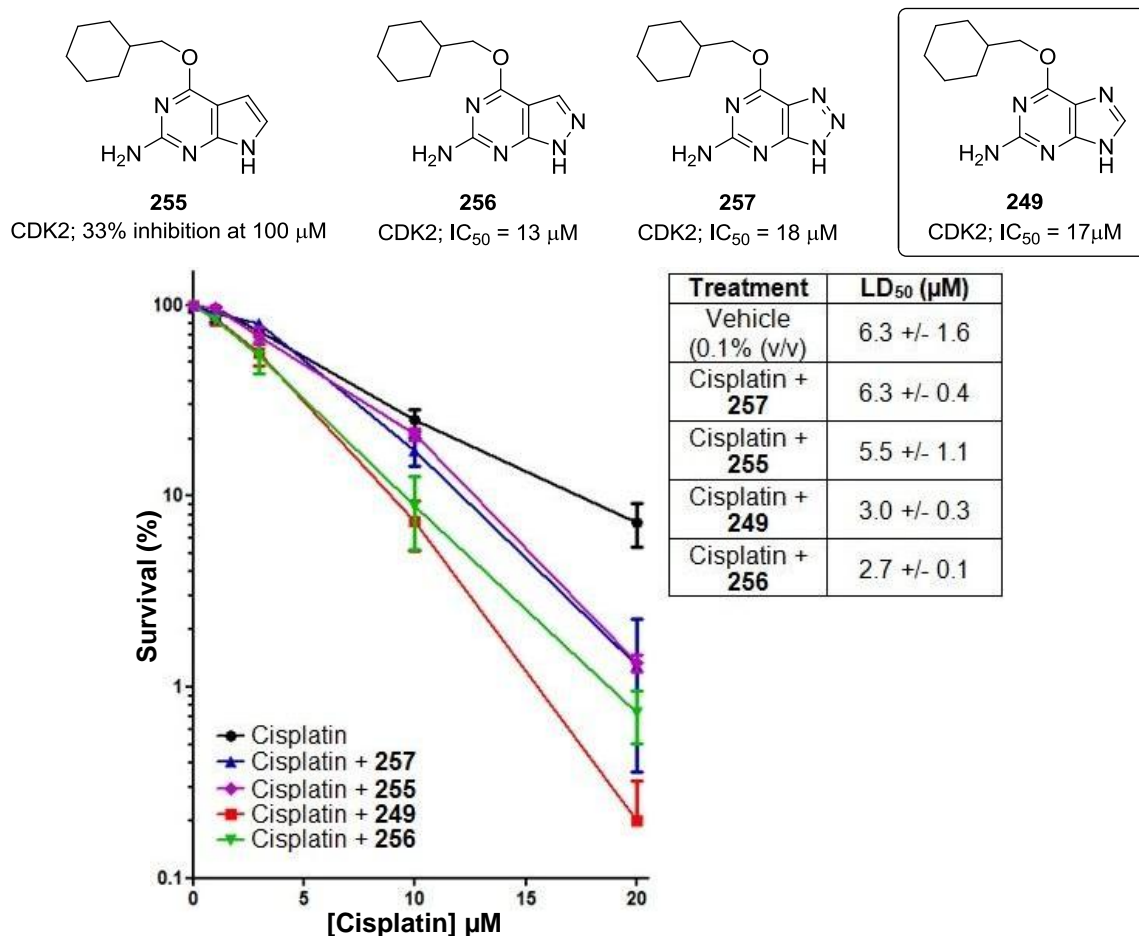


Figure 96 - Cisplatin combination cytotoxicity assay.

Figure 96 shows the results from the cisplatin combined cytotoxicity assay. Whereas triazolopyrimidine **257** and pyrrolopyrimidine **255** did not potentiate cisplatin cytotoxicity, treatment with pyrazolopyrimidine **256** led to an increase in cisplatin cytotoxicity comparable with the parent purine **249** (DMF values = 2.3 and 3.0, respectively). The fact that pyrazolopyrimidine **256** and triazolopyrimidine **257** have similar CDK2 inhibitory activity, yet different cytotoxicity when co-administrated with cisplatin, suggests that the observed synergistic effects are independent of CDK2 inhibition, which supports the previous results.²⁸⁵

Future studies including CDK2 cell-based assays of all inhibitors will determine if these compounds inhibit CDK2 in cells. Furthermore, an investigation into the mechanism by which pyrazolopyrimidine **256** causes potentiation of cisplatin cytotoxicity, and a comparison of this compound with purine **249** would be of interest. Finally, imidazopyridine **254**, which has similar CDK2 inhibitory activity to NU2058 (26 μM vs. 17 μM , respectively), remains to be investigated for potentiation of cisplatin cytotoxicity.

Chapter Nine: Conclusions and Future Work

9.1 Design and Synthesis of Irreversible Inactivators of Nek2

6-Ethynylpurine **39** was identified as a sub-micromolar ATP-competitive irreversible inhibitor of Nek2 with growth-inhibitory activity in cells. This compound forms a non-covalent binding interaction with the Nek2 hinge region at the ATP-binding domain *via* a triplet of H-bonds, which is thought to facilitate covalent modification of the 6-ethynyl group by Cys-22. A series of derivatives of **39** were synthesised (Figure 97) for structure activity studies of the N^9 and 2-amino H-bond donor groups. *N*-methylated derivatives **52-54**, phoxypurine **55**, and benzylpurine **56** were significantly less potent ($IC_{50} > 10 \mu M$) than **39** ($IC_{50} = 150 \text{ nM}$), due to loss of an essential H-bond interaction with the Nek2 hinge region.

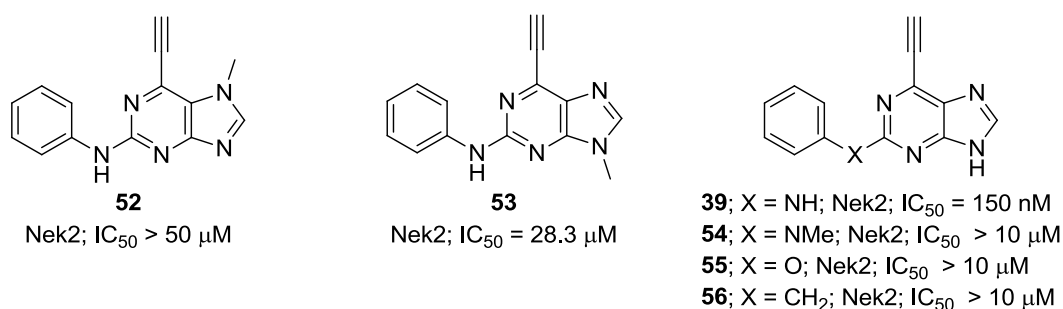


Figure 97 – Purine based derivatives of **39** for Nek2 structure activity studies.

Growth inhibition studies were performed upon the weakly active Nek2 inhibitors **52** (GI_{50} ; SKBR3 = $0.31 \mu M$) and **53** (GI_{50} ; SKBR3 = $0.22 \mu M$), which revealed that these compounds had similar cellular potency as the parent purine **39** (GI_{50} ; SKBR3 = $0.33 \mu M$) despite poor Nek2 inhibitory activity. These findings suggested that the cytotoxicity of **52** and **53** was independent of Nek2 inhibition and possibly due to binding of an as yet undetermined target.

A series of structurally similar heterocyclic derivatives of purine **39** (Figure 98) were synthesised to investigate the influence of the conjugated heterocycle upon ethynyl reactivity and hence irreversible Nek2 inhibitory activity. These compounds were designed to mimic the triplet of H-bond interactions between **39** and the Nek2 hinge region, which is essential for Nek2 inactivation by 6-ethynyl purines.

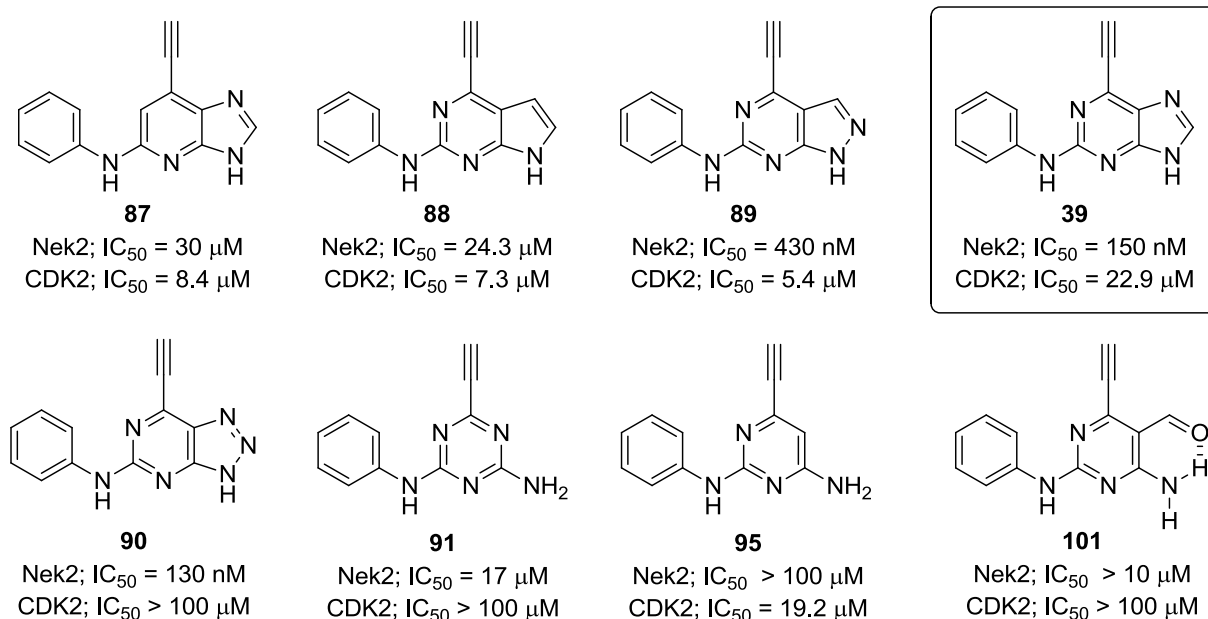
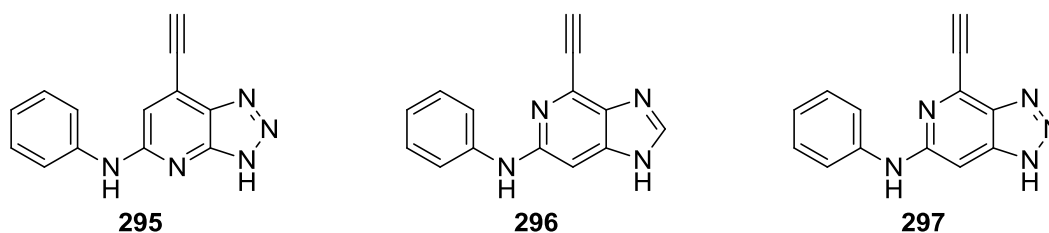


Figure 98 – Heterocyclic derivatives of purine **39**.

Deazapurines **87** and **88** were significantly less potent (IC₅₀ = 30 μM and 24.3 μM, respectively) than purine **39** (IC₅₀ = 150 nM), which was attributed to attenuation of ethynyl reactivity due to the increased electron density of these heterocycles. It was unclear whether **87** and **88** were irreversible inactivators of Nek2 or ATP-competitive reversible inhibitors, as such, future work should include time-dependent inhibition studies. By contrast, Pyrazolopyrimidine **89** and triazolopyrimidine **90** were sub-micromolar (IC₅₀ = 430 nM and 130 nM, respectively) irreversible inactivators of Nek2 with growth inhibitory activity comparable with **39**. These two series may prove a viable alternative to the purine heterocycle and should be investigated further through the synthesis of a small library of substituted aniline derivatives of **89** and **90** for use in comparative studies.

Finally, a series of 6-membered heterocycles based upon **39** was investigated, which included triazine **91**, pyrimidine **95**, and 5-formylpyrimidine **101**. Pyrimidine **95** was found to be weakly active (IC₅₀ > 100 μM), whilst triazine **91** and 5-formylpyrimidine **101** were modest Nek2 inhibitors (IC₅₀ = 17 μM and > 10 μM, respectively). These findings, in addition to the limited patent space of both triazines and pyrimidines, led to these series being abandoned in favour of more appealing targets.



Future work should include the synthesis and biological evaluation of triazolopyridine **295**, imidazopyridine **296**, and triazolopyridine **297**, which were not synthesised due to time-constraints. Synthesis of triazolopyridine **295** would allow further investigation into the role of the pyrimidine N^1 of purine **39** whilst retaining the electron-deficiency of the heterocycle. This compound may demonstrate greater potency than imidazopyridine **87** due to increased ethynyl reactivity, which could lead to the discovery of a new series of Nek2 inhibitors. Compounds **296** and **297** allow investigation into the role of the N^3 -position of **39**, which is thought to be partially protonated *via* a H-bond with Cys-89 of the Nek2 hinge region, which is thought to facilitate covalent modification of the ethynyl group (Figure 27, p70). Additionally, it would be interesting to observe the difference in potency between **296** and **297**, which has increased electron-deficiency.

9.2 qNMR Kinetic Analysis of Irreversible Nek2 Inhibitors

^1H -qNMR studies of irreversible Nek2 inhibitors **54**, **56** and **88-90** (Figure 99) was performed at 24 °C using *N*-acetylcysteine methyl ester (**239**) in $\text{DMSO-}d_6$ with a catalytic amount of DABCO. Analysis of purines **54** and **56** revealed that modification of the 2-position through *N*-methylation or replacement of the 2-amino group with a benzyl group, did not significantly alter ethynyl reactivity, which confirmed that the reduced Nek2 inhibitory activity observed for **54** and **56** relative to purine **39** was due to loss of the 2-amino H-bond. Additional experiments with the heterocyclic derivatives **88**, **89** and **90** revealed that the pyrrolopyrimidine was substantially less reactive than **39**, whereas pyrazolopyrimidine **89** and triazolopyrimidine **90** had increased reactivity and required 0.03 equivalents of DABCO rather than 0.30 equivalents, which was used in previous experiments.

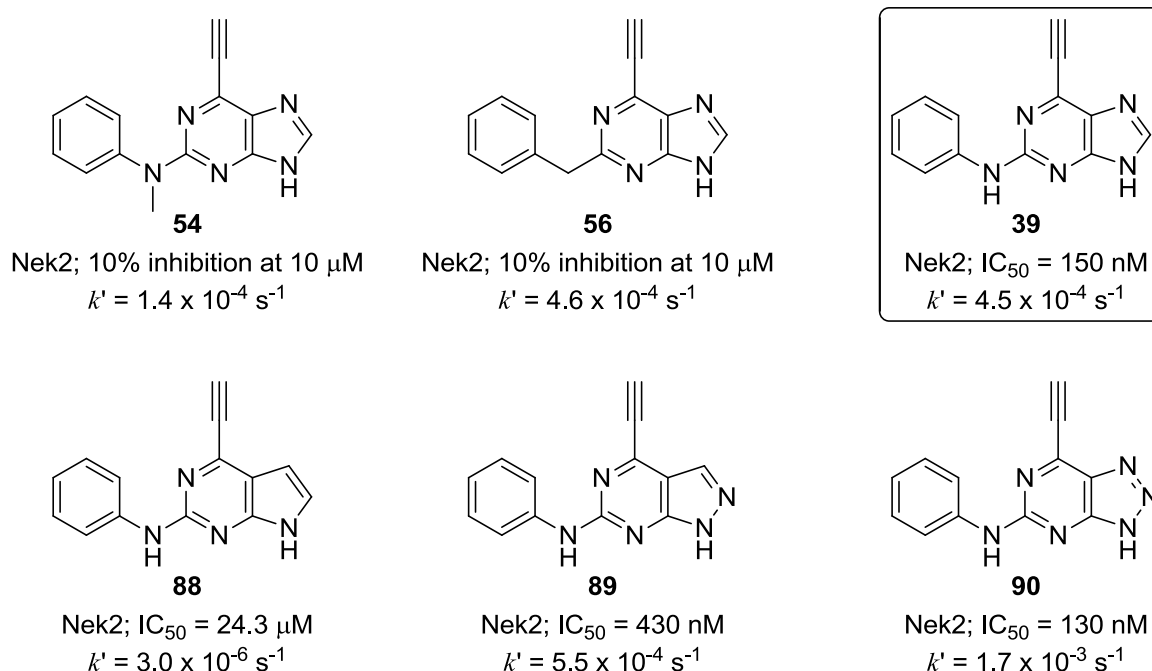


Figure 99 - ^1H -qNMR spectroscopy of selected ethynyl-compounds.

^1H -qNMR spectroscopy proved a valuable tool for the evaluation of ethynyl reactivity towards thiol **239**. However, a limitation of this analysis technique is the requirement of DABCO as a base, which would not be present in a biological system. A possible alternative approach that should be investigated is to use an acidic catalyst, which could accelerate the reaction through protonation of the heterocyclic nitrogen atoms. It is hoped that this would more closely mimic the H-bond mediated partial-protonation of purine **39**, which is believed to facilitate covalent modification of Cys-22 within the Nek2 ATP-binding domain (Figure 27).

9.3 Design and Synthesis of ATP-Competitive CDK2 Inhibitors

It was discovered that the heterocyclic Nek2 inhibitors **87-89** had enhanced CDK2 inhibitory activity when compared with **39**, whereas triazolopyrimidine **90** was essentially inactive in the CDK2 assay ($\text{IC}_{50} > 100 \text{ } \mu\text{M}$). To further investigate this, heterocyclic derivatives of known purine based CDK2 inhibitors **249** ($\text{IC}_{50} = 17 \text{ } \mu\text{M}$) and **37** ($\text{IC}_{50} = 5 \text{ nM}$) were prepared and evaluated for CDK2 inhibitory activity (Figure 100).



249, Purine; CDK2; IC_{50} = 17 μ M
(X = CH, Y = N, Z = N)

254, Imidazopyridine; CDK2; IC_{50} = 18 μ M
(X = CH, Y = N, Z = CH)

255, Pyrrolopyrimidine; CDK2; > 100 μ M
(X = CH, Y = CH, Z = N)

256, Pyrazolopyrimidine; CDK2; IC_{50} = 13 μ M
(X = N, Y = CH, Z = N)

257, Triazolopyrimidine; CDK2; IC_{50} = 18 μ M
(X = N, Y = N, Z = N)

37, Purine; CDK2; IC_{50} = 5 nM
(X = CH, Y = N, Z = N)

250, Imidazopyridine; CDK2; IC_{50} = 140 nM
(X = CH, Y = N, Z = CH)

251, Pyrrolopyrimidine; CDK2; IC_{50} = 26 nM
(X = CH, Y = CH, Z = N)

252, Pyrazolopyrimidine; CDK2; IC_{50} = 18 nM
(X = N, Y = CH, Z = N)

253, Triazolopyrimidine; CDK2; IC_{50} = 3 nM
(X = N, Y = N, Z = N)

Figure 100 – Heterocyclic derivatives of purines **249** and **37**.

CDK2 inhibitors based on the pyrazolopyrimidine and triazolopyrimidine heterocycles (**256**, **252**, **257** and **253**) had similar potency to purines **249** and **37**, with the most potent compound being triazolopyrimidine **253** (IC_{50} = 3 nM). There was a significant difference in the potency of the functionalised imidazopyridine **250** (IC_{50} = 140 nM) and purine **37** (IC_{50} = 5 nM); however, imidazopyridine **254** (IC_{50} = 18 μ M) was of similar potency as purine **249** (IC_{50} = 17 μ M). Additionally, the pyrrolopyrimidine **255** was only weakly active (IC_{50} > 100 μ M), whereas the functionalised pyrrolopyrimidine **251** had potent CDK2 inhibitory activity (IC_{50} = 26 nM). Cisplatin combined cytotoxicity studies of the non-functionalised heterocycles (**255-257**) revealed pyrazolopyrimidine **256** increased cisplatin cytotoxicity, comparable to purine **249**, whereas pyrrolopyrimidine **255** and triazolopyrimidine **257** did not, for reasons that remain unclear.

Future work includes kinase selectivity screens and biological testing of heterocyclic derivatives **250-253** to further evaluate CDK2 as a target of cancer therapeutic interest. Additionally, the mechanism of cisplatin potentiation by pyrazolopyrimidine **256** and purine **249** should be further investigated through additional biological studies.

Chapter Ten: Experimental Section

10.1 Solvents and Reagents

All reagents used were purchased from Sigma-Aldrich, Apollo Scientific or Alfa-Aesar and were in excess of 95% purity unless stated otherwise. Solvents were purchased from Fisher-scientific. Solvents stated as dry or anhydrous were stored in sealed glass bottles containing a SureSeal™ or AcroSeal^(R) septum. When required, solvent was removed from these bottles under dry nitrogen gas and used immediately. Deuterated solvent for NMR analyses were purchased from Sigma-Aldrich.

10.2 Equipment and Analysis

10.2.1 Analytical Techniques

¹H- and ¹³C-NMR spectra were obtained from samples dissolved in deuterated solvents; chloroform (CDCl₃), dimethylsulfoxide (DMSO-*d*₆) or CD₃OD using a Bruker Avance III 500 MHz Spectrometer (125 MHz for ¹³C). Chemical shift values (δ) are reported in parts per million (ppm) with splitting patterns abbreviated to: s (singlet), br s (broad singlet), d (doublet), t (triplet) and m (multiplet). The coupling constant (*J*) is given in Hz and was calculated using the software package Topspin™ developed by Bruker Biospin. When ¹³C values have not been quoted it is due to inability to visualise quaternary carbons. Attempts were made using high concentrations of analyte and increased scan times however in most cases signals for these carbons remained elusive.

Fourier Transform Infrared (FTIR) spectra were obtained using a Bio-Rad FTS 3000mx diamond attenuated total reflectance spectrometer on purified samples with no further preparation. Ultraviolet (UV) analysis was performed in EtOH using a Hitachi UV U2800A spectrophotometer with an analysis range of 800-200 nm.

LC-MS analysis was performed using a Micromass Platform LC electrospray mass spectrometer in positive ionisation mode (ES+) with a PDA 240-400 nm UV detector and a Waters Symmetry Shield RP18 3 µm, 4.6 x 20 mm column at a flow rate of 3

mL/min or a Waters Acquity UPLC system with PDA and ELSD employing both positive and negative ionisation modes and an Acquity UPLC BEH C18 1.7 μ m 2.1 x 50 mm column. The mobile phase consisted of 0.1% v/v formic acid_(aq) / MeCN. Samples analysed by high-resolution mass spectrometry (HRMS) were submitted to the EPSRC national mass spectrometry service centre in Swansea.

Melting points were determined using either a Stuart Scientific SMP3 or Stuart SMP40 automatic melting point apparatus and were observed manually.

cLog P and tPSA values were determined using CS ChemDrawTM Ultra 12.0

10.2.2 Microwave Reactions

Microwave assisted synthesis was performed in sealed Biotage microwave vials, using the Biotage Initiator Sixty microwave system.

10.2.3 Chromatography

Medium pressure automated flash chromatography (MPLC) was performed using a Biotage SP4 or a Varian IntelliFlash 310 flash chromatography system with a solvent gradient calculated from TLC R_f values. MPLC performed on these systems used prepacked columns (KP-Sil, KP-NH or KP-C18). Thin layer chromatography (TLC) was performed using Merck TLC silica gel 60 F₂₅₄ or NH₂F_{254s} plates on aluminium and were visualised under UV light at 245 nm.

10.2.4 Analytical High Performance Liquid Chromatography

All compounds submitted for biological evaluation were in excess of 95% purity which was determined using a Waters XTerra RP18, 5 μ m (4.6 x 150 mm) column at 1 mL/min in both basic (0.1% aqueous ammonia and acetonitrile) and acidic (0.1% formic acid and acetonitrile) conditions with a gradient of 5-100% over 15 min.

10.2.5 Small-Molecule X-ray Crystallography

X-ray crystal structures were obtained by Dr. Ross W. Harrington at X-ray, Crystallography, School of Chemistry, Bedson Building, Newcastle University, Newcastle upon Tyne, NE1 7RU.

10.3 Biological Evaluation of Nek2 and CDK2 inhibitors²⁶⁰

Synthesised inhibitors were evaluated for Nek2 inhibitory activity and counter-screened by Kathy Boxall, Sam Burns, Yvette Newblatt and Maura Westlake under the supervision of Dr. Wynne Aherne in the Analytical Screening and Technology Laboratory of the CR UK Centre for Cancer Therapeutics, The Institute for Cancer Research, Sutton, Surrey, UK, SM2 5NG. The determined inhibitory concentrations are reported as inhibition coefficients for 50% inhibition (IC_{50}) or percentage inhibition as appropriate.

Evaluation of inhibitors for CDK2/cyclin A3 inhibitory activity was conducted by Lan-Zhen Wang at The Northern Institute for Cancer Research, Paul O’Gorman Building, Medical School, Newcastle University, Framlington Place, Newcastle upon Tyne, NE2 4HH.

10.3.1 Nek2 Biochemical Assay

Nek2 inhibitory activities were determined using a Caliper EZ Reader II instrument with either a 4 or 12 sipper microfluidic chip (Caliper Life Sciences Ltd, Runcorn, UK). The assay format employs an electrophoretic method which separates a phosphorylated peptide substrate of Nek2 from the non-phosphorylated substrate after incubation in the assay medium for a defined time in the presence of a chemical inhibitor. The separation is based on charge, with the negatively charged phosphopeptide migrating more rapidly towards a positively charged terminal. The extent of phosphorylation is proportional to the extent of functional Nek2 enzymatic activity in the assay solution and its ability to bind ATP to phosphorylate the peptide substrate. The Caliper instrument readout gives an estimate of the proportion of peptide substrate which is phosphorylated by uninhibited Nek2. Therefore, the

greater the affinity of an inhibitor for Nek2, the lower the proportion of phosphopeptide as detected by a fluorescence sensor.

The assay was conducted by 1:4 dilution of a 10 mM stock solution of an inhibitor in DMSO by taking 15 μ L of inhibitor solution and adding this to 45 μ L of DMSO in the first row of a 384 well polypropylene assay plate (Greiner). Seven further successive 1:3 dilutions were performed by taking 20 μ L of the inhibitor solution and adding this to 60 μ L of 100% DMSO in the well directly below, to give a 250 μ M top concentration in DMSO. The 100% DMSO solutions were each diluted 20-fold by adding 2.5 μ L of each well to 47.5 μ L of a stock kinase buffer (25 mL, consisting of: stock Cisbio buffer (5 mL), 1,4-dithiothreitol (25 μ L, 1 mM), $MgCl_2$ (125 μ L, 5 mM solution in water), Tween₂₀ (25 μ L, 0.1%) and HPLC grade water (20 mL)) to give a top concentration of 125 μ M in 5% DMSO. To a second 384 well assay plate was added 4 μ L of 5% DMSO solution from each well of the first assay plate to give a top concentration of 50 μ M in 2% DMSO after a 1:2.5 dilution. To each well was added Nek2 enzyme (2 μ L of 0.28 mg/mL aqueous solution, giving a 4 nM final concentration, PV3360 Invitrogen), substrate 'peptide-11' (5-FAM-KKLNRTLSVA-COOH, 2 μ L of 1.5 mM aqueous solution, giving a 1 μ M final concentration, #760355 Caliper Life Sciences) and finally ATP (2 μ L aqueous 10 mM solution, giving a 30 μ M final concentration) was added to initiate the reaction. The plate was immediately sealed and centrifuged for 1 minute to mix all of the reagents before incubation at room temperature for 60 min.

The reaction was stopped after the required time by addition of 90 μ L of separation buffer (#760367 Caliper Life Sciences). The amount of peptide 11 phosphorylation was then determined using the Caliper EZ Reader II instrument (1.5 psi, 1750 ΔV). The percentage conversion of substrate protein was measured and the percentage inhibition was thus calculated relative to blank wells, which contained no enzyme and 2% DMSO, and totals wells which contained all reagents and 2% DMSO replacing the inhibitor.

IC₅₀ values were determined in duplicate over a range of 8 concentrations using GraphPad Prism 5, employing a non-linear regression fit of log[inhibitor] versus response (% inhibition) with a variable slope equation. It is noteworthy that IC₅₀

values presented for the irreversible inhibitor series are the values obtained as above, after 60 minute incubation of the inhibitor with Nek2.

10.3.2 CellTiter-Blue Assay for Cell Growth Inhibition

U2OS human osteosarcoma cells (American Type Culture Collection, Manassas, Virginia, United States) were grown in McCoy's 5A medium supplemented with 1.5 mM L-glutamine, 25 mM HEPES, 2% penicillin/streptomycin (Invitrogen, Paisley, United Kingdom) and 10% foetal bovine serum (Biosera, Ringmer, East Sussex, United Kingdom). MDA-MB-231 human breast cancer cells (American Type Culture Collection, Manassas, Virginia, United States) were grown in RPMI 1640 medium (Invitrogen) supplemented with 2 mM L-glutamine, 25 mM HEPES, 2% penicillin/streptomycin and 10% foetal bovine serum. HeLa cells were grown in Dulbecco's Modified Eagle Medium (D-MEM) (Invitrogen) supplemented with 2% penicillin/streptomycin and 10% foetal bovine serum. All three cell lines were maintained in a humidified atmosphere of 5% CO₂ at 37°C. The medium was aspirated and the cells were washed with PBS (Invitrogen), trypsinized (Internal supply, 0.25% versene trypsin with EDTA), neutralised and counted. Cells were seeded into 384-well clear tissue culture treated microtiter plates (Corning B.V. Life Sciences, Amsterdam, The Netherlands) at 200 cells per well in a 45 µL volume of the respective media. Columns 1 and 24 had no cells added and were plated with 45 µL of media alone. Cells were incubated at 37°C / 5% CO₂. At 24 hours after plating, compounds were three-fold serially diluted in large volume V-shape 384-well microplates (Greiner Bio-One, Stonehouse, Gloucestershire, United Kingdom) using an Evolution plate handling system (PerkinElmer Life Sciences, Waltham, Massachusetts, USA). Then 5 µL of diluted test compounds, Etoposide as positive control (Sigma-Aldrich, Gillingham, Dorset, United Kingdom), or DMSO at 1% v/v final concentration (Fisher Scientific, Loughborough, Leicestershire, United Kingdom) were added to the wells using a MiniTrack V plate handling system (PerkinElmer Life Sciences). There were four replicates of each compound concentration, 32 replicates of DMSO wells, and 32 replicates of wells containing no cells. Test compounds were screened at final concentrations of 100 µM, 33.33 µM, 11.11 µM, 3.70 µM, 1.23 µM, 0.41 µM, 0.14 µM, and 0.05 µM. Etoposide was screened at final concentrations of

10 μ M, 3.33 μ M, 1.11 μ M, 0.37 μ M, 0.12 μ M, 0.041 μ M, 0.014 μ M, and 0.005 μ M. After 92 hours, 5 μ L of CellTiter-Blue Reagent (Promega, Southampton, United Kingdom) was added to the cells using a Multidrop dispenser (Thermo Electron, Basingstoke, Hants, United Kingdom) and incubated for 4 hours in a humidified atmosphere of 5% CO₂ at 37°C. After the incubation, the plates were placed at room temperature for 40 minutes before fluorescence was recorded (560_{Ex}/590_{Em}) on an EnVision 2103 plate reader (PerkinElmer Life Sciences). Data were plotted as percentage of DMSO control against compound concentration using *GraphPad Prism* 5 Software. The 50% growth inhibition (GI₅₀) was calculated as the compound concentration required to reduce the cell number by 50% compared with the DMSO control.

10.3.3 CDK2/Cyclin A3 Biochemical Assay

Inhibition of human CDK2/Cyclin A3 was assayed as previously described¹⁸⁷ using recombinant CDK2/cyclin A3 (10 μ L) with 1 mg/mL histone H1 (150 μ L, Sigma type III-S), in the presence of [γ -³²P] ATP (1-5 μ L, 3000 Ci/mmol, Cat number NEG002A Perkin Elmer) and cold ATP (13.13 μ L, 1 mM) in a final volume of 30 μ L. The assay buffer (500 μ L total volume) contained Tris-HCl pH 7.5 (50 mM) and MgCl₂ (5 mM). The final DMSO concentration in the assay was 1% (V/V), after inhibitors stocks in 100% DMSO were diluted 1:10 in the appropriate assay buffer (3 μ L + 27 μ L buffer), followed by addition of 3 μ L of 10% inhibitor solution to a total assay volume of 30 μ L. Therefore, the final DMSO concentration was 1%, final inhibitor concentration was 1/100 of the original stock solution and the final ATP concentration in the assay was 12.5 μ M. After incubation for 10 min at 30 °C, 25 μ L aliquots were spotted onto 2.5 cm \times 3 cm pieces of Whatman P81 phosphocellulose paper, and after 20 s, the filters were washed five times (> 5 min each time) in 1% phosphoric acid. The dry filters were transferred into 6 ml plastic scintillation vials, 5ml scintillation fluid (Amersham) was added, and the radioactivity was measured using a scintillation counter.

10.3.4 Nek2 Protein Crystallography

Nek2 purine co-crystal structures were solved by Dr Richard Bayliss and Dr Corine Mas-Droux at the Section of Structural Biology, The Institute for Cancer Research, 237 Fulham Road, London, SW3 6JB. Crystal structures of novel ethynyl heterocycles were solved as part of a 4-week placement under the supervision of Dr Richard Bayliss and Dr Sharon Yeoh at the University of Leicester, Henry Welcome Building, Lancaster Rd, Leicester, LE1 9HN.

10.4 Index of Synthesised Compounds

	Page
6-Chloro-2-fluoro-9 <i>H</i> -purine (58)	205
6-Chloro-2-fluoro-9-methyl-9 <i>H</i> -purine (60) and 6-chloro-2-fluoro-7-methyl-7 <i>H</i> -purine (59)	206
2-Fluoro-9-methyl-6-((triisopropylsilyl)ethynyl)-9 <i>H</i> -purine (62) and 2-fluoro-7-methyl-6-((triisopropylsilyl)ethynyl)-7 <i>H</i> -purine (61)	207
9-Methyl- <i>N</i> -phenyl-6-((triisopropylsilyl)ethynyl)-9 <i>H</i> -purin-2-amine (64)	208
7-Methyl- <i>N</i> -phenyl-6-((triisopropylsilyl)ethynyl)-7 <i>H</i> -purin-2-amine (63)	209
6-Ethynyl-9-methyl- <i>N</i> -phenyl-9 <i>H</i> -purin-2-amine (53)	210
6-Ethynyl-7-methyl- <i>N</i> -phenyl-7 <i>H</i> -purin-2-amine (52)	211
1 <i>H</i> -Pyrrolo[2,3- <i>d</i>]pyrimidine-2,4(3 <i>H</i> ,7 <i>H</i>)-dione (128)	212
2,4-Dichloro-7 <i>H</i> -pyrrolo[2,3- <i>d</i>]pyrimidine (129)	213
2,4-Dichloro-7-tosyl-7 <i>H</i> -pyrrolo[2,3- <i>d</i>]pyrimidine (130)	214
2-Chloro-7-tosyl-4-((triisopropylsilyl)ethynyl)-7 <i>H</i> -pyrrolo[2,3- <i>d</i>]pyrimidine (131)	215
<i>N</i> -Phenyl-7-tosyl-4-((triisopropylsilyl)ethynyl)-7 <i>H</i> -pyrrolo[2,3- <i>d</i>]pyrimidin-2-amine (132)	216
<i>N</i> -Phenyl-4-((triisopropylsilyl)ethynyl)-7 <i>H</i> -pyrrolo[2,3- <i>d</i>]pyrimidin-2-amine (140)	217
4-Ethynyl- <i>N</i> -phenyl-7 <i>H</i> -pyrrolo[2,3- <i>d</i>]pyrimidin-2-amine (88)	218
2-(3-Aminophenyl)acetamide (290)	219
2-(3-((7-Tosyl-4-((triisopropylsilyl)ethynyl)-7 <i>H</i> -pyrrolo[2,3- <i>d</i>]pyrimidin-2-yl)amino)phenyl)acetamide (141)	220
2-(3-((4-((Triisopropylsilyl)ethynyl)-7 <i>H</i> -pyrrolo[2,3- <i>d</i>]pyrimidin-2-yl)amino) phenyl)acetamide (291)	221
2-(3-((4-Ethynyl-7 <i>H</i> -pyrrolo[2,3- <i>d</i>]pyrimidin-2-yl)amino)phenyl)acetamide (231)	222
3 <i>H</i> -Imidazo[4,5- <i>b</i>]pyridine (103)	223

	Page
3 <i>H</i> -Imidazo[4,5- <i>b</i>]pyridine 4-oxide (104)	224
7-Chloro-3 <i>H</i> -imidazo[4,5- <i>b</i>]pyridine (105)	225
<i>tert</i> -Butyl 7-chloro-3 <i>H</i> -imidazo[4,5- <i>b</i>]pyridine-3-carboxylate (106)	226
<i>tert</i> -Butyl 7-chloro-5-nitro-3 <i>H</i> -imidazo[4,5- <i>b</i>]pyridine-3-carboxylate (107)	227
<i>tert</i> -Butyl 5-amino-7-chloro-3 <i>H</i> -imidazo[4,5- <i>b</i>]pyridine-3-carboxylate (108)	228
7-Chloro-5-fluoro-3 <i>H</i> -imidazo[4,5- <i>b</i>]pyridine (109)	229
Chloro-5-fluoro-3-(tetrahydro-2 <i>H</i> -pyran-2-yl)-3 <i>H</i> -imidazo[4,5- <i>b</i>]pyridine (110)	230
5-Fluoro-3-(tetrahydro-2 <i>H</i> -pyran-2-yl)-7-((triisopropylsilyl)ethynyl)-3 <i>H</i> -imidazo [4,5- <i>b</i>]pyridine (111)	231
5-Fluoro-7-((triisopropylsilyl)ethynyl)-3 <i>H</i> -imidazo[4,5- <i>b</i>]pyridine (112)	232
<i>N</i> -Phenyl-7-((triisopropylsilyl)ethynyl)-3 <i>H</i> -imidazo[4,5- <i>b</i>]pyridin-5-amine (113)	233
7-Ethynyl- <i>N</i> -phenyl-3 <i>H</i> -imidazo[4,5- <i>b</i>]pyridin-5-amine (87)	234
2,4,6-Trichloropyrimidine-5-carbaldehyde (144)	235
4,6-Dichloro-1 <i>H</i> -pyrazolo[3,4- <i>d</i>]pyrimidine (145)	236
4,6-Dichloro-1-(tetrahydro-2 <i>H</i> -pyran-2-yl)-1 <i>H</i> -pyrazolo[3,4- <i>d</i>]pyrimidine (146)	237
6-Chloro-1-(tetrahydro-2 <i>H</i> -pyran-2-yl)-4-((triisopropylsilyl)ethynyl)-1 <i>H</i> -pyrazolo[3,4- <i>d</i>]pyrimidine (147)	238
6-Chloro-4-((triisopropylsilyl)ethynyl)-1 <i>H</i> -pyrazolo[3,4- <i>d</i>]pyrimidine (148)	239
<i>N</i> -Phenyl-4-((triisopropylsilyl)ethynyl)-1 <i>H</i> -pyrazolo[3,4- <i>d</i>]pyrimidin-6-amine (149)	240
4-Ethynyl- <i>N</i> -phenyl-1 <i>H</i> -pyrazolo[3,4- <i>d</i>]pyrimidin-6-amine (89)	241
1-(2,4,6-Trichloropyrimidin-5-yl)ethanol (158)	242
1-(2,4,6-Trichloropyrimidin-5-yl)ethanone (159)	243
4,6-Dichloro-3-methyl-1 <i>H</i> -pyrazolo[3,4- <i>d</i>]pyrimidine (160)	244
4,6-Dichloro-3-methyl-1-(tetrahydro-2 <i>H</i> -pyran-2-yl)-1 <i>H</i> -pyrazolo[3,4- <i>d</i>] pyrimidine (161)	245
6-Chloro-3-methyl-1-(tetrahydro-2 <i>H</i> -pyran-2-yl)-4-((triisopropylsilyl)ethynyl)-1 <i>H</i> -pyrazolo[3,4- <i>d</i>]pyrimidine (162)	246
6-Chloro-3-methyl-4-((triisopropylsilyl)ethynyl)-1 <i>H</i> -pyrazolo[3,4- <i>d</i>]pyrimidine (163)	247
3-Methyl- <i>N</i> -phenyl-4-((triisopropylsilyl)ethynyl)-1 <i>H</i> -pyrazolo[3,4- <i>d</i>]pyrimidin-6-amine (164)	248
4-Ethynyl-3-methyl- <i>N</i> -phenyl-1 <i>H</i> -pyrazolo[3,4- <i>d</i>]pyrimidin-6-amine (165)	249
6-Chloro-5-((4-chlorophenyl)diazenyl)pyrimidine-2,4-diamine (171)	250
6-Chloropyrimidine-2,4,5-triamine (172)	251

	Page
7-Chloro-3 <i>H</i> -[1,2,3]triazolo[4,5- <i>d</i>]pyrimidin-5-amine (173)	252
<i>tert</i> -Butyl 5-amino-7-chloro-3 <i>H</i> -[1,2,3]triazolo[4,5- <i>d</i>]pyrimidine-3-carboxylate (174)	253
<i>tert</i> -Butyl 5-amino-7-((triisopropylsilyl)ethynyl)-3 <i>H</i> -[1,2,3]triazolo[4,5- <i>d</i>] pyrimidine-3-carboxylate (179)	254
7-((Triisopropylsilyl)ethynyl)-3 <i>H</i> -[1,2,3]triazolo[4,5- <i>d</i>]pyrimidin-5-amine (175)	255
2-(3-((7-((Triisopropylsilyl)ethynyl)-3 <i>H</i> -[1,2,3]triazolo[4,5- <i>d</i>]pyrimidin-5-yl) amino)phenyl) acetamide (292)	256
2-(3-((7-Ethynyl-3 <i>H</i> -[1,2,3]triazolo[4,5- <i>d</i>]pyrimidin-5-yl)amino)phenyl) acetamide (232)	257
4,6-Dichloro- <i>N</i> -phenyl-1,3,5-triazin-2-amine (184)	258
4-Chloro- <i>N</i> -phenyl-6-((triisopropylsilyl)ethynyl)-1,3,5-triazin-2-amine (185)	258
<i>N</i> ² -Methyl- <i>N</i> ⁴ -phenyl-6-((triisopropylsilyl)ethynyl)-1,3,5-triazine-2,4-diamine (186)	259
<i>N</i> ² -Ethyl- <i>N</i> ⁴ -phenyl-6-((triisopropylsilyl)ethynyl)-1,3,5-triazine-2,4-diamine (187)	260
<i>N</i> ² -(4-Methoxybenzyl)- <i>N</i> ⁴ -phenyl-6-((triisopropylsilyl)ethynyl)-1,3,5-triazine-2,4-diamine (188)	261
6-Ethynyl- <i>N</i> ² -methyl- <i>N</i> ⁴ -phenyl-1,3,5-triazine-2,4-diamine (92)	262
6-Ethynyl- <i>N</i> ² -ethyl- <i>N</i> ⁴ -phenyl-1,3,5-triazine-2,4-diamine (93)	262
6-Ethynyl- <i>N</i> ² -(4-methoxybenzyl)- <i>N</i> ⁴ -phenyl-1,3,5-triazine-2,4-diamine (94)	263
<i>N</i> ² -Phenyl-6-((triisopropylsilyl)ethynyl)-1,3,5-triazine-2,4-diamine (293)	264
6-Ethynyl- <i>N</i> ² -phenyl-1,3,5-triazine-2,4-diamine (91)	264
Phenylguanidine nitrate (204)	265
6-Hydroxy-2-(phenylamino)pyrimidin-4(1 <i>H</i>)-one (206)	266
4,6-Dichloro- <i>N</i> -phenylpyrimidin-2-amine (207)	266
6-Chloro- <i>N</i> ⁴ -methyl- <i>N</i> ² -phenylpyrimidine-2,4-diamine (208)	267
6-Chloro- <i>N</i> ⁴ -ethyl- <i>N</i> ² -phenylpyrimidine-2,4-diamine (209)	268
6-Chloro- <i>N</i> ⁴ -(4-methoxybenzyl)- <i>N</i> ² -phenylpyrimidine-2,4-diamine (210)	268
6-((<i>tert</i> -Butyldimethylsilyl)ethynyl)- <i>N</i> ⁴ -methyl- <i>N</i> ² -phenylpyrimidine-2,4-diamine (211)	269
6-((<i>tert</i> -Butyldimethylsilyl)ethynyl)- <i>N</i> ⁴ -ethyl- <i>N</i> ² -phenylpyrimidine-2,4-diamine (212)	270
6-((<i>tert</i> -Butyldimethylsilyl)ethynyl)- <i>N</i> ⁴ -(4-methoxybenzyl)- <i>N</i> ² -phenylpyrimidine-2,4-diamine (213)	271
6-((<i>tert</i> -Butyldimethylsilyl)ethynyl)- <i>N</i> ² -phenylpyrimidine-2,4-diamine (220)	272
5-Bromo-6-((<i>tert</i> -butyldimethylsilyl)ethynyl)- <i>N</i> ² -phenylpyrimidine-2,4-diamine (222)	273
6-((<i>tert</i> -Butyldimethylsilyl)ethynyl)-5-chloro- <i>N</i> ² -phenylpyrimidine-2,4-diamine (221)	274

	Page
6-Ethynyl- <i>N</i> ⁴ -methyl- <i>N</i> ² -phenylpyrimidine-2,4-diamine (96)	275
<i>N</i> ⁴ -Ethyl-6-ethynyl- <i>N</i> ² -phenylpyrimidine-2,4-diamine (67)	275
6-Ethynyl- <i>N</i> ⁴ -(4-methoxybenzyl)- <i>N</i> ² -phenylpyrimidine-2,4-diamine (98)	276
6-Ethynyl- <i>N</i> ² -phenylpyrimidine-2,4-diamine (95)	277
5-Bromo-6-ethynyl- <i>N</i> ² -phenylpyrimidine-2,4-diamine (100)	277
5-Chloro-6-ethynyl- <i>N</i> ² -phenylpyrimidine-2,4-diamine (99)	278
7-(Cyclohexylmethoxy)-3 <i>H</i> -[1,2,3]triazolo[4,5- <i>d</i>]pyrimidin-5-amine (257)	279
4-((7-(Cyclohexylmethoxy)-3 <i>H</i> -[1,2,3]triazolo[4,5- <i>d</i>]pyrimidin-5-yl)amino)benzenesulfonamide (253)	280
2-Amino-4,6-dichloropyrimidine-5-carbaldehyde (285)	281
4-Chloro-1 <i>H</i> -pyrazolo[3,4- <i>d</i>]pyrimidin-6-amine (286)	282
4-(Cyclohexylmethoxy)-1 <i>H</i> -pyrazolo[3,4- <i>d</i>]pyrimidin-6-amine (256)	282
6-Chloro-4-(cyclohexylmethoxy)-1 <i>H</i> -pyrazolo[3,4- <i>d</i>]pyrimidine (287)	283
4-((4-(Cyclohexylmethoxy)-1 <i>H</i> -pyrazolo[3,4- <i>d</i>]pyrimidin-6-yl)amino)benzene sulfonamide (252)	284
2-Amino-3 <i>H</i> -pyrrolo[2,3- <i>d</i>]pyrimidin-4(7 <i>H</i>)-one (264)	285
4-Chloro-7 <i>H</i> -pyrrolo[2,3- <i>d</i>]pyrimidin-2-amine (265)	286
4-(Cyclohexylmethoxy)-7 <i>H</i> -pyrrolo[2,3- <i>d</i>]pyrimidin-2-amine (255)	286
4-Chloro-7-((2-(trimethylsilyl)ethoxy)methyl)-7 <i>H</i> -pyrrolo[2,3- <i>d</i>]pyrimidin-2-amine (279)	287
4-(Cyclohexylmethoxy)-7-((2-(trimethylsilyl)ethoxy)methyl)-7 <i>H</i> -pyrrolo[2,3- <i>d</i>]pyrimidin-2-amine (280)	288
2-Chloro-4-(cyclohexylmethoxy)-7-((2-(trimethylsilyl)ethoxy)methyl)-7 <i>H</i> -pyrrolo[2,3- <i>d</i>]pyrimidine (281)	289
4-((4-(Cyclohexylmethoxy)-7-((2-(trimethylsilyl)ethoxy)methyl)-7 <i>H</i> -pyrrolo[2,3- <i>d</i>]pyrimidin-2-yl)amino)benzenesulfonamide (282)	290
4-((4-(Cyclohexylmethoxy)-7 <i>H</i> -pyrrolo[2,3- <i>d</i>]pyrimidin-2-yl)amino) benzenesulfonamide (251)	291
<i>N</i> -Phenyl-7-((triisopropylsilyl)ethynyl)-3 <i>H</i> -[1,2,3]triazolo[4,5- <i>d</i>]pyrimidin-5-amine (176)	292
7-Ethynyl- <i>N</i> -phenyl-3 <i>H</i> -[1,2,3]triazolo[4,5- <i>d</i>]pyrimidin-5-amine (90)	293
2-Benzyl-1 <i>H</i> -purin-6(9 <i>H</i>)-one (81)	294
2-Benzyl-6-chloro-9 <i>H</i> -purine (82)	294
<i>tert</i> -Butyl 2-benzyl-6-chloro-9 <i>H</i> -purine-9-carboxylate (83)	295
<i>tert</i> -Butyl 2-benzyl-6-((triisopropylsilyl)ethynyl)-9 <i>H</i> -purine-9-carboxylate (82)	296

	Page
2-Benzyl-6-((triisopropylsilyl)ethynyl)-9 <i>H</i> -purine (85)	297
2-Benzyl-6-ethynyl-9 <i>H</i> -purine (56)	298
<i>N</i> -Methyl- <i>N</i> -phenyl-6-((triisopropylsilyl)ethynyl)-9 <i>H</i> -purin-2-amine (66)	298
6-Ethynyl- <i>N</i> -methyl- <i>N</i> -phenyl-9 <i>H</i> -purin-2-amine (54)	299
6-Chloro-9-(4-methoxybenzyl)-9 <i>H</i> -purin-2-amine (70)	300
9-(4-Methoxybenzyl)-6-((triisopropylsilyl)ethynyl)-9 <i>H</i> -purin-2-amine (71)	301
2-Chloro-9-(4-methoxybenzyl)-6-((triisopropylsilyl)ethynyl)-9 <i>H</i> -purine (72)	302
9-(4-Methoxybenzyl)-2-phenoxy-6-((triisopropylsilyl)ethynyl)-9 <i>H</i> -purine (73)	303
2-Phenoxy-6-((triisopropylsilyl)ethynyl)-9 <i>H</i> -purine (68)	304
6-Ethynyl-2-phenoxy-9 <i>H</i> -purine (55)	305
<i>N</i> -Benzyltriethylammonium nitrite (294)	305
4,6-Dichloro-2-(phenylamino)pyrimidine-5-carbaldehyde (228)	306
4-Chloro-6-((4-methoxybenzyl)amino)-2-(phenylamino)pyrimidine-5-carbaldehyde (229)	307
4-((<i>tert</i> -Butyldimethylsilyl)ethynyl)-6-((4-methoxybenzyl)amino)-2-(phenylamino)pyrimidine-5-carbaldehyde (230)	308
4-Amino-6-((<i>tert</i> -butyldimethylsilyl)ethynyl)-2-(phenylamino)pyrimidine-5-carbaldehyde (226)	309
4-Amino-6-ethynyl-2-(phenylamino)pyrimidine-5-carbaldehyde (101)	310
7-Chloro-5-nitro-3 <i>H</i> -imidazo[4,5- <i>b</i>]pyridine (258)	311
7-Chloro-3 <i>H</i> -imidazo[4,5- <i>b</i>]pyridin-5-amine (259)	311
7-Chloro-3-(4-methoxybenzyl)-3 <i>H</i> -imidazo[4,5- <i>b</i>]pyridin-5-amine (260)	312
7-(Cyclohexylmethoxy)-3-(4-methoxybenzyl)-3 <i>H</i> -imidazo[4,5- <i>b</i>]pyridin-5-amine (261)	313
7-(Cyclohexylmethoxy)-5-iodo-3-(4-methoxybenzyl)-3 <i>H</i> -imidazo[4,5- <i>b</i>]pyridine (262)	314
4-((7-(Cyclohexylmethoxy)-3-(4-methoxybenzyl)-3 <i>H</i> -imidazo[4,5- <i>b</i>]pyridin-5-yl)amino)benzenesulfonamide (263)	315
4-((7-(Cyclohexylmethoxy)-3 <i>H</i> -imidazo[4,5- <i>b</i>]pyridin-5-yl)amino) benzenesulfonamide (250)	316
7-(Cyclohexylmethoxy)-3 <i>H</i> -imidazo[4,5- <i>b</i>]pyridin-5-amine (254)	317

10.5 General Procedures

10.5.1 General Procedure A: TBAF Mediated Silyl Deprotection of Terminal Acetylenes

To a solution of the appropriate silyl protected acetylene in THF (50 mL/g) was added TBAF solution (1 M in THF, 1.1 equiv.). The reaction mixture was stirred (RT, 15 min) then TBAF scavenger beads were added (10 equiv. by weight). The reaction mixture was stirred overnight, filtered then the solvent was removed *in vacuo*. The crude product was redissolved (EtOAc) then dry loaded onto silica and purified as indicated.

10.5.2 General Procedure B: Nucleophilic Aromatic Substitution of 4-Chloro-*N*-Phenyl-6-((Triisopropylsilyl)ethynyl)-1,3,5-Triazin-2-Amine (185)

To a stirred solution of 4-chloro-*N*-phenyl-6-((triisopropylsilyl)ethynyl)-1,3,5-triazin-2-amine (20 mg, 0.052 mmol) in THF (50 mL/g) was added the appropriate amine (3 equiv.). The resulting mixture was stirred (RT, 1 h). The solvent was removed *in vacuo* and the crude product redissolved in EtOAc (15 mL). The resulting solution was washed with water (3 x 15 mL) then dried (Na₂SO₄). The crude product was dry loaded onto silica and purified as indicated.

10.5.3 General Procedure C: Nucleophilic Aromatic Substitution of 4,6-Dichloro-*N*-Phenylpyrimidin-2-Amine (207)

To a stirred solution of 4,6-dichloro-*N*-phenylpyrimidin-2-amine (200 mg, 0.83 mmol) in THF (15 mL/g) was added the appropriate amine (2 equiv.) followed by KHCO₃ (100 mg, 1.0 mmol). The resulting mixture was heated (80 °C, 6 h) resulting in consumption of the starting material. The reaction mixture was acidified with aqueous HCl_(aq) (1 M) (30 mL) then extracted with EtOAc (3 x 30 mL). The combined organic layers were washed with NaHCO_{3(aq)} (45 mL) and water (2 x 45 mL) then dried (Na₂SO₄). The crude product was dry loaded onto silica and purified as indicated.

10.5.4 General Procedure D: Suzuki Coupling of *tert*-Butyldimethylsilyl Acetylene Boronic Acid Pinacol Ester to Functionalised Pyrimidines

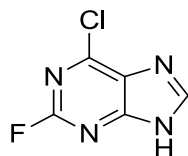
To a solution of the appropriate chloro pyrimidine (1 equiv.) in anhydrous dioxane (40 mL/g) was added *tert*-butyldimethylsilyl acetylene boronic acid pinacol ester (1.5 equiv.), Cs_2CO_3 (1.5 equiv.) and tetrakis(triphenylphosphine)palladium(0) ($\text{Pd}(\text{PPh}_3)_4$) (0.1 equiv.). The reaction mixture was degassed (N_2 , 30 min) then heated under microwave irradiation (2 h, 140 °C). The reaction mixture was filtered through Celite and EtOAc (100 mL/g) was added. The resulting solution was washed with water (3 x 50 mL/g), dried (Na_2SO_4) and dry loaded onto silica and purified as indicated.

10.5.5 General Procedure E: TFA Catalysed Coupling of Aromatic Amines with Halogenated Heterocycles

To a solution of the appropriate fluoro or chloro heterocycle (1 equiv.) in TFE (10 mL/g) was added the aromatic amine (3 equiv.) and TFA (2.5 equiv.). The resulting solution was heated (110 °C, 18h) then cooled (RT) and added to $\text{NaHCO}_{3(\text{aq})}$ (100 mL/g). The aqueous mixture was extracted with EtOAc (3 x 100 mL/g) and the combined organic layers were washed with water (2 x 150 mL/g), dried (Na_2SO_4) and purified as indicated.

10.5.6 General Procedure F: ^1H -qNMR Studies²⁶⁰

The ethynyl heterocycle (690 μL from a stock solution in $\text{DMSO}-d_6$ containing 4.2 μmol of compound) was added to a 10-fold excess of *N*-acetylcysteine methyl ester **239** (7.48 mg, 42 μmol). The solution temperature was maintained at approximately 24 °C (water-bath) before addition of a $\text{DMSO}-d_6$ solution (10 μL) containing DABCO (0.14 mg, 1.26 μmol) and DMF (0.33 μL , 4.2 μmol) to afford a final ethynyl substituted compound in a concentration of 6 mM in a total volume of 700 μL . The NMR tube containing the reagents was inverted several times to aid mixing and dissolution of reagents. The thoroughly mixed solution was inserted into the NMR machine cavity and the acquisition of quantitative ^1H NMR data was immediately initiated. The time between the addition of the DABCO/DMF-solution and the completion of the first ^1H -qNMR experiment was monitored and subsequent time intervals between experiments were calculated based on the defined parameters.

6-Chloro-2-fluoro-9H-purine (58)

A polytetrafluoroethylene (PFTE) conical flask was charged with tetrafluoroboric acid (180 mL) and 2-amino-6-chloro purine (9.0 g, 53.1 mmol). The resulting mixture was cooled to 0 °C and an aqueous solution of sodium nitrite (7.3 g, 0.106 mol) was introduced dropwise with stirring over a period of 75 min. The reaction mixture was then warmed (RT) and stirred for an additional 20 min before being cooled to -15 °C and neutralised (NaOH). The resulting aqueous solution was extracted with EtOAc (2 x 500 mL) and the solvent removed under vacuum to give the title compound (**54**) as a pale yellow solid (6.0 g, 0.035 mol, 66%) which was used in the next reaction without any further purification.

R_f = 0.41 (1:9 MeOH/DCM); m.p. 169-173 °C; UV λ_{max} (EtOH/nm) 270.0; IR ν_{max}/cm^{-1} : 3488, 2961, 2802, 2569, 2155, 1584; 1H NMR (500 MHz, DMSO- d_6) δ 8.62 (1H, s, C⁸-H), 14.01 (1H, br s, N⁹-H); ^{13}C NMR (125 MHz, DMSO- d_6) δ 128.1 (Ar-C), 147.5 (Ar-C), 148.6 (Ar-C), 156.0 (C-Cl), 162.3 (C-F); ^{19}F NMR (500 MHz, DMSO- d_6) δ -52.8; LRMS (ES+) m/z 173.1 [M+H]⁺.

6-Chloro-2-fluoro-9-methyl-9*H*-purine (60) and 6-chloro-2-fluoro-7-methyl-7*H*-purine (59)



To a solution of chloro-2-fluoro-9*H*-purine (**58**) (1.00 g, 6.37 mmol) in anhydrous DMF (14 mL) was added K_2CO_3 (0.88 g, 6.37 mmol). The reaction mixture was stirred (RT, 5 min) then iodomethane (435 μ L, 6.37 mmol) was added dropwise to the reaction mixture and the vessel sealed. The reaction mixture was stirred at RT for 18 h. The iodomethane was removed by vacuum distillation into a rotary evaporator containing a 3:1 mixture of MeOH/ NH_4OH (32%), and residual DMF was removed under high vacuum. The crude product was redissolved in EtOAc (30 mL), dry loaded onto silica and purified by MPLC on silica (2:98 MeOH/DCM) to give a mixture of non-separable regioisomers (**60**) and (**59**) (ratio of 2:1 respectively (NMR)) as an off-white crystalline solid (0.81 g, 4.32 mmol, 75%).

*N*⁹-Methylated compound (**60**)

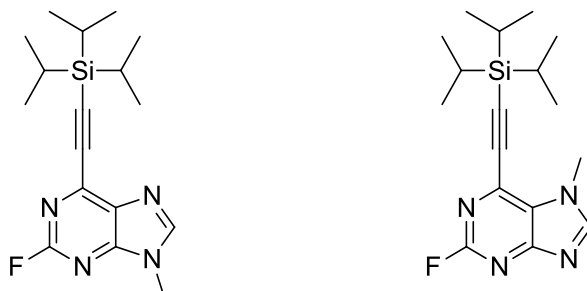
R_f 0.45 (5:95 MeOH/DCM); 1H NMR (500 MHz, DMSO- d_6) δ 3.82 (3H, s, CH_3), 8.66 (1H, s, C^8 -H); LRMS (ES+) m/z 187.1 $[M+H]^+$.

*N*⁷-Methylated compound (**59**)

R_f 0.45 (5:95 MeOH/DCM); 1H NMR (500 MHz, DMSO- d_6) δ 4.13 (3H, s, CH_3), 8.87 (1H, s, C^8 -H); ^{19}F NMR (500 MHz, DMSO- d_6) δ -52.9, -52.4

Note: Compound was not fully characterised due to inseparable mixture of regioisomers.

2-Fluoro-9-methyl-6-((triisopropylsilyl)ethynyl)-9*H*-purine (62) and 2-fluoro-7-methyl-6-((triisopropylsilyl)ethynyl)-7*H*-purine (61)



The inseparable mixture of 6-chloro-2-fluoro-9-methyl-9*H*-purine (**60**) and 6-chloro-2-fluoro-7-methyl-7*H*-purine (**59**) (0.74 g, 3.97 mmol) was dissolved in anhydrous THF (16 mL). (Triisopropylsilyl)acetylene (996 μ L, 4.44 mmol) was added followed by Pd(PPh₃)₂Cl₂ (56 mg, 0.08 mmol), Cul (15 mg, 0.08 mmol) and triethylamine (1.38 mL, 9.92 mmol). The reaction mixture was degassed (20 min, N₂) and shielded from light. The reaction mixture was then stirred (RT, 18 h) resulting in a colour change from yellow to brown. The crude product was filtered over a pad of Celite then dry loaded onto silica. 2-Fluoro-9-methyl-6-((triisopropylsilyl)ethynyl)-9*H*-purine (**62**) was purified by MPLC (3:2 EtOAc/petrol) as a yellow solid (624 mg, 1.87 mmol, 47%).

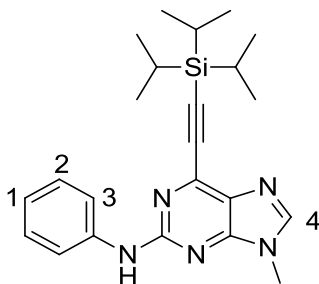
R_f = 0.43 (3:2 EtOAc/petrol); m.p. 114-115 °C; UV λ_{max} (EtOH/nm) 301.0; IR ν_{max}/cm^{-1} : 2944, 2866, 1581, 1509; ¹H NMR (500 MHz, CDCl₃) δ 1.11-1.20 (21H, m, SiCH and CH₃), 3.85 (3H, s, CH₃), 8.06 (1H, s, C⁸-H); ¹³C NMR (125 MHz, CDCl₃) δ 11.3 ((Si(CH(CH₃)₂)₃), 18.7 ((Si(CH(CH₃)₂)₃), 30.1 (N⁹CH₃), 99.9 (C \equiv C-Si), 105.3 (C \equiv C-Si), 133.7 (Ar-C), 133.8 (Ar-C), 143.0 (Ar-C), 143.2 (Ar-C), 146.6 (Ar-C), 157.8 (C⁸-C), 159.5 (C-F); ¹⁹F NMR (500 MHz, DMSO-*d*₆) δ -52.4; LRMS (ES+) m/z 333.1 [M+H]⁺.

2-Fluoro-7-methyl-6-((triisopropylsilyl)ethynyl)-7*H*-purine (**61**) was purified by preparative TLC (1:1 EtOAc/petrol) and obtained as a yellow solid (385 mg, 1.16 mmol, 29%).

R_f = 0.18 (3:2 EtOAc/petrol); m.p. 98-99 °C; UV λ_{max} (EtOH/nm) 298.0; IR ν_{max}/cm^{-1} : 3101, 3077, 2943, 2924, 2866; ¹H NMR (500 MHz, CDCl₃) δ 1.10-1.16 (21H, m, SiCH and CH₃), 3.95 (3H, s, CH₃), 7.96 (1H, s, C⁸-H); ¹³C NMR (125 MHz, CDCl₃) δ

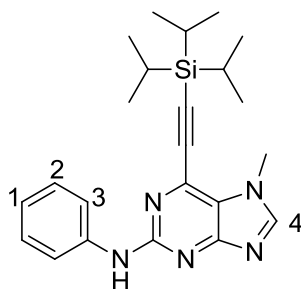
11.5 ((Si(CH(CH₃)₂)₃), 19.7 ((Si(CH(CH₃)₂)₃), 30.4 (N⁷CH₃), 100.1 (C≡C-Si), 104.2 (C≡C-Si), 134.2 (Ar-C), 135.0 (Ar-C), 141.0 (Ar-C), 142.6 (Ar-C), 148.0 (Ar-C), 160.1 (Ar-C), 161.2 (C-F); ¹⁹F NMR (500 MHz, DMSO-*d*₆) δ -52.58; LRMS (ES+) *m/z* 333.1 [M+H]⁺.

9-Methyl-*N*-phenyl-6-((triisopropylsilyl)ethynyl)-9*H*-purin-2-amine (**64**)



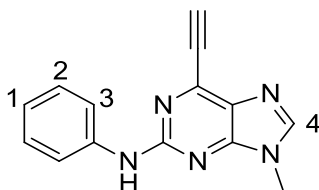
The title compound was prepared following **general procedure E** using: 2-fluoro-9-methyl-6-((triisopropylsilyl)ethynyl)-9*H*-purine (**62**) (300 mg, 0.911 mmol), aniline (166 μL, 1.82 mmol) and TFA (351 μL, 4.56 mmol) in TFE (10 mL). The resulting dark orange oil was purified by MPLC on silica (2:3 EtOAc/petrol) to give the title compound (**64**) as a yellow oil (270 mg, 0.67 mmol, 74%).

*R*_f = 0.27 (2:3 EtOAc/petrol); UV λ_{max} (EtOH/nm) 276.0; IR ν_{max}/cm⁻¹: 2944, 2866, 1581, 1509; ¹H NMR (500 MHz, CDCl₃) δ 1.13-1.28 (21H, m, SiCH and CH₃), 3.80 (3H, s, CH₃), 7.03 (1H, tt, *J* = 7.4 and 1.1 Hz, C¹-H), 7.32 (2H, app. t, *J* = 8.0 Hz, C²-H), 7.38 (1H, br s, ArNHAr), 7.70 (1H, d, *J* = 7.3 Hz, C³-H), 7.82 (1H, s, C⁴-H); ¹³C NMR (125 MHz, CDCl₃) δ 11.4 ((Si(CH(CH₃)₂)₃), 18.8 ((Si(CH(CH₃)₂)₃), 29.6 (N⁹CH₃), 101.1 (C≡C-Si), 101.2 (C≡C-Si), 118.6 (Ar-C), 122.2 (Ar-C), 129.0 (Ar-C), 129.6 (Ar-C), 140.0 (Ar-C), 142.1 (Ar-C), 143.6 (Ar-C), 153.5 (Ar-C), 156.4 (Ar-C); LRMS (ES+) *m/z* 406.3 [M+H]⁺.

7-Methyl-*N*-phenyl-6-((triisopropylsilyl)ethynyl)-7*H*-purin-2-amine (63)

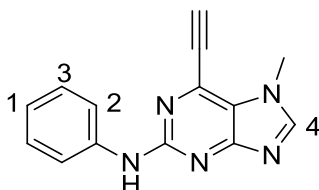
The title compound was prepared following **general procedure E** using: 2-fluoro-7-methyl-6-((triisopropylsilyl)ethynyl)-7*H*-purine (**61**) (385 mg, 1.16 mmol), aniline (211 μ L, 2.32 mmol) and TFA (446 μ L, 5.79 mmol) in TFE (10 mL). The resulting dark orange oil was purified by MPLC on silica (2:3 EtOAc/petrol) to give the title compound (**63**) as a yellow oil (233 mg, 0.58 mmol, 50%).

R_f = 0.18 (2:3 EtOAc/petrol); UV λ_{\max} (EtOH/nm) 268.0; IR $\nu_{\max}/\text{cm}^{-1}$: 2946, 2868, 1579; ^1H NMR (500 MHz, DMSO- d_6) δ 1.13-1.27 (21H, m), 4.09 (3H, s, CH_3), 7.00 (1H, tt, J = 7.4 and 1.1 Hz, $\text{C}^1\text{-H}$), 7.28 (1H, br s, ArNHAr), 7.32 (2H, dd, J = 8.4 and 7.4 Hz, $\text{C}^2\text{-H}$), 7.77 (1H, d, J = 7.6, $\text{C}^3\text{-H}$), 7.96 (1H, s, $\text{C}^4\text{-H}$); ^{13}C NMR (125 MHz, DMSO- d_6) δ 10.5 ((Si(CH(CH $_3$) $_2$) $_3$), 20.1 ((Si(CH(CH $_3$) $_2$) $_3$), 31.7 (N^7CH_3), 104.2 ($\text{C}\equiv\text{C-Si}$), 105.1 ($\text{C}\equiv\text{C-Si}$), 120.6 (Ar-C), 124.2 (Ar-C), 131.0 (Ar-C), 132.4 (Ar-C), 141.1 (Ar-C), 143.2 (Ar-C), 145.1 (Ar-C), 155.4 (Ar-C), 157.9 (Ar-C); LRMS (ES+) m/z 406.3 $[\text{M}+\text{H}]^+$.

6-Ethynyl-9-methyl-*N*-phenyl-9*H*-purin-2-amine (53)

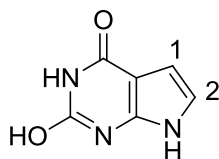
The title compound was prepared following **general procedure A** using: 9-methyl-*N*-phenyl-6-((triisopropylsilyl)ethynyl)-9*H*-purin-2-amine (**64**) (273 mg, 0.67 mmol) and TBAF (1 M in THF (1.00 mL, 1.00 mmol) in THF (15 mL). The crude product was purified by MPLC on silica (4:1 EtOAc/petrol) to give the title compound (**53**) as a yellow solid (165 mg, 0.66 mmol, 98%).

R_f = 0.27 (2:3 EtOAc/petrol); m.p. 200 °C (dec.); UV λ_{max} (EtOH/nm) 261.0; IR $\nu_{\text{max}}/\text{cm}^{-1}$: 3302, 3263, 3188, 3111, 3083, 3047, 2866, 2115, 1791; ^1H NMR (500 MHz, CDCl_3) δ 3.64 (1H, s, CH ethynyl), 3.85 (1H, s, CH_3), 7.05 (1H, tt, J = 7.1 and 1.1 Hz, $\text{C}^1\text{-H}$), 7.31 (1H, br s, ArNHAr), 7.36 (2H, dd, J = 8.4 and 7.4 Hz, $\text{C}^2\text{-H}$), 7.70 (2H, d, J = 7.6 Hz), 7.84 (1H, s, $\text{C}^4\text{-H}$); ^{13}C NMR (125 MHz, $\text{DMSO-}d_6$) δ 29.3 (N^9CH_3), 78.9 ($\text{C}\equiv\text{C-H}$), 87.2 ($\text{C}\equiv\text{C}$), 118.3 (Ar-C), 121.1 (Ar-C), 128.5 (Ar-C), 128.9 (Ar-C), 145.3 (Ar-C), 153.4 (Ar-C), 156.1 (Ar-C); HRMS calcd for $\text{C}_{14}\text{H}_{12}\text{N}_5\text{O}$ $[\text{M}+\text{H}]^+$ 250.1087, Found 250.1087.

6-Ethynyl-7-methyl-*N*-phenyl-7*H*-purin-2-amine (52)

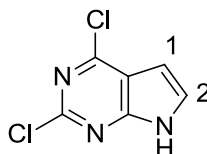
The title compound was prepared following **general procedure A** using: 7-methyl-*N*-phenyl-6-((triisopropylsilyl)ethynyl)-7*H*-purin-2-amine (**63**) (223 mg, 0.55 mmol) and TBAF (1 M in THF (825 μ L, 0.825 mmol) in THF (15 mL). The crude product was purified by MPLC on silica (4:1 EtOAc/petrol) to give the title compound (**52**) as a yellow solid (64 mg, 0.26 mmol, 47%).

R_f = 0.27 (2:3 EtOAc/petrol); m.p. 240 $^{\circ}$ C (dec.); UV λ_{max} (EtOH/nm) 271.0; IR $\nu_{\text{max}}/\text{cm}^{-1}$: 3302, 3263, 3188, 3111, 3083, 3047, 2866, 2115, 1791; ^1H NMR (500 MHz, DMSO- d_6) δ 3.99 (3H, s, CH_3), 5.00 (1H, s, CH ethynyl), 6.91 (1H, tt, J = 7.3 and 1.1 Hz, $\text{C}^1\text{-H}$), 7.28 (2H, dd, J = 8.5 and 7.9 Hz, $\text{C}^2\text{-H}$), 7.81 (2H, d, J = 7.70 Hz, $\text{C}^3\text{-H}$), 8.45 (1H, s, $\text{C}^4\text{-H}$), 9.62 (1H, br s, ArNHAr); ^{13}C NMR (125 MHz, DMSO- d_6) δ 32.8 (N^7CH_3), 78.2 ($\text{C}\equiv\text{C-H}$), 87.5 ($\text{C}\equiv\text{C}$), 118.0 (Ar-C), 120.4 (Ar-C), 120.7 (Ar-C), 128.4 (Ar-C), 133.1 (Ar-C), 141.0 (Ar-C), 150.3 (Ar-C), 156.4 (Ar-C), 162.5 (Ar-C); HRMS calcd for $\text{C}_{14}\text{H}_{12}\text{N}_5\text{O}$ $[\text{M}+\text{H}]^+$ 250.1087, Found 250.1087.

1*H*-Pyrrolo[2,3-*d*]pyrimidine-2,4(3*H*,7*H*)-dione (128)^{289,290}

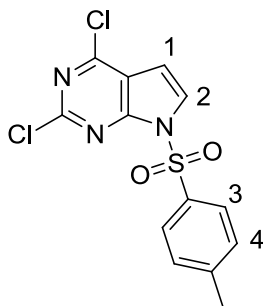
To a mixture of bromoacetaldehyde diethyl acetal (596 μL , 4.0 mmol) and water (1.75 mL) was added $\text{HCl}_{(\text{aq})}$ (2 M) (450 μL , 0.91 mmol). The biphasic mixture rapidly stirred with heating until a homogenous solution was formed (90 $^{\circ}\text{C}$, 30 min). The solution was cooled (RT) and NaOAc (338 mg, 4.12 mmol) was added. In a separate flask a suspension of 6-aminouracil (503 mg, 4.0 mmol) and NaOAc (175 mg, 2.13 mmol) in water (3.75 mL) was stirred (RT). The freshly prepared bromoacetaldehyde solution was added in a single portion and the reaction was heated (80 $^{\circ}\text{C}$, 4h) resulting in a light brown precipitate. The reaction mixture was cooled to 0 $^{\circ}\text{C}$ for 90 min resulting in further precipitation which was collected by filtration. The solid was washed with cold water (2 x 25 mL) and acetone (25 mL) to give the title compound (**128**) as a light brown solid (403 mg, 2.7 mmol, 67%) which was used in the next reaction without further purification.

m.p. 280 $^{\circ}\text{C}$ (dec.) (Lit > 250 $^{\circ}\text{C}$); ^1H NMR (500 MHz, $\text{DMSO}-d_6$) δ 6.22 (1H, dd, J = 2.0 and 2.1 Hz, $\text{C}^1\text{-H}$), 6.56 (1H, dd, J = 2.0 and 2.1 Hz, $\text{C}^2\text{-H}$), 10.47 (1H, br s, NH), 11.09 (1H, br s, NH), 11.44 (1H, br s, NH); ^{13}C NMR (125 MHz, $\text{DMSO}-d_6$) δ 98.6 (C^5H), 102.8 (Ar-C), 116.5 (Ar-C), 138.8 (C^6H), 151.0 (Ar-C), 159.9 (Ar-C); LRMS (ES+) m/z = 152.1 $[\text{M}+\text{H}]^+$

2,4-Dichloro-7H-pyrrolo[2,3-*d*]pyrimidine (129)^{184,291}

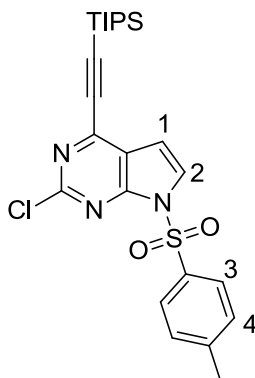
A suspension of 1*H*-pyrrolo[2,3-*d*]pyrimidine-2,4(3*H*,7*H*)-dione (**128**) (77 mg, 0.51 mmol) in phenylphosphoric dichloride (713 μ L, 5.1 mmol) was heated using microwave irradiation (185 °C, 30 min). The resulting dark brown oil was added dropwise to a rapidly stirred beaker of ice-water (50 ml) which was then neutralised (NaOH) and extracted with EtOAc (3 x 50 mL). The combined organic layers were dried (MgSO₄) and dry loaded onto silica. The crude product was purified by MPLC (3:7 EtOAc/petrol) to give the title compound (**129**) as an off-white solid (48 mg, 0.26 mmol, 50%).

R_f = 0.40 (3:7 EtOAc/petrol); m.p. 248 °C (Lit 247-249 °C); ¹H NMR (500 MHz, DMSO-*d*₆) δ 6.67 (1H, d, J = 3.6 Hz, C¹-H), 7.74 (1H, d, J = 3.6 Hz, C²-H), 12.78 (1H, br s, NH); LRMS (ES+) m/z = 188.0 [M+H]⁺.

2,4-Dichloro-7-tosyl-7H-pyrrolo[2,3-d]pyrimidine (130)^{292,293}

To a solution of 2,4-dichloro-7H-pyrrolo[2,3-d]pyrimidine (**129**) (146 mg, 0.78 mmol) and *p*-toluenesulfonyl chloride (296 mg, 0.93 mmol) in DCM (1.5 ml) was added triethylamine (215 μ L, 1.55 mmol) and 4-dimethylaminopyridine (DMAP) (2.5 mg, 2.02×10^{-2} mmol). The resulting solution was stirred (RT, 1 h) then diluted with DCM (40 mL). The reaction mixture was washed with $\text{HCl}_{(\text{aq})}$ (1 M) (40 mL) and $\text{NaHCO}_{3(\text{aq})}$ (2 x 40 mL) then dried (MgSO_4) and dry loaded onto silica. The title compound (**130**) was purified by MPLC on silica (3:7 EtOAc/petrol) and obtained as an off-white crystalline solid (235 mg, 0.69 mmol, 88%).

R_f = 0.60 (3:7 EtOAc/petrol); m.p. 127–130 $^{\circ}\text{C}$; UV λ_{max} (EtOH/nm) 229; IR $\nu_{\text{max}}/\text{cm}^{-1}$: 3142, 2979, 2940, 2869, 2410, 2027, 1934, 1818, 1624, 1596, 1578, 1539; ^1H NMR (500 MHz, $\text{DMSO}-d_6$) δ 6.99 (1H, d, J = 4.1 Hz, $\text{C}^1\text{-H}$), 7.50 (2H, d, J = 8.0 Hz, $\text{C}^4\text{-H}$), 8.03 (2H, d, J = 8.0 Hz, $\text{C}^3\text{-H}$), 8.12 (1H, d, J = 4.1 Hz, $\text{C}^2\text{-H}$); LRMS (ES+) m/z = 342.0 $[\text{M}+\text{H}]^+$.

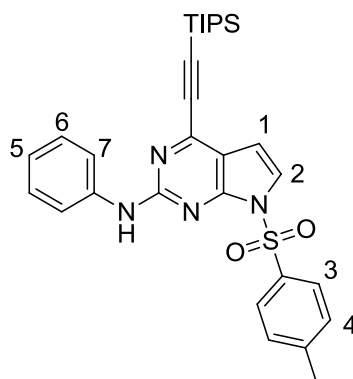
2-Chloro-7-tosyl-4-((triisopropylsilyl)ethynyl)-7H-pyrrolo[2,3-d]pyrimidine (131)

To a suspension of 2,4-dichloro-7-tosyl-7H-pyrrolo[2,3-d]pyrimidine (**130**) (50 mg, 0.15 mmol) copper(I) iodide (0.6 mg, 2.9×10^{-3} mmol) and $\text{Pd}(\text{PPh}_3)_2\text{Cl}_2$ (2.1 mg, 2.9×10^{-3} mmol) in anhydrous THF (1 mL) was added triisopropylsilyl acetylene (37 μL , 0.17 mmol) followed by triethylamine (128 μL , 0.92 mmol). The vessel was capped and degassed (15 min, N_2) then shielded from light and stirred (RT, 18 h). The reaction mixture was filtered through Celite, dried (MgSO_4) and dry loaded onto silica. The crude mixture was purified by MPLC (15:85 EtOAc/petrol) to give the title compound (**131**) as a clear yellow oil (45 mg, 0.09 mmol, 63%).

R_f = 0.53 (15:85 EtOAc/petrol); UV λ_{max} (EtOH/nm) 269; IR $\nu_{\text{max}}/\text{cm}^{-1}$: 2944, 2865, 1766, 1556, 1505, 1461; ^1H NMR (500 MHz, CDCl_3) δ 1.07-1.27 (21H, m, CH_2CH_3), 2.41 (3H, s, CH_3), 6.65 (1H, d, J = 4.1, $\text{C}^1\text{-H}$), 7.34 (2H, d, J = 8.0, $\text{C}^4\text{-H}$), 7.71 (1H, d, J = 3.9, $\text{C}^2\text{-H}$), 8.09 (2H, d, J = 8.0, $\text{C}^3\text{-H}$); ^{13}C NMR (125 MHz, CDCl_3) δ 11.1 ($(\text{Si}(\text{CH}(\text{CH}_3)_2)_3$), 18.6 ($(\text{Si}(\text{CH}(\text{CH}_3)_2)_3$), 103.6 ($\text{C}\equiv\text{C-Si}$), 127.7 (Ar-C), 128.6 (Ar-C), 130.0 (Ar-C), 146.5 (Ar-C), 184.7; HRMS Calcd for $\text{C}_{24}\text{H}_{30}\text{ClN}_3\text{O}_2\text{SSi}$ m/z = 488.1560 $[\text{M}+\text{H}]^+$, Found m/z = 488.1574 $[\text{M}+\text{H}]^+$.

Note: Not all carbon atoms were visible

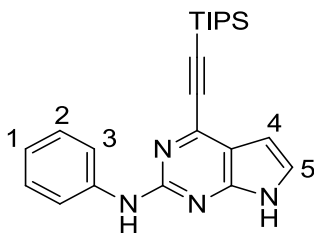
N-Phenyl-7-tosyl-4-((triisopropylsilyl)ethynyl)-7H-pyrrolo[2,3-d]pyrimidin-2-amine (132)



To a solution of 2-chloro-7-tosyl-4-((triisopropylsilyl)ethynyl)-7H-pyrrolo[2,3-d]pyrimidine (**131**) (110 mg, 0.23 mmol) in *n*-BuOH (2.5 mL) was added trimethylsilyl chloride (TMSCl) (58 μ L, 0.45 mmol). Aniline (41 μ L, 0.45 mmol) was added in one portion and vessel was capped. The reaction mixture was heated (116 $^{\circ}$ C, 72 h) resulting in consumption of the starting material (TLC). The reaction mixture was diluted with EtOAc (40 mL) then washed sequentially with HCl_(aq) (1 M) (40 mL), NaHCO_{3(aq)} (40 mL) and brine (40 mL). The crude product was dried (MgSO₄), dry loaded onto silica and purified by MPLC on silica (15:85 EtOAc/petrol) to give compound (**132**) as a yellow oil (110 mg, 0.20 mmol, 89%).

R_f = 0.37 (15:85 EtOAc/petrol); UV λ_{max} (EtOH/nm) 271; IR ν_{max}/cm^{-1} : 3258, 2942, 2864, 1568, 1540, 1508; 1H NMR (500 MHz, CDCl₃) δ 1.08-1.27 (21H, m, CH₂CH₃), 2.33 (3H, s, CH₃), 6.55 (1H, d, J = 4.0 Hz, C¹-H), 7.11 (1H, tt, J = 7.4 and 1.1 Hz, C⁵-H), 7.17 (2H, d, J = 8.5, C⁶-H), 7.41 (2H, app. t, J = 7.4 Hz, C⁷-H), 7.46 (1H, d, J = 4.0 Hz, C²-H), 7.76 (2H, d, J = 8.0 Hz, C⁴-H), 7.97 (2H, d, J = 8.4 Hz, C³-H).; ^{13}C NMR (125 MHz, CDCl₃) δ 11.1 ((Si(CH(CH₃)₂)₃), 18.6 ((Si(CH(CH₃)₂)₃), 33.6 Ar-CH₃), 128.1 (Ar-C), 184.7 (Ar-C); HRMS Calcd for C₃₀H₃₇N₄O₂SSi m/z = 545.2401 [M+H]⁺, Found m/z = 545.2385 [M+H]⁺.

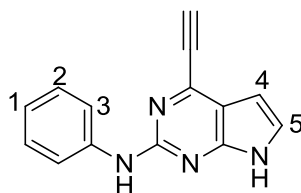
Note: Not all carbon atoms observed

***N*-Phenyl-4-((triisopropylsilyl)ethynyl)-7*H*-pyrrolo[2,3-*d*]pyrimidin-2-amine (140)**

A solution of *N*-phenyl-7-tosyl-4-((triisopropylsilyl)ethynyl)-7*H*-pyrrolo[2,3-*d*]pyrimidin-2-amine (**19**) (100 mg, 0.18 mmol) in anhydrous THF (800 μ L) was cooled to 0 $^{\circ}$ C. Anhydrous MeOH (400 μ L) was added followed by Cs_2CO_3 (120 mg, 0.37 mmol). The reaction vessel was flushed with nitrogen and stirred (0 $^{\circ}$ C, 18 h) after which no starting material remained (LC-MS). The reaction mixture was added to $\text{HCl}_{(\text{aq})}$ (1 M) (15 mL) which was then extracted with DCM (3 x 15 mL). The organic layers were pooled and washed with $\text{NaHCO}_{3(\text{aq})}$ (45 mL) then dried (phase separator) and dry loaded onto silica. The title compound (**20**) was purified by MPLC on silica (5:95 MeOH/DCM) and obtained as a yellow crystalline solid (66 mg, 0.17 mmol, 96%).

R_f = 0.33 (1:3 EtOAc/petrol); m.p. 170 $^{\circ}$ C; UV λ_{max} (EtOH/nm) 255; IR $\nu_{\text{max}}/\text{cm}^{-1}$: 3228, 2943, 2863, 2167, 1600, 1573, 1535; ^1H NMR (500 MHz, CDCl_3) δ 1.08-1.27 (21H, m, CH_2CH_3), 6.51 (1H, d, J = 3.6 Hz, $\text{C}^4\text{-H}$), 7.06 (3H, m, $\text{C}^1\text{-H}$ and NH), 7.30-7.38 (3H, m, $\text{C}^2\text{-H}$ and $\text{C}^5\text{-H}$), 7.64 (2H, d, J = 8.5 Hz, $\text{C}^3\text{-H}$), 8.73 (1H, br s, NH pyrrolopyrimidine); ^{13}C NMR (125 MHz, CDCl_3) δ 11.2 (($\text{Si}(\text{CH}(\text{CH}_3)_2)_3$), 18.7 (($\text{Si}(\text{CH}(\text{CH}_3)_2)_3$), 68.8 ($\text{C}\equiv\text{C-Si}$), 129.0 (Ar-C), 160.2 (Ar-C); HRMS Calcd for $\text{C}_{23}\text{H}_{31}\text{N}_4\text{Si}$ m/z = 391.2313 $[\text{M}+\text{H}]^+$, Found m/z = 391.2309 $[\text{M}+\text{H}]^+$.

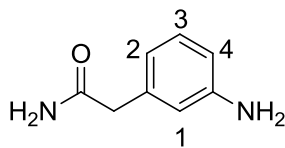
Note: not all carbon atoms were visible

4-Ethynyl-*N*-phenyl-7*H*-pyrrolo[2,3-*d*]pyrimidin-2-amine (88)

The title compound was prepared following **general procedure A** using: *N*-phenyl-4-((triisopropylsilyl)ethynyl)-7*H*-pyrrolo[2,3-*d*]pyrimidin-2-amine (**20**) (30 mg, 7.69×10^{-2} mmol) and TBAF (1 M in THF) (77 μ L, 7.69×10^{-2} mmol) in THF (3 mL). The crude product was purified by MPLC on silica (5:95 MeOH/DCM) to give the title compound (**21**) as a yellow solid (14 mg, 5.98×10^{-2} mmol, 78%).

R_f = 0.30 (5:95 MeOH/DCM); m.p. 230 °C (dec.); UV λ_{\max} (EtOH/nm) 277; IR $\nu_{\max}/\text{cm}^{-1}$: 3569, 3278, 2188, 2149, 2031, 1972, 1611, 1575, 1536; ^1H NMR (500 MHz, DMSO- d_6) δ 4.71 (1H, s, CH ethynyl), 6.39 (1H, d, J = 3.3 Hz, C¹-H), 6.88-6.95 (1H, m, C¹-H), 7.26 (2H, dd, J = 7.6 and J = 7.7 Hz, C²-H), 7.27 (1H, d, J = 3.3 Hz, C⁵-H), 7.81 (2H, d, J = 7.7 Hz, C³-H), 9.47 (1H, br s, NH), 11.75 (1H, br s, NH); ^{13}C NMR (125 MHz, CDCl₃) δ 68.3 (C-H), 84.7 (Ar-C \equiv C), 118.1 (Ar-C), 128.4 (Ar-C); LRMS (ES+) m/z = 234.95 [$\text{M}+\text{H}$]⁺; HRMS Calcd for C₁₄H₁₁N₄ m/z = 235.0978 [$\text{M}+\text{H}$]⁺, Found m/z = 235.0984 [$\text{M}+\text{H}$]⁺.

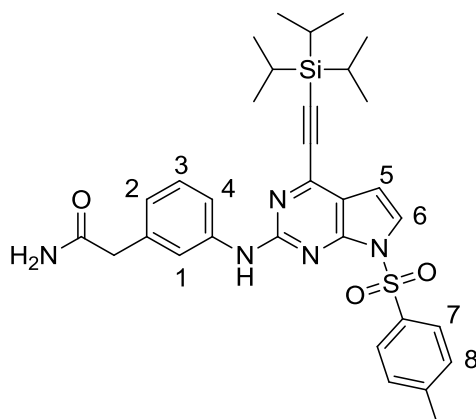
Note: Not all carbon atoms observed

2-(3-Aminophenyl)acetamide (290)

A solution of 3-aminophenylacetic acid (700 mg, 4.63 mmol) in MeOH (10 mL) was cooled to $-10\text{ }^{\circ}\text{C}$. SOCl_2 (673 μL , 9.26 mmol) was then added dropwise with stirring. The reaction mixture was heated to reflux ($90\text{ }^{\circ}\text{C}$, 120 min) then cooled (RT). The solvent was removed *in vacuo* and aqueous ammonia (32%) (10 mL) was added. The reaction mixture was stirred (RT, 18 h) and the solvent was removed *in vacuo*. The crude product was redissolved in MeOH (20 mL) and the resulting solution was dry loaded onto silica then purified by MPLC (2:8 MeOH/DCM) to give the title compound (**290**) as an off-white crystalline solid (483 mg, 3.2 mmol, 70%).

$R_f = 0.53$ (2:8 MeOH/DCM); m.p. $157\text{--}158\text{ }^{\circ}\text{C}$; UV λ_{max} (EtOH/nm) 238; IR $\nu_{\text{max}}/\text{cm}^{-1}$: 3410, 3304, 3176, 2567, 2160, 2029, 1976, 1666, 1607; ^1H NMR (500 MHz, $\text{DMSO-}d_6$) δ 3.19 (2H, s, CH_2), 5.00 (2H, br s, NH_2), 6.40–6.42 (2H, m, $\text{C}^2\text{-H}$ and $\text{C}^4\text{-H}$), 6.47 (1H, s, $\text{C}^1\text{-H}$), 6.81 (1H, br s, NH_2), 6.92 (1H, app. t, $J = 7.7\text{ Hz}$, $\text{C}^3\text{-H}$), 7.34 (1H, br s, NH_2); ^{13}C NMR (125 MHz, $\text{DMSO-}d_6$) δ 42.6 (CH_2), 112.0 (Ar-C), 114.6 (Ar-C), 116.6 (Ar-C), 128.6 (Ar-C), 136.9 (Ar-C), 148.4 (ArC- NH_2), 172.4 (H_2NCOCH_2); LRMS (ES+) $m/z = 151.1$ $[\text{M}+\text{H}]^+$; HRMS Calcd for $\text{C}_8\text{H}_{11}\text{N}_2\text{O}$ $m/z = 151.0866$ $[\text{M}+\text{H}]^+$, Found $m/z = 151.0863$ $[\text{M}+\text{H}]^+$.

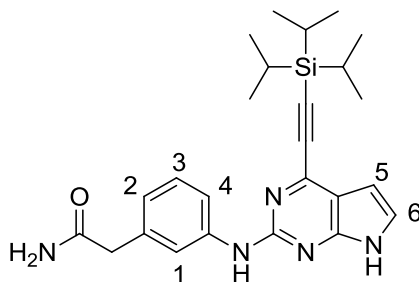
2-(3-((7-Tosyl-4-((triisopropylsilyl)ethynyl)-7H-pyrrolo[2,3-d]pyrimidin-2-yl)amino)phenyl)acetamide (141)



To a solution of 2-chloro-7-tosyl-4-((triisopropylsilyl)ethynyl)-7H-pyrrolo[2,3-d]pyrimidine (**131**) (500 mg, 1.03 mmol) in anhydrous MeCN (15 mL) was added 2-(3-aminophenyl)acetamide (**290**) (170 mg, 1.1 mmol), anhydrous K₂CO₃ (284 mg, 2.1 mmol), Pd₂(dba)₃ (38 mg, 4.1 x 10⁻² mmol) and XPhos (20 mg, 4.1 x 10⁻² mmol). The reaction mixture was capped and degassed (N₂, 30 min) then heated (80 °C, 2 h). The reaction mixture was cooled (RT) and filtered (Celite) then diluted with EtOAc (50 mL). The resulting organic solution was washed sequentially with HCl_(aq) (1 M) (30 mL), NaHCO₃ (30 mL) and brine (30 mL) then dried (Na₂SO₄) and dry loaded onto silica. The title compound (**141**) was purified by MPLC (8:2 EtOAc/petrol) and obtained as a yellow crystalline solid (215 mg, 0.36 mmol, 35%).

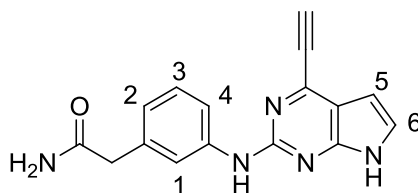
R_f = 0.35 (8:2 EtOAc/petrol); m.p. 200-201 °C; UV λ_{max} (EtOH/nm) 240.0 and 281.5; IR ν_{max}/cm^{-1} : 3476, 3269, 3206, 3150, 3062, 2952, 2864, 1665, 1625, 1578; ¹H NMR (500 MHz, CDCl₃) δ 1.08-1.22 (21H, m, SiCH and CH₃), 2.39 (3H, s, Ar-CH₃), 3.72 (1H, br s, NH Amide), 4.00 (2H, s, CH₂), 6.59 (1H, d, J = 4.0 Hz, C⁵-H), 6.61 (1H, d, J = 7.6 Hz, C²-H), 6.70 (1H, br s, Ar-NH-Ar), 6.75 (1H, d, J = 7.4 Hz, C⁴-H), 7.14 (1H, t, J = 7.6 Hz, C³-H), 7.29 (2H, d, J = 8.2 Hz, C⁷-H), 7.61 (1H, d, J = 4.1 Hz, C⁶-H), 8.01 (1H, br s, NH Amide), 8.18 (2H, d, J = 8.2 Hz, C⁸-H); ¹³C NMR (125 MHz, CDCl₃) δ 11.1 ((Si(CH(CH₃)₂)₃), 18.6 ((Si(CH(CH₃)₂)₃), 21.7 (Ar-CH₃), 43.9 (COCH₂Ar), 60.4 (C \equiv C-Si), 101.3 (C⁵), 101.7 (C \equiv C), 103.6 (Ar-C), 114.2 (Ar-C), 116.2 (Ar-C), 118.9 (Ar-C), 119.9 (Ar-C), 126.3 (C⁶), 128.8 (Ar-C), 129.9 (Ar-C), 134.3 (Ar-C), 135.2 (Ar-C), 143.6 (Ar-C), 146.0 (Ar-C), 146.9 (Ar-C), 151.9 (Ar-C), 153.0 (Ar-C), 173.3 (C=O); HRMS Calcd for C₃₂H₄₀N₅O₃SSi m/z = 602.2616 [M+H]⁺, Found m/z = 602.2601 [M+H]⁺.

2-(3-((4-((Triisopropylsilyl)ethynyl)-7*H*-pyrrolo[2,3-*d*]pyrimidin-2-yl)amino)phenyl)acetamide (291**)**



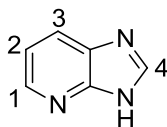
A solution of 2-(3-((7-tosyl-4-((triisopropylsilyl)ethynyl)-7*H*-pyrrolo[2,3-*d*]pyrimidin-2-yl)amino)phenyl)acetamide (**141**) (204 mg, 0.34 mmol) in anhydrous THF (2 mL) was cooled to 0 °C. Anhydrous MeOH (1 mL) was added followed by Cs₂CO₃ (220 mg, 0.68 mmol). The reaction vessel was flushed with nitrogen and stirred (0 °C, 18 h) after which no starting material remained (LC-MS). The reaction mixture was added to HCl_(aq) (1 M) (20 mL) and then extracted with DCM (3 x 20 mL). The combined organic layers were washed with NaHCO_{3(aq)} (30 mL) then dried (phase separator) and dry loaded onto silica. The title compound (**291**) was purified by MPLC on silica (5:95 MeOH/DCM) and obtained as a yellow solid (116 mg, 0.26 mmol, 75%).

R_f = 0.57 (5:95 MeOH/DCM); m.p. 212-213 °C; UV λ_{max} (EtOH/nm) 279.0; IR ν_{max}/cm^{-1} : 3214, 3174, 3073, 3020, 2941, 2890, 2864, 2360, 2339, 1660, 1608, 1594; ¹H NMR (500 MHz, CDCl₃) δ 1.13-1.23 (21H, m, SiCH and CH₃), 3.57 (2H, s, CH₂), 5.51 (1H, br s, NH Amide), 6.33 (1H, br s, NH pyrrolopyrimidine), 6.49 (1H, dd, J = 3.6 and 2.0 Hz, C⁵-H), 6.87 (1H, d, J = 7.7 Hz, C²-H), 7.03 (1H, dd, J = 3.6 and 2.2 Hz, C⁶-H), 7.26 (1H, t, J = 7.8 Hz, C³-H), 7.37 (1H, d, J = 8.10 Hz, C⁴-H) 7.42 (1H, br s, ArNHAr), 7.67 (1H, s, C¹-H), 9.79 (1H br s, NH Amide). ¹³C NMR (125 MHz, DMSO-*d*₆) δ 10.6 ((Si(CH(CH₃)₂)₃), 18.5 ((Si(CH(CH₃)₂)₃), 30.4 (Ar-CH₃), 42.5 (COCH₂Ar), 95.5 (C \equiv C-Si), 98.9 (C⁵), 103.3 (C \equiv C), 113.8 (Ar-C), 116.2 (Ar-C), 119.1 (Ar-C), 121.4 (Ar-C), 125.0 (C⁶), 128.1 (Ar-C), 136.5 (Ar-C), 140.9 (Ar-C), 141.0 (Ar-C), 153.1 (Ar-C), 156.0 (Ar-C), 172.2 (C=O); HRMS Calcd for C₂₅H₃₄N₅O₃SSi m/z = 448.2527 [M+H]⁺, Found m/z = 448.2518 [M+H]⁺.

2-(3-((4-Ethynyl-7H-pyrrolo[2,3-*d*]pyrimidin-2-yl)amino)phenyl)acetamide (231)

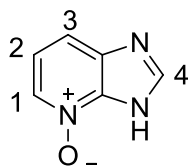
The title compound was prepared following **general procedure A** using: 2-(3-((4-((triisopropylsilyl)ethynyl)-7*H*-pyrrolo[2,3-*d*]pyrimidin-2-yl)amino)phenyl)acetamide (**24**) (58 mg, 0.13 mmol) and TBAF (1 M in THF) (142 μ L, 1.42 mmol) in THF (6 mL). The crude product was purified by MPLC on silica (1:9 MeOH/DCM) to give the title compound (**25**) as a yellow solid (29 mg, 0.10 mmol, 77%).

R_f = 0.48 (1:9 MeOH/DCM); m.p. 227 °C (dec.); UV λ_{max} (EtOH/nm) 277.5; IR ν_{max}/cm^{-1} : 3376, 3266, 3109, 2360, 2337, 2114, 1663, 1604, 1575, 1538, 1471, 1391; 1H NMR (500 MHz, DMSO- d_6) 3.32 (2H, s, CH_2), 4.70 (1H, s, CH Ethynyl), 6.39 (1H, d, J = 3.5 Hz, C^5 -H), 6.82 (1H, d, J = 7.6 Hz, C^2 -H), 6.87 (1H, br s, ArNHAr), 7.20 (1H, t, J = 7.6 Hz, C^3 -H), 7.27 (1H, d, J = 3.5 Hz, C^6 -H), 7.40 (1H, br s, NH pyrrolopyrimidine), 7.52 (1H, s, C^1 -H), 7.80 (1H, d, J = 7.6 Hz, C^4 -H), 9.42 (1H, br s, NH Amide), 11.72 (1H, br s, NH Amide); ^{13}C NMR (125 MHz, DMSO- d_6) δ 42.5 (CH_2), 80.4 ($C\equiv C$ -H), 84.7 ($C\equiv C$), 99.1, (C^5), 113.8 (Ar-C), 116.3 (Ar-C), 119.2 (Ar-C), 121.5 (Ar-C), 125.0 (C^6), 128.1 (Ar-C), 136.5 (Ar-C), 140.7 (Ar-C), 141.0 (Ar-C), 153.1 (Ar-C), 155.9 (Ar-C), 172.2 (H_2NCOCH_2); HRMS Calcd for $C_{16}H_{14}N_5O$ m/z = 292.1198 $[M+H]^+$, Found m/z = 292.1198 $[M+H]^+$.

3*H*-Imidazo[4,5-*b*]pyridine (103)^{294,295}

To a solution of 2,3-diaminopyridine (2.00 g, 18.3 mmol) in TFE (15 mL) was added triethylorthoformate (3.66 mL, 22 mmol). TFA (71 μ L, 0.915 mmol) was added and the reaction mixture was heated *via* microwave irradiation (140 $^{\circ}$ C, 15 min) after which no starting material remained (TLC). The solvent was removed *in vacuo* and the crude product was redissolved in EtOAc (50 mL) then washed sequentially with NaHCO_3 (1 x 50 mL) and brine (2 x 50 mL) then dried (Na_2SO_4). The crude product was dry loaded onto silica and purified by MPLC (3:7 MeOH/EtOAc) to give the title compound (**103**) as an orange crystalline solid (2.13 g, 17.8 mmol, 97%).

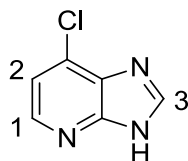
R_f = 0.50 (3:7 MeOH/EtOAc); m.p. 148-150 $^{\circ}$ C (Lit 148-151 $^{\circ}$ C); UV λ_{max} (EtOH/nm) 281.0; IR $\nu_{\text{max}}/\text{cm}^{-1}$: 3062, 3022, 2980, 2921, 2851, 2807, 2769, 2711; ^1H NMR (500 MHz, $\text{DMSO}-d_6$) δ 7.23 (1H, dd, J = 8.0 and 4.7 Hz, $\text{C}^2\text{-H}$), 8.02 (1H, d, J = 7.6, $\text{C}^3\text{-H}$), 8.35 (1H, d, J = 2, $\text{C}^1\text{-H}$), 8.42 (1H, s, $\text{C}^4\text{-H}$), 12.90 (1H, br s, NH imidazopyridine); LRMS (ES+) m/z 120.04 $[\text{M}+\text{H}]^+$.

3*H*-Imidazo[4,5-*b*]pyridine 4-oxide (104)²⁹⁶

To a suspension of 3*H*-imidazo[4,5-*b*]pyridine (**103**) (1.60 g, 13.4 mmol) in chloroform (30 mL) was added 3-chloroperbenzoic acid* (*m*CPBA) (62%) (4.45 g, 18.7 mmol). A slight exotherm was observed alongside dissolution of the starting material. The mixture was stirred (RT, 18 h) resulting in a light yellow precipitate which was removed by filtration then washed with DCM (30 mL) to leave the crude product. The title compound was purified by recrystallisation from acetic acid (20 mL) to give the title compound (**104**) as pale yellow crystals (1.47 g, 11.9 mmol, 81%).

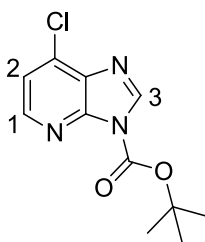
**m*CPBA purity determined by titration against sodium thiosulfate

m.p. 262-263 °C (AcOH) (Lit 252 °C MeOH); UV λ_{max} (EtOH/nm) 299.0; IR ν_{max} /cm⁻¹: 3163, 3128, 3084, 2877, 2783, 2740, 2559, 1227 (*N*-oxide); ¹H NMR (500 MHz, DMSO-*d*₆) δ 7.21 (1H, dd, *J* = 8.3 and 6.4 Hz, C²-H), 7.60 (1H, d, *J* = 7.9 Hz, C³-H), 8.19 (1H, d, *J* = 6.3 Hz, C¹-H), 8.41 (1H, s, C⁴-H), 13.25 (1H, br s, *N*³-H); LRMS (ES+) *m/z* 136.03 [M+H]⁺.

7-Chloro-3*H*-imidazo[4,5-*b*]pyridine (105)²⁹⁷

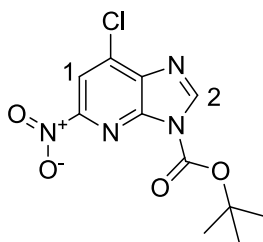
A suspension of 3*H*-imidazo[4,5-*b*]pyridine 4-oxide (**104**) (500 mg, 3.70 mmol) in POCl₃ (3.73 mL, 40.7 mmol) was heated *via* microwave irradiation (140 °C, 15 min) after which the starting material had been consumed (TLC). The reaction was repeated seven times and the crude products were combined. Residual POCl₃ was neutralised by dropwise addition of the reaction mixture to rapidly stirring ice water. The resulting solution was cooled (0 °C) and the pH adjusted to 7 (NaOH). The aqueous solution was extracted with EtOAc (3 x 300 mL) and the organic layers were combined and dried (Na₂SO₄) to give the crude product as a mixture of both the *ortho*- and the desired *para*-chloro regioisomers (1:3 respectively). The crude product was dry loaded onto NH silica and purified by NH MPLC on silica (7:1 EtOAc/MeOH) to give the title compound (**105**) as a white solid (1.64 g, 10.7 mmol, 41%).

R_f = 0.18 (NH silica 1:7 MeOH/EtOAc); m.p. 176-177 °C (Lit 178 °C); UV λ_{max} (EtOH/nm) 278.0; IR ν_{max} /cm⁻¹: 3203, 3117, 3075, 3053, 2965, 2914, 2821, 2755, 2479, 2410, 2163; ¹H NMR (500 MHz, DMSO-*d*₆) δ 7.38 (1H, d, J = 5.3 Hz, C²-H), 8.29 (1H, d, J = 5.3 Hz, C¹-H), 8.51 (1H, s, C³-H), 13.41 (1H, br s, NH imidazopyridine); LRMS (ES+) m/z 120.04 [M+H]⁺.

***tert*-Butyl 7-chloro-3*H*-imidazo[4,5-*b*]pyridine-3-carboxylate (**106**)**²⁹⁷

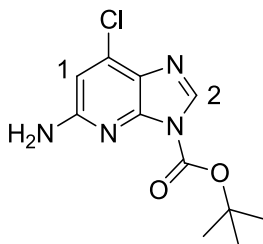
To a solution of 7-chloro-3*H*-imidazo[4,5-*b*]pyridine (**105**) (1.64 g, 10.7 mmol) in anhydrous THF (100 mL) was added di-*tert*-butyl dicarbonate (Boc₂O) (3.27 g, 15.0 mmol). 4-Dimethylaminopyridine (DMAP) (13 mg, 0.11 mmol) was then added and the resulting mixture was stirred (RT, 3 h) resulting in consumption of the starting material (LC-MS). The solvent was removed *in vacuo* and the residual yellow oil was redissolved in EtOAc (50 mL), washed with brine (3 x 50 mL) then dried (Na₂SO₄) and dry loaded onto silica. The title compound (**106**) was purified by MPLC on silica (7:3 petrol/EtOAc) and obtained as a colourless oil (2.31 g, 9.12 mmol, 85 %).

R_f = 0.44 (3:7 EtOAc/Hexane); m.p. 184 °C (Lit 184 °C); ¹H NMR (500 MHz, CDCl₃) δ 1.71 (9H, s, CH₃), 7.38 (1H, d, J = 5.3 Hz, C²-H), 8.45 (1H, d, J = 5.3 Hz, C¹-H), 8.52 (1H, s, C³-H); LRMS (ES+) m/z 154.07 (Boc removed) [M+H]⁺;

***tert*-Butyl 7-chloro-5-nitro-3*H*-imidazo[4,5-*b*]pyridine-3-carboxylate (**107**)²⁹⁷**

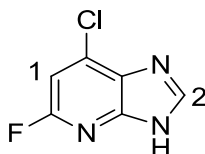
A solution of *tert*-butyl 7-chloro-3*H*-imidazo[4,5-*b*]pyridine-3-carboxylate (**106**) (337 mg, 1.33 mmol) in DCM (6 mL) was cooled to 0 °C. In a separate flask the nitration mixture was prepared by addition of tetrabutylammonium nitrate (1.21 g, 4.00 mmol) to a stirred solution of trifluoroacetic anhydride (554 µL, 4.00 mmol) in DCM (6 mL) at 0 °C. The nitration mixture was stirred for 10 min, before being added dropwise to the solution of *tert*-butyl 7-chloro-3*H*-imidazo[4,5-*b*]pyridine-3-carboxylate (**106**). Upon addition the mixture immediately turned yellow and after 15 min the starting material had been consumed (LC-MS). The reaction mixture was washed with NaHCO_{3(aq)} (1 x 20 mL) and water (2 x 20 mL), dried (Na₂SO₄) then dry loaded onto silica. The title product (**107**) was purified by MPLC (3:7 EtOAc/petrol) and obtained as a pale yellow crystalline solid (280 mg, 0.94 mmol, 71%).

R_f = 0.60 (3:7 EtOAc/Hexane); m.p. 131-132 °C (Lit 288.2 - 290 °C); UV λ_{max} (EtOH/nm) 287.0; IR ν_{max}/cm^{-1} : 3197, 3116, 3001, 2983 2945, 1751 (C=O stretch), 1545 (Asym NO₂ stretch), 1369 (sym NO₂ stretch), 1154 (nitro C-N); ¹H NMR (500 MHz, CDCl₃) δ 1.75 (9H, s, CH₃), 8.39 (1H, s, C²-H), 8.81 (1H, s, C¹-H); LRMS (ES+) m/z 199.05 (Boc removed) [M+H]⁺.

***tert*-Butyl 5-amino-7-chloro-3*H*-imidazo[4,5-*b*]pyridine-3-carboxylate (**108**)**

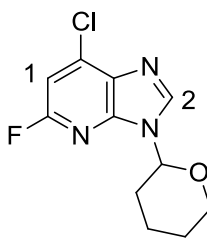
A 0.05 M solution of *tert*-butyl 7-chloro-5-nitro-3*H*-imidazo[4,5-*b*]pyridine-3-carboxylate (**107**) (250 mg, 0.84 mmol) in DCM (17 mL) was reduced using an H-Cube[®] continuous flow reactor (Thalesnano Inc.) with a Raney Nickel CatCart (40 °C, 1 mL/min). After 3 cycles LC-MS confirmed complete conversion of starting material to the title product. The solvent was removed *in vacuo* to give the title compound (**108**) as a colourless oil (188 mg, 0.70 mmol, 84%).

R_f = 0.45 (2:3 EtOAc/petrol); UV λ_{max} (EtOH/nm) 279; IR ν_{max}/cm^{-1} : 3491 (asym NH_2), 3315 (sym NH_2), 3194, 3157, 3049, 3006, 2978, 1769 (C=O stretch); 1H NMR (500 MHz, DMSO- d_6) δ 1.60 (9H, s, CH_3), 6.45 (2H, br s, NH_2), 6.56 (1H, s, C^1 -H), 8.31 (1H, s, C^2 -H); ^{13}C NMR (125 MHz, DMSO- d_6) δ 27.5 (CH_3), 84.8 (OC(CH_3)₃), 105.0 (Ar-C), 124.9 (Ar-C), 134.9 (Ar-C), 139.0 (Ar-C), 145.5 (Ar-C), 145.9 (Ar-C), 158.4 (C=O); LRMS (ES+) m/z 269.07 (Boc removed) $[M+H]^+$; HRMS Calcd for $C_{11}H_{14}ClN_4O_2$ m/z = 269.0800 $[M+H]^+$, Found m/z = 269.0805 $[M+H]^+$.

7-Chloro-5-fluoro-3*H*-imidazo[4,5-*b*]pyridine (109)

A polytetrafluoroethylene (PFTE) conical flask was charged with tetrafluoroboric acid (1 mL, 15.7 mmol) and *tert*-butyl-5-amino-7-chloro-3*H*-imidazo[4,5-*b*]pyridine-3-carboxylate (**108**) (78 mg, 0.29 mmol). The reaction mixture was cooled to 0 °C and an aqueous solution of sodium nitrite (40 mg, 0.58 mmol) was introduced dropwise over a period of 10 min. The resulting mixture was stirred (2h, 0 °C) then allowed to warm (RT, 20 min). The reaction mixture was cooled to -15 °C, neutralised with aqueous NaOH (2 M) and extracted with EtOAc (3 x 30 mL). The combined organic layers were dried (Na₂SO₄), dry loaded onto silica and purified by MPLC on silica (3:2 EtOAc/petrol) to give the title compound (**109**) as a pale yellow solid (22 mg, 0.13 mmol, 44%).

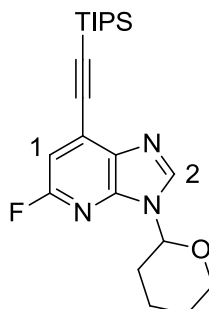
R_f = 0.40 (3:2 EtOAc/petrol); m.p. 210 °C; UV λ_{\max} (EtOH/nm) 281; IR $\nu_{\max}/\text{cm}^{-1}$: 3117, 3083, 3024, 2895, 2772, 2703, 2631, 2501, 2462, 2387, 1034 (C-F stretch); ¹H NMR (500 MHz, DMSO-*d*₆) δ 7.23 (1H, s, C¹-H), 8.51 (1H, s, C²-H), 13.58 (1H, br s, NH); ¹³C NMR (125 MHz, DMSO-*d*₆) δ 103.5 (Ar-C), 103.9 (Ar-C), 144.8 (Ar-C), 158.1 (Ar-C), 160.0 (Ar-C); ¹⁹F NMR (470 MHz, DMSO-*d*₆) δ -73.69; LRMS (ES+) m/z 171 [M+H]⁺; HRMS Calcd for C₆H₄ClFN₃ m/z = 172.0071 [M+H]⁺, Found m/z = 172.0071 [M+H]⁺.

Chloro-5-fluoro-3-(tetrahydro-2H-pyran-2-yl)-3H-imidazo[4,5-b]pyridine (110)

To a solution of 7-chloro-5-fluoro-3H-imidazo[4,5-b]pyridine (**109**) (76 mg, 0.44 mmol) in anhydrous EtOAc (15 mL) was added (*Rac*)-camphor sulfonic acid (3.5 mg, 1.5×10^{-2} mmol). The reaction mixture was heated to 60 °C at which point 3,4-dihydro-2H-pyran (44 μ L, 0.49 mmol) was added. The reaction mixture was heated for a further 18 h then cooled to RT and neutralised ($\text{NH}_4\text{OH}_{(\text{aq})}$ (32%)). The reaction mixture was washed with brine (15 mL) and water (2 x 15 mL) then dried (Na_2SO_4) and dry loaded onto silica. The title compound (**110**) was purified by MPLC (2:3 EtOAc/petrol) and obtained as a colourless oil (106 mg, 0.42 mmol, 94%).

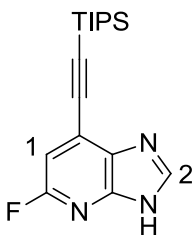
R_f = 0.31 (2:3 EtOAc/petrol); UV λ_{max} (EtOH/nm) 265; IR $\nu_{\text{max}}/\text{cm}^{-1}$: 3115, 2874, 2415, 2318, 1035 (C-F stretch); ^1H NMR (500 MHz, CDCl_3) δ 1.5-2.2 (6H, m, 3 x CH_2), 3.75-3.81 (1H, td, J = 5.9 and 2.6 Hz, CH_2), 4.15-4.20 (1H, td, J = 11.8 and 2.1, CH_2), 5.72 (1H, dd, J = 10.6 and 2.4, CH), 6.97 (1H, s, $\text{C}^1\text{-H}$), 8.28 (1H, s, $\text{C}^2\text{-H}$); ^{13}C NMR (125 MHz, $\text{DMSO-}d_6$) δ 22.9 (CH_2), 24.7 (CH_2), 30.1 (CH_2), 68.2 (OCH_2), 97.5 (ArCH-O-CH_2), 101.9 (Ar-C), 110.2 (Ar-C), 122.5 (Ar-C), 138.1 (Ar-C), 159.1 (Ar-C), 160.2 (Ar-C); ^{19}F NMR (470 MHz, $\text{DMSO-}d_6$) δ -72.97; HRMS Calcd for $\text{C}_{11}\text{H}_{12}\text{ClFN}_3\text{O}$ m/z = 256.0647 $[\text{M}+\text{H}]^+$, Found m/z = 256.0651 $[\text{M}+\text{H}]^+$.

5-Fluoro-3-(tetrahydro-2*H*-pyran-2-yl)-7-((triisopropylsilyl)ethynyl)-3*H*-imidazo[4,5-*b*]pyridine (111)



A suspension of caesium carbonate (159 mg, 0.49 mmol), triisopropylsilyl acetylene (38 μ L, 0.25 mmol), 2-dicyclohexylphosphonio-2,4,6-triisopropylbiphenyl (XPhos) (2.8 mg, 5.9×10^{-3} mmol) and $\text{PdCl}_2(\text{CH}_3\text{CN})_2$ (0.5 mg, 2.0×10^{-3} mmol) was prepared in anhydrous acetonitrile (1 mL). A solution of 7-chloro-5-fluoro-3-(tetrahydro-2*H*-pyran-2-yl)-3*H*-imidazo[4,5-*b*]pyridine (**110**) (50 mg, 0.20 mmol) in anhydrous acetonitrile (1 mL) was added to the reaction mixture. The vial was capped and the reaction mixture was degassed (20 min, N_2) then heated (80 $^\circ\text{C}$, 2 h) resulting in a colour change from yellow to dark red. The reaction mixture was cooled and filtered through Celite before being diluted with EtOAc (10 mL) and washed with water (3 x 10 mL). The resulting solution was dried (MgSO_4) then dry loaded onto silica and purified by MPLC on silica (3:7 EtOAc/ petrol 3:7) to give compound (**111**) as a colourless oil (53 mg, 0.13 mmol, 67%).

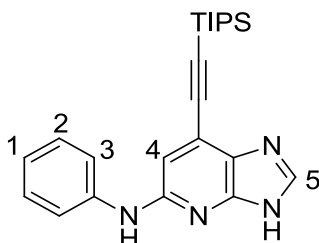
R_f = 0.68 (3:7 EtOAc/petrol); UV λ_{max} (EtOH/nm) 271; IR $\nu_{\text{max}}/\text{cm}^{-1}$: 3124, 2915, 2792, 2162, 1651; ^1H NMR (500 MHz, CDCl_3) δ 1.14-1.19 (21H, m, CH_2CH_3), 1.59-2.21 (6H, m, 3 x CH_2), 3.75-3.81 (1H, td, J = 11.9 and 2.6 Hz, CH_2), 4.12-4.19 (1H, m, CH_2), 5.72 (1H, dd, J = 10.4 and 2.3 Hz, CH), 6.95 (1H, s, $\text{C}^1\text{-H}$), 8.26 (1H, s, $\text{C}^2\text{-H}$); ^{13}C NMR (125 MHz, $\text{DMSO-}d_6$) δ 11.1 (($\text{Si}(\text{CH}(\text{CH}_3)_2)_3$), 18.6 (($\text{Si}(\text{CH}(\text{CH}_3)_2)_3$), 22.1 (CH_2), 24.4 (CH_2) 31.5 (CH_2) 68.1 (OCH_2) 95.1 (ArCH-O-CH_2), 95.2 ($\text{C}\equiv\text{C-Si}$), 101.3 ($\text{C}\equiv\text{C}$), 101.7 (Ar-C), 110.2 (Ar-C), 116.1 (Ar-C), 119.4 (Ar-C), 126.7 (Ar-C), 141.8 (Ar-C), 162.2 (Ar-C); HRMS Calcd for $\text{C}_{22}\text{H}_{33}\text{FN}_3\text{OSi}$ m/z = 402.2371 [$\text{M}+\text{H}$] $^+$, Found m/z = 402.2368 [$\text{M}+\text{H}$] $^+$.

5-Fluoro-7-((triisopropylsilyl)ethynyl)-3*H*-imidazo[4,5-*b*]pyridine (112)

5-Fluoro-7-((triisopropylsilyl)ethynyl)-3*H*-imidazo[4,5-*b*]pyridine (**111**) (20 mg, 0.05 mmol) was dissolved in 2-propanol (0.5 mL). Trifluoroacetic acid (77 μ L, 1 mmol) was added followed by water (77 μ L). The reaction mixture was heated (100 $^{\circ}$ C, 2 h), cooled to RT and diluted in EtOAc (10 mL). The resulting solution was washed sequentially with $\text{NaHCO}_{3(\text{aq})}$ (10 mL) and water (3 x 10 mL) then dried (MgSO_4) and dry loaded onto NH silica. The title compound (**112**) was purified by MPLC (NH silica; 5:95 MeOH/DCM) and obtained as a yellow oil (14.6 mg, 4.6×10^{-2} mmol, 92%).

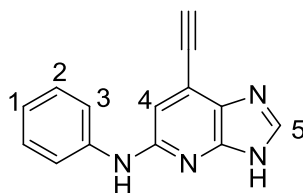
R_f = 0.40 (2:3 EtOAc/petrol); UV λ_{max} (EtOH/nm) 279; IR $\nu_{\text{max}}/\text{cm}^{-1}$: 2944, 2891, 2866, 2798, 2712, 2639, 2362, 2166, 1616, 1602, 1590, 1574, 1494, 1463, 1350; ^1H NMR (500 MHz, MeOD) δ 1.16-1.24 (21H, m, ($\text{Si}(\text{CH}(\text{CH}_3)_2)_3$), 7.00 (1H, s, $\text{C}^1\text{-H}$), 8.38 (1H, s, $\text{C}^2\text{-H}$); ^{13}C NMR (125 MHz, $\text{DMSO-}d_6$) δ 10.6 (($\text{Si}(\text{CH}(\text{CH}_3)_2)_3$), 18.5 (($\text{Si}(\text{CH}(\text{CH}_3)_2)_3$), 158.2 (Ar-C); ^{19}F NMR (500 MHz, CDCl_3) δ -71.71 and -74.17 (imidazole isomers); HRMS Calcd for $\text{C}_{17}\text{H}_{25}\text{FN}_3\text{Si}$ m/z = 318.1796 $[\text{M}+\text{H}]^+$, Found m/z = 318.1796 $[\text{M}+\text{H}]^+$.

Note: not all carbon atoms were visible

N-Phenyl-7-((triisopropylsilyl)ethynyl)-3H-imidazo[4,5-b]pyridin-5-amine (113)

Aniline hydrochloride (114 mg, 0.88 mmol) was added to a solution of 5-fluoro-7-((triisopropylsilyl)ethynyl)-3H-imidazo[4,5-b]pyridine (**112**) (70 mg, 0.22 mmol) in trifluoroethanol (1 mL). The reaction mixture was heated (78 °C, 7 days) after which it had neared completion (TLC). The solvent was removed *in vacuo* and DCM (25 mL) was added. The resulting solution was washed with HCl_(aq) (1 M) (10 mL) and NaHCO_{3(aq)} (1 x 25 mL) then dried (phase separator) and dry loaded onto NH silica. The crude product was purified by MPLC (NH silica; 5:95 MeOH/DCM 5:95) to give (**113**) as a yellow oil (67 mg, 0.17 mmol, 78%).

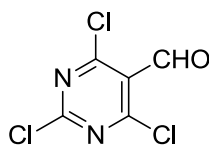
R_f = 0.50 (NH silica 5:95 MeOH/DCM); UV λ_{max} (EtOH/nm) 268; IR ν_{max}/cm^{-1} : 3105, 3046, 2942, 2864, 2562, 2249, 2159, 2024, 2021, 1714, 1613, 1597; 1H NMR (500 MHz, MeOD) δ 1.16-1.24 (21H, m, CH₃CH), 6.86 (1H, s, C⁴-H), 6.91 (1H, tt, J = 7.4 and 1.1 Hz, C¹-H), 7.22-7.28 (2H, app. t, J = 7.4 Hz, C²-H), 7.71 (2H, d, J = 7.8 Hz, C³-H) 8.02 (1H, s, C⁵-H); ^{13}C NMR (125 MHz, DMSO-*d*₆) δ 10.7 ((Si(CH(CH₃)₂)₃), 18.5 ((Si(CH(CH₃)₂)₃), 96.6 (C \equiv C-Si), 102.5 (C \equiv C), 109.6 (Ar-C), 117.6 (Ar-C), 120.3 (Ar-C), 122.3 (Ar-C), 127.6 (Ar-C), 128.6 (Ar-C), 139.9 (Ar-C), 141.7 (Ar-C), 146.0 (Ar-C), 152.1 (Ar-C); HRMS Calcd for C₂₃H₃₀N₄Si m/z = 391.2313 [M+H]⁺, Found m/z = 391.2317 [M+H]⁺.

7-Ethynyl-*N*-phenyl-3*H*-imidazo[4,5-*b*]pyridin-5-amine (87)

The title compound was prepared following **general procedure A** using: *N*-phenyl-7-((triisopropylsilyl)ethynyl)-3*H*-imidazo[4,5-*b*]pyridin-5-amine (**113**) (29 mg, 7.42×10^{-2} mmol) and TBAF (1 M in THF) (111 μ L, 0.11 mmol) in THF (3mL). The crude product was purified by NH MPLC on silica (5:95 MeOH/DCM) to give the title compound (**87**) as a yellow solid (12 mg, 5.12×10^{-2} mmol, 69%).

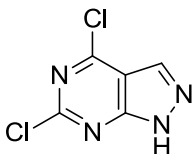
R_f = 0.24 (5:95 MeOH/DCM); m.p. 200 °C (dec.); UV λ_{\max} (EtOH/nm) 260; IR $\nu_{\max}/\text{cm}^{-1}$: 3407, 3283, 3117, 3051, 2856, 2577, 2357, 2344, 2265, 2201, 2161, 1979, 1597, 1580, 1495, 1438, 1380; ^1H NMR (500 MHz, MeOD) δ 4.63 (1H, br s, Ethynyl CH), 6.82 (1H, s, C⁴-H), 6.89 (1H, tt, J = 7.4 and 1.2 Hz, C¹-H), 7.26 (2H, app. t, J = 7.4 Hz, C²-H), 7.73 (2H, d, J = 7.9 Hz, C³-H), 8.09 (1H, s, C⁵-H), 9.11 (1H, br s, ArNHAr), 12.82 (1H, br s, NH imidazopyridine); LRMS (ES+) m/z = 235.2 $[\text{M}+\text{H}]^+$; HRMS Calcd for C₁₄H₁₁N₄ m/z = 235.0978 $[\text{M}+\text{H}]^+$, Found m/z = 235.0980 $[\text{M}+\text{H}]^+$

Note: insufficient sample for ^{13}C NMR analysis

2,4,6-Trichloropyrimidine-5-carbaldehyde (144)²⁹⁸

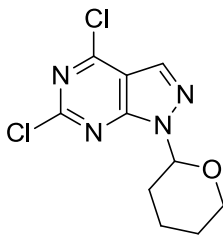
To a flask containing anhydrous DMF (733 μL , 9.5 mmol) cooled to 0 $^{\circ}\text{C}$ was added POCl_3 (7 mL, 76 mmol) dropwise with stirring (0 $^{\circ}\text{C}$ 30 min). Barbituric acid (1 g, 7.8 mmol) was added and the resulting suspension was stirred (RT, 60 min). The reaction mixture was heated to reflux (110 $^{\circ}\text{C}$, 4 h) after which half of the POCl_3 was removed *via* vacuum distillation. The remaining solution was neutralised by drop wise addition over rapidly stirred ice water. A yellow precipitate formed and was collected by filtration, washed with water (50 mL) and dissolved in DCM (25 mL). The resulting yellow solution was washed with $\text{NaHCO}_{3(\text{aq})}$ (50 mL) and water (50 mL) then dried (phase separator) and the solvent was removed *in vacuo* to leave an orange solid. The crude product was purified by triturating with hot 2-propanol (3 x 50 mL) to give the title compound (**144**) as a light yellow crystalline solid (907 mg, 4.3 mmol, 55%).

R_f = 0.62 (DCM); m.p. 128-131 $^{\circ}\text{C}$ (Lit 130-132 $^{\circ}\text{C}$); UV λ_{max} (EtOH/nm) 251; ^1H NMR (500 MHz, CDCl_3) δ 10.42 (1H, s, CHO); IR $\nu_{\text{max}}/\text{cm}^{-1}$: 1704 (CO), 1521, 1495, 1414, 1314, 1296, 1201, 1116; LRMS (ES+) m/z = 211.8 $[\text{M}+\text{H}]^+$

4,6-Dichloro-1*H*-pyrazolo[3,4-*d*]pyrimidine (145)^{299,300}

A solution of 2,4,6-trichloropyrimidine-5-carbaldehyde (**144**) (3 g, 14.2 mmol) in MeOH (75 mL) was cooled to -30 °C. In solution of hydrazine hydrate (710 μ L, 14.6 mmol) in MeOH (18 mL) at -30 °C was prepared added dropwise followed by a solution of triethylamine (2.1 mL, 14.2 mmol) in MeOH (18 mL) at -30 °C. The reaction mixture was stirred (-30 °C, 6 hours) and the solvent was removed *in vacuo* to leave a crude brown deposit. The solid was heated to reflux in 2-propanol (100 mL) and filtered whilst hot. The filtrate was evaporated to dryness, redissolved in EtOAc (100 mL) then dry loaded onto silica. The crude product was purified by MPLC on silica (5:95 MeOH/DCM) to give the title compound (**145**) as an orange/yellow solid (2.15 g, 11.4 mmol, 80%).

R_f = 0.40 (5:95 MeOH/DCM); m.p. 320 °C (dec.) (Lit 145 °C dec.); UV λ_{\max} (EtOH/nm) 270; IR $\nu_{\max}/\text{cm}^{-1}$: 3254, 3211, 3188, 2828, 2392, 2296, 2266, 2216, 2176, 2131, 1989, 1865, 1686, 1596; ^1H NMR (500 MHz, DMSO- d_6) δ 8.52 (1H, s, CH), 14.65 (1H, br s, NH).

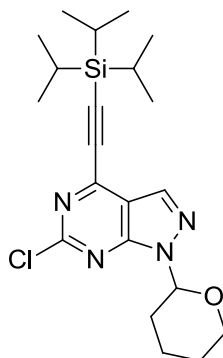
4,6-Dichloro-1-(tetrahydro-2H-pyran-2-yl)-1H-pyrazolo[3,4-d]pyrimidine (146**)**²⁹⁹

To a solution of 4,6-dichloro-1H-pyrazolo[3,4-d]pyrimidine (**145**) (50 mg, 0.27 mmol) in EtOAc (2 mL) was added (*Rac*)-camphor sulfonic acid (2.1 mg, 9.0×10^{-3} mmol). The reaction mixture was heated to 60 °C and 3,4-dihydro-2H-pyran (26 μ L, 0.29 mmol) was added. The resulting solution was heated (60 °C, 18 h) then cooled to RT and washed with $\text{NaHCO}_{3(\text{aq})}$. EtOAc (15 mL) was added and the resulting organic solution was washed with brine (15 mL) and water (2 x 15 mL) then dried (Na_2SO_4) and dry loaded onto silica. The title compound (**146**) was purified by MPLC on silica (DCM) as a white solid (57 mg, 0.21 mmol, 79%).

R_f = 0.49 (DCM); m.p. 64-66 °C; UV λ_{max} (EtOH/nm) 214; IR $\nu_{\text{max}}/\text{cm}^{-1}$: 3098, 2956, 2931, 2870, 2426, 2158, 2035, 1973, 1770, 1591, 1542, 1476; ^1H NMR (500 MHz, CDCl_3) δ 1.59-2.56 (6H, m, 3 x CH_2), 3.81 (1H, m, CH), 4.12 (1H, m, CH), 6.00 (1H, dd, J = 10.4 and 2.5 Hz, CH), 8.19 (1H, s, pyrazolopyrimidine CH); ^{13}C NMR (125 MHz, CDCl_3) δ 22.7 (CH_2), 24.8 (CH_2), 29.4 (CH_2), 68.5 (CH_2), 83.0 (N-CH), 113.3 ($\text{C}^3\text{-H}$); HRMS Calcd for $\text{C}_{10}\text{H}_{11}\text{Cl}_2\text{N}_4\text{O}$ m/z = 273.0310 $[\text{M}+\text{H}]^+$, Found m/z = 273.0309 $[\text{M}+\text{H}]^+$.

Note: not all carbon atoms visible

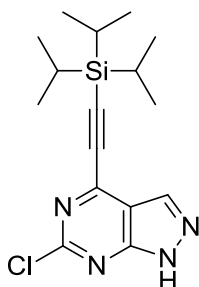
6-Chloro-1-(tetrahydro-2H-pyran-2-yl)-4-((triisopropylsilyl)ethynyl)-1H-pyrazolo[3,4-d]pyrimidine (147)



4,6-Dichloro-1-(tetrahydro-2H-pyran-2-yl)-1H-pyrazolo[3,4-d]pyrimidine (**146**) (50 mg, 0.18 mmol), caesium carbonate (119 mg, 0.37 mmol), Pd(PPh₃)₂Cl₂ (2.8 mg, 4.02 x 10⁻³ mmol) and CuI (1.5 mg, 8.04 x 10⁻³ mmol) were added to a flask. Anhydrous DMF (1 mL) was then added followed by triisopropylsilyl acetylene (45 µL, 0.20 mmol). The reaction vessel was capped and degassed (15 min, N₂) then heated *via* microwave irradiation (45 °C, 10 min). The reaction mixture was diluted with EtOAc (50 mL) then filtered through Celite, washed with water (3 x 50 mL) and dried (MgSO₄). The crude product was dry loaded onto silica and purified by MPLC on silica (15:85 EtOAc/petrol) to give compound (**147**) as a colourless oil (53 mg, 0.13 mmol, 69%).

R_f = 0.52 (15:85 EtOAc/petrol); UV λ_{max} (EtOH/nm) 217; IR ν_{max}/cm^{-1} : 2943, 2892, 2865, 2165, 1559, 1464, 1440, 1381; ¹H NMR (500 MHz, CDCl₃) δ 1.10-1.26 (21H, m, CH₂CH₃), 1.59-2.56 (6H, m, 3 x CH₂), 3.80 (1H, m, CH), 4.12 (1H, m, CH), 6.00 (1H, dd, J = 10.4 and 2.5 Hz, CH), 8.16 (1H, s, CH pyrazolopyrimidine); ¹³C NMR (125 MHz, CDCl₃) δ 10.9 ((Si(CH(CH₃)₂)₃), 18.6 ((Si(CH(CH₃)₂)₃), 22.4 (CH₂), 24.7 (CH₂), 29.3 (CH₂), 68.5 (OCH₂), 83.0 (Ar-CH-O), 113.3 (C³-H), HRMS Calcd for C₂₁H₃₂ClN₄OSi m/z = 419.2028 [M+H]⁺, Found m/z = 419.2029 [M+H]⁺.

Note: not all carbon atoms visible

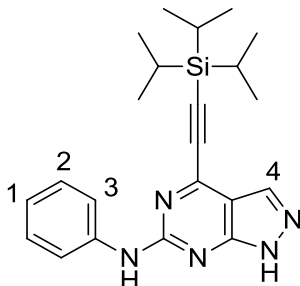
6-Chloro-4-((triisopropylsilyl)ethynyl)-1H-pyrazolo[3,4-d]pyrimidine (148)

To a solution of 6-chloro-1-(tetrahydro-2H-pyran-2-yl)-4-((triisopropylsilyl)ethynyl)-1H-pyrazolo[3,4-d]pyrimidine (**147**) (170 mg, 0.41 mmol) in TFE (8 mL) was added TFA (156 μ L, 2.03 mmol) and water (156 μ L). The reaction mixture was heated (100 $^{\circ}$ C, 4 h) then diluted with $\text{NaHCO}_{3(\text{aq})}$ (50 mL) and extracted with DCM (2 x 50 mL). The DCM layers were combined then washed with water (2 x 50 mL) and dried (phase separator). The crude product was dry loaded onto silica and purified by MPLC on silica (15:85 EtOAc/petrol) to give the compound (**148**) as a white solid (101 mg, 0.30 mmol, 75%).

R_f = 0.40 (15:85 EtOAc/petrol); m.p. 108-111 $^{\circ}$ C; UV λ_{max} (EtOH/nm) 216; IR $\nu_{\text{max}}/\text{cm}^{-1}$: 3192, 3131, 3111, 3016, 2943, 2865, 2892, 2808, 2728, 2360, 2168, 1701, 1565, 1461; ^1H NMR (500 MHz, CDCl_3) δ 1.08-1.29 (21H, m, CH_2CH_3), 8.19 (1H, s, CH pyrazolopyrimidine), 10.67 (1H, br s, NH pyrazolopyrimidine); ^{13}C NMR (125 MHz, CDCl_3) 11.1 ((Si(CH(CH $_3$) $_2$) $_3$), 18.6 (Si(CH(CH $_3$) $_2$) $_3$), 100.6 ($\text{C}\equiv\text{C-Si}$), 106.0 ($\text{C}\equiv\text{C-Si}$), 134.7 (C^3H), 146.7 (Ar-C). HRMS Calcd for $\text{C}_{16}\text{H}_{24}\text{ClN}_4\text{Si}$ m/z = 335.1453 $[\text{M}+\text{H}]^+$, Found m/z = 335.1458 $[\text{M}+\text{H}]^+$.

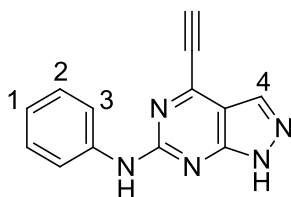
Note: Not all carbon atoms were visible

***N*-Phenyl-4-((triisopropylsilyl)ethynyl)-1*H*-pyrazolo[3,4-*d*]pyrimidin-6-amine (149)**



The title compound was prepared following **general procedure E** using: 6-chloro-4-((triisopropylsilyl)ethynyl)-1*H*-pyrazolo[3,4-*d*]pyrimidine (**148**) (105 mg, 0.31 mmol), aniline (86 μ L, 0.94 mmol) and TFA (60 μ L, 0.79 mmol) in TFE (6 mL). The crude product was dry loaded onto silica and purified by MPLC on silica (15:85 EtOAc/petrol) to give (**149**) as a light yellow solid (90 mg, 0.23 mmol, 73%).

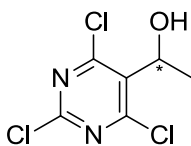
R_f = 0.55 (15:85 EtOAc/petrol); m.p. 153-156 $^{\circ}$ C; UV λ_{\max} (EtOH/nm) 214; IR $\nu_{\max}/\text{cm}^{-1}$: 3125, 3027, 2943, 2864, 2794, 2726, 2388, 2279, 2242, 1967, 1933, 1596, 1572, 1532, 1487; ^1H NMR (500 MHz, CDCl_3) δ 1.1-1.3 (21H, m, CH_2CH_3), 7.09 (1H, tt, J = 7.4 and 1.1 Hz, $\text{C}^1\text{-H}$), 7.37 (2H, app. t, J = 7.37 Hz, $\text{C}^2\text{-H}$), 7.41 (1H, br s, ArNHAr), 7.66 (2H, d, J = 7.6, $\text{C}^3\text{-H}$), 7.91 (1H, s, $\text{C}^4\text{-H}$), 10.05 (1H, br s, NH pyrazolopyrimidine); ^{13}C NMR (125 MHz, CDCl_3) δ 18.7 ($\text{Si}(\text{CH}(\text{CH}_3)_2)_3$), 36.5 ($\text{Si}(\text{CH}(\text{CH}_3)_2)_3$), 99.1 ($\text{C}\equiv\text{C-Si}$), 110.2 ($\text{C}\equiv\text{C}$), 116.9 (Ar-H), 122.5 (Ar-H), 129.3 (Ar-H), 134.1 ($\text{C}^4\text{-H}$); HRMS Calcd for $\text{C}_{22}\text{H}_{30}\text{N}_5\text{Si}$ m/z = 392.2265 $[\text{M}+\text{H}]^+$, Found m/z = 392.2265 $[\text{M}+\text{H}]^+$.

4-Ethynyl-*N*-phenyl-1*H*-pyrazolo[3,4-*d*]pyrimidin-6-amine (89)

The title compound was prepared following **general procedure A** using: *N*-phenyl-4-((triisopropylsilyl)ethynyl)-1*H*-pyrazolo[3,4-*d*]pyrimidin-6-amine (**149**) (45 mg, 0.12 mmol) and TBAF (1 M in THF) (172 μ L, 0.17 mmol) in THF (3 mL). The crude product was purified by MPLC on silica (5:95 MeOH/DCM) to give the title compound (**89**) as an orange solid (17 mg, 7.23×10^{-2} mmol, 63%).

R_f = 0.70 (5:95 MeOH/DCM); m.p. 240 $^{\circ}$ C (dec.); UV λ_{\max} (EtOH/nm) 269; IR $\nu_{\max}/\text{cm}^{-1}$: 3289, 2119, 2030, 1593, 1556, 1497, 1448, 1413, 1310, 1286, 1239; ^1H NMR (500 MHz, DMSO- d_6) δ 4.98 (1H, s, CH ethynyl), 6.98 (2H, m, C¹-H), 7.31 (2H, app. t, J = 7.5 Hz, C²-H), 7.83 (2H, d, J = 7.7 Hz, C³-H), 8.08 (1H, s, C⁴-H), 9.99 (1H, br s, ArNHAr), 13.54 (1H, br s, NH pyrazolopyrimidine); ^{13}C NMR (125 MHz, DMSO- d_6) δ 74.1 (C \equiv C-H), 85.9 (C \equiv C-Ar), 116.9 (Ar-C), 122.2 (Ar-C), 128.7 (Ar-C), 132.5 (C⁴); LRMS (ES+) m/z = 236.20 [M+H]⁺; HRMS Calcd for C₁₄H₁₂N₅ m/z = 236.0931 [M+H]⁺, Found m/z = 236.0928 [M+H]⁺.

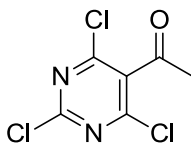
Note: Not all carbon atoms visible

1-(2,4,6-Trichloropyrimidin-5-yl)ethanol (158)

A solution of 2,4,6-trichloropyrimidine-5-carbaldehyde (**144**) (100 mg, 0.47 mmol) was made in anhydrous THF (1 mL). The reaction vessel was capped and flushed with nitrogen then cooled to 0 °C. Methyl magnesium bromide (3M in diethylether) (173 μ L, 0.52 mmol) was added dropwise and the resulting yellow solution was stirred (0 °C, 30 min) then allowed to warm (RT, 30 min). Water (2 mL) was added followed by EtOAc (30 mL). A fine white precipitate formed which was removed by filtering through Celite. The filtrate was washed with brine (3 x 30 mL), dried (MgSO_4) then dry loaded onto silica and purified by MPLC on silica (3:7 EtOAc/petrol) resulting in the title compound (**158**) as a white crystalline solid (80 mg, 0.35 mmol, 74%).

R_f = 0.35 (3:7 EtOAc/petrol); m.p. 148-149 °C; UV λ_{max} (EtOH/nm) 267; IR ν_{max} /cm⁻¹: 3432 (br, OH), 2990, 2931, 2715, 2476, 2405, 2360, 2238, 1896, 1515, 1454; ¹H NMR (500 MHz, DMSO- d_6) δ 1.46 (3H, d, J = 6.8 Hz, CH_3), 5.28 (1H, dq, J = 4.2, 6.8 and 13.6, ArCHOHCH₃), 5.67 (1H, d, J = 4.1, OH); LRMS (ES+) m/z = 227.0 $[\text{M}+\text{H}]^+$.

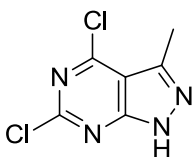
Note: HRMS and ¹³C NMR unsuccessful due to compound degradation

1-(2,4,6-Trichloropyrimidin-5-yl)ethanone (159)

A solution of 1-(2,4,6-trichloropyrimidin-5-yl)ethanol (**158**) (60 mg, 0.26 mmol) was made in anhydrous DCM (2.5 mL). The flask was flushed with nitrogen and a solution of Dess-Martin periodinane (130 mg, 0.31 mmol) in anhydrous DCM (3.5 mL) was added dropwise with stirring. The mixture was stirred (RT, 2 h) after which a white suspension had formed. Ether (10 mL) was added and resulting solution was washed with NaOH_(aq) (1.3M) (2 x 2.5 mL) and water (2 x 10 mL). The organic solution was dried (MgSO₄) then dry loaded onto silica and purified by MPLC on silica (3:7 EtOAc/petrol) to give compound (**159**) as a white crystalline solid (53 mg, 0.23 mmol, 89%).

R_f = 0.35 (3:7 EtOAc/petrol); m.p. 76-79 °C; UV λ_{max} (EtOH/nm) 225; IR ν_{max}/cm^{-1} : 2362, 2337, 1713 (CO), 1541, 1497; ¹H NMR (500 MHz, CDCl₃) δ 2.63 (3H, s, CH₃); LRMS (ES+) m/z = 224.9 [M+H]⁺.

Note: HRMS and ¹³C NMR unsuccessful due to compound degradation

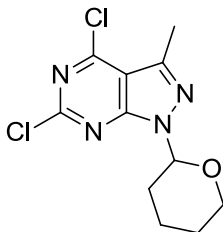
4,6-Dichloro-3-methyl-1H-pyrazolo[3,4-d]pyrimidine (160)

1-(2,4,6-trichloropyrimidin-5-yl)ethanone (**159**) (475 mg, 2.10 mmol) was dissolved in MeOH (15 mL) and cooled to -15 °C. A solution of hydrazine hydrate (105 μ L, 2.17 mmol) in MeOH (5 mL) at -15 °C was added dropwise followed by a solution of triethylamine (316 μ L, 2.10 mmol) in MeOH (5 mL) at -15 °C. The reaction mixture was stirred (-15 °C, 6 h) then warmed to RT. The solvent was removed *in vacuo* and the crude product was redissolved in EtOAc (50 mL). The resulting solution was washed with water (3 x 50 mL), dried (MgSO₄) and dry loaded onto silica. The crude product was purified by MPLC on silica (3:7 EtOAc/petrol) followed by C18 reverse phase MPLC (3:7 MeOH (0.1% HCOOH)/Water (0.1% HCOOH)) to give the title compound (**160**) as a yellow crystalline solid (192 mg, 0.95 mmol, 45%).

R_f = 0.45 (3:7 EtOAc/petrol); m.p. 80-82 °C; UV λ_{max} (EtOH/nm) 203.1; IR ν_{max}/cm^{-1} : 3118, 3085, 3047, 2996, 2963, 2901, 2866, 2816, 2778, 2693, 2027, 1980, 1608, 1556; ¹H NMR (500 MHz, DMSO-*d*₆) δ 3.30 (3H, s, CH₃), 14.23 (1H, br s, NH pyrazolopyrimidine); ¹³C NMR (125 MHz, CDCl₃) δ 14.1 (Ar-CH₃), 111.1 (Ar-C), 144.3 (Ar-C), 156.1 (Ar-C), 156.7 (Ar-C), 157.1 (Ar-C); LRMS (ES+) m/z = 203.1 [M+H]⁺.

Note: HRMS unsuccessful due to compound degradation.

4,6-Dichloro-3-methyl-1-(tetrahydro-2H-pyran-2-yl)-1H-pyrazolo[3,4-d]pyrimidine (161)

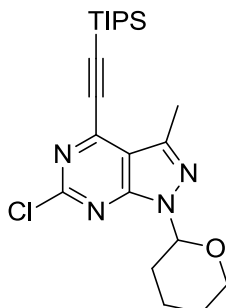


To a solution of 4,6-dichloro-3-methyl-1H-pyrazolo[3,4-d]pyrimidine (**160**) (190 mg, 0.94 mmol) in EtOAc (20 mL) was added (*Rac*)-camphor sulfonic acid (8.0 mg, 3.4 x 10⁻² mmol). The reaction mixture was heated to 60 °C at which point 3,4-dihydro-2H-pyran (128 µL, 1.41 mmol) was added. The reaction mixture was heated (60 °C, 18 h) then cooled to RT and washed with NaHCO_{3(aq)} (40 mL). EtOAc (20 mL) was added and the resulting organic solution was washed with brine (40 mL) and water (2 x 40 mL) then dried (Na₂SO₄) and dry loaded onto silica. The title compound (**161**) was purified by MPLC on silica (15:85 EtOAc/petrol) as a white crystalline solid (290 mg, 0.94 mmol, >99%).

R_f = 0.34 (15:85 EtOAc/petrol); m.p. 106-108 °C; UV λ_{max} (EtOH/nm) 220; IR ν_{max}/cm^{-1} : 2955, 2863, 2159, 1977, 1915, 1584, 1541, 1507, 1458; ¹H NMR (500 MHz, CDCl₃) δ 1.59-2.16 (6H, m, 3 x CH₂), 2.71 (3H, s, CH₃), 3.79 (1H, m, CH), 4.09-4.16 (1H, m, CH), 5.93 (1H, dd, J = 2.5 and 9.7, CH); LRMS (ES+) m/z = 287.1 [M+H]⁺; ¹³C NMR (125 MHz, DMSO-*d*₆) δ 13.1 (CH₃), 22.9 (CH₂), 25.1 (CH₂), 28.9 (CH₂), 105.1 (CH); HRMS Calcd for C₁₁H₁₃Cl₂N₄O m/z = 287.0461 [M+H]⁺, Found m/z = 287.0466 [M+H]⁺.

Note: not all carbon atoms visible

6-Chloro-3-methyl-1-(tetrahydro-2*H*-pyran-2-yl)-4-((triisopropylsilyl)ethynyl)-1*H*-pyrazolo[3,4-*d*]pyrimidine (162**)**

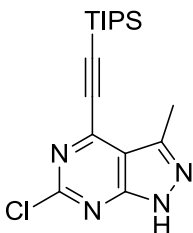


A flask was charged with 4,6-dichloro-3-methyl-1-(tetrahydro-2*H*-pyran-2-yl)-1*H*-pyrazolo[3,4-*d*]pyrimidine (**161**) (50 mg, 0.17 mmol), copper(I) iodide (0.7 mg, 3.48 x 10⁻³ mmol) and Pd(PPh₃)₂Cl₂ (2.5 mg, 3.48 x 10⁻³ mmol). THF (1 mL) was added followed by triisopropylsilyl acetylene (44 µL, 0.19 mmol) and triethylamine (66 µL, 0.44 mmol). The vessel was capped and degassed (15 min, N₂) then shielded from light and stirred (RT, 18 h). The reaction mixture was filtered through Celite, dried (MgSO₄) and dry loaded onto silica then purified by MPLC (1:9 EtOAc/petrol) to give the title compound (**162**) as a colourless oil (73 mg, 0.74 mmol, >99%).

*R*_f = 0.40 (15:85 EtOAc/petrol); UV λ_{max} (EtOH/nm) 223; IR ν_{max}/cm⁻¹: 2944, 2893, 2865, 1557, 1508, 1461, 1377; ¹H NMR (500 MHz CDCl₃) δ 1.14-1.24 (21H, m, CH₂CH₃), 1.59-2.60 (6H, m, 3 x CH₂), 2.73 (3H, s, CH₃), 3.79 (1H, m, CH), 4.12 (1H, m, CH), 5.93 (1H, dd, *J* = 10.7 and 2.4, CH); ¹³C NMR (125 MHz, DMSO-*d*₆) δ 11.1 (Si(CH(CH₃)₂)₃), 13.7 (CH₃), 18.9 (Si(CH(CH₃)₂)₃), 23.1 (CH₂), 25.1 (CH₂), 28.7 (CH₂), 70.1 (OCH₂) 105.1 (CH); HRMS Calcd for C₂₂H₃₄ClN₄OSi *m/z* = 433.2185 [M+H]⁺, Found *m/z* = 433.2185 [M+H]⁺.

Note: not all carbon atoms visible

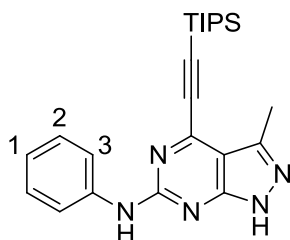
6-Chloro-3-methyl-4-((triisopropylsilyl)ethynyl)-1*H*-pyrazolo[3,4-*d*]pyrimidine (163)



To a solution of 6-chloro-3-methyl-1-(tetrahydro-2*H*-pyran-2-yl)-4-((triisopropylsilyl)ethynyl)-1*H*-pyrazolo[3,4-*d*]pyrimidine (**162**) (73 mg, 0.17 mmol) in 2-propanol (540 μ L) was added TFA (268 μ L, 3.48 mmol) and water (268 μ L). The reaction mixture was heated (100 $^{\circ}$ C, 18 h) then diluted with $\text{NaHCO}_{3(\text{aq})}$ (15 mL). The aqueous mixture was extracted with DCM (2 x 15 mL). The combined organic layers were washed with water (2 x 15 mL) and dried (phase separator). The crude product was dry loaded onto NH silica and purified by NH MPLC on silica (5:95 MeOH/DCM) to give the title compound (**163**) as a white solid (28 mg, 5.4×10^{-2} mmol, 48%).

R_f = 0.23 (NH silica 5:95 MeOH/DCM); m.p. 126-127 $^{\circ}$ C; UV λ_{max} (EtOH/nm) 220; IR $\nu_{\text{max}}/\text{cm}^{-1}$: 3196, 3115, 2945, 2927, 2893, 2867, 2804, 2276, 2160, 2045, 2019, 1682, 1600, 1558; ^1H NMR (500 MHz, CDCl_3) δ 1.10-1.28 (21H, m, CH_2CH_3), 2.75 (3H, s, CH_3), 10.40 (1H, br s, NH pyrazolopyrimidine); HRMS Calcd for $\text{C}_{17}\text{H}_{26}\text{ClN}_4\text{Si}$ m/z = 349.1610 $[\text{M}+\text{H}]^+$, Found m/z = 349.1610 $[\text{M}+\text{H}]^+$.

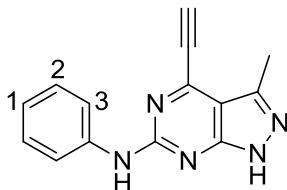
3-Methyl-*N*-phenyl-4-((triisopropylsilyl)ethynyl)-1*H*-pyrazolo[3,4-*d*]pyrimidin-6-amine (164)



The title compound was prepared following **general procedure E** using: 6-chloro-3-methyl-4-((triisopropylsilyl)ethynyl)-1*H*-pyrazolo[3,4-*d*]pyrimidine (**163**) (110 mg, 0.32 mmol), aniline (86 μ L, 0.95 mmol) and TFA (62 μ L, 0.80 mmol) in TFE (6 mL). The crude product was dry loaded onto silica and purified by MPLC on silica (15:85 EtOAc/petrol) to give (**164**) as a light yellow solid (90 mg, 0.23 mmol, 73%).

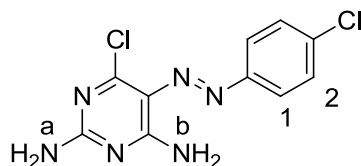
R_f = 0.44 (5:95 MeOH/DCM); m.p. 147-149 $^{\circ}$ C; UV λ_{\max} (EtOH/nm) 272; IR $\nu_{\max}/\text{cm}^{-1}$: 3277, 3205, 3127, 3031, 2942, 2891, 2865, 2772, 2732, 2686, 2120, 2100, 1885, 1853, 1696, 1595, 1570, 1528; ^1H NMR (500 MHz, CDCl_3) δ 1.09-1.30 (21H, m, CH_2CH_3), 2.66 (3H, s, CH_3), 7.07 (1H, tt, J = 7.3 and 1.1 Hz, $\text{C}^1\text{-H}$), 7.35 (2H, dd, J = 8.5 and 7.7 Hz, $\text{C}^2\text{-H}$), 7.36 (1H, br s, ArNHAr), 7.66 (1H, d, J = 8.5 Hz, $\text{C}^3\text{-H}$) 9.72 (1H, br s, NH pyrazolopyrimidine); ^{13}C NMR (125 MHz, CDCl_3) δ 10.8 ($(\text{Si}(\text{CH}(\text{CH}_3)_2)_3$), 13.2 (Ar- CH_3), 18.4 ($(\text{Si}(\text{CH}(\text{CH}_3)_2)_3$), 95.1 ($\text{C}\equiv\text{C-Si}$), 101.3 (Ar-C), 110.1 ($\text{C}\equiv\text{C}$), 117.9 (Ar-C), 120.2 (Ar-C), 122.8 (Ar-C), 129.6 (Ar-C), 139.8 (Ar-C), 147.2 (Ar-C), 149.8 (Ar-C), 160.6 (Ar-C); HRMS Calcd for $\text{C}_{23}\text{H}_{32}\text{N}_5\text{Si}$ m/z = 406.2421 $[\text{M}+\text{H}]^+$, Found m/z = 406.2417 $[\text{M}+\text{H}]^+$.

Note: not all carbon atoms were visible

4-Ethynyl-3-methyl-*N*-phenyl-1*H*-pyrazolo[3,4-*d*]pyrimidin-6-amine (165)

The title compound was prepared following **general procedure A** using: 3-methyl-*N*-phenyl-4-((triisopropylsilyl)ethynyl)-1*H*-pyrazolo[3,4-*d*]pyrimidin-6-amine (**164**) (224 mg, 0.6 mmol) and TBAF (1 M in THF) (903 μ L, 0.90 mmol) in THF (30 mL). The crude product was purified by MPLC on silica (5:95 MeOH/DCM) to give the title compound (**165**) as a yellow solid (73 mg, 0.29 mmol, 49%).

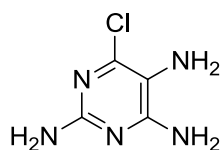
R_f = 0.36 (5:95 MeOH/DCM); m.p. 230 °C (dec.); UV λ_{\max} (EtOH/nm) 270; IR $\nu_{\max}/\text{cm}^{-1}$: 3278, 3207, 3091, 3049, 2989, 2926, 2855, 2804, 2251, 2211, 2160, 2123, 2037, 1975, 1720, 1598, 1575, 1548; ^1H NMR (500 MHz, DMSO- d_6) δ 2.53 (3H, s, CH₃), 4.97 (1H, s, ethynyl CH), 6.97 (1H, tt, J = 7.4 and 1.0 Hz, C¹-H), 7.30 (2H, app. t, J = 7.4 Hz, C²-H), 7.81 (2H, d, J = 7.6 Hz, C³-H); LRMS (ES+) m/z = 250.1 [M+H]⁺; HRMS Calcd for C₁₄H₁₂N₅ m/z = 250.1087 [M+H]⁺, Found m/z = 250.1087 [M+H]⁺.

6-Chloro-5-((4-chlorophenyl)diazenyl)pyrimidine-2,4-diamine (171)^{232,301,302}

A suspension of 4-chloroaniline (10.35 g, 0.081 mol) in water (75 mL) was cooled to 0 °C. HCl_(aq) (12 M) (22.5 mL, 0.27 mol) was added dropwise with stirring until the mixture had fully dissolved. A solution of NaNO₂ (5.66 g, 0.082 mol) in water (75 mL) was then added *via* a dropping funnel over a 30 min period to give a solution of 4-chlorobenzene diazonium chloride which was kept at 0 °C until required.

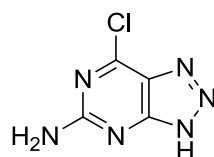
4-Chloro-2,6-diaminopyrimidine (10.60 g, 0.073 mol) was dissolved in a mixture of water (365 mL) and glacial AcOH (365 mL, 6.38 mol). The mixture was stirred until all of the 4-chloro-2,6-diaminopyrimidine had dissolved (~30 min) at which point NaOAc (147 g, 1.79 mol) was added. The cooled solution of 4-chlorobenzene diazonium chloride synthesised previously was then added dropwise with stirring (RT, 30 min). The resulting bright yellow solution was stirred (RT, 18 h) resulting in a yellow precipitate. The precipitate was collected *via* Buchner filtration then washed with water (50 mL) and dried under vacuum to give compound (**171**) as a yellow solid (16.0 g, 0.057 mol, 78%). The filtrate was cooled to 5 °C overnight resulting in a further 3.5 g of the desired product (**171**), which gave a total yield of 19.5 g, 0.069 mol, 95%.

R_f = 0.34 (5:95 MeOH/DCM); m.p. 280 °C (dec.) (Lit m.p. > 230 °C (dec.)); UV λ_{max} (EtOH/nm) 379; IR ν_{max}/cm^{-1} : 3406, 3288, 3136, 2801, 2657, 2430, 2218, 2195, 2170, 2122, 4886, 1647, 1622, 1564, 1517; ¹H NMR (500 MHz, DMSO-*d*₆) δ 7.32 and 7.53 (2H, 2 x br s, NH₂ a), 7.58 (2H, d, J = 8.8 Hz, C¹-H), 7.83 (2H, d, J = 8.8 Hz, C²-H), 8.19 and 9.25 (2H, 2 x br s, NH₂ b).

6-Chloropyrimidine-2,4,5-triamine (172)^{232,302}

A suspension of 6-chloro-5-((4-chlorophenyl)diazenyl)pyrimidine-2,4-diamine (**171**) (9.45 g, 33.5 mmol) in THF (100 mL) was cooled to 0 °C. Glacial acetic acid (15 mL) was added and the reaction vessel was placed under nitrogen. Zinc powder (4.73 g) was added in portions with stirring (0 °C, 15 min). The reaction mixture was warmed to (RT, 15 min) resulting in consumption of the starting material (**171**) (LC-MS). The reaction mixture was filtered through Celite and the resulting red filtrate dry loaded onto silica. The crude product was purified by MPLC on silica (5:95 MeOH/DCM) to give the title compound (**172**) as an off-white crystalline solid (5.93 g, 30.2 mmol, 90%).

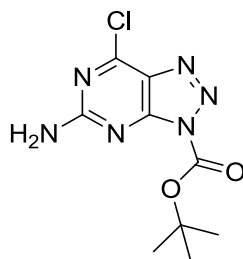
R_f = 0.36 (5:95 MeOH/DCM); m.p. 225-227 °C (Lit m.p. 226-227 °C); UV λ_{\max} (EtOH/nm) 219; IR $\nu_{\max}/\text{cm}^{-1}$: 3365, 3267, 3169, 3123, 3084, 1626, 1579, 1540, 1449; ^1H NMR (500 MHz, DMSO- d_6) δ 3.89 (2H, br s, NH_2), 5.51 (2H, br s, NH_2), 6.35 (2H, br s, NH_2).

7-Chloro-3*H*-[1,2,3]triazolo[4,5-*d*]pyrimidin-5-amine (173)³⁰²

A solution of 6-chloropyrimidine-2,4,5-triamine (**172**) (500 mg, 3.13 mmol) in a mixture of water (45 ml) and glacial AcOH (9.4 mL, 164 mmol) was cooled to 0 °C. A solution of NaNO₂ (238 mg, 3.45 mmol) in water (5 mL) was then added dropwise with stirring over a period of 15 minutes. The mixture was stirred (0 °C, 1 h) after which an orange precipitate had formed. The precipitate was collected by filtration and washed with water (15 ml) then dissolved in EtOH (30 mL). The solvent was removed in vacuo and the crude product was redissolved in EtOAc (30 mL). The resulting solution was washed with brine (3 x 30 mL) and dried (MgSO₄). The solvent was removed to give title compound (**173**) as a yellow solid (360 mg, 2.12 mmol, 68%).

R_f = 0.35 (1:9 MeOH/DCM); m.p. 185 °C (dec.); UV λ_{max} (EtOH/nm) 219; IR ν_{max}/cm^{-1} : 3424, 3386, 3307, 3200, 2954, 2829, 2752, 1659, 1614, 1563, 1508; ¹H NMR (500 MHz, DMSO-*d*₆) δ 7.40 (2H, br s, NH₂), 15.82 (1H, br s, NH triazolopyrimidine).

***tert*-Butyl 5-amino-7-chloro-3*H*-[1,2,3]triazolo[4,5-*d*]pyrimidine-3-carboxylate (174)**

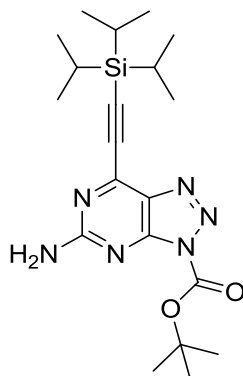


A solution 5-amino-7-chloro-3*H*-[1,2,3]triazolo[4,5-*d*]pyrimidine (**173**) in anhydrous THF (100 ml) was cooled to -10 °C. Di-*tert*-butyl dicarbonate (2.7 g, 12.4 mmol) was then added in one portion followed by 4-dimethylaminopyridine (72 mg, 0.59 mmol). The reaction mixture was stirred under nitrogen (6h, RT) resulting in consumption of the starting material. The solvent was removed *in vacuo* and the crude product was redissolved in EtOAc (50 mL). The organic solution was washed with water (3 x 50 mL), dried (Na₂SO₄) and dry loaded onto silica. The title compound (**174**) was purified by silica based MPCL (5:95 MeOH/DCM) and obtained as an off-white solid (2.37 g, 8.7 mmol, 74%).

R_f = 0.52 (5:95 MeOH/DCM; m.p. 234 °C (dec.); UV λ_{max} (EtOH/nm) 250.5 and 313.0; IR ν_{max}/cm^{-1} : 3496, 3314, 3124, 2988, 1767, 1678, 1617, 1557; ¹H NMR (500 MHz, DMSO-*d*₆) δ 1.75 (9H, s, ^{*t*}Bu), 4.58 (2H, br s, NH₂);

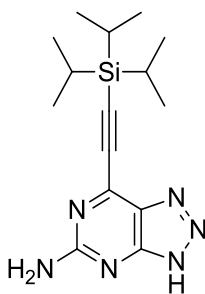
Note: HRMS and ¹³C NMR unsuccessful due to compound degradation

***tert*-Butyl 5-amino-7-((triisopropylsilyl)ethynyl)-3*H*-[1,2,3]triazolo[4,5-*d*]pyrimidine-3-carboxylate (**179**)**



To a solution of *tert*-butyl 5-amino-7-chloro-3*H*-[1,2,3]triazolo[4,5-*d*]pyrimidine-3-carboxylate (**174**) (2.37 g, 8.7 mmol) in anhydrous THF (30 mL) was added triisopropylsilyl acetylene (2.53 mL, 11.0 mmol), copper(I) iodide (66 mg, 0.35 mmol) and PdCl₂(PPh₃)₂ (244 mg, 0.35 mmol) sequentially. Diisopropylethylamine (3.79 mL, 21.8 mmol) was then added and the reaction mixture was degassed (N₂, 30 min). The reaction mixture was stirred (18h, RT) then filtered through Celite. The crude product was dry loaded onto silica and purified by MPLC (2:3 EtOAc/petrol) to give the title compound (**179**) as a yellow oil (2.92 g, 7.01 mmol, 80%).

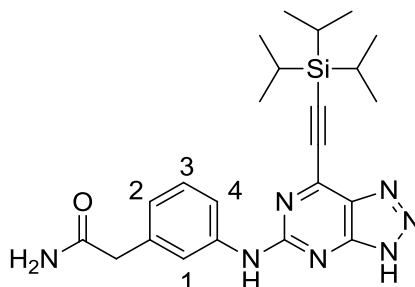
R_f = 0.46 (2:3 EtOAc/petrol); UV λ_{\max} (EtOH/nm) 260.0; IR $\nu_{\max}/\text{cm}^{-1}$: 3513, 3303, 3204, 2944, 2866, 2337, 1765, 1624, 1586, 1561; ¹H NMR (500 MHz, CDCl₃) δ 1.17-1.21 (21H, m, CH₃CH₂), 1.72 (9H, s, ^{*t*}Bu), 5.92 (2H, br s, NH₂); ¹³C NMR (125 MHz, CDCl₃) δ 11.2 ((Si(CH(CH₃)₂)₃), 18.6 ((Si(CH(CH₃)₂)₃), 28.0 ((CH₃)₃), 87.5 (OC(CH₃)₃), 99.3 (C \equiv C-Si), 106.6 (C \equiv C-Si), 132.4 (Ar-C), 146.0 (Ar-C), 146.2 (Ar-C), 152.4 (Ar-C), 163.2 (NCOO); HRMS Calcd for C₂₀H₃₃N₆O₂Si m/z = 417.2429 [M+H]⁺, Found m/z = 417.2426 [M+H]⁺.

7-((Triisopropylsilyl)ethynyl)-3*H*-[1,2,3]triazolo[4,5-*d*]pyrimidin-5-amine (175)

A solution of *tert*-butyl 5-amino-7-((triisopropylsilyl)ethynyl)-3*H*-[1,2,3]triazolo[4,5-*d*]pyrimidine-3-carboxylate (**179**) (2.92 g, 7.01 mmol) in TFE (150 mL) was heated (1h, 80 °C). The solvent was removed and the crude product was redissolved in DCM (50 mL) then dry loaded onto isolate. The crude product was purified by MPLC on silica (1:9 MeOH/DCM) to give the title compound (**175**) as a yellow oil (2.1 g, 6.6 mmol, 95%).

R_f = 0.66 (1:9 MeOH/DCM); UV λ_{\max} (EtOH/nm) 223.5 and 249.5; IR $\nu_{\max}/\text{cm}^{-1}$: 3745, 3314, 2945, 2866, 2364, 2160, 2035, 1937, 1607, 1564; ^1H NMR (500 MHz, CDCl_3) δ 1.10-1.28 (21H, m, SiCH and CH_3), 5.98 (2H, br s, NH_2), 14.22 (1H, br s, NH triazolopyrimidine); ^{13}C NMR (125 MHz, CDCl_3) δ 11.2 ((Si(CH(CH_3) $_2$) $_3$), 18.6 ((Si(CH(CH_3) $_2$) $_3$), 99.7 ($\text{C}\equiv\text{C}$ -Si), 106.1 ($\text{C}\equiv\text{C}$ -Si), 131.6 (Ar-C), 146.1 (Ar-C), 152.6 (Ar-C), 161.8 (Ar-C); HRMS Calcd for $\text{C}_{15}\text{H}_{25}\text{N}_6\text{Si}$ m/z = 317.1904 $[\text{M}+\text{H}]^+$, Found m/z = 317.1909 $[\text{M}+\text{H}]^+$.

2-(3-((7-((Triisopropylsilyl)ethynyl)-3*H*-[1,2,3]triazolo[4,5-*d*]pyrimidin-5-yl) amino)phenyl) acetamide (292)



i) Synthesis of 5-chloro-7-((triisopropylsilyl)ethynyl)-3*H*-[1,2,3]triazolo[4,5-*d*]pyrimidine

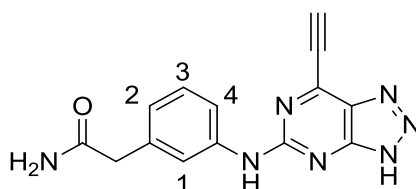
LiCl (134 mg, 3.16 mmol) was added to anhydrous dimethylacetamide (5 mL) and heated until a solution was made. The solution was cooled to 0 °C and 7-((triisopropylsilyl)ethynyl)-3*H*-[1,2,3]triazolo[4,5-*d*]pyrimidin-5-amine (**175**) (250 mg, 0.79 mmol) was added followed by isoamyl nitrite (160 µL, 1.19 mmol) and SOCl₂ (63 µL, 0.87 mmol). The reaction mixture was stirred (0 °C, 1 h) then allowed to warm (RT, 18 h). NaHCO_{3(aq)} (15 mL) was added and the resulting aqueous mixture was extracted with EtOAc (3 x 15 mL). The organic layers were pooled, washed with brine (2 x 30 mL) then dried (Na₂SO₄). The solvent was removed to give the crude product as a brown oil (122 mg, 0.36 mmol, 46 %) which was used without further purification.

ii) Synthesis of 2-(3-((7-((triisopropylsilyl)ethynyl)-3*H*-[1,2,3]triazolo[4,5-*d*]pyrimidin-5-yl) amino)phenyl) acetamide

The title compound was prepared following **general procedure E** using 5-chloro-7-((triisopropylsilyl)ethynyl)-3*H*-[1,2,3]triazolo[4,5-*d*]pyrimidine (122 mg, 0.36 mmol) prepared in **i**), 2-(3-aminophenyl)acetamide (**290**) (109 mg, 0.73 mmol) and TFA (70 µL, 0.91 mmol) in TFE (3 mL). The crude product was dry loaded onto isolate and purified by MPLC on silica (1:9 MeOH/DCM) followed by C18 reverse phase MPLC (9:1 MeOH(0.1% HCOOH)/H₂O (0.1% HCOOH)) to give the title compound (**292**) as a yellow oil (27 mg, 6.01 x 10⁻² mmol, 16%).

$R_f = 0.44$ (1:9 MeOH/DCM); UV λ_{\max} (EtOH/nm) 272.0; IR $\nu_{\max}/\text{cm}^{-1}$: 2942, 2865, 2364, 2335, 1660, 1597, 1540, 1487, 1449; ^1H NMR (500 MHz, CDCl_3) δ 1.15-1.21 (21H, m, SiCH and CH_3), 3.65 (2H, s, CH_2), 5.96 (1H, br s, NH Amide), 6.56 (1H, br s, ArNHAr), 6.98 (1H, d, $J = 7.7$ Hz, $\text{C}^2\text{-H}$), 7.20-7.30 (2H, m, $\text{C}^1\text{-H}$ and $\text{C}^3\text{-H}$), 7.75 (1H, br s, NH triazolopyrimidine), 7.93 (1H, s, $\text{C}^4\text{-H}$), 14.4 (1H, br s, NH Amide); ^{13}C NMR (125 MHz, CDCl_3) δ 11.2 ((Si(CH(CH_3) $_2$) $_3$), 18.6 ((Si(CH(CH_3) $_2$) $_3$), 29.7 (CH_2), 99.8 ($\text{C}\equiv\text{C-Si}$), 105.4 ($\text{C}\equiv\text{C-Si}$), 119.4 (Ar-C), 121.1 (Ar-C), 124.6 (Ar-C), 129.6 (Ar-C), 135.5 (Ar-C), 139.1 (Ar-C), 141.9 (Ar-C), 158.6 (Ar-C), 175.0 (H_2NCOCH_2); HRMS calcd for $\text{C}_{23}\text{H}_{32}\text{N}_7\text{OS}$ $[\text{M}+\text{H}]^+$ 450.2359, Found 450.2424.

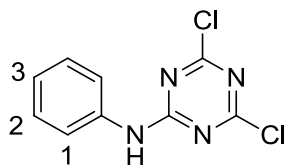
2-(3-((7-Ethynyl-3*H*-[1,2,3]triazolo[4,5-*d*]pyrimidin-5-yl)amino)phenyl)acetamide (232)



The title compound was prepared following **general procedure A** using: 7-((triisopropylsilyl)ethynyl)-3*H*-[1,2,3]triazolo[4,5-*d*]pyrimidin-5-amine (**292**) (25 mg, 5.6×10^{-2} mmol) and TBAF (1 M in THF) (83 μL , 8.3×10^{-2} mmol) in THF (3 mL). The crude product was purified by MPLC on silica (1:9 MeOH/DCM) to give the title compound (**232**) as a yellow solid (12 mg, 4.1×10^{-2} mmol, 74%).

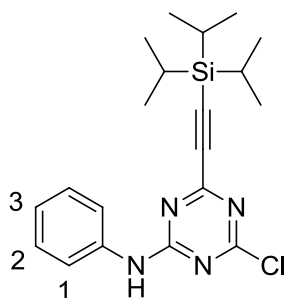
$R_f = 0.24$ (1:9 MeOH/DCM); m.p. 118 °C (dec.); UV λ_{\max} (EtOH/nm) 268.0; IR $\nu_{\max}/\text{cm}^{-1}$: 2959, 2367, 2341, 2333, 2113 (ethynyl), 1655, 1601, 1558, 1493, 1451, 1371; ^1H NMR (500 MHz, $\text{DMSO-}d_6$) δ 3.36 (2H, s, CH_2), 5.14 (1H, s, CH ethynyl), 6.87 (1H, br s, NH), 6.96 (1H, d, $J = 7.4$ Hz, $\text{C}^2\text{-H}$), 7.25 (1H, dd, $J = 8.2$ and 7.6, $\text{C}^3\text{-H}$), 7.43 (1H, br s, NH triazole), 7.58 (1H, s, $\text{C}^1\text{-H}$), 7.74 (1H, d, $J = 8.4$ Hz, $\text{C}^4\text{-H}$), 10.17 (1H, br s, NH Amide), 16.09 (1H, br s, NH Amide); ^{13}C NMR (125 MHz, $\text{DMSO-}d_6$) δ 66.3 (CH_2), 78.3 ($\text{C}\equiv\text{C}$), 89.7 ($\text{C}\equiv\text{C}$), 117.9 (Ar-C), 120.5 (Ar-C), 123.8 (Ar-C), 128.3 (Ar-C), 136.8 (Ar-C), 140.0 (Ar-C), 172.0 (H_2NCOCH_2); HRMS calcd for $\text{C}_{14}\text{H}_{12}\text{N}_7\text{O}$ $[\text{M}+\text{H}]^+$ 294.1098, Found 294.1100.

Note: not all carbon atoms were visible

4,6-Dichloro-*N*-phenyl-1,3,5-triazin-2-amine (184**)**²³⁵

To a cooled (0 °C) solution of cyanuric chloride (1 g, 5.4 mmol) in anhydrous THF (15 mL) was added K₂CO₃ (1.5 g, 0.11 mmol). A solution of aniline (494 µL, 5.4 mmol) in anhydrous THF (5 mL) was then added dropwise with stirring. The reaction mixture was stirred at 0 °C (30 min) then allowed to warm (RT, 1 h). The solvent was removed *in vacuo* and the crude product was redissolved in DCM (10 mL) then filtered and dry loaded on silica. The title compound (**184**) was purified by MPLC on silica (1:9 EtOAc/petrol) as a white crystalline solid (960 mg, 4.0 mmol, 73%).

R_f = 0.40 (1:9 EtOAc/petrol; m.p. 115-116 °C (Lit 136-138 °C); ¹H NMR (500 MHz, CDCl₃) δ 7.23 (1H, tt, C³-H, J = 7.3 and 1.1 Hz) 7.41 (2H, app. t, J = 7.4 Hz, C²-H), 7.49 (1H, br s, ArNHAr), 7.54 (2H, d, J = 8.4 Hz, C¹-H); LRMS (ES+) m/z = 241.0 [M+H]⁺.

4-Chloro-*N*-phenyl-6-((triisopropylsilyl)ethynyl)-1,3,5-triazin-2-amine (185**)**

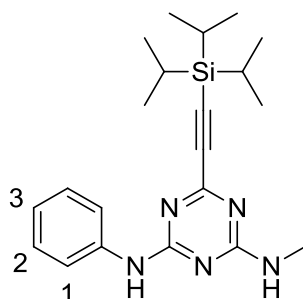
To a solution of 4,6-dichloro-*N*-phenyl-1,3,5-triazin-2-amine (**184**) (2.58 g, 10.7 mmol) in anhydrous THF (30 mL) was added triisopropylsilyl acetylene (2.51 mL, 11.2 mmol), copper(I) iodide (82 mg, 0.43 mmol) and PdCl₂(PPh₃)₂ (300 mg, 0.43 mmol) sequentially. Diisopropylethylamine (4.65 mL, 26.7 mmol) was then added and the reaction mixture was degassed (N₂, 30 min). The reaction mixture was stirred (18h, RT) then filtered through Celite. The crude product was dry loaded onto

Isolute and purified by MPLC on silica (1:9 EtOAc/petrol) to give compound (**185**) a colourless oil (2.64 g, 6.9 mmol, 64%).

R_f = 0.59 (1:9 EtOAc/petrol); UV λ_{\max} (EtOH/nm) 276.0; IR $\nu_{\max}/\text{cm}^{-1}$: 3260, 3203, 3157, 3111, 2944, 2893, 2866, 2170, 1608, 1566, 1516, 1494; ^1H NMR (500 MHz, CDCl_3) δ 1.12-1.26 (21H, m, SiCH and CH_3), 7.17 (1H, tt, J = 7.2 and 1.1 Hz, $\text{C}^3\text{-H}$) 7.38 (2H, app. t, J = 7.6 Hz, $\text{C}^2\text{-H}$), 7.46 (1H, br s, ArNHAr), 7.56 (2H, d, J = 8.4 Hz, $\text{C}^1\text{-H}$); ^{13}C NMR (125 MHz, CDCl_3) δ 17.8 ((Si(CH(CH_3)₂)₃), 18.8 ((Si(CH(CH_3)₂)₃), 121.2 (Ar-C), 130.1 (Ar-C), 164.3 (Ar-C), 171.5 (Ar-C); HRMS Calcd for $\text{C}_{20}\text{H}_{28}\text{ClN}_4\text{Si}$ m/z = 387.1772 $[\text{M}+\text{H}]^+$, Found m/z = 387.177 $[\text{M}+\text{H}]^+$.

Note: not all carbon atoms were visible

***N*²-Methyl-*N*⁴-phenyl-6-((triisopropylsilyl)ethynyl)-1,3,5-triazine-2,4-diamine (**186**)**

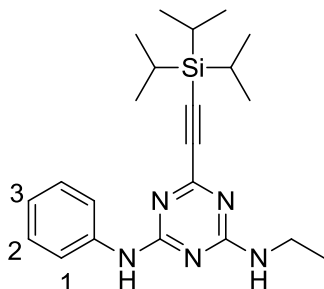


The title compound was prepared following **general procedure B** using: 4-chloro-*N*-phenyl-6-((triisopropylsilyl)ethynyl)-1,3,5-triazin-2-amine (**185**) (20 mg, 0.052 mmol) and methylamine (2 M in THF) (77 μL , 0.16 mmol) in THF (1 mL). The crude product was purified by MPLC on silica (1:4 EtOAc/petrol) to give the title compound (**186**) as a colourless oil (19 mg, 0.05 mmol, 96%).

R_f = 0.36 (1:4 EtOAc/petrol); UV λ_{\max} (EtOH/nm) 269.0; IR $\nu_{\max}/\text{cm}^{-1}$: 3261, 2942, 2892, 2867, 2356, 1937, 1621, 1527, 1496, 1449, 1423; ^1H NMR (500 MHz, CDCl_3) δ 1.12-1.19 (21H, m, SiCH and CH_3), 3.02 (3H, d, J = 4.7 Hz, NHCH_3), 5.23 and 5.61 (1H, br s, ArNHCH₃ rotamers), 7.07 (1H, tt, J = 7.0 and 1.0 Hz, $\text{C}^3\text{-H}$), 7.19 (1H, br s, ArNHAr), 7.32 (2H, app. t, J = 7.6 Hz, $\text{C}^2\text{-H}$), 7.54 and 7.63 (2H, d, J = 7.9 Hz, $\text{C}^1\text{-H}$); ^{13}C NMR (125 MHz, CDCl_3) δ 11.3 ((Si(CH(CH_3)₂)₃), 18.6 ((Si(CH(CH_3)₂)₃), 27.9 (NHCH_3), 60.3 ($\text{C}\equiv\text{C-Si}$), 91.1 ($\text{C}\equiv\text{C-Si}$), 120.0 (Ar-C), 123.3 (Ar-C), 128.9 (Ar-

C), 138.4 (Ar-C), 158.7 (Ar-C), 163.8 (Ar-C), 166.1 (Ar-C); HRMS Calcd for $C_{21}H_{32}N_5Si$ $m/z = 382.2421$ $[M+H]^+$, Found $m/z = 382.2416$ $[M+H]^+$.

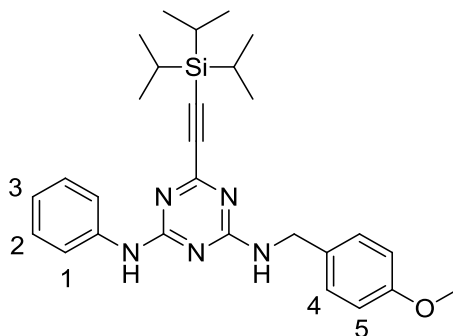
***N*²-Ethyl-*N*⁴-phenyl-6-((triisopropylsilyl)ethynyl)-1,3,5-triazine-2,4-diamine (**187**)**



The title compound was prepared following **general procedure B** using: 4-chloro-*N*-phenyl-6-((triisopropylsilyl)ethynyl)-1,3,5-triazin-2-amine (**185**) (130 mg, 0.34 mmol) and ethylamine (2 M in THF) (513 μ L, 1.03 mmol) in THF (4 mL). The crude product was purified by MPLC on silica (1:4 EtOAc/petrol) to give the title compound (**187**) as a colourless oil (110 mg, 0.28 mmol, 81%).

$R_f = 0.56$ (1:4 EtOAc/petrol); UV λ_{max} (EtOH/nm) 271.0; IR ν_{max}/cm^{-1} : 3262, 3112, 2943, 2893, 2866, 2127, 2097, 1615, 1520; 1H NMR (500 MHz, $CDCl_3$) δ 1.12-1.19 (21H, m, SiCH and CH_3), 1.25 (3H, m, CH_3), 3.48 (2H, m, $NHCH_2$), 5.22 and 5.54 (1H, br s, $ArNHCH_2$ rotamers), 7.06 (1H, tt, $J = 7.0$ and 1.1 Hz, C^3-H), 7.12 (1H, br s, $ArNHAr$), 7.32 (2H, app. t, $J = 7.8$ Hz, C^2-H), 7.54 and 7.61 (1H, d, $J = 7.9$ Hz, C^1-H); ^{13}C NMR (125 MHz, $CDCl_3$) δ 11.3 ((Si($CH(CH_3)_2$)₃), 14.8 (CH_3), 19.4 ((Si($CH(CH_3)_2$)₃), 36.3 ($NHCH_2CH_3$), 60.8 ($C\equiv C-Si$), 91.3 ($C\equiv C-Si$), 120.4 (Ar-C), 123.8 (Ar-C), 128.9 (Ar-C), 139.0 (Ar-C), 159.3 (Ar-C), 164.3 (Ar-C), 165.6 (Ar-C); HRMS Calcd for $C_{22}H_{34}N_5Si$ $m/z = 396.2578$ $[M+H]^+$, Found $m/z = 396.2571$ $[M+H]^+$.

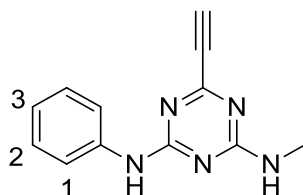
***N*²-(4-Methoxybenzyl)-*N*⁴-phenyl-6-((triisopropylsilyl)ethynyl)-1,3,5-triazine-2,4-diamine (**188**)**



The title compound was prepared following **general procedure B** using: 4-chloro-*N*-phenyl-6-((triisopropylsilyl)ethynyl)-1,3,5-triazin-2-amine (**185**) (342 mg, 0.89 mmol) and 4-methoxybenzylamine (345 μ L, 2.56 mmol) in THF (10 mL). The crude product was purified by MPLC on silica (1:9 EtOAc/petrol) to give the title (**188**) compound as a colourless oil (370 mg, 0.76 mmol, 86%).

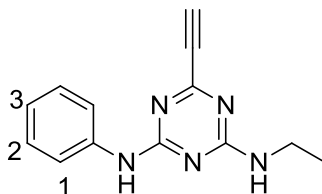
R_f = 0.27 (1:9 EtOAc/petrol); UV λ_{\max} (EtOH/nm) 278.0; IR $\nu_{\max}/\text{cm}^{-1}$: 3342, 3259, 3107, 2911, 2848, 2851, 2119, 2068, 1604; ^1H NMR (500 MHz, DMSO- d_6) δ 1.07-1.13 (21H, m, SiCH and CH₃), 3.71 and 3.72 (3H, s, OCH₃ rotamers), 4.41 and 4.42 (2H, d, J = 6.3 Hz, NHCH₂ Ar rotamers), 7.61 (2H, d, J = 8.7 Hz, C⁴-H), 6.97 (1H, tt, J = 7.3 and 1.1 Hz, C³-H), 7.20-7.28 (4H, m, C²-H and C⁵-H) 7.62 and 7.78 (2H, d, J = 8.7 Hz, C¹-H); ^{13}C NMR (125 MHz, DMSO- d_6) δ 10.5 ((Si(CH(CH₃)₂)₃), 18.4 ((Si(CH(CH₃)₂)₃), 55.0 (OCH₃), 113.7 (Ar-C), 119.9 (Ar-C), 128.2 (Ar-C), 128.4 (Ar-C), 158.2 (Ar-C); HRMS Calcd for C₂₈H₃₈N₅OSi m/z = 488.2840 [M+H]⁺, Found m/z = 488.2835 [M+H]⁺.

Note: not all carbon atoms were visible

6-Ethynyl-*N*²-methyl-*N*⁴-phenyl-1,3,5-triazine-2,4-diamine (92)

The title compound was prepared following **general procedure A** using: *N*²-methyl-*N*⁴-phenyl-6-((triisopropylsilyl)ethynyl)-1,3,5-triazine-2,4-diamine (**186**) (114 mg, 0.30 mmol) and TBAF (1 M in THF) (448 μ L, 0.45 mmol) in THF (4 mL). The crude product was purified by MPLC on silica (5:95 MeOH/DCM) to give the title compound (**92**) as an off-white solid (52 mg, 0.23 mmol, 77%).

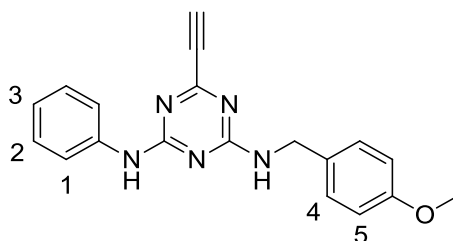
R_f = 0.32 (5:95 MeOH/DCM); m.p. 188-190 °C (dec.); UV λ_{max} (EtOH/nm) 256.5; IR ν_{max}/cm^{-1} : 3298, 3257, 3190, 3120, 3042, 2968, 2127 (ethynyl), 1639 (NH), 1612, 1597, 1566, 1523, 1446, 802; 1H NMR (500 MHz, DMSO- d_6) δ 2.79 and 2.83 (3H, d, J = 4.7 Hz, CH₃ Rotamers), 4.20 and 4.24 (1H, s, CH ethynyl, rotamers), 6.98 and 6.99 (1H, tt, J = 7.2 and 1.1 Hz, C³-H Rotamers), 7.29 and 7.27 (2H, app. t, J = 7.8 Hz, C²-H rotamers), 7.55-7.67 (1H, br s, ArNHCH₃), 7.68-7.79 (2H, m, C¹-H), 9.67 and 9.78 (1H, br s, ArNHAr rotamers); ^{13}C NMR (125 MHz, DMSO- d_6) δ 27.2 (CH₃), 77.4 (C \equiv C-H), 119.9 (Ar-C), 122.4 (Ar-C), 128.5 (Ar-C), 139.4 (Ar-C), 157.6 (Ar-C), 165.3 (Ar-C), 165.4 (Ar-C); HRMS calcd for C₁₂H₁₂N₅ [M+H]⁺ 226.1087, Found 226.1088.

6-Ethynyl-*N*²-ethyl-*N*⁴-phenyl-1,3,5-triazine-2,4-diamine (93)

The title compound was prepared following **general procedure A** using: *N*²-ethyl-*N*⁴-phenyl-6-((triisopropylsilyl)ethynyl)-1,3,5-triazine-2,4-diamine (**187**) (110 mg, 0.28 mmol) and TBAF (1 M in THF) (684 μ L, 0.42 mmol) in THF (5 mL). The crude product was purified by MPLC on silica (5:95 MeOH/DCM) to give the title compound (**93**) as a light orange solid (65 mg, 0.27 mmol, 98%).

R_f = 0.70 (5:95 MeOH/DCM); m.p. 165-167 °C (dec.); UV λ_{\max} (EtOH/nm) 257.0; IR $\nu_{\max}/\text{cm}^{-1}$: 3261, 2975, 2612, 2325, 2306, 2119 (ethynyl), 1613, 1493, 1446; ^1H NMR (500 MHz, DMSO- d_6) δ 1.10 and 1.14 (3H, t, CH₃, J = 7.3 rotamers), 3.24-3.35 (2H, m, NHCH₂, rotamers), 4.19 and 4.23 (1H, s, CH ethynyl, rotamers), 7.02 (1H, dd, J = 6.5 and 7.4, C³-H), 7.30 (2H, m, C²-H rotamers), 7.66-7.77 (2H, m, C¹-H rotamers) 7.83 (1H, br s, ArNHCH₂) 9.67 and 9.77 (1H, br s, ArNHAr, rotamers); ^{13}C NMR (125 MHz, DMSO- d_6) δ 14.3 (CH₃), 34.9 (CH₂), 67.3 (C \equiv C-H), 77.4 (C \equiv C), 119.9 (Ar-C), 122.3 (Ar-C), 128.6 (Ar-C), 139.5 (Ar-C), 158.0 (Ar-C), 164.8 (Ar-C); HRMS calcd for C₁₃H₁₄N₅ [M+H]⁺ 240.1244, Found 240.1245.

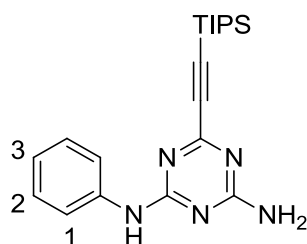
6-Ethynyl-*N*²-(4-methoxybenzyl)-*N*⁴-phenyl-1,3,5-triazine-2,4-diamine (**94**)



The title compound was prepared following **general procedure A** using: *N*²-(4-methoxybenzyl)-*N*⁴-phenyl-6-((triisopropylsilyl)ethynyl)-1,3,5-triazine-2,4-diamine (**188**) (125 mg, 0.26 mmol) and TBAF (1 M in THF) (385 μL , 0.39 mmol) in THF (10 mL). The crude product was purified by MPLC on silica (5:95 MeOH/DCM) then C18 reverse phase MPLC (8:2 MeCN(0.1% HCOOH)/H₂O(0.1% HCOOH)) to give the title compound (**94**) as a dark red solid (55 mg, 0.17 mmol, 65%).

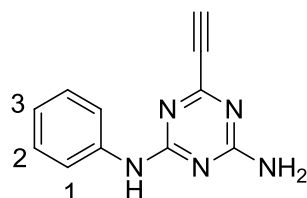
R_f = 0.43 (5:95 MeOH/DCM); m.p. 166-167 °C; UV λ_{\max} (EtOH/nm) 257.5; IR $\nu_{\max}/\text{cm}^{-1}$: 3269, 3001, 2906, 2836, 2343, 2118 (ethynyl), 2083, 1601, 1531, 1510, 1494; ^1H NMR (500 MHz, DMSO- d_6) δ 3.73 and 3.74 (3H, s, OCH₃, rotamers), 4.22 and 4.25 (1H, s, CH ethynyl, rotamers), 4.42 (2H, d, J = 6.2 Hz, CH₂), 6.89 (2H, d, J = 8.6, C⁴-H), 6.98 (H, dd, J = 7.75 and 7.25, C¹-H) 7.20-7.30 (4H, m, C²-H and C⁵-H), 7.61 and 7.75 (2H, d, J = 8.0 Hz, C³-H rotamers), 8.18 and 8.37 (1H, br s, ArNHCH₂, rotamers), 9.76 (1H, br s, ArNHAr); ^{13}C NMR (125 MHz, DMSO- d_6) δ 40.1 (CH₃), 55.0 (NHCH₂Ar), 113.7 (Ar-C), 128.4 (Ar-C), 165.0 (Ar-C); LRMS (ES+) m/z = 332.1 [M+H]⁺.

Note: not all carbon atoms were visible

***N*²-Phenyl-6-((triisopropylsilyl)ethynyl)-1,3,5-triazine-2,4-diamine (293)**

A solution of *N*²-(4-methoxybenzyl)-*N*⁴-phenyl-6-((triisopropylsilyl)ethynyl)-1,3,5-triazine-2,4-diamine (**188**) (246 mg, 0.51 mmol) in TFA (5 mL) was heated to reflux (72 °C) for 18 h. The resulting green solution was allowed to cool to RT and water (10 mL) was added resulting in a green precipitate. The precipitate was collected by filtration, washed with water (2 x 20 mL) then dissolved in EtOAc (20 mL). The resulting solution was washed with saturated NaHCO_{3(aq)} (20 mL) and water (2 x 20 mL). The crude yellow product was dried (Na₂SO₄) the dry loaded onto silica and purified by MPLC (5:95 MeOH/DCM) to give the title compound (**293**) as a yellow oil (183 mg, 0.50 mmol, 99%).

*R*_f = 0.34 (5:95 MeOH/DCM); IR ν_{max} /cm⁻¹: 3499, 3292, 3155, 3107, 2943, 2890, 2865, 1788, 1638, 1604, 1566, 1521, 1494; ¹H NMR (500 MHz, CDCl₃) δ 1.12-1.18 (21H, m, SiCH and CH₃), 5.57 (2H, br s, NH₂), 7.09 (1H, dd, *J* = 7.3 and 7.6, C³-H), 7.32 (2H, dd, *J* = 7.6 and 8.3, C²-H), 7.54 (2H, d, *J* = 8.2 Hz, C¹-H); ¹³C NMR (125 MHz, CDCl₃) δ 11.2 ((Si(CH(CH₃)₂)₃), 18.6 ((Si(CH(CH₃)₂)₃), 120.6 (Ar-C), 123.8 (Ar-C), 128.9 (Ar-C), 137.9 (Ar-C), 164.2 (Ar-C), 166.8 (Ar-C); HRMS calcd for C₂₀H₃₀N₅Si [M+H]⁺ 368.2265, Found 368.2268.

6-Ethynyl-*N*²-phenyl-1,3,5-triazine-2,4-diamine (91)

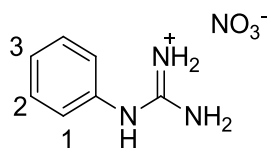
The title compound was prepared following **general procedure A** using: *N*²-phenyl-6-((triisopropylsilyl)ethynyl)-1,3,5-triazine-2,4-diamine (**293**) (90 mg, 0.25 mmol) and

TBAF (1 M in THF) (367 μ L, 0.37 mmol) in THF (5 mL). The crude product was purified by MPLC on silica (5:95 MeOH/DCM) to give the title compound (**91**) as an orange solid (50 mg, 0.24 mmol, 97%).

R_f = 0.25 (5:95 MeOH/DCM); m.p. 170 $^{\circ}$ C (dec.); UV λ_{\max} (EtOH/nm) 255.5; IR $\nu_{\max}/\text{cm}^{-1}$: 3478 (NH_2), 3322, 3264, 2123 (ethynyl), 1638, 1603, 1546, 1532, 1497; ^1H NMR (500 MHz, $\text{DMSO}-d_6$) δ 3.28 (2H, br s, NH_2), 4.20 (1H, s, CH ethynyl), 6.99 (1H, tt, J = 7.5 and 1.1 Hz, $\text{C}^3\text{-H}$), 7.27 (2H, dd J = 7.6 and 8.4 Hz, $\text{C}^2\text{-H}$), 7.73 (2H, d, J = 7.4 Hz, $\text{C}^1\text{-H}$), 9.69 (1H, br s, ArNHAr); ^{13}C NMR (125 MHz, $\text{DMSO}-d_6$) δ 118.1 (Ar-C), 120.0 (Ar-C), 122.4 (Ar-C), 128.4 (Ar-C), 139.4 (Ar-C); HRMS calcd for $\text{C}_{11}\text{H}_{10}\text{N}_5$ $[\text{M}+\text{H}]^+$ 212.0931, Found 212.0931.

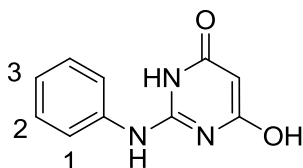
Note: not all carbon atoms were visible

Phenylguanidine nitrate (**204**)³⁰³



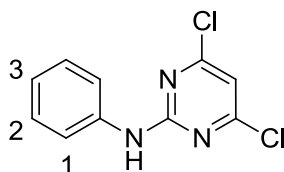
To a solution of aniline (1.28 mL, 14 mmol) in ethanol (14 mL) was added cyanamide (677 mg, 16.1 mmol). HNO_3 (69%) (1 mL, 14 mmol) was added to the reaction mixture dropwise with stirring and the resulting solution was heated to reflux (110 $^{\circ}$ C, 3h) after which almost all of the aniline had been consumed (observed by TLC). The reaction mixture was cooled (0 $^{\circ}$ C) then poured into ether (150 mL) and stirred (20 min, RT) resulting in a grey precipitate. The precipitate was removed by filtration and washed with ether (3 x 20 mL) to give the title compound (**204**) as a grey solid (2.17 g, 10.9 mmol, 78%).

m.p. 111-112 $^{\circ}$ C (Lit. 122 $^{\circ}$ C); ^1H NMR (500 MHz, $\text{DMSO}-d_6$) δ 7.24 (2H, d, J = 7.5 Hz, $\text{C}^1\text{-H}$), 7.29 (1H, tt, J = 7.4 and 1.1 Hz, $\text{C}^3\text{-H}$), 7.37 (4H, br s, NH_2 and NH_2^+), 7.45 (2H, app. t, J = 7.5 Hz, $\text{C}^2\text{-H}$), 9.63 (1H, br s, ArNH).

6-Hydroxy-2-(phenylamino)pyrimidin-4(1*H*)-one (206)³⁰⁴

To a solution of phenylguanidine nitrate (**204**) (5.2 g, 26.2 mmol) in anhydrous methanol (200 mL), was added diethyl malonate (4.38 mL, 28.9 mmol). Freshly prepared sodium methoxide in methanol (50 mL, 78.7 mmol) was added and the resulting solution was stirred overnight (18h, RT). The solvent was removed *in vacuo* and water was added (50 mL). The reaction mixture was acidified (pH 6) with HCl_(aq) (2 M) to give a white precipitate, which was washed with cold water (10 mL) and ether (3 x 30 mL) to give the title compound (**206**) as a white solid (65 mg, 0.32 mmol, 63%).

R_f = 0.50 (2:8 MeOH/DCM); m.p. 224 °C (dec.) (Lit >220); ¹H NMR (500 MHz, DMSO-*d*₆) δ 4.87 (1H, s, pyrimidine C⁵-H), 7.03 (1H, dd, J = 7.3 and 7.6, C³-H), 7.31 (2H, dd, J = 7.6 and 8.5, C²-H), 7.62 (2H, d, J = 7.7 Hz, C¹-H), 8.79 (1H, s, OH), 10.18 (1H, br s, ArNHAr) 10.80 (1H, s, pyrimidine NH). LRMS (ES+) m/z = 204.1 [M+H]⁺.

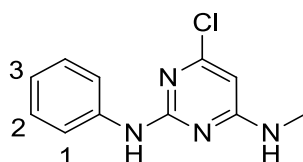
4,6-Dichloro-*N*-phenylpyrimidin-2-amine (207)³⁰⁴

A suspension of 6-hydroxy-2-(phenylamino)pyrimidin-4(1*H*)-one (**206**) (500 mg, 2.46 mmol) in POCl₃ (2.25 mL, 24.6 mmol) was stirred (RT, 30 min). The reaction mixture was heated using microwave irradiation (20 min, 140 °C) to give a dark orange solution, which was quenched over ice water (50 mL). The mixture was cooled (0 °C) and neutralised (NaOH), then extracted with EtOAc (30 mL). The organic layer was then washed with water (3 x 30 mL), dried (MgSO₄) then dry loaded onto silica and

purified by MPLC (3:7 DCM/petrol) to give the title compound (**207**) as a white solid (464 mg, 1.93 mmol, 79%).

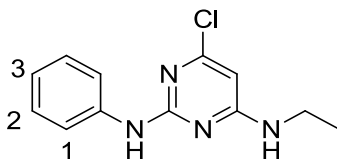
R_f = 0.58 (3:7 DCM/petrol); m.p. 112-113 °C (Lit 112.5); ^1H NMR (500 MHz, CDCl_3) δ 7.11 (1H, dd, J = 7.4 and 7.7, $\text{C}^3\text{-H}$), 7.27 (1H, br s, ArNHAr), 7.36 (2H, dd, J = 7.6 and 8.2, $\text{C}^2\text{-H}$) 7.57 (2H, d, J = 8.0, $\text{C}^1\text{-H}$), LRMS (ES+) m/z = 240.0 $[\text{M}+\text{H}]^+$.

6-Chloro-*N*⁴-methyl-*N*²-phenylpyrimidine-2,4-diamine (**208**)



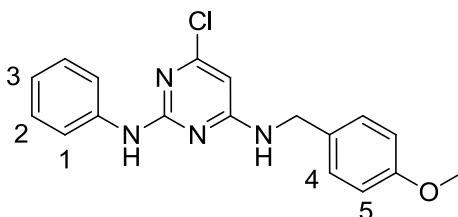
The title compound was prepared following **general procedure C** using: 4,6-dichloro-*N*-phenylpyrimidin-2-amine (**207**) (200 mg, 0.83 mmol), KHCO_3 (100 mg, 1.0 mmol) and methylamine (2 M in THF) (833 μL , 1.67 mmol) in THF (3 mL). The crude product was purified by MPLC on silica (3:7 EtOAc/petrol) to give the title compound (**208**) as a white solid (166 mg, 0.71 mmol, 85%).

R_f = 0.20 (15:85 EtOAc/petrol); m.p. 120-121 °C; UV λ_{max} (EtOH/nm) 237.0 and 268.5; IR $\nu_{\text{max}}/\text{cm}^{-1}$: 3240, 3182, 3108, 3099, 1583, 1524, 1497; ^1H NMR (500 MHz, CDCl_3) δ 3.00 (3H, s, NHCH_3), 4.98 (1H, br s, ArNHCH_3), 5.89 (1H, s, pyrimidine CH), 7.03 (2H, dd and s, J = 7.2 and 7.5, $\text{C}^3\text{-H}$ and ArNHAr), 7.31 (2H, dd, J = 7.5 and 8.6, $\text{C}^2\text{-H}$), 7.58 (2H, d, J = 7.9 Hz, $\text{C}^1\text{-H}$); ^{13}C NMR (125 MHz, CDCl_3) δ 28.5 (CH_3), 119.4 (Ar-C), 122.7 (Ar-C), 128.8 (Ar-C); HRMS calcd for $\text{C}_{11}\text{H}_{12}\text{ClN}_4$ $[\text{M}+\text{H}]^+$ 235.0745, Found 235.0743.

6-Chloro-*N*⁴-ethyl-*N*²-phenylpyrimidine-2,4-diamine (209)

The title compound was prepared following **general procedure C** using: 4,6-dichloro-*N*-phenylpyrimidin-2-amine (**207**) (200 mg, 0.83 mmol), KHCO₃ (100 mg, 1.0 mmol) and ethylamine (2 M in THF) (833 μ L, 1.67 mmol) in THF (3 mL). The crude product was purified by MPLC on silica (3:7 EtOAc/petrol) to give the title compound (**209**) as a white solid (182 mg, 0.73 mmol, 88%).

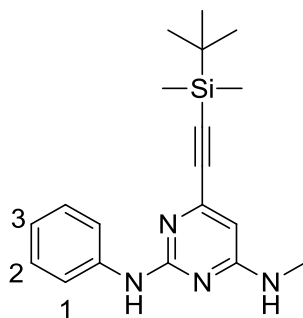
R_f = 0.53 (3:7 EtOAc/petrol); m.p. 102-103 °C; UV λ_{max} (EtOH/nm) 240.0 and 268.0; IR ν_{max}/cm^{-1} : 3254, 3197, 3114, 3043, 2978, 2873, 2367, 1585, 1523, 1497; ¹H NMR (500 MHz, CDCl₃) δ 1.25 (3H, t, J = 7.3 Hz, CH₃), 3.35 (2H, ap. s, CH₂), 4.97 (1H, br s, ArNHCH₂), 5.85 (1H, s, pyrimidine CH), 7.01 (1H, dd, J = 7.3 and 7.6, C³-H), 7.04 (1H, br s, ArNHAr), 7.30 (2H, dd, J = 7.4 and 8.5, C²-H), 7.56 (2H, d, J = 8.0 Hz, C¹-H); ¹³C NMR (125 MHz, CDCl₃) δ 14.6 (CH₃), 36.5 (NHCH₂CH₃), 119.3 (Ar-C), 122.5 (Ar-C), 128.8 (Ar-C), 139.4 (Ar-C), 159.2 (Ar-C), 163.9 (Ar-C); HRMS calcd for C₁₂H₁₄ClN₄ [M+H]⁺ 249.0902, Found 249.0900.

6-Chloro-*N*⁴-(4-methoxybenzyl)-*N*²-phenylpyrimidine-2,4-diamine (210)

The title compound was prepared following **general procedure C** using: 4,6-dichloro-*N*-phenylpyrimidin-2-amine (**207**) (200 mg, 0.83 mmol), KHCO₃ (100 mg, 1.0 mmol) and 4-methoxybenzylamine (216 μ L, 1.67 mmol) in THF (3 mL). The crude product was purified by MPLC on silica (3:7 EtOAc/petrol) to give the title compound (**210**) as a colourless oil (285 mg, 0.83 mmol, >99%).

R_f = 0.55 (3:7 EtOAc/petrol); UV λ_{\max} (EtOH/nm) 239.5 and 269.5; IR $\nu_{\max}/\text{cm}^{-1}$: 3402, 3285, 3200, 3060, 2957, 2908, 2853, 1574, 1510, 1442; ^1H NMR (500 MHz, CDCl_3) δ 3.80 (3H, s, CH_3), 4.46 (2H, s, CH_2), 5.89 (1H, s, pyrimidine CH), 6.89 (2H, d, J = 8.7 Hz, $\text{C}^4\text{-H}$), 7.01 (1H, dd, J = 7.0 and 7.8, $\text{C}^3\text{-H}$), 7.06 (1H, br s, ArNHAr), 7.24 (2H, d, J = 8.7 Hz, $\text{C}^5\text{-H}$), 7.28 (2H, dd, J = 7.6 and 8.5, $\text{C}^2\text{-H}$), 7.53 (2H, d, J = 8.2 Hz, $\text{C}^1\text{-H}$); ^{13}C NMR (125 MHz, CDCl_3) δ 45.3 (NHCH_2Ar), 55.4 (OCH_3), 114.4 (Ar-C), 119.4 (Ar-C), 122.6 (Ar-C), 128.8 (Ar-C), 139.3 (Ar-C), 159.2 (Ar-C), 163.8 (Ar-C). HRMS calcd for $\text{C}_{18}\text{H}_{18}\text{ClN}_4\text{O}$ $[\text{M}+\text{H}]^+$ 341.1164, Found 341.1170.

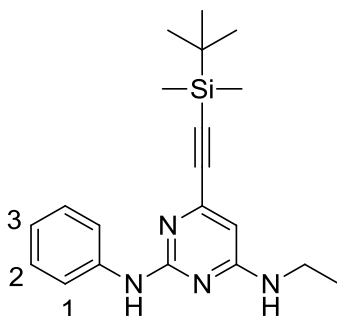
6-((*tert*-Butyldimethylsilyl)ethynyl)-*N*⁴-methyl-*N*²-phenylpyrimidine-2,4-diamine (211)



The title compound was prepared following general **procedure D** using: 6-chloro-*N*⁴-methyl-*N*²-phenylpyrimidine-2,4-diamine (**208**) (83 mg, 0.36 mmol), *tert*-butyldimethylsilyl acetylene boronic acid pinacol ester (142 mg, 0.53 mmol), Cs_2CO_3 (174 mg, 0.53 mmol) and $\text{Pd}(\text{PPh}_3)_4$ (41 mg, 0.036 mmol) in dioxane (4 mL). The title compound (**211**) was purified by MPLC on silica (3:7 EtOAc/petrol) to give the final product as a white crystalline solid (97 mg, 0.29 mmol, 81%).

R_f = 0.14 (3:7 EtOAc/petrol); m.p. 162-163 °C; UV λ_{\max} (EtOH/nm) 235.0 and 269.5; IR $\nu_{\max}/\text{cm}^{-1}$: 3253, 3196, 3117, 3061, 2948, 2927, 2884, 2854, 2360, 2343, 1603, 1585, 1531; ^1H NMR (500 MHz, CDCl_3) δ 0.20 (6H, s, 2 x SiCH_3), 1.00 (9H, s, Si^tBu), 2.97 (3H, d, J = 5.0 Hz, NHCH_3), 4.85 (1H, br s, ArNHCH_3), 6.02 (1H, s, pyrimidine CH), 6.98 (2H, dd and s, J = 7.2 and 7.5, $\text{C}^3\text{-H}$ and ArNHAr), 7.28 (2H, dd, J = 7.4 and 8.7, $\text{C}^2\text{-H}$), 7.59 (2H, d, J = 8.9 Hz, $\text{C}^1\text{-H}$); ^{13}C NMR (125 MHz, CDCl_3) δ -4.75 ($\text{Si}(\text{CH}_3)_2\text{C}$), 16.7 ($\text{SiC}(\text{CH}_3)_3$), 26.2 (CH_3), 103.7 ($\text{C}\equiv\text{C-Si}$), 119.0 (Ar-C), 122.1 (Ar-C), 128.8 (Ar-C), 140.1 (Ar-C), 159.8 (Ar-C), 164.0 (Ar-C); HRMS calcd for $\text{C}_{19}\text{H}_{27}\text{N}_4\text{Si}$ $[\text{M}+\text{H}]^+$ 339.1999, Found 339.1997.

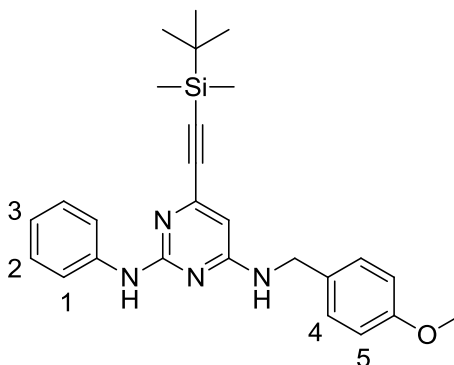
6-((*tert*-Butyldimethylsilyl)ethynyl)-*N*⁴-ethyl-*N*²-phenylpyrimidine-2,4-diamine (212)



The title compound was prepared following general **procedure D** using: 6-chloro-*N*⁴-ethyl-*N*²-phenylpyrimidine-2,4-diamine (**209**) (91 mg, 0.37 mmol), *tert*-butyldimethylsilyl acetylene boronic acid pinacol ester (147 mg, 0.55 mmol), Cs₂CO₃ (180 mg, 0.55 mmol) and Pd(PPh₃)₄ (41 mg, 0.037 mmol) in dioxane (4 mL). The title compound (**212**) was purified by MPLC on silica (3:7 EtOAc/petrol) to give the final product as a white crystalline solid (69 mg, 0.20 mmol, 53%).

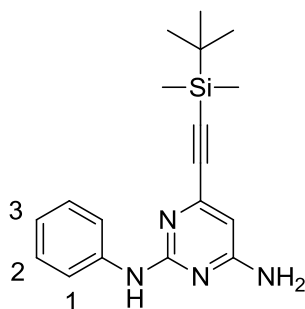
*R*_f = 0.63 (3:7 EtOAc/petrol); m.p. 145-146 °C; UV λ_{max} (EtOH/nm) 236.0 and 269.5; IR ν_{max}/cm⁻¹: 3408, 3335, 3265, 3196, 3123, 3058, 2952, 2928, 2883, 2856, 1606, 1581, 1535; ¹H NMR (500 MHz, CDCl₃) δ 0.20 (6H, s, 2 x SiCH₃), 1.00 (9H, s, Si^tBu), 1.26 (3H, t, *J* = 7.2 Hz, CH₂CH₃) 3.39 (2H, br s, NHCH₂CH₃), 4.78 (1H, br s, ArNHCH₃), 6.02 (1H, s, pyrimidine CH), 6.98 (2H, dd and s, *J* = 7.0 and 7.6, C³-H and ArNHAr), 7.28 (2H, dd, *J* = 7.4 and 8.4, C²-H), 7.57 (2H, d, *J* = 7.6 Hz, C¹-H); ¹³C NMR (125 MHz, CDCl₃) δ -4.6 (Si(CH₃)₂C), 14.9 (SiC(CH₃)₃), 16.9 (CH₃), 26.3 (NHCH₂CH₃), 103.7 (C≡C-Si), 119.1 (Ar-C), 122.1 (Ar-C), 128.9 (Ar-C), 140.0 (Ar-C), 159.8 (Ar-C), 163.1 (Ar-C); HRMS calcd for C₂₀H₂₉N₄Si [M+H]⁺ 353.2156, Found 353.2153.

6-((*tert*-Butyldimethylsilyl)ethynyl)-*N*⁴-(4-methoxybenzyl)-*N*²-phenylpyrimidine-2,4-diamine (213**)**



The title compound was prepared following general **procedure D** using: 6-chloro-*N*⁴-(4-methoxybenzyl)-*N*²-phenylpyrimidine-2,4-diamine (**210**) (248 mg, 0.73 mmol), *tert*-butyldimethylsilyl acetylene boronic acid pinacol ester (291 mg, 1.09 mmol), Cs₂CO₃ (355 mg, 1.09 mmol) and Pd(PPh₃)₄ (84 mg, 0.073 mmol) in dioxane (15 mL). The title compound (**213**) was purified by MPLC on silica (3:7 EtOAc/petrol) to give the final product as a yellow oil (305 mg, 0.69 mmol, 94%).

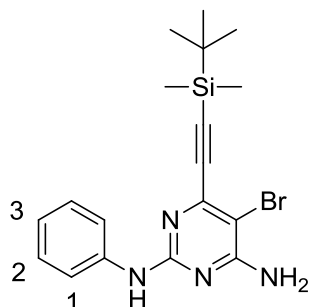
*R*_f = 0.25 (15:75 EtOAc/petrol); UV λ_{max} (EtOH/nm) 235.0 and 272.0; IR ν_{max}/cm⁻¹: 3400, 3265, 3192, 3120, 3036, 2951, 2927, 2896, 2855, 2361, 2341, 1604, 1578, 1536; ¹H NMR (500 MHz, CDCl₃) δ 0.19 (6H, s, 2 x SiCH₃), 1.00 (9H, s, Si^{*t*}Bu), 3.81 (3H, s, CH₃), 4.50 (2H, s, CH₂), 5.04 (1H, br s, ArNHCH₂), 6.05 (1H, s, pyrimidine CH), 6.89 (2H, d, *J* = 8.7 Hz, C⁴-H), 6.97 (1H, dd, *J* = 7.0 and 7.6, C³-H), 7.02 (1H, br s, ArNHAr), 7.21-7.29 (4H, m, C⁵-H and C²-H), 7.55 (2H, d, *J* = 7.89 Hz, C¹-H); ¹³C NMR (125 MHz, CDCl₃) δ -4.5 (Si(CH₃)₂C), 16.9 (SiC(CH₃)₃), 26.6 (OCH₃), 55.8 (NHCH₂Ar), 114.5 (Ar-C), 119.6 (Ar-C), 122.5 (Ar-C), 128.8 (Ar-C), 129.0 (Ar-C), 139.9 (Ar-C), 159.2 (Ar-C), 159.7 (Ar-C), 163.2 (Ar-C); HRMS calcd for C₂₆H₃₃N₄OSi [M+H]⁺ 445.2418, Found 445.2410.

6-((*tert*-Butyldimethylsilyl)ethynyl)-*N*²-phenylpyrimidine-2,4-diamine (**220**)

A solution of 6-((*tert*-butyldimethylsilyl)ethynyl)-*N*⁴-(4-methoxybenzyl)-*N*²-phenyl pyrimidine-2,4-diamine (**213**) (50 mg, 0.11 mmol) in TFA (1 mL) was heated (18 h, 75 °C). The reaction mixture was carefully added to sat. NaHCO_{3(aq)} (30 mL) and extracted with EtOAc (20 mL). The organic layer was removed and washed with water (3 x 30 mL) then dried (Na₂SO₄) and dry loaded onto silica. The title compound (**220**) was purified by MPLC on silica (2:3 EtOAc/petrol) to give a yellow solid (34 mg, 0.10 mmol, 91 %).

R_f = 0.54 (2:3 EtOAc/petrol); m.p. 146-147 °C; UV λ_{max} (EtOH/nm) 225.0 and 268.5; IR ν_{max}/cm^{-1} : 3420, 3284, 3121, 3062, 2950, 2928, 2887, 2856, 1598, 1576, 1538; ¹H NMR (500 MHz, CDCl₃) δ 0.20 (6H, s, 2 x SiCH₃), 1.00 (9H, s, Si^{*t*}Bu), 4.77 (2H, br s, NH₂), 4.85 (1H, br s, ArNHCH₃), 6.10 (1H, s, pyrimidine CH), 7.00 (2H, dd, J = 7.3 and 7.6, C³-H), 7.05 (1H, br s, ArNHAr), 7.29 (2H, dd, J = 7.3 and 8.7, C²-H), 7.56 (2H, d, J = 7.7 Hz, C¹-H); ¹³C NMR (125 MHz, CDCl₃) δ -4.8 (Si(CH₃)₂C), 16.9 (SiC(CH₃)₃), 100.0 (C \equiv C-Si), 119.3 (Ar-C), 122.3 (Ar-C), 128.8 (Ar-C), 139.6 (Ar-C), 163.5 (Ar-C). HRMS calcd for C₁₈H₂₅N₄Si [M+H]⁺ 325.1843, Found 325.1841.

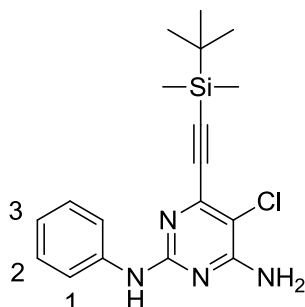
5-Bromo-6-((*tert*-butyldimethylsilyl)ethynyl)-*N*²-phenylpyrimidine-2,4-diamine (222)



A solution of 6-((*tert*-butyldimethylsilyl)ethynyl)-*N*²-phenylpyrimidine-2,4-diamine (**220**) (100 mg, 0.31 mmol) in anhydrous MeCN (10 mL) was cooled to 0 °C. *N*-bromosuccinimide (58 mg, 0.32 mmol) was added in one portion and the reaction mixture was stirred until no starting material remained (0 °C, 45 min). The solvent was removed *in vacuo* and the crude product was redissolved in EtOAc (10 mL) and dry loaded onto isolate HM-N. The title compound (**222**) was purified by C18 reverse phase MPLC (8:2 MeCN (0.1% HCOOH)/H₂O (0.1% HCOOH) as a white crystalline solid (84 mg, 0.21 mmol, 68%).

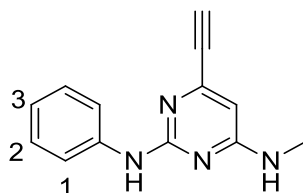
R_f = 0.38 (1:4 EtOAc/petrol); m.p 158-159 °C; UV λ_{max} (EtOH/nm) 272.5; IR ν_{max}/cm^{-1} : 3482, 3422, 3294, 3175, 3055, 3018, 2949, 2927, 2884, 2855, 1622, 1597, 1526; ¹H NMR (500 MHz, CDCl₃) δ 0.23 (6H, s, CH₃), 1.03 (9H, s, *t*Bu), 5.32 (2H, br s, ArNH₂), 6.98 (1H, br s, ArNHAr), 7.02 (1H, tt, J = 7.3 and 1.1 Hz, C³-H), 7.30 (2H, app. t, J = 7.5 Hz, C²-H), 7.51 (2H, d, J = 7.7 Hz, C¹-H); ¹³C NMR (125 MHz, CDCl₃) δ -5.0 (Si(CH₃)₂), 26.1 (SiC(CH₃)₃), 20.8 (C-CH₃), 92.3 (C \equiv C-Si), 101.4 (C \equiv C), 119.1 (Ar-C), 120.5 (Ar-C), 122.3 (Ar-C), 128.5 (Ar-C) 131.5 (Ar-C); HRMS calcd for C₁₈H₂₄BrN₄Si [M+H]⁺ 403.0948, Found 403.0945.

6-((*tert*-Butyldimethylsilyl)ethynyl)-5-chloro-*N*²-phenylpyrimidine-2,4-diamine (221)



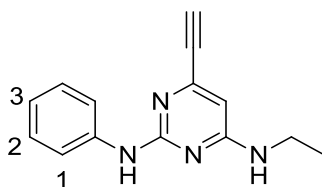
A biotage microwave vessel was charged with 6-((*tert*-butyldimethylsilyl)ethynyl)-*N*²-phenylpyrimidine-2,4-diamine (**220**) (100 mg, 0.31 mmol). Anhydrous MeCN (10 mL) and *N*-chlorosuccinimide (43 mg, 0.32 mmol) were added and the reaction mixture was heated using microwave irradiation (100 °C, 25 min). The solvent was removed *in vacuo* and the crude product was redissolved in EtOAc (10 mL) and dry loaded onto silica. The title compound (**221**) was purified by MPLC on silica (1:4 EtOAc/petrol) as a yellow crystalline solid (84 mg, 0.21 mmol, 87%).

R_f = 0.44 (1:4 EtOAc/petrol); m.p. 149-150 °C; UV λ_{\max} (EtOH/nm) 272.0; IR $\nu_{\max}/\text{cm}^{-1}$: 3247, 3423, 3290, 3165, 2950, 2928, 2856, 2362, 2343, 2362, 2343, 1629, 1599, 1567, 1535; ^1H NMR (500 MHz, CDCl_3) δ 0.23 (6H, s, CH_3), 1.03 (9H, s, *t*Bu), 5.25 (2H, br s, ArNH_2), 6.94 (1H, br s, ArNHAr), 7.01 (1H, tt, J = 7.4 and 1.1 Hz, $\text{C}^3\text{-H}$), 7.30 (2H, app. t, J = 7.4 Hz, $\text{C}^2\text{-H}$), 7.52 (2H, d, J = 7.7 Hz, $\text{C}^1\text{-H}$); ^{13}C NMR (125 MHz, CDCl_3) δ -4.9 ($\text{Si}(\text{CH}_3)_2$), 26.1 ($\text{SiC}(\text{CH}_3)_3$), 100.0 ($\text{C}\equiv\text{C-Si}$), 101.7 ($\text{C}\equiv\text{C-Si}$), 108.7 (Ar-C), 119.3 (Ar-C), 122.5 (Ar-C), 128.9 (Ar-C), 139.4 (Ar-C), 146.8 (Ar-C), 157.3 (Ar-C), 159.6 (Ar-C); HRMS calcd for $\text{C}_{18}\text{H}_{24}\text{ClN}_4\text{Si}$ $[\text{M}+\text{H}]^+$ 359.1453, Found 359.1451.

6-Ethynyl-*N*⁴-methyl-*N*²-phenylpyrimidine-2,4-diamine (96)

The title compound was prepared following **general procedure A** using: 6-((*tert*-butyldimethylsilyl)ethynyl)-*N*⁴-methyl-*N*²-phenylpyrimidine-2,4-diamine (**211**) (50 mg, 0.13 mmol) and TBAF (1 M in THF) (140 μ L, 0.14 mmol) in THF (15 mL). The crude product was purified by MPLC on silica (2:3 EtOAc/petrol) to give the title compound (**96**) as a brown solid (28 mg, 0.13 mmol, 91 %).

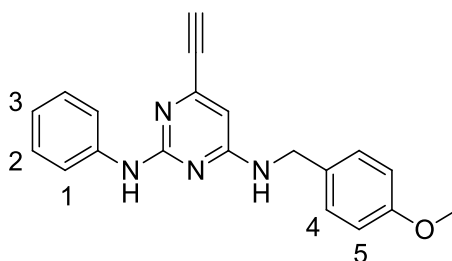
R_f = 0.22 (1:2 EtOAc/petrol); m.p. 80.0-81.0 °C; UV λ_{max} (EtOH/nm) 269.0; IR ν_{max}/cm^{-1} : 3247, 2366, 2153, 1975, 1589, 1528, 1497, 1441, 1389; ¹H NMR (500 MHz, CDCl₃) δ 2.98 (3H, d, J = 3.8 Hz, CH₃), 3.09 (1H, s, CH ethynyl), 4.85 (1H, br s, ArNHCH₃) 6.05 (1H, s, pyrimidine CH), 6.92 (1H, br s, ArNHAr), 6.99 (1H, tt, J = 7.4 and 1.2, C³-H), 7.29 (2H, dd, J = 7.6 and 7.3 Hz, C²-H), 7.60 (2H, d, J = 7.9 Hz, C¹-H); ¹³C NMR (125 MHz, CDCl₃) δ 28.3 (CH₃), 77.5 (C \equiv C-H), 82.0 (C \equiv C), 119.1 (Ar-C), 122.1 (Ar-C), 128.8 (Ar-C), 139.9 (Ar-C), 148.3 (Ar-C), 163.8 (Ar-C), 171.3 (Ar-C); HRMS calcd for C₁₃H₁₃N₄ [M+H]⁺ 225.1135, Found 225.1130.

***N*⁴-Ethyl-6-ethynyl-*N*²-phenylpyrimidine-2,4-diamine (67)**

The title compound was prepared following **general procedure A** using: 6-((*tert*-butyldimethylsilyl)ethynyl)-*N*⁴-ethyl-*N*²-phenylpyrimidine-2,4-diamine (**212**) (60 mg, 0.17 mmol) and TBAF (1 M in THF) (190 μ L, 0.19 mmol) in THF (15 mL). The crude product was purified by MPLC on silica (5:95 MeOH/DCM) to give the title compound (**67**) as an off-white solid (26 mg, 0.11 mmol, 64%).

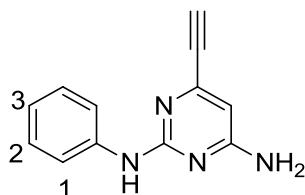
R_f = 0.66 (5:95 MeOH/DCM); m.p. 96.5-97.8 °C; UV λ_{\max} (EtOH/nm) 269; IR $\nu_{\max}/\text{cm}^{-1}$: 3258, 2968, 2356, 2118, 1797, 1575, 1526, 1497, 1410, 1346; ^1H NMR (500 MHz, CDCl_3) δ 1.27 (3H, t, J = 7.3 Hz, CH_3), 3.09 (1H, s, CH ethynyl), 3.39 (2H, m, ArCH_2CH_3), 4.81 (1H, br s, ArNHCH_2), 6.03 (1H, s, pyrimidine CH), 6.95 (1H, br s, ArNHAr), 6.98 (1H, tt, J = 7.3 and 1.1 Hz, $\text{C}^3\text{-H}$), 7.29 (2H, app. t, J = 7.6 Hz, $\text{C}^2\text{-H}$), 7.58 (2H, d, J = 7.6 Hz, $\text{C}^1\text{-H}$); ^{13}C NMR (125 MHz, CDCl_3) δ 14.7 (CH_3), 36.3 (NHCH_2CH_3), 77.6 ($\text{C}\equiv\text{C-H}$), 119.1 (Ar-C), 122.1 (Ar-C), 128.8 (Ar-C), 139.8 (Ar-C), 148.8 (Ar-C), 162.8 (Ar-C); HRMS calcd for $\text{C}_{14}\text{H}_{15}\text{N}_4$ $[\text{M}+\text{H}]^+$ 239.1291, Found 239.1287.

6-Ethynyl- N^4 -(4-methoxybenzyl)- N^2 -phenylpyrimidine-2,4-diamine (**98**)



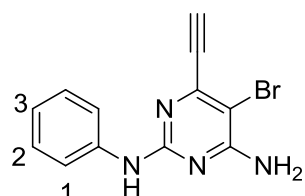
The title compound was prepared following **general procedure A** using: 6-((*tert*-butyldimethylsilyl)ethynyl)- N^4 -(4-methoxybenzyl)- N^2 -phenylpyrimidine-2,4-diamine (**213**) (50 mg, 0.11 mmol) and TBAF (1 M in THF) (120 μL , 0.12 mmol) in THF (15 mL). The crude product was purified by MPLC on silica (2:3 EtOAc/petrol) to give the title (**98**) compound as a brown oil (25 mg, 7.6×10^{-2} mmol, 67%).

R_f = 0.35 (2:3 EtOAc/petrol); UV λ_{\max} (EtOH/nm) 270.5; IR $\nu_{\max}/\text{cm}^{-1}$: 3406, 3282, 2835, 2351, 2114, 1790, 1580, 1536, 1511, 1494, 1456, 1441; ^1H NMR (500 MHz, CDCl_3) δ 3.09 (1H, s, CH ethynyl), 3.80 (3H, s, CH_3), 4.51 (2H, s, CH_2), 5.11 (1H, br s, ArNHCH_2), 6.06 (1H, s, pyrimidine CH), 6.89 (2H, d, J = 8.8 Hz, $\text{C}^4\text{-H}$), 7.01 (1H, tt, J = 7.3 and 1.1, $\text{C}^3\text{-H}$), 6.99 (1H, br s, ArNHAr), 7.25 (2H, d, J = 8.8 Hz, $\text{C}^5\text{-H}$), 7.28 (2H, app. t, J = 7.6 $\text{C}^2\text{-H}$), 7.55 (2H, d, J = 8.7 Hz, $\text{C}^1\text{-H}$); ^{13}C NMR (125 MHz, CDCl_3) δ 45.0 (NHCH_2Ar), 55.6 (OCH_3), 77.6 ($\text{C}\equiv\text{C-H}$), 81.9 ($\text{C}\equiv\text{C}$), 114.2 (Ar-C), 119.2 (Ar-C), 122.1 (Ar-C), 128.8 (Ar-C), 128.9 (Ar-C), 139.7 (Ar-C), 159.2 (Ar-C), 159.8 (Ar-C), 162.8 (Ar-C); HRMS calcd for $\text{C}_{20}\text{H}_{19}\text{N}_4\text{O}$ $[\text{M}+\text{H}]^+$ 331.1553, Found 331.1557.

6-Ethynyl-*N*²-phenylpyrimidine-2,4-diamine (95)

The title compound was prepared following **general procedure A** using: 6-((*tert*-butyldimethylsilyl)ethynyl)-*N*²-phenylpyrimidine-2,4-diamine (**220**) (75 mg, 0.23 mmol) and TBAF (1 M in THF) (250 μ L, 0.25 mmol) in THF (20 mL). The crude product was purified by MPLC on silica (5:95 MeOH/DCM) to give the title compound (**95**) as a yellow oil (38 mg, 0.18 mmol, 78%).

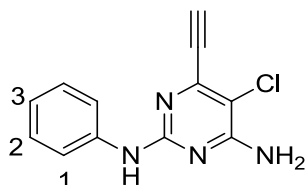
R_f = 0.31 (5:95 MeOH/DCM); UV λ_{\max} (EtOH/nm) 267.5; IR $\nu_{\max}/\text{cm}^{-1}$: 2676, 2337, 2118, 1687, 1615, 1528, 1495, 1403, 1358, 1232, 1173; ^1H NMR (500 MHz, CDCl_3) δ 3.12 (1H, s, CH ethynyl), 4.81 (2H, br s, ArNH_2) 6.13 (1H, s, pyrimidine CH), 6.97 (1H, br s, ArNHAr), 7.01 (1H, tt, J = 7.4 and 1.0 Hz, $\text{C}^3\text{-H}$), 7.30 (2H, app. t, J = 7.4 Hz, $\text{C}^2\text{-H}$), 7.57 (2H, d, J = 7.4 Hz, $\text{C}^1\text{-H}$); ^{13}C NMR (125 MHz, CDCl_3) δ 78.1 ($\text{C}\equiv\text{C-H}$), 81.6 ($\text{C}\equiv\text{C}$), 100.0 (Ar-C), 119.4 (Ar-C), 122.4 (Ar-C), 128.8 (Ar-C), 139.5 (Ar-C), 149.0 (Ar-C), 159.6 (Ar-C), 163.6 (Ar-C); HRMS calcd for $\text{C}_{12}\text{H}_{11}\text{N}_4$ $[\text{M}+\text{H}]^+$ 211.0978, Found 211.0979.

5-Bromo-6-ethynyl-*N*²-phenylpyrimidine-2,4-diamine (100)

The title compound was prepared following **general procedure A** using: 5-bromo-6-((*tert*-butyldimethylsilyl)ethynyl)-*N*²-phenylpyrimidine-2,4-diamine (**222**) (70 mg, 0.17 mmol) and TBAF (1 M in THF) (190 μ L, 0.19 mmol) in THF (15 mL). The crude product was purified by MPLC on silica (5:95 MeOH/DCM) to give the title compound (**100**) as a white solid (48 mg, 0.16 mmol, 95%).

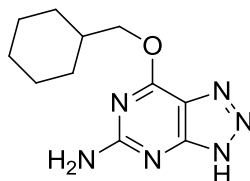
R_f = 0.64 (5:95 MeOH/DCM); m.p 160.9-162.7 °C; UV λ_{max} (EtOH/nm) 271.5; IR $\nu_{\text{max}}/\text{cm}^{-1}$: 3479, 3447, 3401, 3274, 2178, 2033, 1977, 1631, 1596, 1561, 1520; ^1H NMR (500 MHz, CDCl_3) δ 3.36 (1H, s, CH ethynyl), 5.27 (2H, br s, ArNH_2), 6.87 (1H, br s, ArNHAr), 6.96 (1H, tt, J = 7.4 and 1.0 Hz, $\text{C}^3\text{-H}$), 7.24 (2H, app. t, J = 7.6 Hz, $\text{C}^2\text{-H}$), 7.45 (2H, d, J = 7.7 Hz, $\text{C}^1\text{-H}$); ^{13}C NMR (125 MHz, CDCl_3) δ 80.3 ($\text{C}\equiv\text{C-H}$), 82.9 ($\text{C}\equiv\text{C}$), 95.4 (Ar-C), 119.5 (Ar-C), 122.7 (Ar-C), 128.9 (Ar-C), 139.2 (Ar-C), 148.4 (Ar-C), 158.1 (Ar-C), 160.5 (Ar-C); HRMS calcd for $\text{C}_{12}\text{H}_{10}\text{BrN}_4$ $[\text{M}+\text{H}]^+$ 289.0083, Found 289.0089.

5-Chloro-6-ethynyl-*N*²-phenylpyrimidine-2,4-diamine (**99**)



The title compound was prepared following **general procedure A** using: 5-chloro-6-((*tert*-butyldimethylsilyl)ethynyl)-*N*²-phenylpyrimidine-2,4-diamine (**221**) (64 mg, 0.18 mmol) and TBAF (1 M in THF) (196 μL , 0.20 mmol) in THF (10 mL). The crude product was purified by MPLC on silica (5:95 MeOH/DCM) to give the title compound (**99**) as an off-white solid (37 mg, 0.15 mmol, 85%).

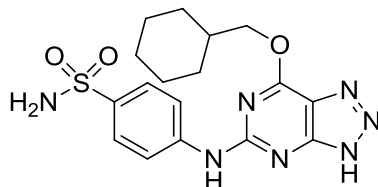
R_f = 0.68 (5:95 MeOH/DCM); m.p 96.5-97.8 °C; UV λ_{max} (EtOH/nm) 270.0; IR $\nu_{\text{max}}/\text{cm}^{-1}$: 3486, 3449, 3397, 3274, 3057, 2121, 1632, 1595, 1564, 1523; ^1H NMR (500 MHz, CDCl_3) δ 3.45 (1H, s, CH ethynyl), 5.29 (2H, br s, ArNH_2), 6.93 (1H, br s, ArNHAr), 6.96 (1H, tt, J = 7.4 and 1.1 Hz, $\text{C}^3\text{-H}$), 7.31 (2H, app. t, J = 7.6 Hz, $\text{C}^2\text{-H}$), 7.52 (2H, d, J = 7.7 Hz, $\text{C}^1\text{-H}$); ^{13}C NMR (125 MHz, CDCl_3) δ 78.8 ($\text{C}\equiv\text{C-H}$), 83.6 ($\text{C}\equiv\text{C}$), 119.4 (Ar-C), 122.7 (Ar-C), 128.7 (Ar-C), 139.2 (Ar-C), 146.1 (Ar-C), 157.3 (Ar-C), 159.6 (Ar-C), 162.8 (Ar-C); HRMS calcd for $\text{C}_{12}\text{H}_{10}\text{ClN}_4$ $[\text{M}+\text{H}]^+$ 245.0589, Found 245.0592.

7-(Cyclohexylmethoxy)-3*H*-[1,2,3]triazolo[4,5-*d*]pyrimidin-5-amine (257)

To a solution of NaH (60% in mineral oil) in anhydrous DMSO (10 mL) was added cyclohexylmethanol (4.34 mL, 35.3 mmol) under nitrogen. The resulting mixture was stirred until no further gas was evolved (45 min) then added to a separate solution of 7-chloro-3*H*-[1,2,3]triazolo[4,5-*d*]pyrimidin-5-amine (**173**) (1.50 g, 8.82 mmol) in anhydrous DMSO (10 mL). The reaction mixture was stirred under nitrogen (RT, 18h) then added to water (100 mL). The aqueous solution was neutralised (AcOH) and stirred for a further hour resulting in a light orange precipitate. The precipitate was filtered then washed with water (50 mL) then ether (2 x 30 mL) and dried under vacuum to give (**257**) as a light orange solid (1.52 g, 6.14 mmol, 70%).

m.p. 214-216 °C; UV λ_{max} (EtOH/nm) 285.0; IR ν_{max} /cm⁻¹: 3494, 3378, 2925, 2780, 2651, 2362, 2329, 2115, 2085, 2013, 1906, 1628, 1608, 1578, 1488; ¹H NMR (500 MHz, DMSO-*d*₆) δ 1.03-1.89 (11H, m, cyclohexyl), 4.30 (2H, d, *J* = 6.5, OCH₂), 6.91 (2H, br s, NH₂), 15.28 (1H, br s, NH triazolopyrimidine); ¹³C NMR (125 MHz, DMSO-*d*₆) δ 25.1 (CH₂), 25.9 (CH₂), 29.1 (CH₂), 36.6 (CH), 71.2 (CH₂), 162.2 (Ar-C); HRMS calcd for C₁₁H₁₇N₆O [M+H]⁺ 249.1458, Found 249.1461.

4-((7-(Cyclohexylmethoxy)-3*H*-[1,2,3]triazolo[4,5-*d*]pyrimidin-5-yl)amino) benzenesulfonamide (253)



i) Synthesis of 5-chloro-7-(cyclohexylmethoxy)-3*H*-[1,2,3]triazolo[4,5-*d*]pyrimidine

LiCl (34 mg, 0.80 mmol) was added to anhydrous dimethylacetamide (500 μ L), which was heated until all LiCl had dissolved. The solution was cooled (0 $^{\circ}$ C) and 7-(cyclohexylmethoxy)-3*H*-[1,2,3]triazolo[4,5-*d*]pyrimidin-5-amine (**257**) (50 mg, 0.20 mmol) was added followed by isoamyl nitrite (61 μ L, 0.30 mmol) and SOCl₂ (16 μ L, 0.22 mmol). The reaction mixture was stirred (0 $^{\circ}$ C, 1 h) then allowed to warm (RT, 18 h). NaHCO_{3(aq)} (15 mL) was added and the resulting aqueous mixture was extracted with EtOAc (3 x 15 mL). The organic layers were pooled, washed with brine (2 x 30 mL) then dried (Na₂SO₄). The solvent was removed to give the crude product as a brown oil (54 mg, 0.20 mmol, >99 %) which was used without further purification.

ii) Synthesis of 4-((7-(Cyclohexylmethoxy)-3*H*-[1,2,3]triazolo[4,5-*d*]pyrimidin-5-yl)amino) benzenesulfonamide

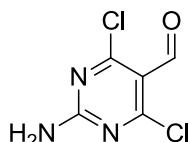
The title compound was prepared following **general procedure E** using crude 5-chloro-7-(cyclohexylmethoxy)-3*H*-[1,2,3]triazolo[4,5-*d*]pyrimidine (54 mg, 0.20 mmol), sulfanilamide (69 mg, 0.40 mmol) and TFA (78 μ L, 1.00 mmol) in TFE (1 mL). The crude product was dry loaded onto isolate HM-N and purified by MPLC on silica (3:7 EtOAc/petrol) followed by C18 reverse phase MPLC (8:2 MeOH(0.1% HCOOH)/H₂O (0.1% HCOOH)) to give the title compound (**253**) as a white solid (28 mg, 6.9×10^{-2} mmol, 35%).

R_f = 0.18 (7:3 EtOAc/petrol), m.p. 217-219 $^{\circ}$ C; UV λ_{max} (EtOH/nm) 310.0; IR ν_{max}/cm^{-1} : 3254, 3121, 2924, 2851, 2363, 2342, 2199, 2140, 1992, 19118, 1700, 1582, 1534, 1492, 1447; ¹H NMR (500 MHz, DMSO-*d*₆) δ 1.04-1.92 (11H, m, Cyclohexyl), 4.36 (2H, d, J = 6.8 Hz, OCH₂), 7.18 (2H, br s, SO₂NH₂), 7.72 (2H, d, J = 8.8 Hz, C²-H), 7.98 (1H, br s, CH triazolopyrimidine), 7.99 (2H, d, J = 9.0 Hz, C¹-

H), 9.92 (1H, br s, ArNHAr) 13.34 (1H, br s, NH triazolopyrimidine); ^{13}C NMR (125 MHz, $\text{DMSO}-d_6$) δ 25.1 (CH_2), 29.1 (CH_2), 35.9 (CH), 118.0 (Ar-C), 126.4 (Ar-C); HRMS calcd for $\text{C}_{17}\text{H}_{22}\text{N}_7\text{O}_3\text{S}$ $[\text{M}+\text{H}]^+$ 404.1499, Found 404.1500.

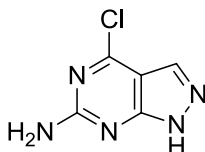
Note: not all carbon atoms were visible

2-Amino-4,6-dichloropyrimidine-5-carbaldehyde (**285**)^{305,306}



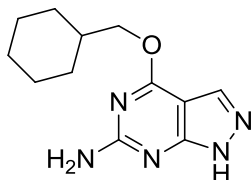
POCl_3 (33 mL, 0.37 mmol) was cooled in an ice bath (0 °C) and placed under nitrogen. To this Anhydrous DMF (3.44 mL, 0.44 mmol) was added dropwise with stirring over 30 min. 2-Amino-4,6-dihydroxy pyrimidine was then added in portions and the resulting mixture was allowed to warm to RT. The reaction mixture was heated (110 °C, 5 h) after which no starting material remained (LC-MS). The resulting brown oil was cooled to RT and the POCl_3 was removed *in vacuo* until the total volume was reduced to approximately 20%. The residual POCl_3 was neutralised by gradual addition to ice water (300 mL) resulting in a yellow precipitate which was filtered, washed with water (3 x 50 mL) and dried under vacuum to give the title compound (**285**) as a yellow solid (4.18 g, 0.22 mmol, 59%) which was sufficiently pure for use in the next reaction.

m.p. 300 °C (dec.) (Lit 208-224 °C); ^1H -NMR ($\text{DMSO}-d_6$) δ 8.55 (2H, br s, NH_2), 10.08 (1H, s, CHO); LRMS (ES-) m/z = 190 $[\text{M}+\text{H}]^+$

4-Chloro-1H-pyrazolo[3,4-d]pyrimidin-6-amine (286)³⁰⁷

A solution of 2-amino-4,6-dichloropyrimidine-5-carbaldehyde (**285**) (500 mg, 2.6 mmol) in a 3:1 mixture of THF/Water (11 mL) was heated to 50 °C. Hydrazine hydrate (252 μ L, 5.2 mmol) in water (3.3 mL) was added resulting in a yellow precipitate. The reaction mixture was cooled to RT and poured into ice-water (12 mL). The volume of solvent was reduced *in vacuo* resulting in further precipitation. The resulting solid was collected by filtration and washed with cold acetone (15 mL) to give the title compound (**286**) as a yellow solid (220 mg, 13.6 mmol, 50%).

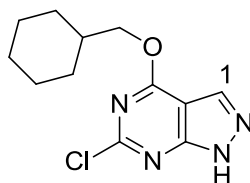
m.p. 201 °C (dec.) (Lit. 210 °C (dec.)); ¹H-NMR (DMSO-*d*₆) δ 8.50 (1H, br s, NH₂), 10.06 (1H, s, CH pyrazolopyrimidine), 11.55 (1H, br s, NH pyrazolopyrimidine), LRMS (ES+) *m/z* = 170.0 [M+H]⁺.

4-(Cyclohexylmethoxy)-1H-pyrazolo[3,4-d]pyrimidin-6-amine (256)

NaH (60% in mineral oil) was added to a solution of cyclohexylmethanol (364 μ L, 3.0 mmol) in anhydrous DMSO (1 mL). The mixture was stirred until no further gas was evolved (RT, 1 h). The resulting solution was added dropwise with stirring, to 4-chloro-1H-pyrazolo[3,4-d]pyrimidin-6-amine (**286**) (125 mg, 0.74 mmol) dissolved in anhydrous DMSO (1 mL). The reaction mixture was heated (100 °C, 30 min) then allowed to cool and added to water (25 mL) which was then neutralised (AcOH) resulting in a yellow precipitate. The precipitate was filtered and washed with water (10 mL) followed by ether (2 x 10 mL). The crude product was purified by MPLC on silica (1:9 MeOH/DCM) to give the title compound (**287**) as an off-white crystalline solid (68 mg, 0.28 mmol, 37%).

R_f = 0.70 (1:9 MeOH/DCM), m.p. 193-195 °C; UV λ_{\max} (EtOH/nm) 275.5; IR $\nu_{\max}/\text{cm}^{-1}$: 3498, 3353, 3232, 3121, 2960, 2921, 2851, 2750, 2667, 2158, 2038, 1902, 1794, 1633, 1578, 1497, 1469, 1441; ^1H NMR (500 MHz, DMSO- d_6) δ 0.98-1.82 (11H, m, cyclohexyl), 4.21 (2H, d, J = 6.5, OCH_2), 6.55 (2H, br s, NH_2), 7.77 (1H, s, CH pyrazolopyrimidine), 12.78 (1H, br s, NH pyrazolopyrimidine); ^{13}C NMR (125 MHz, DMSO- d_6) δ 25.2 (CH_2), 26.0 (CH_2), 29.1 (CH_2), 36.7 (CH), 70.5 (CH_2), 95.4 (Ar-C), 131.6 (Ar-C), 158.9 (Ar-C), 162.0 (Ar-C), 163.4 (Ar-C); HRMS calcd for $\text{C}_{12}\text{H}_{18}\text{N}_5\text{O}$ $[\text{M}+\text{H}]^+$ 248.1506, Found 248.1508.

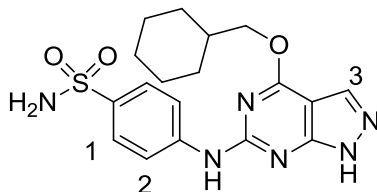
6-Chloro-4-(cyclohexylmethoxy)-1*H*-pyrazolo[3,4-*d*]pyrimidine (**287**)



LiCl (69 mg, 1.62 mmol) was added to anhydrous dimethylacetamide (1 mL), which was heated until the LiCl had fully dissolved. The solution was cooled to 0 °C and 4-(cyclohexylmethoxy)-1*H*-pyrazolo[3,4-*d*]pyrimidin-6-amine (**286**) (100 mg, 0.40 mmol) was added, followed by isoamyl nitrite (123 μL , 0.61 mmol) and SOCl_2 (32 μL , 0.45 mmol). The reaction mixture was stirred (RT, 18 h) then diluted with EtOAc (45 mL). The resulting solution was washed with $\text{NaHCO}_3(\text{aq})$ (45 mL) and brine (2 x 45 mL) then dried (Na_2SO_4) and dry loaded onto silica. The crude product was purified by MPLC (5:95 MeOH/DCM) to give the title compound (**287**) as a yellow solid (65 mg, 0.24 mmol, 60%).

R_f = 0.32 (5:95 MeOH/DCM), m.p. 152-153 °C; UV λ_{\max} (EtOH/nm) 252.5; IR $\nu_{\max}/\text{cm}^{-1}$: 3148, 2922, 2851, 1677, 1579, 1443; ^1H NMR (500 MHz, CDCl_3) δ 0.96-1.95 (11H, m, cyclohexyl), 4.39 (2H, d, J = 6.0 Hz, OCH_2), 8.09 (1H, s, $\text{C}^1\text{-H}$), 11.19 (1H, br s, NH pyrazolopyrimidine); ^{13}C NMR (125 MHz, DMSO- d_6) δ 25.2 (CH_2), 26.0 (CH_2), 29.1 (CH_2), 36.7 (CH), 70.5 (CH_2O), 95.4 (Ar-C), 131.6 ($\text{C}^1\text{-H}$), 158.9 (Ar-C), 162.0 (Ar-C), 163.4 (Ar-C); HRMS calcd for $\text{C}_{12}\text{H}_{16}\text{ClN}_4\text{O}$ $[\text{M}+\text{H}]^+$ 267.1007, Found 267.1012.

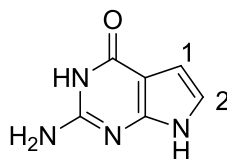
4-((4-(Cyclohexylmethoxy)-1*H*-pyrazolo[3,4-*d*]pyrimidin-6-yl)amino)benzene sulfonamide (252**)**



The title compound was prepared following **general procedure E** using: 6-chloro-4-(cyclohexylmethoxy)-1*H*-pyrazolo[3,4-*d*]pyrimidine (**287**) (42 mg, 0.18 mmol), sulfanilamide (62 mg, 0.36 mmol) and TFA (69 μ L, 0.90 mmol) in TFE (1 mL). The crude product was purified by MPLC on silica (7:3 EtOAc/petrol) followed by C18 reverse phase MPLC (8:2 MeOH(0.1% HCOOH)/H₂O (0.1% HCOOH)) to give the title compound (**252**) as a white solid (20 mg, 5.0×10^{-2} mmol, 28%).

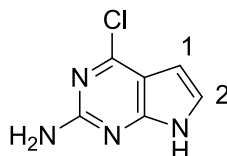
R_f = 0.21 (7:3 EtOAc/petrol), m.p. 268-269 °C; UV λ_{max} (EtOH/nm) 304.5; IR ν_{max}/cm^{-1} : 3367, 3333, 3269, 2922, 2853, 2162, 2012, 1691, 1658, 1624, 1583, 1551, 1524; ¹H NMR (500 MHz, DMSO-*d*₆) δ 1.04-1.92 (11H, m, Cyclohexyl), 4.36 (2H, d, J = 6.8 Hz, OCH₂), 7.18 (2H, br s, SO₂NH₂), 7.72 (2H, d, J = 8.8 Hz, C²-H), 7.98 (1H, br s, C³-H), 7.99 (2H, d, J = 9.0 Hz, C¹-H), 9.92 (1H, br s, ArNHAr) 13.34 (1H, br s, NH Pyrazolopyrimidine); ¹³C NMR (125 MHz, DMSO-*d*₆) δ 25.4 (CH₂), 26.5 (CH₂), 29.5 (CH₂), 37.1 (CH), 71.5 (CH₂) 118.6 (Ar-C), 136.6 (Ar-C), 144.0 (Ar-C); HRMS calcd for C₁₈H₂₃N₆O₃S [M+H]⁺ 403.1547, Found 403.1547.

Note: not all carbon atoms were visible

2-Amino-3*H*-pyrrolo[2,3-*d*]pyrimidin-4(7*H*)-one (264)²²¹

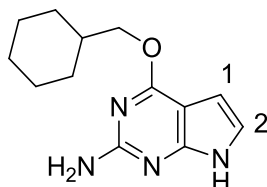
HCl_(aq) (2 M) (450 μ L, 0.91 mmol) was added to a mixture of bromoacetaldehyde diethyl acetal (596 μ L, 4.0 mmol) and water (1.75 mL). The resulting biphasic mixture rapidly stirred with heating until a solution was formed (90 $^{\circ}$ C, 30 min), which was cooled to RT and NaOAc (338 mg, 4.12 mmol) was added. In a separate flask a suspension of 2,6-diamino-4-pyrimidinone (500 mg, 4.0 mmol) in water (3.75 mL) with NaOAc (175 mg, 2.13 mmol) was stirred at RT. The freshly prepared bromoacetaldehyde solution was added in a single portion and the reaction mixture was heated (80 $^{\circ}$ C, 3 h). The reaction mixture was cooled to 0 $^{\circ}$ C for 90 min resulting in an off-white precipitate. The precipitate was filtered and washed with cold water (5 mL) then acetone (2 x 10 mL) to give the title compound (**264**) as a light brown solid (376 mg, 2.5 mmol).

m.p. 325 $^{\circ}$ C (dec.) (Lit >230 $^{\circ}$ C (dec.)); 1 H NMR (500 MHz, DMSO-*d*₆) δ 5.88 (2H, br s, NH₂), 6.17 (1H, d, *J* = 2.1 Hz, C¹-H), 6.60 (1H, d, *J* = 2.1 Hz, C²-H), 10.19 (1H, br s, NH pyrrolopyrimidine), 10.94 (1H, br s, NHCO); LRMS (ES+) *m/z* = 151.1 [M+H]⁺.

4-Chloro-7H-pyrrolo[2,3-d]pyrimidin-2-amine (265)²²¹

A suspension of 2-amino-3H-pyrrolo[2,3-d]pyrimidin-4(7H)-one (**264**) (1.34 g, 8.9 mmol) in POCl₃ (8.15 mL, 89 mmol) was stirred (RT, 30 min). The reaction mixture was then heated to reflux (110 °C, 4h). The volume of POCl₃ was reduced *in vacuo* to approximately 20%. The remaining POCl₃ was quenched over ice water (50 mL) then neutralised (NaHCO_{3(aq)}). The resulting solution was filtered through Celite then extracted with EtOAc (3 x 300 mL) to give the title compound (**264**) as a yellow solid (660 mg, 3.9 mmol, 44%).

m.p. 225 °C (dec.) (Lit 215-217 °C); ¹H NMR (500 MHz, DMSO-*d*₆) δ 6.24 (1H, d, *J* = 2.1 Hz, C¹-H), 6.46 (2H, br s, NH₂), 7.08 (1H, d, *J* = 2.1 Hz, C²-H), 11.44 (1H, br s, NH pyrrolopyrimidine); LRMS (ES+) *m/z* = 169.0 [M+H]⁺.

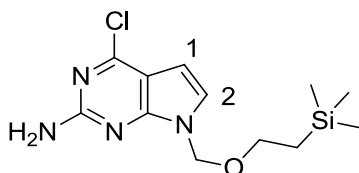
4-(Cyclohexylmethoxy)-7H-pyrrolo[2,3-d]pyrimidin-2-amine (255)

Cyclohexyl methanol (438 μL, 3.6 mmol) was added dropwise under nitrogen to a mixture of NaH (60% in mineral oil) in anhydrous DMSO (1 mL). The resulting mixture was stirred until no further gas was evolved (45 min). A separate solution of 4-chloro-7H-pyrrolo[2,3-d]pyrimidin-2-amine (**254**) (150 mg, 0.89 mmol) in anhydrous DMSO (1 mL) was prepared to which the freshly prepared cyclohexyl methoxide was added dropwise under nitrogen. The reaction mixture was heated using microwave irradiation (170 °C, 5 h), cooled to RT then added to water (20 mL). The aqueous mixture was neutralised (AcOH) then extracted with EtOAc (50 mL) before filtration of the resulting emulsion through Celite to give a biphasic mixture. The organic layer was removed and the aqueous layer was further extracted with EtOAc (2 x 30 mL).

The organic layers were pooled and dried (Na_2SO_4) then dry loaded onto silica. The title compound (**255**) was purified by MPLC on silica (1:9 MeOH/DCM) followed by C18 reverse phase MPLC (8:2 MeOH (0.1% HCOOH)/ Water (0.1% HCOOH) as a white crystalline solid (37 mg, 0.15 mmol, 17%).

R_f = 0.55 (1:9 MeOH/DCM); m.p. 216.3-217.3 °C; UV λ_{max} (EtOH/nm) 221; IR $\nu_{\text{max}}/\text{cm}^{-1}$: 3494, 3362, 3117, 2922, 2851, 2164, 2045, 1968, 1617, 1585, 1499, 1478; ^1H NMR (500 MHz, $\text{DMSO}-d_6$) 0.98-1.83 (11H, m, cyclohexyl), 4.15 (2H, d, J = 6.5, OCH_2), 5.91 (2H, br s, NH_2), 6.17 (1H, dd, J = 1.9 and 3.5, $\text{C}^1\text{-H}$), 6.79 (1H, dd, J = 2.2 and 3.5, $\text{C}^2\text{-H}$), 10.97 (1H, br s, NH pyrrolopyrimidine); ^{13}C NMR (125 MHz, $\text{DMSO}-d_6$) δ 25.2 (CH_2), 26.0 (CH_2), 29.3 (CH_2), 36.8 (CH), 69.9 (CH_2O), 96.9 ($\text{C}^1\text{-H}$), 97.9 (Ar-C), 119.1 ($\text{C}^2\text{-H}$), 155.0 (Ar-C), 159.3 (Ar-C), 162.7 (Ar-C); HRMS calcd for $\text{C}_{13}\text{H}_{19}\text{N}_4\text{O}$ $[\text{M}+\text{H}]^+$ 247.1553, Found 247.1556.

4-Chloro-7-((2-(trimethylsilyl)ethoxy)methyl)-7H-pyrrolo[2,3-d]pyrimidin-2-amine (**279**)

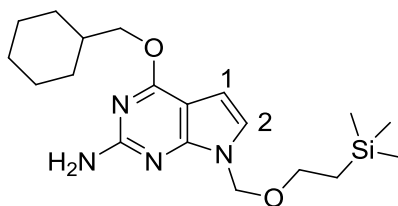


A solution of 4-chloro-7H-pyrrolo[2,3-d]pyrimidin-2-amine (**255**) (100 mg, 0.59 mmol) in anhydrous MeCN (3 mL) was cooled to -30 °C. NaH (60% in mineral oil, 26 mg, 0.65 mmol) was added and the reaction mixture was stirred under nitrogen (45 min). 2-(Trimethylsilyl)ethoxymethyl chloride (SEM-Cl) (90%, 122 μL , 0.62 mmol) was added drop-wise and the reaction mixture was stirred for a further 60 min then allowed to warm to (RT, 2 h). Water (20 mL) was added and the resulting solution was extracted with EtOAc (20 mL). The organic layer was then washed with brine (3 x 20 mL), dried (Na_2SO_4) then dry loaded onto silica. The title compound (**279**) was purified by MPLC on silica (15:85 EtOAc/petrol) as a yellow solid (130 mg, 0.44 mmol, 74%).

R_f = 0.41 (15:85 EtOAc/petrol); m.p. 63-64 °C; UV λ_{max} (EtOH/nm) 234.0 and 317.5; IR $\nu_{\text{max}}/\text{cm}^{-1}$: 3423, 3318, 3212, 3096, 2952, 1631, 1608, 1546, 1493; ^1H NMR (500

MHz, CDCl₃) δ -0.04 (9H, s, CH₃), 0.91 (2H, t, J = 8.0 Hz, CH₂Si), 3.81 (2H, t, J = 8.3 Hz, OCH₂), 4.96 (2H, br s, NH₂), 5.44 (2H, s, ArCH₂), 6.43 (1H, d, J = 3.7 Hz, C¹-H), 6.99 (1H, d, J = 3.7 Hz, C²-H); ¹³C NMR (125 MHz, DMSO-*d*₆) δ 0.0 (Si(CH₃)₃), 19.2 (CH₂CH₂Si), 67.7 (OCH₂CH₂), 74.3 (NCH₂O), 102.2 (C⁵H), 112.2 (Ar-C), 127.0 (C⁶H), 154.2 (Ar-C), 155.6 (Ar-C), 160.2 (Ar-C); HRMS calcd for C₁₂H₂₀ClN₄OSi [M+H]⁺ 299.1089, Found 299.1090.

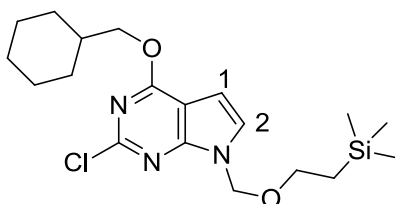
4-(Cyclohexylmethoxy)-7-((2-(trimethylsilyl)ethoxy)methyl)-7H-pyrrolo[2,3-*d*]pyrimidin-2-amine (280)



NaH (60% in mineral oil, 121 mg, 3.03 mmol) was added under nitrogen to a solution of cyclohexylmethanol (496 μ L, 4.03 mmol) in anhydrous THF (5 mL). The resulting mixture was stirred (RT, 45 min) until no further gas was evolved then added dropwise to a solution of 4-chloro-7-((2-(trimethylsilyl)ethoxy)methyl)-7H-pyrrolo[2,3-*d*]pyrimidin-2-amine (**279**) (300 mg, 1.01 mmol) in THF (10 mL). The reaction was stirred (RT, 72 h) then the volume of solvent was reduced *in vacuo* to approximately 2 mL. The resulting solution was added to HCl_(aq) (1 M) (50 mL) which was then extracted with DCM (25 mL) and washed with NaHCO_{3(aq)} (50 mL) and brine (50 mL). The organic layer was dried (phase separator) then dry loaded onto silica. The title compound (**280**) was purified by MPLC on silica (15:85 EtOAc/petrol) as a yellow solid (296 mg, 0.79 mmol, 78%).

R_f = 0.17 (15:85 EtOAc/petrol); m.p. 88-90 °C; UV λ_{max} (EtOH/nm) 223.0, 260.0 and 286.5; IR ν_{max}/cm^{-1} : 3346, 3222, 2926, 2852, 1647, 1602; ¹H NMR (500 MHz, CDCl₃) δ -0.05 (9H, s, CH₃), 0.91 (2H, t, J = 8.3 Hz, CH₂Si), 1.01-1.91 (11H, m cyclohexyl), 3.51 (2H, t, J = 8.3 Hz, OCH₂CH₂), 4.21 (2H, d, J = 6.5 Hz, OCH₂CH), 4.68 (2H, br s, NH₂), 5.41 (2H, s, ArCH₂), 6.40 (1H, d, J = 3.7 Hz, C¹-H), 6.82 (1H, d, J = 3.7 Hz, C²-H); ¹³C NMR (125 MHz, DMSO-*d*₆) δ 0.0 (Si(CH₃)₃), 19.2 (CH₂CH₂Si), 27.2 (CH₂), 28.0 (CH₂), 31.3 (CH₂), 38.8 (CH), 67.4 (OCH₂CH₂), 72.6 (CH₂), 74.1 (NCH₂O), 101.2 (C⁵H), 123.6 (C⁶H), 160.6 (Ar-C), 165.4 (Ar-C); HRMS calcd for C₁₉H₃₃N₄O₂Si [M+H]⁺ 377.2367, Found 377.2367.

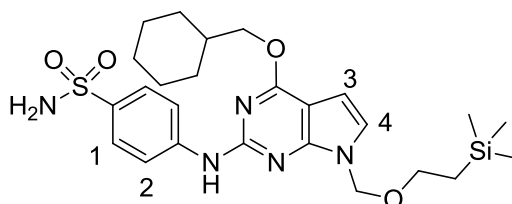
2-Chloro-4-(cyclohexylmethoxy)-7-((2-(trimethylsilyl)ethoxy)methyl)-7H-pyrrolo[2,3-*d*]pyrimidine (281**)**



4-(Cyclohexylmethoxy)-7-((2-(trimethylsilyl)ethoxy)methyl)-7H-pyrrolo[2,3-*d*]pyrimidin-2-amine (**280**) (100 mg, 0.27 mmol) was added to a solution of LiCl in THF (0.5M, 2.13 mL, 1.1 mmol). The reaction mixture was cooled to 0 °C then isoamyl nitrite (81 μ L, 0.40 mmol) and SOCl₂ (21.3 μ L, 0.29 mmol) were added simultaneously. The resulting solution was stirred (RT, 5 h) then added to NH₄Cl_(aq) (30 mL). The aqueous mixture was extracted with EtOAc (30 mL) and the organic layer was washed with water (3 x 30 mL), dried (Na₂SO₄) and dry loaded onto silica. The crude product was purified by MPLC (15:85 EtOAc/petrol) to give the title compound (**281**) as a colourless oil (60 mg, 0.15 mmol, 56%).

R_f = 0.45 (15:85 EtOAc/Petrol); UV λ_{max} (EtOH/nm) 270; IR ν_{max}/cm^{-1} 2924, 2852, 1750, 1661, 1588, 1558, 1506; ¹H NMR (500 MHz, DMSO-*d*₆) δ -0.09 (9H, s, CH₃), 0.82 (2H, t, J = 8.1 Hz, CH₂Si), 0.95-1.89 (11H, m cyclohexyl), 3.50 (2H, t, J = 8.1 Hz, OCH₂CH₂), 4.28 (2H, d, J = 6.0 Hz, OCH₂CH), 5.52 (2H, s, ArCH₂), 6.61 (1H, d, J = 3.6 Hz, C¹-H), 7.55 (1H, d, J = 3.5 Hz, C²-H); ¹³C NMR (125 MHz, DMSO-*d*₆) δ 0.0 (Si(CH₃)₃), 18.5 (CH₂CH₂Si), 26.6 (CH₂), 30.5 (CH₂), 31.8 (CH₂), 38.8 (CH), 67.1 (OCH₂CH₂), 73.3 (CH₂), 74.2 (NCH₂O), 100.4 (C⁵H), 126.4 (C⁶H), 129.7 (Ar-C); HRMS calcd for C₁₉H₃₁ClN₃O₂Si [M+H]⁺ 396.1869, Found 396.1872.

4-((4-(Cyclohexylmethoxy)-7-((2-(trimethylsilyl)ethoxy)methyl)-7H-pyrrolo[2,3-d]pyrimidin-2-yl)amino)benzenesulfonamide (282)

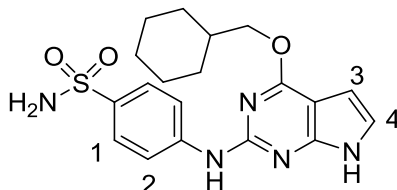


To a solution of 2-chloro-4-(cyclohexylmethoxy)-7-((2-(trimethylsilyl)ethoxy)methyl)-7H-pyrrolo[2,3-d]pyrimidine (**281**) (50 mg, 0.13 mmol) in anhydrous MeCN (2 mL) was added sulfanilamide (24 mg, 0.14 mmol), anhydrous K₂CO₃ (35 mg, 0.25 mmol), Pd₂(dba)₃ (3 mg, 5.0 x 10⁻³ mmol) and XPhos (2.4 mg, 5.0 x 10⁻³ mmol). The reaction mixture was degassed (N₂, 30 min) and heated (80 °C, 2 h) then cooled to RT and filtered (Celite). The resulting solution was diluted with EtOAc (20 mL) and washed sequentially with HCl_(aq) (1 M) (20 mL), NaHCO₃ (20 mL) and brine (30 mL) then dried (Na₂SO₄) and dry loaded onto silica. The title compound (**282**) was purified by MPLC (1:1 EtOAc/petrol) as a yellow oil (33 mg, 6.2 x 10⁻² mmol, 49%).

R_f = 0.63 (1:1 EtOAc/petrol); UV λ_{max} (EtOH/nm) 269; IR ν_{max}/cm^{-1} 3644, 3342, 2924, 2853, 1586, 1528, 1488; ¹H NMR (500 MHz, CDCl₃) δ -0.08 (9H, s, Si(CH₃)₃), 0.88-0.95 (2H, t, J = 8.36 Hz, CH₂Si) 1.04 - 1.93 (11H, m, cyclohexyl), 3.56 (2H, t, J = 3.4 Hz, O-CH₂CH₂Si) 4.29 (2H, d, J = 6.5 Hz, OCH₂), 4.72 (2H, br s, NH₂), 5.52 (2H, s, Ar-CH₂-O), 6.49 (1H, d, J = 3.5 Hz, C³-H), 6.96 (1H, d, J = 3.6 Hz, C⁴-H), 7.20 (1H, br s, Ar-NH-Ar), 7.87 (4H, ap s, C^{1/2}-H); ¹³C NMR (125 MHz, CDCl₃) δ 0.0 (SiCH₃), 15.6 (CH₂Si), 27.2 (CH₂), 27.9 (CH₂), 31.3 (CH₂), 38.8 (CH), 67.8 (CH₂), 73.2 (CH₂), 74.5 (CH₂), 101.5 (Ar-C), 101.9 (Ar-C), 118.8 (Ar-C), 125.0 (Ar-C), 129.3 (Ar-C), 146.2 (Ar-C); HRMS calcd for C₂₅H₃₈N₅O₄SSi [M+H]⁺ 532.2408, Found 532.2406.

Note: Not all carbon atoms visible

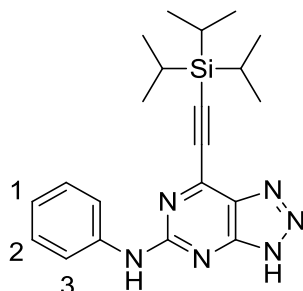
4-((4-(Cyclohexylmethoxy)-7*H*-pyrrolo[2,3-*d*]pyrimidin-2-yl)amino)benzenesulfonamide (251)



A solution of 4-((4-(cyclohexylmethoxy)-7-((2-(trimethylsilyl)ethoxy)methyl)-7*H*-pyrrolo[2,3-*d*]pyrimidin-2-yl)amino)benzenesulfonamide (**282**) (40 mg, 7.5×10^{-2} mmol) in TFA (1.5 mL) was heated to reflux (75 °C, 5 min). The resulting green solution was neutralised over $\text{NaHCO}_{3(\text{aq})}$ (30 mL) then extracted with EtOAc (2 x 30 mL). The combined organic layers were dried (Na_2SO_4) and the solvent was removed to give the hemiaminal as a yellow solid (22.5 mg, 5.2×10^{-2} mmol). MeCN (4 mL) and water (4 mL) were added and the pH was adjusted to 10 with aqueous ammonia (32%). The reaction mixture was stirred (1 h, RT) and the solvent was removed. The crude product was redissolved in EtOAc (20 mL), dried (Na_2CO_3) and dry loaded onto silica. The title compound (**251**) was purified by MPLC on silica (3:7 petrol/EtOAc) as a white solid (12 mg, 3.0×10^{-2} mmol, 40%).

R_f = 0.39 (3:7 petrol/EtOAc); m.p. 251.2-252.0 °C; UV λ_{max} (EtOH/nm) 312.0; IR $\nu_{\text{max}}/\text{cm}^{-1}$: 3374, 3322, 2058, 2924, 2856, 2012, 1615, 1595, 1579; ^1H NMR (500 MHz, $\text{DMSO}-d_6$) δ 1.07-1.95 (11H, m, cyclohexyl), 4.31 (2H, d, J = 6.3 Hz, OCH_2), 6.34 (1H, d, J = 2.1 Hz, $\text{C}^3\text{-H}$), 7.05 (1H, d, J = 2.2 Hz, $\text{C}^4\text{-H}$), 7.13 (2H, br s, SO_2NH_2), 7.68 (2H, d, J = 8.9 Hz, $\text{C}^2\text{-H}$), 7.99 (2H, d, J = 8.8 Hz, $\text{C}^1\text{-H}$), 9.57 (1H, br s, ArNHAr), 11.54 (1H, br s, NH).; ^{13}C NMR (125 MHz, $\text{DMSO}-d_6$) δ 25.2 (CH_2), 26.0 (CH_2), 29.3 (CH_2), 36.8 (CH), 70.6 (CH_2), 98.2 (C^5H), 116.9 (Ar-C), 126.4 (C^6H), 134.9 (Ar-C), 144.6 (Ar-C), 146.4 (Ar-C), 153.6 (Ar-C), 154.4 (Ar-C), 162.4 (Ar-C); HRMS calcd for $\text{C}_{19}\text{H}_{24}\text{N}_5\text{O}_3\text{S}$ $[\text{M}+\text{H}]^+$ 402.1594, Found 402.1596.

***N*-Phenyl-7-((triisopropylsilyl)ethynyl)-3*H*-[1,2,3]triazolo[4,5-*d*]pyrimidin-5-amine (176)**



i) Preparation of 5-chloro-7-((triisopropylsilyl)ethynyl)-3*H*-[1,2,3]triazolo[4,5-*d*]pyrimidine

A solution of trimethylsilyl chloride (100 μ L, 0.79 mmol) in anhydrous DCM (4 mL) was cooled (0 $^{\circ}$ C) and placed under nitrogen. In a separate flask a solution of benzyltriethylammonium nitrite (**294**) (170 mg, 0.71 mmol) in anhydrous DCM (2 mL) was cooled (0 $^{\circ}$ C) and placed under nitrogen. The solution of (**294**) was added dropwise with stirring to the trimethylsilyl chloride solution at 0 $^{\circ}$ C. The resulting mixture was stirred (0 $^{\circ}$ C, 15 min) at which point a cooled (0 $^{\circ}$ C) solution of 7-((triisopropylsilyl)ethynyl)-3*H*-[1,2,3]triazolo[4,5-*d*]pyrimidin-5-amine (**175**) (50 mg, 0.16 mmol) in anhydrous DCM (2 mL) was introduced dropwise with stirring. The reaction mixture was stirred (0 $^{\circ}$ C, 30 min) then warmed to RT (30 min). The resulting solution was washed with $\text{NaHCO}_{3(\text{aq})}$ (4 x 20 mL), dried (phase separator) and the solvent was removed under vacuum (20 $^{\circ}$ C) to give the crude product as a dark orange oil (59 mg, 0.18 mmol, 112%) which was used without any further purification.

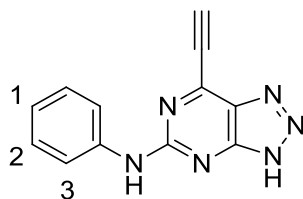
ii) *N*-Phenyl-7-((triisopropylsilyl)ethynyl)-3*H*-[1,2,3]triazolo[4,5-*d*]pyrimidin-5-amine (**105**)

The crude product from i) was dissolved in a 1 M solution of aniline in DMSO (500 μ L, 0.50 mmol) and heated (70 $^{\circ}$ C, 96 h). The resulting solution was poured into 1 M $\text{HCl}_{(\text{aq})}$ (30 mL) which was extracted with EtOAc (2 x 20 mL). The organic layers were combined and washed with 1 M $\text{HCl}_{(\text{aq})}$ (3 x 30 mL), $\text{NaHCO}_{3(\text{aq})}$ (30 mL) and

brine (30 mL) then dried (MgSO₄). The crude product was purified *via* preparative TLC (5:95 MeOH/DCM) to give (**176**) as a yellow oil (48 mg, 0.12 mmol, 81%).

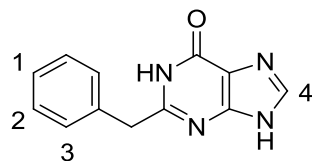
R_f = 0.31 (5:95 MeOH/DCM); UV λ_{\max} (EtOH/nm) 274.0; IR $\nu_{\max}/\text{cm}^{-1}$: 3294, 3209, 3112, 2943, 2865, 1585, 1564, 1516; ¹H NMR (500 MHz, CDCl₃) δ 1.12-1.32 (21H, m, CH₂CH₃), 7.08-7.15 (1H, m, C¹-H), 7.35 (2H, app. t, J = 7.6 Hz, C²-H), 7.63 (2H, d, J = 7.6 Hz, C³-H), 7.73 (1H, br s, ArNHAr), 13.07 (1H, br s, NH triazolopyrimidine); ¹³C NMR (125 MHz, CDCl₃) δ 11.3 (Si(CH(CH₃)₂)₃), 18.6 (Si(CH(CH₃)₂)₃), 99.7 (C \equiv C-Si), 105.7 (C \equiv C), 120.3 (Ar-C), 121.0 (Ar-C), 124.1 (Ar-C), 129.1 (Ar-C), 138.3 (Ar-C), 145.5 (Ar-C), 152.2 (Ar-C), 158.9 (Ar-C); HRMS calcd for C₂₁H₂₉N₆Si [M+H]⁺ 393.2217 Found 393.2219.

7-Ethynyl-*N*-phenyl-3*H*-[1,2,3]triazolo[4,5-*d*]pyrimidin-5-amine (**90**)



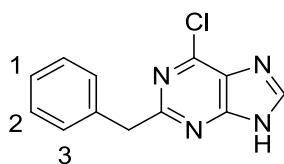
The title compound was prepared following **general procedure A** using: *N*-phenyl-7-((triisopropylsilyl)ethynyl)-3*H*-[1,2,3]triazolo[4,5-*d*]pyrimidin-5-amine (**176**) (40 mg, 0.1 mmol) and TBAF (1 M in THF) (112 μ L, 1.1 mmol) in THF (4 mL) at 0 °C. The crude product was purified by MPLC on silica (5:95 MeOH/DCM) to give the title compound (**90**) as a yellow solid (22 mg, 9.5 x 10⁻² mmol, 92%).

R_f = 0.17 (5:95 MeOH/DCM); m.p. 130 °C (dec); UV λ_{\max} (EtOH/nm) 265.0; IR $\nu_{\max}/\text{cm}^{-1}$: 3303, 3283, 3206, 3144, 3097, 2793, 2121, 1596, 1572, 1553; ¹H NMR (300 MHz, DMSO-*d*₆) δ 5.19 (1H, s, CH ethynyl), 7.03 (1H, tt, J = 7.2 and 1.1 Hz, C¹-H), 7.34 (2H, app. t, J = 7.4 Hz, C²-H), 7.81 (2H, d, J = 8.6 Hz, C³-H), 10.29 (1H, br s, ArNHAr), 16.11 (1H, br s, NH triazolopyrimidine); ¹³C NMR (125 MHz, DMSO-*d*₆) δ 77.8 (C \equiv C-H), 89.6 (C \equiv C), 119.4 (Ar-C), 122.4 (Ar-C), 128.6 (Ar-C), 139.6 (Ar-C); HRMS calcd for C₁₂H₉N₆ [M+H]⁺ 237.0883 Found 237.0886.

2-Benzyl-1*H*-purin-6(9*H*)-one (81)^{289,308}

A solution of 5-amino-4-imidazole carboxamide hydrochloride (500 mg, 3.1 mmol) was prepared in 2:1 mixture of DMF/pyridine (24 mL). Phenylacetic acid (419 mg, 3.1 mmol), *N*-(3-dimethylaminopropyl)-*N*-ethylcarbodiimide hydrochloride (590 mg, 3.1 mmol) and DMAP (376 mg, 3.1 mmol) were added and the mixture was heated (70 °C, 18 h). The solvent was removed *in vacuo* and NaOH_(aq) (2 M) (25 mL) was added. The reaction mixture was heated to reflux (100 °C, 1 h) then cooled (0-5 °C) and neutralised with 2 M HCl_(aq) resulting in a white precipitate. The precipitate was filtered, washed with water (3 x 15 mL) and ether (3 x 15 mL) then dried overnight in a vacuum oven to give (**81**) as an off-white solid (512 mg, 2.3 mmol, 73%).

¹H NMR (300 MHz, DMSO-*d*₆) δ 3.94 (2H, s, CH₂), 7.21-7.35 (5H, m, C¹⁻³-H), 8.04 (1H, s, C⁴-H), 12.34 (1H, br s, N⁹-H), 13.18 (1H, Br s, N¹-H); LRMS (ES+) *m/z* = 227.1 [M+H]⁺.

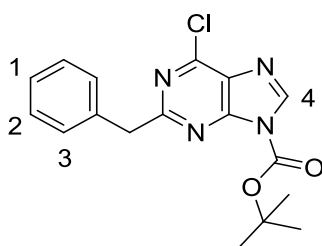
2-Benzyl-6-chloro-9*H*-purine (82)¹⁹⁶

To DMF (anhydrous) (2.6 mL) cooled to 0 °C was added thionyl chloride (2.4 mL, 33 mmol) dropwise with stirring. The resulting mixture was stirred for 15 minutes at 0 °C and kept at this temperature until required. In a separate flask a suspension of (**81**) (1.5 g, 6.6 mmol) in chloroform (30 mL) was prepared. The suspension was heated to reflux and the previously prepared DMF solution was introduced dropwise. The reaction mixture was maintained at reflux (2 h) resulting in a red precipitate. The solvent was removed *in vacuo* and the precipitate was dissolved by adding EtOAc (50 mL) and NaHCO_{3(aq)} (50 mL). The biphasic mixture was filtered and the organic layer was removed. The remaining aqueous layer was extracted with EtOAc (2 x 50

mL) and the organic layers were combined, dried (Na_2SO_4), and dry loaded onto silica. The title compound (**82**) was purified by MPLC on silica (EtOAc) as a light yellow solid (1.2 g, 4.9 mmol, 74%).

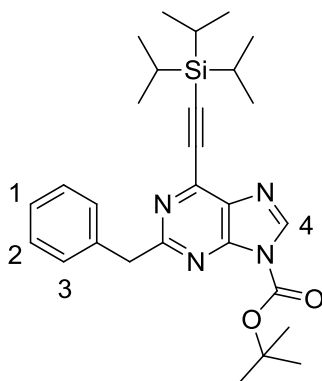
$R_f = 0.38$ (EtOAc); ^1H NMR (300 MHz, $\text{DMSO}-d_6$) δ 4.34 (2H, s, CH_2), 7.11-7.35 (5H, m, $\text{C}^{1-3}\text{-H}$), 8.19 (1H, s, $\text{C}^4\text{-H}$), 13.24 (1H, br s, $\text{N}^9\text{-H}$); LRMS (ES+) $m/z = 245.1$ $[\text{M}+\text{H}]^+$

***tert*-Butyl 2-benzyl-6-chloro-9*H*-purine-9-carboxylate (**83**)**



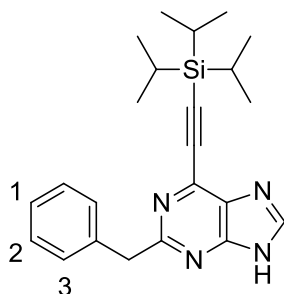
To a solution of (**82**) (1.15 g, 4.7 mmol) in DCM (anhydrous) (50 mL) was added di-*tert*-butyl dicarbonate (1.08 g, 4.9 mmol) and DMAP (29 mg, 0.24 mmol). The reaction mixture was stirred (RT, 1 h) after which no starting material remained (observed by LC-MS). The crude product was dry loaded onto silica and purified by MPLC (3:7 EtOAc/petrol) to give (**83**) as a colourless oil (1.23 g, 3.6 mmol, 76%).

$R_f = 0.51$ (3:7 EtOAc/petrol); UV λ_{max} (EtOH/nm) 254; IR $\nu_{\text{max}}/\text{cm}^{-1}$ 2981, 2934, 1754, 1595, 1552, 1495; ^1H NMR (500 MHz, $\text{DMSO}-d_6$) δ 1.61 (9H, s, $\text{C}(\text{CH}_3)_3$), 4.30 (2H, s, ArCH_2Ar), 7.18-7.39 (5H, m, $\text{C}^{1-3}\text{-H}$), 8.89 (1H, s, $\text{C}^4\text{-H}$); ^{13}C NMR (125 MHz, $\text{DMSO}-d_6$) δ 27.4 ($\text{C}(\text{CH}_3)_3$), 44.5 (CH_2), 86.3 (CCH_3), 126.5 (Ar-C), 128.4 (Ar-C), 129.0 (Ar-C), 130.0 (Ar-C), 137.9 (Ar-C), 138.4 (Ar-C), 145.6 (Ar-C), 151.6 (Ar-C), 164.8 (Ar-C); HRMS calcd for $\text{C}_{17}\text{H}_{18}\text{ClN}_4\text{O}_2$ $[\text{M}+\text{H}]^+$ 345.1113 Found 345.1118.

***tert*-Butyl 2-benzyl-6-((triisopropylsilyl)ethynyl)-9*H*-purine-9-carboxylate (**82**)**

To a solution of *tert*-butyl 2-benzyl-6-chloro-9*H*-purine-9-carboxylate (**83**) (1.23 g, 3.57 mmol) in anhydrous THF (15 mL) was added (triisopropylsilyl)acetylene (897 μ L, 4.00 mmol). Pd(PPh₃)₂Cl₂ (100 mg, 0.14 mmol) and copper iodide (27 mg, 0.14 mmol) were then added followed by triethylamine (1.24 mL, 8.93 mmol). The reaction vessel was stoppered with a septum then degassed (N₂, 20 min) and shielded from light. The reaction mixture was stirred (RT, 18 h) then filtered over a pad of Celite and purified by silica based MPLC (1:9 EtOAc/petrol) resulting in the title compound (**84**) as a colourless oil (1.45 g, 2.95 mmol, 83%).

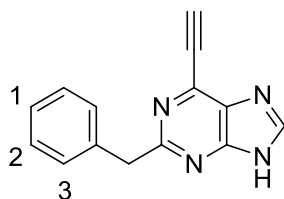
R_f = 0.37 (1:9 EtOAc/Petrol); UV λ_{max} (EtOH/nm) 261; IR ν_{max} /cm⁻¹ 2941, 2864, 1756, 1573, 1495; ¹H NMR (500 MHz, DMSO-*d*₆) δ 1.05-1.24 (21H, m, Si(CH(CH₃)₂)₃), 1.61 (9H, s, C(CH₃)₃), 4.29 (2H, s, ArCH₂Ar), 7.16-7.39 (5H, m, C¹⁻³-H), 8.86 (1H, s, C⁴-H); ¹³C NMR (125 MHz, DMSO-*d*₆) δ 10.6 (Si(CH(CH₃)₂)₃), 18.4 (Si(CH(CH₃)₂)₃), 27.5 (C(CH₃)), 45.0 (CH₂), 86.3 (CCH₃), 100.9 (C \equiv C-Si), 126.3 (C \equiv C), 128.3 (Ar-C), 129.1 (Ar-C), 133.6 (Ar-C), 138.3 (Ar-C), 140.1 (Ar-C), 145.7 (Ar-C), 145.8 (Ar-C), 151.5 (Ar-C), 164.8 (Ar-C); HRMS calcd for C₂₈H₃₉N₄O₂Si [M+H]⁺ 491.2837 Found 491.2831.

2-Benzyl-6-((triisopropylsilyl)ethynyl)-9H-purine (85)

A solution of *tert*-butyl 2-benzyl-6-((triisopropylsilyl)ethynyl)-9H-purine-9-carboxylate (**84**) (1.45 g, 2.95 mmol) in TFE (50 mL) was heated (2h, 80 °C). The solvent was removed and the crude product was redissolved in DCM (50 mL) then dry loaded onto silica. The crude product was purified by MPLC on silica (1:1 EtOAc/petrol) to give the title compound (**85**) as a white solid (1.05 g, 2.69 mmol, 91%).

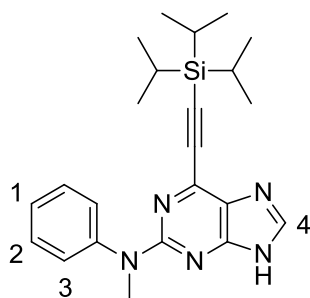
R_f = 0.02 (2:3 EtOAc/Petrol); m.p. 189 °C; UV λ_{max} (EtOH/nm) 272; IR ν_{max}/cm^{-1} 3031, 2941, 2864, 1573, 1462; 1H NMR (500 MHz, DMSO- d_6) δ 1.01-1.22 (21H, m, Si(CH(CH₃)₂)₃), 4.26 (2H, s, ArCH₂Ar), 7.15-7.36 (5H, m, C¹⁻³-H), 8.54 (1H, s, C⁴-H), 13.5 (1H, br s, NH); ^{13}C NMR (125 MHz, DMSO- d_6) δ 10.6 (Si(CH(CH₃)₂)₃), 18.4 (Si(CH(CH₃)₂)₃), 44.8 (CH₂), 99.2 (C \equiv C-Si), 126.2 (C \equiv C), 128.3 (Ar-C), 129.0 (Ar-C), 138.3 (Ar-C), 162.9 (Ar-C); HRMS calcd for C₂₃H₃₁N₄Si [M+H]⁺ 391.2313 Found 391.2318.

Note: not all carbon atoms visible

2-Benzyl-6-ethynyl-9H-purine (56)

The title compound was prepared following **general procedure A** using: 2-Benzyl-6-((triisopropylsilyl)ethynyl)-9H-purine (**86**) (500 mg, 1.28 mmol) and TBAF (1 M in THF (1.41 mL, 1.41 mmol) in THF (40 mL). The crude product was purified by MPLC on silica (1:9 MeOH/DCM) to give the title compound (**56**) as a light yellow solid (295 mg, 1.26 mmol, 98%).

R_f = 0.23 (1:9 MeOH/DCM); m.p. 179.1 °C (dec.); UV λ_{\max} (EtOH/nm) 217.5 and 294.0; IR $\nu_{\max}/\text{cm}^{-1}$ 3142, 3113, 3057, 2993, 2968, 2833, 2795, 2717, 2100, 1606, 1576; ^1H NMR (500 MHz, DMSO- d_6) δ 4.25 (2H, s, CH_2), 4.94 (1H, s, CH ethynyl), 7.14-7.35 (5H, m, $\text{C}^{1-3}\text{-H}$), 8.58 (1H, s, $\text{C}^4\text{-H}$), 13.60 (1H, br s, NH); ^{13}C NMR (125 MHz, DMSO- d_6) δ 44.9 (CH_2), 78.9 ($\text{C}\equiv\text{C-H}$), 88.1 ($\text{C}\equiv\text{C}$), 126.2 (Ar-C), 128.3 (Ar-C), 129.0 (Ar-C), 138.9 (Ar-C), 162.9 (Ar-C); HRMS calcd for $\text{C}_{14}\text{H}_{11}\text{N}_4$ $[\text{M}+\text{H}]^+$ 235.0978 Found 235.098.

N-Methyl-N-phenyl-6-((triisopropylsilyl)ethynyl)-9H-purin-2-amine (66)

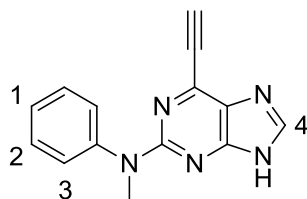
To a solution of 2-fluoro-6-((triisopropylsilyl)ethynyl)-9H-purine (**65**) (100 mg, 0.31 mmol) in anhydrous toluene (2 mL) was added *N*-methylaniline (68 μL , 0.63 mmol) and TFA (61 μL , 0.79 mmol). The reaction mixture was heated (160 °C, 4 h) using microwave irradiation resulting in consumption of the starting material (**65**) (observed by LC-MS). The solvent was removed and the crude product was redissolved in

EtOAc (15 mL) and dry loaded onto silica. The title compound (**66**) was purified by MPLC on silica (5:95 MeOH/DCM) as a yellow oil (85 mg, 0.21 mmol, 67%).

R_f = 0.41 (5:95 MeOH/DCM); UV λ_{\max} (EtOH/nm) 278.0; IR $\nu_{\max}/\text{cm}^{-1}$ 2945, 2864, 1594, 1566, 1493; ^1H NMR (500 MHz, DMSO- d_6) δ 1.07-1.21 (21H, m, Si(CH(CH₃)₂)₃), 3.48 (3H, s, N-CH₃), 7.13 – 7.24 (1H, m, C¹-H), 7.32-7.46 (4H, m, C^{2/3}-H), 8.16 (1H, s, C⁴-H) 12.95 (1H, br s, NH); ^{13}C NMR (125 MHz, DMSO- d_6) δ 10.6 (Si(CH(CH₃)₂)₃), 18.4 (Si(CH(CH₃)₂)₃), 97.7 (C \equiv C-Si), 102.4 (C \equiv C), 125.0 (Ar-C), 126.3 (Ar-C), 128.6 (Ar-C), 128.8 (Ar-C), 139.2 (Ar-C), 142.7 (Ar-C), 146.0 (Ar-C), 154.3 (Ar-C), 158.1 (Ar-C); LRMS (ES+) m/z = 406.2 [M+H]⁺.

Note: N-CH₃ carbon NMR peak obscured by DMSO

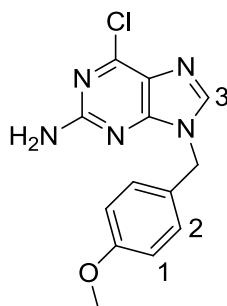
6-Ethynyl-*N*-methyl-*N*-phenyl-9*H*-purin-2-amine (**54**)



The title compound was prepared following **general procedure A** using: *N*-Methyl-*N*-phenyl-6-((triisopropylsilyl)ethynyl)-9*H*-purin-2-amine (**66**) (64 mg, 0.16 mmol) and TBAF (1 M in THF (174 μL , 0.174 mmol) in THF (6 mL). The crude product was purified by MPLC on silica (5:95 MeOH/DCM) to give the title compound (**54**) as a yellow solid (14 mg, 5.62×10^{-2} mmol, 36%).

R_f = 0.32 (5:95 MeOH/DCM); m.p. 249.3 °C; UV λ_{\max} (EtOH/nm) 227 and 254; IR $\nu_{\max}/\text{cm}^{-1}$ 3262, 3091, 3019, 2918, 2848, 2795, 2727, 2112, 1622, 1597; ^1H NMR (500 MHz, DMSO- d_6) 3.46 (3H, s, CH₃), 4.75 (1H, s, CH ethynyl), 7.20 (1H, tt, J = 7.4 and 1.2 Hz, C¹-H), 7.35 (2H, d, J = 7.4 Hz, C³-H), 7.39 (2H, app. t, J = 7.4 Hz, C²-H), 8.20 (1H, s, C⁴-H); ^{13}C NMR (125 MHz, DMSO- d_6) 39.3 (CH₃), 86.8 (C \equiv C-H), 125.0 (Ar-C), 126.4 (Ar-C), 128.9 (Ar-C), 146.0 (Ar-C), 158.2 (Ar-C); HRMS calcd for C₁₄H₁₂N₅ [M+H]⁺ 250.1087 Found 250.1089.

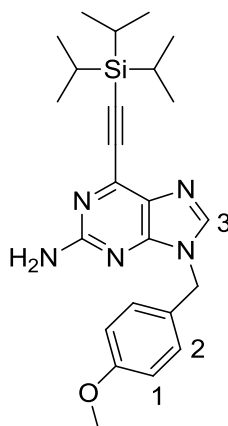
Note: not all carbon atoms visible

6-Chloro-9-(4-methoxybenzyl)-9*H*-purin-2-amine (70)²¹⁹

4-Methoxybenzylchloride (0.88 ml, 6.49 mmol) was added to a solution of 2-amino-6-chloropurine (**69**) (1.00 g, 5.90 mmol) and K_2CO_3 (0.90 g, 6.49 mmol) in dry DMF (30 ml). The reaction mixture was heated at 60 °C for 18 h before being cooled to RT and evaporated to dryness *in vacuo*. The resultant residue was purified by silica gel chromatography (19:1 DCM:MeOH) to give the target compound (**70**) as a pale yellow solid (1.47 g, 5.07 mmol, 86%).

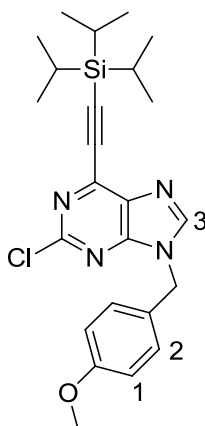
R_f = 0.29 (19:1 DCM:MeOH); m.p. 170-173 °C; UV λ_{max} (EtOH/nm) 224, 310; IR ν_{max}/cm^{-1} 3440, 3310, 3201, 3076, 2957, 2831, 1610, 1561, 1512; 1H NMR (500 MHz, DMSO- d_6) 3.70 (3H, s, OCH₃), 5.19 (1.4 H, s, N⁹-CH₂), 5.46 (0.6 H, s, N⁷-CH₂), 6.64 (0.6 H, s, C²-NH₂ – N⁷-PMB), 6.89 (2H, d, J = 8.8 Hz, Benzyl-H^{3/5}), 6.93 (1.4 H, s, C²-NH₂ – N⁹-PMB), 7.12 (0.6 H, d, J = 8.8 Hz, N⁷-Benzyl-H^{2/6}), 7.23 (1.4 H, d, J = 8.8 Hz, N⁹-Benzyl-H^{2/6}), 8.19 (0.7 H, s, C⁸-H – N⁹-PMB), 8.52 (0.3 H, s, C⁸-H – N⁷-PMB); ^{13}C NMR (125 MHz, DMSO- d_6) 45.6 (N⁹-CH₂), 48.7 (N⁷-CH₂), 55.0 (N⁷-OCH₃), 55.1 (N⁹-OCH₃), 114.1 (Ar-C), 123.2 (Ar-C), 127.9 (Ar-C), 128.1 (Ar-C), 128.5 (Ar-C), 128.8 (Ar-C), 143.1 (Ar-C), 149.4 (Ar-C), 149.8 (Ar-C), 153.9 (Ar-C), 158.8 (Ar-C), 158.9 (Ar-C), 159.9 (Ar-C), 160.0 (Ar-C), 164.4 (Ar-C); HRMS calcd. for C₁₃H₁₃ClN₅O (ES+) m/z 290.0803 [M+H]⁺ found 290.0808.

Note: Greater number of ^{13}C NMR signals than environments due to regioisomers.

9-(4-Methoxybenzyl)-6-((triisopropylsilyl)ethynyl)-9H-purin-2-amine (71)²¹⁹

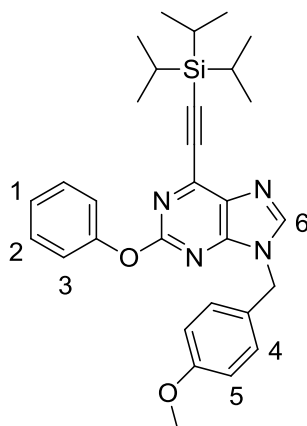
6-Chloropurine intermediate (**70**) (0.50 g, 1.73 mmol), (triisopropylsilyl)acetylene (0.46 ml, 2.07 mmol), copper iodide (6 mg, 0.03 mmol), Pd(PPh₃)₂Cl₂ (21 mg, 0.03 mmol) and triethylamine (0.60 ml, 4.31 mmol) were dissolved in DMF (17 ml). The reaction mixture was degassed (20 min, N₂) and shielded from light then stirred overnight (RT, 18 h). The crude product was filtered over a pad of Celite then dry loaded onto silica. Purification by chromatography on silica (1:1 petrol:EtOAc) gave the target compound (**71**) as a pale yellow solid (0.52 g, 1.19 mmol, 69%).

R_f = 0.59 (1:1 petrol:EtOAc); m.p. 121-124 °C; UV λ_{max} (EtOH/nm) 230, 344; IR $\nu_{\text{max}}/\text{cm}^{-1}$ 3487, 3296, 3183, 2944, 2866, 1594, 1567, 1511; ¹H NMR (500 MHz, DMSO-*d*₆) 1.09-1.17 (21H, m, Si(CH(CH₃)₂)₃), 3.72 (3H, s, -OCH₃), 5.21 (2H, s, N⁹-CH₂), 6.68 (2H, s, C²-NH₂), 6.90 (2H, d, J = 8.7 Hz, C²-H), 7.23 (2H, d, J = 8.7 Hz, C¹-H), 8.19 (1H, s, C³-H); ¹³C NMR (125 MHz, DMSO-*d*₆) 10.6 (Si(CH(CH₃)₂)₃), 18.4 (Si(CH(CH₃)₂)₃), 45.2 (N⁹-CH₂), 55.1 (-OCH₃), 97.1 (C \equiv C-Si), 101.9 (C \equiv C-Si), 114.0 (Ar-C), 127.9 (Ar-C), 128.6 (Ar-C), 128.8 (Ar-C), 140.3 (Ar-C), 143.4 (Ar-C), 153.7 (Ar-C), 158.8 (Ar-C), 160.4 (Ar-C); HRMS calcd. for C₂₄H₃₄N₅OSi (ES+) m/z 436.2527 [M+H]⁺ found 436.2527.

2-Chloro-9-(4-methoxybenzyl)-6-((triisopropylsilyl)ethynyl)-9H-purine (72)

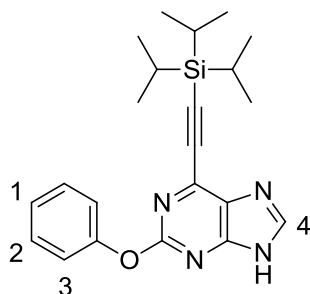
A solution of trimethylsilyl chloride (1.01 mL, 7.95 mmol) in anhydrous DCM (40 mL) was cooled (0 °C) and placed under nitrogen. In a separate flask a solution of benzyltriethylammonium nitrite (**294**) (1.70 g, 7.14 mmol) in anhydrous DCM (15 mL) was cooled (0 °C) and placed under nitrogen. The solution of (**294**) was then added dropwise with stirring to the trimethylsilyl chloride solution at 0 °C. The resulting mixture was stirred (0 °C, 15 min) at which point a cooled (0 °C) solution of 9-(4-methoxybenzyl)-6-((triisopropylsilyl)ethynyl)-9H-purin-2-amine (**71**) (690 mg, 1.59 mmol) in anhydrous DCM (15 mL) was gradually added. The reaction mixture was stirred (0 °C, 30 min) then the ice bath was removed stirring was continued (RT, 30 min). The resulting solution was washed with NaHCO_{3(aq)} (3 x 70 mL), dried (phase separator) and purified by silica based MPCL (1:4 EtOAc/petrol) to give (**72**) as a colourless oil (518 mg, 1.14 mmol, 72%).

R_f = 0.23 (1:4 EtOAc/petrol); UV λ_{\max} (EtOH/nm) 254.1; IR $\nu_{\max}/\text{cm}^{-1}$ 2943, 2865, 1568, 1514; ¹H NMR (500 MHz, DMSO-*d*₆) δ 1.07-1.23 (21H, m, Si(CH(CH₃)₂)₃), 3.72 (3H, s, OCH₃), 5.39 (2H, s, ArCH₂Ar) 6.91 (2H, d, J = 8.6 Hz, C²-H), 7.30 (2H, d, J = 8.6 Hz, C¹-H), 8.78 (1H, s, C³-H); ¹³C NMR (125 MHz, DMSO-*d*₆) δ 10.5 (Si(CH(CH₃)₂)₃), 18.4 (Si(CH(CH₃)₂)₃), 46.3 (N⁹-CH₂), 55.1 (-OCH₃), 100.2 (C \equiv C-Si), 102.5 (C \equiv C), 114.1 (Ar-C), 127.7 (Ar-C), 129.2 (Ar-C), 134.1 (Ar-C), 140.5 (Ar-C), 148.6 (Ar-C), 152.3 (Ar-C), 153.6 (Ar-C), 159.0 (Ar-C); HRMS calcd for C₂₄H₃₂ClN₄OSi [M+H]⁺ 455.2028 Found 455.2031.

9-(4-Methoxybenzyl)-2-phenoxy-6-((triisopropylsilyl)ethynyl)-9H-purine (73)

A vial was charged with phenol (129 mg, 1.37 mmol) and K_3PO_4 (484 mg, 2.28 mmol). A solution of 2-chloro-9-(4-methoxybenzyl)-6-((triisopropylsilyl)ethynyl)-9H-purine (**72**) (518 mg, 1.14 mmol) in anhydrous toluene (6 mL) was then added followed by $Pd(OAc)_2$ (5.1 mg, 2.28×10^{-2} mmol) and XPhos (16.3 mg, 3.42×10^{-2} mmol). The vial was capped and degassed (N_2 , 20 min) then heated (100 °C, 1 h). The crude mixture was cooled and diluted with DCM (30 mL) and filtered through Celite. The resulting solution was washed with $NaHCO_{3(aq)}$ (3 x 30 mL), dried (phase separator) and dry loaded onto silica. The title compound (**73**) was purified by MPLC on silica (1:3 EtOAc/petrol) as a colourless oil (476 mg, 0.93 mmol, 82%).

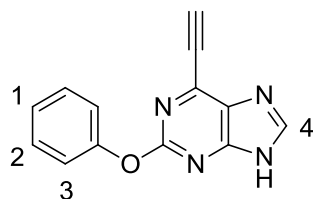
R_f = 0.25 (5:95 MeOH/DCM); UV λ_{max} (EtOH/nm) 273.1; IR ν_{max}/cm^{-1} 3068, 2943, 2864, 1574, 1514, 1490; 1H NMR (500 MHz, $CDCl_3$) 1.07-1.30 (21H, m, $Si(CH(CH_3)_2)_3$), 3.79 (3H, s, OCH_3), 5.12 (2H, s, N^9-CH_2), 6.68 (2H, s, C^2-NH_2), 6.81 (2H, d, J = 8.8 Hz, C^4-H), 7.15 (2H, d, J = 8.9 Hz, C^5-H), 7.22-7.27 (3H, m, $C^{1/3}-H$), 7.38-7.46 (2H, m, C^2-H), 7.91 (1H, s, C^6-H); ^{13}C NMR (125 MHz, $DMSO-d_6$) 11.2 ($Si(CH(CH_3)_2)_3$), 18.7 ($Si(CH(CH_3)_2)_3$), 47.1 (N^9-CH_2), 55.3 (OCH_3), 100.6 ($C\equiv C-Si$), 103.1 ($C\equiv C-Si$), 108.5 (Ar-C), 114.3 (Ar-C), 121.6 (Ar-C), 124.9 (Ar-C), 126.8 (Ar-C), 129.3 (Ar-C), 129.8 (Ar-C), 132.0 (Ar-C), 143.0 (Ar-C), 144.3 (Ar-C), 153.5 (Ar-C), 159.8 (Ar-C), 161.1 (Ar-C); HRMS calcd for $C_{30}H_{37}N_4O_2Si$ $[M+H]^+$ 513.2680 Found 513.2665.

2-Phenoxy-6-((triisopropylsilyl)ethynyl)-9*H*-purine (68)

A solution of 9-(4-methoxybenzyl)-2-phenoxy-6-((triisopropylsilyl)ethynyl)-9*H*-purine (**73**) (476 mg, 0.93 mmol) in TFA (10 mL) was heated to reflux (75 °C, 3 h). The resulting red solution was neutralised over saturated NaHCO_{3(aq)} (50 mL), which was then extracted with EtOAc (3 x 50 mL). The organic layers were pooled then dried (MgSO₄) and dry loaded onto silica. The title compound (**68**) was purified by MPLC on silica (5:95 MeOH/DCM) as a yellow oil (360 mg, 9.2 mmol, 99%).

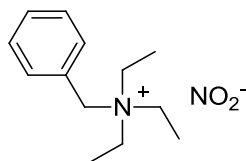
R_f = 0.25 (5:95 MeOH/DCM); UV λ_{max} (EtOH/nm) 254.0; IR ν_{max}/cm^{-1} 3070, 2943, 2865, 1575, 1497; ¹H NMR (500 MHz, DMSO-*d*₆) δ 1.05-1.26 (21H, m, (Si(CH(CH₃)₂)₃), 7.15-7.52 (C¹⁻³-H), 8.46 (1H, C⁴-H); ¹³C NMR (125 MHz, CDCl₃) δ 10.6 (SiCH), 18.4 (CHCH₃), 54.9 (Si-C \equiv C), 100.1 (C \equiv C), 121.4 (Ar-C), 124.9 (Ar-C), 129.7 (Ar-C), 153.4 (Ar-C), 160.4 (Ar-C); HRMS calcd for C₂₂H₂₉N₄OSi [M+H]⁺ 393.2105 Found 393.2106.

Note: not all carbon atoms are visible

6-Ethynyl-2-phenoxy-9H-purine (55)

The title compound was prepared following **general procedure A** using: 2-phenoxy-6-((triisopropylsilyl)ethynyl)-9H-purine (**68**) (300 mg, 0.77 mmol) and TBAF (1 M in THF (842 μ L, 0.84 mmol) in THF (30 mL). The crude product was purified by MPLC on silica (5:95 MeOH/DCM) to give the title compound (**55**) as a white solid (176 mg, 0.75 mmol, 99%).

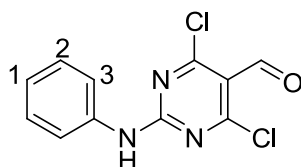
R_f = 0.06 (5:95 MeOH/DCM); m.p. 193 $^{\circ}$ C (dec.); UV λ_{\max} (EtOH/nm) 218; IR $\nu_{\max}/\text{cm}^{-1}$ 3232, 3072, 2775, 2562, 2488, 2110, 1613, 1577, 1491; ^1H NMR (500 MHz, DMSO- d_6) δ 4.99 (1H, s, CH –ethynyl), 7.21 (2H, d, J = 8.5 Hz, C³H), 7.25 (1H, tt, J = 7.2 Hz and 1.1 Hz, C¹-H), 7.44 (2H, app. t, J = 8.4 Hz, C²-H), 8.51 (1H, s, C⁴-H), 13.58 (1H, br s, NH); ^{13}C NMR (125 MHz, DMSO- d_6) δ 88.9, 121.5, 124.9, 129.7, 153.4, 160.4; HRMS calcd for C₁₃H₉N₄O $[M+H]^+$ 237.0771 Found 237.0773.

N-Benzyltriethylammonium nitrite (294)³⁰⁹

To a solution of benzyltriethylammonium tetrafluoroborate (1.4 g, 5.0 mmol) in a mixture of water (7.5 mL) and ethanol (6 mL) was prepared. Potassium nitrite (426 mg, 5.0 mmol) dissolved in water (0.5 mL) was added dropwise at RT and the resulting mixture was stirred overnight then filtered. The solvent was removed *in vacuo* and the resulting crude product was redissolved in DCM and further dried using a phase separator. The DCM was evaporated to give the title compound as an off-white crystalline solid (1.06 g, 4.5 mmol, 89%).

m.p. 137 °C (Lit 132.0-132.3), ^1H NMR (500 MHz, DMSO- d_6) δ 1.30 (9H, t, J = 7.2 Hz, 3 x CH₃), 3.16 (6H, q, J = 7.2 Hz, 3 x CH₂), 4.48 (2H, s, ArCH₂), 7.45-7.61 (5H, m, 5 x Ar-H); LRMS (ES+) m/z = 239.2 [M+H]⁺.

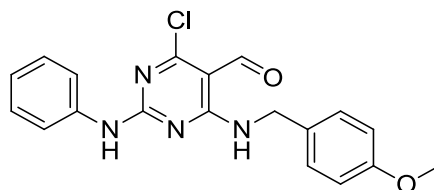
4,6-Dichloro-2-(phenylamino)pyrimidine-5-carbaldehyde (228)



To a flask containing DMF (190 μL , 2.46 mmol) cooled to 0 °C, was carefully added POCl₃ (2.21 mL, 24.10 mmol) dropwise with stirring (10 min). The mixture was allowed to warm (RT, 30 min) after which 6-hydroxy-2-(phenylamino)pyrimidin-4(1*H*)-one (**73**) (500 mg, 2.46 mmol) was added in portions. The resulting suspension was stirred (RT, 1 h), heated to reflux (110 °C, 3 h) then cooled to RT and quenched over rapidly stirred ice water. The pH was adjusted to 7 with solid NaHCO₃ and the resulting aqueous mixture was extracted with DCM (2 x 100 mL). The organic layers were pooled, dried (phase separator) and dry loaded onto silica. The title compound was purified by MPLC on silica (3:7 EtOAc/petrol) as a light yellow solid (323 mg, 1.21 mmol, 49%).

R_f = 0.56 (3:7 EtOAc/petrol); m.p. 135 °C; UV λ_{max} (EtOH/nm) 232.3; IR ν_{max} /cm⁻¹; ^1H NMR (500 MHz, CDCl₃) δ 7.18-7.23 (1H, m, C¹-H), 7.40 (2H, app. t, J = 7.6 Hz, C²-H), 7.60 (2H, d, 7.6 Hz, C³-H), 7.72 (1H, br s, ArNHAr), 10.31 (1H, s, CHO); ^{13}C NMR (125 MHz, CDCl₃) δ 114.7 (Ar-C), 120.9 (Ar-C), 124.5 (Ar-C), 128.9 (Ar-C), 137.5 (Ar-C), 157.7 (Ar-C), 185.0 (CHO); LRMS (ES+) m/z = 168.0 [M+H]⁺.

4-Chloro-6-((4-methoxybenzyl)amino)-2-(phenylamino)pyrimidine-5-carbaldehyde (229)

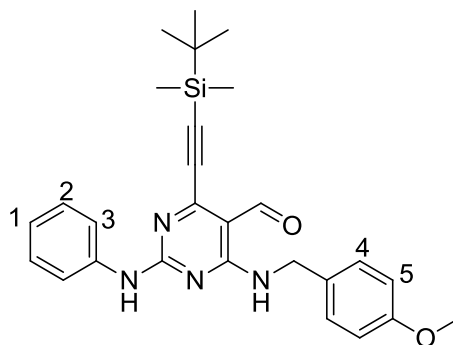


To a solution of 4,6-dichloro-2-(phenylamino)pyrimidine-5-carbaldehyde (**122**) (50 mg, 0.19 mmol) in anhydrous DCM (5 mL) was added 4-methoxybenzylamine (25 μ L, 0.20 mmol) and DIPEA (34 μ L, 0.20 mmol). The reaction mixture was stirred (RT, 1 h) after which no starting material remained (LC-MS). The crude product was dry loaded onto KP-NH silica and purified by KP-NH MPLC on silica (3:7 EtOAc/petrol) to give the target compound as a white solid (59 mg, 0.16 mmol, 85%).

R_f = 0.40 (3:7 EtOAc/petrol, KP-NH silica); m.p. 128 $^{\circ}$ C; UV λ_{max} (EtOH/nm) 249.1; IR ν_{max}/cm^{-1} 3421, 3310, 3281, 3191, 2871, 2121, 1675 (CHO), 1611; 1H NMR (500 MHz, DMSO- d_6) δ 1.35 (3H, s, OCH₃), 4.67 (2H, d, J = 5.9 Hz, NHCH₂), 6.90 (2H, d, J = 8.6 Hz, C⁴-H), 6.99 – 7.09 (1H, m, C¹-H), 7.19 – 7.39 (4H, m, C^{2/3}-H) 7.65 (2H, d, J = 8.5 Hz, C⁵-H), 9.67 (1H, br s, ArNHCH₂), 10.01 (1H, s, CHO), 10.40 (1H, br s, ArNHAr); ^{13}C NMR (125 MHz, CDCl₃) δ 42.1 (CH₂), 56.1 (OCH₃), 114.1 (Ar-C), 118.9 (Ar-C), 122.2 (Ar-C), 129.1 (Ar-C), 130.5 (Ar-C), 189.1 (CHO); HRMS calcd for C₁₉H₁₈ClN₄O₂ [M+H]⁺ 369.1118 Found 369.1110.

Note: not all carbon atoms visible

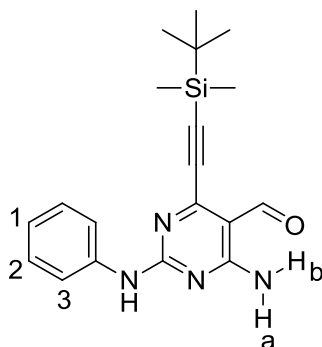
4-((*tert*-Butyldimethylsilyl)ethynyl)-6-((4-methoxybenzyl)amino)-2-(phenylamino)pyrimidine-5-carbaldehyde (230**)**



The title compound was prepared following general **procedure D** using: 4-chloro-6-((4-methoxybenzyl)amino)-2-(phenylamino)pyrimidine-5-carbaldehyde (**123**) (30 mg, 8.15×10^{-2} mmol), *tert*-butyldimethylsilyl acetylene boronic acid pinacol ester (33 mg, 0.12 mmol), Cs_2CO_3 (40 mg, 0.12 mmol) and $\text{Pd}(\text{PPh}_3)_4$ (9.4 mg, 8.15×10^{-3} mmol) in dioxane (1 mL). The title compound (**124**) was purified by KP-NH MPLC on silica (1:4 EtOAc/petrol) to give the final product as a yellow oil (28 mg, 5.92×10^{-2} mmol, 73%).

R_f = 0.41 (1:4 EtOAc/petrol, KP-NH silica); UV λ_{max} (EtOH/nm) 252.1; IR $\nu_{\text{max}}/\text{cm}^{-1}$ 3459, 3299, 3276, 3205, 2843, 2099, 1680 (CHO), 1603, 1571; ^1H NMR (500 MHz, CDCl_3) δ 0.23 (6H, $\text{Si}(\text{CH}_3)_2$), 1.00 (9H, $\text{C}(\text{CH}_3)_3$), 3.80 (3H, s, OCH_3), 4.69 (2H, d, J = 6.9 Hz, $\text{C}^4\text{-H}$), 7.06 (1H, tt, J = 7.4 and 1.3 Hz, $\text{C}^1\text{-H}$), 7.25 (2H, d, J = 7.1 Hz, $\text{C}^5\text{-H}$), 7.29 (2H, app. t, J = 7.6 Hz, $\text{C}^2\text{-H}$), 7.35 (1H, br s, ArNHAr), 7.54 (2H, d, J = 7.8 Hz, $\text{C}^3\text{-H}$), 9.40 (1H, br s, ArNHCH_2), 10.21 (1H, s, CHO); ^{13}C NMR (125 MHz, CDCl_3) δ -4.9 (SiC), 26.2 ($\text{SiC}(\text{CH}_3)_3$), 44.1 (NCH_2Ar), 55.3 (OCH_3), 102.3 (Ar-C), 114.1 (Ar-C), 120.1 (Ar-C), 123.6 (Ar-C), 128.7 (Ar-C), 128.9 (Ar-C), 138.3 (Ar-C), 159.0 (Ar-C), 189.9 (CHO); HRMS calcd for $\text{C}_{27}\text{H}_{33}\text{N}_4\text{O}_2\text{Si}$ $[\text{M}+\text{H}]^+$ 473.2367 Found 473.2361.

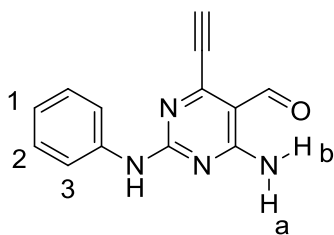
4-Amino-6-((*tert*-butyldimethylsilyl)ethynyl)-2-(phenylamino)pyrimidine-5-carbaldehyde (226**)**



A solution of 4-((*tert*-butyldimethylsilyl)ethynyl)-6-((4-methoxybenzyl)amino)-2-(phenylamino)pyrimidine-5-carbaldehyde (**124**) (25 mg, 5.29×10^{-2} mmol) in TFA (1 mL) was heated (80 °C, 1 h). The resulting solution was added dropwise to $\text{NaHCO}_{3(\text{aq})}$ (30 mL) then extract with DCM (2 x 15 mL). The organic layers were pooled, dried (phase separator) and dry loaded onto silica. The title (**125**) compound was purified by MPLC on silica (3:7 EtOAc/Hexane) as a yellow oil (18 mg, 5.29×10^{-2} mmol, 97%).

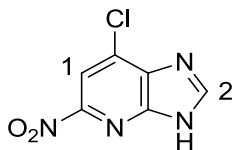
R_f = 0.43 (3:7 EtOAc/petrol); UV λ_{max} (EtOH/nm) 265.3; IR $\nu_{\text{max}}/\text{cm}^{-1}$ 3451, 3310, 3279, 3211, 2839, 2117, 1701 (CHO), 1601, 1533; ^1H NMR (500 MHz, CDCl_3) δ 0.24 (6H, $\text{Si}(\text{CH}_3)_2$), 1.01 (9H, $\text{C}(\text{CH}_3)_3$), 5.66 (1H, br s, N-H a) 7.11 (1H, tt, J = 7.3 Hz and 1.1 Hz), 7.32 (1H, br s, ArNHAr), 7.34 (2H, app. t, J = 7.3 Hz, $\text{C}^2\text{-H}$), 7.59 (2H, d, J = 7.4 Hz), 8.65 (1H, br s, N-H b) 10.24 (1H, s, CHO); ^{13}C NMR (125 MHz, CDCl_3) δ -4.8 (SiC), 26.3 ($\text{SiC}(\text{CH}_3)_3$), 96.3 ($\text{C}\equiv\text{C-Si}$), 113.9 (Ar-C), 121.1 (Ar-C), 122.4 (Ar-C), 129.8 (Ar-C), 130.1 (Ar-C), 137.3 (Ar-C), 159.5 (Ar-C), 189.8 (CHO); HRMS calcd for $\text{C}_{19}\text{H}_{25}\text{N}_4\text{OSi}$ $[\text{M}+\text{H}]^+$ 353.1792 Found 353.1796.

Note: not all carbon atoms visible.

4-Amino-6-ethynyl-2-(phenylamino)pyrimidine-5-carbaldehyde (101)

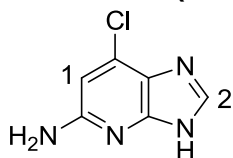
The title compound was prepared following **general procedure A** using: 4-amino-6-((*tert*-butyldimethylsilyl)ethynyl)-2-(phenylamino)pyrimidine-5-carbaldehyde (**125**) (115 mg, 0.33 mmol) and TBAF (1 M in THF) (360 μ L, 0.36 mmol) in THF (23 mL). The crude product was purified by MPLC on silica (3:7 EtOAc/Hexane) to give the title compound (**126**) as a yellow crystalline solid (53 mg, 0.22 mmol, 68%).

R_f = 0.48 (2:3 EtOAc/petrol); m.p. 185 $^{\circ}$ C; UV λ_{max} (EtOH/nm) 234.0, 286.5, 351.5; IR ν_{max}/cm^{-1} 3483, 3307, 3283, 3212, 2859, 2112, 1646 (CHO), 1612, 1565, 1523; 1H NMR (500 MHz, $CDCl_3$) δ 3.48 (1H, s, $C\equiv C-H$), 5.71 (H, br s, C^4-NH a), 7.71 (1H, tt, J = 7.5 and 1.1 Hz, C^3-H), 7.41 (2H, app. t, J = 7.6 Hz, C^2-H), 7.58 (2H, d, J = 7.6 Hz, ^1-H), 7.58 (1H, br s, ArNHAr), 8.63 (1H, br s, C^4-NH b), 10.20 (1H, s, CHO); ^{13}C NMR (125 MHz, $CDCl_3$) δ 77.9 ($C\equiv C-H$), 84.4 ($C\equiv C$), 120.5 (Ar-C), 124.1 (Ar-C), 129.0 (Ar-C), 137.9 (Ar-C), 155.9 (Ar-C), 160.0 (Ar-C), 162.8 (Ar-C), 167.5 (Ar-C), 189.6 (CHO). HRMS calcd. for $C_{13}H_{11}N_4O$ (ES+) m/z 239.0927 $[M+H]^+$ found 239.0931.

7-Chloro-5-nitro-3*H*-imidazo[4,5-*b*]pyridine (258)²⁹⁷

A solution of *tert*-butyl 7-chloro-5-nitro-3*H*-imidazo[4,5-*b*]pyridine-3-carboxylate (**107**) (500 mg, 1.67mmol) in TFE (50 mL) was heated to reflux (85 °C, 3 h) resulting in complete Boc deprotection (observed by LC-MS). The solvent was removed until *ca.* 5 mL remained resulting precipitation of the product as an orange solid. The precipitate was filtered then washed with petrol (3 x 15 mL) then dried under vacuum to give (**258**) as an orange solid (322 mg, 1.63 mmol, 97%).

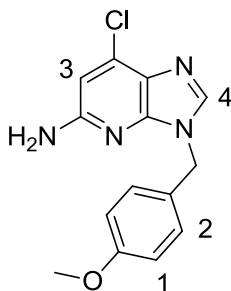
m.p. 250 °C (Lit 249.5); ¹H NMR (500 MHz, DMSO-*d*₆) 8.40 (1H, s, C¹-H), 8.91 (1H, s, C²-H), 14.18 (1H, br s, NH); LRMS (ES+) *m/z* = 199.0 [M+H]⁺.

7-Chloro-3*H*-imidazo[4,5-*b*]pyridin-5-amine (259)³¹⁰

7-Chloro-5-nitro-3*H*-imidazo[4,5-*b*]pyridine (**258**) (500 mg, 2.53 mmol) was dissolved in a mixture of absolute ethanol (15 mL), water (5 mL) and glacial AcOH (1.13 mL, 19.7 mmol). Iron powder (310 mg, 5.56 mmol) was added in one portion with stirring and the reaction mixture was heated (80 °C, 3 h). The resulting dark brown solution was filtered through Celite and the solvent was removed. The crude product was redissolved in MeOH (25 mL) then dry loaded onto silica and purified *via* MPLC on silica (1:4 MeOH/DCM) to give (**259**) as a light yellow solid (370 mg, 2.20 mmol, 87%), which was used immediately in the next reaction.

*R*_f = 0.60 (1:4 MeOH/DCM); m.p. 228-231 °C (Lit 230 °C); ¹H NMR (500 MHz, DMSO-*d*₆) 6.80 (1H, d, C¹-H), 3.30 (2H, br s, NH₂), 8.1 (1H, s, C²-H), 8.9 (1H, br s, NH); ¹H NMR (125 MHz, DMSO-*d*₆) 109 (Ar-C), 150 (Ar-C); HRMS calcd for C₆H₆ClN₄ [M+H]⁺ 169.0276 Found 169.0274.

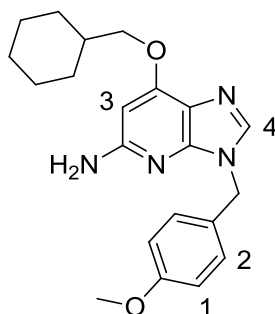
Note: not all carbon atoms visible

7-Chloro-3-(4-methoxybenzyl)-3*H*-imidazo[4,5-*b*]pyridin-5-amine (260)

7-Chloro-5-nitro-3*H*-imidazo[4,5-*b*]pyridine (**259**) (40 mg, 0.24 mmol) was dissolved in anhydrous DMF (1 mL). Anhydrous K₂CO₃ (36 mg, 0.26 mmol) was added followed by 4-methoxybenzyl chloride (34 μ L, 0.25 mmol) with stirring. The reaction mixture was placed under nitrogen and heated (65 °C, 18 h). The solvent was evaporated to dryness and the crude product was redissolved in EtOAc (30 mL) then washed with brine (3 x 30 mL). The organic layer was dried (Na₂SO₄) then dry loaded onto silica and purified by MPLC on silica (2:3 EtOAc/petrol) to give (**260**) as a light yellow solid (29 mg, 0.10 mmol, 42 %).

R_f = 0.21 (3:2 EtOAc/petrol); m.p. 105 °C; UV λ_{\max} (EtOH/nm) 311.0; IR $\nu_{\max}/\text{cm}^{-1}$ 3431, 3312, 3198, 3022, 2940, 2798, 1571, 1513; ¹H NMR (500 MHz DMSO-*d*₆) 3.71 (3H, s, OCH₃), 5.22 (2H, s, Ar-CH₂-Ar), 6.24 (2H, br s, NH₂), 6.48 (1H, s, C³-H), 6.88 (2H, d, J = 8.7 Hz, C²-H), 7.23 (2H, d, J = 8.8 Hz, C¹-H), 8.07 (1H, s, C⁴-H); ¹³C NMR (125 MHz DMSO-*d*₆) 45.4 (Ar-CH₂-Ar), 55.1 (OCH₃), 103.8 (Ar-C), 114.0 (Ar-C), 124.4 (Ar-C), 128.7 (Ar-C), 129.2 (Ar-C), 133.9 (Ar-C), 140.5 (Ar-C), 146.6 (Ar-C), 157.4 (Ar-C), 158.7 (Ar-C); HRMS calcd for C₁₄H₁₄ClN₄O [M+H]⁺ 289.0851 Found 289.0855.

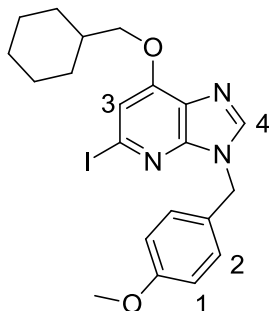
7-(Cyclohexylmethoxy)-3-(4-methoxybenzyl)-3*H*-imidazo[4,5-*b*]pyridin-5-amine (261)



To a solution of NaH (60% in mineral oil) (96 mg, 0.24 mmol) in anhydrous DMSO (1 mL) was added cyclohexylmethanol (442 μ L, 3.59 mmol). The flask was flushed with nitrogen and stirred until no further gas was evolved (*ca.* 30 min). In a separate flask a solution of 7-chloro-3-(4-methoxybenzyl)-3*H*-imidazo[4,5-*b*]pyridin-5-amine (**260**) (172 mg, 0.60 mmol) in anhydrous DMSO (2 mL) was prepared and placed under nitrogen. The freshly prepared cyclohexylmethoxide solution was then introduced dropwise with stirring. The reaction mixture was heated by microwave irradiation (100 $^{\circ}$ C, 2 h) resulting in consumption of the starting material. The reaction mixture was added to water (50 mL) then extracted with ether (3 x 50 mL). The ether layers were combined then washed with water (4 x 50 mL) and brine (50 mL) then dried (MgSO_4) and dry loaded onto isolate. The product (**261**) was purified *via* MPLC on silica (4:1 EtOAc/petrol) as a colourless oil (164 mg, 0.45 mmol, 75%).

R_f = 0.47 (4:1 EtOAc/Petrol); UV λ_{max} (EtOH/nm) 271.0; IR $\nu_{\text{max}}/\text{cm}^{-1}$ 3311, 2954, 2899, 2163, 1672, 1598, 1516; ^1H NMR (500 MHz $\text{DMSO-}d_6$) 0.90-1.87 (11H, m, cyclohexyl), 3.71 (3H, s, OCH_3), 4.00 (2H, d, J = 6.7 Hz, OCH_2), 5.17 (2H, br s, NH_2), 5.90 (1H, s, $\text{C}^3\text{-H}$), 6.87 (2H, d, J = 8.7 Hz, $\text{C}^2\text{-H}$), 7.20 (2H, d, J = 8.8 Hz, $\text{C}^1\text{-H}$), 7.82 (1H, s, $\text{C}^4\text{-H}$); ^{13}C NMR (125 MHz $\text{DMSO-}d_6$) 25.2 (CH_2), 26.0 (CH_2), 29.1 (CH_2), 37.0 (CH), 45.0 (Ar- CH_2), 55.1 (CH_3), 73.3 (CH_2), 87.5 (Ar-C), 113.9 (Ar-C), 118.2 (Ar-C), 128.7 (Ar-C), 129.7 (Ar-C), 137.9 (Ar-C), 147.4 (Ar-C), 157.8 (Ar-C), 158.5 (Ar-C), 158.6 (Ar-C); HRMS calcd for $\text{C}_{21}\text{H}_{27}\text{N}_4\text{O}_2$ $[\text{M}+\text{H}]^+$ 367.2129 Found 367.2132.

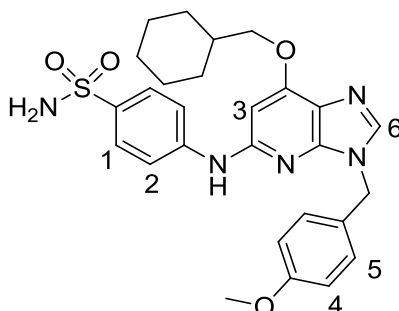
7-(Cyclohexylmethoxy)-5-iodo-3-(4-methoxybenzyl)-3*H*-imidazo[4,5-*b*]pyridine (262)



To a solution of 7-(cyclohexylmethoxy)-3-(4-methoxybenzyl)-3*H*-imidazo[4,5-*b*]pyridin-5-amine (**261**) (112 mg, 0.31 mmol) in anhydrous THF (4 mL) was added diiodomethane (123 μ L, 1.50 mmol) and CuI (59 mg, 0.31 mmol). Isoamyl nitrite (187 μ L, 0.92 mmol) was then introduced with stirring and the reaction mixture was heated to reflux (70 $^{\circ}$ C, 4 h). The dark brown solution was filtered through Celite and diluted with EtOAc (40 mL). The organic solution was washed with sodium thiosulfate solution (10% in H₂O) (2 x 40 mL) and brine (40 mL) then dried (MgSO₄) and dry loaded onto silica. The title compound (**262**) was purified by MPLC on silica (3:7 EtOAc/petrol) as a yellow oil (64 mg, 0.13 mmol, 44%).

R_f = 0.19 (3:7 EtOAc/petrol); UV λ_{\max} (EtOH/nm) 262.0; IR $\nu_{\max}/\text{cm}^{-1}$ 3333, 2951, 2891, 2122, 1672, 1584, 1521; ^1H NMR (500 MHz DMSO-*d*₆) 0.98-1.89 (11H, m, cyclohexyl), 3.71 (3H, s, OCH₃), 4.19 (2H, d, J = 6.5 Hz, OCH₂), 5.17 (2H, s, CH₂), 6.90 (2H, d, J = 8.7 Hz, C²-H), 7.18 (1H, s, C³-H), 7.26 (2H, d, J = 8.8 Hz, C¹-H), 8.31 (1H, s, C⁴-H); ^{13}C NMR (125 MHz DMSO-*d*₆) 25.1 (CH₂), 25.9 (CH₂), 28.9 (CH₂), 37.0 (CH), 45.8 (Ar-CH₂), 55.1 (CH₃), 74.4 (CH₂), 112.0 (Ar-C), 112.7 (Ar-C), 114.1 (Ar-C), 124.6 (Ar-C), 128.8 (Ar-C), 129.0 (Ar-C), 142.6 (Ar-C), 148.5 (Ar-C), 157.0 (Ar-C), 158.8 (Ar-C); HRMS calcd for C₂₁H₂₅IN₃O₂ [M+H]⁺ 478.0986 Found 478.0980.

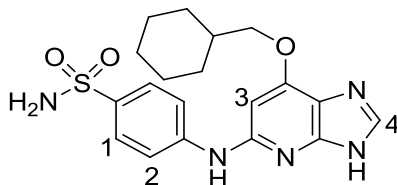
4-((7-(Cyclohexylmethoxy)-3-(4-methoxybenzyl)-3*H*-imidazo[4,5-*b*]pyridin-5-yl)amino)benzenesulfonamide (263)



To a solution of 7-(cyclohexylmethoxy)-5-iodo-3-(4-methoxybenzyl)-3*H*-imidazo[4,5-*b*]pyridine (**262**) (48 mg, 0.10 mmol) in anhydrous MeCN (2 mL) was added sulfanilamide (19 mg, 0.11 mmol), anhydrous K₂CO₃ (28 mg, 0.20 mmol), Pd₂(dba)₃ (2.3 mg, 4.0 × 10⁻³ mmol) and XPhos (1.9 mg, 4.0 × 10⁻³ mmol). The reaction mixture was degassed (N₂, 30 min) then heated (80 °C, 2 h). The resulting solution was cooled to RT and filtered through Celite then diluted with EtOAc (20 mL). The organic solution was washed sequentially with HCl_(aq) (1 M) (20 mL), NaHCO₃ (20 mL) and brine (30 mL) then dried (Na₂SO₄) and dry loaded onto silica. The title compound (**263**) was purified by normal phase MPLC (7:3 EtOAc/petrol) followed by C18 reverse phase MPLC (3:7 water (0.1% HCOOH)/MeOH (0.1% HCOOH)) as a white solid (23 mg, 4.4 × 10⁻² mmol, 43%).

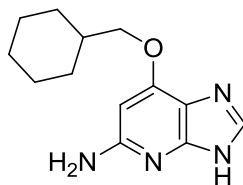
*R*_f = 0.59 (7:3 EtOAc/petrol); m.p. 142 °C; UV λ_{max} (EtOH/nm) 257.0; IR ν_{max}/cm⁻¹ 3329, 2933, 2874, 2158, 1662, 1588, 1501; ¹H NMR (500 MHz, CDCl₃) δ 1.00-1.97 (11H, m, cyclohexyl), 3.79 (3H, s, OCH₃), 4.01 (2H, d, *J* = 6.1 Hz,), 4.76 (2H, br s, NH₂), 5.28 (2H, s, OCH₂), 6.17 (1H, s, C³-H), 6.79 (1H, br s, ArNHAr), 6.88 (2H, d, *J* = 8.8 Hz, C⁵-H), 7.24 (2H, d, *J* = 8.7 Hz, C⁴-H), 7.61 (2H, *J* = 8.8 Hz, C^{1/2}-H), 7.81 (2H, *J* = 8.8 Hz, C^{1/2}-H); ¹³C NMR (125 MHz, CDCl₃) δ 25.7 (CH₂), 26.4 (CH₂), 29.8 (CH₂), 37.6 (CH₂), 46.9 (CH), 55.4 (CH₂), 74.8 (OCH₃), 90.7 (OCH₂), 114.3 (Ar-C), 117.1 (Ar-C), 128.0 (Ar-C), 129.1 (Ar-C), 139.7 (Ar-C), 145.5 (Ar-C), 152.1 (Ar-C); HRMS calcd for C₂₇H₃₂N₅O₄S [M+H]⁺ 522.2170 Found 522.2166.

4-((7-(Cyclohexylmethoxy)-3*H*-imidazo[4,5-*b*]pyridin-5-yl)amino)benzenesulfonamide (250**)**



A solution of 4-((7-(cyclohexylmethoxy)-3-(4-methoxybenzyl)-3*H*-imidazo[4,5-*b*]pyridin-5-yl)amino)benzenesulfonamide (**263**) (22 mg, 4.20×10^{-2} mmol) in TFA (1 mL) was heated to reflux (75 °C, 2 h). The resulting solution was neutralised over saturated $\text{NaHCO}_{3(\text{aq})}$ (25 mL), which was then extracted with EtOAc (3 x 30 mL). The organic layers were pooled then dried (MgSO_4) and dry loaded onto silica. The title compound (**250**) was purified by preparative TLC (5:95 MeOH/DCM) as a white solid (16.7 mg, 4.18×10^{-2} mmol, 99%).

R_f = 0.25 (5:95 MeOH/DCM); m.p. 165-166 °C; UV λ_{max} (EtOH/nm) 274.7 and 324.3; IR $\nu_{\text{max}}/\text{cm}^{-1}$ 3332, 2925, 2852, 2164, 1677, 1583, 1500; ^1H NMR (500 MHz, MeOD) δ 1.07-2.05 (11H, m, cyclohexyl), 4.03 (2H, d, J = 6.2 Hz, OCH_2), 6.33 (1H, s, $\text{C}^3\text{-H}$), 7.77 (2H, d, J = 8.9 Hz, $\text{C}^{1/2}\text{-H}$), 7.92 (2H, d, J = 8.8 Hz, $\text{C}^{1/2}\text{-H}$), 7.96 (1H, s, $\text{C}^4\text{-H}$); ^{13}C NMR (125 MHz, CDCl_3) δ 26.9 (CH_2), 27.6 (CH_2), 30.8 (CH_2), 38.9 (CH), 74.9 (CH_2O), 90.9 (Ar-C), 117.9 (Ar-C), 128.2 (Ar-C); HRMS calcd for $\text{C}_{19}\text{H}_{24}\text{N}_5\text{O}_3\text{S}$ $[\text{M}+\text{H}]^+$ 522.2170 Found 522.2166.

7-(Cyclohexylmethoxy)-3*H*-imidazo[4,5-*b*]pyridin-5-amine (254)

A solution of 7-(cyclohexylmethoxy)-3-(4-methoxybenzyl)-3*H*-imidazo[4,5-*b*]pyridin-5-amine (**261**) (35 mg, 9.55×10^{-2} mmol) in TFA (1 mL) was heated to reflux (75 °C, 2 h). The resulting solution was neutralised over saturated $\text{NaHCO}_{3(\text{aq})}$ (25 mL), which was then extracted with EtOAc (3 x 30 mL). The organic layers were pooled then dried (MgSO_4) and dry loaded onto silica. The title compound (**254**) was purified by MPLC on silica (1:9 MeOH/DCM) as a white solid (16.5 mg, 6.69×10^{-2} mmol, 70%).

R_f = 0.16 (1:9 MeOH/DCM); m.p. 99-102 °C; UV λ_{max} (EtOH/nm) 244.7 and 292.9; IR $\nu_{\text{max}}/\text{cm}^{-1}$ 3447, 3323, 3187, 2923, 2850, 2795, 2026, 1591, 1527; ^1H NMR (500 MHz, CDCl_3) δ 1.03-2.00 (11H, m, cyclohexyl), 4.03 (2H, d, J = 6.1 Hz, OCH_2), 4.37 (1H, br s, NH_2), 5.91 (1H, s, C_6H), 7.77 (1H, s, C_2H), 9.89 (1H, br s, N_3H); ^{13}C NMR (125 MHz, CDCl_3) δ 25.7, 26.4, 29.8, 37.5, 74.4, 88.1, 157.3; HRMS calcd. for $\text{C}_{13}\text{H}_{19}\text{N}_4\text{O}$ (ES+) m/z 247.1553 $[\text{M}+\text{H}]^+$ found 247.1556.

Appendix

i - Small-Molecule X-ray Crystallography Data

Pyrrolopyrimidine **88**Table 9. Crystal data and structure refinement for **88**.

Identification code	88	
Chemical formula (moiety)	C ₁₄ H ₁₀ N ₄	
Chemical formula (total)	C ₁₄ H ₁₀ N ₄	
Formula weight	234.26	
Temperature	150(2) K	
Radiation, wavelength	CuK α , 1.54178 Å	
Crystal system, space group	monoclinic, P12 ₁ /n1	
Unit cell parameters	a = 12.1047(2) Å	$\alpha = 90^\circ$
	b = 10.0066(2) Å	$\beta = 99.405(2)^\circ$
	c = 20.2146(3) Å	$\gamma = 90^\circ$
Cell volume	2415.62(7) Å ³	
Z	8	
Calculated density	1.288 g/cm ³	
Absorption coefficient μ	0.648 mm ⁻¹	
F(000)	976	
Crystal colour and size	colourless, 0.15 × 0.10 × 0.10 mm ³	
Reflections for cell refinement	7206 (θ range 2.2 to 66.6°)	
Data collection method	Oxford Diffraction Gemini A Ultra	
diffractometer	thick-slice ω scans	
θ range for data collection	4.0 to 66.7°	
Index ranges	h -14 to 12, k -11 to 11, l -23 to 22	
Completeness to $\theta = 66.7^\circ$	99.3 %	
Reflections collected	14800	
Independent reflections	4243 ($R_{\text{int}} = 0.0344$)	
Reflections with $F^2 > 2\sigma$	3455	
Absorption correction	semi-empirical from equivalents	
Min. and max. transmission	0.9090 and 0.9380	
Structure solution	direct methods	
Refinement method	Full-matrix least-squares on F^2	
Weighting parameters a, b	0.0525, 0.2814	
Data / restraints / parameters	4243 / 0 / 350	
Final R indices [$F^2 > 2\sigma$]	R1 = 0.0327, wR2 = 0.0841	
R indices (all data)	R1 = 0.0441, wR2 = 0.0897	
Goodness-of-fit on F^2	1.016	
Extinction coefficient	0.00052(12)	
Largest and mean shift/su	0.000 and 0.000	
Largest diff. peak and hole	0.21 and -0.19 e Å ⁻³	

Table 10. Atomic coordinates and equivalent isotropic displacement parameters (\AA^2) for **88**. U_{eq} is defined as one third of the trace of the orthogonalized U^{ij} tensor.

	x	y	z	U_{eq}
N(1)	0.55869(9)	0.21161(12)	0.32823(6)	0.0279(3)
N(2)	0.36752(9)	0.24152(11)	0.27626(5)	0.0271(3)
N(3)	0.33890(9)	0.22219(11)	0.15554(5)	0.0271(3)
N(4)	0.19114(10)	0.25928(13)	0.21068(6)	0.0330(3)
N(5)	0.33497(9)	0.35539(12)	0.40850(6)	0.0298(3)
N(6)	0.50721(9)	0.25982(11)	0.46393(5)	0.0268(3)
N(7)	0.54830(9)	0.30908(11)	0.58187(5)	0.0259(2)
N(8)	0.66868(10)	0.18164(13)	0.53265(6)	0.0306(3)
C(1)	0.65830(11)	0.18643(14)	0.30585(7)	0.0303(3)
C(2)	0.64157(11)	0.17757(14)	0.23799(7)	0.0294(3)
C(3)	0.52424(11)	0.19870(13)	0.21631(6)	0.0258(3)
C(4)	0.47608(11)	0.22002(13)	0.27463(6)	0.0247(3)
C(5)	0.44830(11)	0.20033(13)	0.15651(6)	0.0252(3)
C(6)	0.48575(11)	0.17392(14)	0.09356(6)	0.0276(3)
C(7)	0.52235(13)	0.15161(16)	0.04396(7)	0.0364(3)
C(8)	0.30339(11)	0.23972(13)	0.21537(6)	0.0266(3)
C(9)	0.12930(11)	0.25469(15)	0.26438(6)	0.0286(3)
C(10)	0.14785(12)	0.15757(17)	0.31415(7)	0.0390(4)
C(11)	0.07957(14)	0.1526(2)	0.36267(8)	0.0490(4)
C(12)	−0.00847(14)	0.24150(19)	0.36157(8)	0.0459(4)
C(13)	−0.02709(13)	0.33695(17)	0.31220(8)	0.0409(4)
C(14)	0.04228(12)	0.34454(16)	0.26390(7)	0.0341(3)
C(15)	0.25314(12)	0.43618(15)	0.42796(7)	0.0324(3)
C(16)	0.27880(11)	0.46597(14)	0.49416(7)	0.0301(3)
C(17)	0.38241(11)	0.40014(13)	0.51816(6)	0.0260(3)
C(18)	0.41410(11)	0.33247(13)	0.46281(6)	0.0250(3)
C(19)	0.45495(11)	0.38327(13)	0.57853(6)	0.0255(3)
C(20)	0.43078(11)	0.43714(14)	0.64071(7)	0.0291(3)
C(21)	0.40967(13)	0.47734(16)	0.69217(8)	0.0385(4)
C(22)	0.57029(11)	0.25259(13)	0.52473(6)	0.0250(3)
C(23)	0.70220(11)	0.08893(13)	0.48764(6)	0.0258(3)
C(24)	0.81568(11)	0.07509(14)	0.48601(7)	0.0301(3)
C(25)	0.85354(12)	−0.01941(15)	0.44498(7)	0.0356(3)
C(26)	0.77832(13)	−0.09951(15)	0.40386(7)	0.0366(3)
C(27)	0.66517(12)	−0.08581(14)	0.40540(7)	0.0325(3)
C(28)	0.62649(11)	0.00584(14)	0.44740(6)	0.0286(3)

Table 11. Bond lengths [\AA] and angles [$^\circ$] for **88**.

N(1)–H(1)	0.860(18)	N(1)–C(1)	1.3785(19)
N(1)–C(4)	1.3515(17)	N(2)–C(4)	1.3374(17)
N(2)–C(8)	1.3437(17)	N(3)–C(5)	1.3392(17)
N(3)–C(8)	1.3596(17)	N(4)–H(4)	0.864(19)
N(4)–C(8)	1.3607(18)	N(4)–C(9)	1.4164(18)
N(5)–H(5)	0.925(19)	N(5)–C(15)	1.3846(19)
N(5)–C(18)	1.3534(17)	N(6)–C(18)	1.3383(17)
N(6)–C(22)	1.3386(17)	N(7)–C(19)	1.3444(17)
N(7)–C(22)	1.3510(17)	N(8)–H(8)	0.882(18)
N(8)–C(22)	1.3733(17)	N(8)–C(23)	1.4049(18)
C(1)–H(1A)	0.950	C(1)–C(2)	1.356(2)
C(2)–H(2A)	0.950	C(2)–C(3)	1.4318(19)
C(3)–C(4)	1.4141(19)	C(3)–C(5)	1.3941(18)
C(5)–C(6)	1.4434(19)	C(6)–C(7)	1.182(2)
C(7)–H(7)	0.92(2)	C(9)–C(10)	1.390(2)
C(9)–C(14)	1.384(2)	C(10)–H(10A)	0.950
C(10)–C(11)	1.383(2)	C(11)–H(11A)	0.950
C(11)–C(12)	1.385(3)	C(12)–H(12A)	0.950
C(12)–C(13)	1.373(2)	C(13)–H(13A)	0.950
C(13)–C(14)	1.390(2)	C(14)–H(14A)	0.950
C(15)–H(15A)	0.950	C(15)–C(16)	1.357(2)
C(16)–H(16A)	0.950	C(16)–C(17)	1.4294(19)
C(17)–C(18)	1.4134(18)	C(17)–C(19)	1.3924(18)
C(19)–C(20)	1.4409(19)	C(20)–C(21)	1.182(2)
C(21)–H(21)	0.95(2)	C(23)–C(24)	1.3864(19)
C(23)–C(28)	1.3962(19)	C(24)–H(24A)	0.950
C(24)–C(25)	1.384(2)	C(25)–H(25A)	0.950
C(25)–C(26)	1.384(2)	C(26)–H(26A)	0.950
C(26)–C(27)	1.382(2)	C(27)–H(27A)	0.950
C(27)–C(28)	1.382(2)	C(28)–H(28A)	0.950
H(1)–N(1)–C(1)	127.5(11)	H(1)–N(1)–C(4)	123.8(11)
C(1)–N(1)–C(4)	108.70(11)	C(4)–N(2)–C(8)	113.46(11)
C(5)–N(3)–C(8)	117.62(10)	H(4)–N(4)–C(8)	115.4(12)
H(4)–N(4)–C(9)	115.1(12)	C(8)–N(4)–C(9)	126.07(11)
H(5)–N(5)–C(15)	126.7(11)	H(5)–N(5)–C(18)	125.0(11)
C(15)–N(5)–C(18)	108.23(11)	C(18)–N(6)–C(22)	113.41(11)
C(19)–N(7)–C(22)	118.01(11)	H(8)–N(8)–C(22)	115.6(11)
H(8)–N(8)–C(23)	116.4(11)	C(22)–N(8)–C(23)	127.06(11)
N(1)–C(1)–H(1A)	124.8	N(1)–C(1)–C(2)	110.47(12)
H(1A)–C(1)–C(2)	124.8	C(1)–C(2)–H(2A)	127.0
C(1)–C(2)–C(3)	106.06(12)	H(2A)–C(2)–C(3)	127.0
C(2)–C(3)–C(4)	106.89(11)	C(2)–C(3)–C(5)	138.38(13)
C(4)–C(3)–C(5)	114.70(12)	N(1)–C(4)–N(2)	126.27(12)
N(1)–C(4)–C(3)	107.88(11)	N(2)–C(4)–C(3)	125.83(11)
N(3)–C(5)–C(3)	121.67(12)	N(3)–C(5)–C(6)	117.99(11)
C(3)–C(5)–C(6)	120.32(12)	C(5)–C(6)–C(7)	176.30(14)
C(6)–C(7)–H(7)	178.4(12)	N(2)–C(8)–N(3)	126.69(12)

N(2)–C(8)–N(4)	118.86(12)	N(3)–C(8)–N(4)	114.44(11)
N(4)–C(9)–C(10)	122.28(13)	N(4)–C(9)–C(14)	118.07(12)
C(10)–C(9)–C(14)	119.47(13)	C(9)–C(10)–H(10A)	120.2
C(9)–C(10)–C(11)	119.58(15)	H(10A)–C(10)–C(11)	120.2
C(10)–C(11)–H(11A)	119.6	C(10)–C(11)–C(12)	120.86(15)
H(11A)–C(11)–C(12)	119.6	C(11)–C(12)–H(12A)	120.2
C(11)–C(12)–C(13)	119.51(14)	H(12A)–C(12)–C(13)	120.2
C(12)–C(13)–H(13A)	119.9	C(12)–C(13)–C(14)	120.15(15)
H(13A)–C(13)–C(14)	119.9	C(9)–C(14)–C(13)	120.40(14)
C(9)–C(14)–H(14A)	119.8	C(13)–C(14)–H(14A)	119.8
N(5)–C(15)–H(15A)	124.8	N(5)–C(15)–C(16)	110.46(12)
H(15A)–C(15)–C(16)	124.8	C(15)–C(16)–H(16A)	126.9
C(15)–C(16)–C(17)	106.27(12)	H(16A)–C(16)–C(17)	126.9
C(16)–C(17)–C(18)	106.79(11)	C(16)–C(17)–C(19)	138.24(13)
C(18)–C(17)–C(19)	114.95(12)	N(5)–C(18)–N(6)	126.03(12)
N(5)–C(18)–C(17)	108.26(11)	N(6)–C(18)–C(17)	125.71(11)
N(7)–C(19)–C(17)	121.02(12)	N(7)–C(19)–C(20)	116.85(11)
C(17)–C(19)–C(20)	122.03(12)	C(19)–C(20)–C(21)	177.85(16)
C(20)–C(21)–H(21)	179.4(13)	N(6)–C(22)–N(7)	126.86(12)
N(6)–C(22)–N(8)	119.25(12)	N(7)–C(22)–N(8)	113.88(11)
N(8)–C(23)–C(24)	118.27(12)	N(8)–C(23)–C(28)	122.62(12)
C(24)–C(23)–C(28)	119.03(13)	C(23)–C(24)–H(24A)	119.7
C(23)–C(24)–C(25)	120.59(13)	H(24A)–C(24)–C(25)	119.7
C(24)–C(25)–H(25A)	119.8	C(24)–C(25)–C(26)	120.38(13)
H(25A)–C(25)–C(26)	119.8	C(25)–C(26)–H(26A)	120.5
C(25)–C(26)–C(27)	119.09(14)	H(26A)–C(26)–C(27)	120.5
C(26)–C(27)–H(27A)	119.5	C(26)–C(27)–C(28)	121.07(13)
H(27A)–C(27)–C(28)	119.5	C(23)–C(28)–C(27)	119.80(13)
C(23)–C(28)–H(28A)	120.1	C(27)–C(28)–H(28A)	120.1

Table 12. Anisotropic displacement parameters (\AA^2) for **88**. The anisotropic displacement factor exponent takes the form: $-2\pi^2[h^2a^{*2}U^{11} + \dots + 2hka^*b^*U^{12}]$

	U^{11}	U^{22}	U^{33}	U^{23}	U^{13}	U^{12}
N(1)	0.0273(6)	0.0354(7)	0.0202(6)	0.0015(5)	0.0013(5)	0.0014(5)
N(2)	0.0257(6)	0.0334(6)	0.0215(5)	0.0002(4)	0.0015(4)	-0.0005(5)
N(3)	0.0267(6)	0.0331(6)	0.0210(5)	-0.0009(4)	0.0029(4)	-0.0023(5)
N(4)	0.0242(6)	0.0555(8)	0.0186(6)	-0.0016(5)	0.0009(5)	-0.0009(5)
N(5)	0.0283(6)	0.0367(7)	0.0231(6)	0.0000(5)	0.0002(5)	0.0040(5)
N(6)	0.0251(6)	0.0331(6)	0.0214(5)	-0.0001(4)	0.0012(4)	0.0007(5)
N(7)	0.0235(5)	0.0319(6)	0.0221(5)	-0.0017(4)	0.0033(4)	-0.0010(5)
N(8)	0.0250(6)	0.0433(7)	0.0218(6)	-0.0063(5)	-0.0014(5)	0.0052(5)
C(1)	0.0249(7)	0.0350(8)	0.0294(7)	0.0052(6)	0.0000(5)	0.0026(6)
C(2)	0.0262(7)	0.0338(7)	0.0284(7)	0.0037(6)	0.0055(5)	0.0032(6)
C(3)	0.0275(7)	0.0252(7)	0.0247(6)	0.0022(5)	0.0046(5)	-0.0017(5)
C(4)	0.0260(7)	0.0247(7)	0.0224(6)	0.0013(5)	0.0013(5)	-0.0014(5)
C(5)	0.0268(7)	0.0256(7)	0.0232(6)	0.0006(5)	0.0041(5)	-0.0028(5)
C(6)	0.0262(7)	0.0295(7)	0.0264(7)	0.0010(5)	0.0023(5)	-0.0025(5)
C(7)	0.0390(8)	0.0438(9)	0.0279(8)	-0.0015(6)	0.0098(7)	0.0010(7)
C(8)	0.0261(7)	0.0312(7)	0.0222(6)	-0.0001(5)	0.0027(5)	-0.0019(5)
C(9)	0.0228(7)	0.0412(8)	0.0211(6)	-0.0022(6)	0.0012(5)	-0.0057(6)
C(10)	0.0292(7)	0.0498(9)	0.0373(8)	0.0113(7)	0.0037(6)	0.0010(7)
C(11)	0.0386(9)	0.0709(12)	0.0374(8)	0.0211(8)	0.0056(7)	-0.0053(8)
C(12)	0.0380(9)	0.0713(12)	0.0313(8)	0.0006(8)	0.0138(7)	-0.0088(8)
C(13)	0.0343(8)	0.0478(9)	0.0427(9)	-0.0065(7)	0.0127(7)	0.0003(7)
C(14)	0.0301(7)	0.0407(8)	0.0312(7)	0.0025(6)	0.0042(6)	-0.0001(6)
C(15)	0.0261(7)	0.0366(8)	0.0329(7)	0.0040(6)	0.0005(6)	0.0052(6)
C(16)	0.0274(7)	0.0308(7)	0.0326(7)	0.0011(6)	0.0063(6)	0.0029(6)
C(17)	0.0257(7)	0.0262(7)	0.0267(6)	0.0010(5)	0.0066(5)	-0.0026(5)
C(18)	0.0244(6)	0.0279(7)	0.0221(6)	0.0019(5)	0.0024(5)	-0.0020(5)
C(19)	0.0250(6)	0.0270(7)	0.0247(6)	-0.0007(5)	0.0048(5)	-0.0042(5)
C(20)	0.0275(7)	0.0304(7)	0.0294(7)	-0.0003(6)	0.0044(6)	-0.0011(6)
C(21)	0.0457(9)	0.0392(9)	0.0324(8)	-0.0078(7)	0.0121(7)	-0.0027(7)
C(22)	0.0236(6)	0.0297(7)	0.0212(6)	-0.0008(5)	0.0021(5)	-0.0008(5)
C(23)	0.0285(7)	0.0287(7)	0.0197(6)	0.0038(5)	0.0026(5)	0.0037(5)
C(24)	0.0281(7)	0.0319(7)	0.0287(7)	-0.0019(6)	-0.0002(5)	0.0018(6)
C(25)	0.0280(7)	0.0395(8)	0.0391(8)	-0.0026(6)	0.0048(6)	0.0078(6)
C(26)	0.0427(8)	0.0315(8)	0.0351(7)	-0.0052(6)	0.0048(6)	0.0094(6)
C(27)	0.0388(8)	0.0261(7)	0.0308(7)	0.0007(6)	0.0000(6)	-0.0018(6)
C(28)	0.0272(7)	0.0309(7)	0.0276(7)	0.0054(5)	0.0040(5)	-0.0004(6)

Table 13. Hydrogen coordinates and isotropic displacement parameters (\AA^2) for **88**.

	x	y	z	U
H(1)	0.5486(14)	0.2237(17)	0.3689(9)	0.038(4)
H(4)	0.1524(15)	0.2462(17)	0.1714(9)	0.042(5)
H(5)	0.3351(14)	0.3194(18)	0.3663(9)	0.043(5)
H(8)	0.7205(15)	0.2076(17)	0.5660(9)	0.038(4)
H(1A)	0.7288	0.1767	0.3340	0.036
H(2A)	0.6965	0.1608	0.2104	0.035
H(7)	0.5525(15)	0.1359(19)	0.0056(10)	0.051(5)
H(10A)	0.2070	0.0950	0.3148	0.047
H(11A)	0.0932	0.0875	0.3972	0.059
H(12A)	-0.0556	0.2364	0.3947	0.055
H(13A)	-0.0875	0.3979	0.3110	0.049
H(14A)	0.0299	0.4118	0.2304	0.041
H(15A)	0.1882	0.4665	0.3990	0.039
H(16A)	0.2364	0.5198	0.5195	0.036
H(21)	0.3921(17)	0.509(2)	0.7333(10)	0.063(6)
H(24A)	0.8679	0.1309	0.5133	0.036
H(25A)	0.9316	-0.0293	0.4451	0.043
H(26A)	0.8041	-0.1630	0.3750	0.044
H(27A)	0.6131	-0.1403	0.3771	0.039
H(28A)	0.5486	0.0123	0.4489	0.034

Table 14. Torsion angles [$^\circ$] for **88**.

C(4)–N(1)–C(1)–C(2)	-0.32(17)	N(1)–C(1)–C(2)–C(3)	0.10(16)
C(1)–C(2)–C(3)–C(4)	0.14(15)	C(1)–C(2)–C(3)–C(5)	-177.77(16)
C(8)–N(2)–C(4)–N(1)	-177.46(13)	C(8)–N(2)–C(4)–C(3)	0.84(19)
C(1)–N(1)–C(4)–N(2)	178.95(13)	C(1)–N(1)–C(4)–C(3)	0.40(15)
C(2)–C(3)–C(4)–N(1)	-0.33(15)	C(2)–C(3)–C(4)–N(2)	-178.89(13)
C(5)–C(3)–C(4)–N(1)	178.14(11)	C(5)–C(3)–C(4)–N(2)	-0.4(2)
C(8)–N(3)–C(5)–C(3)	-1.56(19)	C(8)–N(3)–C(5)–C(6)	176.48(12)
C(2)–C(3)–C(5)–N(3)	178.57(15)	C(2)–C(3)–C(5)–C(6)	0.6(3)
C(4)–C(3)–C(5)–N(3)	0.77(19)	C(4)–C(3)–C(5)–C(6)	-177.23(12)
N(3)–C(5)–C(6)–C(7)	-179(100)	C(3)–C(5)–C(6)–C(7)	-1(2)
C(4)–N(2)–C(8)–N(3)	-1.8(2)	C(4)–N(2)–C(8)–N(4)	179.44(12)
C(5)–N(3)–C(8)–N(2)	2.2(2)	C(5)–N(3)–C(8)–N(4)	-178.98(12)
C(9)–N(4)–C(8)–N(2)	-13.9(2)	C(9)–N(4)–C(8)–N(3)	167.15(13)
C(8)–N(4)–C(9)–C(10)	-42.1(2)	C(8)–N(4)–C(9)–C(14)	142.69(15)
N(4)–C(9)–C(10)–C(11)	-175.51(14)	C(14)–C(9)–C(10)–C(11)	-0.4(2)
C(9)–C(10)–C(11)–C(12)	1.3(2)	C(10)–C(11)–C(12)–C(13)	-1.0(3)
C(11)–C(12)–C(13)–C(14)	-0.3(2)	N(4)–C(9)–C(14)–C(13)	174.48(13)
C(10)–C(9)–C(14)–C(13)	-0.8(2)	C(12)–C(13)–C(14)–C(9)	1.2(2)
C(18)–N(5)–C(15)–C(16)	0.20(16)	N(5)–C(15)–C(16)–C(17)	-0.21(16)
C(15)–C(16)–C(17)–C(18)	0.14(15)	C(15)–C(16)–C(17)–C(19)	
	-177.94(16)		

C(22)–N(6)–C(18)–N(5)	–179.35(13)	C(22)–N(6)–C(18)–C(17)	1.62(19)
C(15)–N(5)–C(18)–N(6)	–179.27(13)	C(15)–N(5)–C(18)–C(17)	–0.10(15)
C(16)–C(17)–C(18)–N(5)	–0.03(15)	C(16)–C(17)–C(18)–N(6)	179.14(13)
C(19)–C(17)–C(18)–N(5)	178.57(12)	C(19)–C(17)–C(18)–N(6)	–2.3(2)
C(22)–N(7)–C(19)–C(17)	0.72(19)	C(22)–N(7)–C(19)–C(20)	177.17(12)
C(16)–C(17)–C(19)–N(7)	178.93(15)	C(16)–C(17)–C(19)–C(20)	2.7(3)
C(18)–C(17)–C(19)–N(7)	0.96(18)	C(18)–C(17)–C(19)–C(20)	
	–175.30(12)		
N(7)–C(19)–C(20)–C(21)	–79(4)	C(17)–C(19)–C(20)–C(21)	98(4)
C(18)–N(6)–C(22)–N(7)	0.4(2)	C(18)–N(6)–C(22)–N(8)	–179.56(12)
C(19)–N(7)–C(22)–N(6)	–1.5(2)	C(19)–N(7)–C(22)–N(8)	178.41(11)
C(23)–N(8)–C(22)–N(6)	–15.3(2)	C(23)–N(8)–C(22)–N(7)	164.79(13)
C(22)–N(8)–C(23)–C(24)	149.77(14)	C(22)–N(8)–C(23)–C(28)	–33.7(2)
N(8)–C(23)–C(24)–C(25)	176.81(13)	C(28)–C(23)–C(24)–C(25)	0.2(2)
C(23)–C(24)–C(25)–C(26)	1.4(2)	C(24)–C(25)–C(26)–C(27)	–1.4(2)
C(25)–C(26)–C(27)–C(28)	–0.3(2)	C(26)–C(27)–C(28)–C(23)	1.9(2)
N(8)–C(23)–C(28)–C(27)	–178.28(12)	C(24)–C(23)–C(28)–C(27)	–1.79(19)

Table 15. Hydrogen bonds for **88** [Å and °].

D–H...A	d(D–H)	d(H...A)	d(D...A)	<(DHA)
N(1)–H(1)...N(6)	0.860(18)	2.094(19)	2.9504(17)	174(2)
N(4)–H(4)...N(7A)	0.864(19)	2.103(19)	2.9609(16)	172(2)
N(5)–H(5)...N(2)	0.925(19)	2.076(19)	2.9906(16)	169(1)
N(8)–H(8)...N(3B)	0.882(18)	2.230(18)	3.1096(16)	175(1)

Symmetry operations for equivalent atoms

A $x-1/2, -y+1/2, z-1/2$ B $x+1/2, -y+1/2, z+1/2$

Pyrazolopyrimidine **154**Table 16. Crystal data and structure refinement for **154**.

Identification code	154	
Chemical formula (moiety)	$\text{C}_{19}\text{H}_{20}\text{N}_6\text{O}_2$	
Chemical formula (total)	$\text{C}_{19}\text{H}_{20}\text{N}_6\text{O}_2$	
Formula weight	364.41	
Temperature	150(2) K	
Radiation, wavelength	synchrotron, 0.68890 Å	
Crystal system, space group	monoclinic, $P2_1/n$	
Unit cell parameters	$a = 5.047(3)$ Å	$\alpha = 90^\circ$
	$b = 13.893(7)$ Å	$\beta = 93.969(5)^\circ$
	$c = 25.912(14)$ Å	$\gamma = 90^\circ$
Cell volume	$1812.5(17)$ Å ³	
Z	4	
Calculated density	1.335 g/cm ³	
Absorption coefficient μ	0.091 mm ⁻¹	
F(000)	768	
Crystal colour and size	colourless, $0.08 \times 0.01 \times 0.01$ mm ³	
Data collection method	Rigaku	
	thick-slice ω scans	
θ range for data collection	1.6 to 27.6°	
Index ranges	h -5 to 5 , k 0 to 18 , l 0 to 34	
Completeness to $\theta = 27.6^\circ$	90.4%	
Reflections collected	5548	
Independent reflections	5549 ($R_{\text{int}} = 0.0000$)	
Reflections with $F^2 > 2\sigma$	4298	
Absorption correction	semi-empirical from equivalents	
Min. and max. transmission	0.9927 and 0.9991	
Structure solution	direct methods	
Refinement method	Full-matrix least-squares on F^2	
Weighting parameters a , b	0.1010 , 1.3440	
Data / restraints / parameters	$5549 / 0 / 266$	
Final R indices [$F^2 > 2\sigma$]	$R1 = 0.0778$, $wR2 = 0.2029$	
R indices (all data)	$R1 = 0.0999$, $wR2 = 0.2137$	
Goodness-of-fit on F^2	1.094	
Extinction coefficient	$0.24(3)$	
Largest and mean shift/su	0.000 and 0.000	
Largest diff. peak and hole	0.30 and -0.30 e Å ⁻³	

Table 17. Atomic coordinates and equivalent isotropic displacement parameters (\AA^2) for **154**. U_{eq} is defined as one third of the trace of the orthogonalized U^{ij} tensor.

	x	y	z	U_{eq}
O(1)	0.1328(4)	0.45373(15)	0.44024(7)	0.0322(5)
O(2)	−0.0732(10)	0.1939(4)	0.58266(17)	0.1213(16)
N(1)	−0.2858(6)	0.4457(2)	0.46261(10)	0.0379(7)
N(2)	0.3895(5)	0.14392(18)	0.29956(9)	0.0321(6)
N(3)	0.5400(5)	0.29129(15)	0.26879(8)	0.0279(5)
N(4)	0.7695(6)	0.42374(17)	0.23138(10)	0.0354(7)
N(5)	0.9667(6)	0.43618(17)	0.19810(10)	0.0383(7)
N(6)	0.7058(5)	0.13632(16)	0.24211(8)	0.0292(6)
C(1)	−0.1011(6)	0.43187(18)	0.42930(10)	0.0271(6)
C(2)	−0.1880(6)	0.3876(2)	0.37763(10)	0.0312(7)
C(3)	−0.0825(6)	0.28633(19)	0.37365(10)	0.0303(7)
C(4)	−0.1910(7)	0.2127(2)	0.40094(12)	0.0412(8)
C(5)	−0.1035(8)	0.1189(2)	0.39499(13)	0.0469(9)
C(6)	0.0895(7)	0.0992(2)	0.36180(12)	0.0402(8)
C(7)	0.2032(6)	0.1723(2)	0.33422(10)	0.0312(7)
C(8)	0.1172(6)	0.26711(19)	0.34027(9)	0.0277(6)
C(9)	0.5484(6)	0.19527(18)	0.26966(10)	0.0276(6)
C(10)	0.7156(6)	0.32959(18)	0.23858(10)	0.0278(6)
C(11)	1.0356(7)	0.3499(2)	0.18329(11)	0.0358(7)
C(12)	0.8858(6)	0.27861(19)	0.20769(10)	0.0311(7)
C(13)	0.8685(6)	0.17799(19)	0.21072(10)	0.0285(6)
C(14)	1.0262(6)	0.1174(2)	0.17963(11)	0.0335(7)
C(15)	1.1482(7)	0.0721(2)	0.15135(13)	0.0428(8)
C(16)	−0.0295(15)	0.1257(4)	0.5448(3)	0.119(3)
C(17)	0.2436(12)	0.1385(4)	0.5305(3)	0.0995(19)
C(18)	0.2737(13)	0.2483(4)	0.5346(3)	0.108(2)
C(19)	0.0641(13)	0.2781(4)	0.5689(2)	0.0946(17)

Table 18. Bond lengths [\AA] and angles [$^\circ$] for **154**.

O(1)–C(1)	1.233(3)	O(2)–C(16)	1.392(7)
O(2)–C(19)	1.418(7)	N(1)–H(1A)	0.93(4)
N(1)–H(1B)	0.76(3)	N(1)–C(1)	1.328(4)
N(2)–H(2)	0.81(4)	N(2)–C(7)	1.401(4)
N(2)–C(9)	1.356(4)	N(3)–C(9)	1.335(3)
N(3)–C(10)	1.333(4)	N(4)–H(4)	0.78(4)
N(4)–N(5)	1.372(4)	N(4)–C(10)	1.352(3)
N(5)–C(11)	1.313(4)	N(6)–C(9)	1.375(3)
N(6)–C(13)	1.328(4)	C(1)–C(2)	1.510(4)
C(2)–H(2A)	0.990	C(2)–H(2B)	0.990
C(2)–C(3)	1.511(4)	C(3)–C(4)	1.378(4)
C(3)–C(8)	1.399(4)	C(4)–H(4A)	0.950
C(4)–C(5)	1.388(4)	C(5)–H(5A)	0.950
C(5)–C(6)	1.371(4)	C(6)–H(6A)	0.950
C(6)–C(7)	1.389(4)	C(7)–C(8)	1.399(4)
C(8)–H(8A)	0.950	C(10)–C(12)	1.406(4)
C(11)–H(11A)	0.950	C(11)–C(12)	1.420(4)
C(12)–C(13)	1.403(4)	C(13)–C(14)	1.442(4)
C(14)–C(15)	1.172(4)	C(15)–H(15)	0.99(4)
C(16)–H(16A)	0.990	C(16)–H(16B)	0.990
C(16)–C(17)	1.463(8)	C(17)–H(17A)	0.990
C(17)–H(17B)	0.990	C(17)–C(18)	1.536(8)
C(18)–H(18A)	0.990	C(18)–H(18B)	0.990
C(18)–C(19)	1.488(8)	C(19)–H(19A)	0.990
C(19)–H(19B)	0.990		
C(16)–O(2)–C(19)	106.3(5)	H(1A)–N(1)–H(1B)	124(3)
H(1A)–N(1)–C(1)	116(2)	H(1B)–N(1)–C(1)	120(2)
H(2)–N(2)–C(7)	113(2)	H(2)–N(2)–C(9)	115(2)
C(7)–N(2)–C(9)	131.9(2)	C(9)–N(3)–C(10)	112.8(2)
H(4)–N(4)–N(5)	116(3)	H(4)–N(4)–C(10)	132(3)
N(5)–N(4)–C(10)	111.7(2)	N(4)–N(5)–C(11)	106.7(2)
C(9)–N(6)–C(13)	117.5(2)	O(1)–C(1)–N(1)	121.3(3)
O(1)–C(1)–C(2)	121.3(2)	N(1)–C(1)–C(2)	117.5(3)
C(1)–C(2)–H(2A)	109.5	C(1)–C(2)–H(2B)	109.5
C(1)–C(2)–C(3)	110.9(2)	H(2A)–C(2)–H(2B)	108.0
H(2A)–C(2)–C(3)	109.5	H(2B)–C(2)–C(3)	109.5
C(2)–C(3)–C(4)	120.1(3)	C(2)–C(3)–C(8)	119.5(2)
C(4)–C(3)–C(8)	120.3(3)	C(3)–C(4)–H(4A)	120.0
C(3)–C(4)–C(5)	120.0(3)	H(4A)–C(4)–C(5)	120.0
C(4)–C(5)–H(5A)	119.9	C(4)–C(5)–C(6)	120.2(3)
H(5A)–C(5)–C(6)	119.9	C(5)–C(6)–H(6A)	119.5
C(5)–C(6)–C(7)	120.9(3)	H(6A)–C(6)–C(7)	119.5
N(2)–C(7)–C(6)	116.4(3)	N(2)–C(7)–C(8)	124.3(3)
C(6)–C(7)–C(8)	119.2(3)	C(3)–C(8)–C(7)	119.4(2)
C(3)–C(8)–H(8A)	120.3	C(7)–C(8)–H(8A)	120.3
N(2)–C(9)–N(3)	121.1(3)	N(2)–C(9)–N(6)	111.7(2)
N(3)–C(9)–N(6)	127.3(3)	N(3)–C(10)–N(4)	128.0(2)

N(3)–C(10)–C(12)	126.2(2)	N(4)–C(10)–C(12)	105.8(2)
N(5)–C(11)–H(11A)	124.9	N(5)–C(11)–C(12)	110.3(3)
H(11A)–C(11)–C(12)	124.9	C(10)–C(12)–C(11)	105.5(2)
C(10)–C(12)–C(13)	115.3(2)	C(11)–C(12)–C(13)	139.1(3)
N(6)–C(13)–C(12)	120.8(2)	N(6)–C(13)–C(14)	118.4(2)
C(12)–C(13)–C(14)	120.8(3)	C(13)–C(14)–C(15)	175.2(3)
C(14)–C(15)–H(15)	175(2)	O(2)–C(16)–H(16A)	110.3
O(2)–C(16)–H(16B)	110.3	O(2)–C(16)–C(17)	107.0(6)
H(16A)–C(16)–H(16B)	108.6	H(16A)–C(16)–C(17)	110.3
H(16B)–C(16)–C(17)	110.3	C(16)–C(17)–H(17A)	111.5
C(16)–C(17)–H(17B)	111.5	C(16)–C(17)–C(18)	101.2(5)
H(17A)–C(17)–H(17B)	109.3	H(17A)–C(17)–C(18)	111.5
H(17B)–C(17)–C(18)	111.5	C(17)–C(18)–H(18A)	110.9
C(17)–C(18)–H(18B)	110.9	C(17)–C(18)–C(19)	104.2(5)
H(18A)–C(18)–H(18B)	108.9	H(18A)–C(18)–C(19)	110.9
H(18B)–C(18)–C(19)	110.9	O(2)–C(19)–C(18)	107.5(5)
O(2)–C(19)–H(19A)	110.2	O(2)–C(19)–H(19B)	110.2
C(18)–C(19)–H(19A)	110.2	C(18)–C(19)–H(19B)	110.2
H(19A)–C(19)–H(19B)	108.5		

Table 19. Anisotropic displacement parameters (\AA^2) for **154**. The anisotropic displacement factor exponent takes the form: $-2\pi^2[h^2a^{*2}U^{11} + \dots + 2hka^*b^*U^{12}]$

	U^{11}	U^{22}	U^{33}	U^{23}	U^{13}	U^{12}
O(1)	0.0279(13)	0.0379(11)	0.0313(9)	−0.0069(8)	0.0067(8)	−0.0026(9)
O(2)	0.134(4)	0.136(4)	0.098(3)	0.002(3)	0.035(3)	−0.003(3)
N(1)	0.0256(18)	0.0536(18)	0.0354(13)	−0.0156(12)	0.0091(11)	−0.0039(13)
N(2)	0.0396(17)	0.0221(12)	0.0360(12)	−0.0012(9)	0.0143(11)	0.0039(11)
N(3)	0.0322(15)	0.0226(11)	0.0296(10)	−0.0006(8)	0.0072(10)	0.0027(9)
N(4)	0.0477(19)	0.0203(11)	0.0398(12)	0.0000(9)	0.0144(12)	0.0032(11)
N(5)	0.0490(19)	0.0260(12)	0.0420(13)	0.0029(10)	0.0166(12)	−0.0008(11)
N(6)	0.0349(16)	0.0245(11)	0.0288(11)	−0.0030(8)	0.0067(9)	0.0018(10)
C(1)	0.0314(18)	0.0241(13)	0.0263(12)	−0.0020(9)	0.0046(11)	0.0006(11)
C(2)	0.0308(18)	0.0326(14)	0.0304(12)	−0.0051(10)	0.0034(11)	0.0049(12)
C(3)	0.0343(19)	0.0285(14)	0.0281(12)	−0.0080(10)	0.0017(11)	−0.0007(12)
C(4)	0.050(2)	0.0386(17)	0.0371(14)	−0.0048(12)	0.0200(14)	0.0007(15)
C(5)	0.061(3)	0.0360(16)	0.0471(17)	0.0014(13)	0.0275(17)	−0.0033(16)
C(6)	0.052(2)	0.0276(14)	0.0425(15)	0.0001(12)	0.0165(15)	0.0013(14)
C(7)	0.0336(19)	0.0299(14)	0.0308(13)	−0.0034(10)	0.0072(12)	0.0017(12)
C(8)	0.0305(18)	0.0257(13)	0.0273(12)	−0.0035(9)	0.0037(11)	−0.0024(11)
C(9)	0.0347(18)	0.0201(12)	0.0282(12)	−0.0019(9)	0.0039(11)	0.0009(11)
C(10)	0.0335(18)	0.0222(12)	0.0277(12)	−0.0006(9)	0.0028(11)	0.0024(11)
C(11)	0.046(2)	0.0255(13)	0.0367(14)	0.0029(11)	0.0113(13)	0.0010(13)
C(12)	0.040(2)	0.0257(13)	0.0283(12)	−0.0016(10)	0.0072(12)	−0.0007(12)
C(13)	0.0339(18)	0.0239(13)	0.0278(12)	−0.0041(9)	0.0032(11)	0.0015(11)
C(14)	0.039(2)	0.0261(13)	0.0368(14)	−0.0004(10)	0.0087(13)	−0.0041(12)
C(15)	0.047(2)	0.0380(17)	0.0451(16)	−0.0083(13)	0.0178(15)	0.0017(15)

C(16)	0.148(7)	0.073(4)	0.142(6)	0.017(4)	0.066(5)	0.016(4)
C(17)	0.092(5)	0.100(5)	0.109(4)	−0.008(3)	0.021(4)	0.002(3)
C(18)	0.097(5)	0.100(5)	0.128(5)	0.043(4)	0.007(4)	−0.014(4)
C(19)	0.103(5)	0.082(4)	0.097(4)	−0.002(3)	−0.002(4)	−0.005(3)

Table 20. Hydrogen coordinates and isotropic displacement parameters (\AA^2) for **154**.

	x	y	z	U
H(1A)	−0.227(7)	0.473(2)	0.4941(15)	0.045(9)
H(1B)	−0.431(7)	0.434(2)	0.4550(12)	0.023(9)
H(2)	0.418(7)	0.087(3)	0.3005(13)	0.043(10)
H(4)	0.710(7)	0.471(3)	0.2426(15)	0.054(11)
H(2A)	−0.1223	0.4275	0.3495	0.037
H(2B)	−0.3844	0.3866	0.3733	0.037
H(4A)	−0.3255	0.2261	0.4238	0.049
H(5A)	−0.1776	0.0682	0.4140	0.056
H(6A)	0.1462	0.0346	0.3576	0.048
H(8A)	0.1939	0.3180	0.3219	0.033
H(11A)	1.1668	0.3369	0.1596	0.043
H(15)	1.262(8)	0.038(3)	0.1272(17)	0.070(12)
H(16A)	−0.1557	0.1353	0.5143	0.142
H(16B)	−0.0543	0.0599	0.5584	0.142
H(17A)	0.2661	0.1155	0.4949	0.119
H(17B)	0.3719	0.1050	0.5550	0.119
H(18A)	0.4523	0.2660	0.5499	0.130
H(18B)	0.2456	0.2788	0.5001	0.130
H(19A)	0.1452	0.3100	0.6003	0.114
H(19B)	−0.0602	0.3238	0.5506	0.114

Table 21. Torsion angles [$^\circ$] for **154**.

C(10)–N(4)–N(5)–C(11)	1.1(4)	O(1)–C(1)–C(2)–C(3)	69.7(3)
N(1)–C(1)–C(2)–C(3)	−109.9(3)	C(1)–C(2)–C(3)–C(4)	73.4(4)
C(1)–C(2)–C(3)–C(8)	−109.6(3)	C(2)–C(3)–C(4)–C(5)	176.5(3)
C(8)–C(3)–C(4)–C(5)	−0.6(5)	C(3)–C(4)–C(5)–C(6)	−0.4(6)
C(4)–C(5)–C(6)–C(7)	0.9(6)	C(5)–C(6)–C(7)–N(2)	−177.1(3)
C(5)–C(6)–C(7)–C(8)	−0.5(5)	C(9)–N(2)–C(7)–C(6)	−175.0(3)
C(9)–N(2)–C(7)–C(8)	8.6(5)	C(2)–C(3)–C(8)–C(7)	−176.1(3)
C(4)–C(3)–C(8)–C(7)	1.0(4)	N(2)–C(7)–C(8)–C(3)	175.9(3)
C(6)–C(7)–C(8)–C(3)	−0.4(4)	C(10)–N(3)–C(9)–N(2)	178.0(3)
C(10)–N(3)–C(9)–N(6)	−2.7(4)	C(7)–N(2)–C(9)–N(3)	−1.8(5)
C(7)–N(2)–C(9)–N(6)	178.7(3)	C(13)–N(6)–C(9)–N(2)	179.1(3)
C(13)–N(6)–C(9)–N(3)	−0.3(4)	C(9)–N(3)–C(10)–N(4)	−175.9(3)
C(9)–N(3)–C(10)–C(12)	3.6(4)	N(5)–N(4)–C(10)–N(3)	178.8(3)
N(5)–N(4)–C(10)–C(12)	−0.7(3)	N(4)–N(5)–C(11)–C(12)	−1.0(4)
N(3)–C(10)–C(12)–C(11)	−179.5(3)	N(3)–C(10)–C(12)–C(13)	−1.5(4)
N(4)–C(10)–C(12)–C(11)	0.1(3)	N(4)–C(10)–C(12)–C(13)	178.0(3)

N(5)–C(11)–C(12)–C(10)	0.6(4)	N(5)–C(11)–C(12)–C(13)	–176.5(4)
C(9)–N(6)–C(13)–C(12)	2.6(4)	C(9)–N(6)–C(13)–C(14)	–177.1(3)
C(10)–C(12)–C(13)–N(6)	–1.8(4)	C(10)–C(12)–C(13)–C(14)	177.9(3)
C(11)–C(12)–C(13)–N(6)	175.2(3)	C(11)–C(12)–C(13)–C(14)	–5.1(6)
N(6)–C(13)–C(14)–C(15)	131(4)	C(12)–C(13)–C(14)–C(15)	–49(4)
C(19)–O(2)–C(16)–C(17)	37.1(7)	O(2)–C(16)–C(17)–C(18)	–35.8(7)
C(16)–C(17)–C(18)–C(19)	21.1(7)	C(16)–O(2)–C(19)–C(18)	–21.9(7)
C(17)–C(18)–C(19)–O(2)	–0.5(7)		

Table 22. Hydrogen bonds for **154** [Å and °].

D–H...A	d(D–H)	d(H...A)	d(D...A)	<(DHA)
N(1)–H(1A)...O(1A)	0.93(4)	2.01(4)	2.935(4)	173(3)
N(1)–H(1B)...O(1B)	0.76(3)	2.22(3)	2.954(4)	160(3)
N(2)–H(2)...N(5C)	0.81(4)	2.17(4)	2.976(4)	175(3)
N(4)–H(4)...N(6D)	0.78(4)	2.36(4)	3.033(4)	144(4)

Symmetry operations for equivalent atoms

A $-x, -y+1, -z+1$ B $x-1, y, z$ C $-x+3/2, y-1/2, -z+1/2$ D $-x+3/2, y+1/2, -z+1/2$

Triazolopyrimidine **174**Table 23. Crystal data and structure refinement for **174**.

Identification code	174	
Chemical formula (moiety)	C ₉ H ₁₁ ClN ₆ O ₂	
Chemical formula (total)	C ₉ H ₁₁ ClN ₆ O ₂	
Formula weight	270.69	
Temperature	150(2) K	
Radiation, wavelength	MoK α , 0.71073 Å	
Crystal system, space group	monoclinic, P12 ₁ /n1	
Unit cell parameters	a = 9.9614(4) Å	$\alpha = 90^\circ$
	b = 10.7013(4) Å	$\beta = 94.166(3)^\circ$
	c = 11.2291(4) Å	$\gamma = 90^\circ$
Cell volume	1193.86(8) Å ³	
Z	4	
Calculated density	1.506 g/cm ³	
Absorption coefficient μ	0.325 mm ⁻¹	
F(000)	560	
Crystal colour and size	colourless, 0.40 × 0.30 × 0.30 mm ³	
Reflections for cell refinement	4154 (θ range 2.8 to 28.3°)	
Data collection method	Xcalibur, Atlas, Gemini ultra	
	thick-slice ω scans	
θ range for data collection	2.8 to 28.4°	
Index ranges	h -13 to 13, k -14 to 14, l -14 to 14	
Completeness to $\theta = 25.0^\circ$	99.9 %	
Reflections collected	9462	
Independent reflections	2602 ($R_{\text{int}} = 0.0242$)	
Reflections with $F^2 > 2\sigma$	2288	
Absorption correction	semi-empirical from equivalents	
Min. and max. transmission	0.8809 and 0.9087	
Structure solution	direct methods	
Refinement method	Full-matrix least-squares on F^2	
Weighting parameters a, b	0.0354, 0.5961	
Data / restraints / parameters	2602 / 0 / 175	
Final R indices [$F^2 > 2\sigma$]	R1 = 0.0328, wR2 = 0.0795	
R indices (all data)	R1 = 0.0392, wR2 = 0.0840	
Goodness-of-fit on F^2	1.066	
Extinction coefficient	0.0050(12)	
Largest and mean shift/su	0.001 and 0.000	
Largest diff. peak and hole	0.36 and -0.21 e Å ⁻³	

Table 24. Atomic coordinates and equivalent isotropic displacement parameters (\AA^2) for **174**. U_{eq} is defined as one third of the trace of the orthogonalized U^{ij} tensor.

	x	y	z	U_{eq}
N(1)	0.14545(13)	0.41830(12)	0.54332(11)	0.0250(3)
N(2)	0.08966(13)	0.31408(12)	0.56801(11)	0.0242(3)
N(3)	0.04581(12)	0.32162(11)	0.68288(10)	0.0192(3)
N(4)	0.05862(12)	0.48183(11)	0.83823(10)	0.0182(3)
C(5)	0.10482(14)	0.59974(13)	0.85164(12)	0.0191(3)
N(5)	0.08970(16)	0.65617(13)	0.95514(12)	0.0270(3)
Cl(7)	0.25655(4)	0.70625(4)	0.55984(3)	0.02827(13)
C(7)	0.18186(14)	0.61857(13)	0.66548(13)	0.0196(3)
N(6)	0.16551(12)	0.67025(11)	0.76816(11)	0.0209(3)
C(8)	0.14073(14)	0.49645(14)	0.64038(13)	0.0194(3)
C(9)	0.07827(14)	0.43650(13)	0.73077(12)	0.0169(3)
C(10)	-0.02808(14)	0.22429(13)	0.73440(13)	0.0194(3)
O(11)	-0.08992(12)	0.24572(10)	0.81920(10)	0.0292(3)
O(12)	-0.01518(11)	0.11982(9)	0.67679(9)	0.0230(2)
C(13)	-0.09201(16)	0.00726(14)	0.71490(14)	0.0236(3)
C(14)	-0.0389(2)	-0.03077(17)	0.83870(16)	0.0366(4)
C(15)	-0.0588(2)	-0.08972(16)	0.62429(18)	0.0444(5)
C(16)	-0.24037(18)	0.03588(17)	0.70672(19)	0.0401(5)

Table 25. Bond lengths [\AA] and angles [$^\circ$] for **174**.

N(1)–N(2)	1.2853(18)	N(1)–C(8)	1.3773(19)
N(2)–N(3)	1.3939(16)	N(3)–C(9)	1.3710(18)
N(3)–C(10)	1.4225(19)	N(4)–C(5)	1.3477(19)
N(4)–C(9)	1.3281(18)	C(5)–N(5)	1.3280(19)
C(5)–N(6)	1.3769(19)	N(5)–H(5A)	0.82(2)
N(5)–H(5B)	0.84(2)	Cl(7)–C(7)	1.7232(14)
C(7)–N(6)	1.2996(19)	C(7)–C(8)	1.392(2)
C(8)–C(9)	1.386(2)	C(10)–O(11)	1.1933(18)
C(10)–O(12)	1.3027(17)	O(12)–C(13)	1.5058(17)
C(13)–C(14)	1.507(2)	C(13)–C(15)	1.507(2)
C(13)–C(16)	1.506(2)	C(14)–H(14A)	0.980
C(14)–H(14B)	0.980	C(14)–H(14C)	0.980
C(15)–H(15A)	0.980	C(15)–H(15B)	0.980
C(15)–H(15C)	0.980	C(16)–H(16A)	0.980
C(16)–H(16B)	0.980	C(16)–H(16C)	0.980
N(2)–N(1)–C(8)	108.42(12)	N(1)–N(2)–N(3)	108.59(11)
N(2)–N(3)–C(9)	109.52(11)	N(2)–N(3)–C(10)	122.69(11)
C(9)–N(3)–C(10)	127.69(12)	C(5)–N(4)–C(9)	111.83(12)
N(4)–C(5)–N(5)	117.65(13)	N(4)–C(5)–N(6)	126.88(13)
N(5)–C(5)–N(6)	115.46(13)	C(5)–N(5)–H(5A)	118.6(14)
C(5)–N(5)–H(5B)	120.7(13)	H(5A)–N(5)–H(5B)	119.7(19)
Cl(7)–C(7)–N(6)	117.86(11)	Cl(7)–C(7)–C(8)	120.47(11)
N(6)–C(7)–C(8)	121.67(13)	C(5)–N(6)–C(7)	117.41(12)

N(1)–C(8)–C(7)	134.73(14)	N(1)–C(8)–C(9)	109.96(13)
C(7)–C(8)–C(9)	115.30(13)	N(3)–C(9)–N(4)	129.62(13)
N(3)–C(9)–C(8)	103.50(12)	N(4)–C(9)–C(8)	126.86(13)
N(3)–C(10)–O(11)	119.75(13)	N(3)–C(10)–O(12)	110.72(12)
O(11)–C(10)–O(12)	129.53(14)	C(10)–O(12)–C(13)	118.34(11)
O(12)–C(13)–C(14)	109.07(12)	O(12)–C(13)–C(15)	102.59(12)
O(12)–C(13)–C(16)	109.69(13)	C(14)–C(13)–C(15)	110.94(15)
C(14)–C(13)–C(16)	112.85(15)	C(15)–C(13)–C(16)	111.19(15)
C(13)–C(14)–H(14A)	109.5	C(13)–C(14)–H(14B)	109.5
C(13)–C(14)–H(14C)	109.5	H(14A)–C(14)–H(14B)	109.5
H(14A)–C(14)–H(14C)	109.5	H(14B)–C(14)–H(14C)	109.5
C(13)–C(15)–H(15A)	109.5	C(13)–C(15)–H(15B)	109.5
C(13)–C(15)–H(15C)	109.5	H(15A)–C(15)–H(15B)	109.5
H(15A)–C(15)–H(15C)	109.5	H(15B)–C(15)–H(15C)	109.5
C(13)–C(16)–H(16A)	109.5	C(13)–C(16)–H(16B)	109.5
C(13)–C(16)–H(16C)	109.5	H(16A)–C(16)–H(16B)	109.5
H(16A)–C(16)–H(16C)	109.5	H(16B)–C(16)–H(16C)	109.5

Table 26. Anisotropic displacement parameters (\AA^2) for **174**. The anisotropic displacement factor exponent takes the form: $-2\pi^2[h^2a^{*2}U^{11} + \dots + 2hka^*b^*U^{12}]$

	U^{11}	U^{22}	U^{33}	U^{23}	U^{13}	U^{12}
N(1)	0.0311(7)	0.0232(7)	0.0216(6)	−0.0041(5)	0.0068(5)	−0.0039(6)
N(2)	0.0306(7)	0.0231(6)	0.0200(6)	−0.0053(5)	0.0082(5)	−0.0028(5)
N(3)	0.0235(6)	0.0167(6)	0.0178(6)	−0.0041(5)	0.0045(5)	−0.0017(5)
N(4)	0.0206(6)	0.0160(6)	0.0181(6)	−0.0021(5)	0.0020(5)	0.0004(5)
C(5)	0.0213(7)	0.0174(7)	0.0186(7)	−0.0016(6)	0.0005(5)	0.0006(6)
N(5)	0.0435(9)	0.0181(7)	0.0201(7)	−0.0047(6)	0.0067(6)	−0.0075(6)
Cl(7)	0.0344(2)	0.0250(2)	0.0267(2)	0.00194(15)	0.01042(16)	−0.00649(16)
C(7)	0.0186(7)	0.0191(7)	0.0210(7)	0.0024(6)	0.0018(5)	−0.0009(6)
N(6)	0.0234(6)	0.0183(6)	0.0210(6)	−0.0009(5)	0.0025(5)	−0.0014(5)
C(8)	0.0199(7)	0.0198(7)	0.0188(7)	−0.0016(6)	0.0025(5)	0.0001(6)
C(9)	0.0155(6)	0.0154(7)	0.0195(7)	−0.0017(5)	0.0005(5)	0.0009(5)
C(10)	0.0202(7)	0.0175(7)	0.0204(7)	−0.0034(6)	0.0006(5)	−0.0013(6)
O(11)	0.0370(6)	0.0238(6)	0.0287(6)	−0.0092(5)	0.0148(5)	−0.0074(5)
O(12)	0.0308(6)	0.0159(5)	0.0232(5)	−0.0049(4)	0.0093(4)	−0.0041(4)
C(13)	0.0304(8)	0.0166(7)	0.0243(8)	−0.0020(6)	0.0065(6)	−0.0074(6)
C(14)	0.0470(11)	0.0289(9)	0.0331(9)	0.0078(7)	−0.0016(8)	−0.0072(8)
C(15)	0.0736(14)	0.0204(8)	0.0425(11)	−0.0102(8)	0.0274(10)	−0.0121(9)
C(16)	0.0289(9)	0.0314(10)	0.0592(12)	−0.0016(9)	−0.0021(8)	−0.0096(7)

Table 27. Hydrogen coordinates and isotropic displacement parameters (\AA^2) for **174**.

	x	y	z	U
H(14A)	-0.0617	0.0336	0.8960	0.055
H(14B)	0.0591	-0.0402	0.8409	0.055
H(14C)	-0.0796	-0.1104	0.8597	0.055
H(15A)	-0.0934	-0.0626	0.5445	0.067
H(15B)	-0.1005	-0.1695	0.6436	0.067
H(15C)	0.0390	-0.1002	0.6258	0.067
H(16A)	-0.2664	0.0736	0.6289	0.060
H(16B)	-0.2601	0.0943	0.7704	0.060
H(16C)	-0.2912	-0.0416	0.7155	0.060
H(5A)	0.126(2)	0.724(2)	0.9676(17)	0.033(5)
H(5B)	0.0566(19)	0.6176(18)	1.0116(17)	0.029(5)

Table 28. Torsion angles [$^\circ$] for **174**.

C(8)–N(1)–N(2)–N(3)	0.34(16)	N(1)–N(2)–N(3)–C(9)	-0.69(16)
N(1)–N(2)–N(3)–C(10)	175.86(13)	C(9)–N(4)–C(5)–N(5)	179.27(13)
C(9)–N(4)–C(5)–N(6)	0.2(2)	Cl(7)–C(7)–N(6)–C(5)	179.53(10)
C(8)–C(7)–N(6)–C(5)	-0.4(2)	N(4)–C(5)–N(6)–C(7)	-0.7(2)
N(5)–C(5)–N(6)–C(7)	-179.80(13)	N(2)–N(1)–C(8)–C(7)	-178.77(16)
N(2)–N(1)–C(8)–C(9)	0.12(17)	Cl(7)–C(7)–C(8)–N(1)	0.7(2)
Cl(7)–C(7)–C(8)–C(9)	-178.11(11)	N(6)–C(7)–C(8)–N(1)	-179.32(16)
N(6)–C(7)–C(8)–C(9)	1.8(2)	C(5)–N(4)–C(9)–N(3)	-179.91(14)
C(5)–N(4)–C(9)–C(8)	1.5(2)	N(2)–N(3)–C(9)–N(4)	-178.10(14)
N(2)–N(3)–C(9)–C(8)	0.72(15)	C(10)–N(3)–C(9)–N(4)	5.6(2)
C(10)–N(3)–C(9)–C(8)	-175.61(13)	N(1)–C(8)–C(9)–N(3)	-0.52(16)
N(1)–C(8)–C(9)–N(4)	178.34(13)	C(7)–C(8)–C(9)–N(3)	178.61(12)
C(7)–C(8)–C(9)–N(4)	-2.5(2)	N(2)–N(3)–C(10)–O(11)	-162.33(14)
N(2)–N(3)–C(10)–O(12)	17.84(19)	C(9)–N(3)–C(10)–O(11)	13.6(2)
C(9)–N(3)–C(10)–O(12)	-166.26(13)	N(3)–C(10)–O(12)–C(13)	-177.08(11)
O(11)–C(10)–O(12)–C(13)	3.1(2)	C(10)–O(12)–C(13)–C(14)	-65.81(17)
C(10)–O(12)–C(13)–C(15)	176.50(14)	C(10)–O(12)–C(13)–C(16)	58.25(17)

Table 29. Hydrogen bonds for **174** [\AA and $^\circ$].

D–H...A	d(D–H)	d(H...A)	d(D...A)	$\angle(\text{DHA})$
N(5)–H(5B)...N(4A)	0.84(2)	2.36(2)	3.2009(19)	174(2)

Symmetry operations for equivalent atoms

A $-x, -y+1, -z+2$

5-Formylpyrimidine **101**Table 30. Crystal data and structure refinement for **101**.

Identification code	101	
Chemical formula (moiety)	C ₁₃ H ₁₀ N ₄ O	
Chemical formula (total)	C ₁₃ H ₁₀ N ₄ O	
Formula weight	238.25	
Temperature	150(2) K	
Radiation, wavelength	MoK α , 0.71073 Å	
Crystal system, space group	monoclinic, P12 ₁ /c1	
Unit cell parameters	a = 4.6755(3) Å	$\alpha = 90^\circ$
	b = 24.8238(17) Å	$\beta = 94.831(6)^\circ$
	c = 9.8280(7) Å	$\gamma = 90^\circ$
Cell volume	1136.62(13) Å ³	
Z	4	
Calculated density	1.392 g/cm ³	
Absorption coefficient μ	0.094 mm ⁻¹	
F(000)	496	
Crystal colour and size	colourless, 0.30 × 0.20 × 0.10 mm ³	
Reflections for cell refinement	1894 (θ range 3.2 to 28.5°)	
Data collection method	Xcalibur, Atlas, Gemini ultra	
	thick-slice ω scans	
θ range for data collection	3.2 to 28.5°	
Index ranges	h -5 to 6, k -28 to 32, l -13 to 11	
Completeness to $\theta = 25.0^\circ$	99.9 %	
Reflections collected	5145	
Independent reflections	2363 ($R_{\text{int}} = 0.0210$)	
Reflections with $F^2 > 2\sigma$	1894	
Absorption correction	semi-empirical from equivalents	
Min. and max. transmission	0.9724 and 0.9907	
Structure solution	direct methods	
Refinement method	Full-matrix least-squares on F^2	
Weighting parameters a, b	0.0436, 0.2327	
Data / restraints / parameters	2363 / 0 / 217	
Final R indices [$F^2 > 2\sigma$]	R1 = 0.0389, wR2 = 0.0909	
R indices (all data)	R1 = 0.0524, wR2 = 0.0991	
Goodness-of-fit on F^2	1.040	
Extinction coefficient	0.0055(14)	
Largest and mean shift/su	0.001 and 0.000	
Largest diff. peak and hole	0.25 and -0.19 e Å ⁻³	

Table 31. Atomic coordinates and equivalent isotropic displacement parameters (\AA^2) for **101**. U_{eq} is defined as one third of the trace of the orthogonalized U^{ij} tensor.

	x	y	z	U_{eq}
O	0.2051(2)	0.83340(4)	0.51056(10)	0.0312(3)
N(1)	0.2006(3)	0.72288(5)	0.49977(12)	0.0244(3)
N(2)	0.4917(2)	0.68462(4)	0.35331(10)	0.0215(3)
N(3)	0.7834(2)	0.73801(4)	0.21340(11)	0.0199(3)
N(4)	0.7969(2)	0.64658(4)	0.20629(11)	0.0225(3)
C(1)	0.3839(3)	0.83054(5)	0.42645(13)	0.0246(3)
C(2)	0.4827(3)	0.78171(5)	0.36851(12)	0.0197(3)
C(3)	0.3897(3)	0.72952(5)	0.40782(12)	0.0197(3)
C(4)	0.6825(3)	0.69067(5)	0.26186(12)	0.0193(3)
C(5)	0.6792(3)	0.78202(5)	0.26818(12)	0.0190(3)
C(6)	0.7762(3)	0.83275(5)	0.21558(13)	0.0229(3)
C(7)	0.8535(4)	0.87392(6)	0.17104(17)	0.0369(4)
C(8)	0.7275(3)	0.59162(5)	0.22095(13)	0.0217(3)
C(9)	0.9131(8)	0.55568(12)	0.1711(4)	0.0269(8)
C(10)	0.8592(9)	0.50093(12)	0.1769(4)	0.0331(9)
C(9A)	0.7582(8)	0.55736(12)	0.1072(3)	0.0258(8)
C(10A)	0.6997(8)	0.50271(12)	0.1156(4)	0.0293(8)
C(11)	0.6176(3)	0.48165(6)	0.23479(15)	0.0303(3)
C(12)	0.4330(8)	0.51843(12)	0.2835(4)	0.0292(8)
C(13)	0.4833(8)	0.57360(11)	0.2787(3)	0.0265(8)
C(12A)	0.5862(9)	0.51431(12)	0.3461(4)	0.0316(9)
C(13A)	0.6419(8)	0.56931(12)	0.3384(3)	0.0283(8)

Table 32. Bond lengths [\AA] and angles [$^\circ$] for **101**.

O–C(1)	1.2263(17)	N(1)–H(1A)	0.892(19)
N(1)–H(1B)	0.874(18)	N(1)–C(3)	1.3266(18)
N(2)–C(3)	1.3416(17)	N(2)–C(4)	1.3270(17)
N(3)–C(4)	1.3670(16)	N(3)–C(5)	1.3285(16)
N(4)–H(4)	0.907(16)	N(4)–C(4)	1.3534(16)
N(4)–C(8)	1.4126(17)	C(1)–H(1C)	0.950
C(1)–C(2)	1.4321(18)	C(2)–C(3)	1.4301(18)
C(2)–C(5)	1.4033(19)	C(5)–C(6)	1.4483(18)
C(6)–C(7)	1.180(2)	C(7)–H(7)	0.93(2)
C(8)–C(9)	1.364(3)	C(8)–C(9A)	1.421(3)
C(8)–C(13)	1.391(3)	C(8)–C(13A)	1.370(3)
C(9)–H(9A)	0.950	C(9)–C(10)	1.384(4)
C(10)–H(10A)	0.950	C(10)–C(11)	1.391(4)
C(9A)–H(9AA)	0.950	C(9A)–C(10A)	1.388(4)
C(10A)–H(10B)	0.950	C(10A)–C(11)	1.367(4)
C(11)–H(11)	0.950	C(11)–C(12)	1.370(4)
C(11)–C(12A)	1.379(4)	C(12)–H(12A)	0.950
C(12)–C(13)	1.391(4)	C(13)–H(13A)	0.950
C(12A)–H(12B)	0.950	C(12A)–C(13A)	1.393(4)
C(13A)–H(13B)	0.950		

H(1A)–N(1)–H(1B)	121.8(16)	H(1A)–N(1)–C(3)	121.6(12)
H(1B)–N(1)–C(3)	116.6(11)	C(3)–N(2)–C(4)	117.28(11)
C(4)–N(3)–C(5)	114.63(11)	H(4)–N(4)–C(4)	114.7(10)
H(4)–N(4)–C(8)	115.5(10)	C(4)–N(4)–C(8)	129.62(12)
O–C(1)–H(1C)	117.3	O–C(1)–C(2)	125.32(13)
H(1C)–C(1)–C(2)	117.3	C(1)–C(2)–C(3)	122.93(12)
C(1)–C(2)–C(5)	121.80(12)	C(3)–C(2)–C(5)	115.26(11)
N(1)–C(3)–N(2)	116.64(12)	N(1)–C(3)–C(2)	122.13(12)
N(2)–C(3)–C(2)	121.23(12)	N(2)–C(4)–N(3)	127.21(12)
N(2)–C(4)–N(4)	119.54(11)	N(3)–C(4)–N(4)	113.25(11)
N(3)–C(5)–C(2)	124.36(11)	N(3)–C(5)–C(6)	115.71(11)
C(2)–C(5)–C(6)	119.92(11)	C(5)–C(6)–C(7)	179.12(15)
C(6)–C(7)–H(7)	179.0(12)	N(4)–C(8)–C(9)	115.87(16)
N(4)–C(8)–C(9A)	117.28(15)	N(4)–C(8)–C(13)	123.78(16)
N(4)–C(8)–C(13A)	124.22(16)	C(9)–C(8)–C(9A)	38.45(15)
C(9)–C(8)–C(13)	120.3(2)	C(9)–C(8)–C(13A)	106.1(2)
C(9A)–C(8)–C(13)	105.62(19)	C(9A)–C(8)–C(13A)	118.5(2)
C(13)–C(8)–C(13A)	38.56(16)	C(8)–C(9)–H(9A)	119.9
C(8)–C(9)–C(10)	120.2(3)	H(9A)–C(9)–C(10)	119.9
C(9)–C(10)–H(10A)	119.6	C(9)–C(10)–C(11)	120.8(3)
H(10A)–C(10)–C(11)	119.6	C(8)–C(9A)–H(9AA)	119.8
C(8)–C(9A)–C(10A)	120.3(2)	H(9AA)–C(9A)–C(10A)	119.8
C(9A)–C(10A)–H(10B)	120.1	C(9A)–C(10A)–C(11)	119.7(3)
H(10B)–C(10A)–C(11)	120.1	C(10)–C(11)–C(10A)	38.93(16)
C(10)–C(11)–H(11)	121.0	C(10)–C(11)–C(12)	118.1(2)
C(10)–C(11)–C(12A)	105.4(2)	C(10A)–C(11)–H(11)	119.3
C(10A)–C(11)–C(12)	106.0(2)	C(10A)–C(11)–C(12A)	120.7(2)
H(11)–C(11)–C(12)	121.0	H(11)–C(11)–C(12A)	120.0
C(12)–C(11)–C(12A)	38.65(16)	C(11)–C(12)–H(12A)	119.0
C(11)–C(12)–C(13)	122.1(3)	H(12A)–C(12)–C(13)	119.0
C(8)–C(13)–C(12)	118.5(3)	C(8)–C(13)–H(13A)	120.7
C(12)–C(13)–H(13A)	120.7	C(11)–C(12A)–H(12B)	120.0
C(11)–C(12A)–C(13A)	120.0(3)	H(12B)–C(12A)–C(13A)	120.0
C(8)–C(13A)–C(12A)	120.7(3)	C(8)–C(13A)–H(13B)	119.6
C(12A)–C(13A)–H(13B)	119.6		

Table 33. Anisotropic displacement parameters (\AA^2) for **101**. The anisotropic displacement factor exponent takes the form: $-2\pi^2[h^2a^{*2}U^{11} + \dots + 2hka^*b^*U^{12}]$

	U^{11}	U^{22}	U^{33}	U^{23}	U^{13}	U^{12}
O	0.0311(6)	0.0352(6)	0.0290(5)	−0.0038(4)	0.0124(4)	0.0029(5)
N(1)	0.0238(6)	0.0263(6)	0.0242(6)	0.0010(5)	0.0087(5)	−0.0010(5)
N(2)	0.0207(6)	0.0231(6)	0.0213(5)	0.0009(4)	0.0053(5)	−0.0022(5)
N(3)	0.0180(6)	0.0202(6)	0.0218(5)	0.0010(4)	0.0040(4)	0.0002(4)
N(4)	0.0208(6)	0.0199(6)	0.0281(6)	0.0009(5)	0.0105(5)	−0.0005(5)
C(1)	0.0268(7)	0.0246(7)	0.0229(6)	0.0007(5)	0.0058(6)	0.0005(6)
C(2)	0.0184(7)	0.0223(7)	0.0183(6)	0.0007(5)	0.0007(5)	0.0002(5)

C(3)	0.0163(6)	0.0249(7)	0.0177(6)	0.0007(5)	0.0006(5)	−0.0002(5)
C(4)	0.0170(6)	0.0213(6)	0.0195(6)	0.0009(5)	0.0007(5)	−0.0011(5)
C(5)	0.0159(6)	0.0219(7)	0.0189(6)	0.0011(5)	−0.0002(5)	−0.0001(5)
C(6)	0.0212(7)	0.0231(7)	0.0255(7)	−0.0030(6)	0.0069(6)	0.0018(6)
C(7)	0.0410(9)	0.0227(8)	0.0498(9)	0.0017(7)	0.0212(8)	−0.0005(7)
C(8)	0.0195(7)	0.0205(6)	0.0252(6)	0.0014(5)	0.0030(5)	0.0003(5)
C(9)	0.0227(18)	0.0243(15)	0.0350(17)	0.0004(13)	0.0105(16)	−0.0011(13)
C(10)	0.032(2)	0.0228(15)	0.045(2)	−0.0052(14)	0.0097(18)	0.0046(14)
C(9A)	0.0252(19)	0.0283(15)	0.0249(15)	0.0017(12)	0.0083(15)	0.0032(13)
C(10A)	0.028(2)	0.0254(15)	0.0349(17)	−0.0067(13)	0.0052(16)	0.0021(13)
C(11)	0.0316(8)	0.0192(7)	0.0405(8)	0.0006(6)	0.0058(7)	−0.0021(6)
C(12)	0.0305(19)	0.0272(16)	0.0310(17)	0.0027(13)	0.0088(16)	−0.0077(14)
C(13)	0.0253(18)	0.0224(14)	0.0330(17)	−0.0013(13)	0.0094(15)	−0.0014(13)
C(12A)	0.037(2)	0.0263(16)	0.0324(17)	0.0063(13)	0.0089(17)	−0.0025(14)
C(13A)	0.032(2)	0.0275(16)	0.0265(15)	−0.0012(12)	0.0054(15)	−0.0001(14)

Table 34. Hydrogen coordinates and isotropic displacement parameters (\AA^2) for **101**.

	x	y	z	U
H(1A)	0.123(4)	0.7509(7)	0.5399(18)	0.042(5)
H(1B)	0.159(4)	0.6897(7)	0.5201(16)	0.037(5)
H(4)	0.928(3)	0.6538(6)	0.1459(15)	0.030(4)
H(1C)	0.4634	0.8634	0.3974	0.029
H(7)	0.916(4)	0.9061(8)	0.1349(18)	0.056(5)
H(9A)	1.0800	0.5683	0.1323	0.032
H(10A)	0.9886	0.4762	0.1410	0.040
H(9AA)	0.8190	0.5719	0.0251	0.031
H(10B)	0.7167	0.4800	0.0388	0.035
H(11)	0.5818	0.4441	0.2404	0.036
H(12A)	0.2653	0.5059	0.3216	0.035
H(13A)	0.3538	0.5984	0.3141	0.032
H(12B)	0.5266	0.4993	0.4280	0.038
H(13B)	0.6202	0.5916	0.4154	0.034

Table 35. Torsion angles [°] for **101**.

O–C(1)–C(2)–C(3)	–2.8(2)	O–C(1)–C(2)–C(5)	177.19(13)
C(4)–N(2)–C(3)–N(1)	–179.56(11)	C(4)–N(2)–C(3)–C(2)	0.16(17)
C(1)–C(2)–C(3)–N(1)	1.1(2)	C(1)–C(2)–C(3)–N(2)	–178.58(11)
C(5)–C(2)–C(3)–N(1)	–178.83(11)	C(5)–C(2)–C(3)–N(2)	1.48(17)
C(3)–N(2)–C(4)–N(3)	–1.82(19)	C(3)–N(2)–C(4)–N(4)	178.44(11)
C(8)–N(4)–C(4)–N(2)	6.2(2)	C(8)–N(4)–C(4)–N(3)	–173.53(11)
C(5)–N(3)–C(4)–N(2)	1.55(18)	C(5)–N(3)–C(4)–N(4)	–178.69(10)
C(4)–N(3)–C(5)–C(2)	0.40(18)	C(4)–N(3)–C(5)–C(6)	–178.21(10)
C(1)–C(2)–C(5)–N(3)	178.27(11)	C(1)–C(2)–C(5)–C(6)	–3.17(18)
C(3)–C(2)–C(5)–N(3)	–1.78(18)	C(3)–C(2)–C(5)–C(6)	176.77(11)
N(3)–C(5)–C(6)–C(7)	64(10)	C(2)–C(5)–C(6)–C(7)	–115(10)
C(4)–N(4)–C(8)–C(9)	–169.1(2)	C(4)–N(4)–C(8)–C(9A)	147.7(2)
C(4)–N(4)–C(8)–C(13)	12.5(3)	C(4)–N(4)–C(8)–C(13A)	–34.5(3)
N(4)–C(8)–C(9)–C(10)	–178.1(3)	C(9A)–C(8)–C(9)–C(10)	–76.0(4)
C(13)–C(8)–C(9)–C(10)	0.4(4)	C(13A)–C(8)–C(9)–C(10)	39.7(4)
C(8)–C(9)–C(10)–C(11)	–0.7(5)	N(4)–C(8)–C(9A)–C(10A)	178.6(3)
C(9)–C(8)–C(9A)–C(10A)	80.5(4)	C(13)–C(8)–C(9A)–C(10A)	–38.9(4)
C(13A)–C(8)–C(9A)–C(10A)	0.6(4)	C(8)–C(9A)–C(10A)–C(11)	–1.3(5)
C(9A)–C(10A)–C(11)–C(10)	–74.5(4)	C(9A)–C(10A)–C(11)–C(12)	40.6(4)
C(9A)–C(10A)–C(11)–C(12A)	1.4(4)	C(9)–C(10)–C(11)–C(10A)	81.7(4)
C(9)–C(10)–C(11)–C(12)	1.1(4)	C(9)–C(10)–C(11)–C(12A)	–38.5(4)
C(10)–C(11)–C(12)–C(13)	–1.2(4)	C(10A)–C(11)–C(12)–C(13)	–41.3(4)
C(12A)–C(11)–C(12)–C(13)	78.3(4)	N(4)–C(8)–C(13)–C(12)	177.9(2)
C(9)–C(8)–C(13)–C(12)	–0.4(4)	C(9A)–C(8)–C(13)–C(12)	38.5(4)
C(13A)–C(8)–C(13)–C(12)	–77.9(4)	C(11)–C(12)–C(13)–C(8)	0.8(5)
C(10)–C(11)–C(12A)–C(13A)	38.4(4)	C(10A)–C(11)–C(12A)–C(13A)	
	–0.8(5)		
C(12)–C(11)–C(12A)–C(13A)	–77.5(4)	N(4)–C(8)–C(13A)–C(12A)	–177.9(3)
C(9)–C(8)–C(13A)–C(12A)	–39.6(4)	C(9A)–C(8)–C(13A)–C(12A)	0.0(4)
C(13)–C(8)–C(13A)–C(12A)	79.1(4)	C(11)–C(12A)–C(13A)–C(8)	0.1(5)

Table 36. Hydrogen bonds for **101** [Å and °].

D–H...A	d(D–H)	d(H...A)	d(D...A)	<(DHA)
N(4)–H(4)...OA	0.907(16)	1.959(17)	2.8647(15)	177(1)
N(1)–H(1A)...O	0.892(19)	2.108(18)	2.7456(17)	128(1)
N(1)–H(1A)...N(3B)	0.892(19)	2.441(19)	3.1378(17)	135(1)

Symmetry operations for equivalent atoms

A $x+1, -y+3/2, z-1/2$ B $x-1, -y+3/2, z+1/2$

ii - ^1H -qNMR Experimental Data

2-Benzylpurine 52 – 0.30 mole equivalents of DABCO

Experiment 1 ($R^2 = 0.9832$; $k' = 5.0 \times 10^{-4} \text{ s}^{-1}$; $t_{1/2} = 1386 \text{ s}$)

Time (s)	Integration of Ethynyl C-H (Baseline Corrected)	[52] (mM)	ln[52]
975	0.6539	3.92	-5.54
1575	0.4082	2.45	-6.01
2175	0.2874	1.72	-6.36
2775	0.2053	1.23	-6.70
3375	0.1554	0.93	-6.98
3975	0.1257	0.75	-7.19
4575	0.0751	0.45	-7.70
5175	0.0779	0.47	-7.67
5775	0.0568	0.34	-7.98
6375	0.0407	0.24	-8.32

Experiment 2 ($R^2 = 0.9203$; $k' = 4.9 \times 10^{-4} \text{ s}^{-1}$; $t_{1/2} = 1415 \text{ s}$)

Time (s)	Integration of Ethynyl C-H (Baseline Corrected)	[52] (mM)	ln[52]
1044	0.4157	2.49	-5.99
1644	0.2658	1.59	-6.44
2244	0.1960	1.18	-6.75
2844	0.1475	0.89	-7.03
3444	0.1278	0.77	-7.17
4044	0.0684	0.41	-7.80
4644	0.0594	0.36	-7.94
5244	0.0550	0.33	-8.02
5844	0.0690	0.41	-7.79
6444	0.0412	0.25	-8.31

Experiment 3 ($R^2 = 0.9564$; $k' = 4.8 \times 10^{-4} \text{ s}^{-1}$; $t_{1/2} = 1444 \text{ s}$)

Time (s)	Integration of Ethynyl C-H (Baseline Corrected)	[52] (mM)	ln[52]
984	0.6446	3.87	-5.56
1584	0.4950	2.97	-5.82
2184	0.3238	1.94	-6.24
2784	0.2476	1.49	-6.51
3384	0.1926	1.16	-6.76
3984	0.1740	1.04	-6.86
4584	0.0951	0.57	-7.47
5184	0.0545	0.33	-8.03
5784	0.0696	0.42	-7.78
6384	0.0590	0.35	-7.95

2-Methylanilinopurine **54** – 0.30 mole equivalents of DABCO

Experiment 1 ($R^2 = 0.9895$; $k' = 1.5 \times 10^{-4} \text{ s}^{-1}$; $t_{1/2} = 4621 \text{ s}$)

Time (s)	Integration of Ethynyl C-H (Baseline Corrected)	[54] (mM)	ln[54]
985	0.7330	4.40	-5.43
1585	0.7319	4.39	-5.43
2185	0.6414	3.85	-5.56
2785	0.6102	3.66	-5.61
3385	0.5033	3.02	-5.80
3985	0.4996	3.00	-5.81
4585	0.4504	2.70	-5.91
5185	0.3983	2.39	-6.04
5785	0.3596	2.16	-6.14
6385	0.3045	1.83	-6.31
6985	0.3103	1.86	-6.29
7585	0.2755	1.65	-6.41
8185	0.2779	1.67	-6.40
8785	0.2379	1.43	-6.55
9385	0.2043	1.23	-6.70
9985	0.1928	1.16	-6.76

Experiment 2 ($R^2 = 0.8869$; $k' = 1.3 \times 10^{-4} \text{ s}^{-1}$; $t_{1/2} = 5332 \text{ s}$)

Time (s)	Integration of Ethynyl C-H (Baseline Corrected)	[54] (mM)	ln[54]
985	0.6333	3.80	-5.57
1585	0.5270	3.16	-5.76
2185	0.4887	2.93	-5.83
2785	0.4304	2.58	-5.96
3385	0.4084	2.45	-6.01
3985	0.3432	2.06	-6.19
4585	0.3058	1.83	-6.30
5185	0.2785	1.67	-6.39
5785	0.2431	1.46	-6.53
6385	0.2618	1.57	-6.46
6985	0.2014	1.21	-6.72
7585	0.2414	1.45	-6.54
8185	0.2089	1.25	-6.68
8785	0.1726	1.04	-6.87
9385	0.2015	1.21	-6.72
9985	0.2287	1.37	-6.59

Experiment 3 ($R^2 = 0.9141$; $k' = 1.3 \times 10^{-4} \text{ s}^{-1}$; $t_{1/2} = 5332 \text{ s}$)

Time (s)	Integration of Ethynyl C-H (Baseline Corrected)	[54] (mM)	ln[54]
846	0.8411	5.05	-5.29
1446	0.7693	4.62	-5.38
2046	0.7014	4.21	-5.47
2646	0.5982	3.59	-5.63
3246	0.5317	3.19	-5.75
3846	0.5016	3.01	-5.81
4446	0.4156	2.49	-5.99
5046	0.4217	2.53	-5.98
5646	0.3869	2.32	-6.07
6246	0.5035	3.02	-5.80
6846	0.4199	2.52	-5.98
7446	0.3640	2.18	-6.13
8046	0.3166	1.90	-6.27
8646	0.2949	1.77	-6.34
9246	0.2160	1.30	-6.65
9846	0.2214	1.33	-6.62

Pyrrolopyrimidine **88** – 0.30 mole equivalents of DABCO

Experiment 1 ($R^2 = 0.9939$; $k' = 3.1 \times 10^{-5} \text{ s}^{-1}$; $t_{1/2} = 22360 \text{ s}$)

Time (s)	Integration of Ethynyl C-H (Baseline Corrected)	[88] (mM)	ln[88]
972	0.9908	5.94	-5.13
1572	0.9701	5.82	-5.15
2172	0.9453	5.67	-5.17
2772	0.9280	5.57	-5.19
3372	0.9107	5.46	-5.21
3972	0.8912	5.35	-5.23
4572	0.8787	5.27	-5.25
5172	0.8495	5.10	-5.28
5772	0.8397	5.04	-5.29
6372	0.8224	4.93	-5.31
6972	0.8089	4.85	-5.33
7572	0.7980	4.79	-5.34
8172	0.7935	4.76	-5.35
8772	0.7777	4.67	-5.37
9372	0.7448	4.47	-5.41
9972	0.7528	4.52	-5.40
10572	0.7517	4.51	-5.40
11172	0.7365	4.42	-5.42
11772	0.6941	4.16	-5.48
12372	0.6890	4.13	-5.49

12972	0.6691	4.01	-5.52
13572	0.6689	4.01	-5.52
14172	0.6429	3.86	-5.56
14772	0.6357	3.81	-5.57
15372	0.6155	3.69	-5.60
15972	0.6115	3.67	-5.61
16572	0.6114	3.67	-5.61
17172	0.6044	3.63	-5.62
17772	0.5715	3.43	-5.68
18372	0.5644	3.39	-5.69

Experiment 2 ($R^2 = 0.9187$; $k' = 3.0 \times 10^{-5} \text{ s}^{-1}$; $t_{1/2} = 23105 \text{ s}$)

Time (s)	Integration of Ethynyl C-H (Baseline Corrected)	[88] (mM)	ln[88]
990	0.8023	4.81	-5.34
1590	0.7438	4.46	-5.41
2190	0.6481	3.89	-5.55
2790	0.6703	4.02	-5.52
3390	0.6830	4.10	-5.50
3990	0.6534	3.92	-5.54
4590	0.6292	3.78	-5.58
5190	0.6545	3.93	-5.54
5790	0.6009	3.61	-5.63
6390	0.6236	3.74	-5.59
6990	0.5573	3.34	-5.70
7590	0.6311	3.79	-5.58
8190	0.5776	3.47	-5.66
8790	0.5744	3.45	-5.67
9390	0.5439	3.26	-5.72
9990	0.5820	3.49	-5.66
10590	0.5225	3.14	-5.77
11190	0.5528	3.32	-5.71
11790	0.5310	3.19	-5.75
12390	0.5521	3.31	-5.71
12990	0.4827	2.90	-5.84
13590	0.4993	3.00	-5.81
14190	0.4853	2.91	-5.84
14790	0.4507	2.70	-5.91
15390	0.4950	2.97	-5.82
15990	0.4684	2.81	-5.87
16590	0.4602	2.76	-5.89
17190	0.4687	2.81	-5.87
17790	0.4109	2.47	-6.01
18390	0.4527	2.72	-5.91

Experiment 3 ($R^2 = 0.9951$; $k' = 2.8 \times 10^{-5} \text{ s}^{-1}$; $t_{1/2} = 24755 \text{ s}$)

Time (s)	Integration of Ethynyl C-H (Baseline Corrected)	[88] (mM)	ln[88]
978	0.8463	5.08	-5.28
1578	0.8432	5.06	-5.29
2178	0.8180	4.91	-5.32
2778	0.8001	4.80	-5.34
3378	0.7953	4.77	-5.35
3978	0.7747	4.65	-5.37
4578	0.7537	4.52	-5.40
5178	0.7448	4.47	-5.41
5778	0.7352	4.41	-5.42
6378	0.7300	4.38	-5.43
6978	0.7176	4.31	-5.45
7578	0.6965	4.18	-5.48
8178	0.6842	4.11	-5.50
8778	0.6994	4.20	-5.47
9378	0.6655	3.99	-5.52
9978	0.6490	3.89	-5.55
10578	0.6428	3.86	-5.56
11178	0.6399	3.84	-5.56
11778	0.6304	3.78	-5.58
12378	0.6205	3.72	-5.59
12978	0.6147	3.69	-5.60
13578	0.5821	3.49	-5.66
14178	0.5841	3.50	-5.65
14778	0.5659	3.40	-5.69
15378	0.5610	3.37	-5.69
15978	0.5545	3.33	-5.71
16578	0.5391	3.23	-5.73
17178	0.5362	3.22	-5.74
17778	0.5316	3.19	-5.75
18378	0.5173	3.10	-5.78

Pyrazolopyrimidine **89** – 0.03 mole equivalents of DABCO

Experiment 1 ($R^2 = 0.9408$; $k' = 5.7 \times 10^{-4} \text{ s}^{-1}$; $t_{1/2} = 1218 \text{ s}$)

Time (s)	Integration of Ethynyl C-H (Baseline Corrected)	[89] (mM)	ln[89]
1044	0.4709	2.83	-5.87
1644	0.3177	1.91	-6.26
2244	0.2076	1.25	-6.69
2844	0.1357	0.81	-7.11
3444	0.0999	0.60	-7.42
4044	0.0663	0.40	-7.83
4644	0.0382	0.23	-8.38
5244	0.0244	0.15	-8.83
5844	0.0128	0.08	-9.47
6444	0.0199	0.12	-9.03
7044	0.0169	0.10	-9.20
7644	0.0145	0.09	-9.35

Experiment 2 ($R^2 = 0.9937$; $k' = 5.3 \times 10^{-4} \text{ s}^{-1}$; $t_{1/2} = 1310 \text{ s}$)

Time (s)	Integration of Ethynyl C-H (Baseline Corrected)	[89] (mM)	ln[89]
858	0.5965	3.58	-5.64
1458	0.4416	2.65	-5.93
2058	0.3520	2.11	-6.16
2658	0.2331	1.40	-6.57
3258	0.1594	0.96	-6.95
3858	0.1134	0.68	-7.29
4458	0.0769	0.46	-7.68
5058	0.0571	0.34	-7.98
5658	0.0451	0.27	-8.21
6258	0.0309	0.19	-8.59
6858	0.0265	0.16	-8.75
7458	0.0211	0.13	-8.97

Triazolopyrimidine **90** – 0.03 mole equivalents of DABCO

Experiment 1 ($R^2 = 0.9524$; $k' = 16.5 \times 10^{-4} \text{ s}^{-1}$; $t_{1/2} = 420 \text{ s}$)

Time (s)	Integration of Ethynyl C-H (Baseline Corrected)	[90] (mM)	ln[90]
564	0.5923	3.55	-5.64
744	0.4565	2.74	-5.90
924	0.3316	1.99	-6.22
1104	0.2354	1.41	-6.56
1284	0.1540	0.92	-6.99
1464	0.1265	0.76	-7.18
1644	0.0886	0.53	-7.54
1824	0.0448	0.27	-8.22
2004	0.0698	0.42	-7.78
2184	0.0480	0.29	-8.15

Experiment 2 ($R^2 = 0.8291$; $k' = 16.6 \times 10^{-4} \text{ s}^{-1}$; $t_{1/2} = 418 \text{ s}$)

Time (s)	Integration of Ethynyl C-H (Baseline Corrected)	[90] (mM)	ln[90]
552	0.5931	3.56	-5.64
732	0.4095	2.46	-6.01
912	0.2756	1.65	-6.40
1092	0.1630	0.98	-6.93
1272	0.0590	0.35	-7.95
1452	0.0608	0.36	-7.92
1632	0.0456	0.27	-8.20
1812	0.0543	0.33	-8.03
1992	0.0538	0.32	-8.04
2172	0.0452	0.27	-8.21

Experiment 3 ($R^2 = 0.8882$; $k' = 19.0 \times 10^{-4} \text{ s}^{-1}$; $t_{1/2} = 401 \text{ s}$)

Time (s)	Integration of Ethynyl C-H (Baseline Corrected)	[90] (mM)	ln[90]
528	0.6458	3.87	-5.55
708	0.4391	2.63	-5.94
888	0.2840	1.70	-6.37
1068	0.1689	1.01	-6.89
1248	0.1139	0.68	-7.29
1428	0.0731	0.44	-7.73
1608	0.0513	0.31	-8.09
1788	0.0482	0.29	-8.15
1620	0.0361	0.22	-8.44
2148	0.0473	0.28	-8.17

Bibliography

1. Rang, H. P.; Dale, M. *Rang and Dale's Pharmacology*. 6th ed.; Elsevier Limited, Oxford: **2007**.
2. WHO Cancer. <http://www.who.int/mediacentre/factsheets/fs297/en/> (09th January 2013).
3. Cancer in the UK, December 2011. http://www.cancerresearchuk.org/cancer-info/prod_consump/groups/cr_common/@nre/@sta/documents/generalcontent/018070.pdf (09th January 2013).
4. Avendano, C.; Menendez, J. C. *Medicinal Chemistry of Anticancer Drugs*. Elsevier Science: **2008**; p 1-8.
5. Hanahan, D.; Weinberg, Robert A. Hallmarks of Cancer: The Next Generation. *Cell* **2011**, *144*, 646-674.
6. Miller, J. H.; Lewontin, R. C.; Gelbart, W. M.; Griffiths, A. J. F. *Molecular Cell Biology 4th Edition*. Macmillan Higher Education: **2002**.
7. Hanahan, D.; Weinberg, R. A. The Hallmarks of Cancer. *Cell* **2000**, *100*, 57-70.
8. Witsch, E.; Sela, M.; Yarden, Y. Roles for growth factors in cancer progression. *Physiology* **2010**, *25*, 85-101.
9. Sporn, M. B.; Todaro, G. J. Autocrine secretion and malignant transformation of cells. *N. Engl. J. Med.* **1980**, *303*, 878-880.
10. Habib, A. A.; Chun, S. J.; Neel, B. G.; Vartanian, T. Increased expression of epidermal growth factor receptor induces sequestration of extracellular signal-related kinases and selective attenuation of specific epidermal growth factor-mediated signal transduction pathways. *Mol. Cancer Res.* **2003**, *1*, 219-233.
11. Bennisroune, A.; Gardin, A.; Aunis, D.; Cremel, G.; Hubert, P. Tyrosine kinase receptors as attractive targets of cancer therapy. *Crit. Rev. Oncol. Hematol.* **2004**, *50*, 23-38.
12. Di Fiore, P.; Pierce, J.; Kraus, M.; Segatto, O.; King, C.; Aaronson, S. erbB-2 is a potent oncogene when overexpressed in NIH/3T3 cells. *Science* **1987**, *237*, 178-182.
13. Schito, L.; Rey, S.; Tafani, M.; Zhang, H.; Wong, C. C.-L.; Russo, A.; Russo, M. A.; Semenza, G. L. Hypoxia-inducible factor 1-dependent expression of platelet-derived growth factor B promotes lymphatic metastasis of hypoxic breast cancer cells. *Proc. Nat. Acad. Sci.* **2012**, *109*, 2707-2716.
14. Davies, M. A.; Samuels, Y. Analysis of the genome to personalize therapy for melanoma. *Oncogene* **2010**, *29*, 5545-5555.
15. Burkhart, D. L.; Sage, J. Cellular mechanisms of tumour suppression by the retinoblastoma gene. *Nat. Rev. Cancer* **2008**, *8*, 671-682.
16. Zheng, L.; Lee, W.-H. The Retinoblastoma Gene: A Prototypic and Multifunctional Tumor Suppressor. *Exp. Cell Res.* **2001**, *264*, 2-18.
17. Jain, M. V.; Paczulla, A. M.; Klonisch, T.; Dimgba, F. N.; Rao, S. B.; Roberg, K.; Schweizer, F.; Lengerke, C.; Davoodpour, P.; Palicharla, V. R.; Maddika, S.; Łos, M. Interconnections between apoptotic, autophagic and necrotic pathways: implications for cancer therapy development. *J. Cell. Mol. Med.* **2012**, 12-29.
18. Olivier, M.; Hollstein, M.; Hainaut, P. TP53 Mutations in Human Cancers: Origins, Consequences, and Clinical Use. *Cold Spring Harb. Perspect. Biol.* **2010**, *2*.

19. Chambers, A. F.; Groom, A. C.; MacDonald, I. C. Metastasis: Dissemination and growth of cancer cells in metastatic sites. *Nat. Rev. Cancer* **2002**, *2*, 563-572.
20. Wyckoff, J. B.; Jones, J. G.; Condeelis, J. S.; Segall, J. E. A Critical Step in Metastasis: In Vivo Analysis of Intravasation at the Primary Tumor. *Cancer Res.* **2000**, *60*, 2504-2511.
21. Chaffer, C. L.; Weinberg, R. A. A Perspective on Cancer Cell Metastasis. *Science* **2011**, *331*, 1559-1564.
22. Steeg, P. S. Tumor metastasis: mechanistic insights and clinical challenges. *Nat. Med.* **2006**, *12*, 895-904.
23. Guo, W.; Giancotti, F. G. Integrin signalling during tumour progression. *Nat. Rev. Mol. Cell Biol.* **2004**, *5*, 816-826.
24. Cavallaro, U.; Christofori, G. Cell adhesion and signalling by cadherins and Ig-CAMs in cancer. *Nat. Rev. Cancer.* **2004**, *4*, 118-132.
25. Pai, S. I.; Lin, Y. Y.; Macaes, B.; Meneshian, A.; Hung, C. F.; Wu, T. C. Prospects of RNA interference therapy for cancer. *Gene Ther.* **2006**, *13*, 464-477.
26. Donate, L. E.; Blasco, M. A. Telomeres in cancer and ageing. *Phil. Trans. R. Soc. B* **2011**, *366*, 76-84.
27. Campbell, Peter J. Telomeres and Cancer: From Crisis to Stability to Crisis to Stability. *Cell* **2012**, *148*, 633-635.
28. Raynaud, C. M.; Hernandez, J.; Llorca, F. P.; Nuciforo, P.; Mathieu, M. C.; Commo, F.; Delaloge, S.; Sabatier, L.; Andre, F.; Soria, J. C. DNA damage repair and telomere length in normal breast, preneoplastic lesions, and invasive cancer. *Am. J. Clin. Oncol.* **2010**, *33*, 341-345.
29. Papetti, M.; Herman, I. M. Mechanisms of normal and tumor-derived angiogenesis. *Am. J. Physiol. Cell Physiol* **2002**, *282*, 947-970.
30. Folkman, J. *Tumor Angiogenesis*. Academic Press: **1985**; Vol. 43, p 175-203.
31. Kerbel, R. S. Tumor angiogenesis: past, present and the near future. *Carcinogenesis* **2000**, *21*, 505-515.
32. Siemann, D. W. Vascular Targeting Agents. *Horizons in Cancer Therapeutics: From Bench to Bedside* **2002**, *3*, 4-15.
33. Risau, W. Mechanisms of angiogenesis. *Nature* **1997**, *386*, 671-674.
34. Bergers, G.; Benjamin, L. E. Tumorigenesis and the angiogenic switch. *Nat. Rev. Cancer* **2003**, *3*, 401-410.
35. Kazerounian, S.; Yee, K. O.; Lawler, J. Thrombospondins in cancer. *Cell Mol. Life Sci.* **2008**, *65*, 700-712.
36. Takahashi, Y.; Kitadai, Y.; Bucana, C. D.; Cleary, K. R.; Ellis, L. M. Expression of vascular endothelial growth factor and its receptor, KDR, correlates with vascularity, metastasis, and proliferation of human colon cancer. *Cancer Res.* **1995**, *55*, 3964-3968.
37. Hoeben, A.; Landuyt, B.; Highley, M. S.; Wildiers, H.; Van Oosterom, A. T.; De Bruijn, E. A. Vascular Endothelial Growth Factor and Angiogenesis. *Pharmacol. Rev.* **2004**, *56*, 549-580.
38. Ellis, L. M.; Hicklin, D. J. VEGF-targeted therapy: mechanisms of anti-tumour activity. *Nat. Rev. Cancer* **2008**, *8*, 579-591.
39. Chen, H.; Herndon, M. E.; Lawler, J. The cell biology of thrombospondin-1. *Matrix Biology* **2000**, *19*, 597-614.
40. Levine, A. J.; Oren, M. The first 30 years of p53: growing ever more complex. *Nat. Rev. Cancer* **2009**, *9*, 749-758.

41. Ravi, R.; Mookerjee, B.; Bhujwalla, Z. M.; Sutter, C. H.; Artemov, D.; Zeng, Q.; Dillehay, L. E.; Madan, A.; Semenza, G. L.; Bedi, A. Regulation of tumor angiogenesis by p53-induced degradation of hypoxia-inducible factor 1alpha. *Genes Dev.* **2000**, *14*, 34-44.
42. Reed, J. C. Mechanisms of apoptosis. *Am. J. Pathol.* **2000**, *157*, 1415-1430.
43. Adams, J. M.; Cory, S. Bcl-2-regulated apoptosis: mechanism and therapeutic potential. *Curr. Opin. Immunol.* **2007**, *19*, 488-496.
44. Olsson, M.; Zhivotovsky, B. Caspases and cancer. *Cell Death Differ.* **2011**, *18*, 1441-1449.
45. Prendergast, G. C. Mechanisms of apoptosis by c-Myc. *Oncogene* **1999**, *18*, 2967-2987.
46. Bartek, J.; Lukas, J. Chk1 and Chk2 kinases in checkpoint control and cancer. *Cancer cell* **2003**, *3*, 421-429.
47. Ocker, M.; Höpfner, M. Apoptosis-Modulating Drugs for Improved Cancer Therapy. *Eur. Surg. Res.* **2012**, *48*, 111-120.
48. Chabner, B. A.; Roberts, T. G. Chemotherapy and the war on cancer. *Nat. Rev. Cancer* **2005**, *5*, 65-72.
49. Gerber, D. E. Targeted therapies: a new generation of cancer treatments. *Am. Fam. Physician.* **2008**, *77*, 311-319.
50. Arora, A.; Scholar, E. M. Role of Tyrosine Kinase Inhibitors in Cancer Therapy. *J. Pharmacol. Exp. Ther.* **2005**, *315*, 971-979.
51. Nygren, P.; Larsson, R. Overview of the clinical efficacy of investigational anticancer drugs. *J. Intern. Med.* **2003**, *253*, 46-75.
52. Rosa, D. D.; Ismael, G.; Lago, L. D.; Awada, A. Molecular-targeted therapies: Lessons from years of clinical development. *Cancer Treat. Rev.* **2008**, *34*, 61-80.
53. Katsios, C.; Ziogas, D. E.; Roukos, D. H.; Baltogiannis, G. Targeted therapy for colorectal cancer resistance to EGF receptor antibodies and new trends. *Expert Rev Gastroenterol Hepatol.* **2012**, *7*, 5-8.
54. Cavalli, F.; Hansen, H. H.; Kaye, S. B.; Oncology, E. S. f. M. *Textbook of Medical Oncology*. 3rd ed.; Taylor & Francis Group: **2004**.
55. Rixe, O.; Fojo, T. Is Cell Death a Critical End Point for Anticancer Therapies or Is Cytostasis Sufficient? *Clin. Cancer Res.* **2007**, *13*, 7280-7287.
56. Morphy, J. R.; Harris, C. J. *Designing Multi-Target Drugs*. Royal Society of Chemistry: **2012**; p 155-180.
57. Kummar, S.; Chen, A.; Ji, J.; Zhang, Y.; Reid, J. M.; Ames, M.; Jia, L.; Weil, M.; Speranza, G.; Murgo, A. J.; Kinders, R.; Wang, L.; Parchment, R. E.; Carter, J.; Stotler, H.; Rubinstein, L.; Hollingshead, M.; Melillo, G.; Pommier, Y.; Bonner, W.; Tomaszewski, J. E.; Doroshow, J. H. Phase I study of PARP inhibitor ABT-888 in combination with topotecan in adults with refractory solid tumors and lymphomas. *Cancer Res.* **2011**, *71*, 5626-5634.
58. Thomas, H. D.; Calabrese, C. R.; Batey, M. A.; Canan, S.; Hostomsky, Z.; Kyle, S.; Maegley, K. A.; Newell, D. R.; Skalitzky, D.; Wang, L.-Z.; Webber, S. E.; Curtin, N. J. Preclinical selection of a novel poly(ADP-ribose) polymerase inhibitor for clinical trial. *Mol. Cancer Ther.* **2007**, *6*, 945-956.
59. Kummar, S.; Chen, A.; Parchment, R.; Kinders, R.; Ji, J.; Tomaszewski, J.; Doroshow, J. Advances in using PARP inhibitors to treat cancer. *BMC Med.* **2012**, *10*, 25.
60. IHGSC. Finishing the euchromatic sequence of the human genome. *Nature* **2004**, *431*, 931-945.

61. Fedorov, O.; Sundström, M.; Marsden, B.; Knapp, S. Insights for the development of specific kinase inhibitors by targeted structural genomics. *Drug Discovery Today* **2007**, *12*, 365-372.
62. Matthews, D. J.; Gerritsen, M. E. *Targeting Protein Kinases for Cancer Therapy*. Wiley: **2011**.
63. Tsatsanis, C.; Spandidos, D. A. The role of oncogenic kinases in human cancer (Review). *Int. J. Mol. Med.* **2000**, *5*, 583-590.
64. Capra, M.; Nuciforo, P. G.; Confalonieri, S.; Quarto, M.; Bianchi, M.; Nebuloni, M.; Boldorini, R.; Pallotti, F.; Viale, G.; Gishizky, M. L.; Draetta, G. F.; Di Fiore, P. P. Frequent Alterations in the Expression of Serine/Threonine Kinases in Human Cancers. *Cancer Research* **2006**, *66*, 8147-8154.
65. Endicott, J. A.; Noble, M. E. M.; Johnson, L. N. The Structural Basis for Control of Eukaryotic Protein Kinases. *Annu. Rev. Biochem.* **2012**, *81*, 587-613.
66. Melnikova, I.; Golden, J. Targeting protein kinases. *Nat. Rev. Drug Discov.* **2004**, *3*, 993-994.
67. Cohen, P. Protein kinases - the major drug targets of the twenty-first century? *Nat. Rev. Drug Discov.* **2002**, *1*, 309-315.
68. Dar, A. C.; Shokat, K. M. The evolution of protein kinase inhibitors from antagonists to agonists of cellular signaling. *Annu. Rev. Biochem.* **2011**, *80*, 769-795.
69. Karaman, M. W.; Herrgard, S.; Treiber, D. K.; Gallant, P.; Atteridge, C. E.; Campbell, B. T.; Chan, K. W.; Ciceri, P.; Davis, M. I.; Edeen, P. T.; Faraoni, R.; Floyd, M.; Hunt, J. P.; Lockhart, D. J.; Milanov, Z. V.; Morrison, M. J.; Pallares, G.; Patel, H. K.; Pritchard, S.; Wodicka, L. M.; Zarrinkar, P. P. A quantitative analysis of kinase inhibitor selectivity. *Nat. Biotechnol.* **2008**, *26*, 127-132.
70. Quintas-Cardama, A.; Kantarjian, H.; Cortes, J. Flying under the radar: the new wave of BCR-ABL inhibitors. *Nat. Rev. Drug Discov.* **2007**, *6*, 834-848.
71. Hantschel, O.; Grebien, F.; Superti-Furga, G. The growing arsenal of ATP-competitive and allosteric inhibitors of BCR-ABL. *Cancer Res.* **2012**, *72*, 4890-4895.
72. Liu, Y.; Gray, N. S. Rational design of inhibitors that bind to inactive kinase conformations. *Nat. Chem. Biol.* **2006**, *2*, 358-364.
73. Zhang, J.; Yang, P. L.; Gray, N. S. Targeting cancer with small molecule kinase inhibitors. *Nat. Rev. Cancer* **2009**, *9*, 28-39.
74. Johnson, D. S.; Weerapana, E.; Cravatt, B. F. Strategies for discovering and derisking covalent, irreversible enzyme inhibitors. *Future Med. Chem.* **2010**, *2*, 949-964.
75. Silverman, R. B. *The Organic Chemistry of Drug Design and Drug Action*. 2nd ed.; Elsevier Academic Press: **2004**; p 274-303.
76. Singh, J.; Petter, R. C.; Baillie, T. A.; Whitty, A. The resurgence of covalent drugs. *Nat. Rev. Drug Discov.* **2011**, *10*, 307-317.
77. Barf, T.; Kaptein, A. Irreversible Protein Kinase Inhibitors: Balancing the Benefits and Risks. *J. Med. Chem.* **2012**, *55*, 6243-6262.
78. Kumar, S.; Mitra, K.; Kassahun, K.; Baillie, T. *Approaches for Minimizing Metabolic Activation of New Drug Candidates in Drug Discovery*. Springer Berlin Heidelberg: **2010**; Vol. 196, p 511-544.
79. Uetrecht, J. Immune-Mediated Adverse Drug Reactions. *Chem. Res. Toxicol.* **2008**, *22*, 24-34.

80. Kwak, E. L.; Sordella, R.; Bell, D. W.; Godin-Heymann, N.; Okimoto, R. A.; Brannigan, B. W.; Harris, P. L.; Driscoll, D. R.; Fidias, P.; Lynch, T. J.; Rabindran, S. K.; McGinnis, J. P.; Wissner, A.; Sharma, S. V.; Isselbacher, K. J.; Settleman, J.; Haber, D. A. Irreversible inhibitors of the EGF receptor may circumvent acquired resistance to gefitinib. *Proc. Nat. Acad. Sci.* **2005**, *102*, 7665-7670.
81. Colman, R. F. Affinity Labeling of Purine Nucleotide Sites in Proteins. *Annu. Rev. Biochem.* **1983**, *52*, 67-91.
82. Tummino, P. J.; Copeland, R. A. Residence time of receptor-ligand complexes and its effect on biological function. *Biochemistry* **2008**, *47*, 5481-5492.
83. Marino, S. M.; Gladyshev, V. N. Analysis and Functional Prediction of Reactive Cysteine Residues. *J. Biol. Chem.* **2012**, *287*, 4419-4425.
84. Sevier, C. S.; Kaiser, C. A. Formation and transfer of disulphide bonds in living cells. *Nat. Rev. Mol. Cell Biol.* **2002**, *3*, 836-847.
85. Marino, S. M.; Li, Y.; Fomenko, D. E.; Agisheva, N.; Cerny, R. L.; Gladyshev, V. N. Characterization of Surface-Exposed Reactive Cysteine Residues in *Saccharomyces cerevisiae*. *Biochemistry* **2010**, *49*, 7709-7721.
86. Nakamura, H.; Nakamura, K.; Yodoi, J. Redox regulation of cellular activation. *Annu Rev Immunol* **1997**, *15*, 351-369.
87. Kirkland, L. O.; McInnes, C. Non-ATP competitive protein kinase inhibitors as anti-tumor therapeutics. *Biochem. Pharmacol.* **2009**, *77*, 1561-1571.
88. Sadowsky, J. D.; Burlingame, M. A.; Wolan, D. W.; McClendon, C. L.; Jacobson, M. P.; Wells, J. A. Turning a protein kinase on or off from a single allosteric site via disulfide trapping. *Proc. Nat. Acad. Sci.* **2011**, *108*, 6056-6061.
89. Lewis, J. A.; Lebois, E. P.; Lindsley, C. W. Allosteric modulation of kinases and GPCRs: design principles and structural diversity. *Curr. Opin. Cell Biol.* **2008**, *12*, 269-280.
90. White, A. W.; Westwell, A. D.; Brahemi, G. Protein-protein interactions as targets for small-molecule therapeutics in cancer. *Expert Rev. Mol. Med.* **2008**, *19*.
91. Fry, D. C.; Vassilev, L. T. Targeting protein-protein interactions for cancer therapy. *J. Mol. Med.* **2005**, *83*, 955-963.
92. Clackson, T.; Wells, J. A. A hot spot of binding energy in a hormone-receptor interface. *Science* **1995**, *267*, 383-386.
93. Chène, P. Inhibition of the p53-MDM2 Interaction: Targeting a Protein-Protein Interface. *Mol. Cancer Res.* **2004**, *2*, 20-28.
94. Momand, J.; Jung, D.; Wilczynski, S.; Niland, J. The MDM2 gene amplification database. *Nucl. Acids Res.* **1998**, *26*, 3453-3459.
95. Vassilev, L. T.; Vu, B. T.; Graves, B.; Carvajal, D.; Podlaski, F.; Filipovic, Z.; Kong, N.; Kammlott, U.; Lukacs, C.; Klein, C.; Fotouhi, N.; Liu, E. A. In Vivo Activation of the p53 Pathway by Small-Molecule Antagonists of MDM2. *Science* **2004**, *303*, 844-848.
96. Künkele, A.; De Preter, K.; Heukamp, L.; Thor, T.; Pajtler, K. W.; Hartmann, W.; Mittelbronn, M.; Grotzer, M. A.; Deubzer, H. E.; Speleman, F.; Schramm, A.; Eggert, A.; Schulte, J. H. Pharmacological activation of the p53 pathway by nutlin-3 exerts anti-tumoral effects in medulloblastomas. *Neuro Oncol.* **2012**, 859-869.

97. Daub, H.; Specht, K.; Ullrich, A. Strategies to overcome resistance to targeted protein kinase inhibitors. *Nat. Rev. Drug Discov.* **2004**, 3, 1001-1010.
98. Krishnamurty, R.; Maly, D. J. Biochemical Mechanisms of Resistance to Small-Molecule Protein Kinase Inhibitors. *ACS Chem. Biol.* **2010**, 5, 121-138.
99. Sierra, J. R.; Cepero, V.; Giordano, S. Molecular mechanisms of acquired resistance to tyrosine kinase targeted therapy. *Mol. Cancer* **2010**, 9, 75.
100. Chen, F. L.; Xia, W.; Spector, N. L. Acquired Resistance to Small Molecule ErbB2 Tyrosine Kinase Inhibitors. *Clin. Cancer Res.* **2008**, 14, 6730-6734.
101. Bikker, J. A.; Brooijmans, N.; Wissner, A.; Mansour, T. S. Kinase domain mutations in cancer: implications for small molecule drug design strategies. *J. Med. Chem.* **2009**, 52, 1493-1509.
102. Lee, F.; Fandi, A.; Voi, M. Overcoming kinase resistance in chronic myeloid leukemia. *Int. J. Biochem. Cell Biol.* **2008**, 40, 334-343.
103. Legraverend, M.; Grierson, D. S. The purines: Potent and versatile small molecule inhibitors and modulators of key biological targets. *Bioorg. Med. Chem.* **2006**, 14, 3987-4006.
104. Meijer, L.; Raymond, E. Roscovitine and Other Purines as Kinase Inhibitors. From Starfish Oocytes to Clinical Trials. *Acc. Chem. Res.* **2003**, 36, 417-425.
105. Klebe, G. Recent developments in structure-based drug design. *J. Mol. Med.* **2000**, 78, 269-281.
106. Collins, K.; Jacks, T.; Pavletich, N. P. The cell cycle and cancer. *Proc. Natl. Acad. Sci.* **1997**, 94, 2776-2778.
107. Sherr, C. J. Cancer cell cycles. *Science* **1996**, 274, 1672-1677.
108. Williams, G. H.; Stoeber, K. The cell cycle and cancer. *J. Pathol.* **2012**, 226, 352-364.
109. Pardee, A. G1 events and regulation of cell proliferation. *Science* **1989**, 246, 603-608.
110. Skaar, J. R.; Pagano, M. Cdh1: a master G0/G1 regulator. *Nat. Cell Biol.* **2008**, 10, 755-757.
111. Nigg, E. A. Mitotic kinases as regulators of cell division and its checkpoints. *Nat. Rev. Mol. Cell Biol.* **2001**, 2, 21-32.
112. Agarwal, M. L.; Agarwal, A.; Taylor, W. R.; Stark, G. R. p53 controls both the G2/M and the G1 cell cycle checkpoints and mediates reversible growth arrest in human fibroblasts. *Proc. Natl. Acad. Sci.* **1995**, 92, 8493-8497.
113. http://kvhs.nbed.nb.ca/gallant/biology/mitosis_phases.html (28th January 2013).
114. McIntosh, J. R.; Molodtsov, M. I.; Ataullakhanov, F. I. Biophysics of mitosis. *Q. Rev. Biophys.* **2012**, 45, 147-207.
115. Belmont, A. S. Mitotic chromosome structure and condensation. *Curr. Opin. Cell Biol.* **2006**, 18, 632-638.
116. Lodish, H.; Berk, A.; Zipursky, S. L. Molecular Cell Biology. 4th edition. In *Section 19.5, Microtubule Dynamics and Motor Proteins during Mitosis*, W. H. Freeman: New York, 2000.
117. Bayliss, R.; Fry, A.; Haq, T.; Yeoh, S. On the molecular mechanisms of mitotic kinase activation. *Open Biol.* **2012**, 2, 120136.
118. Uhlmann, F.; Wernic, D.; Poupart, M.-A.; Koonin, E. V.; Nasmyth, K. Cleavage of Cohesin by the CD Clan Protease Separin Triggers Anaphase in Yeast. *Cell* **2000**, 103, 375-386.
119. Amon, A. Together until separin do us part. *Nat. Cell Biol.* **2001**, 3, 12-14.

120. FitzHarris, G. Anaphase B Precedes Anaphase A in the Mouse Egg. *Curr. Biol.* **2012**, 22, 437-444.
121. Maiato, H.; Lince-Faria, M. The perpetual movements of anaphase. *Cell Mol. Life Sci.* **2010**, 67, 2251-2269.
122. Centrosome. <http://www.genome.gov/Glossary/resources/centrosome.pdf> (16th January 2013).
123. Fry, A. M. The Nek2 protein kinase: a novel regulator of centrosome structure. *Oncogene* **2002**, 21, 6184-6194.
124. Lange, B. M.; Gull, K. A molecular marker for centriole maturation in the mammalian cell cycle. *J. Cell Biol.* **1995**, 130, 919-927.
125. Meraldi, P.; Nigg, E. A. The centrosome cycle. *FEBS Lett.* **2002**, 521, 9-13.
126. Baumann, K. Cell cycle: Order in the pericentriolar material. *Nat. Rev. Mol. Cell Biol.* **2012**, 13, 749.
127. Crasta, K.; Surana, U. Disjunction of conjoined twins: Cdk1, Cdh1 and separation of centrosomes. *Cell Div.* **2006**, 1, 12.
128. Hinchcliffe, E. H.; Sluder, G. Two for two: Cdk2 and its role in centrosome doubling. *Oncogene* **2002**, 21, 6154-6160.
129. Brinkley, B. R. Managing the centrosome numbers game: from chaos to stability in cancer cell division. *Trends Cell Biol.* **2001**, 11, 18-21.
130. Hinchcliffe, E. H.; Sluder, G. "It Takes Two to Tango": understanding how centrosome duplication is regulated throughout the cell cycle. *Genes Dev.* **2001**, 15, 1167-1181.
131. Khodjakov, A.; Cole, R. W.; Oakley, B. R.; Rieder, C. L. Centrosome-independent mitotic spindle formation in vertebrates. *Curr. Biol.* **2000**, 10, 59-67.
132. Chan, K. S.; Koh, C. G.; Li, H. Y. Mitosis-targeted anti-cancer therapies: where they stand. *Cell Death Dis.* **2012**, 18, 148.
133. Schmidt, M.; Bastians, H. Mitotic drug targets and the development of novel anti-mitotic anticancer drugs. *Drug Resist. Update* **2007**, 10, 162-181.
134. Thomas, H. D.; Wang, L.-Z.; Roche, C.; Bentley, J.; Cheng, Y.; Hardcastle, I. R.; Golding, B. T.; Griffin, R. J.; Curtin, N. J.; Newell, D. R. Preclinical in vitro and in vivo evaluation of the potent and specific cyclin-dependent kinase 2 inhibitor NU6102 and a water soluble prodrug NU6301. *Eur. J. Cancer* **2011**, 47, 2052-2059.
135. Huwe, A.; Mazitschek, R.; Giannis, A. Small molecules as inhibitors of cyclin-dependent kinases. *Angew. Chem., Int. Ed.* **2003**, 42, 2122-2138.
136. Schwartz, G. K.; Shah, M. A. Targeting the cell cycle: a new approach to cancer therapy. *J. Clin. Oncol.* **2005**, 23, 9408-9421.
137. Johnson, L. Protein kinases and their therapeutic exploitation. *Biochem. Soc. Trans.* **2007**, 35, 7-11.
138. Nebreda, A. R. CDK activation by non-cyclin proteins. *Curr. Opin. Cell Biol.* **2006**, 18, 192-198.
139. Heitz, F.; Morris, M. C.; Fesquet, D.; Cavadore, J. C.; Doree, M.; Divita, G. Interactions of cyclins with cyclin-dependent kinases: a common interactive mechanism. *Biochemistry* **1997**, 36, 4995-5003.
140. Ortega, S.; Prieto, I.; Odajima, J.; Martin, A.; Dubus, P.; Sotillo, R.; Barbero, J. L.; Malumbres, M.; Barbacid, M. Cyclin-dependent kinase 2 is essential for meiosis but not for mitotic cell division in mice. *Nat. Genet.* **2003**, 35, 25-31.
141. Fajas, L.; Blanchet, E.; Annicotte, J.-S. CDK4, pRB and E2F1: connected to insulin. *Cell Div.* **2010**, 5, 6.

142. Hu, M. G.; Deshpande, A.; Schlichting, N.; Hinds, E. A.; Mao, C.; Dose, M.; Hu, G. F.; Van Etten, R. A.; Gounari, F.; Hinds, P. W. CDK6 kinase activity is required for thymocyte development. *Blood* **2011**, *117*, 6120-6131.
143. Zoubir, M.; Flament, C.; Gdoura, A.; Bahleda, R.; Litvinova, E.; Soumelis, V.; Conforti, R.; Viaud, S.; Soria, J.-C.; Kroemer, G.; Zitvogel, L.; Chaput, N. An inhibitor of cyclin-dependent kinases suppresses TLR signaling and increases the susceptibility of cancer patients to herpes viridae. *Cell Cycle* **2011**, *10*, 118-126.
144. Malumbres, M.; Barbacid, M. Cell cycle, CDKs and cancer: a changing paradigm. *Nat. Rev. Cancer* **2009**, *9*, 153-166.
145. Mountzios, G.; Terpos, E.; Dimopoulos, M. A. Aurora kinases as targets for cancer therapy. *Cancer Treat. Rev.* **2008**, *34*, 175-182.
146. Sausville, E. A. Aurora kinases dawn as cancer drug targets. *Nat. Med.* **2004**, *10*, 234-235.
147. Barr, A. R.; Gergely, F. Aurora-A: the maker and breaker of spindle poles. *J. Cell Sci.* **2007**, *120*, 2987-2996.
148. Carmena, M.; Wheelock, M.; Funabiki, H.; Earnshaw, W. C. The chromosomal passenger complex (CPC): from easy rider to the godfather of mitosis. *Nat. Rev. Mol. Cell Biol.* **2012**, *13*, 789-803.
149. Nair, J. S.; Ho, A. L.; Tse, A. N.; Coward, J.; Cheema, H.; Ambrosini, G.; Keen, N.; Schwartz, G. K. Aurora B Kinase Regulates the Postmitotic Endoreduplication Checkpoint via Phosphorylation of the Retinoblastoma Protein at Serine 780. *Mol. Biol. Cell* **2009**, *20*, 2218-2228.
150. Kallio, M. J.; McClelland, M. L.; Stukenberg, P. T.; Gorbsky, G. J. Inhibition of aurora B kinase blocks chromosome segregation, overrides the spindle checkpoint, and perturbs microtubule dynamics in mitosis. *Curr. Biol.* **2002**, *12*, 900-905.
151. Takai, N.; Hamanaka, R.; Yoshimatsu, J.; Miyakawa, I. Polo-like kinases (Plks) and cancer. *Oncogene* **2005**, *24*, 287-291.
152. Taylor, S.; Peters, J. M. Polo and Aurora kinases: lessons derived from chemical biology. *Curr. Opin. Cell Biol.* **2008**, *20*, 77-84.
153. Bowers, A. J.; Boylan, J. F. Nek8, a NIMA family kinase member, is overexpressed in primary human breast tumors. *Gene* **2004**, *328*, 135-142.
154. Hayward, D. G.; Fry, A. M. Nek2 kinase in chromosome instability and cancer. *Cancer Lett.* **2006**, *237*, 155-166.
155. Liu, S.; Lu, W.; Obara, T.; Kuida, S.; Lehoczky, J.; Dewar, K.; Drummond, I. A.; Beier, D. R. A defect in a novel Nek-family kinase causes cystic kidney disease in the mouse and in zebrafish. *Development* **2002**, *129*, 5839-5846.
156. Quarmby, L. M.; Mahjoub, M. R. Caught Nek-ing: cilia and centrioles. *J. Cell Sci.* **2005**, *118*, 5161-5169.
157. Richards, M. W.; O'Regan, L.; Mas-Droux, C.; Blot, J. M.; Cheung, J.; Hoelder, S.; Fry, A. M.; Bayliss, R. An autoinhibitory tyrosine motif in the cell-cycle-regulated Nek7 kinase is released through binding of Nek9. *Mol. Cell* **2009**, *36*, 560-570.
158. Belham, C.; Roig, J.; Caldwell, J. A.; Aoyama, Y.; Kemp, B. E.; Comb, M.; Avruch, J. A mitotic cascade of NIMA family kinases. Ncc1/Nek9 activates the Nek6 and Nek7 kinases. *J. Biol. Chem.* **2003**, *278*, 34897-34909.
159. Noguchi, K.; Fukazawa, H.; Murakami, Y.; Uehara, Y. Nek11, a new member of the NIMA family of kinases, involved in DNA replication and genotoxic stress responses. *J. Biol. Chem.* **2002**, *277*, 39655-39665.

160. Thompson, S. L.; Bakhoum, S. F.; Compton, D. A. Mechanisms of Chromosomal Instability. *Curr. Biol.* **2010**, *20*, 285-295.
161. Mayor, T.; Meraldi, P.; Stierhof, Y. D.; Nigg, E. A.; Fry, A. M. Protein kinases in control of the centrosome cycle. *FEBS Lett.* **1999**, *452*, 92-95.
162. Schultz, S. J.; Fry, A. M.; Sutterlin, C.; Ried, T.; Nigg, E. A. Cell cycle-dependent expression of Nek2, a novel human protein kinase related to the NIMA mitotic regulator of *Aspergillus nidulans*. *Cell Growth Differ.* **1994**, *5*, 625-635.
163. O'Regan, L.; Blot, J.; Fry, A. M. Mitotic regulation by NIMA-related kinases. *Cell Div.* **2007**, *2*, 25.
164. Mardin, B. R.; Lange, C.; Baxter, J. E.; Hardy, T.; Scholz, S. R.; Fry, A. M.; Schiebel, E. Components of the Hippo pathway cooperate with Nek2 kinase to regulate centrosome disjunction. *Nat. Cell Biol.* **2010**, *12*, 1166-1176.
165. Hames, R. S.; Fry, A. M. Alternative splice variants of the human centrosome kinase Nek2 exhibit distinct patterns of expression in mitosis. *Biochem. J.* **2002**, *361*, 77-85.
166. Casenghi, M.; Meraldi, P.; Weinhart, U.; Duncan, P. I.; Korner, R.; Nigg, E. A. Polo-like kinase 1 regulates Nlp, a centrosome protein involved in microtubule nucleation. *Dev. Cell* **2003**, *5*, 113-125.
167. Li, J.; Zhan, Q. The role of centrosomal Nlp in the control of mitotic progression and tumorigenesis. *Br. J. Cancer* **2011**, *104*, 1523-1528.
168. Qu, D.; Qu, H.; Fu, M.; Zhao, X.; Liu, R.; Sui, L.; Zhan, Q. Increased expression of Nlp, a potential oncogene in ovarian cancer, and its implication in carcinogenesis. *Gynecol. Oncol.* **2008**, *110*, 230-236.
169. Shao, S.; Liu, R.; Wang, Y.; Song, Y.; Zuo, L.; Xue, L.; Lu, N.; Hou, N.; Wang, M.; Yang, X.; Zhan, Q. Centrosomal Nlp is an oncogenic protein that is gene-amplified in human tumors and causes spontaneous tumorigenesis in transgenic mice. *J. Clin. Invest.* **2010**, *120*, 498-507.
170. Rapley, J.; Baxter, J. E.; Blot, J.; Wattam, S. L.; Casenghi, M.; Meraldi, P.; Nigg, E. A.; Fry, A. M. Coordinate regulation of the mother centriole component nlp by nek2 and plk1 protein kinases. *Mol. Cell Biol.* **2005**, *25*, 1309-1324.
171. Fry, A. M.; Arnaud, L.; Nigg, E. A. Activity of the human centrosomal kinase, Nek2, depends on an unusual leucine zipper dimerization motif. *J. Biol. Chem.* **1999**, *274*, 16304-16310.
172. Kops, G. J. P. L.; Weaver, B. A. A.; Cleveland, D. W. On the road to cancer: aneuploidy and the mitotic checkpoint. *Nat. Rev. Cancer* **2005**, *5*, 773-785.
173. Chen, Y.; Riley, D. J.; Zheng, L.; Chen, P. L.; Lee, W. H. Phosphorylation of the mitotic regulator protein Hec1 by Nek2 kinase is essential for faithful chromosome segregation. *J. Biol. Chem.* **2002**, *277*, 49408-49416.
174. Qiu, X. L.; Li, G.; Wu, G.; Zhu, J.; Zhou, L.; Chen, P. L.; Chamberlin, A. R.; Lee, W. H. Synthesis and biological evaluation of a series of novel inhibitor of Nek2/Hec1 analogues. *J. Med. Chem.* **2009**, *52*, 1757-1767.
175. Wu, G.; Qiu, X. L.; Zhou, L.; Zhu, J.; Chamberlin, R.; Lau, J.; Chen, P. L.; Lee, W. H. Small molecule targeting the Hec1/Nek2 mitotic pathway suppresses tumor cell growth in culture and in animal. *Cancer Res.* **2008**, *68*, 8393-8399.
176. Liu, Q.; Hirohashi, Y.; Du, X.; Greene, M. I.; Wang, Q. Nek2 targets the mitotic checkpoint proteins Mad2 and Cdc20: a mechanism for aneuploidy in cancer. *Exp. Mol. Pathol.* **2010**, *88*, 225-233.

177. Di Agostino, S.; Fedele, M.; Chieffi, P.; Fusco, A.; Rossi, P.; Geremia, R.; Sette, C. Phosphorylation of high-mobility group protein A2 by Nek2 kinase during the first meiotic division in mouse spermatocytes. *Mol. Biol. Cell* **2004**, *15*, 1224-1232.
178. Di Agostino, S.; Botti, F.; Di Carlo, A.; Sette, C.; Geremia, R. Meiotic progression of isolated mouse spermatocytes under simulated microgravity. *Reproduction* **2004**, *128*, 25-32.
179. Sette, C.; Barchi, M.; Bianchini, A.; Conti, M.; Rossi, P.; Geremia, R. Activation of the mitogen-activated protein kinase ERK1 during meiotic progression of mouse pachytene spermatocytes. *J. Biol. Chem.* **1999**, *274*, 33571-33579.
180. Fedele, M.; Battista, S.; Kenyon, L.; Baldassarre, G.; Fidanza, V.; Klein-Szanto, A. J.; Parlow, A. F.; Visone, R.; Pierantoni, G. M.; Outwater, E.; Santoro, M.; Croce, C. M.; Fusco, A. Overexpression of the HMGA2 gene in transgenic mice leads to the onset of pituitary adenomas. *Oncogene* **2002**, *21*, 3190-3198.
181. Kokuryo, T.; Senga, T.; Yokoyama, Y.; Nagino, M.; Nimura, Y.; Hamaguchi, M. Nek2 as an effective target for inhibition of tumorigenic growth and peritoneal dissemination of cholangiocarcinoma. *Cancer Res.* **2007**, *67*, 9637-9642.
182. Whelligan, D. K.; Solanki, S.; Taylor, D.; Thomson, D. W.; Cheung, K.-M. J.; Boxall, K.; Mas-Droux, C.; Barillari, C.; Burns, S.; Grummitt, C. G.; Collins, I.; van Montfort, R. L. M.; Aherne, G. W.; Bayliss, R.; Hoelder, S. Aminopyrazine Inhibitors Binding to an Unusual Inactive Conformation of the Mitotic Kinase Nek2: SAR and Structural Characterization. *J. Med. Chem.* **2010**, *53*, 7682-7698.
183. Solanki, S.; Innocenti, P.; Mas-Droux, C.; Boxall, K.; Barillari, C.; van Montfort, R. L. M.; Aherne, G. W.; Bayliss, R.; Hoelder, S. Benzimidazole Inhibitors Induce a DFG-Out Conformation of Never in Mitosis Gene A-Related Kinase 2 (Nek2) without Binding to the Back Pocket and Reveal a Nonlinear Structure–Activity Relationship. *J. Med. Chem.* **2011**, *54*, 1626-1639.
184. Innocenti, P.; Cheung, K.-M. J.; Solanki, S.; Mas-Droux, C.; Rowan, F.; Yeoh, S.; Boxall, K.; Westlake, M.; Pickard, L.; Hardy, T.; Baxter, J. E.; Aherne, G. W.; Bayliss, R.; Fry, A. M.; Hoelder, S. Design of Potent and Selective Hybrid Inhibitors of the Mitotic Kinase Nek2: Structure–Activity Relationship, Structural Biology, and Cellular Activity. *J. Med. Chem.* **2012**, *55*, 3228-3241.
185. Henise, J. C.; Taunton, J. Irreversible Nek2 kinase inhibitors with cellular activity. *J. Med. Chem.* **2011**, *54*, 4133-4146.
186. Rellos, P.; Ivins, F. J.; Baxter, J. E.; Pike, A.; Nott, T. J.; Parkinson, D. M.; Das, S.; Howell, S.; Fedorov, O.; Shen, Q. Y.; Fry, A. M.; Knapp, S.; Smerdon, S. J. Structure and regulation of the human Nek2 centrosomal kinase. *J. Biol. Chem.* **2007**, *282*, 6833-42.
187. Arris, C. E.; Boyle, F. T.; Calvert, A. H.; Curtin, N. J.; Endicott, J. A.; Garman, E. F.; Gibson, A. E.; Golding, B. T.; Grant, S.; Griffin, R. J.; Jewsbury, P.; Johnson, L. N.; Lawrie, A. M.; Newell, D. R.; Noble, M. E.; Sausville, E. A.; Schultz, R.; Yu, W. Identification of novel purine and pyrimidine cyclin-dependent kinase inhibitors with distinct molecular interactions and tumor cell growth inhibition profiles. *J. Med. Chem.* **2000**, *43*, 2797-2804.
188. Hocek, M.; Nauš, P.; Pohl, R.; Votruba, I.; Furman, P. A.; Tharnish, P. M.; Otto, M. J. Cytostatic 6-Arylpyrimidine Nucleosides 6. SAR in Anti-HCV and

- Cytostatic Activity of Extended Series of 6-Hetarylpurine Ribonucleosides. *J. Med. Chem.* **2005**, *48*, 5869-5873.
189. Lacal, J. C. Intelligent drug design come of age: STI571 as the start a of a new era in cancer research and treatment. *Rev. Oncología* **2001**, *3*, 229-230.
 190. Gilmore, K.; Alabugin, I. V. Cyclizations of alkynes: revisiting Baldwin's rules for ring closure. *Chem. Rev.* **2011**, *111*, 6513-6556.
 191. Knowles, R. R.; Jacobsen, E. N. Attractive noncovalent interactions in asymmetric catalysis: Links between enzymes and small molecule catalysts. *Proc. Natl. Acad. Sci. USA* **2010**, *107*, 20678-20685.
 192. Daunderer, M. Physostigmine salicylate as an antidote. *Int. J. Clin. Pharmacol. Ther. Toxicol.* **1980**, *18*, 523-535.
 193. Fukuto, T. R. Mechanism of action of organophosphorus and carbamate insecticides. *Environ. Health Perspect.* **1990**, *87*, 245-254.
 194. Pritchard, R. B.; Lough, C. E.; Currie, D. J.; Holmes, H. L. Equilibrium reactions of n-butanethiol with some conjugated heteroenoid compounds. *Can. J. Chem.* **1968**, *46*, 775-781.
 195. Serafimova, I. M.; Pufall, M. A.; Krishnan, S.; Duda, K.; Cohen, M. S.; Maglathlin, R. L.; McFarland, J. M.; Miller, R. M.; Frödin, M.; Taunton, J. Reversible targeting of noncatalytic cysteines with chemically tuned electrophiles. *Nat. Chem. Biol.* **2012**, *8*, 471-476.
 196. Wong, C. Purine-Based Inhibitors of Nek2 Kinase; *PhD Thesis*. Newcastle University, 2010.
 197. Furuya, T.; Klein, J. E.; Ritter, T. C-F Bond Formation for the Synthesis of Aryl Fluorides. *Synthesis* **2010**, *1*, 1804-1821.
 198. Smith, M. B.; March, J. *March's Advanced Organic Chemistry: Reactions, Mechanisms, and Structure*. Wiley: **2007**.
 199. Chinchilla, R.; Nájera, C. The Sonogashira Reaction: A Booming Methodology in Synthetic Organic Chemistry. *Chem. Rev.* **2007**, *107*, 874-922.
 200. Whitfield, H. J.; Griffin, R. J.; Hardcastle, I. R.; Henderson, A.; Meneyrol, J.; Mesguiche, V.; Sayle, K. L.; Golding, B. T. Facilitation of addition-elimination reactions in pyrimidines and purines using trifluoroacetic acid in trifluoroethanol. *Chem. Commun.* **2003**, 2802-2803.
 201. Liu, J.; Robins, M. J. SNAr Displacements with 6-(Fluoro, Chloro, Bromo, Iodo, and Alkylsulfonyl)purine Nucleosides: Synthesis, Kinetics, and Mechanism¹. *J. Am. Chem. Soc.* **2007**, *129*, 5962-5968.
 202. Brændvang, M.; Gundersen, L.-L. Synthesis, biological activity, and SAR of antimycobacterial 2- and 8-substituted 6-(2-furyl)-9-(p-methoxybenzyl)purines. *Bioorg. Med. Chem.* **2007**, *15*, 7144-7165.
 203. Francom, P.; Robins, M. J. Nucleic Acid Related Compounds. 118. Nonaqueous Diazotization of Aminopurine Derivatives. Convenient Access to 6-Halo- and 2,6-Dihalopurine Nucleosides and 2'-Deoxynucleosides with Acyl or Silyl Halides. *J. Org. Chem.* **2002**, *68*, 666-669.
 204. Francom, P.; Janeba, Z.; Shibuya, S.; Robins, M. J. Nucleic Acid Related Compounds. 116. Nonaqueous Diazotization of Aminopurine Nucleosides. Mechanistic Considerations and Efficient Procedures with tert-Butyl Nitrite or Sodium Nitrite. *J. Org. Chem.* **2002**, *67*, 6788-6796.
 205. Burgos, C. H.; Barder, T. E.; Huang, X.; Buchwald, S. L. Significantly Improved Method for the Pd-Catalyzed Coupling of Phenols with Aryl Halides: Understanding Ligand Effects. *Angw. Chem. Int. Ed.* **2006**, *45*, 4321-4326.

206. Crespo, M. I.; Pages, L.; Vega, A.; Segarra, V.; Lopez, M.; Domenech, T.; Miralpeix, M.; Beleta, J.; Ryder, H.; Palacios, J. M. Design, synthesis, and biological activities of new thieno[3,2-*d*] pyrimidines as selective type 4 phosphodiesterase inhibitors. *J. Med. Chem.* **1998**, *41*, 4021-4035.
207. Caron, S. *Practical Synthetic Organic Chemistry: Reactions, Principles, and Techniques*. Wiley: **2011**.
208. Choy, J.; Jaime-Figueroa, S.; Jiang, L.; Wagner, P. Novel Practical Deprotection of *N*-Boc Compounds Using Fluorinated Alcohols. *Synth. Commun.* **2008**, *38*, 3840-3853.
209. Schelling, J. E.; Salemink, C. A. Deazapurine derivatives. X: Synthesis and reactions of 5,7-disubstituted imidazo[4,5-*b*]pyridines. *Recl. Trav. Chim. Pays-Bas* **1972**, *91*, 650-656.
210. Deghati, P. Y. F.; Wanner, M. J.; Koomen, G.-J. Regioselective nitration of purine nucleosides: synthesis of 2-nitroadenosine and 2-nitroinosine. *Tetrahedron Lett.* **2000**, *41*, 1291-1295.
211. Tedder, M. E.; Nie, Z.; Margosiak, S.; Chu, S.; Feher, V. A.; Almassy, R.; Appelt, K.; Yager, K. M. Structure-based design, synthesis, and antimicrobial activity of purine derived SAH/MTA nucleosidase inhibitors. *Bioorg. Med. Chem. Lett.* **2004**, *14*, 3165-3168.
212. Zeinyeh, W.; Pilmé, J.; Radix, S.; Walchshofer, N. Regioselective *N*-alkylation of imidazo[4,5-*b*]pyridine-4-oxide derivatives: an experimental and DFT study. *Tetrahedron Lett.* **2009**, *50*, 1828-1833.
213. Ochiai, E. Recent japanese work on the chemistry of pyridine 1-oxide and related compounds. *J. Org. Chem.* **1953**, *18*, 534-551.
214. Rodenko, B.; Koch, M.; van der Burg, A. M.; Wanner, M. J.; Koomen, G.-J. The Mechanism of Selective Purine C-Nitration Revealed: NMR Studies Demonstrate Formation and Radical Rearrangement of an N7-Nitramine Intermediate. *J. Am. Chem. Soc.* **2005**, *127*, 5957-5963.
215. Gelman, D.; Buchwald, S. L. Efficient Palladium-Catalyzed Coupling of Aryl Chlorides and Tosylates with Terminal Alkynes: Use of a Copper Cocatalyst Inhibits the Reaction. *Angw. Chem. Int. Ed.* **2003**, *42*, 5993-5996.
216. Li, J. J.; Corey, E. J.; Gribble, G. W. *Name Reactions for Homologation*. Wiley: **2009**.
217. Chinchilla, R.; Najera, C. Recent advances in Sonogashira reactions. *Chem. Soc. Rev.* **2011**, *40*, 5084-5121.
218. Challenger, S.; Dessi, Y.; Fox, D. E.; Hesmondhalgh, L. C.; Pascal, P.; Pettman, A. J.; Smith, J. D. Development of a Scalable Process for the Synthesis of the A2a Agonist, UK-371,104. *Org. Process Res. Dev.* **2008**, *12*, 575-583.
219. Matheson, C. M. Chemical and Biological Studies with Nek2 Kinase Inhibitors; *PhD Thesis*. Newcastle University, 2012.
220. Parlow, J. J.; Vazquez, M. L.; Flynn, D. L. A mixed resin bed for the quenching and purification of tetrabutylammonium fluoride mediated desilylating reactions. *Bioorg. Med. Chem. Lett.* **1998**, *8*, 2391-2394.
221. Brückl, T.; Thoma, I.; Wagner, A. J.; Knochel, P.; Carell, T. Efficient Synthesis of Deazaguanosine-Derived tRNA Nucleosides PreQ0, PreQ1, and Archaeosine Using the Turbo-Grignard Method. *Eur. J. Org. Chem.* **2010**, *2010*, 6517-6519.
222. Robison, M. M. Chlorodehydroxylation of Nitrogen Heterocycles with Phenylphosphonic Dichloride. *J. Am. Chem. Soc.* **1958**, *80*, 5481-5483.

223. Mangalagiu, I.; Benneche, T.; Undheim, K. Ethenylation and Alkynylation in Palladium-Catalyzed Carbosubstitution in Heteroazine. *Acta. Chem. Scand.* **1996**, *50*, 914-917.
224. Bajwa, J. S.; Chen, G.-P.; Prasad, K.; Repič, O.; Blacklock, T. J. Deprotection of N-tosylated indoles and related structures using cesium carbonate. *Tetrahedron Lett.* **2006**, *47*, 6425-6427.
225. Surry, D. S.; Buchwald, S. L. Dialkylbiaryl phosphines in Pd-catalyzed amination: a user's guide. *Chem. Sci.* **2011**, *2*, 27-50.
226. Slavish, P. J.; Price, J. E.; Hanumesh, P.; Webb, T. R. Efficient Synthesis of Pyrazolopyrimidine Libraries. *ACS. Comb. Sci.* **2010**, *12*, 807-809.
227. Evans, L. E.; Cheeseman, M. D.; Jones, K. N–N Bond-Forming Cyclization for the One-Pot Synthesis of N-Aryl[3,4-d]pyrazolopyrimidines. *Org. Lett.* **2012**, *14*, 3546-3549.
228. Congxin, L.; Zhigang, L. PI3K/MTOR Kinase Inhibitors. WO2010/56320 A2, 2010.
229. Uyanik, M.; Ishihara, K. 2-Iodoxybenzenesulfonic Acid (IBS) Catalysed Oxidation of alcohols. *Aldrichimica Acta* **2010**, *43*, 83-90.
230. Dess, D. B.; Martin, J. C. A Useful 12-I-5 Triacetoxypersulfonane (the Dess-Martin Persulfonane) for the Selective Oxidation of Primary or Secondary Alcohols and a Variety of Related 12-I-5 Species. *J. Am. Chem. Soc.* **1991**, *113*, 7277-7287.
231. Fuller, R.; Chavez, B. Ticagrelor (brilinta), an antiplatelet drug for acute coronary syndrome. *P T* **2012**, *37*, 562-568.
232. Israel, M.; Protopapa, H. K.; Schlein, H. N.; Modest, E. J. Pyrimidine Derivatives. VI. 2,4,5-Triamino-6-chloro- and -6-mercaptopyrimidine and Related Compounds. *J. Med. Chem.* **1964**, *7*, 792-799.
233. Gowda, S.; Abiraj, K.; Gowda, D. C. Reductive cleavage of azo compounds catalyzed by commercial zinc dust using ammonium formate or formic acid. *Tetrahedron Lett.* **2002**, *43*, 1329-1331.
234. Masai, N.; Hayashi, T.; Kumazawa, Y.; Nishikawa, J.; Barta, I.; Kawakami, T. Process for producing 2,6-dihalogenopurine US2003/0144508 a1, 2003.
235. Kumar, A.; Srivastava, K.; Kumar, S. R.; Siddiqi, M. I.; Puri, S. K.; Sexana, J. K.; Chauhan, P. M. 4-Anilinoquinoline triazines: a novel class of hybrid antimalarial agents. *Eur. J. Med. Chem.* **2011**, *46*, 676-690.
236. Sonoda, M.; Inaba, A.; Itahashi, K.; Tobe, Y. Synthesis of Differentially Substituted Hexaethynylbenzenes Based on Tandem Sonogashira and Negishi Cross-Coupling Reactions. *Org. Lett.* **2001**, *3*, 2419-2421.
237. Brown, D. J.; Manson, S. F. *Introduction to the Pyrimidines*. John Wiley & Sons, Inc.: **2008**; Vol. 16, p 1-30.
238. Shewchuk, L. M.; Hassell, A. M.; Holmes, W. D.; Veal, J. M.; Emerson, H. K.; Musso, D. L.; Chamberlain, S. D.; Peckham, G. E. Crystal structure of liganded cFMS kinase domain. US7491731, 2009.
239. Naik, T. A.; Chikhalia, K. H. Studies on Synthesis of Pyrimidine Derivatives and their Pharmacological Evaluation. *E-Journal of Chem.* **2006**, *4*, 60-66.
240. Fluorinating Reagents, Building Blocks & Fluorinated Bioactive Compounds. http://www.tcichemicals.com/eshop/en/us/category_index/00205/ (30th November 2012).
241. Filler, R.; Saha, R. Fluorine in medicinal chemistry: a century of progress and a 60-year retrospective of selected highlights. *Future Med. Chem.* **2009**, *1*, 777-791.

242. Marchetti, F.; Cano, C.; Curtin, N. J.; Golding, B. T.; Griffin, R. J.; Haggerty, K.; Newell, D. R.; Parsons, R. J.; Payne, S. L.; Wang, L. Z.; Hardcastle, I. R. Synthesis and biological evaluation of 5-substituted O⁴-alkylpyrimidines as CDK2 inhibitors. *Org. Biomol. Chem.* **2010**, *8*, 2397-2407.
243. Mohamed, A. J.; Yu, L.; Backesjo, C. M.; Vargas, L.; Faryal, R.; Aints, A.; Christensson, B.; Berglof, A.; Vihinen, M.; Nore, B. F.; Smith, C. I. Bruton's tyrosine kinase (Btk): function, regulation, and transformation with special emphasis on the PH domain. *Immunol. Rev.* **2009**, *228*, 58-73.
244. Wiestner, A. Targeting B-Cell Receptor Signaling for Anticancer Therapy: The Bruton's Tyrosine Kinase Inhibitor Ibrutinib Induces Impressive Responses in B-Cell Malignancies. *J. Clin. Oncol.* **2013**, *31*, 128-130.
245. Honigberg, L. A.; Smith, A. M.; Sirisawad, M.; Verner, E.; Loury, D.; Chang, B.; Li, S.; Pan, Z.; Thamm, D. H.; Miller, R. A.; Buggy, J. J. The Bruton tyrosine kinase inhibitor PCI-32765 blocks B-cell activation and is efficacious in models of autoimmune disease and B-cell malignancy. *Proc. Nat. Acad. Sci.* **2010**.
246. Pan, Z.; Scheerens, H.; Li, S.-J.; Schultz, B. E.; Sprengeler, P. A.; Burrill, L. C.; Mendonca, R. V.; Sweeney, M. D.; Scott, K. C. K.; Grothaus, P. G.; Jeffery, D. A.; Spoerke, J. M.; Honigberg, L. A.; Young, P. R.; Dalrymple, S. A.; Palmer, J. T. Discovery of Selective Irreversible Inhibitors for Bruton's Tyrosine Kinase. *ChemMedChem* **2007**, *2*, 58-61.
247. Kaidanovich-Beilin, O.; Woodgett, J. R. GSK-3: functional insights from cell biology and animal models. *Front. Mol. Neurosci.* **2011**, *4*.
248. Cohen, P.; Frame, S. The renaissance of GSK3. *Nat. Rev. Mol. Cell Biol.* **2001**, *2*, 769-776.
249. Perez, D. I.; Palomo, V.; Pérez, C. n.; Gil, C.; Dans, P. D.; Luque, F. J.; Conde, S.; Martínez, A. Switching Reversibility to Irreversibility in Glycogen Synthase Kinase 3 Inhibitors: Clues for Specific Design of New Compounds. *J. Med. Chem.* **2011**, *54*, 4042-4056.
250. Perez, D. I.; Conde, S.; Pérez, C.; Gil, C.; Simon, D.; Wandosell, F.; Moreno, F. J.; Gelpí, J. L.; Luque, F. J.; Martínez, A. Thienylhalomethylketones: Irreversible glycogen synthase kinase 3 inhibitors as useful pharmacological tools. *Bioorg. Med. Chem.* **2009**, *17*, 6914-6925.
251. Sale, E. M.; Sale, G. J. Protein kinase B: signalling roles and therapeutic targeting. *Cell. Mol. Life Sci.* **2008**, *65*, 113-127.
252. Yang, L.; Dan, H. C.; Sun, M.; Liu, Q.; Sun, X.-m.; Feldman, R. I.; Hamilton, A. D.; Polokoff, M.; Nicosia, S. V.; Herlyn, M.; Sebt, S. M.; Cheng, J. Q. Akt/Protein Kinase B Signaling Inhibitor-2, a Selective Small Molecule Inhibitor of Akt Signaling with Antitumor Activity in Cancer Cells Overexpressing Akt. *Cancer Res.* **2004**, *64*, 4394-4399.
253. Kumar, C. C.; Madison, V. AKT crystal structure and AKT-specific inhibitors. *Oncogene* **2005**, *24*, 7493-7501.
254. Holzgrabe, U. Quantitative NMR spectroscopy in pharmaceutical applications. *Prog. Nucl. Magn. Reson. Spectrosc.* **2010**, *57*, 229-240.
255. Hollis, D. P. Quantitative Analysis of Aspirin, Phenacetin, and Caffeine Mixtures by Nuclear Magnetic Resonance Spectrometry. *Anal. Chem.* **1963**, *35*, 1682-1684.
256. Rundlöf, T.; Mathiasson, M.; Bekiroglu, S.; Hakkarainen, B.; Bowden, T.; Arvidsson, T. Survey and qualification of internal standards for quantification by ¹H NMR spectroscopy. *J. Pharmaceut. Biomed. Anal.* **2010**, *52*, 645-651.

257. Wawer, I.; Diehl, B.; Holzgrabe, U. *NMR Spectroscopy in Pharmaceutical Analysis*. Elsevier Science: **2008**.
258. Bawn, C. Personal Communication. Newcastle University, Newcastle upon Tyne. In December 2012.
259. Claridge, T. D. W. *High-Resolution NMR Techniques in Organic Chemistry*. Elsevier Science Limited: **2009**; p 21-24.
260. Coxon, C. R. Design and Synthesis of Irreversible Inhibitors of Nek2 Kinase; *PhD Thesis*. Newcastle University, 2010.
261. Connors, K. A. *Chemical Kinetics: The Study of Reaction Rates in Solution*. John Wiley & Sons, Incorporated: **1990**; p 1-32.
262. Arnaut, L. G.; Formosinho, S. J.; Burrows, H. *Chemical Kinetics: From Molecular Structure to Chemical Reactivity*. Elsevier Science: **2006**; p 29-30.
263. Neganova, I.; Vilella, F.; Atkinson, S. P.; Lloret, M.; Passos, J. F.; von Zglinicki, T.; O'Connor, J. E.; Burks, D.; Jones, R.; Armstrong, L.; Lako, M. An important role for CDK2 in G1 to S checkpoint activation and DNA damage response in human embryonic stem cells. *Stem Cells* **2011**, 29, 651-659.
264. Lundberg, A. S.; Weinberg, R. A. Functional inactivation of the retinoblastoma protein requires sequential modification by at least two distinct cyclin-cdk complexes. *Mol. Cell Biol.* **1998**, 18, 753-761.
265. Koepp, D. M.; Schaefer, L. K.; Ye, X.; Keyomarsi, K.; Chu, C.; Harper, J. W.; Elledge, S. J. Phosphorylation-Dependent Ubiquitination of Cyclin E by the SCFFbw7 Ubiquitin Ligase. *Science* **2001**, 294, 173-177.
266. Petersen, B. O.; Lukas, J.; Sorensen, C. S.; Bartek, J.; Helin, K. Phosphorylation of mammalian CDC6 by Cyclin A/CDK2 regulates its subcellular localization. *EMBO J.* **1999**, 18, 396-410.
267. Sorensen, C. S.; Lukas, C.; Kramer, E. R.; Peters, J. M.; Bartek, J.; Lukas, J. A conserved cyclin-binding domain determines functional interplay between anaphase-promoting complex-Cdh1 and cyclin A-Cdk2 during cell cycle progression. *Mol. Cell Biol.* **2001**, 21, 3692-3703.
268. Adon, A. M.; Zeng, X.; Harrison, M. K.; Sannem, S.; Kiyokawa, H.; Kaldis, P.; Saavedra, H. I. Cdk2 and Cdk4 regulate the centrosome cycle and are critical mediators of centrosome amplification in p53-null cells. *Mol. Cell Biol.* **2010**, 30, 694-710.
269. Matsumoto, Y.; Hayashi, K.; Nishida, E. Cyclin-dependent kinase 2 (Cdk2) is required for centrosome duplication in mammalian cells. *Curr. Biol.* **1999**, 9, 429-432.
270. Satyanarayana, A.; Kaldis, P. A dual role of Cdk2 in DNA damage response. *Cell Div.* **2009**, 4, 9.
271. Giono, L. E.; Manfredi, J. J. The p53 tumor suppressor participates in multiple cell cycle checkpoints. *J. Cell Physiol.* **2006**, 209, 13-20.
272. Satyanarayana, A.; Hilton, M. B.; Kaldis, P. p21 Inhibits Cdk1 in the absence of Cdk2 to maintain the G1/S phase DNA damage checkpoint. *Mol. Biol. Cell* **2008**, 19, 65-77.
273. Hu, B.; Mitra, J.; van den Heuvel, S.; Enders, G. H. S and G2 Phase Roles for Cdk2 Revealed by Inducible Expression of a Dominant-Negative Mutant in Human Cells. *Mol. Cell Biol.* **2001**, 21, 2755-2766.
274. Tetsu, O.; McCormick, F. Proliferation of cancer cells despite CDK2 inhibition. *Cancer cell* **2003**, 3, 233-245.
275. Berthet, C.; Aleem, E.; Coppola, V.; Tessarollo, L.; Kaldis, P. Cdk2 Knockout Mice Are Viable. *Curr. biol.* **2003**, 13, 1775-1785.

276. L'Italien, L.; Tanudji, M.; Russell, L.; Schebye, X. M. Unmasking the redundancy between Cdk1 and Cdk2 at G2 phase in human cancer cell lines. *Cell Cycle* **2006**, *5*, 984-993.
277. Davies, T. G.; Bentley, J.; Arris, C. E.; Boyle, F. T.; Curtin, N. J.; Endicott, J. A.; Gibson, A. E.; Golding, B. T.; Griffin, R. J.; Hardcastle, I. R.; Jewsbury, P.; Johnson, L. N.; Mesguiche, V.; Newell, D. R.; Noble, M. E. M.; Tucker, J. A.; Wang, L.; Whitfield, H. J. Structure-based design of a potent purine-based cyclin-dependent kinase inhibitor. *Nat. Struct. Mol. Biol.* **2002**, *9*, 745-749.
278. Griffin, R. J.; Arris, C. E.; Bleasdale, C.; Boyle, F. T.; Calvert, A. H.; Curtin, N. J.; Dalby, C.; Kanugula, S.; Lembicz, N. K.; Newell, D. R.; Pegg, A. E.; Golding, B. T. Resistance-modifying agents. 8. Inhibition of O(6)-alkylguanine-DNA alkyltransferase by O(6)-alkenyl-, O(6)-cycloalkenyl-, and O(6)-(2-oxoalkyl)guanines and potentiation of temozolomide cytotoxicity in vitro by O(6)-(1-cyclopentenylmethyl)guanine. *J. Med. Chem.* **2000**, *43*, 4071-4083.
279. K. Lembicz, N.; Grant, S.; Clegg, W.; J. Griffin, R.; L. Heath, S.; T. Golding, B. Facilitation of displacements at the 6-position of purines by the use of 1,4-diazabicyclo[2.2.2]octane as leaving group. *J. Chem. Soc., Perkin Trans. 1* **1997**, 185-186.
280. Harada, H.; Asano, O.; Hoshino, Y.; Yoshikawa, S.; Matsukura, M.; Kabasawa, Y.; Nijima, J.; Kotake, Y.; Watanabe, N.; Kawata, T.; Inoue, T.; Horizoe, T.; Yasuda, N.; Minami, H.; Nagata, K.; Murakami, M.; Nagaoka, J.; Kobayashi, S.; Tanaka, I.; Abe, S. 2-Alkynyl-8-aryl-9-methyladenines as Novel Adenosine Receptor Antagonists: Their Synthesis and Structure-Activity Relationships toward Hepatic Glucose Production Induced via Agonism of the A2B Receptor. *J. Med. Chem.* **2000**, *44*, 170-179.
281. Aujard, I.; Benbrahim, C.; Gouget, M.; Ruel, O.; Baudin, J.-B.; Neveu, P.; Jullien, L. o-Nitrobenzyl Photolabile Protecting Groups with Red-Shifted Absorption: Syntheses and Uncaging Cross-Sections for One- and Two-Photon Excitation. *Chem. Eur. J.* **2006**, *12*, 6865-6879.
282. Il'ichev, Y. V.; Schworer, M. A.; Wirz, J. Photochemical reaction mechanisms of 2-nitrobenzyl compounds: methyl ethers and caged ATP. *J. Am. Chem. Soc.* **2004**, *126*, 4581-4595.
283. Myers, S. Discovery and Optimisation of Small-Molecule ERK5 Inhibitors as Cancer Therapeutics; *PhD Thesis*. Newcastle University, 2012.
284. Yasunori, T.; Kimihiro, S. Novel pyrrolo[2,3-d]pyrimidine compound. WO2011145718 (A1), 2009.
285. Harrison, L. R. E.; Ottley, C. J.; Pearson, D. G.; Roche, C.; Wedge, S. R.; Dolan, M. E.; Newell, D. R.; Tilby, M. J. The kinase inhibitor O⁶-cyclohexylmethylguanine (NU2058) potentiates the cytotoxicity of cisplatin by mechanisms that are independent of its effect upon CDK2. *Biochem. Pharmacol.* **2009**, *77*, 1586-1592.
286. Wang, D.; Lippard, S. J. Cellular processing of platinum anticancer drugs. *Nat. Rev. Drug Discov.* **2005**, *4*, 307-320.
287. Wong, E.; Giandomenico, C. M. Current Status of Platinum-Based Antitumor Drugs. *Chem. Rev.* **1999**, *99*, 2451-2466.
288. Fishel, M. L.; Newell, D. R.; Griffin, R. J.; Davison, R.; Wang, L.-Z.; Curtin, N. J.; Zuhowski, E. G.; Kasza, K.; Egorin, M. J.; Moschel, R. C.; Dolan, M. E. Effect of Cell Cycle Inhibition on Cisplatin-Induced Cytotoxicity. *J. Pharmacol. Exp. Ther.* **2005**, *312*, 206-213.
289. Vernalis. Pyrrolopyrimidine Compounds. WO2009/37467 A1, **2009**.

290. Han, B.; Rajwanshi, V.; Nandy, J.; Krishnamurthy, R.; Eschenmoser, A. Mannich-Type C-Nucleosidations with 7-Carba-purines and 4-Aminopyrimidines. *Synlett* **2005**, 2005, 744-750.
291. Kazimierczuk, Z.; Cottam, H. B.; Revankar, G. R.; Robins, R. K. Synthesis of 2'-deoxytubercidin, 2'-deoxyadenosine, and related 2'-deoxynucleosides via a novel direct stereospecific sodium salt glycosylation procedure. *J. Am. Chem. Soc.* **1984**, 106, 6379-6382.
292. Chuaqui, C. E.; Huang, S.; Ioannidis, S.; Shi, J.; Su, M.; Su, Q. Heterocyclic JAK Kinase Inhibitors. WO/2010/038060, **2010**.
293. GlaxoSmithKline. Pyrrolopyrimidine Derivatives as SYK Inhibitors. WO2007/42298 A1, **2007**.
294. Itoh, T.; Ono, K.; Sugawara, T.; Mizuno, Y. Studies on the chemical synthesis of potential antimetabolites. 30. Regioselective introduction of a chlorine atom into the imidazo[4,5-*b*]pyridine nucleus. *J. Heterocycl. Chem.* **1982**, 19, 513-517.
295. Wenzel, T.; Seela, F. Synthesis of 6-Substituted 1-Deazapurine 2' - Deoxyribonucleosides. *Helv. Chim. Acta* **1996**, 79, 169-178.
296. Chang, L. C. W.; von Frijtag Drabbe Künzel, J. K.; Mulder-Krieger, T.; Westerhout, J.; Spangenberg, T.; Brussee, J.; Ijzerman, A. P. 2,6,8-Trisubstituted 1-Deazapurines as Adenosine Receptor Antagonists. *J. Med. Chem.* **2007**, 50, 828-834.
297. Solvay-Pharmaceuticals. 2-Substituted-1-Deaza Purine Derivatives with Adenosine Receptor Modulating Activity US2006/52412 A1, **2006**.
298. Nowak, P.; Cole, D. C.; Brooijmans, N.; Bursavich, M. G.; Curran, K. J.; Ellingboe, J. W.; Gibbons, J. J.; Hollander, I.; Hu, Y.; Kaplan, J.; Malwitz, D. J.; Toral-Barza, L.; Verheijen, J. C.; Zask, A.; Zhang, W.-G.; Yu, K. Discovery of Potent and Selective Inhibitors of the Mammalian Target of Rapamycin (mTOR) Kinase. *J. Med. Chem.* **2009**, 52, 7081-7089.
299. Tyrogenex Inc.; Liang, C.; Li, Z. WO2010/56320 A2, **2010**.
300. Robins, R. K. Potential Purine Antagonists. IX. Further Studies of Some 4,6-Disubstituted Pyrazolo[3,4-*d*]pyrimidines. *J. Am. Chem. Soc.* **1957**, 79, 6407-6415.
301. Frohlich, L. G.; Kotsonis, P.; Traub, H.; Taghavi-Moghadam, S.; Al-Masoudi, N.; Hofmann, H.; Strobel, H.; Matter, H.; Pfeleiderer, W.; Schmidt, H. H. Inhibition of neuronal nitric oxide synthase by 4-amino pteridine derivatives: structure-activity relationship of antagonists of (6*R*)-5,6,7,8-tetrahydrobiopterin cofactor. *J. Med. Chem.* **1999**, 42, 4108-4121.
302. Shealy, Y. F.; Clayton, J. D.; O'Dell, C. A.; Montgomery, J. A. v-Triazolo[4,5-*d*]pyrimidines. II. O-Substituted Derivatives of 8-Azaguanine and 8-Azahypoxanthine. *J. Org. Chem.* **1962**, 27, 4518-4523.
303. Johns, B. A.; Gudmundsson, K. S.; Turner, E. M.; Allen, S. H.; Samano, V. A.; Ray, J. A.; Freeman, G. A.; Boyd, F. L., Jr.; Sexton, C. J.; Selleseth, D. W.; Creech, K. L.; Moniri, K. R. Pyrazolopyridine antiherpetics: SAR of C2' and C7 amine substituents. *Bioorg. Med. Chem.* **2005**, 13, 2397-2411.
304. Han, A.; Qi; Wang, E.; Gauss, C.; Xie, W.; Coburn, G.; Demuys, J.-M. Antiviral Pyrimidines. WO2010/118367 A2, **2010**.
305. Ortíz, A.; Insuasty, B.; Torres, M. R.; Herranz, M. Á.; Martín, N.; Viruela, R.; Ortí, E. Aminopyrimidine-Based Donor–Acceptor Chromophores: Push–Pull versus Aromatic Behaviour. *Eur. J. Org. Chem.* **2008**, 2008, 99-108.

- 306. Parsons, R. J. The design and synthesis of pyrimidine based cyclin-dependent kinase (CDK) inhibitors; *PhD Thesis*. Newcastle University, **2001**.
- 307. Seela, F.; Steker, H. Synthesis of 2'-Deoxyribofuranosides of 8-Aza-7-deazaguanine and Related Pyrazolo[3,4-*d*]pyrimidines. *Helv. Chim. Acta* **1986**, *69*, 1602-1613.
- 308. Klepper, F.; Jahn, E.-M.; Hickmann, V.; Carell, T. Synthesis of the Transfer-RNA Nucleoside Queuosine by Using a Chiral Allyl Azide Intermediate. *Angw. Chem. Int. Ed.* **2007**, *46*, 2325-2327.
- 309. Nakatani, Y.; Koizumi, Y.; Yamasaki, R.; Saito, S. Copper-catalyzed synthesis of esters from ketones. Alkyl group as a leaving group. *Org. Lett.* **2008**, *10*, 2067-2070.
- 310. Temple, C.; Smith, B. H.; Montgomery, J. A. Preparation of 5,7-diamino-3H-imidazo[4,5-*b*]pyridine-2,6-diamino-1-deazapurine. *J. Org. Chem.* **1973**, *38*, 613-615.